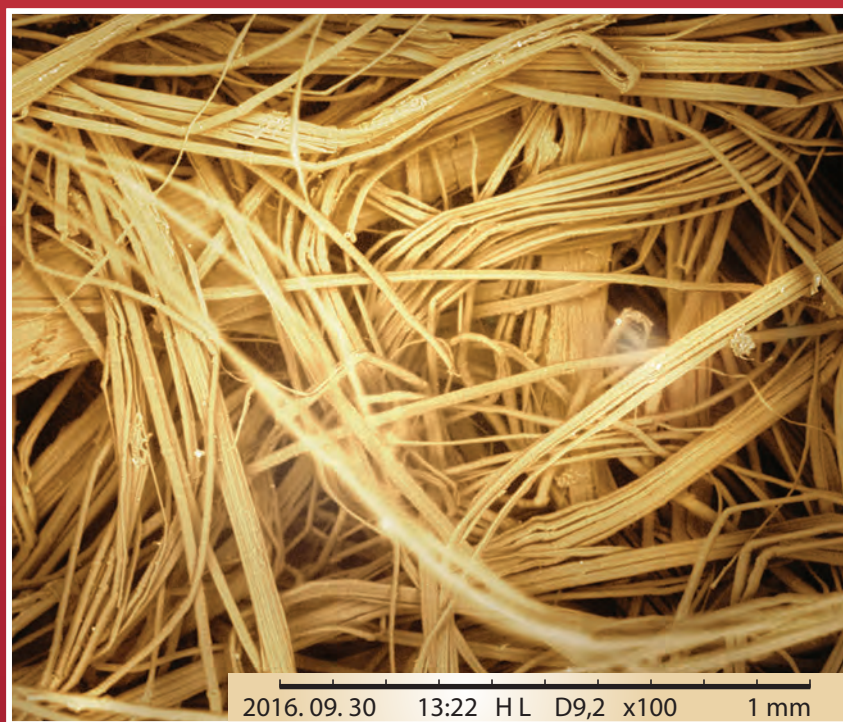




# Acta Chimica Slo Acta Chimica Slo Slovenica Acta C 2

64/2017



Selected titles: Electroanalytical Determination of Escitalopram Oxalate Using Nickel Nanoparticles Modified Carbon Paste Sensor ■ New Bioactive Heteroleptic Copper(II) Carboxylates: Structure, Enzymatic and DNA-Binding Studies ■ A Natural Based Method for Hydrophobic Treatment of Natural Fiber Material ■ Microwave-assisted Synthesis of Hybrid Heterocycles as Potential Anticancer Agents ■ AB Initio Prediction of Stable Conformer Polymorphs of Benzocaine Molecule- a Local Anaesthetic Molecule

<http://acta.chem-soc.si>

---

## EDITOR-IN-CHIEF

**ALEKSANDER PAVKO**

Slovenian Chemical Society, Hajdrihova 19, SI-1000 Ljubljana, Slovenija,  
E-mail: ACSi@fkk.uni-lj.si, Telephone: (+386)-1-476-0252; Fax: (+386)-1-1-476-0300

## ASSOCIATE EDITORS

**Marija Bešter-Rogač**, University of Ljubljana, Slovenia  
**Janez Cerkovnik**, University of Ljubljana, Slovenia  
**Krištof Kranjc**, University of Ljubljana, Slovenia  
**Franc Perdih**, University of Ljubljana, Slovenia  
**Helena Prosen**, University of Ljubljana, Slovenia  
**Damjana Rozman**, University of Ljubljana, Slovenia

**Melita Tramšek**, Jožef Stefan Institute, Slovenia  
**Irena Vovk**, National Institute of Chemistry, Slovenia

## ADMINISTRATIVE ASSISTANT

**Marjana Gantar Albreht** National Institute of Chemistry, Slovenia

---

## EDITORIAL BOARD

**Wolfgang Buchberger**, Johannes Kepler University, Austria  
**Alojz Demšar**, University of Ljubljana, Slovenia  
**Stanislav Gobec**, University of Ljubljana, Slovenia  
**Marko Goličnik**, University of Ljubljana, Slovenia  
**Günter Grampp**, Graz University of Technology, Austria  
**Wojciech Grochala**, University of Warsaw, Poland  
**Danijel Kikelj**, Faculty of Pharmacy, Slovenia  
**Ksenija Kogej**, University of Ljubljana, Slovenia  
**Janez Košmrlj**, University of Ljubljana, Slovenia  
**Blaž Likozar**, National Institute of Chemistry, Slovenia

**Mahesh K. Lakshman**, The City College and  
The City University of New York, USA  
**Janez Mavri**, National Institute of Chemistry, Slovenia  
**Friedrich Sreinc**, University of Minnesota, USA  
**Walter Steiner**, Graz University of Technology, Austria  
**Jurij Svete**, University of Ljubljana, Slovenia  
**Ivan Švancara**, University of Pardubice, Czech Republic  
**Jiri Pinkas**, Masaryk University Brno, Czech Republic  
**Gašper Tavčar**, Jožef Stefan Institute, Slovenia  
**Christine Wandrey**, EPFL Lausanne, Switzerland  
**Ennio Zangrando**, University of Trieste, Italy

---

## ADVISORY EDITORIAL BOARD

### Chairman

Branko Stanovnik, Slovenia

### Members

Josef Barthel, Germany  
Udo A. Th. Brinkman, The Netherlands  
Attilio Cesaro, Italy  
Dušan Hadži, Slovenia  
Vida Hudnik, Slovenia  
Venčeslav Kaučič, Slovenia

Željko Knez, Slovenia

Radovan Komel, Slovenia

Janez Levec, Slovenia

Stane Pejovnik, Slovenia

Anton Perdih, Slovenia

Slavko Pečar, Slovenia

Andrej Petrič, Slovenia

Boris Pihlar, Slovenia

Milan Randić, Des Moines, USA

Jože Škerjanc, Slovenia

Miha Tišler, Slovenia

Đurđa Vasić-Rački, Croatia

Marjan Veber, Slovenia

Gorazd Vesnaver, Slovenia

Jure Zupan, Slovenia

Boris Žemva, Slovenia

Majda Žigon, Slovenia

---

*Acta Chimica Slovenica* is indexed in: *Chemical Abstracts Plus*, *Current Contents (Physical, Chemical and Earth Sciences)*, *PubMed*, *Science Citation Index Expanded* and *Scopus*. Impact factor for 2015 is IF = 1,167.



Articles in this journal are published under Creative Commons Attribution 3.0 License  
<http://creativecommons.org/licenses/by/3.0/>

*Izdaja – Published by:*

SLOVENSKO KEMIJSKO DRUŠTVO – SLOVENIAN CHEMICAL SOCIETY

Naslov redakcije in uprave – Address of the Editorial Board and Administration

Hajdrihova 19, SI-1000 Ljubljana, Slovenija

Tel.: (+386)-1-476-0252; Fax: (+386)-1-476-0300; E-mail: chem.soc@ki.si

Slovensko kemijsko društvo  
Slovenian Chemical Society



*Izdajanje sofinancirajo – Financially supported by:*

Slovenian Research Agency, Ljubljana, Slovenia

National Institute of Chemistry, Ljubljana, Slovenia

Jožef Stefan Institute, Ljubljana, Slovenia

Faculty of Chemistry and Chemical Technology at University of Ljubljana, Slovenia

Faculty of Chemistry and Chemical Engineering at University of Maribor, Slovenia

Faculty of Pharmacy at University of Ljubljana, Slovenia

University of Nova Gorica, Nova Gorica, Slovenia

Chamber of Commerce and Industry of Slovenia – Chemical and Rubber Industry Association, Slovenia

Članom je revija na voljo brezplačno. Za nečlane in pravne osebe znaša letna naročnina 50 EUR, za inozemstvo 110 EUR vključno s poštnino.

Annual subscription: 110 EUR including postage.

Transakcijski račun: 02053-0013322846

Bank Account No.: SI56020530013322846-Nova Ljubljanska banka d. d., Trg republike 2, SI-1520 Ljubljana, Slovenia, SWIFT Code: LJBA SI 2X

Na podlagi Zakona o davku na dodano vrednost sodi revija *Acta Chimica Slovenica* med proizvode, od katerih se obračunava DDV po stopnji 9,5 %.

*Acta Chimica Slovenica* izhaja štirikrat letno v 200 izvodih – *Acta Chimica Slovenica* appears quarterly in 200 copies

Oblikovanje ovitka – Design cover: KULT, oblikovalski studio, Simon KAJTNA, s. p. Grafična priprava za tisk: Majanafin, d. o. o. Tisk – Printed by: Tiskarna Skušek, Ljubljana

© Copyright by Slovenian Chemical Society

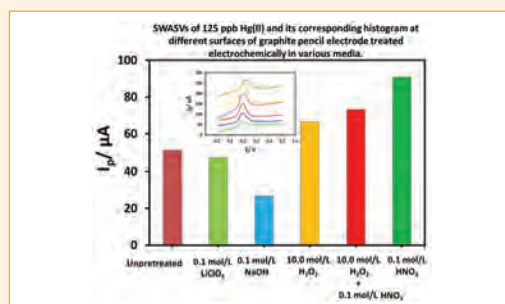


## SCIENTIFIC PAPER

267–275 Analytical chemistry

### Trace Determination of Hg(II) in Human Saliva Using Disposable Electrochemically Pretreated Graphite Pencil Electrode Surfaces

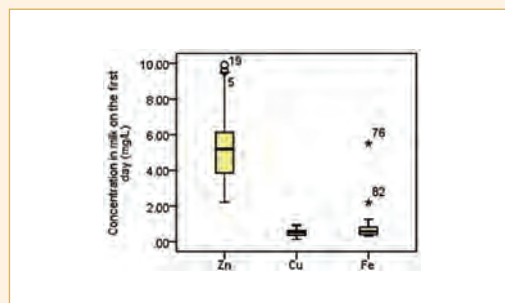
Abdel-Nasser Kawde



276–282 Analytical chemistry

### Determination of Microelements in Human Milk and Infant Formula Without Digestion by ICP-OES

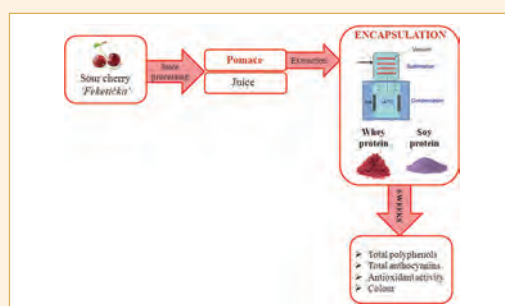
Dijana Đurović, Branka Milisavljević, Mirjana Nedović-Vuković, Branislav Potkonjak, Snežana Spasić and Miroslav M. Vrvčić



283–289 Applied chemistry

### Encapsulation of Sour Cherry Pomace Extract by Freeze Drying: Characterization and Storage Stability

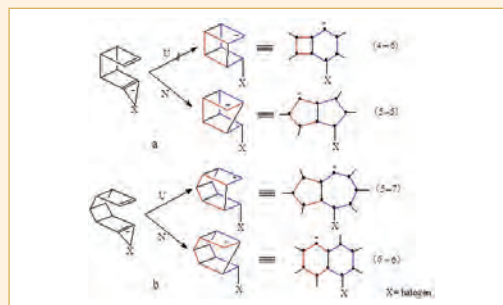
Vesna Tumbas Šaponjac, Gordana Četković, Jasna Čanadanović-Brunet, Sonja Dilas, Biljana Pajin, Jovana Petrović, Slađana Stajčić and Jelena Vulić



290–298 Physical chemistry

## Theoretical Investigation of Electrophilic Transannular Addition Reactions of Bromine to Face-to-Face (Juxtaposed) Double Bonds in Strained Polycyclic Hydrocarbons

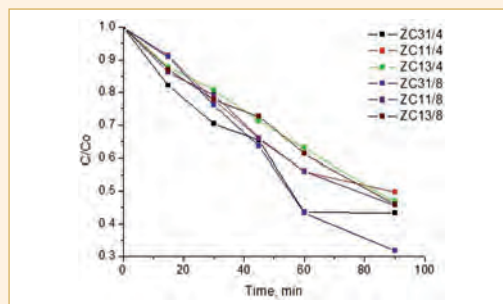
Rza Abbasoglu



299–311 Materials science

## Mixed Metal Oxides of the Type $\text{Co}_x\text{Zn}_{1-x}\text{Fe}_2\text{O}_4$ as Photocatalysts for Malachite Green Degradation Under UV Light Irradiation

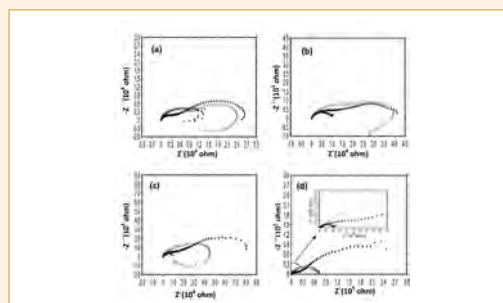
Martin Tzvetkov, Maria Milanova, Zara Cherkezova-Zheleva, Ivanka Spassova, Evgenia Valcheva, Joana Zaharieva and Ivan Mitov



312–318 Materials science

## Poly(N-methylpyrrole) Film on ZnNi Plated Carbon Steel Electrode

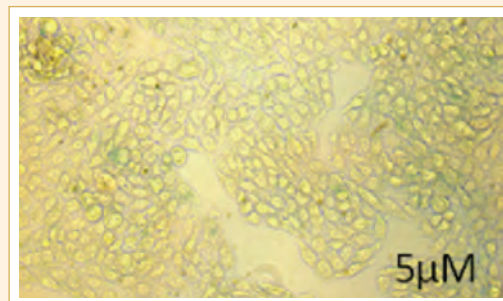
Abdurrahman Akdag and Ali Tuncay Ozyilmaz



319–331 Organic chemistry

## Microwave-assisted Synthesis of Hybrid Heterocycles as Potential Anticancer Agents

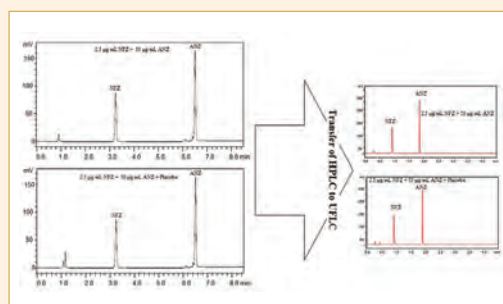
Avula Srinivas, Malladi Sunitha, Kammachichu Raju, Banothu Ravinder, Siluveru Anusha, Thallapalli Rajasri, Pothuganti Swapna, Dupa Sushmitha, Deva Swaroopa, Gurala Nikitha and Chakunta Govind Rao



332–341 Analytical chemistry

## Stability Indicating UHPLC-PDA Assay for Simultaneous Determination of Antazoline Hydrochloride and Naphazoline Hydrochloride in Ophthalmic Formulations

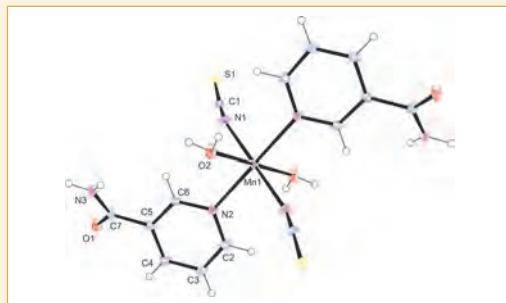
Amir Ali, Umar Farooq, Mahmood Ahmed, Muhammad Makshoof Athar, Kashif Nadeem and Ghulam Murtaza



342–348 Inorganic chemistry

## $[M^{II}(NCS)_2(nia)_2(OH_2)_2]$ : Preparation, Crystal Structure and Thermal Properties ( $M^{II} = Mn, Fe$ ; nia = nicotinamide)

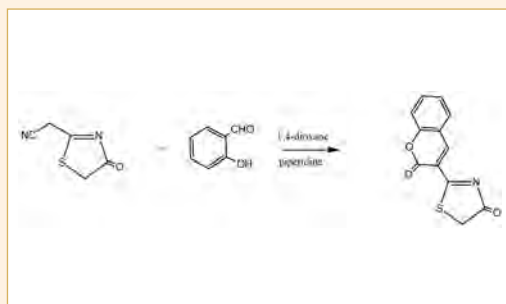
Marta Počkaj, Nives Kitanovski, Boris Čeh and Romana Cerc-Korošec



349–364 Organic chemistry

## Anti-inflammatory and Anti-ulcer Activities of New Fused Thiazole Derivatives Derived from 2-(2-Oxo-2H-chromen-3-yl)thiazol-4(5H)-one

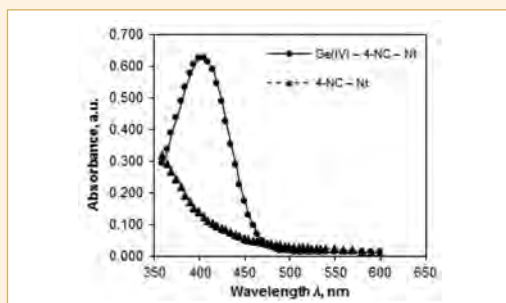
Rafat M. Mohareb, Fatima Al-Omran, Mahmoud A. Abdelaziz and Rehab A. Ibrahim



365–372 Inorganic chemistry

## Study on the Equilibria of the Complex Formation of the Ion-pair of Germanium(IV) with 4-Nitrocatechol and 1,4-Diphenyl-3-(phenylamino)-1H-1,2,4-triazole

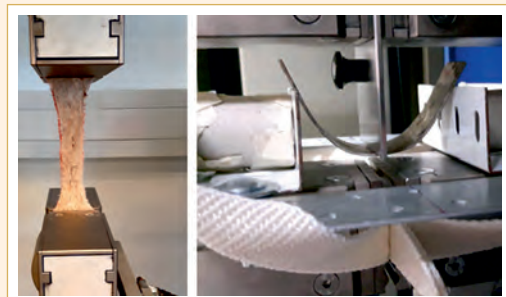
Petya Racheva, Kirila Stojnova, Vidka Divarova and Vanya Lekova



373–380 Materials science

## A Natural Based Method for Hydrophobic Treatment of Natural Fiber Material

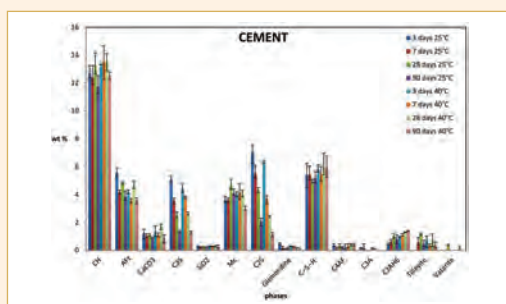
Thomas Kick, Thomas Grethe and Boris Mahltig



381–396 Materials science

## Influence of Various Soluble Carbonates on the Hydration of Portland Cement studied by X-ray Diffraction

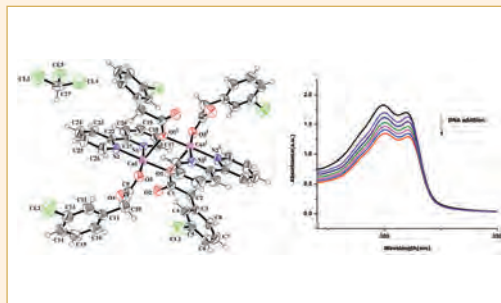
Simona Medvešček, Venčeslav Kaučič and Anton Meden



397–408 Inorganic chemistry

## New Bioactive Heteroleptic Copper(II) Carboxylates: Structure, Enzymatic and DNA-Binding Studies

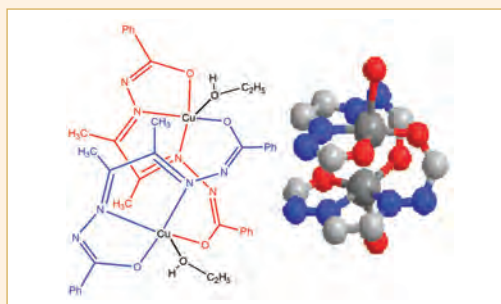
Afifa Mushtaq, Saqib Ali, Muhammad Nawaz Tahir, Hammad Ismail, Bushra Mirza, Muhammad Saadiq, Muhammad Abdul Haleem and Muhammad Iqbal



409–414 Inorganic chemistry

## Synthesis and Structural Characterization of a Double Helical Dinuclear Copper(II) Complex With Tetradentate Biacetyl Bis(benzoylhydrazone)

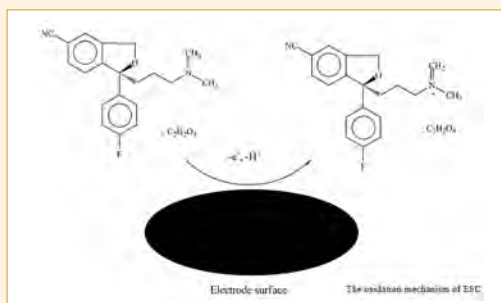
Rasoul Vafazadeh, Najmeh Abdollahi and Anthony C. Willis



415–421 Analytical chemistry

## Electroanalytical Determination of Escitalopram Oxalate Using Nickel Nanoparticles Modified Carbon Paste Sensor

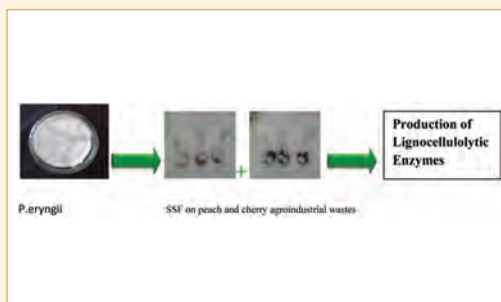
Ali Kamal Attia, Mona A. Mohamed and Amany M. Fekry



422–430 Analytical chemistry

## Peach and Cherry Agroindustrial Wastes: New and Economic Sources for the Production of Lignocellulolytic Enzymes

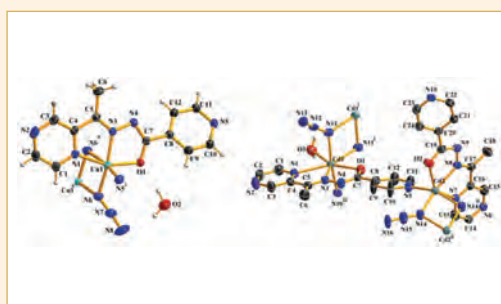
Merve Akpinar and Raziye Ozturk Urek



431–437 Inorganic chemistry

## 2D Frameworks Self-assembled From a Hydrazone Ligand and Azide Salts: Synthesis, Structures, and Luminescent Property

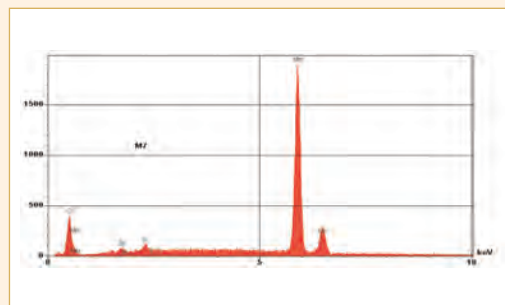
Peng Wang, Yu-Shan Wu, Xiao-Meng Han, Shan-Shan Zhao and Jie Qin



438–448 General chemistry

## Synthesis of $\text{MnO}_2$ on Activated Carbon and its Potential Application in the Adsorption of $\text{As(V)}$ and $\text{Pb(II)}$ in Aqueous Solutions

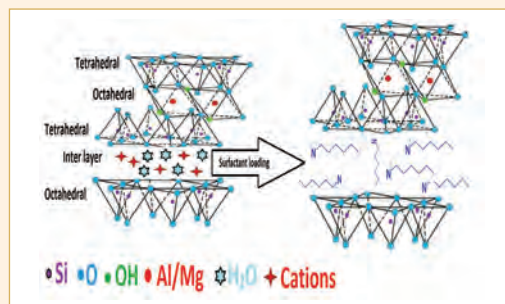
Roberto Contreras-Bustos, E. Manríquez-Reza, Jaime Jiménez-Becerril, Melania Jiménez-Reyes and Bibiana Cercado-Quezada



449–460 Chemical, biochemical and environmental engineering

## Adsorption Kinetics of Malachite Green and Methylene Blue from Aqueous Solutions Using Surfactant-modified Organoclays

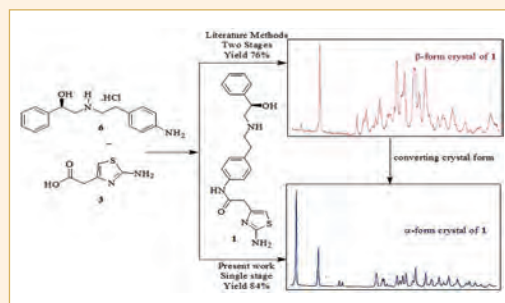
Haseeb Ullah, Muhammad Nafees, Farhat Iqbal, Muhammad Saifullah Awan, Afzal Shah and Amir Waseem



461–466 Organic chemistry

## First Direct Isolation of Stable $\alpha$ -Form Crystals of Mirabegron, a Selective $\beta_3$ -Adrenoceptor Agonist

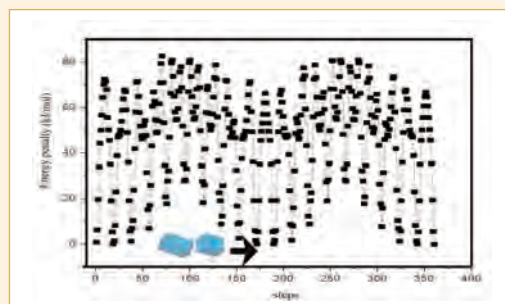
Dattatray G. Deshmukh, Mukund N. Bangal, Anil C. Mali, Vijay J. Medhane and Vijayavithal T. Mathad



467–478 Materials science

## AB Initio Prediction of Stable Conformational Polymorphs of Benzocaine Molecule- a Local Anaesthetic Molecule

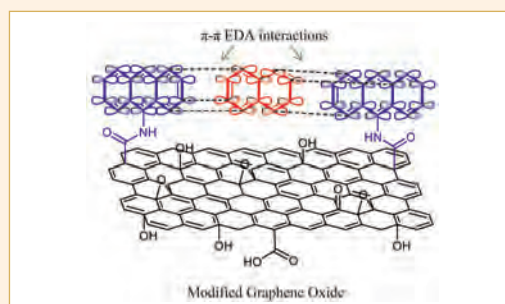
Pallipurath Veleelath Nidhin, Arputharaj David Stephen and Charles Selvaraj Arun Paul



479–490 Chemical, biochemical and environmental engineering

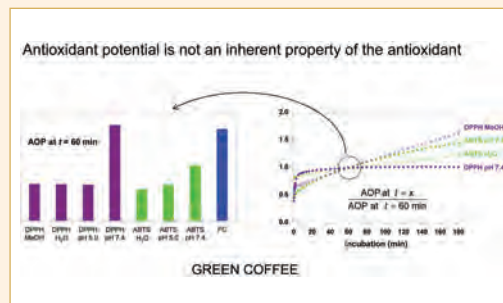
## Functionalization of Graphene Oxide with 9-aminoanthracene for the Adsorptive Removal of Persistent Aromatic Pollutants from Aqueous Solution

Ali Balati, Mohammad Ghanbari, Sara Karimi Behzad and Mostafa M. Amini



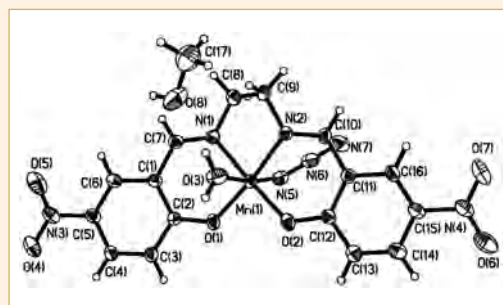
## The Methodology Applied in DPPH, ABTS and Folin-Ciocalteu Assays Has a Large Influence on the Determined Antioxidant Potential

Helena Abramovič, Blaž Grobin, Nataša Poklar Ulrih and Blaž Cigić



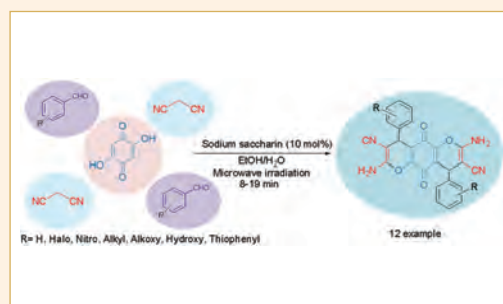
## Synthesis, Crystal Structures and Catalytic Oxidation of Manganese(III) Complexes Derived from Salen-Type Schiff Base *N,N'*-Bis(5-nitrosalicylidene)ethane-1,2-diamine

Qing-Bin Li, Yong-Jun Han, Gan-Qing Zhao and Ling-Wei Xue



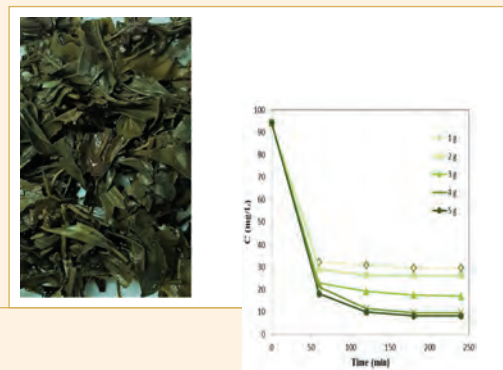
## Sodium Saccharin as an Effective Catalyst for Rapid One-pot Pseudo-five Component Synthesis of Dihydropyrano[2,3-g]chromenes under Microwave Irradiation

Leila Moradi and Maryam Aghamohammad Sadegh



## Adsorptive Removal of Malachite Green from Model Aqueous Solutions by Chemically Modified Waste Green Tea Biomass

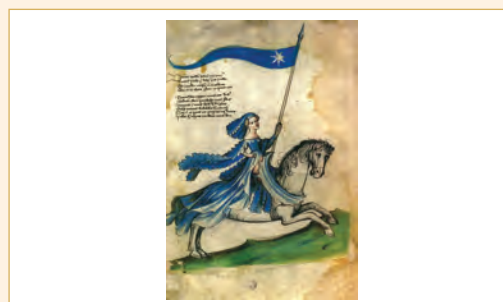
Cerasella Indolean, Silvia Burcă and Andrada Măicăneanu



## DRUŠTVENE VESTI

## Kemijski laboratorij celjske kraljice (ob 580 letnici kronanja češke kraljice Barbare Celjske)

Stanislav Južnič





Scientific paper

# Trace Determination of Hg(II) in Human Saliva Using Disposable Electrochemically Pretreated Graphite Pencil Electrode Surfaces

Abdel-Nasser Kawde\*

Chemistry Department, College of Sciences, King Fahd University of Petroleum and Minerals,  
Dhahran 31261, Saudi Arabia

\* Corresponding author: E-mail: akawde@kfupm.edu.sa  
Tel. No. +966 1 3 860 2145; Fax: +966 1 3 860 4277

Received: 20-04-2016

## Abstract

An electrochemically pretreated graphite pencil electrode (PGPE) was designed to assay trace levels of Hg(II) in human saliva. The GPE was pretreated in 0.1 mol/L nitric acid by cycling the potential between  $-1.6$  and  $-0.6$  V for 60 cycles at a scan rate of 50 mV/s. The effects of pretreatment conditions, including media constituents, pH, and various electrochemical techniques and parameters, were analyzed and optimum conditions determined. Square wave anodic stripping voltammetry (SWASV) was used for the determination of Hg(II). The calibration curve obtained under optimum conditions showed that the linear range of the PGPE was from  $10.0 \times 10^{-9}$  mol/L to  $175.0 \times 10^{-9}$  mol/L with a detection limit of  $3.0 \times 10^{-9}$  mol/L ( $S/N = 3$ ). Relative to non-pretreated GPE surfaces, electrochemical pretreatment improved the electrochemical performance of GPE surfaces in detecting Hg(II). The present analytical method was used to measure Hg(II) released from dental amalgam in human saliva.

**Keywords:** Pretreated graphite pencil electrode, Mercury (II), Square wave anodic stripping voltammetry, Human saliva

## 1. Introduction

Mercury is a long-standing occupational hazard, especially in dental offices and health care institutions, as well as in some homes.<sup>1,2</sup> The major manifestations of mercury poisoning include nephrotoxicity, primarily proteinuria and tubular necrosis, and neurotoxicity, which can be profound with high exposure.<sup>3</sup> The most important symptoms of mercury toxicity include tremors, nail changes, hair loss, oral and gingival inflammation, ataxia, excessive and uncontrollable salivation, anorexia and weight loss, labile affect and irritability, pathologic shyness and avoidance of people, and acrodynia (erythema and painful desquamative dermatitis of the hands and feet).<sup>4–14</sup> Individuals with congenital mercury toxicity will have severe mental retardation and motor abnormalities, including disturbances in swallowing.<sup>15,16</sup>

Various methods have been developed recently to determine mercury in body fluids, including urine,<sup>17</sup> serum,<sup>18</sup> and saliva.<sup>19,20</sup> Trace levels of mercury can be measured by techniques including atomic absorption spectroscopy,<sup>21</sup> cold vapor atomic emission,<sup>22</sup> X-ray fluorescence,<sup>23</sup> mass spectrometry,<sup>24</sup> and ICP-OES.<sup>25</sup> However, all of these methods have limitations in the routine analysis of mercury, including high costs, complex instrumentation, long duration and poor selectivity.

Electrochemical methods are frequently used in analytical chemistry due to their high sensitivity, low cost, fast response, simple instrumentation and portability.<sup>26,27</sup> The poor electrocatalytic properties of conventional electrodes, however, limit their use in measuring mercury concentrations. These electrocatalytic properties of electrodes can be improved by electrochemical pretreatment,<sup>28</sup> modifying the electrode with a suitable electrocatalyst or electron mediator,<sup>29,30</sup> and using a solution that enhances electrochemical reactions. Various types of modified electrodes have been developed to detect and measure mercury concentrations. These include silica modified electrodes,<sup>31</sup> bimetallic Au-Pt inorganic-organic hybrid nanocomposite-modified electrodes,<sup>32</sup> mercaptoacetic acid modified gold microwire electrodes,<sup>33</sup> organic-inorganic pillared montmorillonite-modified electrodes,<sup>34</sup> electro-

des modified with 5-methyl-2-thiouracil, graphene oxide and gold nanoparticles,<sup>35</sup> carbon nanotube modified electrodes,<sup>36</sup> and DNA-modified electrodes.<sup>37</sup> Despite the selectivity of these voltammetric techniques, methods that are cheaper and/or more sensitive and selective are needed to detect mercury. Electrochemical pretreatment of pencil graphite electrodes is a simpler, less time consuming and more applicable strategy compared with other procedures. This method eliminates the use of some toxic compounds required in the modification of the electrode surface.

Trace metals in saliva may be biomarkers for exposure to and metabolism of trace metals.<sup>38</sup> Blood flow in salivary glands is high, with chemicals and metabolites distributed in saliva by several mechanisms, including passive diffusion, active transport, and ultrafiltration.<sup>39</sup> Previous studies on the use of saliva for biomonitoring have focused on herbicides,<sup>40</sup> lead,<sup>41</sup> phthalate,<sup>42</sup> and fluoride ions,<sup>43</sup> in humans, animals or artificial models. The concentrations of chemical contaminants in saliva have been shown to reflect their concentrations in plasma. Saliva sampling is non-invasive and has advantages over urine and blood collection, particularly from newborns and infants. The present study describes a simple sensor, based on an electrochemically pretreated graphite pencil electrode (PGPE), for the detection of trace levels of mercury (II) in human saliva. The analytical performance of this sensor was evaluated by anodic stripping square wave voltammetry.

## 2. Experimental

### 2.1. Reagents

All chemicals used in this study were analytical reagent grade and used without further purification. Hydrogen peroxide (30%), sodium hydroxide, lithium chlorate and sodium acetate buffer (3.0 mol/L, pH 5.2) were obtained from Sigma Aldrich® (USA). Nitric acid was obtained from AnalaR® (England). A standard stock solution of mercury ( $5.0 \times 10^{-3}$  mol/L, plasma emission standard solution) was obtained from BDH, ARISTAR® (England) and diluted as required. Hi-polymer graphite pencil HB black leads were obtained from Pentel (Japan). All leads had a total length of 60.0 mm and a diameter of 0.5 mm and were used as received.

### 2.2. Apparatus and Procedures

A Jedo mechanical pencil (Korea) was used to hold both bare and pretreated graphite pencil leads. Electrical contact with the lead was achieved by soldering a copper wire to the metallic part that holds the lead in place inside the pencil. The pencil was fixed vertically with 15 mm of the lead extruded outside, and 10 mm of the lead immersed in the solution, corresponding to an electrode area of ca. 16 mm<sup>2</sup>. An electrochemical analyzer (CHI 660C model, CH Instruments, USA), was used in all electroche-

mical experiments. The electrochemical cell contained a PGPE as a working electrode, a Pt wire counter electrode, and an Ag/AgCl (Sat. KCl) reference electrode. Saliva samples were analyzed using an ICP-OES (iCAP 6000 series) spectrometer (Thermo Scientific, USA).

### 2.3. Pretreatment of GPE

A 10.0 mm length of GPE extruded from the pencil, an Ag/AgCl reference electrode, and a Pt counter electrode were immersed in a cell containing HNO<sub>3</sub> or other solutions at different concentrations, and different potential ranges were applied to pretreat the GPE surface. The pretreated electrodes were washed by gently dipping them twice in deionized water, and all entire electrochemical measurements were performed right after preparation of the pretreated electrodes.

### 2.4. Saliva Collection

Saliva was collected according to the recommendations of the World Medical Association Declaration of Helsinki for International Health Research. Saliva samples were obtained from volunteers living in Dhahran, Saudi Arabia, at least one hour after food consumption and after participants rinsed their mouths with water at least three times to remove any food residue. The samples were spat into detergent washed collection vials and examined for the presence of food, blood or nasal discharge. Contaminated samples were discarded, and retained samples were stored at -20.0 °C until analyzed.

### 2.5. Digestion of Saliva

Prior to sample preparation, the saliva samples were thawed and allowed to equilibrate to room temperature before being rechecked for any trace contaminants. A 5.0 ml aliquot of saliva was placed in a beaker, to which 20.0 ml of 2% nitric acid and 5.0 ml of 10.0 mol/L hydrogen peroxide were added. This solution was filtered through a Whatman no. 42 filter paper into a 100.0 ml volumetric flask and diluted to a final volume with distilled deionized water (DDW). These samples were stored until analyzed.

### 2.6. Electrochemical Procedure

The GPE, a working electrode in a three electrochemical cell, was immersed in 0.1 mol/L HNO<sub>3</sub> solution and treated electrochemically using cyclic voltammetric technique at a scan rate of 50 mV/s, with a potential range of -1.6 to -0.6 V, for 60 segments. The SWASV measurements of Hg(II) were completed after a deposition time of 300 s at -1.6 V from a stirred 0.1 mol/L pH 5.5 acetate buffer solution. The electrode was stripped after a 10 s rest period (without stirring) at an amplitude of 0.06 V and a frequency of 100 Hz, the experimentally determined opti-

mal parameters for Hg(II) determination by the SWASV method using PGPE (Table 1).

### 3. Results and Discussion

#### 3.1. Evaluation of the Electrode and Pretreatment Solution

The electrochemical oxidation of Hg(II) was assessed by recording SWASVs of different electrode materials, including glassy carbon, graphite pencil, carbon paste, Pt disc and gold disc electrodes, in acetate buffer (0.1 mol/L, pH 5.5) (Figure 1a). Carbon paste, Pt disc and gold disc electrodes did not respond well to  $6.2 \times 10^{-7}$  mol/L Hg(II) solution. This may have been due to differences among the various types of carbon electrodes (i.e. carbon paste, glassy carbon, and graphite electrodes), and to the effect of the electrochemical treatment in 0.1 mol/L HNO<sub>3</sub>. Both GCE and GPE gave a relatively well-defined SWASV signal, with the highest obtained signal at the GPE (Figure 1b).

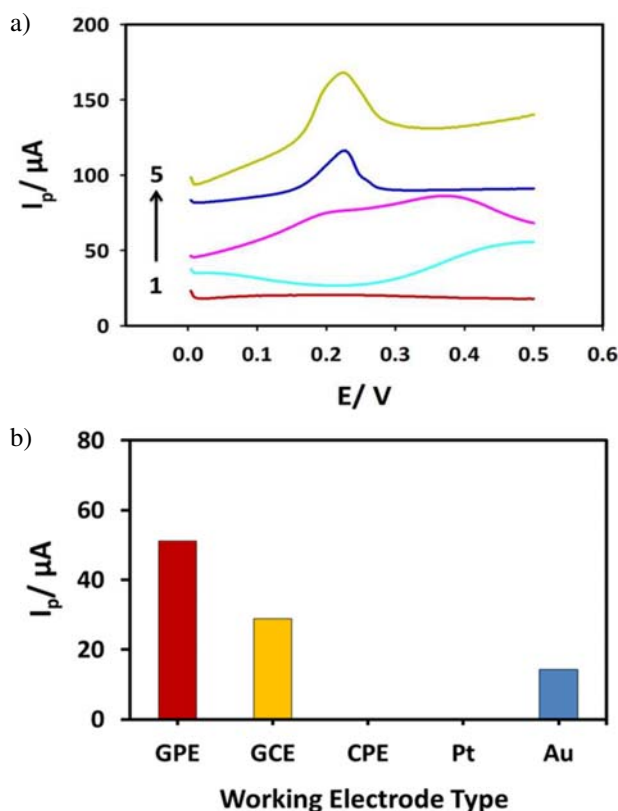


**Figure 1:** a) Square wave anodic stripping voltammograms (SWASVs) and b) corresponding histograms of  $6.2 \times 10^{-7}$  mol/L Hg(II) in acetate buffer (0.1 mol/L, pH 5.5) at 1) carbon paste, 2) Pt, 3) Au, 4) glassy carbon and 5) graphite pencil electrode. Working conditions: deposition potential,  $-1.6$  V; deposition time, 120 s; frequency, 100 Hz; scan rate, 100 mV/s; amplitude, 0.06 V

The differences in behavior among these five electrodes, in particular between the Pt- and Au-electrodes illustrated in Figure 1b, are observed. This may be due to amalgam formation with gold, as gold-mercury amalgam formation is well-known and even used in the extraction of gold from ore; platinum, by contrast, does not form such an amalgam. Various types of gold electrodes, including solid gold,<sup>44</sup> gold fiber,<sup>45</sup> and plated gold,<sup>46–48</sup> electrodes have been used for the determination of mercury; however, to the best of our knowledge, no study to date has examined platinum electrodes for this purpose.

Because a high electrochemical oxidation signal is essential for the fabrication of an ultrasensitive electroanalytical sensor, GPE was chosen as the transducer material for the electroanalytical determination of Hg(II).

The effect of GPE pretreatment solution was evaluated in NaOH, LiClO<sub>4</sub>, HNO<sub>3</sub>, H<sub>2</sub>O<sub>2</sub> and a mixture of H<sub>2</sub>O<sub>2</sub> and HNO<sub>3</sub> (Figure 2a). The potential pretreatment range was between  $-1.6$  to  $-0.6$  V of cyclic voltammetry (CV) with 20 pretreatment scans at a scan rate of 100 mV/s, followed by detection of Hg(II) in acetate buffer (0.1 mol/L, pH 5.5). Pretreatment of the pencil graphite electrode in

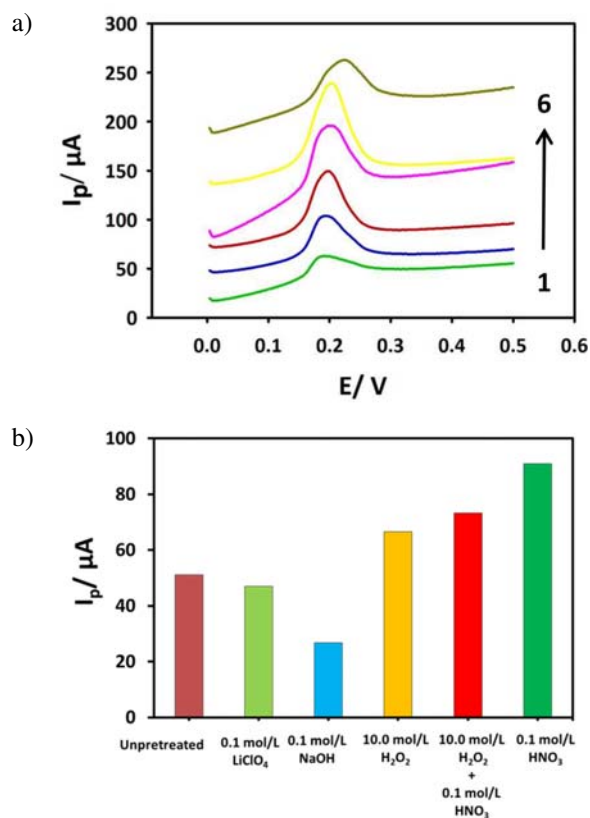


**Figure 2:** a) Square wave anodic stripping voltammograms (SWASVs) and b) corresponding histograms of  $6.2 \times 10^{-7}$  mol/L Hg(II) in acetate buffer (0.1 mol/L, pH 5.5) at 1) unpretreated (6) and pretreated GPEs in 1) NaOH, 2) LiClO<sub>4</sub>, 3) H<sub>2</sub>O<sub>2</sub> and HNO<sub>3</sub> and 5) HNO<sub>3</sub>, each at a concentration of 0.1 mol/L. Working conditions: deposition potential,  $-1.6$  V; deposition time, 120 s; frequency, 100 Hz; amplitude, 0.06 V

$\text{LiClO}_4$  and  $\text{NaOH}$  did not increase the SWASV response of  $\text{Hg(II)}$ . In contrast, both  $\text{H}_2\text{O}_2$  and  $\text{HNO}_3$  prominently increased the peak current for  $\text{Hg(II)}$ , with 0.1 mol/L  $\text{HNO}_3$  showing the highest peak current of  $\text{Hg(II)}$ . This may be attributed to an increase in surface roughness and a corresponding increase in electrode surface area. GPEs electrochemically pretreated with 0.1 mol/L  $\text{HNO}_3$  were used in further experiments.

### 3. 2. Effect of Electrochemical Pretreatment

The main constituents of pencil graphite electrodes are graphite (65%), clay (nearly 30%) and an electro-inactive polymer acting as a binder (5%). Graphite is a form of carbon in which atoms are connected by weak bonds between planes. Clay is a naturally occurring aluminosilicate with ion exchange properties. However, the graphite part of a pencil in contact with the pretreatment solution, such as  $\text{HNO}_3$ , is cleaned and linked to various oxygen-containing functional groups. An increased GPE signal after pretreatment can be attributed to an increase in the num-

ber of oxygen-containing groups on the electrode surface or to the formation of a graphite oxide film.

To determine the effect of the concentration of pretreatment solution ( $\text{HNO}_3$ ) on the PGPE, GPEs were pretreated with different concentrations of  $\text{HNO}_3$ , ranging from 0.05 mol/L to 0.8 mol/L, in a potential range of  $-1.6$  to  $-0.6$  V at a fixed scan rate of 100 mV/s, and  $\text{Hg(II)}$  concentrations were measured with the pretreated electrodes. Figure 3a shows SWASVs obtained using these electrodes in acetate buffer (0.1 mol/L, pH 5.5). As its concentration increased, the peak current for  $6.2 \times 10^{-7}$  mol/L  $\text{Hg(II)}$  also increased, with a maximum peak current obtained at 0.1 mol/L  $\text{HNO}_3$  (Figure 3b).

To evaluate the number of CV segments, GPEs were potentiodynamically pretreated by altering the number of scans between  $-1.6$  and  $-0.6$  V, at a scan rate of 100 mV/s. The maximum  $i_p$  was observed after 60 pretreatment scans, making the optimum number of pretreatment scans 60 segments (Figure 4).

We also assessed the effect of potential scan range on GPE. Figure 5a shows the influence of scanning poten-

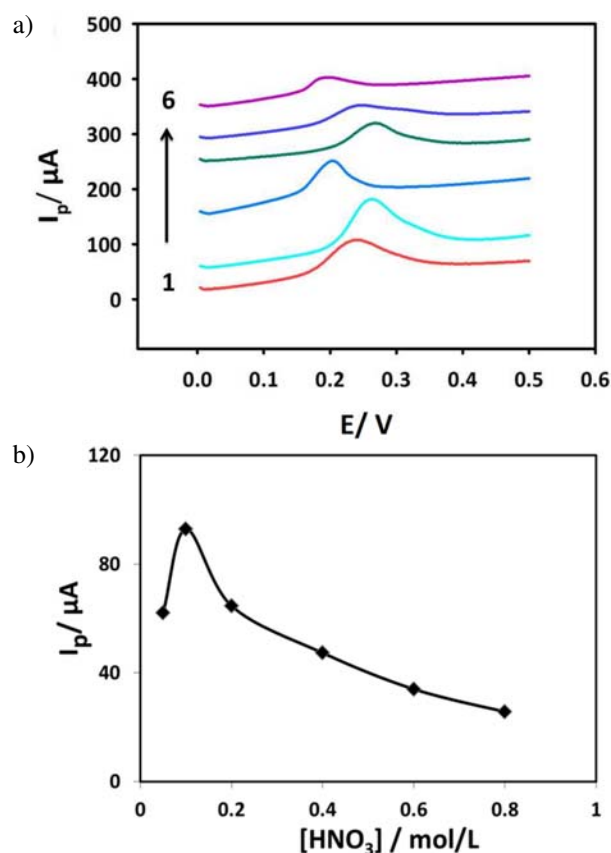


**Figure 3:** a) Square wave anodic stripping voltammograms (SWASVs) of  $6.2 \times 10^{-7}$  mol/L  $\text{Hg(II)}$  in 0.1 mol/L acetate buffer, pH 5.5 at GPE surfaces pretreated in 1) 0.05, 2) 0.1, 3) 0.2, 4) 0.4, 5) 0.6 and 6) 0.8 mol/L  $\text{HNO}_3$ . Working conditions: Pretreatment CV segments, 20; pretreatment potential,  $-1.6$  to  $-0.6$ ; deposition potential,  $-1.6$  V; deposition time, 120 s; frequency, 100 Hz; amplitude, 0.06 V. b) Corresponding plot of peak currents  $i_p$  ( $\mu\text{A}$ ) vs.  $\text{HNO}_3$  concentrations.

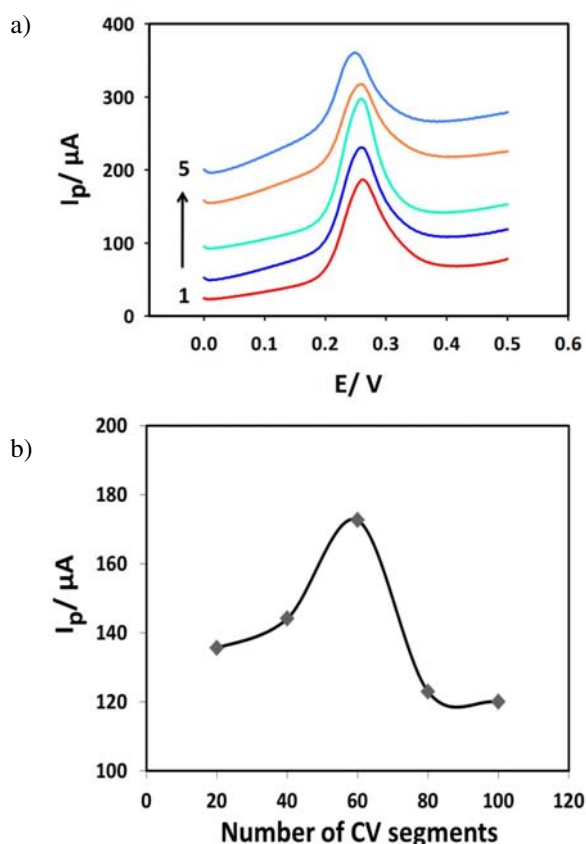


**Figure 4:** a) Square wave anodic stripping voltammograms (SWASVs) of  $6.2 \times 10^{-7}$  mol/L  $\text{Hg(II)}$  in 0.1 mol/L acetate buffer, pH 5.5 as a function of number of pretreated CV segments on GPE surfaces: 1) 20, 2) 40, 3) 60, 4) 80 and 5) 100 segments. Working conditions: Pretreatment potential,  $-1.6$  to  $-0.6$ ; pretreatment solution, 0.1 mol/L  $\text{HNO}_3$ ; deposition potential,  $-1.6$  V; deposition time, 120 s; frequency, 100 Hz; amplitude, 0.06 V. b) Corresponding plot of  $i_p$  vs number of pretreated CV segments.

tial range used during GPE pretreatment on SWV in a 0.1 mol/L solution of acetate buffer (pH 5.5) containing  $6.2 \times 10^{-7}$  mol/L Hg(II). The potential range of  $-1.6$  to  $-0.6$  V showed the highest peak current (Figure 5b).

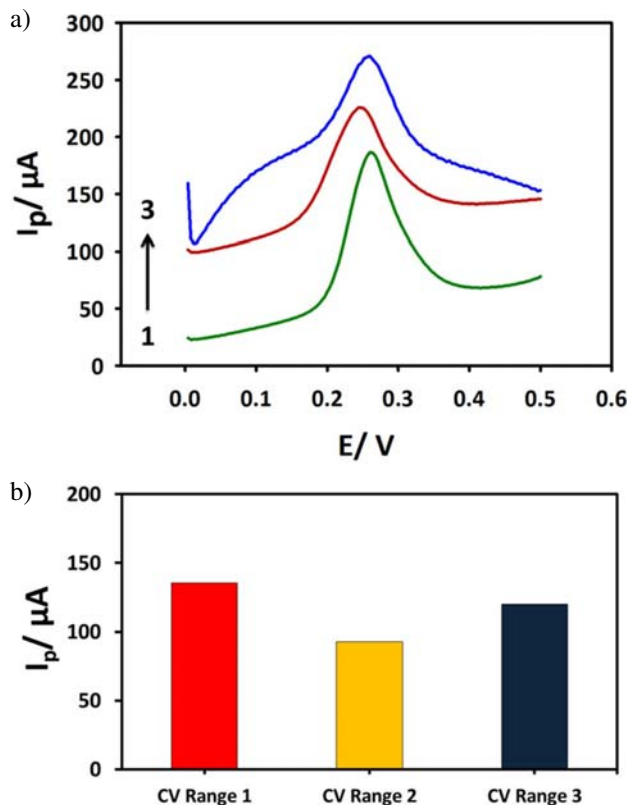


**Figure 5:** a) Square wave anodic stripping voltammograms (SWASVs) and b) corresponding histograms of  $6.2 \times 10^{-7}$  mol/L Hg(II) in 0.1 mol/L acetate buffer, pH 5.5 at GPE surfaces and after pretreatment potential ranges of 1)  $-1.6$  to  $-0.6$ , 2)  $-0.6$  to  $0.6$  and 3)  $0.6$  to  $1.6$  V. Twenty CV segments were pretreated; other working conditions were identical to those in Fig. 4a.

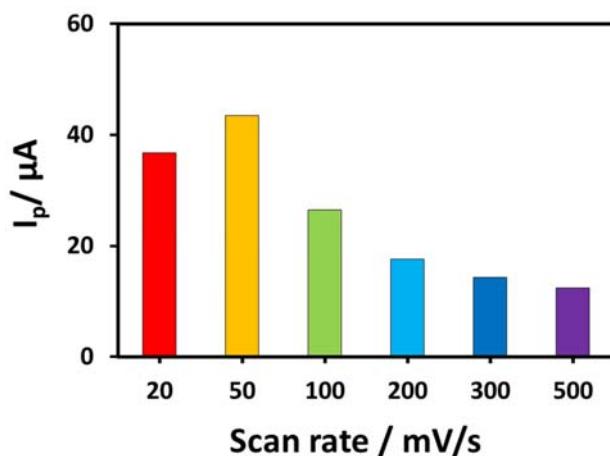


**Figure 6:** Histograms showing the effect of pretreatment scan rate on the detection of  $6.2 \times 10^{-7}$  mol/L Hg(II) in 0.1 mol/L acetate buffer (pH 5.5) at GPE surfaces. Pretreatment CV segments, 20; other working conditions are described in Fig. 4a.

Figure 6 shows the effect of scan rate on Hg(II) response at the electrochemically pretreated GPE, with a scan rate of 50 mV/s showing the maximum response.

### 3. 3. Optimization of SWASV Parameters

To select a suitable voltammetric technique for the detection of Hg(II) using the developed GPE, different voltammetric techniques were tested, including differential pulse, square wave, differential normal pulse, linear sweep, staircase, and normal pulse voltammetry. Of these methods, square wave voltammetry showed the highest peak current for the same concentration of Hg(II) (Figure 7).

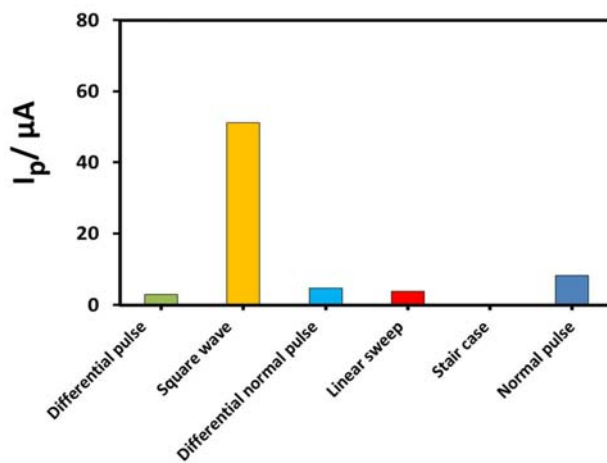


**Figure 7:** Histograms showing the effect of various voltammetric techniques at GPE surfaces on the detection of  $6.2 \times 10^{-7}$  mol/L Hg(II) in 0.1 mol/L acetate buffer (pH 5.5). Working conditions: deposition potential  $-1.6$  V, amplitude 0.06 V, frequency 100 Hz, deposition time 120 s.

To select the best medium for detecting Hg(II), various solutions were tested, including  $\text{HNO}_3$ , NaOH, and acetate and phosphate buffers, all at the same concentration, 0.1 mol/L. NaOH and phosphate buffer showed no peak for  $6.2 \times 10^{-7}$  mol/L Hg(II), whereas  $\text{HNO}_3$  and acetate buffer showed well-defined peaks (Figure 8a). Because the peak current for Hg(II) was the highest in 0.1 mol/L acetate buffer (Figure 8b), further optimizations were completed in acetate buffer solution.

The pH of the aqueous medium and the SWASV parameters can significantly influence the detection limit of any analyte. Thus, the effects of pH and SWASV parameters on Hg(II) electro-oxidation by PGPE were analyzed.

The SWV response to the electro-oxidation of  $6.2 \times 10^{-7}$  mol/L Hg(II) in acetate buffer at the PGPE was systematically studied over the pH range 3.2–6.5. As the pH increased, the electro-oxidation peak potential ( $E_p$ ) of Hg(II) became less positive (Figure 9a). The highest electro-oxidation signal was obtained at pH 5.5 (Figure 9b), making this the optimum pH.

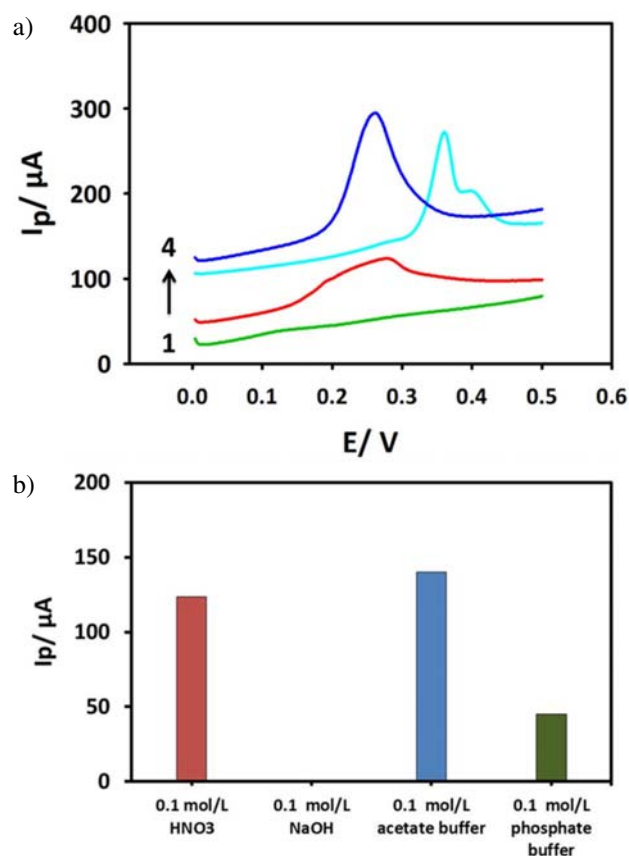


**Figure 8:** a) Square wave anodic stripping voltammograms (SWASVs) and b) corresponding histograms of  $6.2 \times 10^{-7}$  mol/L Hg(II) at GPE surfaces in a) 0.1 mol/L NaOH b) 0.1 mol/L phosphate buffer, c) 0.1 mol/L HNO<sub>3</sub> and d) 0.1 mol/L acetate buffer. Pretreatment CV segments, 20; other working conditions are identical to those in Fig. 4a.

To determine the effect of amplitude variation on the activity of the PGPE, Hg(II) was measured at different amplitudes. The SWV curves showed variations in peak current and peak potential, with an amplitude of 0.06 V being optimal for Hg(II) detection (Figure 10a).

To test the effect of frequency on PGPE activity, different frequencies were applied to detect of  $6.2 \times 10^{-7}$  mol/L Hg(II), while maintaining all other parameters con-

**Table 1:** Optimal parameters for Hg(II) determination by the SWASV method using PGPE.

Parameter	Optimum Parameter
Electrode type	PGPE
Pretreatment solution	0.1 mol/L HNO <sub>3</sub>
Pretreatment potential range, V	-1.6 to -0.6
Pretreatment CV scan segments	60
Pretreatment CV scan rate, V/s	50
Sensing solution, mol/L	0.1 acetate buffer
Sensing pH	pH 5.5
Amplitude, V	0.06
Frequency, Hz	100
Deposition time, s	300

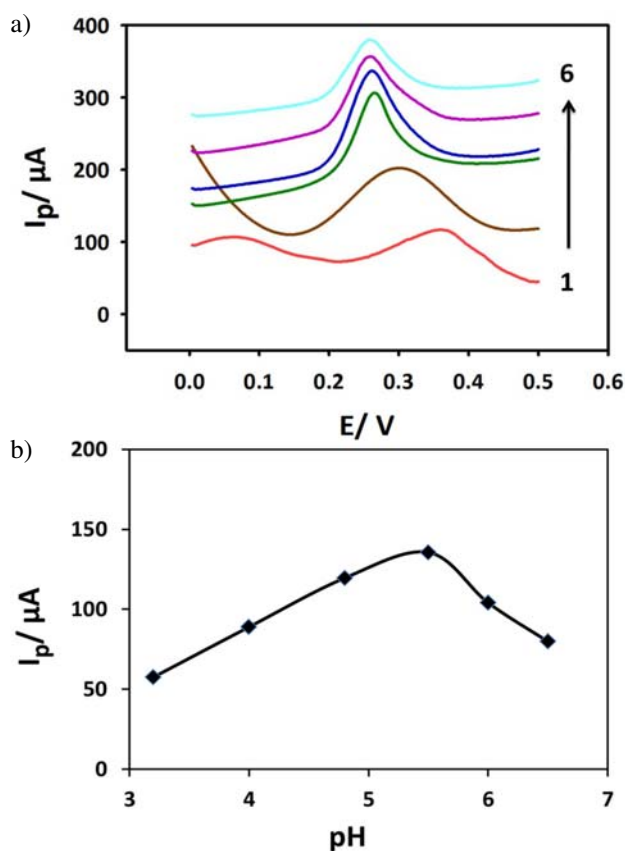


**Figure 9:** a) Square wave anodic stripping voltammograms (SWASVs) of  $6.2 \times 10^{-7}$  mol/L Hg(II) at GPE surfaces in 0.1 mol/L acetate buffer at pH 1) 3.2, 2) 4.0, 3) 4.8, 4) 5.5, 5) 6.0 and 6) 6.5. Pretreatment CV segments, 20; other working conditions are identical to those in Fig. 2a. b) Corresponding plot of pH vs peak current.

stant. The highest peak current was obtained when a 100.0 Hz frequency was applied (Figure 10b), making 100.0 Hz the optimum frequency for Hg(II) detection.

We also attempted to optimize the deposition time required for the detection of Hg(II) at the PGPE. Peak current increased at deposition times of 0–300 s, but later became nearly constant (Figure 10c). Finally, we attempted to optimize the deposition potential for  $6.2 \times 10^{-7}$  mol/L Hg(II) at the PGPE. The deposition potential was varied from -1.4 V to -2.0 V, with the peak current highest for -1.6 V (Figure 10d). The optimal SWASV parameters are summarized in Table 1.

### 3. 4. Calibration

The dependence of Hg(II) peak currents on their concentrations are presented in Figure 11. Under the optimum conditions described in Table 1, the peak currents were linearly proportional to Hg(II) concentration ranging from  $5.0 \times 10^{-9}$  mol/L to  $1.75 \times 10^{-7}$  mol/L ( $R^2 = 0.994$ ; Figure 11, inset). Thus the limit of quantification was  $10.0 \times 10^{-9}$  mol/L and the limit of detection was ( $S/N = 3$ )  $3.0$

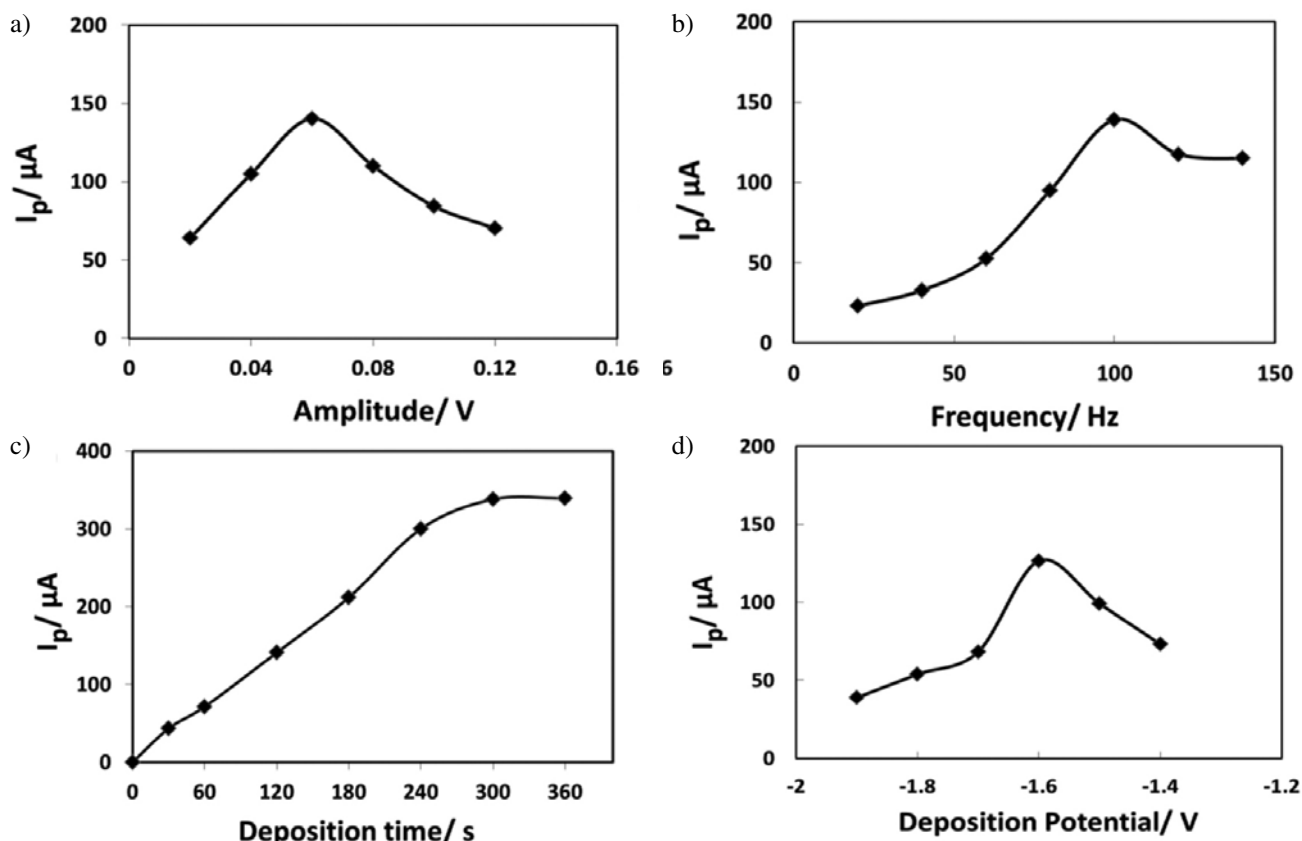


**Figure 10:** Plots of peak current vs. a) amplitude, b) frequency, c) deposition time, and d) deposition potential of the square wave voltammograms of  $6.2 \times 10^{-7}$  mol/L Hg(II) solution in 0.1 mol/L acetate buffer (pH 5.5) at GPE surfaces. Other conditions are identical to those described in Fig. 2a.

$\times 10^{-9}$  mol/L for Hg(II) at the PGPE. The relationship between  $i_p$  and Hg(II) concentration can be represented by the equation  $i_p = aC + b$ , where  $a$  and  $b$  are the slope and

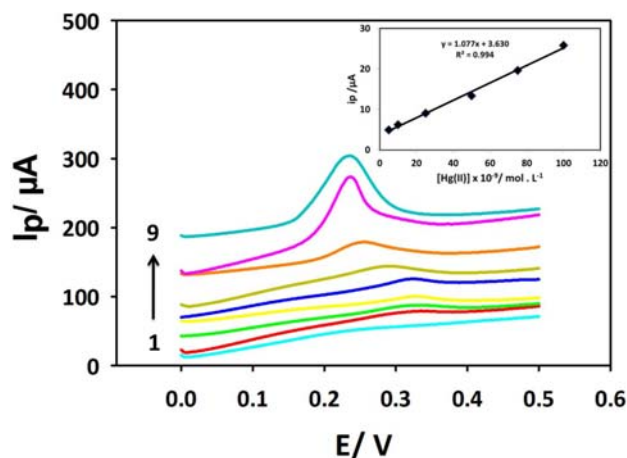


**Figure 11:** Square wave anodic stripping voltammograms (SWASVs) in 0.1 mol/L acetate buffer, pH 5.5, containing 1) 0.0, 2)  $5.0 \times 10^{-9}$ , 3)  $1.0 \times 10^{-8}$ , 4)  $2.5 \times 10^{-8}$ , 5)  $5.0 \times 10^{-8}$ , 6)  $7.5 \times 10^{-8}$ , 7)  $1.0 \times 10^{-7}$ , 8)  $1.5 \times 10^{-7}$ , and 9)  $1.75 \times 10^{-7}$  mol/L of Hg(II) at the pretreated GPE. Other working conditions were identical to those in Table 1. The inset shows the corresponding calibration curve from  $1.0 \times 10^{-8}$  to  $1.0 \times 10^{-7}$  mol/L Hg(II).

intercept of the straight line respectively. These results indicate that our method based on square wave adsorption stripping voltammetry using inexpensive and renewable graphite pencil electrodes is both convenient and efficient for quantitation of Hg(II).

### 3. 5. Determination of Hg(II) in Human Saliva

Because of their low electroactivity, non-pretreated GPEs cannot detect Hg(II) in human saliva. The ability of the PGPE to detect low Hg(II) concentrations in saliva was determined. PGPE yielded promising results (Table 2), similar to ICP-OES for the same Hg(II) concentrations.

## 4. Conclusions

This study showed that pretreatment of GPE electrode surfaces enhanced the electrochemical catalytic activity of these electrodes towards the oxidation of Hg(II). Comparison of non-pretreated GPEs and PGPEs showed that the latter are highly sensitive, with a low limit of detection ( $S/N = 3$ ) of  $3.0 \times 10^{-9}$  mol/L. Moreover, PGPEs are sensors that

**Table 2:** Concentrations of Hg(II) in spiked saliva samples measured by PGPE and inductively coupled plasma (ICP-OES).

Saliva Sample	Hg(II) Concentration after Addition	Hg(II) Concentration Detected by ICP-OES	Hg(II) Concentration Detected by the Electrochemical Method	Recovery of the Electrochemical Method
1	25.0 nmol/L	25.0 ± 10.0 nmol/L	25.0 ± 4.0 nmol/L	100.0%
2	50.0 nmol/L	41.0 ± 6.0 nmol/L	47.0 ± 5.5 nmol/L	94.0%
3	100.0 nmol/L	96.0 ± 4.9 nmol/L	99.5 ± 3.5 nmol/L	99.5%

(where n = 3)

are both inexpensive and easy to manufacture. These sensors give satisfactory results when used to detect low concentrations of Hg(II) in human saliva samples. As saliva can be easily and non-invasively collected, the development of these sensors can allow the use of human saliva as a biomonitoring matrix to electrochemically measure Hg(II).

## 5. Acknowledgement

The author would like to acknowledge the support received from King Fahd University of Petroleum and Minerals (KFUPM) through Project No. IN161046.

## 6. References

1. P. W. Davidson, G. J. Myers, B. Weiss, *Pediatrics* **2004**, *113*, 1023–1029.
2. A. A. Tinkov, O.P. Ajsuvakova, M. G. Skalnaya, E. V. Popova, A. I. Sinitskii, O. N. Nemereshina, E. R. Gatiatulina, A. A. Nikonorov, A. V. Skalny, *Biometals* **2015**, *28*, 231–254. <https://doi.org/10.1007/s10534-015-9823-2>
3. J. K. Nicholson, M. D. Kendall, D. Osborn, *Nature* **1983**, *304*, 633–635. <https://doi.org/10.1038/304633a0>
4. H. Wüstner, C.E. Orfanos, H. Steinbach, H. Käferstein, H. Herpers, *Dtsch. Medizinische Wochenschrift*. **1975**, *100*, 1694. <https://doi.org/10.1055/s-0028-1106446>
5. A. Marenduzzo, M. D'Urso, F. Caruso, F. Gombos, *Arch. Stomatol.* **1972**, *13*, 59–67.
6. J. B. Rocha, M. Aschner, J. G. Dórea, S. Ceccatelli, M. Farina, L.C.L. Silveira, *J. Biomed. Biotechnol.* **2012**, *2012*, 831–890.
7. P. J. Landrigan, R. O. Wright, L.S. Birnbaum, *Science* **2013**, *342*, 1447. <https://doi.org/10.1126/science.342.6165.1447>
8. F. Zahir, S. J. Rizwi, S. K. Haq, R. H. Khan, *Environ. Toxicol. Pharmacol.* **2005**, *20*, 351–360. <https://doi.org/10.1016/j.etap.2005.03.007>
9. A. B. Akcan, O. Dursun, *Güncel Pediatr.* **2008**, *6*, 72–75.
10. N. Langford, R. Ferner, *J. Hum. Hypertens* **1999**, *13*, 651–656. <https://doi.org/10.1038/sj.jhh.1000896>
11. D. Ravneet, S. Paradiso, *Am. J. Psychiatry* **2008**, *165*, 1489–1490. <https://doi.org/10.1176/appi.ajp.2008.08020233>
12. V. Vardhan, S. Garg, *Med. J. Armed Forces India* **2005**, *61*, 76–78. [https://doi.org/10.1016/S0377-1237\(05\)80127-3](https://doi.org/10.1016/S0377-1237(05)80127-3)
13. M. Schner, S. J. Walker, *Mol. Psychiatry*. **2002**, *7*, S40–41. <https://doi.org/10.1038/sj.mp.4001176>
14. S. D. Burt, *AAOHN J.* **1986**, *34*, 543–546.
15. G. J. Myers, D. O. Marsh: The role of Methylmercury Toxicity in Mental Retardation, Academic Press Inc., USA, **1990**, pp. 33–50. [https://doi.org/10.1016/s0074-7750\(08\)60091-9](https://doi.org/10.1016/s0074-7750(08)60091-9)
16. M. Dell'Ormo, G. Muzi, A. Bernard, R.R. Lauwerys, G. Abbritti, *Lancet*. **1996**, *348*, 64. [https://doi.org/10.1016/S0140-6736\(05\)64395-4](https://doi.org/10.1016/S0140-6736(05)64395-4)
17. M. A. Padilla Millán, F. Granados Correa, *J. Radioanal. Nucl. Chem.* **2002**, *254*, 305–309. <https://doi.org/10.1023/A:1021675900453>
18. P. R. Aranda, R. A. Gil, S. Moyano, I. De Vito, L. D. Martinez, *J. Hazard. Mater.* **2009**, *161*, 1399–1403. <https://doi.org/10.1016/j.jhazmat.2008.04.129>
19. C. Yuan, J. Wang, Y. Jin, *Microchim. Acta.* **2012**, *177*, 153–158. <https://doi.org/10.1007/s00604-012-0768-7>
20. V. A. Lemos, L. O. dos Santos, *Food Chem.* **2014**, *144*, 203. <https://doi.org/10.1016/j.foodchem.2013.10.109>
21. N. A. Panichev, S. E. Panicheva, *Food Chem.* **2015**, *166*, 432–441. <https://doi.org/10.1016/j.foodchem.2014.06.032>
22. X. Yuan, G. Yang, Y. Ding, X. Li, X. Zhan, Z. Zhao, *Spectrochim. Acta Part B At. Spectrosc.* **2014**, *93*, 1–7.
23. V. S. Hatzistavros, N. G. Kallithrakas-Kontos, *Anal. Chim. Acta* **2014**, *809*, 25–29. <https://doi.org/10.1016/j.aca.2013.11.045>
24. S. Drennan-Harris, L. R. Wongwilawan, J. F. Tyson, *J. Anal. At. Spectrom.* **2013**, *28*, 259–265. <https://doi.org/10.1039/C2JA30278K>
25. G. Jarzynska, J. Falandysz, *J. Environ. Sci. Heal. A, Toxic/hazardous Subst. Environ. Eng.* **2011**, *46*, 569–573.
26. Q. Zhang, G. Lu, L. Jiao, Y. Yuan, P. Li, J. Wang, *Micro Nano Lett.* **2013**, *8*, 903–905. <https://doi.org/10.1049/mnl.2013.0626>
27. M. K. Sezgintürk, E. Dinçkaya, *Int. J. Pept. Res. Ther.* **2011**, *17*, 87–92. <https://doi.org/10.1007/s10989-011-9243-2>
28. Z. Ye, Y. Li, J. Wen, K. Li, B. Ye, *Talanta* **2014**, *126*, 38–45. <https://doi.org/10.1016/j.talanta.2014.03.026>
29. F. Mirkhalaf, J. E. Graves, *Chem. Pap.* **2012**, *66*, 472–483.
30. C. M. Silveira, M. G. Almeida, *Anal. Bioanal. Chem.* **2013**, *405*, 3619–3635. <https://doi.org/10.1007/s00216-013-6786-4>
31. A. Walcarius, J. Devoy, J. Bessiere, *J. Solid State Electrochem.* **2000**, *4*, 330–336. <https://doi.org/10.1007/s100080000109>



32. J. Gong, T. Zhou, D. Song, L. Zhang, X. Hu, *Anal. Chem.* **2010**, 82, 567. <https://doi.org/10.1021/ac901846a>
33. A. Widmann, C. van den Berg, *Electroanalysis* **2005**, 17, 825–831. <https://doi.org/10.1002/elan.200403159>
34. B. Chen, L. Wang, X. Huang, P. Wu, *Microchim. Acta* **2011**, 172, 335–341. <https://doi.org/10.1007/s00604-010-0457-3>
35. N. Zhou, H. Chen, J. Li, L. Chen, *Microchim. Acta* **2013**, 180, 493–499. <https://doi.org/10.1007/s00604-013-0956-0>
36. X. Fu, J. Wu, L. Nie, C. Xie, J. Liu, X. Huang, *Anal. Chim. Acta* **2012**, 720, 29–37. <https://doi.org/10.1016/j.aca.2011.12.071>
37. Z. Zhao, X. Zhou, *Sensors & Actuators: B.Chemical.* **2012**, 171–172, 860–865. <https://doi.org/10.1016/j.snb.2012.05.084>
38. P. B. Patil, B. R. Patil, *J. Indian Soc. Periodontol.* **2011**, 15, 310–317. <https://doi.org/10.4103/0972-124X.92560>
39. N. Spielmann, D.T. Wong, *Oral Dis.* **2011**, 17, 345–354. <https://doi.org/10.1111/j.1601-0825.2010.01773.x>
40. L. A. Denovan, C. Lu, C. J. Hines, R. A. Fenske, *Int. Arch. Occup. Environ. Health.* **2000**, 73, 457–462. <https://doi.org/10.1007/s004200000174>
41. A. Iskandar, S. A. Seri Masran, A. R. Ishak, *Int. J. Environ. Sci. Dev.* **2014**, 5, 45.
42. M. J. Silva, J. A. Reidy, E. Samandar, A. R. Herbert, L. L. Needham, A. M. Calafat, *Arch. Toxicol.* **2005**, 79, 647–652. <https://doi.org/10.1007/s00204-005-0674-4>
43. I. Milosev, B. Kapun, and V.S. Selih, *Acta Chim. Slov.* **2013**, 60, 543–555.
44. L. Sipos, H.W. Nurnberg, P. Valenta, and M. Branica, *Anal. Chim. Acta* **1980**, 115, 25–42. [https://doi.org/10.1016/S0003-2670\(01\)93140-X](https://doi.org/10.1016/S0003-2670(01)93140-X)
45. H. Huiliang, D. Jagner, and L. Renman, *Anal. Chim. Acta* **1987**, 202, 117–122. [https://doi.org/10.1016/S0003-2670\(00\)85906-1](https://doi.org/10.1016/S0003-2670(00)85906-1)
46. E. Gil, and P. Ostapczuk, *Anal. Chim. Acta* **1994**, 293, 55–65. [https://doi.org/10.1016/0003-2670\(94\)00075-1](https://doi.org/10.1016/0003-2670(94)00075-1)
47. I. Svancara, M. Matousek, E. Sikora, K. Shachl, K. Kalcher, and K. Vytras, *Electroanalysis* **1997**, 9, 827–833. <https://doi.org/10.1002/elan.1140091105>
48. E. Viltchinskaya, L. Zeigman, D. Garcia, and P. Santos, *Electroanalysis* **1997**, 9, 633–640. <https://doi.org/10.1002/elan.1140090811>

## Povzetek

Pripravili smo elektrokemijsko obdelano elektrodo iz grafitnega svinčnika (PGPE) za analizo sledov Hg (II) v humani slini. Obdelavo GPE smo izvedli z uporabo 0,1 mol/L dušikove kisline in ciklanje potenciala med –1,6 in –0,6 V v 60 ciklih pri hitrosti skeniranja 50 mV/s. Optimalne pogoje smo določili na osnovi analize vplivov sestavin medija, pH in različnih elektrokemijskih tehnik in parametrov. Za določanje Hg (II) smo uporabili anodno inverzno voltometrijo s pravokotnimi pulzi («square wave anodic stripping voltammetry», SWASV). Pri optimalnih pogojih je bila kalibracijska krivulja linearna v območju od  $10 \times 10^{-9}$  mol/L do  $175 \times 10^{-9}$  mol/L, meja zaznave pa  $3,0 \times 10^{-9}$  mol/L (S/N = 3). Metodo smo uporabili za merjenje Hg (II) v slini, kamor prehaja iz amalgamskih zalivk.

Scientific paper

# Determination of Microelements in Human Milk and Infant Formula Without Digestion by ICP-OES

Dijana Đurović,<sup>1,\*</sup> Branka Milisavljević,<sup>2</sup> Mirjana Nedović-Vuković,<sup>1</sup>  
Branislav Potkonjak,<sup>3</sup> Snežana Spasić<sup>3</sup> and Miroslav M. Vrvic<sup>4</sup>

<sup>1</sup> Institute of Public Health of Montenegro, Džona Džeksona bb, 81000 Podgorica, Montenegro,

<sup>2</sup> Department of Neonatology, Subotica Hospital, Izvorska 3, 24000 Subotica, Serbia,

<sup>3</sup> Department of Chemistry, Institute of Chemistry, Technology and Metallurgy, University of Belgrade, Njegoševa 1, Belgrade, Serbia,

<sup>4</sup> Faculty of Chemistry, University of Belgrade, Studentski trg 12-16, Belgrade, Serbia

\* Corresponding author: E-mail: dil@t-com.me

Tel/Fax ++ 382 (0) 20 412 888

Received: 11-05-2016

## Abstract

The concentrations of zinc (Zn), iron (Fe) and copper (Cu) in both human milk and infant formula were determined using a new sample preparation method, by inductively coupled plasma – optical emission spectrometry (ICP-OES) and flame atomic absorption spectrometry (FAAS). Human milk samples were diluted in ultrapure water. The infant formula of powder samples (suitable for an infant 1–6 months of age) and standard reference material (SRM-1849) were analyzed in parallel.

The results have shown that FAAS method was more sensitive for Fe determination in human milk while ICP-OES was more sensitive for both Zn and Cu detection. The limit of quantification for both Zn and Cu was  $5 \mu\text{g L}^{-1}$  and  $10 \mu\text{g L}^{-1}$  for Fe and the recovery for Zn, Fe and Cu was ranged from 90% to 94%, 97% to 103% and 90% to 102%, respectively. Mean concentrations of Zn, Fe, and Cu in human milk samples were 5.35, 0.47 and 0.83  $\text{mg L}^{-1}$ , respectively while these values in infant formula were ranged from 3.52–4.75  $\text{mg L}^{-1}$ , 3.37–4.56  $\text{mg L}^{-1}$  and 0.28–0.41  $\text{mg L}^{-1}$ , respectively. Despite the sample complexity, the proposed method using dilution of milk samples with water was simple, rapid, effective and accurate. ICP-OES was a better method for Zn determination while FAAS was a better method for Fe determination. In the case of Cu both methods were comparable.

**Keywords:** Microelements, human milk, method validation, sample preparation

## 1. In trodution

Human breast milk is a complex mixture of nutrients. The World Health Organization recommends breast milk as the ideal food for the growth of infants under 12 months of age.<sup>1</sup> Human milk contains almost all the essential components (minerals, vitamins, essential amino and fatty acids) required for normal growth and development of newborns.<sup>2–4</sup> Microelements are important constituents of a large number of molecules including structural proteins and catalytic enzymes. Zinc (Zn), iron (Fe), and copper (Cu) are essential microelements for the normal growth of an infant. The European Society for Pe-

diatric Gastroenterology, Hepatology and Nutrition (ESPGHAN) proposed standards for infant formula composition, specifically 0.5–1.5 mg of Zn and 0.3–1.3 mg of Fe in 100 kcal of infant formula.<sup>5</sup> Human milk during early childhood (the first few months of a baby's life), provides both protection for the immune system and healthy development.<sup>6</sup> Zn is an essential microelement for many biochemical processes, especially for infants as it is a cofactor and constituent of almost 300 enzymes. Zn participates in nucleic acid metabolism, synthesis and turnover of proteins, lipids, carbohydrates, cell replication and gene regulation.<sup>7</sup> During pregnancy, childhood and adolescence Zn supports healthy development and normal

growth.<sup>8–10</sup> Copper (Cu) is another very important microelement for enzyme catalysis crucial for balanced metabolism.<sup>11</sup> Moreover, Cu regulate myelin sheath production in the nervous system, melanin synthesis and normal thyroid gland function.<sup>12</sup> Cu has both, antioxidant and pro-oxidant properties. Another trace element of interest is iron (Fe) which is absolutely required for hemoglobin synthesis and red blood cell formation and for regulation of oxidative reactions.<sup>9–14</sup> Human milk demonstrates some bacteriostatic properties most likely due to the content and/or bioavailability of Fe in breast milk. Many *in vivo* and *in vitro* studies have confirmed that Fe is a key factor in breast milk to protect against pediatric pathogens.<sup>15</sup> Therefore, a deficiency or excess of these microelements could threaten enzyme activities and biological processes in the human body.<sup>16,17</sup>

Definition of nutritional requirements as well as physiology of milk secretion for infants is based on appropriate date of micronutrient content in human milk during lactation. Determination of trace elements content is very important since the examined matrix is very complex emulsion, with low metal ions concentration. Previous studies using a number of different methods have been published.<sup>18–20</sup> Atomic absorption spectrometry was one of the first techniques employed and it is still used in clinical and dairy product analysis.<sup>21</sup> ICP-OES, FAAS, electrothermal atomic absorption spectrometry (EAAS) and inductively coupled plasma – mass spectrometry (ICP-MS) are standard techniques nowadays.<sup>22,23</sup> A new method for Cu determination, zeeman electrothermal atomic absorption spectrophotometry (ZEAAS), was recently established. It does not require sample digestion, requires minimal preparation and uses two chemical modifiers.<sup>24</sup> Determination by inductively coupled plasma – atomic emission spectroscopy (ICP-AES) and ICP-MS of major and minor elements has used milk dilution procedures with 5 or 10% v/v water-soluble extract mixed with tertiary amine reagent at pH 8.<sup>25</sup>

Despite the fact that ICP-MS is highly sensitive, accurate and precise, it is the least used technique in clinical laboratories due to high instrument cost and demanding protocols.<sup>26–28</sup> Neutron activation analysis (NAA) is one of the most sensitive techniques for applications in clinical biology. However, analyses are time consuming and therefore largely inappropriate.<sup>29</sup>

Microwave-assisted digestion is the most common sample preparation method for clinical and dairy samples.<sup>30</sup> Despite the fact that the technique is fast and simple, strong acids for sample degradation are needed. There is a lack of information regarding a unified human sample preparation procedure. Accordingly, the first aim of our study was to introduce a new method for human milk and infant formula sample preparation based on simple water-based dilution without chemical consumption. This could be considered as an environmentally-friendly “green method” for clinical and dairy sample preparation.

This is similar to inorganic ion determination using minimal nitric acid consumption and water dilution in donkey’s milk by ion chromatography.<sup>31</sup>

The second aim of this study was to optimize microelement analysis using ICP-OES via an easy, rapid, cost-effective and environmentally acceptable procedure amenable to most laboratories.

## 2. Material and Methods

### 2.1. Sample Collection and Storage

Twenty-eight human milk samples (10–20 ml) were obtained from healthy mothers (aged  $31.2 \pm 6$  years) on a first day after on-term delivery at the Department of Neonatology in Subotica Hospital in January 2013. All the mothers gave written consent for milk sampling. The Ethical Committee of the Faculty of Medicine in Belgrade approved the study (No.01-434/4, dated 22/05/2012). The study protocol adhered to general guidelines laid down by the Ethical Committee of the Faculty of Medicine.

Every mother cleaned her breast and nipple with ultrapure water (Milli-Q, conductivity  $<1 \mu\text{S}/\text{cm}$ ) using protective gloves prior to milk sampling using a manual breast milk pump and/or a passive breast milk sampler. The women were instructed to sample milk both at the beginning and at the end of the breast-feeding session. Milk samples were collected in clean plastic vessels which were previously washed with ultrapure water. Human milk samples were labeled and stored at  $-20^\circ\text{C}$  before analysis. Random samples of infant formula were obtained from the local market (five different manufacturers) in Montenegro (APTAMIL 1, BEBELAC 1, HIPPI, NAN 1 and IMPAMIL<sup>®</sup>MIL1). IMPAMIL<sup>®</sup>MIL1 was produced in Serbia. Others originated from EU countries. Formulae were purchased in triplicate from January to April, 2013. The samples were stored in a dark and dry location until analysis, which was performed before the expiry date.

Human milk samples were defrosted at room temperature and diluted 10 times with ultrapure water. Infant formulae samples were prepared as follows: 1 g was made up to 100 ml of ultrapure water, due to the higher concentrations of the microelements and higher density of the resulting solutions in comparison to diluted human milk samples. This procedure allowed analyses to fall within the linear ranges of the analytical standard calibration curves. Our methodology allowed direct analysis of samples without digestion and took into consideration possible interference from organic matter during the detection of the microelements. Using the above-mentioned dilution procedures, the samples were prepared in such a way to be very similar (fat and protein content) and enabled us to correctly validate the method. The content of the analyzed microelements in the samples was similar to the chosen reference material.

## 2. 2. Reagents

All chemicals used were purchased as analytical grade. Zn, Fe and Cu analytical solutions were prepared after serial dilutions of stock reference solutions containing 1000 mg L<sup>-1</sup> of each element (LGC-ICP-OES stock solution). Reference material from the National Institute of Standards and Technology (NIST), and infant/adult nutritional formula SRM-1849 were used as calibrators.

## 2. 3. Equipment

The ICP-OES instrument (with axial configuration) was purchased from Spectro Analytical Instruments GmbH (Kleve, Germany). It was controlled using Smart Analyzer Vision Software (version 5.01.0928) and connected to an ASX-520 auto sampler (CETAC). Spectro ICA solution (10x concentrate, Berd Kraft Der Standard) was used for self-checking and self-adjustment of the instrument (over the entire polychromator). ICP-OES instrument parameter settings are shown in Table 1.

Table 1. ICP-OES instrument parameter settings

Parameter	Setting
Plasma Power	1.4 KW
Pump Speed	30 Rpm
Coolant Flow	14 L min <sup>-1</sup>
Auxiliary Flow	0.7 L min <sup>-1</sup>
Nebulizer Flow	0.9 L min <sup>-1</sup>
Spray chamber	Cyclonic
Plasma viewing mode	Axial
Processing mode	Area
Metal (wavelength, nm)	Zn (213.857), Fe (238.204), Cu (327.396)
Correlation Coefficient	0.999
Number of replicates	3
Rinse delay	30 s
Read delay	30 s

## 2. 4. Statistical Analysis

Statistical analyses were conducted using SPSS Version 17.0 for Windows. Correlation coefficients for Zn, Fe and Cu in human milk samples were established (Pearson coefficient). The results were considered to be statistically significant if *p* was < 0.05. Linear regression was used to

evaluate the differences between FAAS and ICP-OES. Descriptive statistics was used for data evaluation. The results are presented as tables and box plots. The boxes represent the median and the 25<sup>th</sup> and 75<sup>th</sup> percentiles; the whiskers represent the non-outlier range. Outliers and extremes were defined as data point values that were more than 1.5× and 3× the interquartile range (IQR) outside of the box.

## 3. Results and Discussion

### 3. 1. Method validation

Table 2 summarizes sensitivity and linearity. The linearity of the measurement was assessed by analyzing five standard solutions prepared by diluting the standard mixture solution (1000 mg L<sup>-1</sup>) in ultrapure water. All standards (0, 0.05, 0.1, 0.5 and 1.0 mg L<sup>-1</sup>) were measured in triplicate. Standards were analyzed on a regular basis for the purpose of monitoring instrument drift. In order to monitor cross-contamination and sample loss blank solutions were analyzed on a regular basis.<sup>32</sup> Surface area vs. metal ion concentration was plotted and calibration curves were constructed. The aim of the study was to obtain a correlation coefficient of  $R^2 > 0.999$  for linearity.<sup>32</sup> Since the correlation coefficients for Zn, Fe and Cu were  $R^2 > 0.9999$ , the aim of study was met. Within the measurement range deviations from theoretical values did not exceed 5% which demonstrated good correlation between element concentration and surface area. To evaluate sensitivity of the analytical method the limits of detection (LOD) and limits of quantification (LOQ) were used. Their values were determined as (3  $\sigma$ /S) and (10  $\sigma$ /S), respectively. According to International Union of Pure and Applied Chemistry (IUPAC) recommendations, detection and quantification limits were calculated where  $\sigma$  was the standard deviation (SD) of the response to ten calibration blanks and S was the slope of the analytical curve. The highest detection limit was for Fe, 3.0 mg L<sup>-1</sup>. Precision was evaluated through the determination of the coefficient of variation (CV) by measuring the relative standard deviation.<sup>33</sup> For each sample duplicate measurements were repeated as six replicates per day for intra-assay variation. The standard deviations (SDs) of intra-assay variation were 4% for Zn, 8% for Fe and 1% for Cu by ICP-OES and 3% for Zn, 3% for Fe and 0.6% for Cu by FAAS. Coefficients of variation (CVs) were acceptable for clinical sample detection (CV < 7%). CV values were lower from FAAS, whereas the recovery of Zn and Cu was superior from ICP-OES.

Table 2. Analytical method validation

Element	Relative precision (%)	R <sup>2</sup>	Linearity range ( $\mu\text{g L}^{-1}$ )	LOD ( $\mu\text{g L}^{-1}$ )	LOQ ( $\mu\text{g L}^{-1}$ )
Zn	4	0.99994	0.9–2400	1.5	5
Fe	8	0.99971	0.7–2400	1.5	5
Cu	1	0.99957	1.2–2400	3.0	10

### 3. 1. 2. Accuracy

There was no suitable and available reference material for human milk. Accordingly, the method accuracy was assessed using the SRM. Quality control was verified by recovery experiments for the three selected microelements. Recoveries of the analyzed microelements by ICP-OES and FAAS for SRM NIST-1849 are presented in Table 3. Although milk is a complex matrix composed of proteins, carbohydrates and lipids accuracy indicated good recovery from two different microelement spiked concentrations (10 and 50  $\mu\text{g L}^{-1}$ ) in human milk pools (Table 4).<sup>28</sup> Specifically, average recovery ranged from 90% to 94% for Zn, 90% to 102% for Cu by ICP-OES and 97% to 103% for Fe by FAAS (Table 4). Blank samples and the 0.25  $\text{mg L}^{-1}$  control standard were evaluated together with samples in each batch (Table 5).

**Table 3.** Recovery (%) of NIST 1849 by ICP-OES and FAAS

Element	ICP-OES	FAAS
Zn	91	85
Fe	93	100
Cu	99	98

**Table 4.** Recoveries of spiked (10 and 50  $\mu\text{g L}^{-1}$ ) Zn, Fe and Cu in milk samples from lactating mothers

Element	Min %	Max %
Zn	90	94
Fe	97	103
Cu	90	102

**Table 5.** Recovery and precision for control standard 0.25  $\text{mg L}^{-1}$

Element	Mean $\pm$ SD	Recovery (%)	RSD (%)
Zn	0.2632 $\pm$ 0.0085	105.3	3.40
Fe	0.2592 $\pm$ 0.0043	103.7	1.65
Cu	0.2583 $\pm$ 0.0032	103.3	1.23

ICP-OES and FAAS analysis of Zn, Fe and Cu in SRM-1849 infant/adult Nutritional Formula and infant formula (Aptamil, Bebelac, NAN1, HIPP and Impamil Mil1) are summarized in Tables 6 and 7. The concentrations of Zn, Fe and Cu in SRM-1849 obtained by FAAS and ICP-OES were similar with the stated reference values. Better results for Zn and Cu were obtained by ICP-OES whereas FAAS provided a better result for Fe. For each sample, duplicate tests were repeated 6 times per day for intra-assay comparison. Analytical characteristics (linearity, sensitivity, precision and accuracy) were considered satisfactory for analysis of clinical and infant formula samples by ICP-OES.

### 3. 1. 3. Clinical Sample Detection

After method validation 28 samples of human milk were analyzed for Zn and Cu content by ICP-OES while Fe content was measured by FAAS. Results of human milk analysis are shown in Table 8, while concentration correlation with dietary reference intake of Institute of Medicine<sup>34</sup> between Zn, Fe and Cu is to be found in Table 9.

The results reported in Table 8 showed that Zn concentration on a first day after delivery ( $5.35 \pm 2.15$

**Table 6.** Detected (by ICP-OES) and certified and labeled values of microelements in infant formula and SRM. Minimum and maximum values are expressed as mean values (n = 12)

		Detected values mg/100g of powder			Certified and labeled values mg/100g of powder
		Min	Max	Mean $\pm$ SD	
Zn	SRM	12.89	14.25	<b>13.93 <math>\pm</math> 0.4</b>	15.23 $\pm$ 0.5
	Aptamil 1	3.49	3.71	<b>3.52 <math>\pm</math> 0.2</b>	3.6
	Bebelac 1	3.28	3.55	<b>3.48 <math>\pm</math> 0.3</b>	3.6
	HIPP	3.75	4.10	<b>3.86 <math>\pm</math> 0.4</b>	4.0
	NAN 1	4.65	5.10	<b>4.75 <math>\pm</math> 0.4</b>	5.4
	Impamil <sup>®</sup> Mil1	4.25	4.85	<b>4.45 <math>\pm</math> 0.2</b>	4.3
Fe	SRM	13.88	17.04	<b>16.47 <math>\pm</math> 0.8</b>	17.71 $\pm$ 0.3
	Aptamil 1	3.59	3.94	<b>3.78 <math>\pm</math> 0.4</b>	3.9
	Bebelac 1	3.38	3.71	<b>3.63 <math>\pm</math> 0.3</b>	3.9
	HIPP	3.73	4.21	<b>3.89 <math>\pm</math> 0.5</b>	4.0
	NAN 1	4.45	4.95	<b>4.56 <math>\pm</math> 0.4</b>	5.2
	Impamil <sup>®</sup> Mil1	3.26	4.00	<b>3.37 <math>\pm</math> 0.1</b>	3.6
Cu	SRM	1.83	2.07	<b>2.01 <math>\pm</math> 0.10</b>	2.03 $\pm$ 0.04
	Aptamil 1	0.26	0.33	<b>0.30 <math>\pm</math> 0.05</b>	0.29
	Bebelac 1	0.26	0.31	<b>0.28 <math>\pm</math> 0.03</b>	0.29
	HIPP	0.25	0.28	<b>0.26 <math>\pm</math> 0.05</b>	0.27
	NAN 1	0.34	0.41	<b>0.38 <math>\pm</math> 0.05</b>	0.40
	Impamil <sup>®</sup> Mil1	0.30	0.36	<b>0.32 <math>\pm</math> 0.06</b>	0.36

**Table 7.** Detected (by FAAS) and certified and labeled values of microelements in infant formula and SRM. Minimum and maximum values are expressed as mean values (n = 12)

		Detected values mg/100g of powder			Certified and labeled values mg/100g of powder
		Min	Max	Mean $\pm$ SD	
Zn	SRM	12.74	13.14	<b>12.90 <math>\pm</math> 0.3</b>	15.23 $\pm$ 0.5
	Aptamil 1	2.75	3.21	<b>3.10 <math>\pm</math> 0.4</b>	3.6
	Bebelac 1	2.85	3.15	<b>3.09 <math>\pm</math> 0.4</b>	3.6
	HIPP	3.37	3.75	<b>3.58 <math>\pm</math> 0.3</b>	4.0
	NAN 1	4.12	5.00	<b>4.55 <math>\pm</math> 0.5</b>	5.4
	Impamil <sup>®</sup> Mil1	3.89	4.15	<b>4.01 <math>\pm</math> 0.1</b>	4.3
Fe	SRM	17.23	18.30	<b>17.74 <math>\pm</math> 0.3</b>	17.71 $\pm$ 0.3
	Aptamil 1	3.55	3.85	<b>3.61 <math>\pm</math> 0.3</b>	3.9
	Bebelac 1	3.67	3.90	<b>3.75 <math>\pm</math> 0.3</b>	3.9
	HIPP	3.78	4.10	<b>3.95 <math>\pm</math> 0.3</b>	4.0
	NAN 1	4.98	5.29	<b>5.05 <math>\pm</math> 0.5</b>	5.2
	Impamil <sup>®</sup> Mil1	3.25	3.75	<b>3.55 <math>\pm</math> 0.1</b>	3.6
Cu	SRM	1.82	2.21	<b>1.99 <math>\pm</math> 0.06</b>	2.03 $\pm$ 0.04
	Aptamil 1	0.27	0.32	<b>0.29 <math>\pm</math> 0.03</b>	0.29
	Bebelac 1	0.25	0.30	<b>0.27 <math>\pm</math> 0.03</b>	0.29
	HIPP	0.21	0.27	<b>0.24 <math>\pm</math> 0.04</b>	0.27
	NAN 1	0.34	0.40	<b>0.37 <math>\pm</math> 0.02</b>	0.40
	Impamil <sup>®</sup> Mil1	0.31	0.37	<b>0.33 <math>\pm</math> 0.08</b>	0.36

mg L<sup>-1</sup>) was higher than in the previously reported study.<sup>35</sup> Mean values for Zn in a study reported by Honda were very similar to our study and it was 5.32 mg L<sup>-1</sup>.<sup>36</sup> Based on this data Zn concentration on a first day after delivery are in accordance to the Daily Recommended Intake (DRI) and can satisfied infant needs. The mean concentration of Zn reported for donkey milk, that is considered as a best replacement for human milk, reported in some studies are comparable to our human milk study.<sup>23,37,38</sup>

The mean Fe concentration determined for clinical samples was 0.83  $\pm$  0.99 mg L<sup>-1</sup> and as such it was lower than the value reported in the previous studies as well as

in some studies for donkey milk.<sup>23,35,37,39</sup> The mean concentration of Cu in human milk samples was 0.47  $\pm$  0.20 mg L<sup>-1</sup>. The obtained data pointed out that Fe content showed the same trend as Zn, which is a lower concentration in both, human and donkey milk as it has been established in the previous studies.<sup>37,39</sup> It could be concluded that on a first day of delivery level of Zn, Fe and Cu human milk is sufficient to meet the recommended values.

There is no statistically significant correlation between Zn, Fe and Cu content in human milk samples ( $p > 0.05$ ).

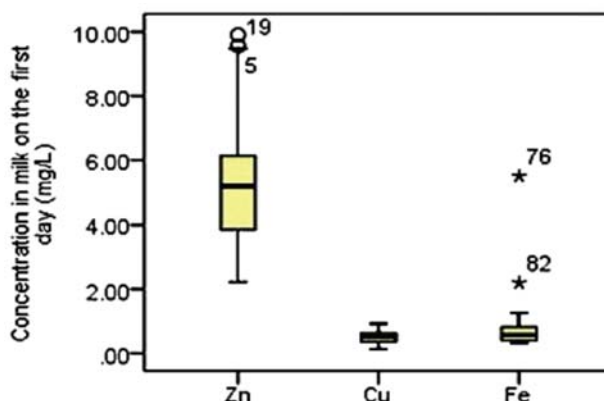
The obtained data showed that ICP-OES method provided statistically significantly higher average values

**Table 8.** Descriptive analysis of for Zn, Fe and Cu in human milk samples

Element	Concentration, (mg L <sup>-1</sup> )			
	Min.	Max.	Mean $\pm$ SD	DRI (mg)
Zn	2.22	9.91	5.35 $\pm$ 2.15	2.00
Fe	0.32	5.50	0.83 $\pm$ 0.99	0.27
Cu	0.12	0.92	0.47 $\pm$ 0.20	0.20
N			28	

**Table 9.** Correlation concentration coefficient for Zn, Fe and Cu in human milk samples

Element	Cu	Zn	Fe
Cu	1		
Zn	-0.135	1	
Fe	0.116	-0.069	1

**Figure 1.** Concentration of Zn, Fe and Cu in human milk samples on a first day after the delivery. The boxes represent the median and the 25th and 75th percentiles; the whiskers represent the non-outlier range.

for 9.5 mg L<sup>-1</sup> for Zn when compared to FAAS (p = 0.001). Method FAAS provided statistically significantly higher average values of 23.25 mg L<sup>-1</sup> for Fe when compared to ICP-OES (p < 0.001). For Cu, there was no statistically significant difference between both methods (p = 0.671). Figure 1 shows changes of Zn, Cu and Fe concentration in human milk samples on the first day after the delivery.

## 4. Conclusion

In this study, a fast, easy, economical and simple method for sample preparation was developed (no degradation) in order to determine the essential trace elements in human breast milk. Method evaluation and clinical sample detection on ICP-OES were used for validation of accuracy, reliability and practicality. The main advantage of presented sample preparation method is the fact that there is no chemical consumption and it is considered to be a green chemical method, i.e. it is environmentally acceptable. In conclusion, the proposed method is simple, economical, accurate, and highly reliable and as such, it can be applied to the clinical detection of trace elements in biological samples. There is no statistically significant correlation between Zn, Fe and Cu concentrations in human milk samples. Based on the obtained data and linear regression, it could be concluded that ICP-OES is a better method for Zn determination, FAAS for Fe, while there is no statistically significant difference between these two methods, when Cu is concerned.

## 5. Acknowledgments

This work was partially financed by the Ministry of Education, Science and Technological Development of the Republic of Serbia (Grants No. III 43004).

**Conflict of Interest:** All authors declare no conflict of interest.

**Ethical approval:** “All procedures performed in studies involving human participants were in accordance with the ethical standards of the institutional and/or national research committee and with the 1964 Helsinki declaration and its later amendments or comparable ethical standards.”

**Informed consent:** Informed consent was obtained from all mothers that donated milk samples.

## 6. References

1. R. Mahdavi, L. Nikniaz, B. P. Gargari, S. G. Hezaveh, *Iran. Biol. Trace. Elem. Res.* **2010**, *135*, 174–181  
<https://doi.org/10.1007/s12011-009-8510-y>
2. K. Ljung, B. Palm, M. Grandér, M. Vahter, *Food Chem.* **2011**, *127*, 943–951.  
<https://doi.org/10.1016/j.foodchem.2011.01.062>
3. M. L. Cross, H. S. Gill, *Br. J. Nutr.* **2000**, *84*, 81–89.  
<https://doi.org/10.1017/S0007114500002294>
4. B. Lonnerdal, *Nutrition.* **2000**, *16*, 509–511.
5. B. Koletzko, S. Baker, G. N. Cleghorn, F. Ulysses, S. Gopalan, O. Hernell, Q. S. Hock, P. Jirapinyo, B. Lonnerdal, P. Pencharz, H. Pzyrembel, J. Ramirez-Mayans, R. Shamir, D. Turck, Y. Yamashiro, D. Zong-Yi, *J. Pediatr. Gastroenterol. Nutr.* **2005**, *41*, 584–599.  
<https://doi.org/10.1097/01.mpg.0000187817.38836.42>
6. O. T. Oftedal, *Animal.* **2012**, *6*, 355–368.  
<https://doi.org/10.1017/S1751731111001935>
7. EFSA Panel on Dietetic Products Nutrition and Allergies (NDA)s Scientific Opinion on the substantiation of health claims related to zinc. *EFSA* **2009**, *J7* (9): 122:34.
8. R. Gibson, A.-L. Heath, *Nutr. Diet.* **2011**, *68*, 97–108.  
<https://doi.org/10.1111/j.1747-0080.2011.01516.x>
9. J. Bryan, S. Osendarp, D. Hughes, E. Calvaresi, K. Baghurst, J.-W. Van Klinken, *Nutr. Rev.* **2004**, *62*, 295–306.  
<https://doi.org/10.1111/j.1753-4887.2004.tb00055.x>
10. W. Maret, H. H. Sandstead, *J. Trace. Elem. Med. Biol.* **2006**, *20*, 3–18. <https://doi.org/10.1016/j.jtemb.2006.01.006>
11. E. D. Harris, *Nutr. Rev.* **2001**, *59*, 281–285.  
<https://doi.org/10.1111/j.1753-4887.2001.tb07017.x>
12. J. Osredkar, N. Sustar, *J. Clin. Toxicol.* **2011**, *S3*, S3-001.
13. B. Lozoff, M. K. Georgieff, *Semin. Pediatr. Neurol.* **2006**, *13*, 158–165. <https://doi.org/10.1016/j.spen.2006.08.004>
14. F. M. Rioux, J. Bélanger-Plourde, C. P. Leblanc, F. Vigneau, *Can. J. Diet. Pract. Res.* **2011**, *72*, e140-e146.
15. J. G. Dorea, *Nutrition.* **2000**, *16*, 209–20.  
[https://doi.org/10.1016/S0899-9007\(99\)00287-7](https://doi.org/10.1016/S0899-9007(99)00287-7)
16. J. Koolman, K. H. Roehm, *Color Atlas of Biochemistry*. 2<sup>nd</sup> Edition, Thieme **2005**, pp 362–363.
17. M. Hannan, B. Faraji, J. Tanguma, N. Longoria, R. C. M. Rodriguez, *Biol. Trace. Elem. Res.* **2009**, *127*, 6–15.  
<https://doi.org/10.1007/s12011-008-8221-9>
18. D. Silvestre, M. J. Lagarda, R. Farré, C. Martínez-Costa, J. Brines. *Food Chem.* **2000**, *68*, 95–99.  
[https://doi.org/10.1016/S0308-8146\(99\)00160-0](https://doi.org/10.1016/S0308-8146(99)00160-0)
19. R. Melø, K. Gellein, L. Evje, T. Syversen, *Food Chem. Toxicol.* **2008**, *46*, 3339–42.  
<https://doi.org/10.1016/j.fct.2008.08.007>
20. K. Ljung Björklund, M. Vahter, B. Palm, M. Grandér, S. Lignell, M. Berglund, *Environ Heal.* **2012**, *11*, 92.  
<https://doi.org/10.1186/1476-069X-11-92>
21. Y. Luo, B. Zhang, M. Chen, J. Wang, X. Zhang, W. Y. Gao, J. F. Huang, W. L. Fu, *J. Agric. Food. Chem.* **2010**, *58*, 9396–9400. <https://doi.org/10.1021/jf100940e>
22. R. S. Nascimento, R. E. S. Froes, N. O. C. Silva, R. L. P. Naveira, D. B. C. Mendes, W. B. Neto, J. B. B. Silva, *At. Spectrosc.* **2010**, *43*, 960–971.
23. A. G. Potortì, G. Di Bella, V. Lo Turco, R. R., R. Rando, G. Dugo, *J. Food Compos. Ana.* **2013**, *31*, 161–172.  
<https://doi.org/10.1016/j.jfca.2013.05.006>
24. A. Pineau, B. Fauconneau, A. Marraud, A. Lebeau, R. Han-

- kard, O. Guillard, *Biol. Trace. Elem. Res.* **2015**, *166*, 119–122. <https://doi.org/10.1007/s12011-015-0249-z>
25. J. A. Nobrega, Y. Gelinas, A. Krushevska, R. M. Barnes, *J. Anal. At. Spectrom.* **1997**, *12*, 1243–1246. <https://doi.org/10.1039/A607492H>
26. W. Wasowicz, J. Gromadzinska, K. Szram, K. Rydzynski, J. Cieslak, Z. Pietrzak, *Biol. Trace. Elem. Res.* **2001**, *79*, 221–33. <https://doi.org/10.1385/BTER:79:3:221>
27. M. Krachler, T. Prohaska, G. Koellensperger, E. Rossipal, G. Stingeder, *Biol. Trace. Elem. Res.* **2000**, *76*, 97–112. <https://doi.org/10.1385/BTER:76:2:97>
28. Khan N, Jeong IS, Hwang IM, J. S. Kim, S. H. Choi, E. Y. Nho, J. Y. Cho, K. S. Park, K. S. Kim, (2014) *Food Chem.* **2014**, *147*, 220–224. <https://doi.org/10.1016/j.foodchem.2013.09.147>
29. M. Hannan, N. N. Dogadkin, I. Ashur I, W. M. Markus, *Biol. Trace. Elem. Res.* **2005**, *107*, 11–20. <https://doi.org/10.1385/BTER:107:1:011>
30. M. Yaman, N. Çokol, *At. Spectrosc.* **2004**, *25*, 185–190.
31. G. Di Bella, V. Lo Turco, A. G. Potortì, R. R. Luppino, V. Fofia, F. Conte, G. Dugo, *Food Addit. Contam. A.* **2012**, *29*, 1021–1029. <https://doi.org/10.1080/19440049.2012.674979>
32. N. Khan, I. S. Jeong, I. M. Hwang, J. S. Kim, S. H. Choi, E. Y. Nho, J. Y. Choi, B.-M. Kwak, J.-H. Ahn, T. Yoon, K. S. Kim. *Food Chem.* **2013**, *141*, 3566–3570. <https://doi.org/10.1016/j.foodchem.2013.06.034>
33. M. Chudzinska, D. Baralkiewicz, *Food Chem. Toxicol.* **2011**, *49*, 2741–2749. <https://doi.org/10.1016/j.fct.2011.08.014>
34. Institute of Medicine, Dietary Reference Intakes; the Essential Guide to Nutrient Requirements, National Academy Press, Washington DC, **2006**,
35. M. T. S. Andrade, L. A. Del Ciampo, I. R. Lopes Del Ciampo, I. S. Ferraz, Fernando Barbosa Junior, *Food Nutr Sci.* **2014**, *1196*–1201. <https://doi.org/10.4236/fns.2014.513130>
36. R. Honda, K. Tawara, M. Nishijo, H. Nakagawa, K. Tanebe, S. Saito, *Toxicology*, **2003**, *186*, 255–259. [https://doi.org/10.1016/S0300-483X\(03\)00002-7](https://doi.org/10.1016/S0300-483X(03)00002-7)
37. E. Salimei, F. Fantuz, *Int. Dairy J.* **2012**, *24*, 146–152. <https://doi.org/10.1016/j.idairyj.2011.11.008>
38. V. A. Soares, M. M. M. Kus, A. L. C. Peixoto, J. S. Carrocci, R. F. S. Salazar, H. J. I. Filho, *Food Control.* **2010**, *21*, 45–49. <https://doi.org/10.1016/j.foodcont.2009.03.010>
39. N. Yamawaki, M. Yamada, T. Kan-no, T. Kojima, T. Kaneko, A. Yonekubo, *J. Trace. Elem. Med. Biol.* **2005**, *19*, 171–181. <https://doi.org/10.1016/j.jtemb.2005.05.001>

## Povzetek

Z uporabo optične emisijske spektrometrije z induktivno sklopljeno plazmo (ICP-OES) in plamenske atomske absorpcijske spektrometrije (FAAS) smo v vzorcih humanega mleka in vzorcih mlečnih formul za dojenčke določili koncentracije cinka, železa in bakra. Poleg mlečnih formul za dojenčke stare od 1 do 6 mesecev smo analizirali tudi standardni referenčni material SRM-1849. Za Fe smo najboljšo občutljivost določili s FAAS, za Zn in Cu pa z ICP-OES. Meja določanja za Zn in Cu je  $5 \mu\text{g L}^{-1}$  in  $10 \mu\text{g L}^{-1}$  za Fe. Izkoristki za Zn, Fe in Cu so v območjih od 90 % do 94 %, 97 % do 103 % in 90 % do 102 %. V vzorcih humanega mleka so bile povprečne koncentracije Zn, Fe in Cu  $5,35$ ,  $0,47$  in  $0,83 \text{ mg L}^{-1}$ , medtem ko so bile v mlečnih formulah za dojenčke v območjih od  $3,52$ – $4,75 \text{ mg L}^{-1}$ ,  $3,37$ – $4,56 \text{ mg L}^{-1}$  in  $0,28$ – $0,41 \text{ mg L}^{-1}$ . Kljub kompleksnosti vzorcev je predlagana metoda preprosta, hitra in učinkovita. Za določanje Zn je boljša ICP-OES metoda, za določanje Fe pa FAAS. V primeru Cu sta metodi primerljivi.



*Scientific paper*

# Encapsulation of Sour Cherry Pomace Extract by Freeze Drying: Characterization and Storage Stability

Vesna Tumbas Šaponjac,\* Gordana Četković, Jasna Čanadanović-Brunet, Sonja Đilas, Biljana Pajin, Jovana Petrović, Slađana Stajčić and Jelena Vulić

University of Novi Sad, Faculty of Technology, Bulevar cara Lazara 1, 21000 Novi Sad, Serbia

\* Corresponding author: E-mail: vesnat@uns.ac.rs  
Tel: +381 21 4853763; Fax: +381 21 450 413

Received: 03-08-2016

## Abstract

In this study sour cherry pomace was extracted with food-grade solvent (50% ethanol), concentrated and stabilized in whey and soy proteins by encapsulation. Soy proteins exhibited higher encapsulation efficiency (94.90%), but not significantly ( $p < 0.05$ ), from whey (90.10%). Storage properties of whey (WP) and soy protein (SP) encapsulates in terms of total polyphenols, anthocyanins and antioxidant activity were tested for 6 weeks. At the end of storage period the retention of polyphenols in SP and WP was similar (67.33 and 69.30%, respectively), while the content of anthocyanins has increased in SP (for 47.97%) and decreased in WP (for 1.45%). The decrease in antioxidant activity in SP (12.22%) was lower than in WP (35.04%). Colour parameters of encapsulates have followed the similar trend as anthocyanin change during storage. The technique reported herewith can be used for obtaining quality encapsulates for their use as functional food additives, as a way of fruit waste valorization.

**Keywords:** Sour cherry, encapsulation, polyphenols, antioxidant activity, colour

## 1. Introduction

Polyphenols have attracted the interest of many researchers and the general public due to the potential health benefits to humans, resulting from their antioxidant, anti-inflammatory, cardioprotective, and neuroprotective activities, inhibition of bacterial, viral, or fungal infections, development of tumors, and interaction with proteins, such as enzymes, tissue proteins, and membrane receptors. Based on these facts employment of polyphenols in food, pharmaceutical and biomedical fields is suggested.<sup>1</sup> The fate of dietary polyphenols during thermal food processing is associated with destruction of some primary compounds and introduction of many new compounds, and can lead to alterations in foods' organoleptic properties and, more importantly, biological activities. It was suggested that during future functional food development by means of dietary polyphenol fortification before food processing, cautious measures

are required to efficiently retain the primary chemical structure and the structure-associated health-beneficial bioactivities of polyphenols during thermal treatment.<sup>2</sup> Some polyphenols show low water solubility and low stability to other environmental conditions (exposure to light, oxygen, and enzymatic activities) and may undergo degradation in water or oxidation, with a consequent loss in activity. Also, some of them have a high rate of metabolism and rapid elimination from the human body (e.g. non-conjugated polyphenols).<sup>3</sup> Additionally, high molecular weight polyphenols (tannins, proanthocyanidins etc.) cannot be easily absorbed.<sup>1,3,4</sup> Further, phenolics are unstable in various solutions and therefore it is necessary to coat them in order to stabilize them which can be achieved by the process of encapsulation. This process prolongates the shelf life of the phenolics and accompanied biochemical functionalities, and eases the incorporation of such components into certain food products due to prevention of lumping, improving flow ability, compression and mi-

xing properties, reducing core particle dustiness and modifying particle density.<sup>5,6</sup>

Polyphenolics from various sources have been encapsulated in predominantly protein and polysaccharide carriers and their mixtures. For example, beetroot juice was encapsulated in maltodextrin, Arabic gum and a mixture of both,<sup>7</sup> saffron and beetroot extracts in maltodextrin, gum Arabic, modified starch and chitosan,<sup>8</sup> pomegranate peel,<sup>5</sup> green tea and olive pomace in maltodextrin,<sup>4,9</sup> cranberry pomace in soy proteins,<sup>10</sup> curcumin in *Saccharomyces cerevisiae*,  $\beta$ -cyclodextrin and modified starch,<sup>11</sup> onion and apple extracts in gum acacia and pea protein isolate or modified starch,<sup>12</sup> blueberry in whey protein isolate,<sup>13</sup> and so on. Ezhilarasi et al.<sup>14</sup> reported that whey protein possesses unsurpassed nutritional quality and inherent functional properties that meet the demands of encapsulation, while Ribnicky et al.<sup>15</sup> showed that polyphenols sorbed to soy protein isolate express higher bioavailability and bioaccessibility. In another study, ethanol extracts of ginkgo leaf were microencapsulated with maltodextrin, gum Arabic, or a soluble soybean protein by spray drying. The volume of core and wall materials had a significant influence on the encapsulation efficiency. This value was equal to 82.4% when the ratio for core material ingredients gum Arabic:maltodextrin:soybean protein was 6.1:2.87:11.75:4.28.<sup>16</sup> Ezhilarasi et al.<sup>14</sup> have determined the efficiency of encapsulation of the extract of *Garcinia cowa* on various protein and carbohydrate matrices (soy protein isolate, maltodextrin, and combinations thereof). All three materials had high encapsulation efficiency, in the range of 90–97%. Umesha et al.<sup>17</sup> examined the effectiveness of encapsulation of *Lepidium sativum* oil on whey proteins. It was found that the entrapment efficiency was significantly lower (64.8%).

There are very few studies on microencapsulation of polyphenols extracted from sour cherry pomace using freeze-drying.<sup>18,19</sup> The Republic of Serbia has very favorable natural and climatic conditions for sweet and sour cherries growing, and is a significant and promising fruit product in Serbia, primarily from the standpoint of exports to the international market. It has considerable nutritional, medicinal, dietetic and technological value. It is used in the fresh state or as a raw material, mainly in soft drinks, less in jams, yoghurt, liqueurs, brandy, compotes, and also serves as a raw material in the confectionery industry. According to the production volume of cherries, Serbia ranks seventh in the world, with a share of 7% of the total production.<sup>20</sup> Processing of sour cherries leaves bulky by-products, such as pomace, behind every year. Sour cherry pomace is still a good source of polyphenols, particularly anthocyanins.<sup>21</sup> According to the literature, sour cherry polyphenols have not been investigated much. Polyphenols identified in sour cherry juices, besides anthocyanins, include (–)-epicatechin (flavanol), neochlorogenic, chlorogenic and 3-coumaroylquinic acids (hydroxycinnamic acids), as well as quercetin and kaempferol

glycosides (flavonols).<sup>22</sup> In this study, sour cherry cv. 'Feketička' was chosen for its more intensive taste and deeper red colour, indicating high anthocyanin content. Although grown exclusively in northern Serbian province Vojvodina, in Feketić, this variety is officially recognized, even at the international level, as a separate high-quality variety.

The present study was aimed at stabilization and concentration of polyphenols extracted from sour cherry pomace by encapsulation using freeze-drying method. Whey and soy protein were used as carriers for sour cherry pomace polyphenols. Further, the effects of storage on microencapsulated phenolics, antioxidant activity and colour parameters of powders were evaluated during 6 weeks.

## 2. Experimental

### 2.1. Chemicals and Instruments

Chemicals used in the study were of analytical grade purchased from Sigma Chemicals Co. (St. Louis, MO, USA), J.T. Baker (Deventer, Holland) and Lachner (Brno, Czech Republic). Distilled water was produced using water purification system DESA 0081 Water Still destillator (POBEL, Madrid, Spain). Soy protein isolate was purchased from "Macrobiotic prom" (Belgrade, Serbia) while whey protein was from "Lučar" (Novi Sad, Serbia).

Spectrophotometric assays were carried out using UV-1800 spectrophotometer (Shimadzu, Kyoto, Japan). Freeze drier, model Christ Alpha 2–4 LSC, was from Martin Christ, Osterode am Harz, Germany. High performance homogenizer (model Silent Crusher M) and shaker (model Unimax 1010) were from Heidolph Instruments GmbH, Kelheim, Germany. Centrifuge, model EBA 21, was from Hettich Zentrifugen, Tuttlingen, Germany.

### 2.2. Plant Material

Ripe sour cherries, variety 'Feketička', were purchased from local producer "Horkai", Feketić, Serbia. Fresh undamaged sour cherries were washed, all of the stones were removed by hand, and stoneless fruits were packed immediately, frozen and stored in a freezer at –20 °C pending further use.

### 2.3. Preparation and Extraction of Sour Cherry Pomace

Sour cherry pomace was obtained by pressing the unfrozen stoneless sour cherries through cheesecloth. The yield of pomace compared to the unfrozen fruits was 22.40%. The obtained pomace was dried in a freeze drier at –40 °C for 120 h. The extraction of phenolic substances from dry pomace was performed using 50% ethanol aqueous solution, according to Roopchand et al.<sup>10</sup> Sample of pomace (100 g) was extracted in three steps. The first step

includes homogenization with 500 ml of 50% ethanol for 3 min on a high performance homogenizer followed by extraction for 60 min on a laboratory shaker (200 rpm). The second and third steps were performed with the same parameters, extraction with 250 ml of 50% ethanol for 30 min on a laboratory shaker (200 rpm). After each step liquid extract was collected after separating the pomace solids by vacuum filtration using Whatman filter paper Ø 47 mm. Obtained three extracts were combined and organic solvent in the collected hydro-alcohol extract was evaporated by rotary evaporation set at 40 °C.

## 2. 4. Encapsulation of Sour Cherry Pomace Extract

Concentrated water pomace extract (100 ml) was mixed with wall material (50 g of soy protein isolate or whey, core:coating ratio 2:1) with additional 200 ml of water for 30 min on laboratory shaker (200 rpm). The homogenized mixtures were iced and then freeze dried at –40 °C for 24 h, yielding red and purple-blue free-flowing powders – whey (WP) and soy protein (SP) encapsulates, respectively.

## 2. 5. Encapsulate Powder Storage Stability Studies

Encapsulate samples (WP and SP) were stored at room temperature (25 °C) in high-density polyethylene bags for 6 weeks to determine the effect of time on the stability of total polyphenols, anthocyanins, antioxidant activity and colour parameters. For determination of the content of polyphenols and anthocyanins, as well as antioxidant activity of WP and SP, three portions of 100 mg of each encapsulate were removed every second week, in triplicate.

### 2. 5. 1. Polyphenol Content

For determination of encapsulation efficiency phenolic content in the core (CPC) and surface (SPC) of encapsulate were determined, according to Saikia et al.<sup>23</sup> For the core phenolic content, as well as for the storage studies, encapsulates were extracted using the following protocol: 100 mg of powders were mixed with 1 ml ethanol, acetic acid and water (50:8:42) on vortex for 1 min, then centrifuged at 6000 rpm for 3 min. Liquid part was collected and filtered through 0.45 µm filter. Similarly, for surface polyphenols, 100 mg of sample was dispersed in 1 ml of ethanol and methanol (1:1) mixture. The mixture was vortexed for 1 min, centrifuged for 2 min, and the supernatant was separated. Total polyphenol contents in encapsulate extracts were determined by Folin–Ciocalteu method given by Singelton et al.<sup>24</sup> Results were expressed as mg gallic acid equivalents per 100 g encapsulate (mg GAE/100 g).

The encapsulating efficiency was determined by using the given equation:

$$EE (\%) = ((CPC-SPC)/CPC) \times 100 \quad (1)$$

where CPC is the phenolic content inside the core of the encapsulate; SPC is the surface phenolic content.

### 2. 5. 2. Anthocyanin Content

For determination of total anthocyanins in encapsulates, the same extraction procedure as for core polyphenols was used. Total anthocyanins were determined according to the pH differential method by Lee et al.<sup>25</sup> Results were expressed as mg cyaniding-3-glycoside per 100 g encapsulate (mg CyGE/100 g).

### 2. 5. 3. Antioxidant Activity

The antioxidant activity of encapsulates, extracted by the aforementioned protocol for core polyphenols, was evaluated using the DPPH assay.<sup>26</sup> Trolox was used as a positive control for callibration. Results were expressed as µmol Trolox equivalents per 100 g encapsulate (µmol TE per 100 g).

### 2. 5. 4. Colour Parameters of Powder Encapsulates

Encapsulate colour was measured in triplicate every second week in the period of six weeks. The CIELab colour coordinates (L\* – lightness, a\* – redness to greenness and b\* – yellowness to blueness)<sup>27</sup> were determined using MINOLTA Chroma Meter CR-400 (Minolta Co., Ltd., Osaka, Japan) using D-65 lighting, a 2° standard observer angle and an 8-mm aperture in the measuring head. The Chroma Meter was calibrated using a Minolta calibration plate (No. 11333090; Y = 92.9, x = 0.3159; y = 0.3322).

## 2. 6. Statistical Analysis

All data are presented as mean values of triplicate analysis along with their standard deviations. Variance analysis (ANOVA) was performed, with a confidence interval of 95% (p < 0.05). Statistical analyses were carried out using STATISTICA 12.0 (StatSoft, Inc., Tulsa, OK, USA).

## 3. Results and Discussion

### 3. 1. Sour Cherry Pomace Encapsulation

A characteristic of bioactive food components is that they are subject to rapid inactivation or degradation. Many bioactive food components would therefore benefit from an encapsulation procedure that slows down the degradation processes and/or prevents degradation until the pro-

duct is delivered at the sites where absorption is desired.<sup>28</sup> Selecting the appropriate carrier for the given bioactives is a critical step. The type of coating affects the encapsulation efficiency as well as its final morphology. It has to be biodegradable, stable, avoid reaction with the bioactive, maintain the bioactive structure and improve functionality during processing and storage at different conditions.<sup>29</sup> For our study we have chosen whey and soy proteins for coating polyphenols extracted from sour cherry pomace. The encapsulation efficiency did not differ significantly ( $p < 0.05$ ) among the two wall materials, being higher in soy proteins (94.90%) than in whey (90.10%). These results show that the procedure of encapsulation of sour cherry pomace polyphenols was very successful.

## 3. 2. Encapsulate Powders Storage Stability Studies

### 3. 2. 1. Bioactive Compounds in Powders

The results of testing the powders' polyphenol and anthocyanin shelf life are presented in Figure 1. During the first 4 weeks the content of total polyphenols has decreased considerably in SP (70%) and WP (80%). However, during the last two weeks of storage, there was a significant ( $p < 0.05$ ) increase in polyphenol contents in both encapsulates, resulting in final retention 67.33% in SP and 69.30% in WP, compared to the initial polyphenol contents.

These results are in accordance with the findings of other authors. An increase in total phenolics from 2 to 2.5 fold was found after 30 days of storage at 22, 37 and 45 °C in spray-dried blueberry pomace extract encapsulated with whey protein isolate as wall material.<sup>30</sup> The total polyphenol contents of black currant encapsulated in maltodextrin increase in the first 6 months at 8 °C, while in inulin-based encapsulates they increase even after 12 months.<sup>31</sup> Saénz et al.<sup>32</sup> reported that cactus pear polyphenols in powders dried with inulin increase after 44 days

storage at 60 °C. During degradation of conjugated polyphenols free hydroxyl groups are released, causing an overestimation of the total polyphenol content determined by Folin-Ciocalteu assay. The decreases in anthocyanin levels in SP happened in the first two weeks of storage, while in WP during four weeks, and after that the content of anthocyanin levels increased, in both encapsulates. Compared to the initial concentrations of anthocyanins in encapsulates, the final concentration after 6 weeks of storage in SP has increased (for 47.97%) and in WP it has decreased very slightly (for 1.45%). This difference in anthocyanin retention in SP and WP encapsulates can be explained by different encapsulation efficiency in these two wall materials. Since the efficiency to encapsulate polyphenols, which includes anthocyanins, was higher in soy proteins (94.90%) than in whey (90.10%), more anthocyanins have remained unbound, on the surface of WP compared to SP, leading to higher degradation rate. Robert et al.<sup>33</sup> found that anthocyanins in fresh pomegranate juice totally degraded in less than 10 days while in juice microencapsulated in SPI and maltodextrin the retention of anthocyanins was above 70% even after 60 days of storage, showing the importance of the encapsulation in preserving the bioactive compounds. In the same study it was reported that when SPI is used as a wall material both polyphenol and anthocyanin retention increase during the first 35 days of storage, possibly due to the hydrolysis of the pomegranate conjugated polyphenols, and then decrease. They showed the first-order degradation rate constant for polyphenols and anthocyanin encapsulated, calculated between 35 and 56 days. Similar behaviour was also reported by other authors.<sup>34,35</sup>

### 3. 2. 2. Antioxidant Activity of Powders

Based on the retention of antioxidant activity presented in Figure 2, tested by DPPH assay, the storage affected this feature of encapsulates as well. The preservation of antioxidant activity was dependent on the material

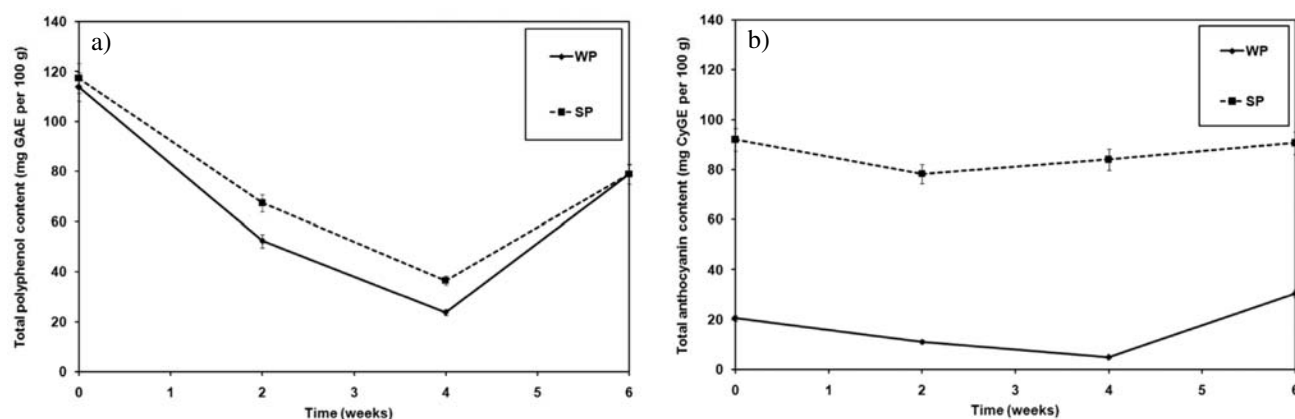
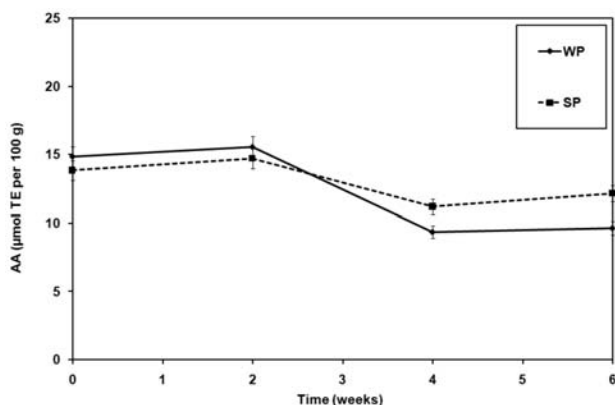


Figure 1. Polyphenol (a) and anthocyanin (b) stability of sour cherry pomace encapsulates during storage



**Figure 2.** Antioxidant activity of sour cherry pomace encapsulates during storage

used for encapsulation, but only after the second week of storage. There was no significant difference ( $p < 0.05$ ) in antioxidant activity of powders during the first two weeks. After 6 weeks the antioxidant activity of SP ( $12.13 \mu\text{mol TE per } 100 \text{ g}$ ) was almost 4-fold higher than WP ( $3.24 \mu\text{mol TE per } 100 \text{ g}$ ). Final decrease in antioxidant activity after 6 weeks of storage compared to the fresh powders in SP ( $12.22\%$ ) was lower than in WP ( $35.04\%$ ). This is in agreement with the results of polyphenol and especially anthocyanin retention in powders showing the superior ability of soy proteins to bind polyphenols and anthocyanins, due to higher content of proteins.

Nori et al.<sup>36</sup> encapsulated propolis extract employing isolated soy protein and pectin as wall materials, with relatively high encapsulation efficiency. They confirmed that encapsulation provided not only protection against degradation of phenolic and flavonoids compounds present in free propolis, but also preservation of their antioxidant properties.

### 3. 2. 3. Colour Parameters of Powders

Encapsulation of natural colours can be an interesting alternative for the replacement of artificial colourants for natural colourants in the food and pharmaceutical industry.<sup>6</sup> Change in colour parameters of sour cherry encapsu-

late powders, measured by CIE  $L^*a^*b^*$  method, during 6 weeks of storage is presented in Table 1.

According to the instrumental measurements of colour parameters it can be observed that the initial colour of WP and SP encapsulates was different (Table 1). SP encapsulate had lower  $L^*$  values (i.e. it was darker) than WP encapsulate, due to the fact that SP encapsulate showed higher initial anthocyanin content (Figure 1). Also, there was a significant difference ( $p < 0.05$ ) in redness (positive  $a^*$  values) and in yellowness/blueness ( $b^*$  values) between SP and WP encapsulates. WP encapsulate had higher  $a^*$  and  $b^*$  values and was coloured red, while SP encapsulate was purple-blue as evidenced by negative  $b^*$  value ( $-1.37$ ). The reason for this is that the colour of anthocyanins depends on pH. Weakly acidic medium, as whey, causes red tone coloration of anthocyanins, while in slightly alkaline conditions in soy protein isolate they change their colour to blue. Storage period and type of encapsulation agent significantly affected the colour change of encapsulates. During the storage, samples changed their colour to less intense red/purple-blue. In both samples, lightness ( $L^*$  values) and redness ( $a^*$  values) decreased significantly ( $p < 0.05$ ), while  $b^*$  values increased. The loss of red colour (decrease in  $a^*$  values) was higher in WP than in SP encapsulate due to higher encapsulation efficiency of soy protein which had superior ability to bind anthocyanins, as mentioned above.

Idham et al.<sup>37</sup> noticed the same trend (decrease in  $L^*$  and  $a^*$  values, and increase in  $b^*$  values during storage) in spray dried encapsulated anthocyanins from *Hibiscus sabdariffa*. They also concluded that colour changes depend on the type of carriers. In SP encapsulate  $a^*$  values decreased in the first two weeks from 16.52 to 15.09, and then increased to 16.25. In WP these values decreased from 25.17 to 19.23 during the first four weeks and then increased slightly to 21.88. The increase in redness after some time could be explained by the increase in anthocyanin levels in encapsulates during storage (Figure 1).

## 4. Conclusions

Sour cherry pomace polyphenols were encapsulated in whey and soy proteins as a protecting core material.

**Table 1.** Colour change of sour cherry pomace encapsulates during storage

Week	$L^*$		$a^*$		$b^*$	
	WP	SP	WP	SP	WP	SP
0	$53.25 \pm 0.01^d$	$47.55 \pm 0.23^d$	$25.17 \pm 0.4^a$	$16.52 \pm 0.01^d$	$1.47 \pm 0.75^a$	$-1.37 \pm 0.03^a$
2	$51.22 \pm 0.58^c$	$46.21 \pm 0.14^c$	$22.34 \pm 0.52^b$	$15.09 \pm 0.23^a$	$4.16 \pm 0.45^b$	$2.54 \pm 0.38^b$
4	$49.41 \pm 1.02^b$	$45.88 \pm 0.13^b$	$19.23 \pm 0.74^d$	$15.95 \pm 0.54^b$	$7.05 \pm 0.33^c$	$4.73 \pm 0.42^c$
6	$48.35 \pm 0.14^a$	$43.75 \pm 0.26^a$	$21.88 \pm 0.85^c$	$16.25 \pm 0.55^c$	$10.35 \pm 1.25^d$	$8.29 \pm 0.35^d$

Values represent average of triplicates  $\pm$  standard deviation. Means with different letters in superscript (a–d) in columns are significantly different ( $p < 0.05$ ).

Free-flowing powders obtained by freeze drying with high encapsulation efficiency had favourable antioxidant features (polyphenol and anthocyanin contents as well as antioxidant activity on DPPH radicals) and colour parameters, even after six weeks of storage. From the results presented herewith it can be concluded that the sour cherry pomace encapsulates represent a promising food ingredient for functional food development, due to both antioxidant content and potential as a colourant. The results of this study also suggest that encapsulation can be regarded as a final stage of high added-value compounds processing from food wastes. Future studies will involve incorporation of encapsulates in a food model system to test the influence of other components as well as food processing parameters on stability of encapsulated bioactive compounds.

## 5. Acknowledgements

This research was supported by the grant from the Ministry of Education, Science and Technological Development of Serbia (project No. TR 31044).

## 6. References

- O. I. Parisi, F. Puoci, D. Restuccia, G. Farina, F. Iemma, N. Picci, in: R. R. Watson, V. R. Preedy, S. Zibadi (Eds.): *Polyphe- nols in Human Health and Disease*, Elsevier, Academic Press, London, **2014**, pp. 29–45.  
<https://doi.org/10.1016/B978-0-12-398456-2.00004-9>
- X. Zhang, F. Chen, M. Wang, *J. Agric. Food Chem.* **2014**, *62*, 1643–1648. <https://doi.org/10.1021/jf4045827>
- A. Scalbert, C. Morand, C. Manach, C. Rémésy, *Biomed. Pharmacother.* **2002**, *56*(6), 276–282.  
[https://doi.org/10.1016/S0753-3322\(02\)00205-6](https://doi.org/10.1016/S0753-3322(02)00205-6)
- M. Paini, B. Aliakbarian, A. A. Casazza, A. Lagazzo, R. Bot- ter, P. Perego, *LWT – Food Sci. Technol.* **2015**, *62*, 177–186.
- M. Çam, N. C. İcyer, F. Erdoğan, *LWT – Food Sci. Technol.* **2014**, *55*, 117–123.
- K. Ravichandran, R. Palaniraj, N. M. M. T. Saw, A. M. M. Gabr, A. R. Ahmed, D. Knorr, I. Smetanska, *J. Food Sci. Tech.* **2014**, *51*(9), 2216–2221.  
<https://doi.org/10.1007/s13197-012-0728-6>
- E. Janiszewska, *Powder Tech.* **2014**, *264*, 190–196.  
<https://doi.org/10.1016/j.powtec.2014.05.032>
- C. Chranioti, A. Nikoloudaki, C. Tzia, *Carbohydr. Polymer* **2015**, *127*, 252–263.  
<https://doi.org/10.1016/j.carbpol.2015.03.049>
- D. Pasrija, P. N. Ezhilarasi, D. Indrani, C. Anandharama- krishnan, *LWT – Food Sci. Technol.* **2015**, *64*, 289–296.
- D. E. Roopchand, C. G. Krueger, K. Moskal, B. Fridlender, M. A. Lila, I. Raskin, *Food Chem.* **2013**, *141*, 3664–3669.  
<https://doi.org/10.1016/j.foodchem.2013.06.050>
- E. I. Paramera, S. J. Konteles, V. T. Karathanos, *Food Chem.* **2011**, *125*, 913–922.  
<https://doi.org/10.1016/j.foodchem.2010.09.071>
- N. Işık, B. Altheld, S. Kühn, N. Schulze-Kaysers, B. Kunz, H. R. Wollseifen, P. Stehle, S. Lesser, *Food Res. Int.* **2014**, *65*, 109–114.  
<https://doi.org/10.1016/j.foodres.2014.02.012>
- F. P. Flores, R. K. Singh, W. L. Kerr, D. R. Phillips, F. Kong, *Food Chem.* **2015**, *168*, 225–232.  
<https://doi.org/10.1016/j.foodchem.2014.07.059>
- P. N. Ezhilarasi, D. Indrani, B. S. Jena, C. Anandharama- krishnan, *J. Food Eng.* **2013**, *117*, 513–520.  
<https://doi.org/10.1016/j.jfoodeng.2013.01.009>
- D. M. Ribnicky, D. E. Roopchand, A. Poulev, P. Kuhn, A. Oren, W. T. Cefalu, I. Raskin, *Nutrition* **2014**, *30*, S4–S10.  
<https://doi.org/10.1016/j.nut.2014.03.009>
- L. Haidong, Y. Fang, T. Zhihong, S. Huanwei, Z. Tiehui, *Carbohydr. Polymer.* **2012**, *88*(2), 435–440.  
<https://doi.org/10.1016/j.carbpol.2011.12.025>
- S. S. Umesh, R. S. Manohar, A. R. Indiramma, S. Akshitha, K. A. Naidu, *LWT – Food Sci. Technol.* **2015**, *62*, 654–661.
- B. Cilek, A. Luca, V. Hasirici, S. Sahin, G. Sumnu, *Eur. Food Res. Technol.* **2012**, *235*, 587–596.  
<https://doi.org/10.1007/s00217-012-1786-8>
- V. Tumbas Šaponjac, G. Četković, J. Čanadanović-Brunet, B. Pajin, S. Djilas, J. Petrović, I. Lončarević, S. Stajčić, J. Vulić, *Food Chem.* **2016**, *207*, 27–33.  
<https://doi.org/10.1016/j.foodchem.2016.03.082>
- Z. Sredojević, D. Milić, M. Jeločnik, *The Petroleum-Gas University of Ploiesti Bulletin* **2011**, *63*(3), 37–49.
- C. Yılmaz, V. Gökmen, *Ind. Crop. Prod.* **2013**, *49*, 130–135.  
<https://doi.org/10.1016/j.indcrop.2013.04.048>
- D. Bonerz, K. Würth, H. Dietrich, F. Will, *Eur. Food Res. Tech.* **2007**, *224*, 355–364.  
<https://doi.org/10.1007/s00217-006-0328-7>
- S. Saikia, N. K. Mahnot, C. L. Mahanta, *Food Chem.* **2015**, *171*, 144–152.  
<https://doi.org/10.1016/j.foodchem.2014.08.064>
- V. L. Singleton, R. Orthofer, R. M. Lamuela-Raventos, in: L. Packer (Ed.): *Methods in Enzymology, Oxidant and Antioxi- dant (Part A)*, vol. 299. Academic Press, San Diego, **1999**, pp. 152–178.  
[https://doi.org/10.1016/S0076-6879\(99\)99017-1](https://doi.org/10.1016/S0076-6879(99)99017-1)
- J. Lee, R. W. Durst, R. E. Wrolstad, *Journal of AOAC (Asso- ciation of Official Analytical Chemists) International* **2005**, *88*(5), 1269–1278.
- V. Tumbas Šaponjac, A. Gironés-Vilaplana, S. Djilas, P. Me- na, G. Četković, D. A. Moreno, J. Čanadanović-Brunet, J. Vulić, S. Stajčić, M. Vinčić, *RSC Adv.* **2015**, *5*, 5397–5405.
- CIE International Commission on Illumination, Colorime- try: Official Recommendation of the International Commis- sion on Illumination, Publication CIE No. (E-1.31), **1976**, Paris, France: Bureau Central de la CIE.
- P. de Vos, M. M. Faas, M. Spasojevic, J. Sikkema, *Int. Dairy J.* **2010**, *20*, 292–302.  
<https://doi.org/10.1016/j.idairyj.2009.11.008>
- M. D. A. Saldana, J. S. dos R. Coimbra, L. Cardozo-Filho,

- Current Opinion in Food Science* **2015**, *5*, 76–85.
30. F. P. Flores, R. K. Singh, F. Kong, *J. Food Eng.* **2014**, *137*, 1–6. <https://doi.org/10.1016/j.jfoodeng.2014.03.034>
31. A. M. Bakowska-Barczak, P. P. Kolodziejczyk, *Ind. Crop. Prod.* **2011**, *34*, 1301–1309. <https://doi.org/10.1016/j.indcrop.2010.10.002>
32. C. Saénz, S. Tapia, J. Chávez, P. Robert, *Food Chem.* **2009**, *114*, 616–622. <https://doi.org/10.1016/j.foodchem.2008.09.095>
33. P. Robert, T. Gorena, N. Romero, E. Sepulveda, J. Chavez, C. Saenz, *Int. J. Food Sci. Tech.* **2010**, *45*, 1386–1394. <https://doi.org/10.1111/j.1365-2621.2010.02270.x>
34. A. Stewart, S. Bozonnet, W. Mullen, G. Jenkins, E. Michael, A. Crozier, *J. Agric. Food Chem.* **2000**, *48*, 2663–2669. <https://doi.org/10.1021/jf000070p>
35. N. Turkmen, F. Sari, Y. Velioglu, *Food Chem.* **2005**, *93*, 713–718. <https://doi.org/10.1016/j.foodchem.2004.12.038>
36. M. P. Nori, C. S. Favaro-Trindade, S. Matias de Alencar, M. Thomazini, J. de Camargo Balieiro, C. J. Contreras Castillo, *LWT – Food Sci. Technol.* **2011**, *44*(2), 429–435.
37. Z. Idham, I. I. Muhamad, M. R. Sarmidi, *J. Food Process. Eng.* **2012**, *3*, 522–542. <https://doi.org/10.1111/j.1745-4530.2010.00605.x>

## Povzetek

V tej študiji smo tropine višenj ekstrahirali s 50 % etanolom, ji koncentrirali in stabilizirali z enkapsulacijo z uporabo sirotkinih in sojinih proteinov. Učinkovitost enkapsulacije je bila večja pri uporabi sojinih proteinov (94,90 %), a ne statistično značilna ( $p < 0,05$ ), kot pri uporabi sirotkinih proteinov (90,10 %). Preverili smo tudi stabilnost enkapsulatov s proteini sirotke (WP) in soje (SP) med skladiščenjem v obdobju šestih tednov, kjer smo se osredotočili na vsebnost celokupnih polifenolov in antocianinov ter antioksidativno aktivnost. Po končanem obdobju skladiščenja je bila vsebnost polifenolov v enkapsulatih SP in WP podobna (67,33 % in 69,30 %), vsebnost antocianinov v SP se je povežala (za 47,97 %), v WP pa zmanjšala (za 1,45 %). Antioksidativna aktivnost enkapsulatov z SP se je znižala (12,22 %), a manj kot v primeru enkapsulatov z WP (35,04 %). Skladno s spremembami, ki smo jih med skladiščenjem zaznali pri antocianinih, se je spreminjala tudi barva enkapsulatov. Opisana tehnika omogoča pripravo kakovostnih enkapsulatov, ki se jih lahko uporabi kot funkcionalne aditive v živilih in se s tem izkoristi vrednost sadnih odpadkov.

Scientific paper

# Theoretical Investigation of Electrophilic Transannular Addition Reactions of Bromine to Face-to-Face (Juxtaposed) Double Bonds in Strained Polycyclic Hydrocarbons

Rza Abbasoglu

Department of Chemistry, Karadeniz Technical University, 61080 Trabzon, Turkey

\* Corresponding author: E-mail: rabbas@ktu.edu.tr

Telephone: +90-462-377-2595, Fax: +90-462-325-319

Received: 14-10-2016

## Abstract

Transannular electrophilic addition reaction of halogens to face-to-face(juxtaposed) double bonded strained alkenes were theoretically investigated. General rules that allow us to stipulate the factors that direct the main steps of the energy hypersurface of reactions as well as the products were established. Direction of the reaction flow is determined by direction of intramolecular skeletal isomerisation of cyclic-bridged halogenium cation and isomerisation takes place to create a more stable skeletal structure. Stability of resultant skeletal structure is determined by the number of  $\sigma$  bonds between isolated double bonds of the alkene and bonding-type of double bonds (N- and U-type). When the number of  $\sigma$  bonds between double bonds of the alkene is three ( $m = 3$ ), the reaction takes place to predominantly give an N-type product, and when four ( $m = 4$ ), N- and U-type products are formed. Structure and stability of cation intermediates (bridged, N- and U-type cations) of electrophilic addition reaction of homohipostrofen molecule, whose double bonds were linked by three  $\sigma$  bonds, with bromine were investigated by DFT methods in detail. Also the addition reaction of endo,endo-tetracyclo[6.2.2.2<sup>3,6</sup>.0<sup>2,7</sup>]tetradeca-4,9-dien molecule, whose double bonds were linked by four  $\sigma$  bonds, with bromine were investigated by quantum chemistry.

**Keywords:** DFT calculations, Strained alkenes, Electrophilic transannular addition, Face-to-face (juxtaposed) double bonds, Intramolecular skeletal rearrangement.

## 1. Introduction

Although theoretical and experimental investigations of the electrophilic additions of halogens to carbon-carbon double bond have been carried out extensively, the structure, the nature and the stability of the reaction intermediates as well as the mechanism of these reactions are still under discussion. The attack of an electrophile to a molecule having two isolated double bonds in spatial proximity usually leads to the transannular bridge formation in either cross (N-type) or parallel (U-type) manner or both.<sup>1-4</sup> Experimental results on this type of reaction have been confusing. In some cases, only the cross or the parallel bridged product is isolated, while in other cases both products are formed simultaneously.<sup>2,3,5-15</sup> Recently Inagaki et al. advanced a perturbation theory to interpret those cases where preferential cross bridging takes place.<sup>16</sup>

While the orbital mixing effect must certainly be working when cross bridging occurs, a general theory must explain why and to what extent parallel addition takes place in other systems. Osawa et al. suggested that this was due to the thermodynamic stability of the N- and U-type products.<sup>2</sup> According to Osawa, it is possible for both products to form when the difference between the thermodynamic stability of N- and U-type products is less than 10 kcal mol<sup>-1</sup>. If the difference is more than 10 kcal mol<sup>-1</sup>, more stable product is obtained.

In order to learn the inner mechanism and dynamic stereochemistry of these reactions in detail, it is crucial to determine the structure and the stability of the intermediates (cyclic-bridged, N- and U-type cations) formed during the course of the reaction and investigate their skeletal isomerization. It is feasible for the cyclic bridged halogenium cation to transform into N- and U-type bridged ca-



tions as a result of the transannular cross (N-type) and parallel (U-type) linkage of the double bonds. Therefore, the stability of N- and U-type cations, into which cyclic bridged halogenium cation isomerized, is important in order to ascertain the direction of the flow of the addition reaction.

The structure and the nature of the alkene play an important role in the display of characteristic behavior of the electrophilic addition reactions of the halogens to parallel face-to-face (juxtaposed) double bonded strained alkenes. The investigation of the geometrical and electronic structure of alkenes is necessary to resolve the link between the structure of the alkenes and their behaviors during the electrophilic addition reactions. The study of the stability and stereochemistry of the different configurations of the reaction products is vital so as to interpret the many features of the electrophilic addition reactions.

The objective of this study is to establish relationships between geometric and electronic structures of face-to-face double bonded strained alkenes and their behaviors during electrophilic transannular addition reactions. Furthermore, we aimed to study unique characteristics of these reactions, identify essential factors that determine the direction of reactions' flow and establish general rules that allow us to stipulate the factors that direct the flow of such reactions, and reaction products considering the results of this investigation and structure-characteristic relationships. In order to prove these suggested rules, electrophilic transannular addition reactions of bromine molecule to two face-to-face double bonded strained alkenes, namely tetracyclo[6.3.0<sup>4,11</sup>.0<sup>5,9</sup>]undeca-2,6-diene (homohipostrofene) and endo,endo-tetracyclo[6.2.2.2<sup>3,6</sup>.0<sup>2,7</sup>]tetradeca-4,9-diene (TCTD) were studied by DFT method.

## 2. Methodology

The geometry and the electronic structure of the tetracyclo[6.3.0<sup>4,11</sup>.0<sup>5,9</sup>]undeca-2,6-diene (homohipostrofene) and endo,endo-tetracyclo[6.2.2.2<sup>3,6</sup>.0<sup>2,7</sup>]tetradeca-4,9-diene (TCTD) molecules were investigated by DFT/B3LYP<sup>17,18</sup> method using the 6-311G(d,p) and 6-311++G(d,p)<sup>19</sup> basis sets. The predicted cationic intermediates and products formed in the addition reactions were investigated using the B3LYP/6-311G(d,p) method. By using the optimized geometries of cations and products by B3LYP/6-311G(d,p) method, their single point energies were calculated at the B3LYP/6-311++G(2d, 2p)<sup>19</sup> level. Solvent effects were calculated at the same theory level as the optimizations by performing single-point calculations on the optimized structures using the CPCM (conducting polarized continuum model)<sup>20,21</sup> method (with UAKS cavities<sup>22</sup>) in chloroform ( $\epsilon = 4.9$ ). All stationary points were characterized by calculating the vibrational frequencies and zero-point vibrational energies have been added for all species. We did not calculate the two TSs of the addi-

tion reaction of the intermediate carbocations because of the complexity of the method; instead we used the energy of the intermediates applying the Hammond-principle to predict the stereoselectivity (ratio of N- and U-type product) of the reaction. The calculations were performed with Gaussian 03<sup>23</sup> program with an IBM PC Pentium IV computer.

## 3. Results and Discussions

### 3. 1. Factors Driving Electrophilic Transannular Addition Reactions of Halogens to Face-to-Face Double Bonded Strained Alkenes and Unique Characteristics of These Reactions

It is important to investigate stability of cyclic-bridged halogenium cations formed as a result of heterolytic decomposition of alkene...halogen molecular complexes formed during first step of electrophilic addition reaction of halogens to face-to-face double bonded strained alkenes as well as their skeletal isomerisation for determination of addition reaction's mechanism. Direction of the addition reaction's flow is determined by direction of intramolecular skeletal isomerisation (intramolecular rearrangement of bonds) of cyclic-bridged halogenium cation and isomerisation takes place to create a more stable skeletal structure. Moreover, the direction of intramolecular skeletal isomerisation of bridged halogenium ions is determined by stability of N- and U-type cations formed as a result of cross (N-type) and parallel (U-type) bonding of double bonds. Therefore, the direction of addition reaction is determined by stability of skeletal structure formed as a result of skeletal isomerisation of bridged halogenium cation.

Skeletal isomerisation of bridged halogenium ion by formation of two different new cyclic structures (having different number of carbon atoms) depending on the number of  $\sigma$  bonds between double bonds of the alkene and bonding type of such double bonds (Chart). The following chart shows skeletal isomerisation of cyclic bridged halogenium cations and new cyclic structures involved in the molecular structure. Hence, stability of skeletal structure formed by skeletal isomerisation of bridged halogenium cation depends on type and stability of new cyclic structures involved in the molecular system as a result of the isomerisation. On the other hand, type and stability of cyclic structures formed as a result of isomerisation are determined by the number ( $m$ ) and type of bonding of  $\sigma$  bonds between double bonds of the alkene, hence, the structure of the alkene. In the case of alkenes with three ( $m = 3$ )  $\sigma$  bonds between its double bonds, four-ring structure (cyclobutane ring) and six-ring structure (cyclohexane ring) are obtained as a result of parallel (U-type) bonding of double bonds whereas two five-ring structures (cyclopentane ring) are obtained as a result of cross (N-type)

bonding (Chart, a). A four-ring structure has high stretching energy so there is a low possibility of formation of U-type cation. Therefore, the possibility of transformation of a cyclic halogenium cation into a U-type cation is low, causing a low possibility that addition reaction will take place over the U-type cation. Compared to a four-ring structure, a five-ring structure has lower stretching energy. Skeletal isomerisation of a cyclic bridged halogenium ion to an N-type cation (having two five-ring structures) has higher possibility. Addition reaction should primarily take place to give N-type cation (N-type product). In the case of alkenes having four  $\sigma$  ( $m = 4$ ) bonds between its double bonds, a five-ring structure (cyclopentane ring) and a six-ring structure (cycloheptane ring) are obtained as a result of parallel (U-type) bonding of double bonds, and two six-ring structures (cyclohexane ring) are obtained as a result of cross(N-type) bonding (Chart, b). Since there isn't a large difference between stretching energies of resultant structures, the difference between stabilities of U-type cation having five-ring and seven-ring structures and of N-type cation having two six-ring structures should be small. In conclusion, during electrophilic addition reaction of halogens to alkenes having four  $\sigma$  bonds between its double bonds, skeletal isomerisation of cyclic bridged halogenium cation should take place to give N- and U-type cations (Chart, b) and thus N- and U-type products.

Hence, general rules that allow us stipulate any factors that direct the flow of electrophilic addition reactions of halogens to face-to-face double bonded strained alkenes as well as possible resultant products by considering the abovementioned suggestions, results of calculations<sup>24–34</sup> and structure-characteristic relationships can be listed as follows:

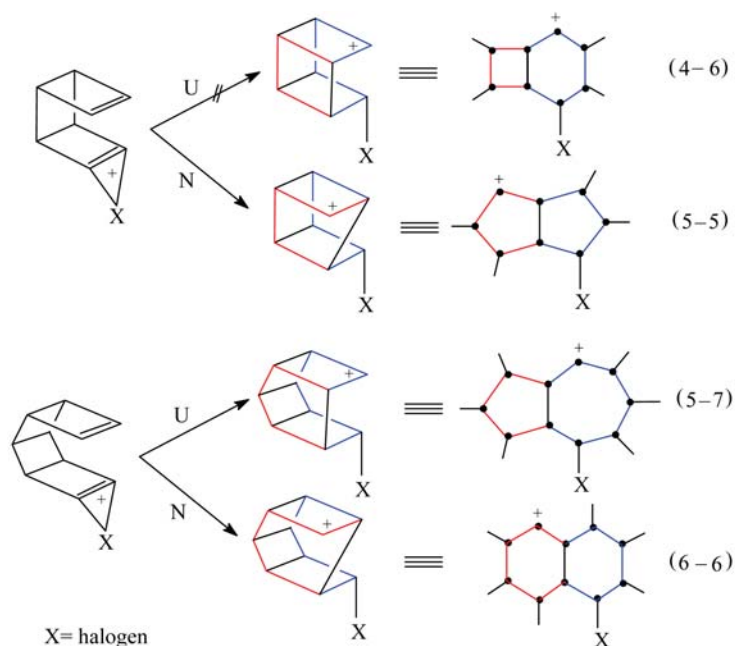
1. Direction of the reaction's flow is determined by the direction of intramolecular skeletal isomerisation (intramolecular rearrangement of bonds) of cyclic bridged halogenium cation.
2. Intramolecular skeletal isomerisation of cyclic bridged cation takes place to give a more stable skeletal structure.
3. Stability of resultant skeletal structure depends on type (Chart) and stability of new cyclic structures involved in the molecular system as a result of isomerisation.
4. Type and stability of cyclic structures formed as a result of isomerisation are determined by the number of  $\sigma$  bonds between double bonds of the alkene and bonding type of double bonds (N- and U-type), thus, by the structure of the alkene.
5. Direction of addition reaction is determined by the number of  $\sigma$  bonds between isolated double bonds of the alkene: When  $m = 3$  (Chart, a), the reaction predominantly takes place to give N-type product and when  $m = 4$  (Chart, b), to give N- and U-type products (Abbasoglu rule).<sup>32–34</sup>

Number of  $\sigma$  bonds ( $m$ ) Bonding type Product

3 N N-type

4 N and U N- and U-type

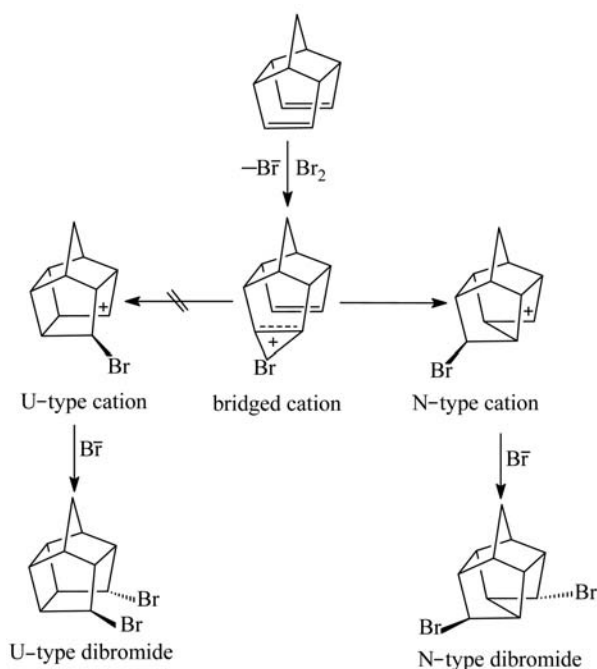
These suggested rules are also confirmed by experimental results of transannular electrophilic addition reactions of halogens to face-to-face double bonded strained alkenes.<sup>2,3,5–15</sup> It is also vital to theoretically investigate electrophilic addition reactions in order to prove such rules. Therefore, electrophilic addition reactions of bromine to tetracyclo[6.3.0<sup>4,11</sup>.0<sup>5,9</sup>]undeca-2,6-diene (homohippofrostene) and endo,endo-tetracyclo[6.2.2.2<sup>3,6</sup>.0<sup>2,7</sup>]tetraca-4,9-diene were investigated by DFT method.



Chart

### 3. 2. DFT Study on the Electrophilic Transannular Addition Reaction of Bromine to Tetracyclo[6.3.0.4.11.05,9]undeca-2,6-diene (Homohipostrofene)

Bromination of the homohipostrofene molecule (ph) gave only the adduct of N-type (Scheme 1).<sup>2,35</sup> However, the formation of U-type adduct can't be observed. To identify the reason for this, it is important to study



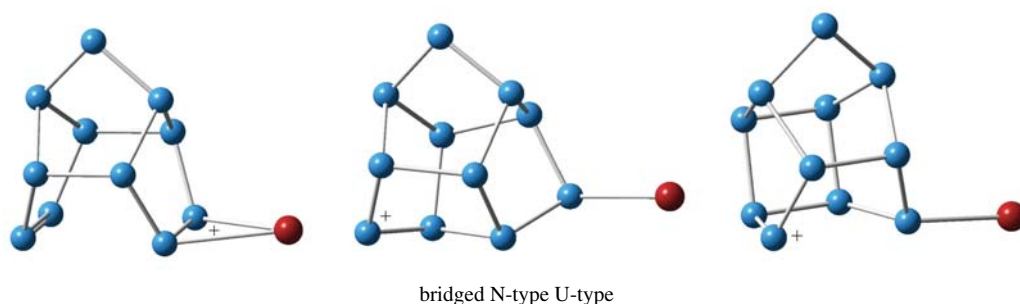
Scheme 1. The electrophilic addition reaction of bromine to ph

structures and stabilities of electrophilic addition reaction intermediates (bridged, N- and U-type cations) as well as geometric and electron structure of homohipostrofene molecule. Full geometric optimization of the ph was performed by DFT/B3LYP method in 6-311G(d,p) and 6-311++G(d,p) basis and the structure of the molecule was also investigated in detail.

Bridged cation and its isomers (N- and U-type cations) are the possible intermediates of the addition reactions of bromine to ph in gas phase and solvent medium (Scheme 2). The structures and relative stabilities of these cations were determined by carrying out geometrical optimization using the B3LYP/6-311G(d,p) method and the total energies ( $E_{tot}$ ) were also calculated. By using the optimized geometries of cations at the B3LYP/6-311G(d,p) level, their single point energies have been computed using B3LYP/6-311++G(2d,2p) and CPCM-B3LYP/6-311++G(2d,2p) methods. The calculated relative energies are given in Table 1.

According to the results of each method, bridged bromonium cation is more stable than U type cation and less stable than N-type cation (Table 1). In other words, bridged bromonium cation transforms into more stable N-type cation by cross-bonding (cross mechanism) of the double bonds (Scheme 1). It is not possible for the bridged bromonium cation to isomerizes skeletally to the unstable U-type cation. As a result, the direction of the electrophilic addition reaction of bromine to ph is determined by the direction of the skeletal isomerization of the bridged bromonium cation into N-type cation and N-type reaction product is preferred to the N-type cation.

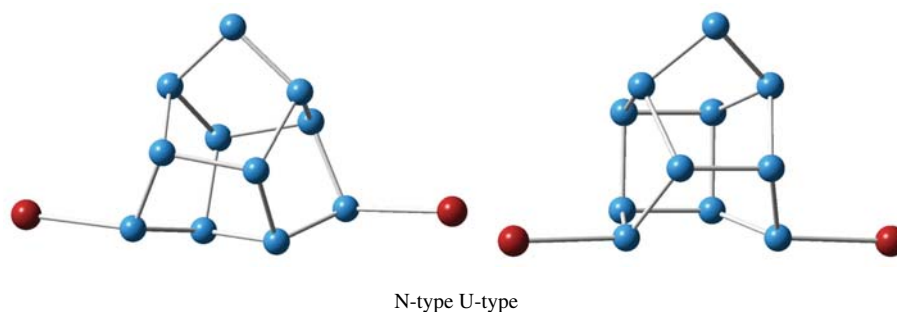
The stereochemistry and the stable configurations of the reaction products were investigated by DFT method.



Scheme 2. The optimized geometries of cations (B3LYP/6-311G(d,p))

Table 1. The calculated relative energies of cations  
Cations Relative energy (kcal mol<sup>-1</sup>)

	B3LYP/6311 G(d,p)	B3LYP/6311++G(2d,2p) //B3LYP/6-311G(d,p)	CPCM-B3LYP/6311++G(2d,2p) //B3LYP/6-311G(d,p)
bridged	3.485	3.242	3.926
N-type	0.0	0.0	0.0
U-type	6.647	6.976	7.252



**Scheme 3.** The optimized geometries of products (B3LYP/6-311G(d,p))

**Table 2.** The calculated relative energies of products  
Products Relative energy (kcal mol<sup>-1</sup>)

	B3LYP/6311 G(d,p)	B3LYP/6311++G(2d,2p) //B3LYP/6-311G(d,p)	CPCM-B3LYP/6311++G(2d,2p) //B3LYP/6-311G(d,p)
N-type	0.0	0.0	0.0
U-type	8.260	8.203	7.896

The geometrical structure of the N- and U-type products (Scheme 3) were optimized by B3LYP/6-311G(d,p) method and their total energies ( $E_{\text{tot}}$ ) were also calculated. The single point energies of products were calculated by using B3LYP/6-311++G(2d,2p)//B3LYP/6-311G(d,p) and CPCM-B3LYP/6-311++G(2d,2p)//B3LYP/6-311G(d,p) methods. The calculated relative energies are given in Table 2. According to the results of each method, the N-

type dibromide molecule was more stable than U-type dibromide molecule (Table 2).

In other words, parallelism exists between the cation and the corresponding product (Figure 1). In Figure 1, the energy diagram of electrophilic addition reaction of bromine to ph is given. As can be seen from the energy diagram, the reaction progresses in the direction of the more stable cation and the skeletal isomerisation of the bridged cation

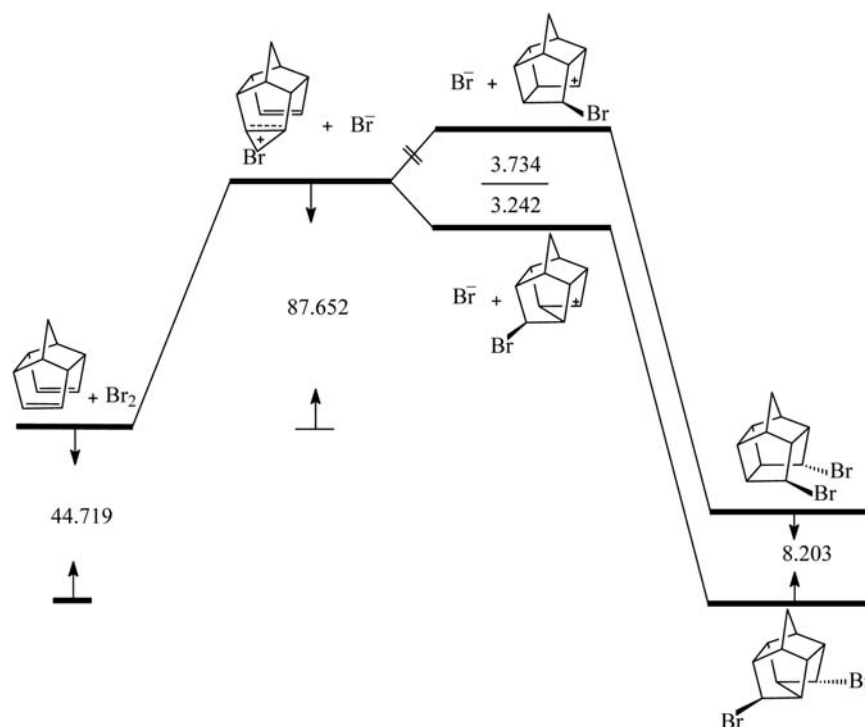
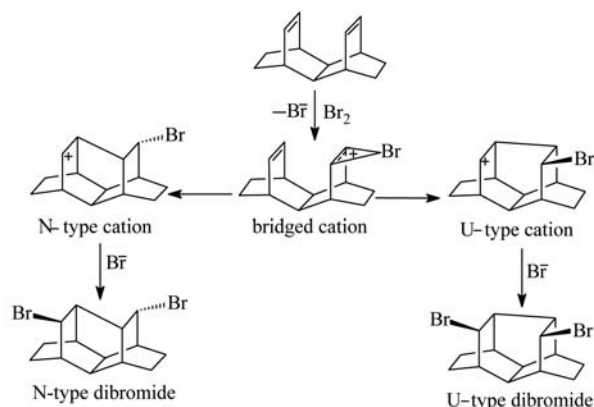


**Figure 1.** The energy diagram of homohipostrofene-Br<sub>2</sub> system (kcalmol<sup>-1</sup>) [B3LYP/6-311++G(2d,2p)//B3LYP/6-311G(d,p)].

into N-type cation and finally an N-type product was obtained. Thus, the reaction occurs by the formation of the most stable intermediate combination (N-type cation). In ph, there are three  $\sigma$  bonds between double bonds and hence N-type product is obtained. Hence, theoretical investigation results of addition of bromine molecule to homohopstufen demonstrate accuracy of the abovementioned rules.

### 3. 3. DFT Investigation of Electrophilic Transannular Addition Reaction of Bromine to Endo,endo-tetracyclo [6.2.2.2.3,6.02,7]tetradeca-4,9-diene (TCTD)

A mixture of N-type and U-type products was obtained in the electrophilic addition reaction of bromine to TCTD molecule (Scheme 4).<sup>2,36</sup> The geometry and the

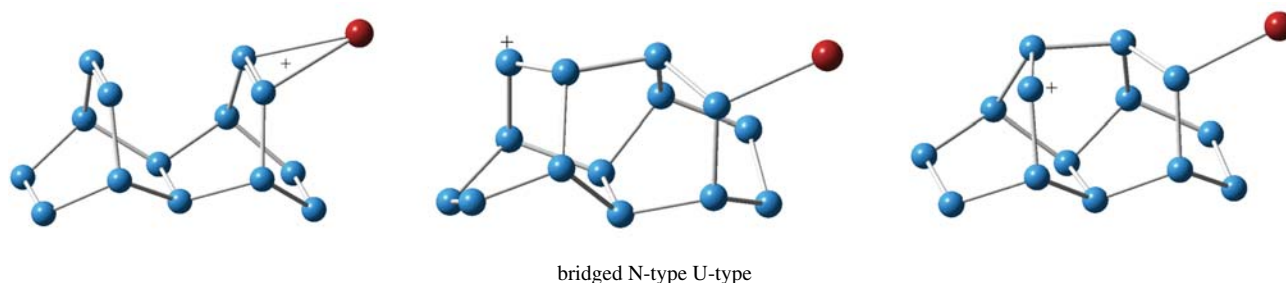


**Scheme 4.** The electrophilic addition reaction of bromine to TCTD molecule

electronic structure of the TCTD molecule were investigated using the B3LYP/6-311G(d,p) and B3LYP/6-311+G(d,p) methods and the structure of the molecule was also investigated in detail.

In order to determine the structures and relative stabilities of the predicted cationic intermediates (bridged, N- and U-type cations) (Scheme 5) formed in the addition reaction, their full geometry optimization was performed at the B3LYP/6-311G(p,d) level and the total energies ( $E_{\text{tot}}$ ) were also calculated. By using the optimized geometries of cations at the B3LYP/6-311++G(d,p) level, their single point energies were computed using B3LYP/6-311++G(2d,2p) and CPCM-B3LYP/6-311++G(2d,2p) methods. The calculated relative energies are given in Table 3.

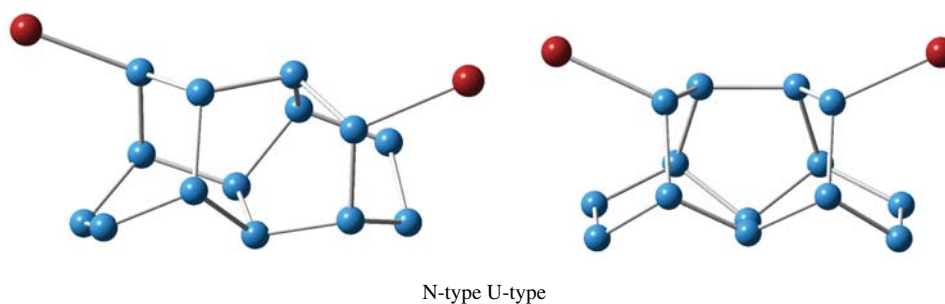
The results of each method showed that the N- and U-type cations are more stable than the bridged bromonium cation. The skeletal isomerization of the bridged bromonium cation into N- and U-type cations is thermodynamically feasible. The total energies of N- and U-type cations differ little and their stabilities are nearly the same. Hence, the bridged bromonium cation transforms into appropriate N- and U-type cations as a result of skeletal isomerization, where crosswise and parallel mechanisms take place. The direction of the addition reaction is determined by the direction of the rearrangement of the bridged bromonium ion into N- and U-type cations. The reaction takes place over the N- and U-type cations in the parallel direction and finally, the N- and U-type reaction products are obtained. In TCTD molecule, there are four  $\sigma$  bonds between double bonds and hence N- and U-type products are obtained. Hence, the results of DFT investigation of addition of bromine molecule to TCTD molecule prove accuracy of the abovementioned rules.



**Scheme 5.** The optimized geometries of cations (B3LYP/6-311G(d,p))

**Table 3.** The calculated relative energies of cations

Cations	Relative energy (kcal mol <sup>-1</sup> )		
	B3LYP/6311 G(d,p)	B3LYP/6311++G(2d,2p) //B3LYP/6-311G(d,p)	CPCM-B3LYP/6311++G(2d,2p) //B3LYP/6-311G(d,p)
bridged	6.253	5.525	8.876
N-type	0.0	0.0	0.0
U-type	1.003	0.590	0.154



**Scheme 6.** The optimized geometries of products (B3LYP/6-311G(d,p))

**Table 4.** The calculated relative energies of products  
Product Relative energy (kcal mol<sup>-1</sup>)

	B3LYP/6311 G(d,p)	B3LYP/6311++G(2d,2p) //B3LYP/6-311G(d,p)	CPCM-B3LYP/6311++G(2d,2p) //B3LYP/6-311G(d,p)
N-type	0.0	0.0	0.0
U-type	3.601	3.977	3.733

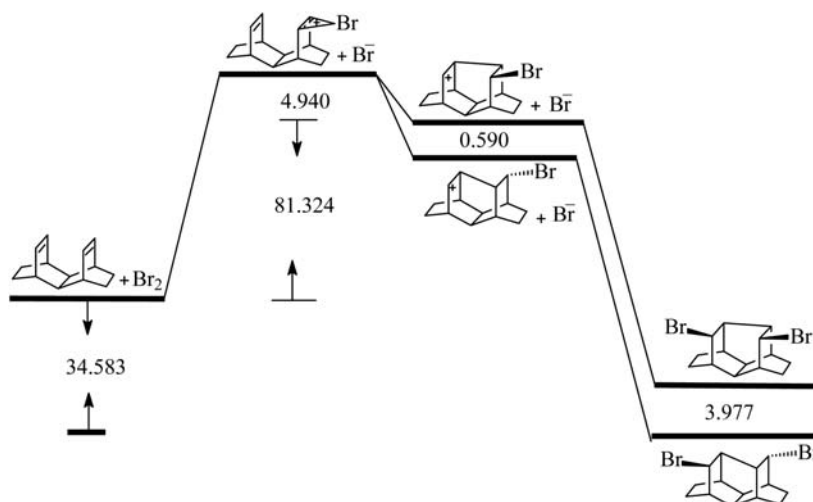
The stereochemistry and the stable configurations of the reaction products were investigated by DFT method. The geometrical structure of the N- and U-type products (Scheme 5) were optimized by B3LYP/6-311G(d,p) method and their total energies were evaluated. By using the optimized geometries of products by B3LYP/6-311G(d,p) method, their single point energies were calculated at the B3LYP/6-311++G(2d, 2p) and CPCM-B3LYP/6311++G(2d,2p) levels. The calculated relative energies are given in Table 4.

Figure 2 shows the energy diagram of the electrophilic addition reaction of bromine to TCTD molecule. As seen from the diagram, the reaction takes place by the

transformation of the bridged bromonium cation into the N- and U-type cations. As the reaction progresses over the N- and U-type cations, the N- and U-type products are obtained. The stabilities of the N- and U-type cation differ little and the stabilities of the N- and U-type products are very close to each other.

## 4. Conclusions

General rules that allow us to stipulate the factors that direct the flow of electrophilic addition reactions of halogens to face-to-face double bonded strained alkenes



**Figure 2.** The energy diagram of TCTD-Br<sub>2</sub> system (kcal mol<sup>-1</sup>) [B3LYP/6-311++G(2d,2p)//B3LYP/6-311G(d,p)] (The formations of N- and U-type products are controlled by the relative energy of N- and U-type cationic intermediates. And also, both products are formed because the relative energies of the cations intermediates are low.)

and reaction products were established by considering the results of the calculations and structure-characteristic relationships. Direction of the addition reaction is determined by direction of isomerisation of bridged halogenium cation and isomerisation takes place to create a more stable skeletal structure. Stability of resultant skeletal structure depends on types and stability of new cyclic structures. Stability of resultant new cyclic structures are determined by the number of  $\sigma$  bonds between isolated double bonds of the alkene and bonding-type of double bonds (N- and U-type), hence by the structure of alkene. When the number of  $\sigma$  bonds between double bonds of the alkene is three ( $m = 3$ ), the reaction takes place to predominantly give an N-type product, and when four ( $m = 4$ ), N- and U-type products. Structure and stability of cation intermediates of electrophilic addition reaction of bromine to homohoprostrofen molecule having double bonds with three  $\sigma$  bonds inbetween, were investigated by DFT methods in detail. The reaction takes place over more stable N-type cation which bridged bromonium cation isomerizes into to give N-type dibromide product. Addition reaction of bromine to endo,endo-tetracyclo [6.2.2.2<sup>3,6</sup>.0<sup>2,7</sup>]tetradeca-4,9-dien molecule, whose double bonds were linked by four  $\sigma$  bonds, was investigated by quantum chemistry. Bridged bromonium cation isomerizes into more stable N- and U-type cations and the reaction takes place over these cations to give N- and U-type dibromide products.

## 5. References

1. C. T. Lin, N. J. Wang, H. Z. Tseng, T. C. Chou, *J. Org. Chem.* **1997**, *62*, 4857–4861. <https://doi.org/10.1021/jo970299c>
2. E. Osawa, K. Aigami, Y. Inamoto, *Tetrahedron* **1978**, *34*, 509–515. [doi.org/10.1016/0040-4020\(78\)00044-1](https://doi.org/10.1016/0040-4020(78)00044-1)
3. C. T. Lin, N. J. Wang, Y. L. Yhe, T. C. Chou, *Tetrahedron*, **1995**, *51*, 2907–2928. [https://doi.org/10.1016/0040-4020\(95\)00044-6](https://doi.org/10.1016/0040-4020(95)00044-6)
4. C. T. Lin, H. C. Hsu, T. C. Chou, *J. Org. Chem.* **1999**, *64*, 7260–7264. <https://doi.org/10.1021/jo990569m>
5. T. Sasaki, K. Kanematsu, A. Kondo, *J. Org. Chem.* **1974**, *39*, 2246–2251. <https://doi.org/10.1021/jo00929a025>
6. M. G. Matturro, R. D. Adams, K. B. Wiberg, *Chem. Commun.* **1981**, *17*, 878–879. <https://doi.org/10.1039/c39810000878>
7. S. Uemura, S. Fukuzawa, A. Toshimitsu, O. Masaya, *J. Org. Chem.* **1983**, *48*, 270–273. <https://doi.org/10.1021/jo00150a029>
8. K. B. Wiberg, R. D. Adams, P. J. Okarma, M. G. Matturro, B. Segmüller, *J. Am. Chem. Soc.* **1984**, *106*, 2200–2206. <https://doi.org/10.1021/ja00319a048>
9. M. Kimura, S. Morosawa, *J. Org. Chem.* **1985**, *50*, 1532–1534. <https://doi.org/10.1021/jo00209>
10. K. J. Shea, A. C. Greeley, S. Nguyen, P. D. Beauchamp, D. H. Aue, J. S. Witzeman, *J. Am. Chem. Soc.* **1986**, *108*, 5901–5908. <https://doi.org/10.1021/ja00279a040>
11. G. Hauße, G. Alvernhe, A. Laurent, *Tetrahedron Lett.* **1986**, *27*, 4449–4452. [https://doi.org/10.1016/S0040-4039\(00\)84975-8](https://doi.org/10.1016/S0040-4039(00)84975-8)
12. C. H. Lee, S. Liang, T. Haumann, R. Boese, A. de Meijere, *Angew. Chem. Int. Edit. Engl.* **1993**, *32*, 559–560. <https://doi.org/0570-0833/93/0404-0559>
13. R. Pinkos, J. P. Melder, K. Weber, D. Hunkler, H. Prinzbach, *J. Am. Chem. Soc.* **1993**, *115*, 7173–7191. <https://doi.org/10.1021/ja00069a015>
14. R. E. Robinson, D. Y. Myers, *Tetrahedron Lett.* **1999**, *40*, 1099–1100. [https://doi.org/10.1016/S0040-4039\(98\)08843-4](https://doi.org/10.1016/S0040-4039(98)08843-4)
15. D. D. Günbaş, F. Algý, T. Hökelek, W. H. Watson, M. Balcý, *Tetrahedron* **2005**, *61*, 11177–11183. <https://doi.org/10.1016/j.tet.2005.09.019>
16. S. Inagaki, H. Fujimoto, K. Fukui, *J. Am. Chem. Soc.* **1976**, *98*, 4054–4061. <https://doi.org/10.1021/ja00430a006>
17. C. Lee, W. Yang, R. G. Parr, *Phys. Rev. B* **1988**, *37*, 785–789. <https://doi.org/10.1103/PhysRevB.37.785>
18. A. D. Becke, *J. Chem. Phys.* **1993**, *98*, 5648–5652. <https://doi.org/10.1063/1.46491319>
19. R. Krishnan, J. S. Binkley, R. Seeger, J. A. Pople, *J. Chem. Phys.* **1980**, *72*, 650–654. <https://doi.org/10.1063/1.438955>
20. V. Barone, M. Cossi, *J. Phys. Chem. A* **1998**, *102*, 1995–2001. <https://doi.org/10.1021/jp9716997>
21. J. Tomasi, B. Mennucci, R. Cami, *Chem. Rev.* **2005**, *105*, 2999–3093. <https://doi.org/10.1021/cr9904009>
22. Y. Takano, K. N. Houk, *J. Chem. Theory Comput.* **2005**, *1*, 70–77. <https://doi.org/10.1021/ct049977a>
23. M. J. Frisch, G. W. Trucks, H. B. Schlegel, G. E. Scuseria, M. A. Robb, J. R. Cheeseman, J. A. J. Montgomery, T. Vreven, K. N. Kudin, J. C. Burant, J. M. Millam, S. S. Iyengar, J. Tomasi, V. Barone, B. Mennucci, M. Cossi, G. Scalmani, N. Rega, G. A. Petersson, H. Nakatsuji, M. Hada, M. Ehara, K. Toyota, R. Fukuda, J. Hasegawa, M. Ishida, T. Nakajima, Y. Honda, O. Kitao, H. Nakai, M. Klene, X. Li, J. E. Knox, H. P. Hratchian, J. B. Cross, C. Adamo, J. Jaramillo, R. Gomperts, R. E. Stratmann, O. Yazyev, A. J. Austin, R. Cammi, C. Pomelli, J. W. Ochterski, P. Y. Ayala, K. Morokuma, G. A. Voth, P. Salvador, J. J. Dannenberg, V. G. Zakrzewski, S. Dapprich, A. D. Daniels, M. C. Strain, O. Farkas, D. K. Mallick, A. D. Rabuck, K. Raghavachari, J. B. Foresman, J. V. Ortiz, Q. Cui, A. Baboul, G. S. Clifford, J. Cioslowski, B. B. Stefanov, G. Liu, A. Liashenko, P. Piskorz, I. Komaromi, R. L. Martin, D. J. Fox, T. Keith, M. A. Al-Laham, C. Y. Peng, A. Nanayakkara, M. Challacombe, P. M. W. Gill, B. Johnson, W. Chen, M. W. Wong, C. Gonzalez, J. A. Pople, Gaussian 03, Revision B.03, Gaussian, Pittsburgh, PA., **2003**.
24. R. Abbasoglu, *J. Mol. Model.* **2006**, *12*, 991–995. <https://doi.org/10.1007/s00894-006-0113-3>
25. R. Abbasoglu, *J. Mol. Model.* **2007**, *13*, 425–430. <https://doi.org/10.1007/s00894-006-0161-8>
26. R. Abbasoglu, *J. Mol. Model.* **2007**, *13*, 1215–1220. <https://doi.org/10.1007/s00894-007-0236-1>

27. R. Abbasoglu, A. Magerramov, *Acta Chim. Slov.* **2007**, *54*, 882–887.
28. R. Abbasoglu, Y. Uygur, *Indian J. Chem. A* **2007**, *46A*, 396–400.
29. R. Abbasoglu, *J. Mol. Model.* **2009**, *15*, 397–403.  
<https://doi.org/10.1007/s00894-008-0388-7>
30. R. Abbasoglu, A. Magerramov, Y. Aşamaz, *Acta Chim. Slov.* **2009**, *56*, 237–245.
31. R. Abbasoglu, A. Yasar, *Turk J. Chem.* **2010**, *34*, 127–134.  
<https://doi.org/10.3906/kim-0812-14>
32. R. Abbasoglu, Y. Aşamaz, A. Magerramov, E. Mamedov, *THEOCHEM* **2010**, *955*, 130–133.  
<https://doi.org/10.1016/j.theochem.2010.06.005>
33. R. Abbasoglu, *Acta Chim. Slov.* **2010**, *57*, 842–848.
34. R. Abbasoglu, M. N. Misir, *Acta Chim. Slov.* **2012**, *59*, 109–116.
35. G. R. Underwood, B. Ramamoorthy, *Tetrahedron Lett.* **1970**, *11*, 4125–4127.  
[https://doi.org/10.1016/S0040-4039\(01\)98683-6](https://doi.org/10.1016/S0040-4039(01)98683-6)
36. E. LeGoff, S. Oka, *J. Am. Chem. Soc.* **1969**, *91*, 5665–5667.  
<https://doi.org/10.1021/ja01048a054>

## Povzetek

Teoretično smo proučevali elektrofilno adicijo halogenov na sosednja mesta v alkenih. Določili smo splošna pravila, ki nam omogočajo določanje dejavnikov pri usmerjanju glavnih stopenj te reakcije. Ugotovili smo, da je smer reakcije odvisna od usmerjenosti intramolekularne skeletne izomerizacije ciklično premoščene halogenskega kationa. Izomerizacija poteče tako, da nastane bolj stabilna skeletna struktura. Njeno stabilnost smo določili s številom  $\sigma$  vezi med izoliranimi dvojnimi vezmi v alkenu in dvojnimi vezmi N- in U-tipa. Če je število  $\sigma$  vezi med dvojnimi vezmi v alkenu tri ( $m = 3$ ), reakcija poteka pretežno tako, da dobimo produkt N-tipa, pri  $m = 4$  pa nastanejo produkti N- in U-tipa. Strukturo in stabilnost kationskih intermediatov (premoščen, N in U-tip) pri elektrofilni adiciji smo natančno preučili z metodo DFT.



Scientific paper

# Mixed Metal Oxides of the Type $\text{Co}_x\text{Zn}_{1-x}\text{Fe}_2\text{O}_4$ as Photocatalysts for Malachite Green Degradation Under UV Light Irradiation

Martin Tzvetkov,<sup>1</sup> Maria Milanova,<sup>1,\*</sup> Zara Cherkezova-Zheleva,<sup>2</sup>  
Ivanka Spassova,<sup>3</sup> Evgenia Valcheva,<sup>4</sup> Joana Zaharieva<sup>1</sup> and Ivan Mitov<sup>2</sup>

<sup>1</sup> Department of Inorganic Chemistry, Faculty of Chemistry and Pharmacy, Sofia University “St. Kliment Ohridski”,  
1, J. Bourchier, 1164 Sofia, Bulgaria

<sup>2</sup> Institute of Catalysis, Bulgarian Academy of Sciences, Acad. G. Bonchev St., Block 11, 1113 Sofia, Bulgaria

<sup>3</sup> Institute of General and Inorganic Chemistry, Bulgarian Academy of Sciences, Acad. G. Bonchev St., Block 11,  
1113 Sofia, Bulgaria

<sup>4</sup> Department of Solid State Physics, Faculty of Physics, Sofia University “St. Kliment Ohridski”, 3, J. Bourchier,  
1164 Sofia, Bulgaria

\* Corresponding author: E-mail: mariamilanova2@abv.bg,  
tel. +35928161322

Received: 07-11-2016

## Abstract

A combination of thermal and mechanical (high energy ball milling) treatment was applied in an attempt to obtain polycrystalline mixed metal binary and ternary oxides of the type  $\text{Co}_x\text{Zn}_{1-x}\text{Fe}_2\text{O}_4$  ( $x = 0; 0.25; 0.5; 0.75; 1$ ). The synthetic procedure used successfully produced single-phased, homogeneous  $\text{ZnFe}_2\text{O}_4$ ,  $\text{CoFe}_2\text{O}_4$ , and  $\text{Co}_{0.75}\text{Zn}_{0.25}\text{Fe}_2\text{O}_4$ , as well as mixed oxides, whose composition depended both on the duration of the high energy ball milling and the ratio Zn(II)/Co(II). The formation of spinel-like structures was proved by XRD, Mössbauer spectroscopy and Raman spectroscopy. For the characterization of the samples low-temperature  $\text{N}_2$  adsorption, UV/Vis spectroscopy and transmission electron microscopy were applied. The energy band gap of the samples was calculated, suggesting they are promising photocatalysts. The decomposition of the Malachite Green in model water solutions under UV-light irradiation was successfully achieved in the presence of the samples as photocatalysts. The highest rate constant was obtained for the sample synthesized at longer milling time in combination with higher Zn(II)/Co(II) ratio. The photocatalytic activity of the ternary mixed oxides was compared with the pure hematite,  $\alpha\text{-Fe}_2\text{O}_3$ , and the binary  $\text{ZnFe}_2\text{O}_4$  and  $\text{CoFe}_2\text{O}_4$  ferrites with spinel structure that were treated in the same way. A synergetic effect of  $\alpha\text{-Fe}_2\text{O}_3$  and the spinel-like structure on the photocatalytic properties of ternary mixed metal oxides was detected.

**Keywords:** ferrites; mechanoactivation, Mossbauer spectroscopy; powder diffraction, photocatalysis, malachite green

## 1. Introduction

Ferrites with spinel-like structure with the formula  $\text{MFe}_2\text{O}_4$ , where M represents a divalent metal ion, are technologically important and have been used in many applications including magnetic recording media and magnetic fluids for the storage and/or retrieval of information, magnetic resonance imaging enhancement, catalysis, magnetically guided drug delivery, sensors, pigments, etc.<sup>1–3</sup>

Among all the properties they possess, ferrites offer the advantage of having a band gap capable of absorbing ultra violet and visible light. Ferrites with spinel-like structure prepared through solid state reaction have been used for photocatalytic hydrogen generation.<sup>4</sup> The spinel crystal structure enhances the efficiency of light absorption due to the available extra sites in the crystal lattice.<sup>5</sup> Some organic molecules have been decomposed under UV irradiation in the presence of different spinels as pho-

tocatalysts, such as methyl orange by  $\text{BaFe}_2\text{O}_4$ ,<sup>6</sup> phenolphthalein by  $\text{CoFe}_2\text{O}_4\text{-ZnO}$ ,<sup>7</sup> rhodamine B by  $\text{Ag/ZnFe}_2\text{O}_4$  nanocomposites,<sup>8</sup> and methylene blue by  $\text{Zn-Fe}_2\text{O}_4$  nanorods.<sup>9</sup> There are not many data available for  $\text{CoFe}_2\text{O}_4$  used as a photocatalyst, but it has been used for decomposition of  $\text{H}_2\text{O}_2$ .<sup>10</sup> The testing of ferrites as photocatalysts for degradation of inorganics, bacteria as well as organic molecules such as methylene blue, methyl orange and rhodamine B has been summarized,<sup>11</sup> but no data are available for malachite green degradation. Malachite Green, MG, is a water-soluble azo dye that is widely used in research laboratories and in the textile, pharmaceutical and food industries. It appears in waste waters, so the water need treatment and purification.

Among the spinel ferrites,  $\text{ZnFe}_2\text{O}_4$  has significant absorbance in the 450–700 nm wavelength range.<sup>12</sup> It is regarded as a promising photocatalyst with a band gap of 1.92 eV (646 nm), which makes it possible to utilize solar energy.<sup>11,12</sup> Possessing photochemical stability and low toxicity,  $\text{ZnFe}_2\text{O}_4$  has been applied to degrade organic pollutants,<sup>13,14</sup> modified by multiwall carbon nanotubes,<sup>15</sup> by  $\text{SrTiO}_3$ ,<sup>16</sup> by  $\text{TiO}_2$ <sup>15,17,18</sup> etc. In those cases no energy band gaps have been calculated, but it can be expected that the modification influences the energy band gap of the samples: for example, for bulk  $\text{CoFe}_2\text{O}_4$ , the band gap was found to be 2.7 eV<sup>4,19</sup> while for modified nanostructure  $\text{CoFe}_2\text{O}_4/\text{ZnO}$  it was found to be 4.5 eV.<sup>7</sup> One can therefore expect that polycrystalline mixed metal ternary oxides of the type  $\text{Co}_x\text{Zn}_{1-x}\text{Fe}_2\text{O}_4$  will have energy band gaps different from that of pure  $\text{CoFe}_2\text{O}_4$  and  $\text{ZnFe}_2\text{O}_4$  and therefore can have different photocatalytic activities for malachite green degradation.

Different methods for synthesis of ferrites have been developed, among them co-precipitation and sol-gel techniques. These usually result in large particles and a broad size distribution.<sup>17,20,21</sup> A combination of mechanical and thermal treatment is often used in a procedure that includes several steps. Mechanical treatment with a ball milling technique has been applied to synthesize Ni-Zn ferrite from initial mixtures of NiO, ZnO and  $\text{Fe}_2\text{O}_3$ ,<sup>22,23</sup> while polycrystalline  $\text{Mn}_{1-x}\text{Zn}_x\text{Fe}_2\text{O}_4$  was prepared by mechanical alloying of stoichiometric mixtures of  $\text{MnO}^{24}$  or  $\text{MnO}_2$ <sup>25</sup> and ZnO and  $\text{Fe}_2\text{O}_3$  powders. Variations of the mechanical treatment method include the duration of the pre-heating process as well as the number and the duration of heating steps to anneal after the mechanical treatment. The annealing of a milled powder is usually applied to reduce the lattice defects and strains and to improve the magnetic properties of the ferrites (internal strain has a negative effect on the magnetic properties).<sup>24,26</sup> The annealing includes heating at a constant rate and isothermal holding, followed by cooling down to room temperature. The milled powders can be annealed at different temperatures to obtain a single-phase powder.<sup>17</sup> During the ball milling, crystal defects can be created so they might have various life times and different natures. The crystal

defects influence the properties of oxides such as electrical,<sup>27,28,29</sup> magnetic<sup>30</sup> and optical,<sup>31</sup> and may act both as a source and as a trap of electrons. In the synthetic procedure applied in the work presented, we tried to preserve the potential defects formed by first pre-grinding the oxides in order to mix them carefully, then calcining them at high temperature and finally ball milling them in order to stimulate crystal defects in the structure. The later should be preserved if further annealing is not applied.

Shortly, in the work presented, by a two-step procedure combining high temperature treatment and mechanical treatment, polycrystalline binary and ternary mixed metal oxides were synthesized and characterized. The photocatalytic decomposition of Malachite Green under UV irradiation in model water solutions in the presence of the samples obtained was tested. By this an attempt was made to evaluate the application of the synthesized catalysts. Ferrites are seldom used for the decomposition of Malachite Green, so the results obtained increase the range of photocatalysts that can be used for degradation of this dye.

## 2. Experimental

### 2. 1. Materials and Synthetic Procedure

The initial materials used were hematite,  $\alpha\text{-Fe}_2\text{O}_3$  (>99%, p.a), ZnO (>99%, p.a.) and  $\text{Co}(\text{NO}_3)_2 \cdot 6\text{H}_2\text{O}$  (p. a.) (all Alfa Aesar). Cobalt nitrate was used to produce CoO after calcination at 900 °C for 5 hours. The synthetic procedure for the samples used in the work included calcination at 900 °C for 5 h and then milling for two different periods of time (4 or 8 hours). A high energy ball mill (Pulverisette 7, Fritsch) with zirconium oxide vials and balls was used. The milling intensity was 600 rpm and the ball-to-milled powder ratio was 8:1. By treating in the same way the commercial *hematite*  $\alpha\text{-Fe}_2\text{O}_3$ , three different samples were obtained, namely Fe-TS, Fe-4MA and Fe-8MA, where TS is the symbol for the calcined sample and it comes from Thermal Synthesis, MA presents the treatment by milling at 4 or 8 hours, respectively and it means MechanoActivated sample. The *binary* mixed metal oxides  $\text{ZnFe}_2\text{O}_4$  ( $\text{Co}_x\text{Zn}_{1-x}\text{Fe}_2\text{O}_4$  where  $x = 0$ ) and  $\text{CoFe}_2\text{O}_4$  ( $\text{Co}_x\text{Zn}_{1-x}\text{Fe}_2\text{O}_4$  where  $x = 1$ ) were synthesized in two steps. In the first step, the stoichiometric mixture of the oxides was hand-grinded for 30 min to ensure complete homogenization, and then compacted to disks 50 mm in diameter and 1–2 mm thick and finally sintered at 900 °C for 5h. In the second step, the as prepared samples were milled for 4h. For the powders obtained, the symbols ZFO-TS, ZFO-4MA, CFO-TS and CFO-4MA, respectively (TS and MA as mentioned above) are used, where ZFO is for Zinc Ferrite Oxide and CFO for Cobalt Ferrite Oxide. The synthetic procedure for *ternary mixed metal oxides* included the same two steps, and the samples produced can be presented by the stoichiometric formula  $\text{Co}_x\text{Zn}_{1-x}\text{Fe}_2\text{O}_4$  where  $x = 0.25; 0.5; 0.75$  and denoted as

ZC31/4, ZC11/4 and ZC13/4 after 4h milling and ZC31/8, ZC11/8 and ZC13/8 after 8h milling where ZC is for Zinc-Cobalt ferrite. The mole ratio of the ions Zn(II)/Co(II) (3:1, 1:1, 1:3) as well as the duration of the milling (4 or 8 hours) are mentioned in the symbols by 31/4, 11/4, 11/4 and 31/8, 11/8, 11/8.

## 2. 2. Methods for Characterization of the Samples

**X-ray powder diffraction (XRD)** patterns for phase identification were recorded in the angle interval 10–80° (2 $\theta$ ), on a Philips PW 1050 diffractometer, equipped with a Cu K $\alpha$  tube and a scintillation detector. Data for cell refinements were collected in  $\theta$ –2 $\theta$ , step-scan mode in the angle interval from 25 to 70° (2 $\theta$ ), at steps of 0.04° (2 $\theta$ ) and a counting time of 1 s/step. The cell refinement analysis was carried out in BRASS (Bremen Rietveld Analysis and Structure Suite).<sup>32</sup>

**Internal strain** of the samples was estimated by analysis of XRD peaks using the Williamson-Hall formula<sup>33</sup>  $(\beta/2)\cot\theta = 0.45\lambda/(\sin\theta D) + \epsilon$ , where  $\beta$  is the peak width at half maximum,  $\theta$  is the Bragg diffraction angle,  $\lambda$  is the X-ray wavelength,  $D$  is the average crystallite size and  $\epsilon$  is the value of the strain.

**Mössbauer spectra** were recorded with an electro-mechanical spectrometer (Wissenschaftliche Elektronik GmbH) in constant acceleration mode at room temperature. The source of radiation is <sup>57</sup>Co/Rh (activity  $\cong$  50 mCi) and standard  $\alpha$ -Fe. The recorded spectra were used for calculations using software working with the method of least squares. The following parameters of the hyperfine interactions were calculated: isomer shift (IS), quadrupole splitting (QS), effective inner magnetic field in the site of iron nuclei ( $H_{\text{eff}}$ ), as well as the full width at half maximum (FWHM) and relative weights (G) of the components.

**The texture characteristics** were determined by low-temperature (77.4 K) nitrogen adsorption using a Quantachrome Instruments NOVA 1200e apparatus. The specific surface area ( $S_{\text{BET}}$ ) was calculated using the Brunauer–Emmett–Teller (BET) surface area method.

**Raman spectroscopy** – The measurements were carried out in a HORIBA Jobin Yvon Labram HR 800 micro-Raman spectrometer with a He–Ne (633nm) laser, the absolute measurement accuracy being 0.5 cm<sup>-1</sup> or better.

**UV-VIS absorption spectroscopy** – an Evolution 300 UV-Vis spectrometer (Thermo Scientific) was used for measuring the absorption of the samples in the range 200–900 nm.

**Transmission electron microscopy (HRTEM)** was done using a JEM 2100 (JEOL), with an accelerator voltage of 200 kV and up to 1 500 000 times magnification, to follow the morphology of the samples.

**Band gap energy calculations.** The optical properties (absorption and optical band gap energy) of the sam-

ples were studied using UV-Vis absorption spectra. In all cases broad absorption was registered in the 300–900 nm range of the spectra. The UV-Vis data were analysed for the relation between the optical band gap, absorption coefficient and energy ( $h\nu$ ) of the incident photon for near edge optical absorption in semiconductors. The band gap energy was calculated from the measured curves by fits according to Tauc's equation<sup>34</sup>  $\alpha h\nu = A(h\nu - E_g)^n$ , where  $A$  is a constant independent of  $h\nu$ ,  $E_g$  is the semiconductor band gap and  $n$  depends on the type of transition. In addition, the well-known approach for semiconductor band gap energy determination from the intersection of linear fits of  $(\alpha h\nu)^{1/n}$  versus  $h\nu$  on the x-axis was used,  $n$  being 1/2 and 2 for direct and indirect band gap, respectively.

## 2. 3. Photocatalytic Activity

The photocatalytic tests were performed in a slurry (1 g catalyst/l), using a 10<sup>-5</sup> M aqueous solution of Malachite Green oxalate (Chroma GmbH) as a model pollutant. After a 30-min “dark” period (in order to establish the equilibrium of the sorption process), the system was UV-illuminated by a lamp (Sylvania 18 W BLB T8, emission in the 345–400-nm region with a maximum at 365 nm), situated at 9.5 cm distance above the slurry (illumination intensity 0.5 W/m<sup>2</sup>), under continuous magnetic stirring (400 min<sup>-1</sup>) and bubbling with air (45 L/h). The initial pH of the solutions were between 5.8 and 5.9. Periodically, a 5-ml aliquot was taken from the solution and filtered through a 0.20- $\mu$  Minisart filter. The dye concentration was determined spectrophotometrically using the band at 622 nm. The data obtained were plotted in coordinates  $(C/C_0)/t$  and  $-\ln(C/C_0)/t$  (where  $C_0$  is the concentration after the “dark” period, and  $C$  is the concentration after  $t$  min irradiation), and apparent rate constants of the degradation process were determined assuming first-order kinetics. The sorption capacity was calculated as the ratio  $(C_{00}-C_0)/C_{00}$ , where  $C_{00}$  is the starting solution concentration (before the “dark” period). The malachite green degradation at moment  $t$  is determined by the formula: degradation, % =  $(A_0 - A_t)/A_0 \times 100$ , where  $A_0$  is the initial absorption of the malachite green solution at moment  $t = 0$  min, and  $A_t$  is the absorption at moment  $t$  min.

## 3. Results

### 3. 1.Characterization of the Samples

#### 3. 1. 1. Phase Composition and Crystal Structure of the Hematite and the Binary Mixed Oxides With Spinel-like Structure (ferrites).

The XRD patterns of the samples Fe-TS, Fe-4MA, Fe-8MA (Figure S1), those of the binary metal oxides ZF-TS, ZF-4MA (Figure S2, a), and CF-TS and CF-4MA

(Figure S2, *b*) reveal a single phase without detectable secondary phase (within the limit of X-ray detection, typically 5 %). The calculated unit cell parameters are in good agreement with the data from the crystallographic databases (ZFO 8.4430 Å, ICSD 98-002-8511; CFO 8.3550 Å, ICSD 98-018-4063) (Table 1). The data for the crystallite sizes for ZF-4MA and CF-4MA are close and are similar to those for the ternary oxides milled for 4h (Table 1). For CF-TS and CF-4MA, the unit cell parameters slightly decrease with the milling time, although they are bigger in comparison with the literature data (CFO 8.3550 Å, ICSD 98-018-4063). The intensity of the reflex is slightly higher for the TS (only calcined) samples compared with those for the MA (calcined and milled) samples (Figure S2). With increasing milling time, the unit cell parameters and the crystallites size decrease for both the zinc and cobalt ferrites, while the lattice distortion increases. An inducing of cation redistribution in spinel ferrites by the high energy ball milling<sup>35,36</sup> as well as contraction of the lattice caused by lattice defects<sup>35</sup> have been pointed out as probable reasons for reduction of lattice parameters.

The experimental Mössbauer spectra of the samples ZF-TS and ZF-MA analysed contain a typical doublet spectrum for the spinel ferrite paramagnetic phase (Figure S3 *a, b*). The experimental Mössbauer spectra of CF-TS and CF-MA include only components expressing super-fine magnetic structure i.e. sextets (Figure S3 *c, d*) that correspond to tetrahedral and octahedral sites of Fe<sup>3+</sup>, indicating the inverse spinel structure of CoFe<sub>2</sub>O<sub>4</sub> at ambient temperature (the inverse spinel structure of CoFe<sub>2</sub>O<sub>4</sub> has oxygen atoms which make up an fcc lattice, with half of the Fe<sup>3+</sup> ions occupying the tetrahedral A sites and the other half, together with the Co<sup>2+</sup> ions located at the octahedral B sites<sup>37</sup>). The third component (Sextet-3) is likely

due to the presence of ferrite spinel particles having a smaller size. So far the analysis confirms that the synthetic procedure used resulted in CoFe<sub>2</sub>O<sub>4</sub> and ZnFe<sub>2</sub>O<sub>4</sub> binary mixed metal oxides with spinel structure both after calcination only and after a combination of calcination and milling for 4 hours.

### 3. 1. 2. Phase Composition and Crystal Structure of Ternary Mixed Metal Oxides

The XRD patterns of the mixed oxides show single phases of well crystallized Co<sub>x</sub>Zn<sub>1-x</sub>Fe<sub>2</sub>O<sub>4</sub> (*x* = 0.25; 0.5; 0.75) (Figure 1). The longer milling time is the reason for the weak amorphous halo in the XRD of the samples ZC11/8 and ZC13/8. The calculated unit cell parameters are smaller than those for pure ZnFe<sub>2</sub>O<sub>4</sub> and bigger than those for pure CoFe<sub>2</sub>O<sub>4</sub>, compared both with the literature data and with the samples synthesized by us. The uncertainty of the calculations for 8h-milled samples is high due to the smaller size of the crystallites, which leads to higher full width at half maximum (FWHM) values.

The results of the Rietveld analysis are summarized in Table 1. The shape factor used for determination of the crystallite size with the Scherrer formula is 1. The samples milled for 4h have bigger crystallite sizes (almost double the size of 8h-milled samples). The tendency in the decrease of the cell parameters with decrease of the ratio Zn(II)/Co(II) is analogous to reported data (8.4210 Å for Zn/Co = 0.6/0.4: (ICSD 98-016-6203); 8.4120 Å for Zn/Co = 0.4/0.6: (ICSD 98-016-6202)).

The Mössbauer spectra of the powdered samples are a result of a superposition of lines of components without resolved hyperfine magnetic structure i.e. *quadruple doublets* and components with expressed superfine magnetic structure, i.e. *sextets* (Figure 2). The models for

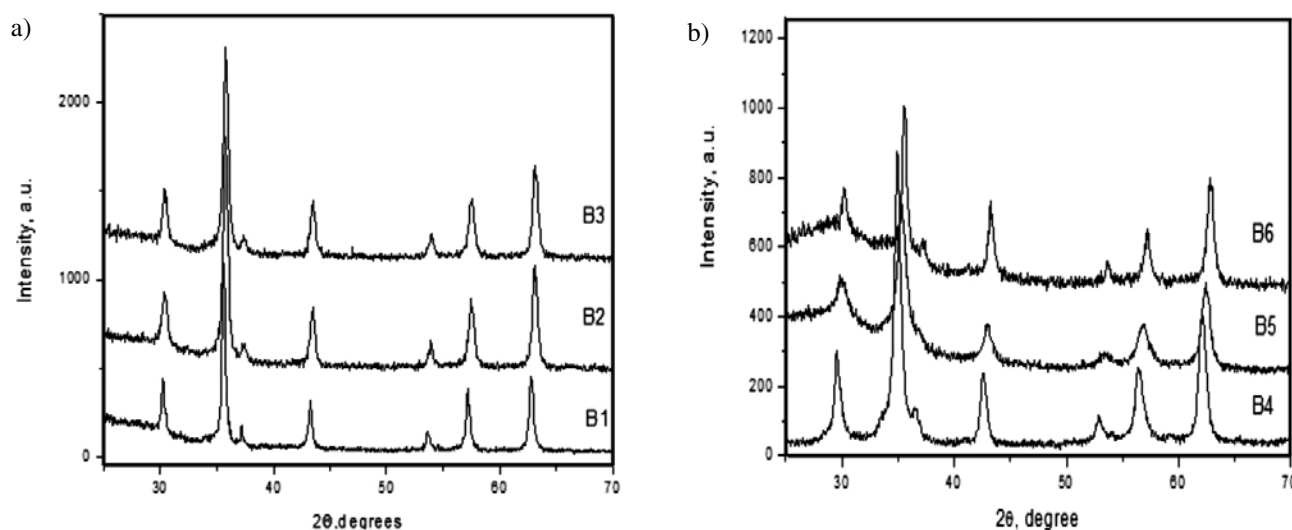


Figure 1. XRD patterns of the samples, from bottom to top (a) ZC31/4, ZC11/4, ZC13/4 and (b) ZC31/8, ZC11/8, ZC13/8, respectively.

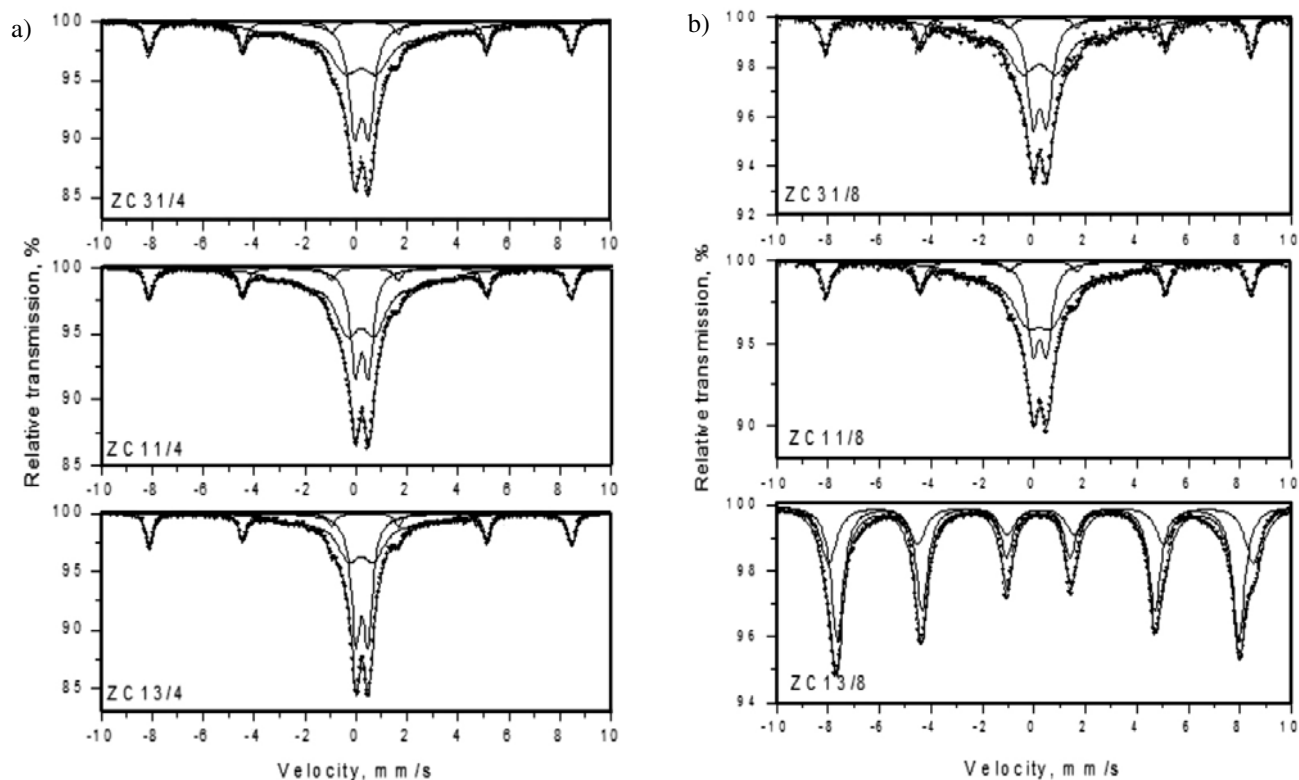
**Table 1.** Unit cell parameter ( $a_0$ ), average crystallite size ( $D$ ) and lattice strain ( $\epsilon$ ).

Sample	$a_0$ (Å)	$D$ , nm	$\epsilon$ , $\times 10^{-3}$ , a.u.
Fe-TS	$a = 5.0352 \pm 0.0001$ $c = 13.7440 \pm 0.0001$	$76.3 \pm 2.7$	0.006
Fe-4MA	$a = 5.0334 \pm 0.0002$ $c = 13.6846 \pm 0.0030$	$21.5 \pm 0.5$	1.20
Fe-8MA	$a = 5.0342 \pm 0.0001$ $c = 13.6940 \pm 0.0025$	$19.8 \pm 1.9$	1.23
ZF-TS	$8.4428 \pm 0.0005$	$77.3 \pm 0.9$	1.70
ZF-4MA	$8.4418 \pm 0.0013$	$53.2 \pm 0.5$	1.90
CF-TS	$8.3840 \pm 0.0022$	$73.5 \pm 0.2$	2.05
CF-4MA	$8.3827 \pm 0.0031$	$57.9 \pm 0.3$	2.31
ZC31/4	$8.4230 \pm 0.0012$	$56.1 \pm 0.2$	1.95
ZC11/4	$8.4160 \pm 0.0013$	$57.4 \pm 0.4$	1.86
ZC13/4	$8.4090 \pm 0.0023$	$56.5 \pm 0.3$	1.96
ZC31/8	$8.4260 \pm 0.0025$	$26.3 \pm 0.5$	0.91
ZC11/8	$8.4173 \pm 0.0031$	$28.0 \pm 0.6$	1.37
ZC13/8	$8.4101 \pm 0.0401$	$24.1 \pm 0.5$	1.00

Mössbauer spectra processing include these two types of components i.e. two sextets and one doublet for samples ZC31/4 to ZC11/8 and two sextets for the sample ZC13/8. In the calculations, both components are included. The results are summarized in Table S1.

The five ternary mixed metal oxides ZC31/4, ZC11/4, ZC13/4, ZC31/8 and ZC11/8 have a similar composition of the three components i.e. Sx1-hematite

(17–20% of the sample), Sx2-spinel (50–55%) and a superparamagnetic component (26–33%). A possible explanation of the presence of hematite is either because of some incompletely reacted initial hematite material or because some partial destruction of the spinel phase during the milling process. The absence of reflections of hematite in the XRD patterns (Figure 1) suggests that the hematite is present as very small crystals. Taking into account

**Figure 2.** Mössbauer spectra of ZC31/4, ZC11/4, ZC13/4 (a) and ZC31/8, ZC11/8, ZC13/8 (b), from top to bottom.

that the oxides in the initial source system were present in stoichiometric ratios for the formation of ferrite, the presence of hematite suggests that unreacted free ZnO and CoO should also be present in the samples. The latter are not registered by XRD either because of their very small crystals (just like the hematite) or because of their low concentration.

The hyperfine parameters of the other two components in the Mossbauer spectra of samples ZC31/4, ZC11/4, ZC13/4, ZC31/8 and ZC11/8 can be attributed to the presence of a spinel phase. Its relatively small particle size gives rise to an incompletely resolved magnetic structure. A bidisperse particle size distribution is evidenced by both sextet and doublet components of bigger particles with collective magnetic excitations behaviour and smaller spinel particles with completely collapsed magnetic structures due to thermally activated reversals of particle magnetisation moments<sup>38</sup>. The lower than typical values of  $H_{\text{eff}}$  of the crystalline spinel phases may also be a result of the mixed nature of the spinel component. The described composition of the samples from ZC31/4 to ZC11/8 can be explained with their heterogeneity. Sample ZC13/8 has a different spectrum, consisting of two sextets of a spinel phase i.e. Sx1 that includes  $\text{Fe}^{3+}$  ions in tetrahedral coordination and Sx2 with  $\text{Fe}^{3+}$  ions in octahedral coordination.

The spinel-like structure of the sample ZC13/8 shown to be homogeneous by Mössbauer spectrum is confirmed by its Raman spectrum (150–1200  $\text{cm}^{-1}$ ) (Figure 3), which shows clear bands at 468, 612 and 682  $\text{cm}^{-1}$ . According to the literature, both Raman modes at 612 and 682  $\text{cm}^{-1}$  are reflecting the local lattice effect in the tetrahedral sublattice, while the peak at 468  $\text{cm}^{-1}$  is probing the local lattice effect in the octahedral sublattice.<sup>39,40</sup> The

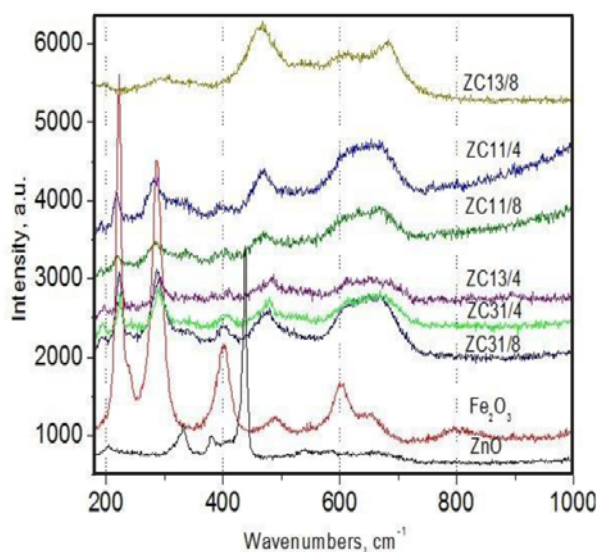


**Figure 3.** Raman spectra of the samples ZC31/4, ZC11/4, ZC13/4, ZC31/8, ZC11/8, ZC13/8 compared with the spectra of pure hematite and ZnO.

same Raman bands mentioned above as well as additional bands at 222  $\text{cm}^{-1}$  and 286  $\text{cm}^{-1}$  can be seen in samples ZC31/4 to ZC11/8; these additional bands can be assigned to  $\alpha\text{-Fe}_2\text{O}_3$ , which has very intense bands at these positions, shown in the Figure 3 for convenience. The Raman data thus confirm the observed significant difference between sample ZC13/8 and samples ZC31/4 to ZC11/8 by Mossbauer spectroscopy, i.e. the presence of  $\alpha\text{-Fe}_2\text{O}_3$ . The broadening and the asymmetry of the Raman peaks may be related to a high degree of cation disorder induced by the milling.<sup>41</sup> No ZnO and CoO are detected as separate phases in the Raman spectra of the samples (no distortion of the lattice cell was observed by XRD either). No peaks induced by CoO could be detected according to literature.<sup>42</sup>

### 3. 1. 3. The Lattice Strain

The influence of the milling on the samples can be evaluated by the lattice strain data. From the data of Table 1, it appears that for the *individual oxide Fe-TS* the annealing at 900 °C causes the biggest relaxation, as the lattice strain observed is insignificant. The milling for 4h leads to a distortion and introduces point defects, but the further milling for 8h does not change crystallites size and the lattice strain. For *the binary oxides* the decrease of the crystallites size leads to higher values of the lattice strain. Between pure CF and ZF, CF shows the higher lattice strain. A possible reason could be the inverse spinel structure of  $\text{CoFe}_2\text{O}_4$  at ambient temperature, as proved by Mossbauer spectroscopy (Table S1). For *the ternary oxides* the shorter milling time (4 h) causes bigger lattice strain than the longer 8 h. The fact that the samples contain three metal cations, with different ratio Zn(II)/Co(II) and a more complicated heterogeneous phase composition makes the interpretation of the values for these samples complicated. In conclusion, the milling introduces energy in the system, which partially dissipates but partially causes point defects i.e. lattice strain.

## 3. 2. Optical Properties and Band Gap Energy Calculation

The absorbance in the UV/Vis range (450–700 nm, spectra not shown here) showed a clear maximum at around 400 nm and a weaker band at around 750 nm. Based on these data, the band gap energy,  $E_g$ , was determined after plotting  $\alpha/E$ , where  $\alpha$  is the absorption coefficient. Examples for ZC31/4 are shown in the range of direct and indirect transitions (Figure 4 a, b).

The crossing point with the x-axis was found after applying different analyses.<sup>34</sup> For the direct transition,  $\alpha^2/E$  was plotted against energy and the linear part of the graph was extrapolated to zero where a value of 1.83 eV was obtained; for the indirect transition,  $\alpha^{1/2}/E$  was plotted against energy and in a similar way, a value of 1.3 eV was

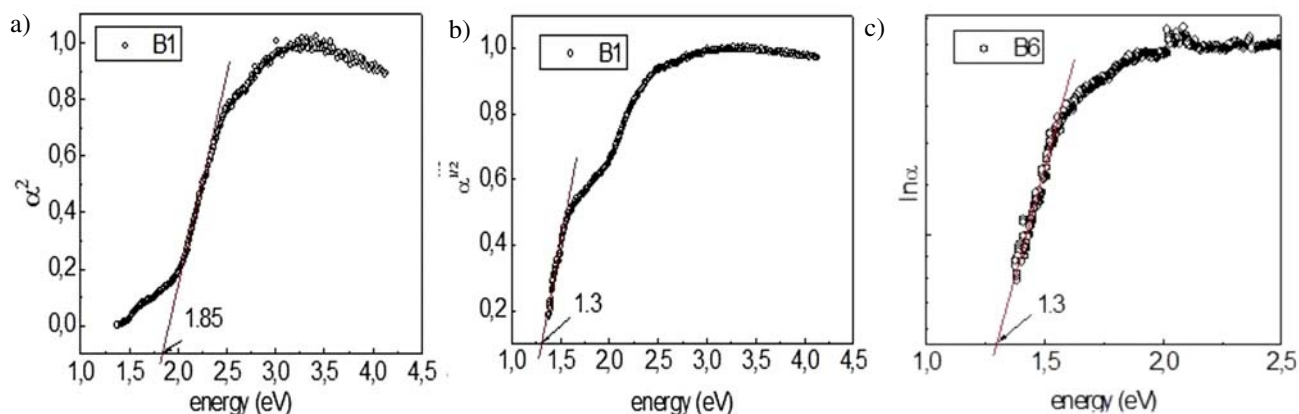


**Figure 3.** Raman spectra of the samples ZC31/4, ZC11/4, ZC13/4, ZC31/8, ZC11/8, ZC13/8 compared with the spectra of pure hematite and ZnO.

found. Similar graphs were obtained for ZC11/4, ZC13/4, ZC31/8, and ZC11/8. However, the data for ZC13/8 are different from the other samples and a linear fit is obtained if the expression accounting for Urbach tails for amorphous material is used,  $\alpha(h\nu) \sim \exp(h\nu/E_u)$ .<sup>43</sup> The fit gives one linear part of the graph and a value of 1.3 eV was obtained by extrapolation of the straight section to the x-axis (Figure 4, c). This model accounts for static disorder in amorphous solids. The fact that sample ZC13/8 has the smallest particle size of all samples (24 nm, Table 1) could be the reason for the similarity of sample ZC13/8 with an amorphous sample. The band gap in the range 1.1–1.3 eV for the samples ZC31/4, ZC11/4, ZC13/4, ZC31/8, ZC11/8 (Table 2) confirms the presence of spinel phase as detected by IR (not included here), Raman and Mössbauer spectroscopy and XRD, along with mono metal oxides like hematite.

**Table 2.** Calculated data for  $E_g1$  and  $E_g2$ .

Sample	$E_g1$ (direct), eV	$E_g2$ (indirect), eV
ZC31/4	1.83	1.3
ZC11/4	1.79	1.3
ZC13/4	1.69	1.21
ZC31/8	1.68	1.22
ZC11/8	1.72	1.11
ZC13/8	–	1.3

It can be speculated that the values found for  $E_g1$  are due to the presence of hematite, ZnO and CoO. The band gap data  $E_g1$  (direct) for ZC31/4, ZC11/4, ZC13/4 show a clear tendency of a decrease upon substitution (according the experimental stoichiometry) by a lighter cation, i.e. Co(II). A similar observation was made for Co(II) doped ZnO,<sup>44,45</sup> an increase is observed for cations such as Al(III) and Ga(III), with a larger mass difference than Zn(II) and Co(II).<sup>46</sup> Considering the literature data for the values of the band gap i.e.  $\alpha$ -Fe<sub>2</sub>O<sub>3</sub> with 2.2 eV<sup>47</sup>, ZnO with 3.77 eV<sup>12</sup> or

3.3 eV, according<sup>45</sup> ZnFe<sub>2</sub>O<sub>4</sub> with 1.92 eV,<sup>11,12</sup> and CoFe<sub>2</sub>O<sub>4</sub> with 2.7 eV<sup>4,19</sup> it is obvious that the resulting ternary oxides have lower values of the band gap than the individual components. It is an indication that the composite oxides can absorb more photons and generate more e<sup>-</sup>/h<sup>+</sup> pairs so the photocatalytic activity can be enhanced. Similar behaviours for composite systems has been reported.<sup>48</sup>

### 3. 3. Specific Surface Area (SSA), Pore Volume and Average Pore Diameter

The BET specific surface areas (Table 3) were found to be low, which is probably caused by the high temperature for calcination during the first step of the synthetic procedure. The value for  $\alpha$ -Fe<sub>2</sub>O<sub>3</sub> calcined, Fe-TS, is the lowest among all the samples and increased with the milling time for Fe-4MA and Fe-8MA, which is to be expected. The highest observed values are those for ZF-4MA, 30 m<sup>2</sup>/g, and for CF-4MA, 21 m<sup>2</sup>/g, in agreement with expectations for higher SSA after the milling

**Table 3.** Specific surface area (SSA), pore volume and average pore diameter of the samples

Sample	$S_{BET}$ , m <sup>2</sup> /g	Pore volume, cm <sup>3</sup> /g	Average pore size, nm
Fe-TS	2		
Fe-4MA	8		
Fe-8MA	12		
ZF-TS	7		
ZF-4MA	30		
CF-TS	9		
CF-4MA	21		
ZC31/4	14	0.02	5.4
ZC11/4	14	0.03	8.1
ZC13/4	14	0.03	9.4
ZC31/8	12	0.02	7.4
ZC11/8	14	0.03	8.0
ZC13/8	22	0.20	32.8

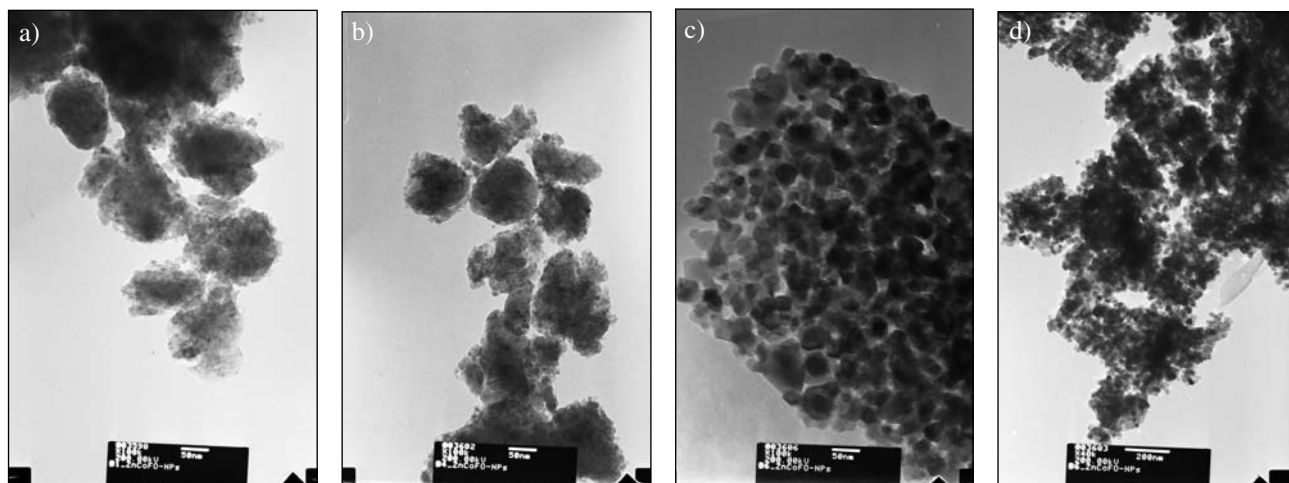


Figure 5. TEM-micrographs of ZC31/4 (a), ZC31/8 (b) x100k and ZC13/8 (c) and (d), respectively at x100k and x 40k.

procedure. Among the ternary oxides the sample ZC13/8 shows a substantially higher  $S_{\text{BET}}$  than the other ternary oxides,  $22 \text{ m}^2/\text{g}$ .

The values for pore volume were determined only for the ternary oxide systems. It was determined from the amount of nitrogen adsorbed at the end of the isotherm at  $p/p_0 = 0.98$  according to the Gurvitch rule. Nitrogen adsorption – desorption isotherms conducted at  $-196^\circ\text{C}$  over powdered samples (Figure S4, a, b) show different shapes. The samples ZC31/4, ZC11/4, ZC13/4, ZC31/8, and ZC11/8, showed II type isotherms according to the IUPAC classification<sup>49</sup> (non-porous or macroporous forms which allow monolayer-multilayer adsorption to occur at high  $p/p_0$ ); the H3 loop is usually assigned to aggregates of plate-like particles which possess non-rigid slit-shaped pores. The isotherm of ZC13/8 is of the II type with H1 loop, which shows well-defined cylindrical pores or agglomerates of approximately uniform spheres appearing probably as secondary intra-particle porosity (Figure S4, b). The hysteresis loops are characteristic of mesoporous solids and their shape reveals a change in the pore structure.

The average pore size is rather close for ZC31/4, ZC11/4, ZC13/4, ZC31/8 and ZC11/8 (Table 3) and different from that of the sample ZC13/8. The  $S_{\text{BET}}$ , pore volume and average pore diameter are changing in the order ZC31/4, ZC11/4, ZC13/4, ZC31/8, ZC11/8, ZC13/8 in the same way. The change of the porous structure is clearly shown (Figure S5) for the pore size distribution of the samples, where ZC13/8 shows a large amount of mesopores in the range 15–100 nm.

### 3. 4. Transmission Electron Microscopy

TEM micrographs show agglomerates for ZC31/4, ZC31/8 (Figure 5, a, b) and crystallites for ZC13/8 (Figure 5 c, d). Agglomeration was present even after sonification, and can be attributed to the mechanotreatment of the

samples without the addition of surfactants. This can lead to partial melting of the edges of the smaller particles during the milling and can play the role of glue between the bigger particles. Because of the agglomeration in the ZC31/4, ZC11/4, ZC13/4, ZC31/8, ZC11/8 samples, evaluation of the particles size distribution on the base of TEM micrograph was attempted only for the ZC13/8 sample (Figure 6). Nanosized particles in the broad range between 5–45 nm can be observed, while sizes between 15–25 nm are the most typical (more than 60% of all particles) (Figure 6).

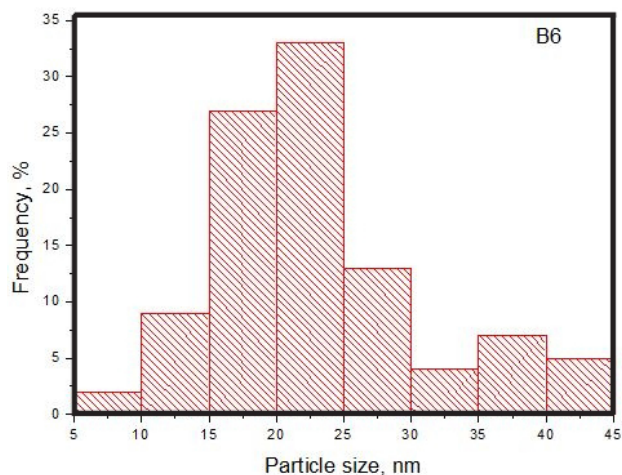


Figure 6. Particles size distribution for ZC13/8 (based on the TEM micrograph, Figure 5, c).

### 3. 5. Photocatalytic Properties of the Samples

$\alpha\text{-Fe}_2\text{O}_3$ : hematite is an n-type semiconductor with a band gap in the region 2.0–2.2 eV.<sup>47</sup> The rate constants



for  $\alpha\text{-Fe}_2\text{O}_3$  shown in Table 4 are decreasing with increasing milling time, so Fe-TS is showing the highest value of  $(6.6 \pm 0.4) \times 10^{-3} \text{ min}^{-1}$ ; the values for the rate constants for Fe-4MA and Fe-8MA are only half of that. The rate constant per unit surface area shows the same tendency i.e. high for Fe-TS, lower for Fe-4MA and Fe-8MA; the difference is bigger here because of the high SSA of Fe-TS. The lattice strain (Table 1) is higher for the less photocatalytically active samples.

**Binary mixed metal oxides  $\text{ZnFe}_2\text{O}_4$  and  $\text{CoFe}_2\text{O}_4$ :** Among the binary mixed oxides, the highest rate constant is observed for ZF-TS,  $(12.7 \pm 0.73) \times 10^{-3} \text{ min}^{-1}$ . The values for ZF-4MA, CF-TS and CF-4MA are smaller and similar. The lattice strain increases with the milling for CF-4MA, but there is no difference in the rate constants for CF-TS and CF-4MA. The very big difference in the rate constants for ZF-TS and ZF-4MA can hardly be explained with the insignificant difference in the lattice strain. The activity per unit surface for ZF-4MA and CF-4MA are the same; apparently the milling is causing the same effect on the surface and on the photocatalytic activity.

**Ternary oxides:** The data in Table 4 show the rate constants and sorption, and those in Table 5 show the degradation of Malachite Green with the time. It is obvious that the samples are active as photocatalysts. They suc-

cessfully degrade more than 50% of the Malachite Green present in the suspension within 90 min. The highest conversion of 68% (Table 5) was obtained by sample ZC31/8 with the highest rate constant observed,  $12.3 \times 10^{-3} \text{ min}^{-1}$  (Figure 7, Table 4).

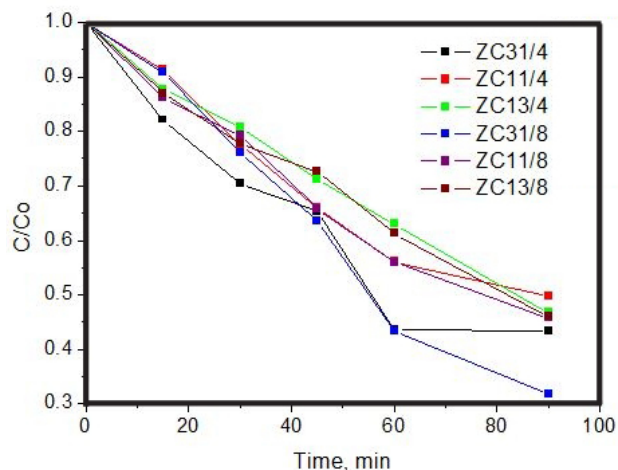


Figure 7. Photocatalytic degradation of Malachite Green by the samples ZC31/4, ZC11/4, ZC13/4, ZC31/8, ZC11/8, ZC13/8 under UV-irradiation

The photocatalytic rate constants (Table 4) increase both with increasing Zn(II)/Co(II) ratio in the samples and with increasing milling time. The values for the rate constants for the ternary oxides ZC31/4,  $10.6 \times 10^{-3}$ , ZC11/4,  $8.4 \times 10^{-3}$ , and ZC13/4,  $8.1 \times 10^{-3} \text{ min}^{-1}$  are higher than those for  $\alpha\text{-Fe}_2\text{O}_3$ ,  $6.6 \times 10^{-3} \text{ min}^{-1}$  (the highest value among Fe-TS, Fe-4MA, Fe-8MA) as well as higher than those for the binary mixed metal oxides made at the same milling time, ZF-4MA,  $6.53 \times 10^{-3}$ , and CF-4MA,  $5.33 \times 10^{-3} \text{ min}^{-1}$ . This may be explained by  $\alpha\text{-Fe}_2\text{O}_3$  and the spinels in the ternary mixed metal oxides having a synergetic effect on the photocatalytic activity.

## 4. Discussion

The aim of the work was to obtain polycrystalline ternary spinel ferrites with different Zn/Co ratios and to test their photocatalytic activity. In order to reveal the inf-

Table 4. Photocatalytic activity: rate constants and sorption

Sample	Rate constant, $\times 10^{-3}, \text{ min}^{-1}$	Rate constant to $S_{\text{BET}}, \times 10^{-4}, \text{ min}^{-1} \cdot \text{g} \cdot \text{m}^{-2}$	Sorption, %
Fe-TS	$6.6 \pm 0.41$	3.30	53.03
Fe-4MA	$2.9 \pm 0.35$	0.37	37.32
Fe-8MA	$3.3 \pm 0.35$	0.28	43.46
ZF-TS	$12.70 \pm 0.73$	1.81	78.13
ZF-4MA	$6.53 \pm 0.40$	0.22	70.82
CF-TS	$5.73 \pm 0.38$	0.64	77.80
CF-4MA	$5.33 \pm 0.31$	0.25	68.34
ZC31/4	$10.6 \pm 0.45$	7.57	78.32
ZC11/4	$8.4 \pm 0.25$	6.00	75.89
ZC13/4	$8.1 \pm 0.25$	5.78	78.18
ZC31/8	$12.3 \pm 0.71$	10.25	82.46
ZC11/8	$9.0 \pm 0.3$	6.43	78.28
ZC13/8	$8.3 \pm 0.25$	3.77	79.35

Table 5. Degradation of Malachite Green with the time, %

Time, min	Samples					
	ZC31/4	ZC11/4	ZC13/4	ZC31/8	ZC11/8	ZC13/8
15	17.76	8.69	12.26	9.16	13.85	12.98
30	29.61	22.46	19.24	23.89	20.72	22.25
45	34.69	33.92	28.71	36.53	34.16	27.41
60	56.31	43.94	36.93	56.56	44.00	38.76
90	56.55	50.35	53.29	68.13	54.26	53.95

fluence of the synthetic procedure on the photocatalytic properties of the samples, a combination of solid state reaction with high-energy ball-milling was applied both to treat a commercial ferric oxide (hematite) and to synthesize oxides with spinel structure of the type  $M'_xM''_{1-x}Fe_2O_4$  ( $M' = Zn$ ,  $M'' = Co$ ;  $x = 0, 0.25, 0.5, 0.75, 1$ ). Homogeneous  $ZnFe_2O_4$  and  $CoFe_2O_4$  ferrites with spinel structure were obtained both by solid state reaction and by a combination of solid state reaction with high-energy ball-milling. The ternary mixed metal oxide  $Co_{0.75}Zn_{0.25}Fe_2O_4$  was obtained as a well-crystallized homogeneous spinel structure after 8 hours of milling. In spite of the XRD data showing single phases of well crystallized oxides  $Co_xZn_{1-x}Fe_2O_4$  ( $x = 0.25; 0.5$ ), the Mössbauer and Raman spectroscopy measurements revealed the presence of both a spinel-like structure and hematite. This illustrates the importance of combining different methods for analysis of the structure in ferrite multicomponent systems, and gives a chance to test a potential synergism in the photocatalytic activity of the spinel structure and hematite, when they are treated at the same experimental conditions. Some considerations on the photocatalytic activity are worth mentioning:

(i) *The composition and the photocatalytic properties of ternary mixed metal oxides:* Considering the composition of the ternary mixed metal oxides presented, they can be divided in two groups, namely ZC31/4, ZC11/4, ZC13/4, ZC31/8, and ZC11/8 in first group and ZC13/8 the other one. The five samples ZC31/4, ZC11/4, ZC13/4, ZC31/8 and ZC11/8 are phases, containing spinel-like ferrite (50–55%) and hematite,  $\alpha-Fe_2O_3$  (17–20%). The hematite, with an energy band gap of 2.2 eV, absorbs light up to 550 nm and (as other iron oxides) possesses photocatalytic activity.<sup>47</sup> Any of the components can be active during the photocatalytic decomposition of Malachite Green; their activity is difficult to be separated, especially because of the fact that they have close energy band gap values. The sample ZC13/8 is the only one with a homogeneous spinel structure,  $Co_{0.75}Zn_{0.25}Fe_2O_4$ , but its photocatalytic behaviour does not differ from the samples ZC31/4, ZC11/4, ZC13/4 and ZC11/8 (containing both hematite and spinel-like ferrite). Taking into account the data from Table 4, an increasing of the rate constant with the increasing of Zn(II) content in the samples is observed for both milling periods applied. The samples ZC31/4 and ZC31/8 show the best activity among the others, with rate constants of  $10.6 \times 10^{-3}$  and  $12.3 \times 10^{-3} \text{ min}^{-1}$ , respectively.

It can be assumed that peculiarities of the synthetic procedure namely a heat treatment, followed by mechano-treatment without annealing in combination with the Zn(II)/Co(II) ratio, favoured the photocatalytic activity. That the highest rate constant was observed for the sample with the longest mechano-treatment and highest Zn(II)/Co(II) ratio, ZC31/8, is an illustration for this. Additional reason for the highest rate constant value for ZC31/8 is the synergetic effect of the spinel-like structure and  $\alpha-Fe_2O_3$ . Considering the data from Mossbauer (Tab-

le S1), the amount of hematite in all five samples ZC31/4, ZC11/4, ZC13/4, ZC31/8, ZC11/8 is very close, so the difference in their activity could be a result of the different Zn/Co ratios and different milling times.

(ii) *The specific surface area,  $S_{BET}$ , and the photocatalytic activity:* The specific surface area is rather low, which is to be expected taking into account the high temperature for heat treatment of the samples, 900 °C. The samples ZC31/4, ZC11/4, ZC13/4, ZC31/8, ZC11/8 have similar values of  $S_{BET}$ , but have different photocatalytic behaviour. The sample ZC13/8 is very different from the others, with a specific surface area twice as high, but it does not show the highest rate constant obtained. It looks like  $S_{BET}$  is not decisive for the photocatalytic activity in our case because no correlation between specific surface area and photocatalytic activity is observed. If the degradation rate constant is divided by the specific surface area (the same approach as applied in<sup>50</sup>) the “normalized” values ( $\text{min}^{-1} \text{ g. m}^{-2}$ , Table 4) show the weakest catalytic activity for ZC13/8 while the best sample is still ZC31/8. According to Bubacz et al.<sup>51</sup> the process of photodegradation is not determined only by the specific surface area,  $S_{BET}$ . The peculiarities of the surface structure are responsible for differences in the catalytic activity. The size of the particles and crystallites is influencing the activity of the catalyst by influencing the processes of recombination of the electron-hole couples.<sup>52,53</sup> The best catalyst among the synthesized, ZC31/8, has the smallest crystallite size. That the crystallite size for ZC31/4 (56 nm) is twice as large as that for ZC31/8 (26 nm) does not reflect in their catalytic activity, which are similar ( $10.3 \times 10^{-3} \text{ min}^{-1}$  for ZC31/4 and  $12.3 \times 10^{-3} \text{ min}^{-1}$  for ZC31/8).

The rate constants for some of the samples (ZC31/4, ZC31/8) are close to those obtained by us for  $TiO_2$  (Degussa P-25) when decomposing Malachite Green with UV light irradiation, namely  $11.6 \times 10^{-3} \text{ min}^{-1}$ , but at higher specific surface area (52  $\text{m}^2/\text{g}$ ).<sup>50</sup> The “normalized” value for Degussa P25 (rate constant/ $S_{BET}$ ) is  $2.2 \times 10^{-4} \text{ min}^{-1} \text{ g. m}^{-2}$ , which is rather low compared with the values for our samples (Table 4), even including our weakest result, the one for the sample ZC13/8. This is in accordance with the values for the energy band gap (Results, 3.2), obtained for our samples that are considerably smaller than the one for Degussa-P25.

(iii) *Comparison of the homogeneous ZC13/8 and the other five inhomogeneous samples ZC31/4, ZC11/4, ZC13/4, ZC31/8, ZC11/8* shows that ZC13/8 has the same UV/Vis and IR spectra as the other samples although it is the only one with a clearly crystallised spinel structure. ZC13/8 differs in some physicochemical parameters such as  $S_{BET}$ , pore volume, average pore size and composition, but its photocatalytic activity is similar to ZC13/4 (and ZC11/4), synthesised at shorter milling time (Table 4). Probably the activity of ZC13/4 (and ZC11/4) is similar to ZC13/8 because of the synergetic effect observed. The photocatalytic activity of sample ZC13/8 is the only one repor-

ted in the literature for a pure spinel-like structure for degradation of Malachite Green under UV light irradiation.

If the reason for inhomogeneity of the five ternary oxides ZC31/4, ZC11/4, ZC13/4, ZC31/8, ZC11/8 is the milling procedure, which could cause some decomposition, the reason to obtain ZC13/8 could be a combination of successful synthesis by the longer mechanotreatment assisted by the stabilizing role of the smaller  $\text{Co}^{2+}$  ions.

(iv) *The relation between the defects in the structure of the samples and their photocatalytic activity:* Apparently the milling increases the defects and the lattice strain for  $\alpha\text{-Fe}_2\text{O}_3$ , but the photocatalytic activity of  $\alpha\text{-Fe}_2\text{O}_3$  decreases, so it looks like for  $\alpha\text{-Fe}_2\text{O}_3$  the defects do not have a positive effect on its activity as a photocatalyst. For the binary mixed metal oxides the one with the lowest strain has the highest activity, i.e. the pure  $\text{Zn-Fe}_2\text{O}_4$ . No positive effect of the lattice strain is observed for the ternary oxides: the sample with the lowest strain possesses the best activity. It is known that cationic vacancies (and/or interstitial atoms) can be observed in the structure of spinels.<sup>54</sup> The possible defects in the powdered samples are evaluated on the base of the calculated lattice strain. In spite of the expectations that the lattice strain induces structural distortion and by that transforms the properties,<sup>55</sup> we did not observe a correlation between the lattice strain and the photocatalytic activity. The sample with the best activity among the ternary oxides, ZC31/8, has the lowest value of lattice strain. We can suggest there are factors which are compensating the lattice strain caused by the defects.

## 5. Conclusions

Polycrystalline spinel-like ferrites were synthesized and tested for degradation of Malachite Green in model solutions under UV light irradiation. The values for the rate constant and the degree of degradation obtained show that these samples have potential to be used as photocatalysts to purify contaminated waters. The rate constants observed are similar to that obtained for  $\text{TiO}_2$  Degussa P25, but at lower specific surface area. Considering all the factors influencing the photocatalytic activity, differences in photocatalytic behavior are observed depending on the duration of high energy ball-milling and  $\text{Zn(II)/Co(II)}$  ratio. A synergetic effect of the  $\alpha\text{-Fe}_2\text{O}_3$  and spinel-like structure on the photocatalytic properties was detected.

*Acknowledgements:* The financial support of Bulgarian Fund for Scientific Investigations (Project DFNI E01/7/2012) is gratefully acknowledged.

## 6. References

1. P. Laokul, V. Amornkitbamrung, S. Seraphin, S. Maensiri, *Curr. Appl. Phys.* **2011**, *11*, 101–108.

2. V. B.-Gutierrez, M. J. T. - Fernandez, R. Saez-Puche, *J. Phys. Chem. C* **2010**, *114*, 1789–1795.
3. Y. B. Li, R. Yi, A. G. Yan, L. W. Deng, K. C. Zhou, X. H. Liu, *Solid State Sci.* **2009**, *11*, 1319–1324.  
<https://doi.org/10.1016/j.solidstatesciences.2009.04.014>
4. S. Saadi, A. Bouguelia, M. Trari, *Renew. Energy* **2006**, *31*, 2245–2256. <https://doi.org/10.1016/j.renene.2005.10.014>
5. A. V. Ravindra, P. Padhan, W. Prellier, *Appl. Phys. Lett.* **2012**, *101*, 161902.  
<https://doi.org/10.1063/1.4759001>
6. Y. Yang, Y. Jiang, Y. Wang, Y. Sun, L. Liu, J. Zhang, *Mat. Chem. Phys.* **2007**, *105*, 154–156.  
<https://doi.org/10.1016/j.matchemphys.2007.04.050>
7. C. Borgohain, K. K. Senapati, K. C. Sarma, P. Phukana, *J. Mol. Catal. A: Chem.* **2012**, *363–364*, 495–500.  
<https://doi.org/10.1016/j.molcata.2012.07.032>
8. X. Cao, Li Gu, X. Lan, C. Zhao, D. Yao, W. Sheng, *Mat. Chem. Phys.* **2007**, *106*, 175–180.  
<https://doi.org/10.1016/j.matchemphys.2007.05.033>
9. Z. Jia, D. Ren, Y. Liang, R. Zhu, *Mat. Lett.* **2011**, *65*, 3116–3119. <https://doi.org/10.1016/j.matlet.2011.06.101>
10. G. A. El-Shobaky, A. M. Turky, N. Y. Mostafa, S. K. Mohamed, *J. Alloys Compd.* **2010**, *493*, 415–422.  
<https://doi.org/10.1016/j.jallcom.2009.12.115>
11. E. Casbeer, V. K. Sharma, X. - Zh. Li, *Sep. Purif. Techn.* **2012**, *87*, 1–14.  
<https://doi.org/10.1016/j.seppur.2011.11.034>
12. M. Su, Ch. He, V. K. Sharma, M. A. Asi, D. Xia, X. - Li, H. Deng, Y. Xiong, *J. Hazard. Mater.* **2012**, *211–212*, 95–103.
13. S. H. Xu, D. L. Feng, W. F. Shangguan, *J. Phys. Chem. C* **2009**, *113*, 2463–2467. <https://doi.org/10.1021/jp806704y>
14. S. D. Jadhav, P. P. Hankare, R. P. Patil, R. Sasikala, *Mater. Lett.* **2011**, *65*, 371–373.  
<https://doi.org/10.1016/j.matlet.2010.10.004>
15. C.-H. Chen, Y.-H. Liang, W. - D. Zhang, *J. Alloys Compd.* **2010**, *501*, 168–172.  
<https://doi.org/10.1016/j.jallcom.2010.04.072>
16. S. Boumaza, A. Boudjemaa, A. Bouguelia, R. Bouarab, M. Trari, *Appl. Energy* **2010**, *87*, 2230–2236.  
<https://doi.org/10.1016/j.apenergy.2009.12.016>
17. B. P. Zhang, J. L. Zhang, F. Chen, *Res. Chem. Intermed.* **2008**, *34*, 375–380.  
<https://doi.org/10.1163/156856708784040669>
18. G. Y. Zhang, Y. Q. Sun, D. Z. Gao, Y. Y. Xu, *Mater. Res. Bull.* **2010**, *45*, 755–760.  
<https://doi.org/10.1016/j.materresbull.2010.03.025>
19. R. S. Gaikwad, S. - Y. Chae, R. S. Mane, S. - H. Han, O. - S. Joo, *Int. J. Electrochem.* **2011**, *ID 729141*, 6 pages,  
<https://doi.org/10.4061/2011/729141>
20. M. Yokoyama, T. Oku, T. Taniyama, T. Sato, E. Ohta, T. Sato, K. Haneda, S. Itoh, K. Kurahashi, M. Takeda, *Phys. B* **1995**, *213–214*, 251–253.  
[https://doi.org/10.1016/0921-4526\(95\)00121-O](https://doi.org/10.1016/0921-4526(95)00121-O)
21. P. P. Hankare, R. P. Patil, R. Sasikala, *Mater. Lett.* **2011**, *65*, 371–373. <https://doi.org/10.1016/j.matlet.2010.10.004>

22. M. Jalaly, M. H. Enayati, F. Karimzadeh, P. Kameli, *Powder Techn.* **2009**, *193*, 150–153.  
<https://doi.org/10.1016/j.powtec.2009.03.008>
23. N. H. Vasoya, L. H. Vanpariya, P. N. Sakariya, M. D. Timbadiya, T. K. Pathak, V. K. Lakhani, K. B. Modi, *Ceram. Int.* **2010**, *36*, 947–954.  
<https://doi.org/10.1016/j.ceramint.2009.10.024>
24. S. Dasgupta, K. B. Kim, J. Ellrich, J. Eckert, I. Manna, *J. Alloys Compd.* **2006**, *424*, 13–20.  
<https://doi.org/10.1016/j.jallcom.2005.12.078>
25. M. Mozaffari, F. Ebrahimi, S. Daneshfozon, J. Amighian, *J. Alloys Compd.* **2008**, *449*, 65–67.  
<https://doi.org/10.1016/j.jallcom.2006.03.107>
26. K. Maaz, A. Mumtaz, S. K. Hasanain, A. Ceylan, *J. Magn. Mater.* **2007**, *308*, 289–295.  
<https://doi.org/10.1016/j.jmmm.2006.06.003>
27. Z. Q. Liu, C. J. Li, W. M. Lü, X. H. Huang, Z. Huang, S. W. Zeng, X. P. Qiu, L. S. Huang, A. Annadi, J. S. Chen, J. M. D. Coey, T. Venkatesan, Ariando, *Phys. Rev. X* **2013**, *3*, 021010.  
<https://doi.org/10.1103/PhysRevX.3.021010>
28. Z. Q. Liu, D. P. Leusink, X. Wang, W. M. Lü, K. Gopinadhan, A. Annadi, Y. L. Zhao, X. H. Huang, S. W. Zeng, Z. Huang, A. Srivastava, S. Dhar, T. Venkatesan, Ariando, *Phys. Rev. Lett.* **2011**, *107*, 146802.  
<https://doi.org/10.1103/PhysRevLett.107.146802>
29. Z. Q. Liu, D. P. Leusink, W. M. Lü, X. Wang, X. P. Yang, K. Gopinadhan, Y. T. Lin, A. Annadi, Y. L. Zhao, A. Roy Barman, S. Dhar, Y. P. Feng, H. B. Su, G. Xiong, T. Venkatesan, Ariando, *Phys. Rev. B* **2011**, *84*, 165106.  
<https://doi.org/10.1103/PhysRevB.84.165106>
30. Z. Q. Liu, W. M. Lü, S. L. Lim, X. P. Qiu, N. N. Bao, M. Motapothula, J. B. Yi, M. Yang, S. Dhar, T. Venkatesan, Ariando, *Phys. Rev. B* **2013**, *87*, 220405(R).  
<https://doi.org/10.1103/PhysRevB.87.220405>
31. Z. Q. Liu, W. Lu, S. W. Zeng, J. W. Deng, Z. Huang, C. J. Li, M. Motapothula, W. M. Lü, L. Sun, K. Han, J. Q. Zhong, P. Yang, N. N. Bao, W. Chen, J. S. Chen, Y. P. Feng, J. M. D. Coey, T. Venkatesan, Ariando, *Adv. Mater. Interfaces* **2014**, *1*, 1400155. <https://doi.org/10.1002/admi.201400155>
32. J. Birkenstock, R. X. Fisher, T. Messner, BRASS, Ber. DMG, Beih, *Eur. J. Mineral.* **2003**, *15*, 21–28.
33. K. Wiliamson, W. H. Hall, *Acta Metall.* **1953**, *1*, 22–31.  
[https://doi.org/10.1016/0001-6160\(53\)90006-6](https://doi.org/10.1016/0001-6160(53)90006-6)
34. J. Tauc, R. Grigorovici, A. Vancu, *Phys. Status Solidi* **1966**, *15*, 627–637. <https://doi.org/10.1002/pssb.19660150224>
35. S. D. Shenoy, P. A. Joy, M. R. Anantharaman, *J. Magn. Mater.* **2004**, *269*, 217.  
[https://doi.org/10.1016/S0304-8853\(03\)00596-1](https://doi.org/10.1016/S0304-8853(03)00596-1)
36. K. B. Modi, S. N. Dolia, P. U. Sharma, *Indian J. Phys.* **2015**, *89*, 425–436.  
<https://doi.org/10.1007/s12648-014-0604-5>
37. P. D. Thang, G. Rijnders, D. H. A. Blanket, *J. Magn. Mater.* **2005**, *295*, 251–256.  
<https://doi.org/10.1016/j.jmmm.2005.01.011>
38. F. Bodker, S. Morup, C. A. Oxborrow, S. Linderroth, M. B. Madsen, J. W. Niemantsverdriet, *J. Phys. Condens. Mat.* **1992**, *4*, 6555–6568.  
<https://doi.org/10.1088/0953-8984/4/31/008>
39. J. Kreisel, G. Lucazeau, J. Vincent, *J. Solid State Chem.* **1999**, *137*, 127–137.  
<https://doi.org/10.1006/jssc.1997.7737>
40. F. Nakagomi, S. W. da Silva, V. K. Garg, A. C. Oliveira, P. C. Morais, A. F. Junior, E. C. D. Lima, *J. Appl. Phys.* **2007**, *101*, 09M514.
41. L. Ben Tahar, L. S. Smiri, M. Artus, A. - L. Joudrier, F. Herbst, M. J. Vaulay, S. Ammar, F. Feivet, *Mater. Res. Bull.* **2007**, *42*, 1888.  
<https://doi.org/10.1016/j.materresbull.2006.12.014>
42. C. - W. Tang, C. - B. Wang, S. - H. Chien, *Thermochim. Acta* **2008**, *473*, 68–73.  
<https://doi.org/10.1016/j.tca.2008.04.015>
43. D. L. Wood, J. S. Tauc, *Phys Rev B* **1972**, *5*, 3144.  
<https://doi.org/10.1103/PhysRevB.5.3144>
44. M. Bouloudeine, N. Viart, S. Colis, A. Dinia, *Chem. Phys. Lett.* **2004**, *397*, 73.  
<https://doi.org/10.1016/j.cplett.2004.08.064>
45. S. V. Bhat, F. L. Deepak, *Solid State Commun.* **2005**, *135*, 345–347. <https://doi.org/10.1016/j.ssc.2005.05.051>
46. H. Dixit, N. Tandon, S. Cottenier, R. Saniz, D. Lamoen, B. Partoens, V. Van Speybroeck, M. Waroquier, *New J. Phys.* **2011**, *13*, 063002.  
<https://doi.org/10.1088/1367-2630/13/6/063002>
47. J. Bandara, J. A. Mielczarski, A. Lopez, J. Kiwi, *Appl. Catal. B: Environ.* **2001**, *34*, 321–333.  
[https://doi.org/10.1016/S0926-3373\(01\)00225-9](https://doi.org/10.1016/S0926-3373(01)00225-9)
48. L. Zhang, Y. He, P. Ye, Y. Wu, T. Wu, *Catal. Commun.* **2013**, *30*, 14–18. <https://doi.org/10.1016/j.catcom.2012.10.013>
49. F. Rouquerol, J. Rouquerol, K. Sing, Adsorption by powders and porous solids: Principles, methodology and applications, Acad. Press, San Diego, **1999**.
50. R. Kralchevska, M. Milanova, D. Hristov, A. Pintar, D. Todorovsky, *Mater. Res. Bull.* **2012**, *47*, 2165–2177.  
<https://doi.org/10.1016/j.materresbull.2012.06.009>
51. K. Bubacz, J. Choina, D. Dolat, E. Borowiak-Paleń, D. Moszyński, A. W. Morawski, *Mater. Res. Bull.* **2010**, *45*, 1085–1091.  
<https://doi.org/10.1016/j.materresbull.2010.06.024>
52. R. Scotti, M. D'Arienzo, F. Morazzoni, I. R. Bellobono, *Appl. Catal. B* **2009**, *88*, 323–330.  
<https://doi.org/10.1016/j.apcatb.2008.11.012>
53. A. Testino, I. R. Bellobono, V. Buscaglia, C. Canevali, M. D'Arienzo, S. Polizzi, R. Scotti, F. Morazzoni, *J. Am. Chem. Soc.* **2007**, *129*, 3564–3575.  
<https://doi.org/10.1021/ja067050+>
54. M. Gaudon, N. Pailhe, A. Wattiaux, A. Demourgues, *Mat. Res. Bull.* **2009**, *44*, 479–484.  
<https://doi.org/10.1016/j.materresbull.2008.12.005>
55. L. Zhao, H. Yang, X. Zhao, L. Yu, Y. Cui, S. Feng, *Mat. Lett.* **2006**, *60*, 1–6.  
<https://doi.org/10.1016/j.matlet.2005.07.017>

## Povzetek

Kombinacijo toplotne in mehanske (krogelni mlini) obdelave smo uporabili pri pripravi polikristalničnih mešanih binarnih in ternarnih kovinskih oksidov tipa  $\text{Co}_x\text{Zn}_{1-x}\text{Fe}_2\text{O}_4$  ( $x = 0, 0.25, 0.5, 0.75, 1$ ). S takšnim sinteznim pristopom smo uspešno pripravili homogene  $\text{ZnFe}_2\text{O}_4$ ,  $\text{CoFe}_2\text{O}_4$ , in  $\text{Co}_{0.75}\text{Zn}_{0.25}\text{Fe}_2\text{O}_4$  ter tudi mešane okside, katerih sestava je odvisna tako od trajanja mletja s kroglicami in razmerja  $\text{Zn(II)/Co(II)}$ . Tvorbo spinelu podobnih struktur smo dokazali z rentgensko praškovno difrakcijo (XRD), Mössbauerjevo spektroskopijo in Ramansko spektroskopijo. Za nadaljnjo karakterizacijo vzorcev smo uporabili nizko-temperaturno adsorpcijo  $\text{N}_2$ , UV/VIS spektroskopijo in transmisijsko elektronsko mikroskopijo (TEM). Izračunana energija prepovedanega pasu (band gap) vzorcev kaže, da so materiali potencialni fotokatalizatorji. V prisotnosti vzorcev, ki smo jih uporabili kot fotokatalizatorje, je barvilo malahitno zeleno v modelnih vodnih raztopinah pri obsevanju z UV svetlobo razpadlo. Najboljšo fotokatalitsko učinkovitost smo opazili pri vzorcu za katerega smo pri sintezi uporabili daljši čas mletja in višje razmerje  $\text{Zn(II)/Co(II)}$ . Primerjali smo tudi fotokatalitsko aktivnost ternarnih mešanih oksidov s čistim hematitom  $\alpha\text{-Fe}_2\text{O}_3$  in binarnima  $\text{ZnFe}_2\text{O}_4$  in  $\text{CoFe}_2\text{O}_4$  feritoma s spinelno strukturo, ki smo jih pripravili na enak način. Zaznali smo sinergijski učinek  $\alpha\text{-Fe}_2\text{O}_3$  in strukture podobne spinelu na fotokatalitske lastnosti ternarnih mešanih kovinskih oksidov.

Scientific paper

# Poly(N-methylpyrrole) Film on ZnNi Plated Carbon Steel Electrode

Abdurrahman Akdag<sup>1,\*</sup> and Ali Tuncay Ozyilmaz<sup>2</sup>

<sup>1</sup> Department of Medical Laboratory Techniques, Vocational School of Health Services, Harran University, 63300, Sanliurfa, Turkey

<sup>2</sup> Department of Chemistry, Faculty of Arts and Sciences, Mustafa Kemal University, 31040, Hatay, Turkey

\* Corresponding author: E-mail: ab.ak@hotmail.com

Phone: +90-414-3183209, Fax: +90-414-3183211

Received: 02-12-2016

## Abstract

In this study, zinc–nickel (ZnNi) particles were electrochemically deposited on carbon steel (CS) electrode applying constant current of 1 mA with chronopotentiometry technique. Poly(N-methylpyrrole) (PNMP) film on CS/ZnNi electrode was synthesized with cyclic voltammetry technique from 0.10 M N-methylpyrrole containing 0.20 M sodium oxalate solution. The corrosion performances of coated and uncoated electrodes in 3.5% NaCl solution were evaluated with the help of AC impedance spectroscopy (EIS) and anodic polarisation curves. Scanning electron microscopy (SEM) and linear sweep voltammetry (LSV) were used to characterization of coatings. It was shown that the ZnNi particles exhibited important barrier effect on CS substrate. The highest 298350 ohm value of polarization resistance showed that PNMP film on the CS/ZnNi electrode exhibited an effective barrier property and electrocatalytic behaviour protection of substrate for longer exposure time.

**Keywords:** Alloy plating, corrosion, conducting polymer, poly(N-methylpyrrole)

## 1. Introduction

Corrosion of the metals is one of the most serious problems in industry.<sup>1</sup> Zinc coating provides good protection for ferrous substrates. Zinc and zinc alloys (Zn-Co, ZnNi) are widely used in the corrosion protection of steel.<sup>2–8</sup> But these zinc alloys exhibit a significantly higher corrosion resistance than pure zinc coating.<sup>9–16</sup> Conducting polymers like polyaniline, polythiophene and polypyrrole have shown wide range of applications due to their very interesting physical properties. Some of their important properties include electrical conductivity, electroactivity, electrochromism, environmental stability, chemical stability and corrosion inhibitive property.<sup>17</sup> Conducting polymers act as anodic protection and constitute effective physical barrier against corrosive products in the protection of metals. These polymers significantly reduce the rate of corrosion.<sup>18–21</sup> Introduced advantages by these organic coatings are a good adhe-

sion at the metal surface and nontoxic corrosion problems as than occurs in the commonly painting systems.<sup>22</sup> Due to these properties polypyrrole and polyaniline and its derivatives are most extensively studied conducting polymers.<sup>22–33</sup>

Ozyilmaz et al. studied comparative study of passivation of ZnFe and ZnFeCo alloy platings on carbon steel from oxalate and tartrate medium and the results were showing that in oxalate medium passivation exhibited better physical barrier behavior.<sup>34</sup>

The purpose of the present study was to synthesize electrochemically PNMP film on thin zinc–nickel (ZnNi) plated carbon steel in sodium oxalate (NaOX) solution. The corrosion behaviors of ZnNi deposited carbon steel electrodes with and without PNMP film have been investigated in 3.5% NaCl and compared by using AC impedance spectroscopy (EIS) technique, open circuit potential-time measurements linear sweep voltammetry (LCV) technique and anodic polarization curves.

## 2. Experimental

All electrochemical experiments were performed in a standard one-compartment three-electrode cell. The reference electrode was Ag/AgCl (3 M, KCl) and the counter electrode was a platinum sheet. Surface area of platinum sheet and working electrode were 0.18 cm<sup>2</sup> and 0.05 cm<sup>2</sup>, respectively. The working electrode used in this study was carbon steel with the composition: 0.0561% C, 0.4498% Mn, 0.0103% P, 0.0036% S, 0.14085 Si and 99.3394% Fe. The surface of this electrode was carefully polished with abrasive paper (1200 grid), degreased with 1/1 ethanol/acetone mixture, washed with distilled water and dried. CHI 606C and CHI 660B model digital electrochemical analyzers were used for all electrochemical measurements. Zinc-nickel plating was carried out in a bath including 200 gl<sup>-1</sup> ZnSO<sub>4</sub>·7H<sub>2</sub>O, 140 gl<sup>-1</sup> NiSO<sub>4</sub>·6H<sub>2</sub>O, 20 gl<sup>-1</sup> H<sub>3</sub>BO<sub>3</sub>, 2 gl<sup>-1</sup> CH<sub>3</sub>C<sub>6</sub>H<sub>4</sub>SO<sub>3</sub>H·H<sub>2</sub>O. Meanwhile pH was approximately 5.5. The plating time was 400 sec applying 1 mA constant current. ZnNi plating was accomplished under atmospheric condition without stirring the solution. The thickness of alloy plating was determined by estimation of the passing charge amount applying 1 mA constant current and the thickness of ZnNi alloy plating was estimated to be between approx. 2.73–3.80 μm. Poly(N-methylpyrrole) film was electrochemically synthesized using cyclic voltammetry technique. Electrochemical impedance measurements were obtained at measured open circuit potential values applying 7 mV of amplitude in frequency range from 10<sup>5</sup> to 10<sup>-3</sup> Hz. The anodic polarization curves were recorded after 168 h of immersion time in corrosive test solution. The scan rate was 4 mV/s and the measured open circuit potential value was the initial potential for the scan. SEM was employed to characterize the surface morphology with a JEOL JSM-5500LV scanning electron microscope at 10 kV.

## 3. Results and Discussion

In this study, zinc-nickel (ZnNi) plating was electrochemically deposited on carbon steel (CS) electrode applying constant current of 1 mA with chronopotentiometry technique. After deposition, the composition ZnNi plating was mechanically removed from the surface of the electrode and dissolved in 0.10 M HCl solution. The chemical composition of the ZnNi alloy was analyzed by atomic absorption spectroscopy (AAS). The percentage metal ratio was determined as 20.27% Ni and 79.73% Zn.

The cyclic voltammograms recorded for zinc-nickel plated carbon steel (CS/ZnNi) in monomer containing NaOX solution are given in Fig. 1. PNMP coating was synthesized in two steps. The first cycle was obtained in the potential range from -1.10 to +1.80 V. Then the film

growth was carried out in the potential range between 0.00 and 1.80 V. Fifty segment were employed for the preparation of PNMP covered CS/ZnNi electrode. The scan rate was 100 mVs<sup>-1</sup> for both cases. The thickness of synthesized PNMP coating was estimated as 5.59 μm by the sum of the charge amount passed in the monomer oxidation potential region.<sup>32</sup> In Fig. 1a, anodic current values started to increase at approximately -0.70 V due to the zinc and nickel dissolution process, which continued in a wide potential range. The passivation of the surface was observed to terminate at approximately 0.56 V. The passivation mechanism resulted from the formation of insoluble zinc and nickel oxalate compounds. Ozyilmaz et al. have reported the influence of anion and concentration on the passivation of ZnFe and ZnFeCo alloy plating on carbon steel using an aqueous bath of sodium tartrate and sodium oxalate with different concentrations, resulting in a lower corrosion rate by 0.20 M sodium oxalate.<sup>34</sup> In Fig. 1b, there are growth curves of PNMP film synthesized on the surface of CS/ZnNi electrode. At anodic scan, the current waves observed at around 1.07 V were attributed to monomer oxidation. The current values of these waves decreased proportional number of cycles. This case showed that the PNMP film covered the CS/ZnNi electrode surface. The adherence of synthesized PNMP coating was tested by a simple sello tape test, where perfect results were obtained.

SEM images of bare CS, CS/ZnNi and CS/ZnNi/PNMP electrodes are given in Fig. 2. The bare electro-

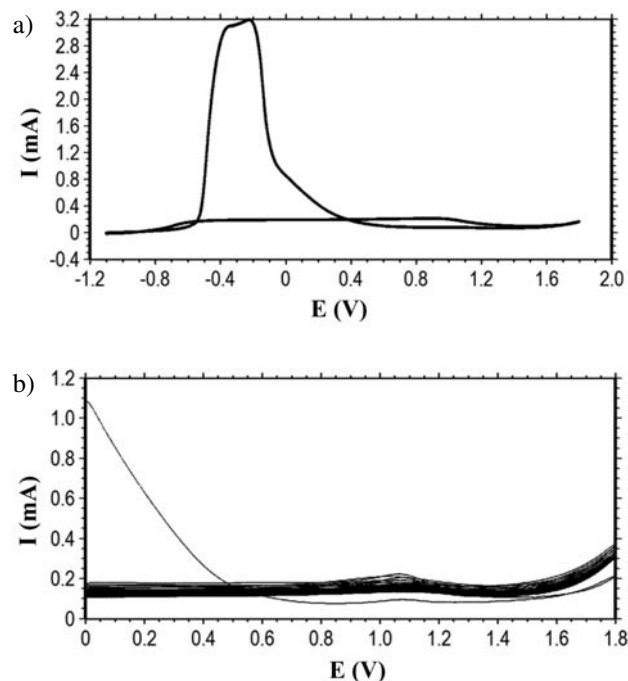


**Fig. 1.** First CV (a) and film growth curves (b) recorded for CS/ZnNi electrode 0.10 M N-methylpyrrole containing 0.20 M NaOX solution, scan rate: 100 mVs<sup>-1</sup>

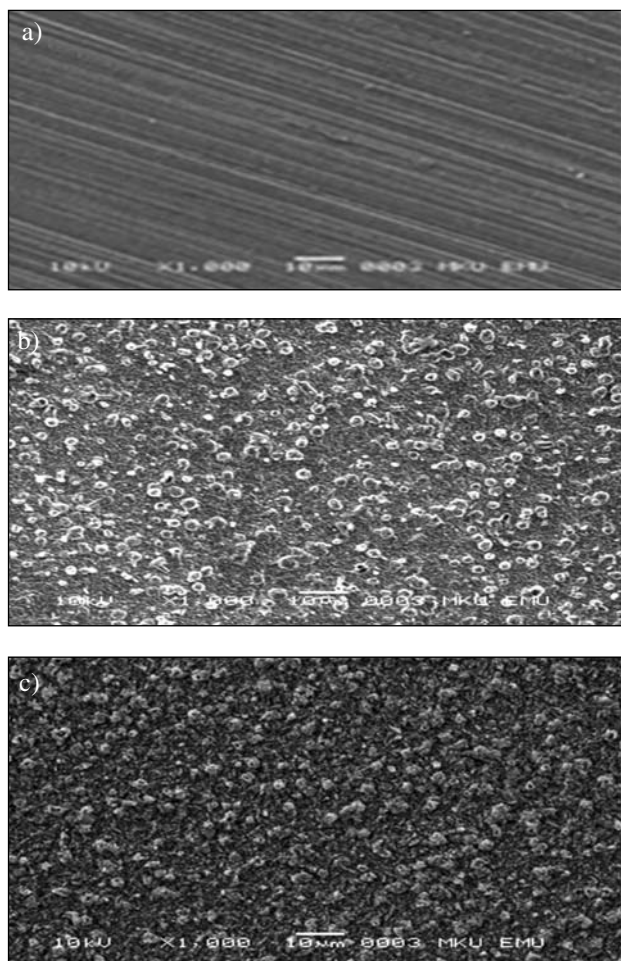


Fig. 2. SEM images of bare CS (a), CS/ZnNi (b) and CS/ZnNi/PNMP (c) electrodes.

de showed the evidence of emery. The emery traces observed for CS electrode disappeared for CS/ZnNi and CS/ZnNi/PNMP electrodes. It can be seen that CS/ZnNi electrode was smooth structure. The surface of CS/ZnNi electrode was covered with granular structure of PNMP film.

The Nyquist diagrams recorded for CS, CS/ZnNi and CS/ZnNi/PNMP electrodes in 3.5% NaCl solution are given in Fig. 3, after various immersion times. As seen from Fig. 3, there were one depressed semicircle at high frequency and an inductive loop at low frequency region, in presence of CS electrode, while these plots for CS/ZnNi and CS/ZnNi/PNMP electrodes consisted two depressed semicircles which could not be well resolved from each other at high and mid frequency regions, after 2 h of exposure time. The depressed semicircle at high frequency region obtained for CS electrode was related to the charge transfer resistance ( $R_{ct}$ ) that was responsible for the anodic dissolution of bare metal and oxide layer resistance ( $R_o$ ). On the other hand, there were  $R_{ct}$  at high frequency region and alloy plating ( $R_{ZnNi}$ ) +  $R_o$  or  $R_{ZnNi}$  +  $R_o$

+ polymer film resistance ( $R_{pf}$ ) for CS/ZnNi or CS/ZnNi/PNMP electrodes, respectively. The inductive loop at low frequency region was related to adsorption of different corrosion intermediates. In this study,  $R_p$  values were used in stern-Geary equation for calculation of corrosion current ( $I_{corr}$ ).<sup>32</sup>

$$I_{corr} = \frac{B}{R_p} \quad (1)$$

In this equation, B value was equal to  $(\beta_a \times \beta_c) / (\beta_a + \beta_c) \times 2.303$ ;  $\beta_a$  and  $\beta_c$  were anodic and cathodic Tafel slopes, respectively. The value of B was taken as 0.026 V for uncoated electrode and 0.052 V for coated electrode. The protection efficiency values (E %) were calculated by using the following equation.<sup>34</sup>

$$E\% = \frac{R_{p(uncoated)}^{-1} - R_{p(coated)}^{-1}}{R_{p(uncoated)}^{-1}} \times 100 \quad (2)$$

After 2h of exposure time,  $R_p$  values for CS/ZnNi and CS/ZnNi/PNMP electrodes were found to be higher than CS electrode, while the highest  $R_p$  value was obtained for CS/ZnNi/PNMP electrode. This case was related to barrier effect of PNMP film and supported that the value of  $I_{corr}$  and E% are presented in Table 1. After 48 h,  $R_p$  values of all electrodes were greater than those of 2 h exposure times. This case showed that oxide layers formed with time. Protection efficiency value of CS/ZnNi/PNMP electrode was 75.36% that it was relatively higher value than that of CS/ZnNi electrode. After 96 h,  $I_{corr}$  value obtained for CS/ZnNi/PNMP electrode was 0.63  $\mu A$  that the lowest value when compared with those of all electrodes. At the same time,  $R_p$  value increased from 40578 to 82115  $\Omega$  for CS/ZnNi/PNMP electrode. This increase in  $R_p$  value of CS/ZnNi/PNMP electrode was related to electrocatalytic behaviour of polymer film. Electrocatalytic property of polymer film contributed to the polarization resistance due to the formation of protective oxide layers and the reduction of polymer film. When the ions diffused the pores of the coating, zinc and nickel were oxidized thereby yielding the formation of their oxide layers. Then, polymer film was reduced at metal/polymer interface.<sup>32</sup> After 168 h of immersion time, the  $R_p$  value observed for CS/ZnNi/PNMP electrode was approx. 298350  $\Omega$ . Ozyilmaz et al reported corrosion protection of passivated carbon steel substrate by oxalate ions. It was clearly observed that the  $I_{corr}$  decreased and  $E_{corr}$  increased for CS/ZnNi/PNMP electrode when compared with that of CS/ZnNi/FeCo/OX electrode, after 168 h of exposure times. The positive shift in  $E_{corr}$  indicated the protection of the alloy plating surface by the PNMP coating. The corrosion rate (CR) decreased significantly as a result of the reduction in the  $I_{corr}$ .<sup>34</sup>

This value is fairly higher than those of CS and CS/ZnNi electrode values. The results clearly showed that



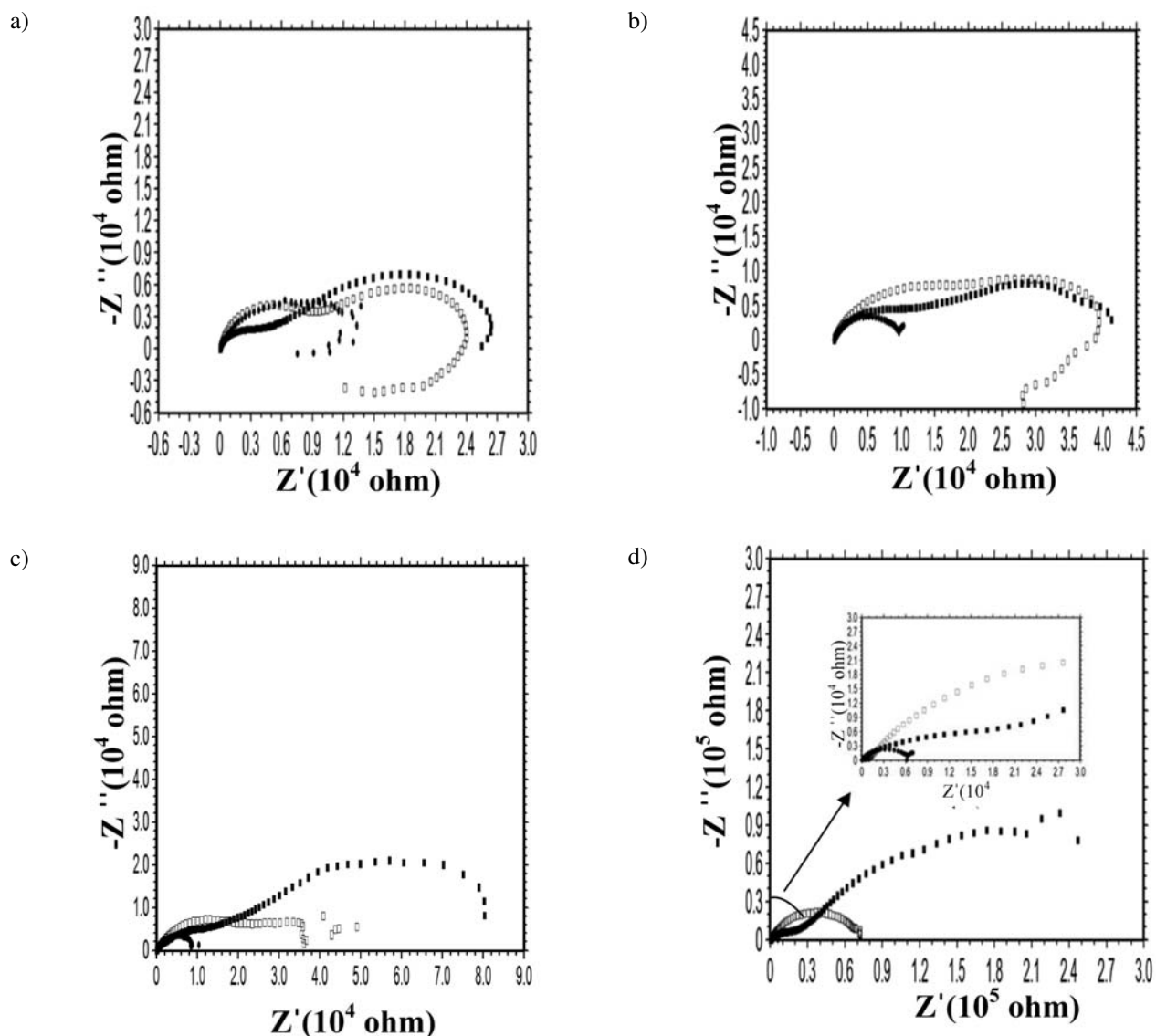


**Fig. 3.** The Nyquist plots recorded for CS (●), CS/ZnNi (□) and CS/ZnNi/PNMP (■) electrodes after 2 (a), 48 (b), 96 (c) and 168 h (d) of exposure time in 3.5% NaCl solution.

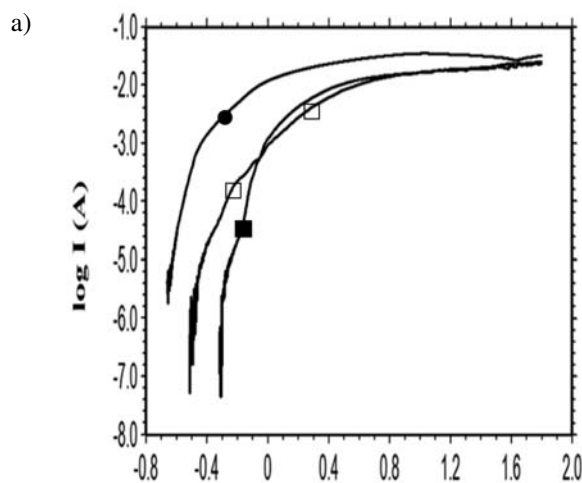
**Table 1.** The  $R_p$ ,  $E_{ocp}$ ,  $I_{corr}$  and E% values recorded for CS, CS/ZnNi and CS/ZnNi/PNMP electrodes after various exposure times in 3.5% NaCl.

Samples	t (h)	$E_{ocp}$ (V)	$R_p$ ( $\Omega$ )	$I_{corr}$ ( $\mu$ A)	E%
CS	2	-0.585	7504	3.46	–
	48	-0.669	10000	2.60	–
	96	-0.665	9413	2.76	–
	168	-0.655	6776	3.84	–
CS/ZnNi	2	-0.974	12163	4.28	38.30
	48	-0.968	27980	1.86	64.26
	96	-0.891	39240	1.33	76.01
	168	-0.598	71250	0.73	90.49
CS/ZnNi/PNMP	2	-0.981	25620	2.03	70.71
	48	-0.964	40578	1.28	75.36
	96	-0.945	82115	0.63	88.54
	168	-0.572	298350	0.17	97.66

the PNMP coating on ZnNi plated carbon steel exhibited an effective anticorrosive property on ZnNi plated carbon steel.

Fig. 4a compares the anodic polarization curves of CS, CS/ZnNi and CS/ZnNi/PNMP electrodes after 168 h of immersion time in 3.5% NaCl corrosive solution. In the case of CS electrode, the corrosion potential ( $E_{\text{corr}}$ ) value was measured to be  $-0.652$  V. Current values increased so rapidly that there was not any possibility for passivation of the CS electrode under the corrosive condition. The  $E_{\text{corr}}$  values recorded for CS/ZnNi and CS/ZnNi/PNMP electrodes were measured  $-0.507$  V and  $-0.314$  V, respectively. It was clearly seen that both electrodes exhibited significantly lower current values and  $E_{\text{corr}}$  values shifted towards nobler potential regions with respect to the bare CS electrode. But it must be noted that much lower current values in near the  $E_{\text{corr}}$  region were recorded for CS/ZnNi/PNMP electrode with respect to CS/ZnNi electrode. At the same time, Ozyilmaz et al.<sup>34</sup> reported anodic polarization curves of both ZnFe and ZnFeCo alloy plating passivated oxalate layer, immersed in 3.5% NaCl. The polarization curve for PNMP coated ZnNi alloy deposited carbon steel showed a smaller corrosion current and a more noble corrosion potential than that observed with CS/ZnFe/OX and CS/ZnNiCo/OX electrode. These results showed that PNMP coating provided much better barrier efficiency against the attack of corrosive species like dissolved oxygen and chloride ions.

Immediately after the immersion time, open circuit potential ( $E_{\text{ocp}}$ ) – time curves of CS, CS/ZnNi and CS/ZnNi/PNMP electrodes in 3.5% NaCl solution are given in Fig. 4b. It was clearly seen that  $E_{\text{ocp}}$  values of CS/ZnNi and CS/ZnNi/PNMP electrodes were the negative direction when compared with CS electrode. Consequently, this behaviour of coated electrodes showed the presence of a layer on CS substrate. Those of CS electrode were at



approx.  $-0.640$  V, while  $E_{\text{ocp}}$  values recorded for coated electrodes were generally  $E_{\text{ocp}}$  observed at approx.  $-0.985$  V. These values obtained for coated electrodes indicated the presence of Zn metal on CS electrode. The  $E_{\text{ocp}}$  values of coated electrodes were closely each other, after 1800 s of immersion time. But, it was shown in Table 1 that  $E_{\text{ocp}}$  values of PNMP coated CS/ZnNi electrode was relatively higher than that of ZnNi coated CS electrode, after 48, 96 and 168 h of exposure times. This case was related to anodic protection behavior of polymer film.

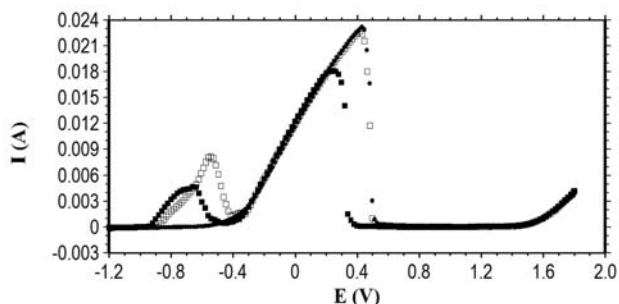


Fig. 5. The linear sweep voltammograms recorded for CS (●), CS/ZnNi (□) CS/ZnNi/PNMP (■) electrodes in 0.05 M EDTA containing 0.50 M sodium sulphate solution.

Anodic linear sweep voltammograms obtained for CS, CS/ZnNi and CS/ZnNi/PNMP electrodes in 0.05 M EDTA containing 0.50 M sodium sulphate are given in Fig. 5. All measurements were taken at scan rate of  $5 \text{ mV s}^{-1}$ . In the anodic linear sweep voltammetry technique, different phase structures and chemical forms existing in the metal and metal alloy plating will lead to dissolution at present potential values depending on their equilibrium an kinetic properties. Hence, the peak properties produced

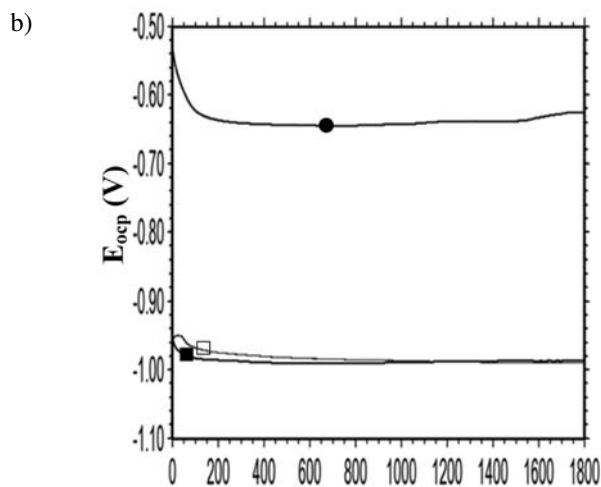


Fig. 4. The anodic polarization (a) and  $E_{\text{ocp}}$ -time curves (b) recorded for CS (●), CS/ZnNi (□) and CS/ZnNi/PNMP (■) electrodes in 3.5% NaCl solution.

are the characteristics of the alloy substrates and phase structure of the coating. There were only single anodic peak for bare CS electrode and two anodic dissolution peaks for CS/ZnNi and CS/ZnNi/PNMP electrodes. The peaks at approximately  $-0.65$  V for CS/ZnNi and  $-0.55$  V for CS/ZnNi/PNMP electrodes were due to dissolution of zinc and nickel and formation of zinc and nickel complex with EDTA. This peak in this potential was not seen for bare CS electrode. Therefore, this behavior of CS/ZnNi/PNMP electrode indicated the presence of alloy coating underlying the PNMP homopolymer film. The peaks at approximately  $0.43$  V for CS and CS/ZnNi and  $0.25$  V for CS/ZnNi/PNMP electrodes were anodic dissolution of iron substrate. The current values recorded for dissolution peak of iron were the lowest in presence of PNMP film. It was clear that PNMP coating on CS/ZnNi electrode provided an adequate physical protection to metal between the corrosive environment and ZnNi alloy plating.

## 4. Conclusions

ZnNi alloy plating was successfully deposited on the CS electrode. PNMP film was synthesized on ZnNi alloy deposited carbon steel electrode with cyclic voltammetry techniques from  $0.20$  M *N*-methylpyrrole containing  $0.20$  M NaOX solution. It was shown that ZnNi alloy plating contributed to the corrosion resistance of CS electrode. Compared with CS/ZnNi electrode, the CS/ZnNi/PNMP electrode exhibited the  $193$  mV more anodic potential value and about 19 times more lower current values near corrosion potential, in anodic polarization curves. The corrosion test showed that CS/ZnNi/PNMP electrode exhibited the highest protection efficiency and the lowest corrosion current values. The polarization resistance of PNMP coated CS/ZnNi electrode was fairly higher when compared with CS and CS/ZnNi electrodes. The protective effect of PNMP film formed on CS/ZnNi grew in parallel extended exposure time by its electrocatalytic behavior.

## 5. References

1. I. Milošev, N. Kovačević, A. Kokalj. *Acta Chim.Slov.* **2016**, 63, 544–559. <https://doi.org/10.17344/acsi.2016.2326>
2. A. C. Hegde, K. Venkatakrishna, N. Eliaz. *Surf. & Coat. Techn.* **2010**, 205, 2031–2041. <https://doi.org/10.1016/j.surfcoat.2010.08.102>
3. J. B. Bajat, S. Stankovic, B. M. Jokic, *J. Sol. St. Electrochem.* **2009**, 13, 755–762. <https://doi.org/10.1007/s10008-008-0604-5>
4. A. P. Ordine, S. L. Diaz, I. C. P. Margarit, O. R. Mattos. *Electrochim. Acta.* **2004**, 49, 2815–2823. <https://doi.org/10.1016/j.electacta.2004.01.044>
5. R. Ramanauskas, P. Quintana, L. Maldonado, R. Porn, M. A. *Surf. & Coat. Techn.* **1997**, 92, 16–21. [https://doi.org/10.1016/S0257-8972\(96\)03125-8](https://doi.org/10.1016/S0257-8972(96)03125-8)
6. N. R. Short, S. Zhou, J. K. Dennis. *Surf. & Coat. Techn.* **1996**, 79, 218–224. [https://doi.org/10.1016/0257-8972\(95\)02428-X](https://doi.org/10.1016/0257-8972(95)02428-X)
7. A. El Hajjami, M. P. Gigandet, M. De Petris-Wery, J. C. Cantonne, J. J. Duprat, L. Thiery, F. Raulin, N. Pommier, B. Starck, P. Remy. *Appl. Surf. Sci.* **2007**, 254, 480–489. <https://doi.org/10.1016/j.apsusc.2007.06.016>
8. H. Park, J.A. Szpunar. *Corr. Sci.* **1998**, 40, (4/5), 525–545. [https://doi.org/10.1016/S0010-938X\(97\)00148-0](https://doi.org/10.1016/S0010-938X(97)00148-0)
9. Z. L. Wang, Y. X. Yang, Y. R. Chen. *Jour. Corros. Sci. Eng.* **2005**, 7, 18.
10. M. A. Pech-Canul, R. Ramanauskas, L. Maldonado. *Electrochim. Acta*, **1997**, 42, (2), 255–260. [https://doi.org/10.1016/0013-4686\(96\)00152-1](https://doi.org/10.1016/0013-4686(96)00152-1)
11. I. Kirilova, I. Ivanov, S. Rashkov. *Jour. Appl. Electrochem.* **1997**, 27, (12), 1380–1384. <https://doi.org/10.1023/A:1018425129532>
12. G. Roventi, T. Bellezze, R. Fratesi. *Electrochim. Acta.* **2006**, 51, 2691–2697. <https://doi.org/10.1016/j.electacta.2005.08.002>
13. Z. F. Lodhi, J. M. C. Mol, W. J. Hamer, H.A. Terryn, J. H. W. De Wit. *Electrochim. Acta*, **2007**, 52, 5444–5452. <https://doi.org/10.1016/j.electacta.2007.02.077>
14. I. H. Karahan, O. Karabulut, U. Alver. *Phys. Scr.* **2009**, 79, 55801. <https://doi.org/10.1088/0031-8949/79/05/055801>
15. P. D. L. Neto, A. N. Correia, R. P. Colares, W. S. Araujo. *J. Braz. Chem. Soc.* **2007**, 18, (6), 1164–1175. <https://doi.org/10.1590/S0103-50532007000600010>
16. N. Boshkov, K. Petrov, S. Vitkova, S. Nemska, G. Raichevsky. *Surf. & Coat. Techn.* **2002**, 157, 171–178. [https://doi.org/10.1016/S0257-8972\(02\)00161-5](https://doi.org/10.1016/S0257-8972(02)00161-5)
17. R. Rajagopalan, J. O. Iroh. *Appl. Surf. Sci.* **2003**, 218, 58–69. [https://doi.org/10.1016/S0169-4332\(03\)00579-8](https://doi.org/10.1016/S0169-4332(03)00579-8)
18. J. O. Iroh, W. Su. *Electrochim. Acta.* **2000**, 46, 15–24. [https://doi.org/10.1016/S0013-4686\(00\)00519-3](https://doi.org/10.1016/S0013-4686(00)00519-3)
19. S. Toprak Doşlu, B. Dođru Mert, B. Yazıcı, *Corros. Sci.* **2013**, 66, 51–58. <https://doi.org/10.1016/j.corsci.2012.08.067>
20. M. Ates, A. T. Özyılmaz. *Prog. Org. Coat.* **2015**, 84, 50–58. <https://doi.org/10.1016/j.porgcoat.2015.02.013>
21. M. Ates. *J. Adhes. Sci. Technol.* **2016**, 30(14), 1510–1536. <https://doi.org/10.1080/01694243.2016.1150662>
22. J. I. Martins, T. C. Reis, M. Bazzouai, E. A. Bazzouai, L. Martins. *Corros. Sci.* **2004**, 46, 2361–2381. <https://doi.org/10.1016/j.corsci.2004.02.006>
23. A. T. Özyılmaz, A. Akdag. *Trans. IMF.* **2011**, 89 (4), 215–224. <https://doi.org/10.1179/174591911X13077162170188>
24. A. T. Özyılmaz, A. Akdag. *Trans. IMF.* **2013**, 91 (1), 44–51. <https://doi.org/10.1179/0020296712Z.00000000063>
25. N. M. Martyak, P. Mc Andrew, J. E. McCaskie, D. Dijon. *Sci. Tech. Advan. Mat.* **2002**, 3, 345–352. [https://doi.org/10.1016/S1468-6996\(02\)00040-2](https://doi.org/10.1016/S1468-6996(02)00040-2)
26. D. J. Shirale, V. K. Gade, P. D. Gaikwad, H. J. Kharat, K. P. Kakde, P. A. *Mat. Letters*, **2006**, 60, 1407–1411. <https://doi.org/10.1016/j.matlet.2005.11.040>

27. S.U. Rahman. *Surf. & Coat. Techn.* **2011**, 205, 3035–3042.  
<https://doi.org/10.1016/j.surfcoat.2010.11.018>
28. A. T. Ozyilmaz, A. Akdag, I. H. Karahan, G. Ozyilmaz. *Prog. Org. Coat.* **2014**, 77, 872–879.  
<https://doi.org/10.1016/j.porgcoat.2014.01.020>
29. A. T. Ozyilmaz, A. E. Aydin, A. Akdag. *Trans. IMF.* **2014**, 92, (1), 34–40.  
<https://doi.org/10.1179/0020296713Z.000000000134>
30. R. Singh, A. K. Narula, R. P. Tandon, S. U. M. Rao, V. S. Panwar, S. Chandra, A. Mansingh. *Synt. Met.* **1996**, 79, (1), 1–6. [https://doi.org/10.1016/0379-6779\(96\)80121-4](https://doi.org/10.1016/0379-6779(96)80121-4)
31. S.B. Saidman *Electrochim. Acta*, **2003**, 48, 1719–1726.  
[https://doi.org/10.1016/S0013-4686\(03\)00110-5](https://doi.org/10.1016/S0013-4686(03)00110-5)
32. A.T. Özyilmaz, G. Ozyilmaz, N. Çolak, *Surf. & Coat. Techn.* **2006**, 201, 2484–2490.  
<https://doi.org/10.1016/j.surfcoat.2006.04.008>
33. A.T. Ozyilmaz, B. Avsar, G. Ozyilmaz, I. H. Karahan, Taskin Camurcu, F. Colak *Appl. Surf. Sci.* **2014**, 318, 262–268.  
<https://doi.org/10.1016/j.apsusc.2014.04.177>
34. A.T. Ozyilmaz, G. Ozyilmaz, I. H. Karahan, *Acta Chim.Slov.* **2016**, 63, 809–821.  
<https://doi.org/10.17344/acsi.2016.2690>
35. Walter, G. W. *Corros. Sci.* **1986**, 26, (9), 681–703.  
[https://doi.org/10.1016/0010-938X\(86\)90033-8](https://doi.org/10.1016/0010-938X(86)90033-8)

## Povzetek

V študiji predstavljamo elektrokemijsko depozicijo delcev cink-nikelj (ZnNi) na elektrodo iz ogljikovega jekla (CS) s kronopotenciometrično tehniko in uporabo toka 1 mA. Na elektrodo CS/ZnNi smo poli(N-metilpirol) (PNMP) film nanesli s pomočjo ciklične voltametrije iz raztopine 0.01 M N-pirola in 0.2 M natrijevega oksalata. Korozijske lastnosti elektrode CS/ZnNi in prevlečene elektrode (CS/ZnNi/PNMP) v 3.5% raztopini NaCl smo določali s pomočjo elektrokemijske impendancne spektroskopije (EIS) in anodnih polarizacijskih krivulj. Vrstično elektronsko mikroskopijo (SEM) in elektrokemijsko metodo (linear sweep voltammetry (LSV)) smo uporabili za karakterizacijo prevleke. Pokazali smo, da delci ZnNi predstavljajo pomembno bariero na CS noslicu. Najvišja vrednost polarizacijske upornosti 298350 ohm je bila določena v primeru CS/ZnNi elektrode prevlečene s PNMP filmom, kar kaže na učinkovito bariero in boljšo korozijsko zaščito nosilca tudi v primeru daljše izpostavljenosti le tega.

Scientific paper

# Microwave-assisted Synthesis of Hybrid Heterocycles as Potential Anticancer Agents

Avula Srinivas,\* Malladi Sunitha, Kammachichu Raju, Banothu Ravinder, Siluveru Anusha, Thallapalli Rajasri, Pothuganti Swapna, Dupa Sushmitha, Deva Swaroopa, Gurala Nikitha and Chakunta Govind Rao

Department of Chemistry, Vaagdevi Degree & PG College  
Kishanpura, Warangal, Telangana, India 506001

\* Corresponding author: E-mail: avula.sathwikreddy@gmail.com

Received: 24-12-2016

## Abstract

In a one pot procedure, a series of novel hybrid heterocycles **6a–g** and **7a–g** were prepared by condensation of (3a*S*,4*S*,6*S*,6a*S*)-6-((1-(4-chlorophenyl)-1*H*-1,2,3-triazol-4-yl)methoxy)-2,2-dimethyltetrahydrofuro[3,4-*d*][1,3]dioxole-4-carbaldehyde **5** with mercapto acids and primary amines in the presence of ZnCl<sub>2</sub> under both microwave irradiation and conventional heating conditions. Compound **5** was prepared from di-acetone D-mannose *via* a click reaction, primary acetonide deprotection and oxidative cleavage. Characterization of new compounds has been done by IR, NMR, MS and elemental analysis. Anticancer activity of the compounds has also been evaluated.

**Keywords:** D-mannose, click reaction, cyclisation, anticancer activity

## 1. Introduction

1,2,3-Triazoles are one of the most important classes of heterocyclic organic compounds, which are reported to be present in a plethora of biologically active compounds, useful for diverse therapeutic areas.<sup>1</sup> The 1,2,3-triazole motif is associated with diverse pharmacological activities, such as antibacterial, antifungal, hypoglycemic, antihypertensive and analgesic properties. Polysubstituted five-membered aza heterocycles rank as the most potent glycosidase inhibitors.<sup>2</sup> Further, this nucleus in combination with or in linking with various other classes of compounds such as amino acids, steroids, aromatic compounds, carbohydrates etc., became prominent in having various pharmacological properties.<sup>3</sup> 1,2,3-Triazole modified carbohydrates have become easily available after the discovery of the Cu(I)-catalyzed azide-alkynes 1,3-dipolar cycloaddition reaction<sup>4</sup> and quickly became a prominent class of non-natural sugar derivatives. The chemistry and biology of triazole modified sugars is dominated by triazole glycosides.<sup>5</sup> Therefore, the synthesis and investigation of biological activity of 1,2,3-triazole glycosides is an important objective, which also received a considerable attention by the medicinal chemists.

Thiazolidinones and 1,2,3-triazoles represent important classes of drugs in medicinal chemistry. They are among the most extensively investigated compounds by biochemists and medicinal chemists.<sup>6</sup> Thiazolidinones in particular show interesting anticancer,<sup>7</sup> anti-HIV,<sup>8</sup> tuberculostatic,<sup>9</sup> antihistaminic,<sup>10</sup> anticonvulsant,<sup>11</sup> antibacterial,<sup>12</sup> and anti arrhythmic<sup>13</sup> activities.

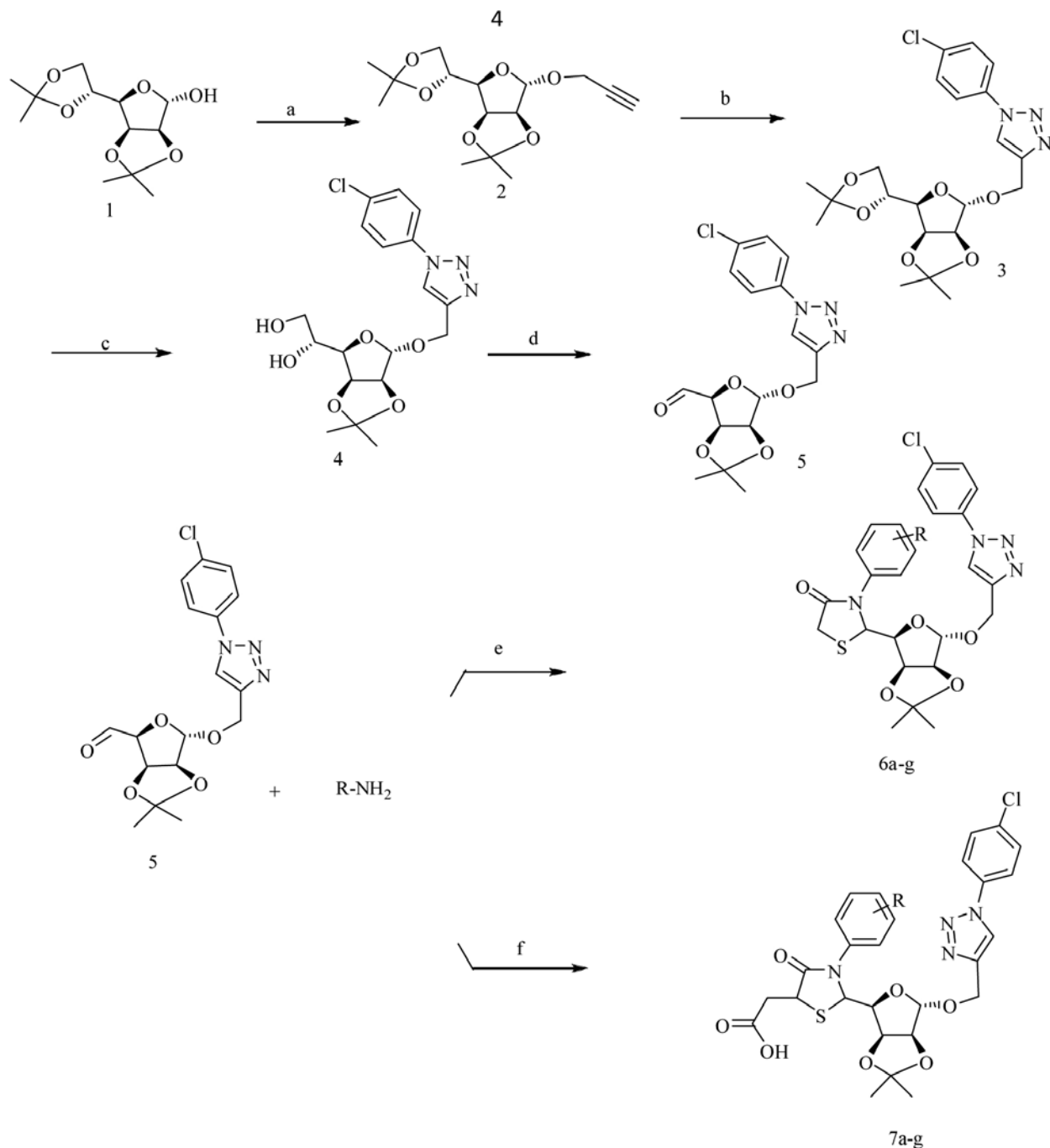
So called hybrid molecules have been shown to be highly active and effective in medicinal chemistry. Synergistic effects are obtained *via* hybridization of two different bioactive moieties with complementary pharmacophoric functions, or with different modes of action.<sup>14</sup> The confirmation of this hypothesis has been well established in previous studies of 4-thiazolidinones coupled with other heterocyclic fragments,<sup>15</sup> *i.e.* resulting in high anti tumor activity.

Microwave irradiation is an alternative heating technique based on the transformation of electromagnetic energy into heat. Often this method increases the rate of chemical reactions<sup>16</sup> and results in higher yields. In recent years, multi component reactions (MCRs)<sup>17</sup> have received interesting attention due to their simplicity, efficiency, atom economy, shortened reaction times, and the possibility for diversity oriented synthesis.

Following the successful introduction of triazoles and thiazolidinones, microwave-assisted MCR reactions, inspired by the biological profile of triazoles, thiazolidinones, and in the continuation of our work on biologically active heterocycles<sup>18–29</sup> we have developed a series of novel triazole-linked thiazolidenone derivatives, we have investigated the application of microwave irradiation for the synthesis of our hybrid molecules and evaluated their anticancer activity.

## 2. Result and Discussion

Di-acetone D-mannose (**1**), prepared from D-(+)-mannose by treating with acetone in the presence of a catalytic amount of sulphuric acid according to the literature procedure,<sup>30</sup> on subsequent propargylation in DMF in the presence of NaH in 1 h afforded propargyl ether **2** (80%). Next, the propargyl ether was converted into triazole **3**



**Scheme 2. Reagents and conditions:** (a) Propargyl bromide, NaH, DMF, 0 °C → rt; (b) p-Chlorophenyl azide, glucose,  $\text{CuSO}_4 \cdot 5\text{H}_2\text{O}$ , THF/ $\text{H}_2\text{O}$ ; (c) 60% AcOH; (d)  $\text{NaIO}_4$ ,  $\text{CH}_2\text{Cl}_2$ ; (e)  $\text{Ar-NH}_2$ ,  $\text{SHCH}_2\text{COOH}$ ,  $\text{ZnCl}_2$ , toluene, 80 °C, MW 110 °C; (f)  $\text{Ar-NH}_2$ , thio malic acid,  $\text{ZnCl}_2$ , toluene, 80 °C, MW 110 °C.

Table 1. Synthesis of compounds 6a–g and 7a–g

Compound	R	Mol. formula	Reaction time		Yield	
			A (h)	B (min)	A	B
6a	C <sub>6</sub> H <sub>5</sub>	C <sub>25</sub> H <sub>25</sub> ClN <sub>4</sub> O <sub>5</sub> S	3.5	5	62	80
6b	4-Cl-C <sub>6</sub> H <sub>4</sub>	C <sub>25</sub> H <sub>24</sub> Cl <sub>2</sub> N <sub>4</sub> O <sub>5</sub> S	2.5	6	75	89
6c	4-NO <sub>2</sub> -C <sub>6</sub> H <sub>4</sub>	C <sub>25</sub> H <sub>24</sub> ClN <sub>5</sub> O <sub>7</sub> S	3.0	6	65	82
6d	2-CH <sub>3</sub> -C <sub>6</sub> H <sub>4</sub>	C <sub>26</sub> H <sub>27</sub> ClN <sub>4</sub> O <sub>5</sub> S	2.0	5	65	86
6e	4-CH <sub>3</sub> -C <sub>6</sub> H <sub>4</sub>	C <sub>26</sub> H <sub>27</sub> ClN <sub>4</sub> O <sub>5</sub> S	2.5	5	69	88
6f	3-OH-C <sub>6</sub> H <sub>4</sub>	C <sub>25</sub> H <sub>25</sub> ClN <sub>4</sub> O <sub>6</sub> S	3.0	5	74	86
6g	4-OH-C <sub>6</sub> H <sub>4</sub>	C <sub>25</sub> H <sub>25</sub> ClN <sub>4</sub> O <sub>6</sub> S	2.0	3	82	91
7a	C <sub>6</sub> H <sub>5</sub>	C <sub>27</sub> H <sub>27</sub> ClN <sub>4</sub> O <sub>7</sub> S	3.5	5	61	79
7b	4-Cl-C <sub>6</sub> H <sub>4</sub>	C <sub>27</sub> H <sub>26</sub> Cl <sub>2</sub> N <sub>4</sub> O <sub>7</sub> S	2.5	6	68	82
7c	4-NO <sub>2</sub> -C <sub>6</sub> H <sub>4</sub>	C <sub>27</sub> H <sub>26</sub> Cl <sub>2</sub> N <sub>5</sub> O <sub>9</sub> S	3.0	7	60	79
7d	2-CH <sub>3</sub> -C <sub>6</sub> H <sub>4</sub>	C <sub>28</sub> H <sub>29</sub> ClN <sub>4</sub> O <sub>7</sub> S	2.5	5	72	81
7e	4-CH <sub>3</sub> -C <sub>6</sub> H <sub>4</sub>	C <sub>28</sub> H <sub>29</sub> ClN <sub>4</sub> O <sub>7</sub> S	2.0	5	64	82
7f	3-OH-C <sub>6</sub> H <sub>4</sub>	C <sub>27</sub> H <sub>27</sub> ClN <sub>4</sub> O <sub>8</sub> S	3.0	5	79	87
7g	4-OH-C <sub>6</sub> H <sub>4</sub>	C <sub>27</sub> H <sub>27</sub> ClN <sub>4</sub> O <sub>8</sub> S	2.5	4	69	90

A: conventional heating; B: microwave irradiation.

(82%) by using a 1,3-dipolar cycloaddition with *p*-chlorophenyl azide, which was carried out at ambient temperature in the presence of CuSO<sub>4</sub> and glucose which reduced CuSO<sub>4</sub> in a mixture of 1:1 *t*-BuOH–H<sub>2</sub>O. Acid hydrolysis of 5,6-acetonide **3** in 60% AcOH furnished the diol **4** (85%), which on oxidative cleavage with NaIO<sub>4</sub> gave the aldehyde **5** (Scheme 1). Subsequently one pot synthesis of triazole-linked thiazolidinone glycosides was carried out by the condensation reaction between **5**, primary aromatic amine and a thioglycolic acid and thiomalic acid in the presence of ZnCl<sub>2</sub> under microwave irradiation or conventional heating (Scheme 2). In the classic method, the reactions were performed in dry toluene at reflux for a long time (2–4 h), often leading to degradation processes and consequent low yields of isolated products, whereas upon the application of microwave-assisted technology the reaction was completed in only 5–10 minutes and the compounds, isolated by conventional work-up, were obtained in satisfactory yields, often higher than those achieved by traditional methods (Table 1). The structures of synthesized compounds were confirmed by IR, NMR, MS and elemental analysis. Further, the compounds were subject to anticancer testing.

### 3. Cytotoxicity Evaluation Against Different Cancer Cell Lines

The cytotoxic effect of the compounds was tested by performing a Sulforhodamine B Assay (SRB) on different representative cell lines. Initially, the cell line of interest was seeded in a flat bottom 96-well plate (5000 cells/100 μL) in a medium containing 10% serum, followed by incubation for 18–20 h in an incubator continuously supplied with 5% CO<sub>2</sub>, so as to ensure proper adherence of the cells to the surface bottom of the wells. After 18 h the

cells were treated with the compound. Working dilutions of concentration of the compounds were prepared, of which 2 μL aliquot was added to each well, thereby making the final concentration of compound 0 to 100 μM. Each compound was tested in triplicate and the cytotoxicity was determined as the average of that triplicate. DM-SO and doxorubicin (as standard control anti cancer drug) were taken as vehicle and positive controls, respectively. Further, the plates were incubated for another 48 h in an incubator maintained at 37 °C with a constant supply of 5% CO<sub>2</sub>. After the period of 48 h, the cells were fixed using 10% TCA solution and incubated for 1 h at 4 °C after which the plate was rinsed carefully with MQ water and air dried; this was followed by addition of 0.057% SRB solution which was kept for approx. 30 min before it was rinsed off using 1% acetic acid. The plates were then air dried and the absorbance was measured using Perkin–Elmer Multimode Reader at 510 nm. To measure the absorbance, 100 μL of 10 mM Tris Base was added to each well to solubilize the SRB. The value of absorbance is directly proportional to cell growth and is thus used to calculate the IC<sub>50</sub> values. In this study for initial screening, four types of cancer cell lines, *i.e.* human lung cancer (A549), human breast cancer (MCF-7), prostate cancer (DU145) and HeLa cell lines were tested for the cytotoxic effect of the series of compounds. Based on the IC<sub>50</sub> values obtained, the compound **7b** was picked for further assays to ascertain its effect on prostate cancer cell line (DU145).

#### 3. 1. Change in Morphology

Based on the cytotoxic ability of the compound, its effect on the morphology of the cells was also ascertained. To achieve this, a 24-well plate was seeded with cells in a manner previously described and incubated for 18–20 h. Then, the cells were treated with increasing concentra-

tions of **7b**. After another 48 h of incubation, the experiment was terminated and the cells were observed under the microscope and images were captured using Olympus Xi71 microscope.

### 3. 2. Colony Formation Assay

The long term effect of the **7b** on the anchorage independent nature of cancer cells was further tested in the following experiment. The experiment was a soft agar assay which was conducted as reported previously with minor modifications. In the experiment, base agar was prepared by mixing 1% of agarose (Bacto Agar: Becton, Dickinson, Sparks, MD) with 2 × DMEM along with 20% FBS and 2X antibiotics in 6-well plates in order to achieve final concentration of 0.5% of agar in 1X growth medium with 10% serum concentration. After the solidification of the base agar, 2.5 × 10<sup>4</sup> cells were mixed with cultivation medium containing compound at varying concentrations along with agar solution to obtain a final concentration of 0.35% agar. This was spread on top of the base agar previously solidified. The plate was incubated for 9 days with periodic replenishment every 3 days with medium and compound. Over the period of time, plates were monitored regularly for appearance of colonies. After 9 days of incubation the plates were stained with 0.005% crystal violet solution until colonies turned purple in color. The excessive stain was washed off using MQ water and the colonies were photographed and counted using a microscope.

### 3. 3. Determination of Caspase-3 and Caspase-9 Activities

Caspase activity, specifically, caspase-9 and caspase-3 activities were analyzed in the cell lysates obtained

from DU 145 cells previously treated with compound **7b**. The activity was observed using fluorogenic substrates, namely Ac-DEVD-AMC and Ac-LEHD-AFC for caspase-3 and caspase-9, respectively. After 48 h treatment of cells with compound **7b**, harvested cells were lysed directly in caspase lyses buffer (50 mM HEPES, 5 mM CHAPS, 5 mM DTT, pH 7.5). The lysates were incubated with the respective substrate (Ac-DEVD-AFC/Ac-LEHD-AMC) in 20 mM HEPES (pH 7.5), 0.1% CHAPS, 2 mM EDTA and 5 mM DTT at 37 °C for 2 h. The release of AFC and AMC was analyzed by a fluorimeter using an excitation/emission wavelength of 400/505 nm (for AFC) and 380/460 nm (for AMC) which is directly proportional to caspase-9 and caspase-3 activity, respectively. The observed fluorescence values were normalized with total protein concentration estimated by Bradford method and the relative caspase activities were calculated as the ratio of values between mock treated (DMSO) and treated cells.

### 3. 4. Senescence Assay

Compounds with anti-cancer potential may have the possibility to induce senescence in cells, thus limiting their proliferation. The ability to induce cellular senescence was determined by measuring senescence-associated beta-galactosidase (SA-βgal) activity (pH 6.0) in DU145 cells exposed to compound **7b**. A 24-well plate was seeded with DU 145 cells as previously described and treated with the compound and subsequently incubated for 48 h. After 48 h, the media was aspirated and the cells were washed with PBS (2 × 1 min) and fixed by adding enough volume of fixation solution (2% formaldehyde and 0.2% glutaraldehyde in PBS solution) to submerge the cells in solution. After incubation for 5 min at room temperature

**Table 2.** Four representative cell lines were tested with the series of compounds to determine their cytotoxicity. Table shows the IC<sub>50</sub> values of the compounds against the cell lines.

S.No.	Sample codes	DU145		A549		HELA		MCF 7	
		IC <sub>50</sub>	Std. Dev	IC <sub>50</sub>	Std. Dev	IC <sub>50</sub>	Std. Dev	IC <sub>50</sub>	Std. Dev
1	<b>6a</b>	17.99	3.27	31.15	13.78	>100	–	40.97	21.06
2	<b>6b</b>	15.98	3.10	37.29	0.00	>100	–	57.16	5.33
3	<b>6c</b>	12.25	0.85	15.18	1.12	58.34	15.39	63.60	29.26
4	<b>6d</b>	37.71	18.26	33.64	6.64	>100	–	>100	–
5	<b>6e</b>	>100	–	29.81	0.62	>100	–	66.30	8.84
6	<b>6f</b>	16.91	2.37	21.84	4.68	67.07	42.33	18.73	2.11
7	<b>6g</b>	8.76	0.68	10.70	1.11	24.29	1.02	19.51	0.48
8	<b>7a</b>	>100	–	43.67	6.33	>100	19.62	>100	–
9	<b>7b</b>	8.76	0.68	10.7	1.11	24.29	1.02	19.5	0.48
10	<b>7c</b>	23.87	1.06	49.98	7.33	>100	–	>100	–
11	<b>7d</b>	>100	–	25.19	5.72	>100	–	>100	–
12	<b>7e</b>	53.48	9.73	39.94	30.16	52.74	16.02	29.87	0.00
13	<b>7f</b>	39.94	7.30	36.04	16.40	77.81	47.77	60.07	29.73
14	<b>7g</b>	25.09	3.39	33.96	9.95	33.55	6.11	37.28	14.04
15	Doxorubicin	6.70	0.10	8.49	0.13	10.89	0.09	8.62	1.52



the fixation solution was removed and the cells were washed twice with PBS ( $2 \times 1$  min). The resultant fixed cells were then stained with freshly prepared staining solution (40 mM citric acid/Na phosphate buffer, 5 mM  $K_4[Fe(CN)_6] \cdot 3H_2O$ , 5 mM  $K_3[Fe(CN)_6]$ , 150 mM sodium chloride, 2 mM magnesium chloride and 1 mg X-gal in 1 mL distilled water) overnight at 37 °C. The excess stain was removed by repeated washings with PBS and plate was allowed to dry at room temperature. The cells stained with SA- $\beta$ gal levels were observed and photographed under an Olympus Xi71 microscope.

### 3. 5. PI Uptake for Analysis of Cell Death

Cell death induced by compound **7b** was determined as a measure of PI uptake. Cells were harvested after treatment with compound at desired concentration and fixed in 70% ethanol at  $-20$  °C overnight. The cells were then collected in the form of pellet. All cells in the form of a pellet were then resuspended in PI solution (RNase 0.1 mg/mL, Triton X-100 0.05%, PI 50  $\mu$ g/mL) and incu-

bated for 1 h in dark at room temperature. The excess PI solution was washed away by repeated washings with PBS buffer. The resultant PI uptake was analyzed by fluorescence activated cell sorting (FACS Caliber System; BD Bio-science, Erembodegem, Belgium) in a FL-2 fluorescence detector (10000 events were recorded

**Table 3.** Compound **7b** induced G0/G1 phase cell cycle arrest in DU145 cells. Cells were treated with varying concentrations of compound **7b** (5, 10, 15, 20 and 25  $\mu$ M) for 48 h and cell cycle progression was examined by flow cytometry. Table shows the percentage cell fractions in G0/G1, S and G2/M phases of compound **7b** treated DU145 cells.

	G0/G1	S	G2/M
DMSO	71.36	5.02	22.74
5 $\mu$ M	63.92	8.10	22.16
10 $\mu$ M	69.15	5.54	24.65
15 $\mu$ M	71.86	3.92	22.51
20 $\mu$ M	72.11	3.89	20.05
25 $\mu$ M	76.48	2.99	18.77

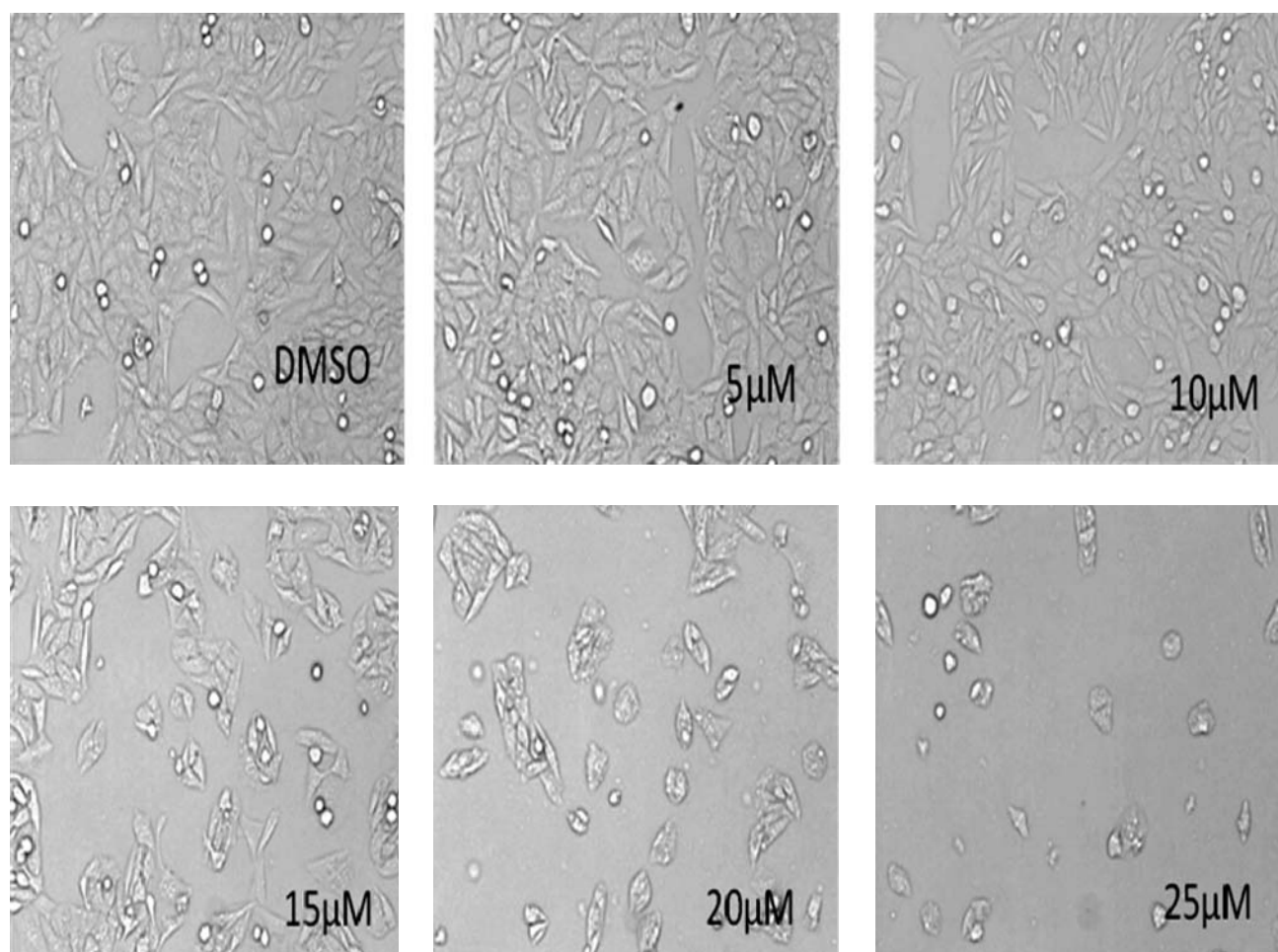


**Figure 1.** DU145 cell were treated with compound **7b** at indicated concentration or DMSO. Upon exposure of DU145 cells to compound **7b** the extent of change in cell morphology of cells is observed with increasing concentration.

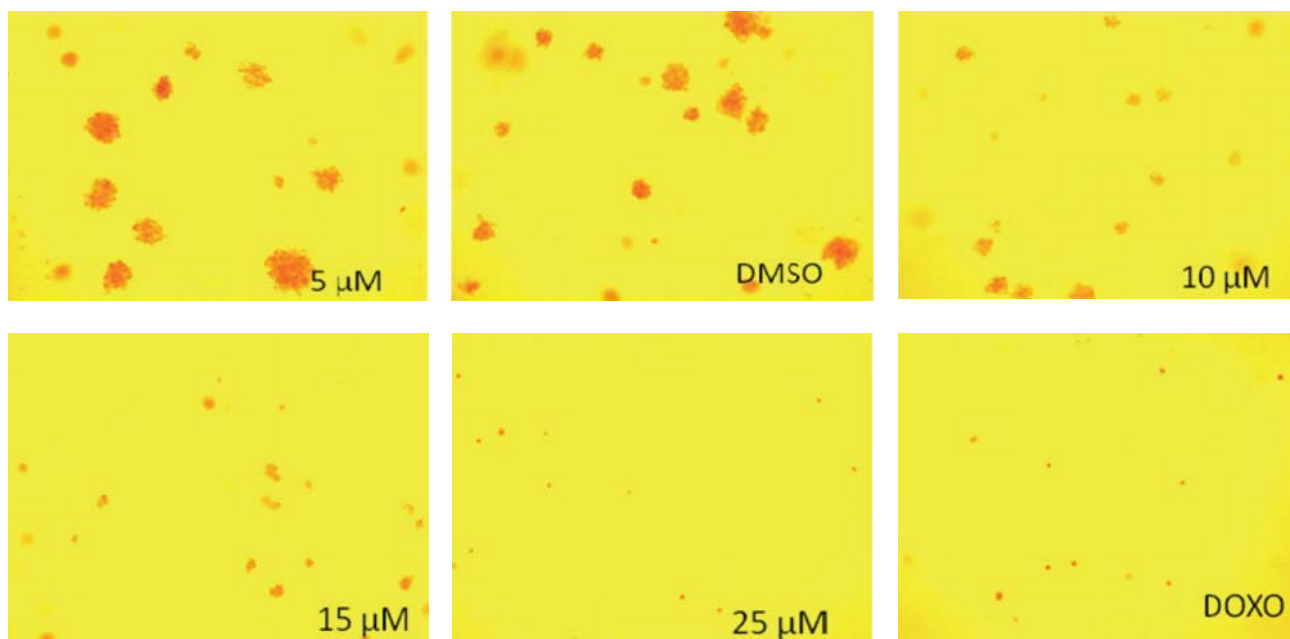


**Figure 2.** Long term effect of compound **7b** on the number of colony-forming DU145 cells. DU145 cells were treated with desired concentration of **7b** (0–25  $\mu\text{M}$ ) and allowed to grow for 9 days to form colonies. Representative images of the colony-forming assay are shown here. Number of colonies and their size formed by DU145 in soft agar is decreased on exposure to compound **7b**.

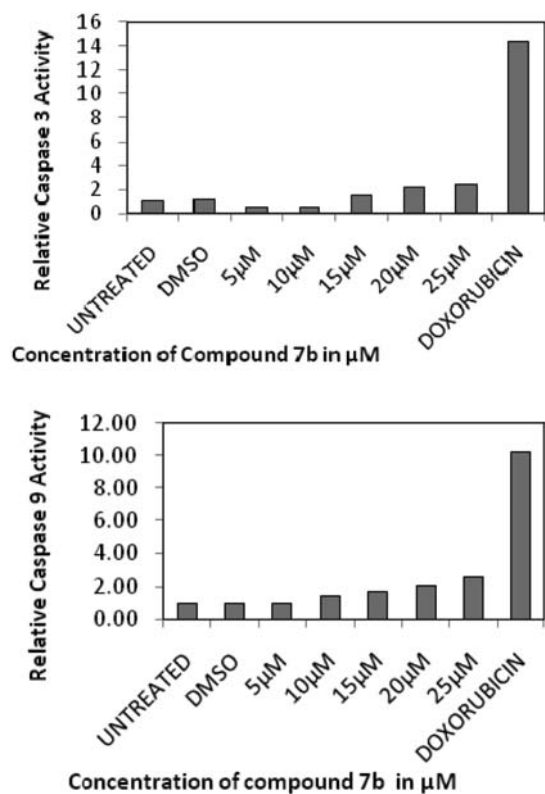


**Figure 3.** The ability of the compound to activate caspases in DU145 cells was observed. Treatment of DU145 cells with different concentration of **7b** for 48 h induced activation of caspase-3 (A) and caspase-9 (B) significantly in concentration dependent manner. Doxorubicin was used as control for activation of both caspases. All experiments were carried out in triplicates and mean values are presented here.

for each condition). Flow cytometry data was analyzed using FCS express 4 software (De Novo Software, Los Angeles, CA).

## 4. Experimental

Commercial grade reagents were used as supplied. Solvents, except those of analytical grade, were dried and purified according to literature when necessary. Reaction progress and purity of the compounds were checked by thin-layer chromatography (TLC) on pre-coated silica gel F254 plates from Merck and compounds visualized either by exposure to UV light or dipping in 1% aqueous potassium permanganate solution. Silica gel chromatographic columns (60–120 mesh) were used for separations. Microwave reactions were carried out in mini lab microwave catalytic reactor (ZZKD, WBFY-201) and reaction mixture temperatures were measured through an immersed fibre-optic sensor. All melting points are uncorrected and measured using Fisher–Johns apparatus. IR spectra were recorded as KBr disks on a Perkin–Elmer FT IR spectrometer. The  $^1\text{H}$  NMR and  $^{13}\text{C}$  NMR spectra were recorded on a Varian Gemini spectrometer (300 MHz for  $^1\text{H}$  and 75 MHz for  $^{13}\text{C}$ ). Chemical shifts are reported as  $\delta$  ppm against TMS as internal reference and coupling constants ( $J$ ) are reported in Hz units. Mass spectra were recorded on a VG micro mass 7070H spectrometer. Elemental analyses (C, H, N) determined by a Perkin–Elmer 240 CHN elemental analyzer, were within  $\pm 0.4\%$  of theoretical.

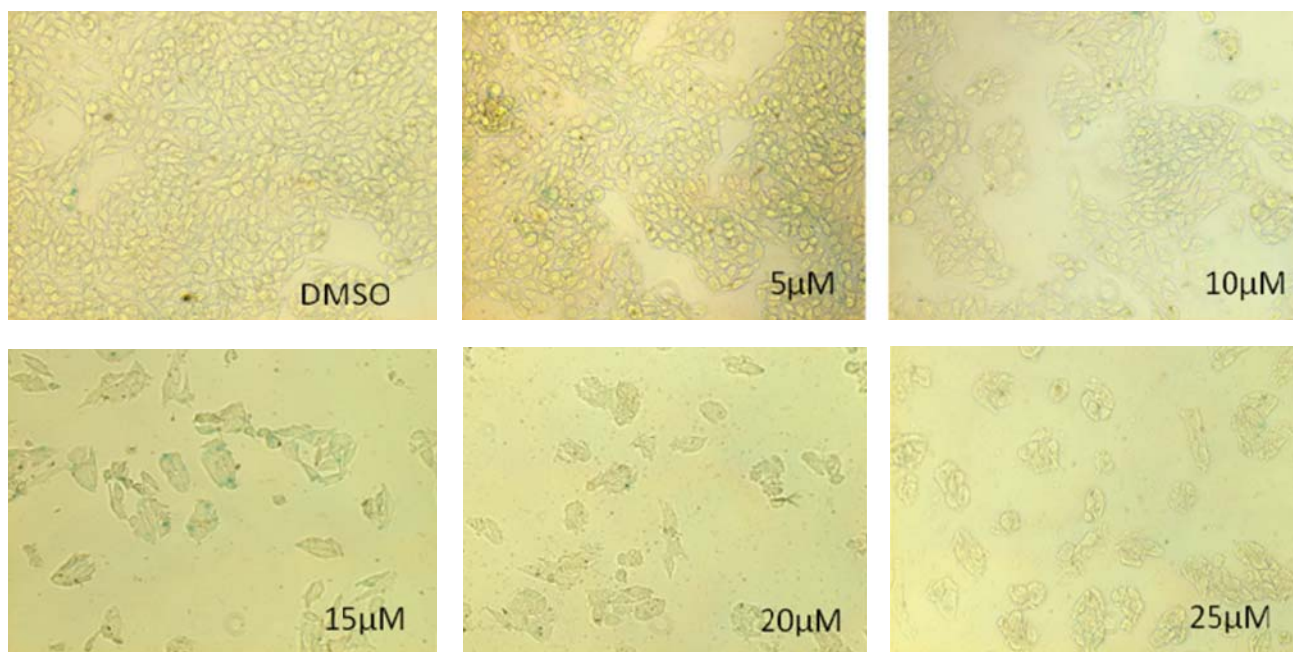


**Figure 4.** Senescence induced by compound **7b** was quantified using SA- $\beta$ gal-staining. As shown in the figure, **7b** did not induce senescence in cells as at higher concentrations the cells underwent apoptosis

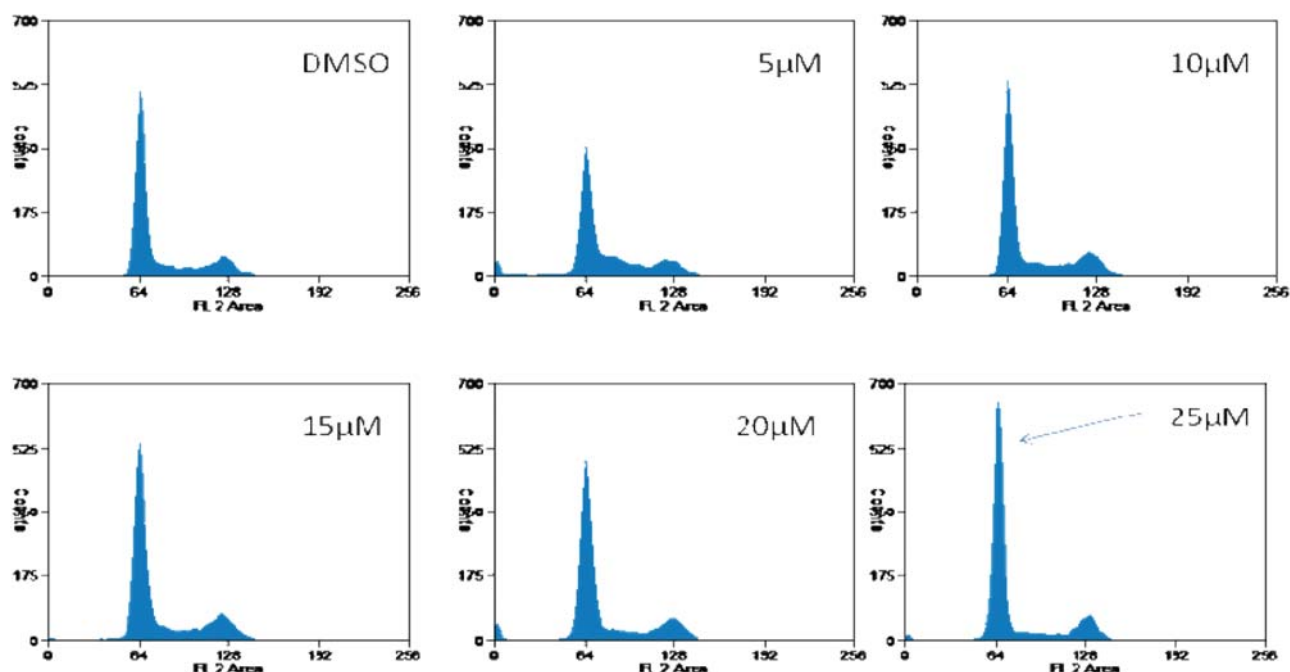


**Figure 5.** Cell cycle analysis of DU145 cells treated with compound **7b**. Cells were treated with either DMSO or **7b** and the DNA content was measured by propidium iodide staining to determine the distribution of cells in various phases of cell cycle. DMSO was taken as reference.

(3a*S*,4*R*,6*S*,6a*S*)-4-((*R*)-2,2-Dimethyl-1,3-dioxolan-4-yl)-2,2-dimethyl-6-(prop-2-ynyloxy)tetrahydrofuro[3,4-*d*][1,3]dioxole (**2**). Sodium hydride (60% in mineral oil, 0.64 g) was added to a stirred solution of **3** (3.6 g, 13.84 mmol) in DMF (80 mL) at 0 °C and allowed to stir

for 30 min. This yellow mixture was cooled to 0 °C and treated with propargyl bromide (4.2 g) in DMF (20 mL). The dark brown reaction mixture was allowed to stir for an hour at room temperature and quenched (at 5–10 °C) with saturated aqueous ammonium chloride (20 mL). The

crude product was extracted with  $\text{CH}_2\text{Cl}_2$  ( $3 \times 30$  mL), dried ( $\text{Na}_2\text{SO}_4$ ) and concentrated. The residue was purified by column chromatography on silica gel (5% EtOAc : hexane) to afford **4** (3.1 g, 75%) as viscous oil. IR (KBr):  $\nu$  3312, 2997, 2929, 2266, 1632, 1377, 1222, 1162, 1074, 1016  $\text{cm}^{-1}$ ;  $^1\text{H}$  NMR (300 MHz,  $\text{CDCl}_3$ ):  $\delta$  5.52 (d,  $J = 3.7$  Hz, 1H,  $\text{C}_1\text{H}$ ), 4.59 (t,  $J = 3.9$  Hz, 1H,  $\text{C}_2\text{H}$ ), 4.26 (dt,  $J = 3.1, 7.3$  Hz, 1H,  $\text{C}_5\text{H}$ ), 4.19 (s, 2H,  $\text{CH}_2$ ), 4.07–3.94 (m, 3H,  $\text{C}_4\text{H}$ ,  $2 \times \text{C}_6\text{H}$ ), 3.65 (dd,  $J = 8.9, 4.1$  Hz, 1H,  $\text{C}_3\text{H}$ ), 3.16 (s, 1H, CH), 1.53 (s, 3H,  $\text{CH}_3$ ), 1.40 (s, 3H,  $\text{CH}_3$ ), 1.32 (s, 6H,  $2 \times \text{CH}_3$ );  $^{13}\text{C}$  NMR (75 MHz,  $\text{CDCl}_3$ ): 112.5, 109.4, 103.6, 80.1, 76.6, 75.2, 73.6, 65.2, 56.2, 25.6, 24.2. MS:  $m/z$  ( $\text{M}^+\text{Na}$ ) 321.

**1-(4-Chlorophenyl)-4-(((3aS,4S,6R,6aS)-6-((R)-2,2-dimethyl-1,3-dioxolan-4-yl)-2,2-dimethyltetrahydrofuro[3,4-d][1,3]dioxol-4-yloxy)methyl)-1H-1,2,3-triazole (3)**. To solution containing (3 g, 10.06 mmol) of the alkyne **4**, *p*-chlorophenyl azide (1.8 g, 11.76 mmol) in tetrahydrofuran (30 mL) and water (1 mL) were added  $\text{CuSO}_4 \cdot 5\text{H}_2\text{O}$  (1.8 g, 8.15 mmol) and glucose (0.2 g). The resulting suspension was stirred at room temperature for 4–6 h. After this time, the mixture was diluted with 20 mL  $\text{CH}_2\text{Cl}_2$  and 20 mL water. The organic phase was separated, dried with sodium sulfate and concentrated at reduced pressure, the crude residue was purified by column chromatography silica gel (60–120 mesh, 35% EtOAc : hexane) to afford **5** (3.2 g, 75%) as a white powder. mp 149–151 °C. IR (KBr):  $\nu$  3252, 2974, 2926, 1631, 1551, 1512, 1372, 1225, 1164, 1070, 1019, 734  $\text{cm}^{-1}$ ;  $^1\text{H}$  NMR (300 MHz,  $\text{CDCl}_3$ ):  $\delta$  8.04 (s, 1H, Ar-H), 7.55 (d,  $J = 9.2$  Hz, 2H, ArH), 7.43 (d,  $J = 8.9$  Hz, 2H, Ar-H) 5.56 (d,  $J = 3.7$  Hz, 1H,  $\text{C}_1\text{H}$ ), 4.62 (t,  $J = 3.9$  Hz, 1H,  $\text{C}_2\text{H}$ ), 4.55 (s, 2H,  $\text{CH}_2$ ), 4.36 (dt,  $J = 3.1, 7.3$  Hz, 1H,  $\text{C}_5\text{H}$ ), 4.08–3.98 (m, 3H,  $\text{C}_4\text{H}$ ,  $2 \times \text{C}_6\text{H}$ ), 3.69 (dd,  $J = 8.9, 4.1$  Hz, 1H,  $\text{C}_3\text{H}$ ), 1.52 (s, 3H,  $\text{CH}_3$ ), 1.39 (s, 3H,  $\text{CH}_3$ ), 1.33 (s, 6H,  $2 \times \text{CH}_3$ );  $^{13}\text{C}$  NMR (75 MHz,  $\text{CDCl}_3$ ): 143.6, 133.6, 122.1, 118.9, 111.9, 108.6, 103.2, 80.0, 76.9, 73.9, 66.9, 65.9, 26.2, 25.9, 24.9. MS:  $m/z$  ( $\text{M}^+\text{H}$ ) 452. Anal. Calcd for  $\text{C}_{21}\text{H}_{26}\text{ClN}_3\text{O}_6$ : C, 55.81; H, 5.80; N, 9.30. Found: C, 55.75; H, 5.75; N, 9.21.

**(R)-1-(((3aS,4R,6S,6aS)-6-((1-(4-Chlorophenyl)-1H-1,2,3-triazol-4-yl)methoxy)-2,2-dimethyltetrahydrofuro[3,4-d][1,3]dioxol-4-yl)ethane-1,2-diol (4)**. A mixture of **3** (3 g, 6.65 mmol) in 60% aq. AcOH (25 mL) was stirred at room temperature for 12 h. Reaction mixture was neutralized with anhy.  $\text{NaHCO}_3$  (15 g) and extracted with EtOAc ( $3 \times 41$  mL). The combined organic layers were dried ( $\text{Na}_2\text{SO}_4$ ), evaporated and residue purified by column chromatography (60–120 mesh silica gel, 41% ethyl acetate in pet. ether) to afford **4** (2.6 g, 82%) as a pale yellow solid; mp 168–171 °C. IR (KBr)  $\nu$  3218, 3486, 3362, 2992, 2965, 2936, 2922, 1630, 1544, 1510, 1212, 1161, 1022, 732  $\text{cm}^{-1}$ ;  $^1\text{H}$  NMR (300 MHz,  $\text{CDCl}_3$ ):  $\delta$  8.01 (s, 1H, Ar-H), 7.51 (d,  $J = 9.2$  Hz, 2H, ArH), 7.40 (d,  $J = 8.9$

Hz, 2H, Ar-H) 5.49 (d,  $J = 3.7$  Hz, 1H,  $\text{C}_1\text{H}$ ), 4.52 (t,  $J = 3.9$  Hz, 1H,  $\text{C}_2\text{H}$ ), 4.58 (s, 2H,  $\text{OCH}_2$ ), 3.88–3.81 (m, 2H,  $\text{C}_4\text{H}$ ,  $\text{C}_5\text{H}$ ), 4.01–3.92 (m, 3H,  $\text{C}_3\text{H}$ ,  $2 \times \text{C}_6\text{H}$ ), 2.42 (bs, 1H, OH), 1.50 (s, 3H,  $\text{CH}_3$ ), 1.45 (bs, 1H, OH), 1.34 (s, 3H,  $\text{CH}_3$ );  $^{13}\text{C}$  NMR (75 MHz,  $\text{CDCl}_3$ ):  $\delta$  143.2, 133.2, 122.1, 117.2, 110.2, 109.2, 102.1, 78.8, 77.1, 75.1, 70.6, 67.2, 65.2, 63.2, 26.6, 26.2, 24.9. MS:  $m/z$  ( $\text{M}^+\text{H}$ ) 412. Anal. Calcd for  $\text{C}_{18}\text{H}_{22}\text{ClN}_3\text{O}_6$ : C, 52.49; H, 5.38; N, 10.21. Found: C, 52.35; H, 5.25; N, 10.211.

**2-(((3aR,4S,6S,6aS)-6-((1-(4-Chlorophenyl)-1H-1,2,3-triazol-4-yl)methoxy)-2,2-dimethyltetrahydrofuro[3,4-d][1,3]dioxol-4-yl)-3-phenylthiazolidin-4-one 6a-g**. To a solution of diol **4** (0.200 g, 0.48 mmol) in  $\text{CH}_2\text{Cl}_2$  (5 mL),  $\text{NaIO}_4$  (0.130 g, 0.61 mmol) was added at 0 °C and stirred at room temperature for 6 h. The reaction mixture was filtered and washed with  $\text{CH}_2\text{Cl}_2$  ( $2 \times 10$  mL). It was dried ( $\text{Na}_2\text{SO}_4$ ) and evaporated to give aldehyde **5** (0.150 g) in quantitative yield as a yellow liquid, which was used as such for the next reaction.

To a stirred mixture of **5** (0.150 g, 0.395 mmol), aromatic amine (0.395 mmol) and anhydrous thioglycolic acid (0.160 g, 0.211 mmol) in dry toluene (5 mL),  $\text{ZnCl}_2$  (0.100 g, 0.751 mmol) was added after 2 min and irradiated in microwave bath reactor at 280 W for 4–7 minutes at 110 °C. After cooling, the filtrate was concentrated to dryness under reduced pressure and the residue was taken up in ethyl acetate. The ethyl acetate layer was washed with 5% sodium bicarbonate solution and finally with brine. The organic layer was dried over  $\text{Na}_2\text{SO}_4$  and evaporated to dryness at reduced pressure. The crude product thus obtained was purified by column chromatography on silica gel (60–120 mesh) with hexane – ethyl acetate as eluent. Under conventional method the reaction mixture in toluene (10 mL) was refluxed at 110 °C for the appropriate time (Table 1).

**2-(((3aR,4S,6S,6aS)-6-((1-(4-Chlorophenyl)-1H-1,2,3-triazol-4-yl)methoxy)-2,2-dimethyltetrahydrofuro[3,4-d][1,3]dioxol-4-yl)-3-phenylthiazolidin-4-one (6a)**. mp 137–139 °C, IR (KBr)  $\nu$  3422, 3210, 2984, 2972, 2934, 2831, 1712, 1610, 1541, 1512, 1414, 1225, 683  $\text{cm}^{-1}$ ;  $^1\text{H}$  NMR (300 MHz,  $\text{CDCl}_3$ ):  $\delta$  8.04 (s, 1H, Ar-H), 7.50 (d,  $J = 9.2$  Hz, 2H, Ar-H), 7.39 (d,  $J = 8.9$  Hz, 2H, Ar-H), 7.42–6.95 (5H, m, Ar-H), 5.65 (d,  $J = 3.6$  Hz, 1H,  $\text{C}_1\text{H}$ ), 4.83 (d,  $J = 5.2$  Hz, CH-S), 4.52 (t,  $J = 3.9$  Hz, 1H,  $\text{C}_2\text{H}$ ), 4.48 (s, 2H,  $\text{OCH}_2$ ), 3.98–3.95 (m, 1H,  $\text{C}_5\text{H}$ ), 3.65 (s, 2H,  $\text{CH}_2$ ), 3.29 (dd,  $J = 9.1, 4.2$  Hz, 1H,  $\text{C}_3\text{H}$ ), 1.50 (s, 3H,  $\text{CH}_3$ ), 1.29 (m, 3H,  $\text{CH}_3$ );  $^{13}\text{C}$  NMR (75 MHz,  $\text{CDCl}_3$ ):  $\delta$  170.6, 143.2, 140.2, 133.8, 132.2, 127.9, 126.2, 125.4, 122.2, 118.6, 116.2, 104.8, 81.4, 78.2, 74.1, 65.9, 51.0, 33.6, 25.5; MS:  $m/z$  ( $\text{M}^+\text{Na}$ ) 552. Anal. Calcd for  $\text{C}_{25}\text{H}_{25}\text{ClN}_4\text{O}_5\text{S}$ : C, 56.76; H, 4.76; N, 10.59. Found: C, 56.53; H, 4.55; N, 10.43.

**3-(4-Chlorophenyl)-2-(((3aR,4S,6S,6aS)-6-((1-(4-chlorophenyl)-1H-1,2,3-triazol-4-yl)methoxy)-2,2-di-**

**methyltetrahydrofuro[3,4-*d*][1,3]dioxol-4-yl)thiazolidin-4-one (6b).** mp 206–208 °C; IR (KBr)  $\nu$  3420, 3219, 2974, 2962, 2812, 1710, 1610, 1546, 1510, 1409, 1219, 682  $\text{cm}^{-1}$ ;  $^1\text{H}$  NMR (300 MHz,  $\text{CDCl}_3$ ):  $\delta$  8.01 (s, 1H, Ar-H), 7.46 (d,  $J = 9.2$  Hz, 4H, Ar-H), 7.41 (d,  $J = 8.9$  Hz, 4H, Ar-H), 5.62 (d,  $J = 3.6$  Hz, 1H,  $\text{C}_1\text{H}$ ), 4.84 (d,  $J = 5.2$  Hz, CH-S), 4.50 (t,  $J = 3.9$  Hz, 1H,  $\text{C}_2\text{H}$ ), 4.49 (s, 2H,  $\text{OCH}_2$ ), 3.86–3.71 (m, 1H,  $\text{C}_4\text{H}$ ), 3.66 (s, 2H,  $\text{CH}_2$ ), 3.29 (dd,  $J = 9.1, 4.2$  Hz, 1H,  $\text{C}_3\text{H}$ ), 1.45 (s, 3H,  $\text{CH}_3$ ), 1.32 (m, 3H,  $\text{CH}_3$ );  $^{13}\text{C}$  NMR (75 MHz,  $\text{CDCl}_3$ ): 170.2, 138.4, 134.4, 133.0, 128.4, 127.6, 125.2, 122.1, 118.4, 111.6, 104.3, 80.5, 74.1, 65.3, 52.1, 34.3, 25.5; MS:  $m/z$  ( $\text{M}^+\text{H}$ ) 563. Anal. Calcd for  $\text{C}_{25}\text{H}_{24}\text{Cl}_2\text{N}_4\text{O}_5\text{S}$ : C, 53.29; H, 4.29; N, 9.94. Found: C, 53.21; H, 4.16; N, 9.83.

**2-((3aR,4S,6S,6aS)-6-((1-(4-Chlorophenyl)-1H-1,2,3-triazol-4-yl)methoxy)-2,2-dimethyltetrahydrofuro[3,4-*d*][1,3]dioxol-4-yl)-3-(4-nitrophenyl)thiazolidin-4-one (6c).** mp 201–205 °C; IR (KBr)  $\nu$  3422, 3216, 2984, 2961, 2820, 1710, 1605, 1536, 1512, 1416, 1372, 1210, 863, 630  $\text{cm}^{-1}$ ;  $^1\text{H}$  NMR (300 MHz,  $\text{CDCl}_3$ ):  $\delta$  8.16 (d,  $J = 8.7$  Hz, 2H, Ar-H), 8.02 (s, 1H, Ar-H), 7.49 (d,  $J = 9.2$  Hz, 2H, Ar-H), 7.40 (d,  $J = 8.5$  Hz, 2H, Ar-H), 6.72 (d,  $J = 9.8$  Hz, 2H, Ar-H), 5.69 (d,  $J = 3.6$  Hz, 1H,  $\text{C}_1\text{H}$ ), 4.86 (d,  $J = 5.2$  Hz, CH-S), 4.52 (t,  $J = 3.9$  Hz, 1H,  $\text{C}_2\text{H}$ ), 4.49 (s, 2H,  $\text{OCH}_2$ ), 3.86–3.81 (m, 1H,  $\text{C}_4\text{H}$ ), 3.66 (s, 2H,  $\text{CH}_2$ ), 3.24 (dd,  $J = 9.1, 4.2$  Hz, 1H,  $\text{C}_3\text{H}$ ), 1.50 (s, 3H,  $\text{CH}_3$ ), 1.24 (m, 3H,  $\text{CH}_3$ );  $^{13}\text{C}$  NMR (75 MHz,  $\text{CDCl}_3$ ):  $\delta$  170.2, 145.5, 143.4, 142.2, 134.2, 130.2, 126.6, 124.3, 121.4, 118.8, 111.4, 104.6, 80.5, 77.2, 73.8, 66.4, 52.1, 34.2, 26.2; MS:  $m/z$  ( $\text{M}^+\text{H}$ ) 574. Anal. Calcd for  $\text{C}_{25}\text{H}_{24}\text{ClN}_5\text{O}_7\text{S}$ : C, 52.31; H, 4.21; N, 12.20. Found: C, 52.26; H, 4.19; N, 12.11.

**2-((3aR,4S,6S,6aS)-6-((1-(4-Chlorophenyl)-1H-1,2,3-triazol-4-yl)methoxy)-2,2-dimethyltetrahydrofuro[3,4-*d*][1,3]dioxol-4-yl)-3-*o*-tolylthiazolidin-4-one (6d).** mp 181–183 °C; IR (KBr)  $\nu$  3436, 3234, 2986, 2976, 2834, 1710, 1705, 1610, 1549, 1516, 1418, 1262, 865  $\text{cm}^{-1}$ ;  $^1\text{H}$  NMR (300 MHz,  $\text{CDCl}_3$ ):  $\delta$  8.13 (d,  $J = 8.7$  Hz, 2H, Ar-H), 8.01 (s, 1H, Ar-H), 7.50 (d,  $J = 9.2$  Hz, 2H, Ar-H), 7.35–6.92 (m, 5H, Ar-H), 5.64 (d,  $J = 3.6$  Hz, 1H,  $\text{C}_1\text{H}$ ), 4.84 (d,  $J = 5.2$  Hz, 1H, CH-S), 4.52 (t,  $J = 3.9$  Hz, 1H,  $\text{C}_2\text{H}$ ), 4.44 (s, 2H,  $\text{OCH}_2$ ), 3.86–3.71 (m, 1H,  $\text{C}_4\text{H}$ ), 3.66 (s, 2H,  $\text{CH}_2$ ), 3.16 (dd,  $J = 9.1, 4.2$  Hz, 1H,  $\text{C}_3\text{H}$ ), 2.08 (s, 3H,  $\text{CH}_3$ ), 1.49 (s, 3H,  $\text{CH}_3$ ), 1.26 (m, 3H,  $\text{CH}_3$ );  $^{13}\text{C}$  NMR (75 MHz,  $\text{CDCl}_3$ ):  $\delta$  170.2, 143.6, 136.7, 134.3, 133.3, 130.2, 129.1, 127.6, 125.2, 122.1, 118.8, 111.2, 104.4, 81.4, 78.3, 74.4, 66.1, 52.1, 26.2, 16.3; MS:  $m/z$  ( $\text{M}^+\text{H}$ ) 545. Anal. Calcd for  $\text{C}_{26}\text{H}_{27}\text{ClN}_4\text{O}_5\text{S}$ : C, 57.51; H, 5.51; N, 10.32. Found: C, 56.86; H, 5.39; N, 10.11.

**2-((3aR,4S,6S,6aS)-6-((1-(4-Chlorophenyl)-1H-1,2,3-triazol-4-yl)methoxy)-2,2-dimethyltetrahydrofuro[3,4-*d*][1,3]dioxol-4-yl)-3-*p*-tolylthiazolidin-4-one (6e).** mp 181–183 °C; IR (KBr)  $\nu$  3418, 3220, 2981, 2972, 2830, 1702, 1691, 1610, 1536, 1519, 1412, 1251, 856  $\text{cm}^{-1}$ ;  $^1\text{H}$

NMR (300 MHz,  $\text{CDCl}_3$ ):  $\delta$  8.2 (d,  $J = 8.7$  Hz, 2H, Ar-H), 8.01 (s, 1H, Ar-H), 7.44 (d,  $J = 9.2$  Hz, 2H, Ar-H), 7.36 (d,  $J = 8.3$  Hz, 2H, Ar-H), 7.16 (d,  $J = 8.3$  Hz, 2H, Ar-H), 5.66 (d,  $J = 3.6$  Hz, 1H,  $\text{C}_1\text{H}$ ), 4.86 (d,  $J = 5.2$  Hz, 1H, CH-S), 4.56 (t,  $J = 3.9$  Hz, 1H,  $\text{C}_2\text{H}$ ), 4.54 (s, 2H,  $\text{OCH}_2$ ), 3.86–3.81 (m, 1H,  $\text{C}_4\text{H}$ ), 3.66 (s, 2H,  $\text{CH}_2$ ), 3.16 (dd,  $J = 9.1, 4.2$  Hz, 1H,  $\text{C}_3\text{H}$ ), 2.32 (s, 3H,  $\text{CH}_3$ ), 1.43 (s, 3H,  $\text{CH}_3$ ), 1.36 (m, 3H,  $\text{CH}_3$ );  $^{13}\text{C}$  NMR (75 MHz,  $\text{CDCl}_3$ ):  $\delta$  171.6, 143.1, 136.4, 131.6, 130.3, 129.2, 128.2, 127.9, 124.2, 122.1, 118.2, 110.2, 103.1, 80.9, 78.3, 74.6, 64.9, 51.6, 26.4, 15.1; MS:  $m/z$  ( $\text{M}^+\text{Na}$ ) 565. Anal. Calcd for  $\text{C}_{26}\text{H}_{27}\text{ClN}_4\text{O}_5\text{S}$ : C, 57.51; H, 5.51; N, 10.32. Found: C, 56.82; H, 5.35; N, 10.09.

**2-((3aR,4S,6S,6aS)-6-((1-(4-Chlorophenyl)-1H-1,2,3-triazol-4-yl)methoxy)-2,2-dimethyltetrahydrofuro[3,4-*d*][1,3]dioxol-4-yl)-3-(3-hydroxyphenyl)thiazolidin-4-one (6f).** mp 218–219 °C; IR (KBr)  $\nu$  3525, 3416, 3231, 2975, 2964, 2822, 1710, 1610, 1546, 1512, 1416, 1259, 861  $\text{cm}^{-1}$ ;  $^1\text{H}$  NMR (300 MHz,  $\text{CDCl}_3$ ):  $\delta$  8.16 (d,  $J = 8.7$  Hz, 2H, Ar-H), 8.01 (s, 1H, Ar-H), 7.46 (d,  $J = 9.2$  Hz, 2H, Ar-H), 7.04–6.90 (m, 4H, Ar-H), 5.72 (d,  $J = 3.6$  Hz, 1H,  $\text{C}_1\text{H}$ ), 5.30 (s, 1H, OH), 4.86 (d,  $J = 5.2$  Hz, 1H, CH-S), 4.56 (t,  $J = 3.9$  Hz, 1H,  $\text{C}_2\text{H}$ ), 4.50 (s, 2H,  $\text{OCH}_2$ ), 3.91–3.89 (m, 1H,  $\text{C}_4\text{H}$ ), 3.71 (s, 2H,  $\text{CH}_2$ ), 3.22 (dd,  $J = 9.1, 4.2$  Hz, 1H,  $\text{C}_3\text{H}$ ), 1.50 (s, 3H,  $\text{CH}_3$ ), 1.36 (m, 3H,  $\text{CH}_3$ );  $^{13}\text{C}$  NMR (75 MHz,  $\text{CDCl}_3$ ):  $\delta$  171.2, 157.3, 144.0, 143.6, 133.6, 132.4, 130.6, 128.3, 121.2, 120.4, 119.3, 113.6, 111.1, 107.6, 106.8, 81.8, 77.6, 74.8, 63.9, 54.4, 41.2, 34.3; MS:  $m/z$  ( $\text{M}^+\text{H}$ ) 545. Anal. Calcd for  $\text{C}_{25}\text{H}_{25}\text{ClN}_4\text{O}_6\text{S}$ : C, 55.09; H, 4.62; N, 10.28. Found: C, 54.82; H, 4.55; N, 10.19.

**2-((3aR,4S,6S,6aS)-6-((1-(4-Chlorophenyl)-1H-1,2,3-triazol-4-yl)methoxy)-2,2-dimethyltetrahydrofuro[3,4-*d*][1,3]dioxol-4-yl)-3-(4-hydroxyphenyl)thiazolidin-4-one (6g).** mp 253–255 °C; IR (KBr)  $\nu$  3531, 3415, 3222, 2977, 2960, 2832, 1710, 1614, 1536, 1509, 1412, 1248, 860  $\text{cm}^{-1}$ ;  $^1\text{H}$  NMR (300 MHz,  $\text{CDCl}_3$ ):  $\delta$  8.20 (d,  $J = 8.7$  Hz, 2H, Ar-H), 8.02 (s, 1H, Ar-H), 7.51 (d,  $J = 9.2$  Hz, 2H, Ar-H), 7.02–6.90 (m, 4H, Ar-H), 5.56 (d,  $J = 3.6$  Hz, 1H,  $\text{C}_1\text{H}$ ), 5.18 (s, 1H, OH), 4.90 (d,  $J = 5.2$  Hz, 1H, CH-S), 4.60 (t,  $J = 3.9$  Hz, 1H,  $\text{C}_2\text{H}$ ), 4.49 (s, 2H,  $\text{OCH}_2$ ), 3.81–3.79 (m, 1H,  $\text{C}_4\text{H}$ ), 3.69 (s, 2H,  $\text{CH}_2$ ), 3.24 (dd,  $J = 9.1, 4.2$  Hz, 1H,  $\text{C}_3\text{H}$ ), 1.50 (s, 3H,  $\text{CH}_3$ ), 1.26 (m, 3H,  $\text{CH}_3$ );  $^{13}\text{C}$  NMR (75 MHz,  $\text{CDCl}_3$ ):  $\delta$  170.2, 156.8, 143.2, 142.2, 132.9, 131.4, 130.2, 127.6, 121.9, 120.5, 119.8, 114.2, 111.2, 106.4, 81.4, 78.1, 73.5, 62.4, 54.2, 40.3, 34.6; MS:  $m/z$  ( $\text{M}^+\text{H}$ ) 545. Anal. Calcd for  $\text{C}_{25}\text{H}_{25}\text{ClN}_4\text{O}_6\text{S}$ : C, 55.09; H, 4.62; N, 10.28. Found: C, 54.92; H, 4.59; N, 10.22.

**2-(2-((3aR,4S,6S,6aS)-6-((1-(4-Chlorophenyl)-1H-1,2,3-triazol-4-yl)methoxy)-2,2-dimethyltetrahydrofuro[3,4-*d*][1,3]dioxol-4-yl)-4-oxo-3-phenylthiazolidin-5-yl)acetic acid 7a–g.** To a solution of diol **5** (0.200 g, 0.48

mmol) in  $\text{CH}_2\text{Cl}_2$  (5 mL),  $\text{NaIO}_4$  (0.130 g, 0.61 mmol) was added at 0 °C and stirred at room temperature for 6 h. The reaction mixture was filtered and washed with  $\text{CH}_2\text{Cl}_2$  (2 × 10 mL). It was dried ( $\text{Na}_2\text{SO}_4$ ) and evaporated to give aldehyde **7** (0.150 g) in quantitative yield as a yellow liquid, which was used as such for the next reaction.

To a stirred mixture of **7** (0.150 g, 0.395 mmol), aromatic amine (0.395 mmol) and thiomalic acid (0.125 g, 0.86 mmol) in dry toluene (5 mL), anhydrous  $\text{ZnCl}_2$  (0.100 g, 0.751 mmol) was added after 2 min and irradiated in microwave bath reactor at 280 W for 4–7 minutes at 110 °C. After cooling, the filtrate was concentrated to dryness under reduced pressure and the residue was taken up in ethyl acetate. The ethyl acetate layer was washed with 5% sodium bicarbonate solution and finally with brine. The organic layer was dried over  $\text{Na}_2\text{SO}_4$  and evaporated to dryness at reduced pressure. The crude product thus obtained was purified by column chromatography on silica gel (60–120 mesh) with hexane - ethyl acetate as eluent. Under conventional method the reaction mixture in toluene (10 mL) was refluxed at 110 °C for the appropriate time (Table 1).

**2-(2-((3aR,4S,6S,6aS)-6-((1-(4-Chlorophenyl)-1H-1,2,3-triazol-4-yl)methoxy)-2,2-dimethyltetrahydrofuro[3,4-d][1,3]dioxol-4-yl)-4-oxo-3-phenylthiazolidin-5-yl)acetic acid (7a).** mp 211–214 °C IR (KBr)  $\nu$  3434, 3221, 2984, 2970, 2940, 2822, 1722, 1610, 1539, 1512, 1410, 1214, 684  $\text{cm}^{-1}$ ;  $^1\text{H}$  NMR (300 MHz,  $\text{CDCl}_3$ ):  $\delta$  11.34 (s, 1H,  $\text{CO}_2\text{H}$ ), 8.05 (s, 1H, Ar-H), 7.45 (d,  $J = 9.2$  Hz, 2H, Ar-H), 7.38 (d,  $J = 8.9$  Hz, 2H, Ar-H), 7.32–7.28 (m, 5H, Ar-H), 6.05 (s, 1H, CHS), 5.53 (d,  $J = 4.2$  Hz, 1H,  $\text{C}_1\text{H}$ ), 4.59 (t,  $J = 3.9$  Hz, 1H,  $\text{C}_2\text{H}$ ), 4.55 (t, 1H, CH), 4.42 (s, 2H,  $\text{OCH}_2$ ), 3.82–3.79 (m, 1H,  $\text{C}_4\text{H}$ ), 3.21 (dd,  $J = 9.1, 4.2$  Hz, 1H,  $\text{C}_3\text{H}$ ), 2.28 (d, 2H,  $\text{CH}_2$ ), 1.43 (s, 3H,  $\text{CH}_3$ ), 1.20 (m, 3H,  $\text{CH}_3$ );  $^{13}\text{C}$  NMR (75 MHz,  $\text{CDCl}_3$ ):  $\delta$  170.3, 143.2, 140.2, 133.2, 126.2, 124.8, 121.9, 117.8, 103.2, 80.1, 76.9, 72.8, 65.1, 50.0, 36.2, 32.9, 24.9; MS:  $m/z$  ( $\text{M}^+\text{H}$ ) 545. Anal. Calcd for  $\text{C}_{27}\text{H}_{27}\text{ClN}_4\text{O}_7\text{S}$ : C, 55.24; H, 4.64; N, 9.54. Found: C, 55.12; H, 4.59; N, 9.39.

**2-(3-(4-Chlorophenyl)-2-((3aR,4S,6S,6aS)-6-((1-(4-chlorophenyl)-1H-1,2,3-triazol-4-yl)methoxy)-2,2-dimethyltetrahydrofuro[3,4-d][1,3]dioxol-4-yl)-4-oxothiazolidin-5-yl)acetic acid (7b).** mp 249–251 °C; IR (KBr)  $\nu$  3428, 3421, 3216, 2972, 2819, 1721, 1715, 1606, 1529, 1509, 1410, 1206, 679  $\text{cm}^{-1}$ ;  $^1\text{H}$  NMR (300 MHz,  $\text{CDCl}_3$ ):  $\delta$  11.24 (s, 1H,  $\text{CO}_2\text{H}$ ), 7.88 (s, 1H, Ar-H), 7.35 (d,  $J = 9.2$  Hz, 4H, Ar-H), 7.39 (d,  $J = 8.9$  Hz, 4H, Ar-H), 6.10 (s, 1H, CHS), 5.78 (d,  $J = 4.2$  Hz, 1H,  $\text{C}_1\text{H}$ ), 4.72 (t,  $J = 3.9$  Hz, 1H,  $\text{C}_2\text{H}$ ), 4.55 (t, 1H, CH), 4.52 (s, 2H,  $\text{OCH}_2$ ), 3.92–3.89 (m, 1H,  $\text{C}_4\text{H}$ ), 3.20 (dd,  $J = 9.1, 4.2$  Hz, 1H,  $\text{C}_3\text{H}$ ), 2.34 (d, 2H,  $\text{CH}_2$ ), 1.53 (s, 3H,  $\text{CH}_3$ ), 1.30 (m, 3H,  $\text{CH}_3$ );  $^{13}\text{C}$  NMR (75 MHz,  $\text{CDCl}_3$ ):  $\delta$  170.4, 142.2,

141.6, 132.6, 127.8, 125.9, 121.2, 117.4, 103.5, 80.4, 77.23, 71.2, 66.1, 51.3, 35.9, 31.2, 24.6; MS:  $m/z$  ( $\text{M}^+\text{H}$ ) 621. Anal. Calcd for  $\text{C}_{27}\text{H}_{26}\text{Cl}_2\text{N}_4\text{O}_7\text{S}$ : C, 52.18; H, 4.22; N, 9.01. Found: C, 52.02; H, 4.09; N, 8.95

**2-(2-((3aR,4S,6S,6aS)-6-((1-(4-Chlorophenyl)-1H-1,2,3-triazol-4-yl)methoxy)-2,2-dimethyltetrahydrofuro[3,4-d][1,3]dioxol-4-yl)-3-(4-nitrophenyl)-4-oxothiazolidin-5-yl)acetic acid (7c).** mp 266–268 °C, IR (KBr)  $\nu$  3418, 3424, 3215, 2971, 2986, 2819, 1722, 1710, 1606, 1526, 1510, 1409, 1363, 1210, 861, 635  $\text{cm}^{-1}$ ;  $^1\text{H}$  NMR (300 MHz,  $\text{CDCl}_3$ ):  $\delta$  11.42 (s, 1H,  $\text{CO}_2\text{H}$ ), 8.11 (d,  $J = 8.4$  Hz, 2H), 8.01 (s, 1H, Ar-H), 7.45 (d,  $J = 9.1$  Hz, 2H, Ar-H), 7.41 (d,  $J = 8.5$  Hz, 2H, Ar-H), 6.79 (d,  $J = 9.6$  Hz, 2H, Ar-H), 6.14 (s, 1H, CHS), 5.69 (d,  $J = 4.2$  Hz, 1H,  $\text{C}_1\text{H}$ ), 4.65 (t, 1H, CH), 4.53 (t,  $J = 3.9$  Hz, 1H,  $\text{C}_2\text{H}$ ), 4.52 (s, 2H,  $\text{OCH}_2$ ), 3.90–3.86 (m, 1H,  $\text{C}_4\text{H}$ ), 3.19 (dd,  $J = 9.1, 4.2$  Hz, 1H,  $\text{C}_3\text{H}$ ), 2.30 (d, 2H,  $\text{CH}_2$ ), 1.49 (s, 3H,  $\text{CH}_3$ ), 1.25 (m, 3H,  $\text{CH}_3$ );  $^{13}\text{C}$  NMR (75 MHz,  $\text{CDCl}_3$ ):  $\delta$  190.2, 173.2, 143.6, 141.9, 134.5, 128.2, 126.5, 122.2, 118.2, 104.3, 80.4, 77.2, 73.1, 66.2, 52.1, 36.4, 33.1, 25.4; MS:  $m/z$  ( $\text{M}^+\text{H}$ ) 632. Anal. Calcd for  $\text{C}_{27}\text{H}_{26}\text{Cl}_2\text{N}_5\text{O}_9\text{S}$ : C, 51.31; H, 4.15; N, 11.08. Found: C, 51.19; H, 4.09; N, 10.95.

**2-(2-((3aR,4S,6S,6aS)-6-((1-(4-Chlorophenyl)-1H-1,2,3-triazol-4-yl)methoxy)-2,2-dimethyltetrahydrofuro[3,4-d][1,3]dioxol-4-yl)-4-oxo-3-*o*-tolylthiazolidin-5-yl)acetic acid (7d).** mp 247–249 °C; IR (KBr)  $\nu$  3429, 3219, 2968, 2831, 1704, 1689, 1610, 1549, 1512, 1415, 1260, 850  $\text{cm}^{-1}$ ;  $^1\text{H}$  NMR (300 MHz,  $\text{CDCl}_3$ ):  $\delta$  11.42 (s, 1H,  $\text{CO}_2\text{H}$ ), 8.20 (d,  $J = 8.4$  Hz, 2H, Ar-H), 8.02 (s, 1H, Ar-H), 7.48 (d,  $J = 9.1$  Hz, 2H, Ar-H), 7.32–6.95 (m, 4H, Ar-H), 6.09 (s, 1H, CHS), 5.55 (d,  $J = 4.2$  Hz, 1H,  $\text{C}_1\text{H}$ ), 4.50 (t, 1H, CH), 4.48 (t,  $J = 3.9$  Hz, 1H,  $\text{C}_2\text{H}$ ), 4.44 (s, 2H,  $\text{OCH}_2$ ), 3.82–3.76 (m, 1H,  $\text{C}_4\text{H}$ ), 3.12 (dd,  $J = 9.1, 4.2$  Hz, 1H,  $\text{C}_3\text{H}$ ), 2.24 (d, 2H,  $\text{CH}_2$ ), 2.19 (s, 3H,  $\text{CH}_3$ ), 1.49 (s, 3H,  $\text{CH}_3$ ), 1.19 (m, 3H,  $\text{CH}_3$ );  $^{13}\text{C}$  NMR (75 MHz,  $\text{CDCl}_3$ ): 190.4, 172.4, 143.6, 141.9, 132.9, 124.4, 122.2, 118.2, 104.6, 80.2, 76.4, 72.4, 65.5, 52.1, 35.3, 32.2, 24.2, 16.1; MS:  $m/z$  ( $\text{M}^+\text{H}$ ) 600. Anal. Calcd for  $\text{C}_{28}\text{H}_{29}\text{ClN}_4\text{O}_7\text{S}$ : C, 55.95; H, 4.86; N, 9.32. Found: C, 54.19; H, 4.62; N, 9.15.

**2-(2-((3aR,4S,6S,6aS)-6-((1-(4-Chlorophenyl)-1H-1,2,3-triazol-4-yl)methoxy)-2,2-dimethyltetrahydrofuro[3,4-d][1,3]dioxol-4-yl)-4-oxo-3-*p*-tolylthiazolidin-5-yl)acetic acid (7e).** mp 187–189 °C; IR (KBr)  $\nu$  3425, 3229, 2961, 2820, 1709, 1686, 1615, 1545, 1510, 1424, 1253, 840  $\text{cm}^{-1}$ ;  $^1\text{H}$  NMR (300 MHz,  $\text{CDCl}_3$ ):  $\delta$  11.35 (s, 1H,  $\text{CO}_2\text{H}$ ), 8.19 (d,  $J = 8.4$  Hz, 2H, Ar-H), 8.01 (s, 1H, Ar-H), 7.51 (d,  $J = 9.1$  Hz, 2H, Ar-H), 7.26 (d,  $J = 8.33$  Hz, 2H, Ar-H), 7.10 (d,  $J = 8.3$  Hz, 2H, Ar-H), 6.11 (s, 1H, CHS), 5.60 (d,  $J = 4.2$  Hz, 1H,  $\text{C}_1\text{H}$ ), 4.50 (t, 1H, CH), 4.43 (t,  $J = 3.9$  Hz, 1H,  $\text{C}_2\text{H}$ ), 4.34 (s, 2H,  $\text{OCH}_2$ ), 3.82–3.76 (m, 1H,  $\text{C}_4\text{H}$ ), 3.12 (dd,  $J = 9.1, 4.2$  Hz, 1H,

C<sub>3</sub>H), 2.32 (d, 2H, CH<sub>2</sub>), 2.16 (s, 3H, CH<sub>3</sub>), 1.47 (s, 3H, CH<sub>3</sub>), 1.19 (m, 3H, CH<sub>3</sub>); <sup>13</sup>C NMR (75 MHz, CDCl<sub>3</sub>): 190.4, 172.4, 143.6, 141.9, 132.9, 124.4, 121.2, 117.2, 103.6, 80.6, 76.4, 72.4, 65.5, 52.1, 35.3, 32.2, 24.2, 15.2; MS: *m/z* (M<sup>+</sup>+H) 600. Anal. Calcd for C<sub>28</sub>H<sub>29</sub>ClN<sub>4</sub>O<sub>7</sub>S: C, 55.95; H, 4.86; N, 9.32. Found: C, 54.19; H, 4.62; N, 9.15.

**2-(2-((3*aR*,4*S*,6*S*,6*aS*)-6-((1-(4-Chlorophenyl)-1*H*-1,2,3-triazol-4-yl)methoxy)-2,2-dimethyltetrahydrofuro[3,4-*d*][1,3]dioxol-4-yl)-3-(3-hydroxyphenyl)-4-oxothiazolidin-5-yl)acetic acid (7f).** mp 237–239 °C; IR (KBr)  $\nu$  3525, 3426, 3216, 2965, 2830, 1710, 1612, 1534, 1514, 1414, 1251, 861 cm<sup>-1</sup>; <sup>1</sup>H NMR (300 MHz, CDCl<sub>3</sub>):  $\delta$  11.32 (s, 1H, CO<sub>2</sub>H), 8.21 (d, *J* = 8.7 Hz, 2H, Ar-H), 8.01 (s, 1H, Ar-H), 7.51 (d, *J* = 9.2 Hz, 2H, Ar-H), 7.04–6.90 (m, 4H, Ar-H), 6.11 (s, 1H, CHS), 5.66 (d, *J* = 3.6 Hz, 1H, C<sub>1</sub>H), 5.32 (s, 1H, OH), 4.86 (d, *J* = 5.2 Hz, 1H, CH), 4.49 (t, *J* = 3.9 Hz, 1H, C<sub>2</sub>H), 4.34 (s, 2H, OCH<sub>2</sub>), 3.83–3.76 (m, 1H, C<sub>4</sub>H), 3.26 (dd, *J* = 9.1, 4.2 Hz, 1H, C<sub>3</sub>H), 2.24 (d, 2H, CH<sub>2</sub>), 1.43 (s, 3H, CH<sub>3</sub>), 1.28 (m, 3H, CH<sub>3</sub>); <sup>13</sup>C NMR (75 MHz, CDCl<sub>3</sub>): 174.6, 171.1, 157.3, 143.2, 143.1, 133.6, 133.4, 131.6, 127.6, 121.2, 120.1, 119.1, 114.2, 111.2, 107.2, 106.2, 81.2, 78.2, 74.1, 64.3, 54.2, 41.0, 38.2, 35.1; MS: *m/z* (M<sup>+</sup>+H) 545. Anal. Calcd for C<sub>27</sub>H<sub>27</sub>ClN<sub>4</sub>O<sub>8</sub>S: C, 53.78; H, 4.52; N, 9.29. Found: C, 53.52; H, 4.35; N, 8.99.

**2-(2-((3*aR*,4*S*,6*S*,6*aS*)-6-((1-(4-Chlorophenyl)-1*H*-1,2,3-triazol-4-yl)methoxy)-2,2-dimethyltetrahydrofuro[3,4-*d*][1,3]dioxol-4-yl)-3-(4-hydroxyphenyl)-4-oxothiazolidin-5-yl)acetic acid (7g).** mp 256–258 °C; IR (KBr)  $\nu$  3532, 3430, 3226, 2973, 2830, 1710, 1616, 1534, 1506, 1411, 1258, 854 cm<sup>-1</sup>; <sup>1</sup>H NMR (300 MHz, CDCl<sub>3</sub>):  $\delta$  11.39 (s, 1H, CO<sub>2</sub>H), 8.22 (d, *J* = 8.7 Hz, 2H, Ar-H), 8.06 (s, 1H, Ar-H), 7.52 (d, *J* = 9.2 Hz, 2H, Ar-H), 7.14–6.87 (m, 4H, Ar-H), 6.14 (s, 1H, CHS), 5.76 (d, *J* = 3.6 Hz, 1H, C<sub>1</sub>H), 5.42 (s, 1H, OH), 4.96 (d, *J* = 5.2 Hz, 1H, CH), 4.51 (t, *J* = 3.9 Hz, 1H, C<sub>2</sub>H), 4.54 (s, 2H, OCH<sub>2</sub>), 3.93–3.96 (m, 1H, C<sub>4</sub>H), 3.26 (dd, *J* = 9.1, 4.2 Hz, 1H, C<sub>3</sub>H), 2.34 (d, 2H, CH<sub>2</sub>), 1.53 (s, 3H, CH<sub>3</sub>), 1.38 (m, 3H, CH<sub>3</sub>); <sup>13</sup>C NMR (75 MHz, CDCl<sub>3</sub>):  $\delta$  173.6, 171.6, 154.1, 143.2, 142.1, 133.6, 131.4, 129.6, 128.1, 122.6, 120.5, 115.4, 112.6, 111.8, 107.6, 106.8, 81.8, 78.6, 76.8, 65.9, 56.9, 42.1, 36.9, 34.3; MS: *m/z* (M<sup>+</sup>+H) 545. Anal. Calcd for C<sub>27</sub>H<sub>27</sub>ClN<sub>4</sub>O<sub>8</sub>S: C, 53.78; H, 4.52; N, 9.29. Found: C, 53.42; H, 4.25; N, 8.79.

## 5. Conclusion

A series of novel triazole linked thiazolidenone derivatives **6a–g** and **7a–g** was prepared and evaluated for their anticancer activity. The screened compound **7b** exhibited potent anticancer activity compared to standard drug at the tested concentrations.

## 6. Acknowledgements

The authors are thankful to CSIR-New Delhi for the financial support (Project funding No: 02(247)15/EMR-II). Director, CSIR- IICT, Hyderabad, India, for NMR and MS spectral analysis and Principal Vaagdevi Degree and PG College for his constant encouragement to carry out research work.

## 7. References

- (a) K. D. Hani, D. A. Leigh, *Chem. Soc. Rev.* **2010**, *39*, 1240–1251. <https://doi.org/10.1039/B901974J>  
 (b) C. O. Kappe, Van der Eycken, E. *Chem. Soc. Rev.* **2010**, *39*, 1280–1290. <https://doi.org/10.1039/B901973C>  
 (c) A. H. El-Sagheer, T. Brown, *Chem. Soc. Rev.* **2010**, *39*, 1388–1405. <https://doi.org/10.1039/b901971p>  
 (d) A. Qin, J. W. Y. Lam, B. Z. Tang, *Chem. Soc. Rev.* **2010**, 2522–2544. <https://doi.org/10.1039/b909064a>  
 (e) M. Meldal, C. W. Tornøe, *Chem. Rev.* **2008**, *108*, 2952–3015. <https://doi.org/10.1021/cr0783479>  
 (f) H. Nandivada, X. Jiang, J. Lahann, *Adv. Mater.* **2007**, *19*, 2197–2208. <https://doi.org/10.1002/adma.200602739>  
 (g) Y. L. Angell, K. Burgess, *Chem. Soc. Rev.* **2007**, *36*, 1674–1689. <https://doi.org/10.1039/b701444a>  
 (h) D. Fournier, R. Hoogenboom, U. S. Schubert, *Chem. Soc. Rev.* **2007**, *36*, 1369–1380. <https://doi.org/10.1039/b700809k>  
 (i) J. E. Moses, A. D. Moorhouse. *Chem. Soc. Rev.* **2007**, *36*, 1249–1262. <https://doi.org/10.1039/B613014N>  
 (j) J. F. Lutz, *Angew. Chem. Int. Ed.* **2007**, *46*, 1018–1125. <https://doi.org/10.1002/anie.200604050>  
 (k) A. Dondoni, *Chem.–Asian J.* **2007**, *2*, 700–708. <https://doi.org/10.1002/asia.200700015>  
 (l) H. C. Kolb, K. B. Sharpless, *Drug Discovery Today*, **2003**, *8*, 1128–1137. [https://doi.org/10.1016/S1359-6446\(03\)02933-7](https://doi.org/10.1016/S1359-6446(03)02933-7)
- A. Brick, J. Muldoon, Y.-C. Lin, J. H. Elder, D. S. Goodsell, A. J. Olson, V. V. Fokin, K. B. Sharpless, C.-H. Wong, *ChemBioChem.* **2003**, *4*, 1246–12148.  
 (b) M. J. Soltis, H. J. Yeh, K. A. Cole, N. Whittaker, R. P. Wersto, E. C. Kohn, *Drug Metab. Dispos.* **1996**, *24*, 799–806.
- (a) W.-Q. Fan, A. R. Katritzky, 1,2,3-Triazoles, In *Comprehensive Heterocyclic Chemistry II*. Edited by A. R. Katritzky, C. W. Rees, V. Scriven, Elsevier, Oxford. **1996**, *4*, 1–126, pp. 905–1006. (b) M. Whiting, J. Muldoon, Y.-C. Lin, S. M. Silverman, W. Lindstrom, A. J. Olson, H. C. Kolb, M. G. Finn, K. B. Sharpless, J. H. Elder, V. V. Fokin, *Angew. Chem. Int. Ed.*, **2006**, *45*, 1435–1439. <https://doi.org/10.1002/anie.200502161>  
 (c) Y. Bourne, H. C. Kolb, Z. Radić, K. B. Sharpless, P. Taylor, P. Marchot, *Proc. Natl. Acad. Sci. U. S. A.* **2004**, *101*, 1449–1454. <https://doi.org/10.1073/pnas.0308206100>  
 (d) W. G. Lewis, G. Green, F. Z. Grynspan, Z. Radić, P. R. Carlier, P. Taylor, M. G. Finn, K. B. Sharpless, *Angew.*

- Chem., Int. Ed.* **2002**, *41*, 1053–1057.  
[https://doi.org/10.1002/1521-3773\(20020315\)41:6<1053::AID-ANIE1053>3.0.CO;2-4](https://doi.org/10.1002/1521-3773(20020315)41:6<1053::AID-ANIE1053>3.0.CO;2-4)
4. R. Huisgen, A. Padwa, *1,3-Dipolar Cycloaddition Chemistry*, ed. Wiley, New York, **1984**, *1*, 1–176.
5. (a) N. A. Al-Maoudi, A. Y. Al-Soud, *Tetrahedron Lett.* **2002**, *43*, 4021–4022.  
[https://doi.org/10.1016/S0040-4039\(02\)00733-5](https://doi.org/10.1016/S0040-4039(02)00733-5)  
(b) B. H. M. Kuijpers, S. Groothuys, A. B. R. Keereweer, P. J. L. M. Quaedflieg, R. H. Blaauw, F. L. van Delft, F. P. J. T. Rutjes, *Org. Lett.* **2004**, *6*, 3123–3126.  
<https://doi.org/10.1021/ol048841o>  
(c) C. Srinivas, X. Fang, Q. Wang, *Tetrahedron Lett.* **2005**, *46*, 2331–2334. <https://doi.org/10.1016/j.tetlet.2005.01.175>  
(d) S. Hotha, R. I. Anegundi, A. A. Natu, *Tetrahedron Lett.* **2005**, *46*, 4585–4588.  
<https://doi.org/10.1016/j.tetlet.2005.05.012>  
(e) S. Hotha, S. Kashyap, *J. Org. Chem.* **2006**, *71*, 364–367.  
<https://doi.org/10.1021/jo051731q>
6. (a) A. K. Jain, A. Vaidya, A. Ravichandran, S. Kashaw, R. Agarwak, *Bioorg. Med. Chem.* **2012**, *20*, 3378–3395.  
<https://doi.org/10.1016/j.bmc.2012.03.069>  
(b) A. Verma, S. Saraf, *Eur. J. Med. Chem.* **2008**, *43*, 897–905. <https://doi.org/10.1016/j.ejmech.2007.07.017>
7. Z. Hongyu, S. Wu, S. Zhai, A. Liu, Y. Sun, R. Li, Y. Zhang, S. Ekins, P. W. Swaan, B. Fang, B. Zhang, B. Yan, *J. Med. Chem.* **2008**, *51*, 1242–1251.  
<https://doi.org/10.1021/jm7012024>
8. (a) M. L. Barreca, J. Balzarini, A. Chimmiri, E. Declerq, L. De Luca, H. D. Holtje, M. Holte, A. M. Monforte, P. Monforte, C. Pannecouque, A. Rao, M. Zappala, *J. Med. Chem.* **2002**, *45*, 5410–5413. <https://doi.org/10.1021/jm020977+>  
(b) A. Rao, J. Balzarini, A. Carbone, A. Chimmiri, E. Declerq, A. M. Monforte, P. Monforte, C. Pannecouque, M. Zappala, *Antiviral Res.* **2004**, *63*, 79–84.  
<https://doi.org/10.1016/j.antiviral.2004.03.004>  
(c) R. K. Rawal, R. Tripathi, S. B. Katti, C. Pannecouque, E. Declerq, *Bio. Org. Med. Chem.* **2007**, *15*, 3134–3142.  
<https://doi.org/10.1016/j.bmc.2007.02.044>
9. G. C. Kuckguzel, J. R. Shchulle, A. Kaocapte, E. Declerq, F. Sahniv, M. Gulluce, *Eur. J. Med. Chem.* **2006**, *41*, 353–359.  
<https://doi.org/10.1016/j.ejmech.2005.11.005>
10. M. V. Diurano, O. Mazzoni, P. E. Calignano, F. Giorodano, A. Bolognase, *J. Med. Chem.* **1992**, *35*, 2910–2912.  
<https://doi.org/10.1021/jm00093a025>
11. (a) T. Archana, V. K. Srivastava, K. Kumar, *Eur. J. Med. Chem.* **2002**, *37*, 873–882.  
[https://doi.org/10.1016/S0223-5234\(02\)01389-2](https://doi.org/10.1016/S0223-5234(02)01389-2)  
(b) C. Dwivedi, S. S. Gupta, S. S. Parmer, *J. Med. Chem.* **1972**, *15*, 553–554.  
<https://doi.org/10.1021/jm00275a031>
12. K. G. Desai, K. R. Desai, *J. Sulfur Chem.* **2006**, *27*, 315–328. <https://doi.org/10.1080/17415990600786409>
13. C. M. Jackson, B. Blass, K. Coburn, L. Dijandjighian, G. Fadaye, A. Fluxe, S. J. Hodson, J. M. Janusz, M. Murawsky, J. M. Ridgeway, R. E. White, S. Wu, *Bio. Org. Med. Chem. Lett.* **2007**, *17*, 282–284.  
<https://doi.org/10.1016/j.bmcl.2006.07.007>
14. (a) V. R. Solomon, C. Hu, H. Lee, *Bio. Org. Med. Chem. Lett.* **2009**, *17*, 7585–7592.  
<https://doi.org/10.1016/j.bmc.2009.08.068>  
(b) B. Muenier, *Acc. Chem. Res.* **2008**, *41*, 69–77.  
<https://doi.org/10.1021/ar7000843>
15. (a) D. Havrlyuk, L. Mosula, B. Zimenkovsky, A. Vasylenko, A. Gzella, R. Lesyk, *Eur. J. Med. Chem.* **2010**, *5*, 5012–5021.  
<https://doi.org/10.1016/j.ejmech.2010.08.008>  
(b) R. Lesyk, O. Vladgimiska, S. Holota, L. Zaprutko, A. Gzella, *Eur. J. Med. Chem.* **2007**, *42*, 641–648.  
<https://doi.org/10.1016/j.ejmech.2006.12.006>  
(c) D. Havrlyuk, N. Kovach, B. Zimmenkovesky, O. Vaseylenko, R. Lesyk, *Arch. Pharm. Chem. Life Sci.* **2011**, *344*, 514–522. <https://doi.org/10.1002/ardp.201100055>  
(d) L. Mosula, B. Zimmenkovesky, D. Havrlyuk, A. V. Missir, I. C. Chiritha, R. Lesyk, *Farmacia*, **2009**, *57*, 321–330.  
(e) D. Kaminsky, O. Vasylenko, D. Atamanyuk, A. Gzella, R. Lesyk, *Synlett.* **2011**, *10*, 1385–1388.
16. (a) C. O. Kappe, *Angew. Chem. Int. Ed.* **2004**, *43*, 6250–6284. <https://doi.org/10.1002/anie.200400655>  
(b) C. O. Kappe, D. Dallinger, *Nat. Rev. Drug Discovery.* **2006**, *5*, 51–63. <https://doi.org/10.1038/nrd1926>
17. Y. Kumar, V. Bahadur, A. K. Singh, V. S. Parmer, E. V. van der Eycken, B. K. Singh, *Beilstein J. Org. Chem.* **2014**, *10*, 113–118.
18. A. Srinivas, M. Sunitha, C. Govind Rao, *Acta Chim. Slov.* **2016**, *63*, 344–350. <https://doi.org/10.17344/acsi.2015.2124>
19. A. Srinivas, *Acta Chim. Slov.* **2016**, *63*, 173–179.  
<https://doi.org/10.17344/acsi.2015.2124>
20. A. Srinivas, M. Sunitha, G. Rajesh Kumar, *Org. Commun.* **2016**, *9*, 1–8.
21. A. Srinivas, M. Sunitha, *Indian J. Chemistry sec B.* **2016**, *55B*, 102–109.
22. A. Srinivas, A. Nagaraj, C. S. Reddy, *Eur. J. Med. Chem.* **2010**, *45*, 2353–2358.  
<https://doi.org/10.1016/j.ejmech.2010.02.014>
23. C. S. Reddy, A. Srinivas, M. Sunitha, A. Nagaraj, *J. Heterocycl. Chem.* **2010**, *47*, 1303–1309.  
<https://doi.org/10.1002/jhet.474>
24. C. S. Reddy, A. Nagaraj, A. Srinivas, G. P. Reddy, *Indian J. Chem.* **2010**, *49B*, 617–622.
25. A. Srinivas, C. S. Reddy, A. Nagaraj, *Chem. Pharm. Bull.* **2009**, *57*, 685–693. <https://doi.org/10.1248/cpb.57.685>
26. C. S. Reddy, A. Srinivas, A. Nagaraj, *J. Heterocycl. Chem.* **2009**, *46*, 497–502. <https://doi.org/10.1002/jhet.100>
27. C. S. Reddy, A. Nagaraj, A. Srinivas, G. P. Reddy, *Indian J. Chem.* **2009**, *48B*, 248–254.
28. C. S. Reddy, A. Srinivas, A. Nagaraj, *J. Heterocycl. Chem.* **2008**, *45*, 1121–1125.  
<https://doi.org/10.1002/jhet.5570450428>
29. C. S. Reddy, G. P. Reddy, A. Nagaraj, A. Srinivas, *Org. Commun.* **2008**, *1*, 84–94.
30. P. A. Levene, G. M. Meyer, *J. Biol. Chem.* **1931**, *92*, 257–262.



## Povzetek

S postopkom sinteze v eni sami posodi smo s pomočjo kondenzacije (3a*S*,4*S*,6*S*,6a*S*)-6-((1-(4-klorofenil)-1*H*-1,2,3-triazol-4-il)metoksi)-2,2-dimetiltetrahydrofuro[3,4-*d*][1,3]dioksol-4-karbaldehida **5** z merkaptokislinami in primarnimi amini v prisotnosti ZnCl<sub>2</sub> pripravili serijo novih hibridnih heterociklov **6a–g** in **7a–g**. Sinteze so bile izvedene tako pod mikrovalovnimi kot tudi konvencionalnimi pogoji segrevanja. Spojino **5** smo pripravili iz di-aceton D-manoze s pomočjo »click« reakcije, s sledečo odstranitvijo primarne acetamidne zaščite in z oksidativnim razcepom. Karakterizacijo novih spojin smo izvedli s pomočjo IR, NMR, MS in elementne analize. Za nove spojine smo določili tudi delovanje proti različnim rakastim celicam.

Scientific paper

# Stability Indicating UHPLC-PDA Assay for Simultaneous Determination of Antazoline Hydrochloride and Naphazoline Hydrochloride in Ophthalmic Formulations

Amir Ali,<sup>1</sup> Umar Farooq,<sup>1</sup> Mahmood Ahmed,<sup>1,\*</sup> Muhammad Makshoof Athar,<sup>1</sup> Kashif Nadeem<sup>2</sup> and Ghulam Murtaza<sup>2</sup>

<sup>1</sup> Institute of Chemistry, University of the Punjab, Lahore-Pakistan 54590

<sup>2</sup> Schazoo Pharmaceutical Laboratories, Lahore-Jaranwala Road, Sheikhpura

\* Corresponding author: E-mail: mahmoodresearchscholar@gmail.com  
tel.:0092 300 8819844

Received: 01-01-2017

## Abstract

In the present study, a newly developed method based on ultrahigh performance liquid chromatography (UHPLC) was optimized for the simultaneous determination of antazoline hydrochloride (ANZ) and naphazoline hydrochloride (NFZ) in ophthalmic formulations. Isocratic separation of ANZ and NFZ was performed at 40 °C with an ACE Excel 2 C18-PFP column (2 μm, 2.1 × 100 mm) at a flow rate of 0.6 mL min<sup>-1</sup> whereas the mobile phase consisted of acetonitrile/phosphate buffer (60:40, v/v, pH 3.0) containing 0.5% triethylamine. Both analytes were detected at a wavelength of 285 nm and the injection volume was 1.0 μL. The overall run time per sample was 4.5 min with retention time of 0.92 and 1.86 min for NFZ and ANZ, respectively. The calibration curve was linear from 0.500–100 μg mL<sup>-1</sup> for ANZ and NFZ with a correlation coefficient ≥ 0.9981 while repeatability and reproducibility (expressed as relative standard deviation) were lower than 1.28 and 2.14%, respectively. In comparison with high-performance liquid chromatography (HPLC), the developed UHPLC method had remarkable advantages over HPLC as the run time was significantly reduced by 3.4-fold with a 5-fold decreased solvent consumption. Forced degradation studies indicated a complete separation of the analytes in the presence of their degradation products providing high degree of method specificity. The proposed UHPLC method was demonstrated to be simple and rapid for the determination of ANZ and NFZ in commercially available ophthalmic formulations providing recoveries between 99.6 and 100.4%.

**Keywords:** Antazoline; naphazoline; allergic conjunctivitis; vasoconstrictor; UHPLC

## 1. Introduction

Antazoline hydrochloride (ANZ), chemically known as *N*-benzyl-*N*-(4,5-dihydro-1*H*-imidazol-2-ylmethyl)aniline hydrochloride (C<sub>17</sub>H<sub>20</sub>ClN<sub>3</sub>) is an imidazoline ligand which acts as histamine H1 receptor antagonist. It has not only a high affinity for 2-adrenoceptors in various tissues, but also binds to non-adrenergic imidazoline sites. ANZ is classified as first generation antihistamine used to reduce congestion of nasal passages and in eye drops in combination with naphazoline (NFZ) to reduce allergic conjunctivitis symptoms.<sup>1–3</sup> Another drug belonging to the imidazole group is naphazoline hydrochloride

(NFZ, C<sub>14</sub>H<sub>15</sub>ClN<sub>2</sub>) which is α-symphathomimetic drug with decongestive and vasoconstrictor properties reducing the mucous membrane swelling rapidly.<sup>4–6</sup> The chemical structures for both drugs are depicted in Fig.1. Until now, NFZ was only analyzed in combination with other drugs than ANZ in ophthalmic formulations using capillary electrophoresis,<sup>7</sup> gas chromatography,<sup>8</sup> spectrofluorimetry,<sup>9</sup> phosphometric,<sup>10</sup> electrochemical<sup>11</sup> detectors coupled to HPLC.<sup>12,13</sup>

To the best of our knowledge, only one first-derivative spectrometric assay for the simultaneous determination of ANZ and NFZ in ophthalmic formulations was published in the literature. ANZ in combination with NFZ

was determined by first derivative spectrometry.<sup>6</sup> However, our goal was to optimize and validate an ultrahigh performance liquid chromatography (UHPLC) based method for the direct simultaneous analysis of ANZ and NFZ in ophthalmic preparations. High performance liquid chromatography (HPLC) is prominent technique in laboratories for the last 30 years but did not keep the pace with the growing demand for a reliable analysis in short time. More samples can be analysed in very short time with reliability and accuracy by UHPLC. Eddy and longitudinal diffusion coefficients in Van Deemter equation play an important role regarding the separation of analytes. These coefficients are directly related to particle size of column packing which results in better resolution.<sup>14–17</sup> The developed method was compared with HPLC to prove its adequacy for pharmaceutical studies with minimum consumption of solvents, high resolution and symmetrical peaks. The UHPLC-based method was validated in accordance to guidelines from the International Conference on Harmonization (ICH)<sup>18–21</sup> and forced degradation studies were conducted to demonstrate the applicability of the proposed UHPLC method.

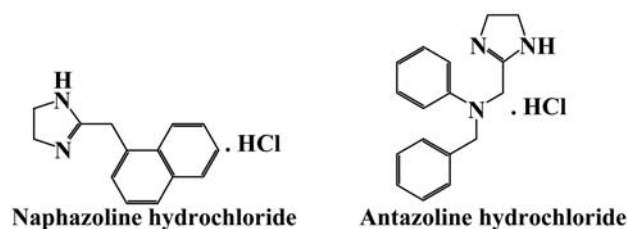


Figure 1. Molecular structures of analytes

## 2. Experimental

### 2.1. Chemicals and Reagents

ANZ, NFZ reference standard were provided by Schazoo Labs (Pakistan). Acetonitrile (ACN), potassium dihydrogen phosphate ( $\text{KH}_2\text{PO}_4$ ), phosphoric acid ( $\text{H}_3\text{PO}_4$ , 85%) and triethylamine (TEA) were supplied by Honeywell (USA). All the chemicals and reagents were of analytical grade while GenPure water system (Thermo Scientific, USA) was used to obtain ultrapure water ( $18 \text{ M}\Omega\cdot\text{cm}^{-1}$ ).

### 2.2. Chromatography

For HPLC analysis, Shimadzu Japan liquid chromatographic system (LC-20A) with diode array detector (SPDM20A), online degasser (DGU-20A5), and equipped with ACE 5 C18 column ( $5 \mu\text{m}$ ,  $4.6 \times 250 \text{ mm}$ ) was used. For UHPLC analysis, Shimadzu Japan, liquid chromatographic system (Nexera 2, LC-30AD), with diode array detector (*i*-DReC, SPD-M30A), online degasser (DGU-20A5), and equipped with ACE Excel 2 C18-PFP column ( $2 \mu\text{m}$ ,  $2.1 \times 100 \text{ mm}$ ) was used. Both systems were equip-

ped with auto sampler (SIL-20AXR) with injection volume ranges between  $0.1\text{--}50 \mu\text{L}$ . Mobile phase comprised of ACN and phosphate buffer pumped in ratio of 60:40 (v/v) at pH 3.0 adjusted by TFA (pH meter, Orion 5 Star, Thermo Scientific, UK).  $5.0 \mu\text{L}$  and  $1.0 \mu\text{L}$  injection volume was injected and flow rate set at  $1.0$  and  $0.6 \text{ mL min}^{-1}$  for HPLC and UHPLC, respectively. The detection was carried out at  $25 \text{ }^\circ\text{C}$  and  $40 \text{ }^\circ\text{C}$ , respectively, for HPLC and UHPLC with best selected wavelength of  $285 \text{ nm}$  by *i*-DReC (detector). Shimadzu LC program (Lab Solutions software) was used to record chromatograms, peak quantification and integration. Mobile phase, standard solutions and samples were filtered through nylon filter ( $0.45 \mu\text{m}$ , Sartorius, Germany) before injection into chromatographic system.

### 2.3. Standard and Working Solutions

Individual stock standard solutions of ANZ and NFZ ( $1000 \mu\text{g mL}^{-1}$ ) were prepared in methanol and placed in an ultrasonic bath for 15 min. Subsequently, working solutions were prepared by serial dilution of the individual stock standard solutions with the mobile phase. Mixed standard solution of ANZ ( $2.50 \mu\text{g mL}^{-1}$ ) and NFZ ( $50.0 \mu\text{g mL}^{-1}$ ) were also prepared in the same manner.

### 2.4. Solution for Forced Degradation Studies

Forced degradation studies were conducted with ANZ or NFZ solutions at a final concentration of  $50.0 \mu\text{g mL}^{-1}$ . For mild stress conditions the solutions were treated with  $0.1 \text{ M HCl}$  and  $0.1 \text{ M NaOH}$  for acidic and basic hydrolysis for 1 h,  $3\% \text{ H}_2\text{O}_2$  was employed for oxidative stress (1 h), while photolytic and thermal stress tests were performed after exposing the solid form for 6 h under UV ( $254 \text{ nm}$ ) or kept at  $100 \text{ }^\circ\text{C}$ , respectively. In contrast for drastic stress conditions,  $1 \text{ M HCl}$  and  $1 \text{ M NaOH}$  were utilized for acidic and basic hydrolysis for 10 h,  $30\% \text{ H}_2\text{O}_2$  was employed for oxidative stress (10 h), whereas photolytic and thermal degradation were evaluated after exposing the solid form for 24 h under UV ( $254 \text{ nm}$ ) or kept at  $100 \text{ }^\circ\text{C}$ , respectively.

### 2.5. Analysis of Ophthalmic Preparation

Curall-A<sup>®</sup> and Orbaclear<sup>®</sup> eye drops both contain  $0.5\%$  of ANZ ( $5.00 \text{ mg mL}^{-1}$ ) and  $0.025\%$  of NFZ ( $0.250 \text{ mg mL}^{-1}$ ). Suitable aliquots of each commercially available product was diluted with methanol, sonicated for 15 min and was further diluted with mobile phase prior to UHPLC analysis.<sup>22,23</sup>

### 2.6. Validation Studies

Validation studies were performed to characterize the proposed analytical method including specificity, linearity, accuracy, precision, limit of detection (LOD), li-

mit of quantitation (LOQ) and conformity of chromatographic parameters (tailing factor, selectivity factor, resolution, theoretical plates). Conformity of chromatographic conditions are basically system suitability tests which are the foremost part of validation studies.

### Specificity

Analysis of placebo (aqueous based sodium chloride and benzalkonium chloride) was performed to assess the specificity of the proposed method. Moreover, the forced degradation study is also another parameter which was performed to prove the specificity of chromatographic method.<sup>21,24</sup>

### 2. 6. 1. Linear Dynamic Range

For both LC-based methods (HPLC and UHPLC), the linear dynamic range was selected within 0.500–100  $\mu\text{g mL}^{-1}$  for both analytes. A linear calibration curve in the form of  $y = ax + b$  was obtained by plotting the peak area  $y$  against the nominal concentration  $x$  of seven concentrations (0.500, 2.50, 12.5, 25.0, 50.0, 75.0 and 100  $\mu\text{g/mL}$ ) whereas  $a$  represented the slope of the calibration curve and  $b$  indicated the intercept.

### 2. 6. 2. Accuracy and Precision

The accuracy of each method was determined in triplicate by spiking a known amount of analyte standard solution in the dosage form resulting in final concentrations of 2.50, 5.00 and 7.50  $\text{mg mL}^{-1}$  for ANZ, whereas NFZ was spiked at 0.125, 0.250 and 0.375  $\text{mg mL}^{-1}$ . This represented 50, 100 and 150% of each analyte in the dosing formulation. For precision determination, ANZ as well as

NFZ were spiked at 4.00, 5.00, 6.00  $\text{mg mL}^{-1}$  and 0.200, 0.250, 0.300  $\text{mg mL}^{-1}$ , respectively, representing 80, 100 and 120% of each analyte. The intra-day precision (repeatability) was evaluated by replicates of five on one day whereas the inter-day precision (reproducibility) was determined over three consecutive days.

### 2. 6. 3. Method's LOD/LOQ

ANZ and NFZ standard solution was injected in replicates of six. The resultant parameters of the linear regression including the standard deviation (SD) of the response based upon the slope  $a$  and intercept  $b$  determined the LOD and LOQ of the UHPLC method. The LOD and LOQ were defined as three times and ten times the SD of the intercept, respectively.<sup>25–28</sup>

### 2. 6. 4. Method Robustness

Small but deliberate changes in chromatographic conditions such as mobile phase, pH, column temperature and flow rate were used to evaluate the robustness of proposed UHPLC method.

## 3. Results and Discussion

### 3. 1. Optimization of Chromatographic Conditions

System suitability tests were performed to optimize both LC-based methods. In the first step, a UV absorption spectrum was acquired in the range of 200–400 nm resulting in a maximum absorbance at 285 nm for both analy-

**Table 1.** Results of tested stationary phases

HPLC					
Column	Drug	$R_s$	$T_f$	$\alpha$	N
Hypersil ODS (250 × 4.6 mm, 5 $\mu\text{m}$ )	ANZ	3.66	1.27	2.14	4521
	NFZ	–	1.36	–	5043
Venusil XBP C18 (250 × 4.6 mm, 5 $\mu\text{m}$ )	ANZ	4.66	1.21	2.35	3203
	NFZ	–	1.34	–	4597
ACE 5 C18 (250 × 4.6 mm, 5 $\mu\text{m}$ )	ANZ	8.92	1.17	2.32	5432
	NFZ	–	1.13	–	6162
Purespher® RP-18 (250 × 4.6 mm, 5 $\mu\text{m}$ )	ANZ	0.89	2.27	1.13	3576
	NFZ	–	1.66	–	3278
UHPLC					
ACE Excel 2 C18-PFP (100 × 2.1 mm, 2 $\mu\text{m}$ )	ANZ	3.43	0.97	2.27	17289
	NFZ	–	0.94	–	18521
Waters ACQUITY 1.7 BEH C 18 (100 × 2.1 mm, 2 $\mu\text{m}$ )	ANZ	1.09	2.07	0.87	13098
	NFZ	–	1.83	–	11832
Agilent Poroshell 2.7 120 EC C18 (100 × 2.1 mm, 2 $\mu\text{m}$ )	ANZ	1.01	2.23	0.88	12094
	NFZ	–	1.45	–	11095
Phenomenex Kinetex 2.6 C18 (100 × 2.1 mm, 2 $\mu\text{m}$ )	ANZ	0.92	2.07	0.93	10654
	NFZ	–	1.44	–	13294

tes. Different compositions (60:40, 50:50, 40:60 and 30:70, *v/v*) of the mobile phase (ACN: phosphate buffer) were examined to optimize the chromatographic conditions including tailing factor, selectivity factor, resolution, theoretical plates to get compliance with the ICH guidelines. Different columns were also tested for HPLC analysis including ACE 5 C18, Venusil XBP C18, Hypersil ODS and Purespher® RP-18 while ACE Excel 2 C18-PFP, Waters ACQUITY 1.7 BEH C 18, Agilent Poroshell 2.7 120 EC C18 and Phenomenex Kinetex 2.6 C18 were employed with UHPLC at different pH (3.0, 4.0, 5.0 and 6.0). Free silanol in column packing could be interacting with drugs of both acidic as well as of basic nature. In order to improve the peak shapes, TEA, a silanol blocker,

was added to the mobile phase (0.5%, *v/v*).<sup>29</sup> Silanol blocker provided additional selectivity by  $\pi$ - $\pi$  and dipole interaction which resulted in achieving the better overall resolution. The summary of the tailing factor, selectivity factor, resolution and theoretical plates for each of the tested columns are presented in Table 1.

In the end, the mobile phase consisting of ACN and phosphate buffer (10 mM) in a ratio of 60:40 (*v/v*) with the addition of 0.5% TEA was found to be excellent using ACE 5 C18 and ACE Excel 2 C18-PFP columns for UHPLC and HPLC analysis, respectively. The chromatographic parameters under final conditions are summarized in Table 2 exhibiting an excellent peak shape, resolution and higher number of theoretical plates.

**Table 2.** System suitability test parameters

Parameters	Analyte/Technique			
	HPLC		UHPLC	
	ANZ	NFZ	ANZ	NFZ
Retention time ( $t_R$ in min)	6.45	3.21	1.86	0.92
Tailing factor (T)	1.17	1.13	0.97	0.94
Resolution (Rs)	8.92	–	3.43	–
Selectivity factor ( $\alpha$ )	2.32	–	2.27	–
Theoretical plates (N)	5432	6182	17289	18521
% RSD of Retention Time ( $t_R$ )	0.003	0.002	0.002	0.004

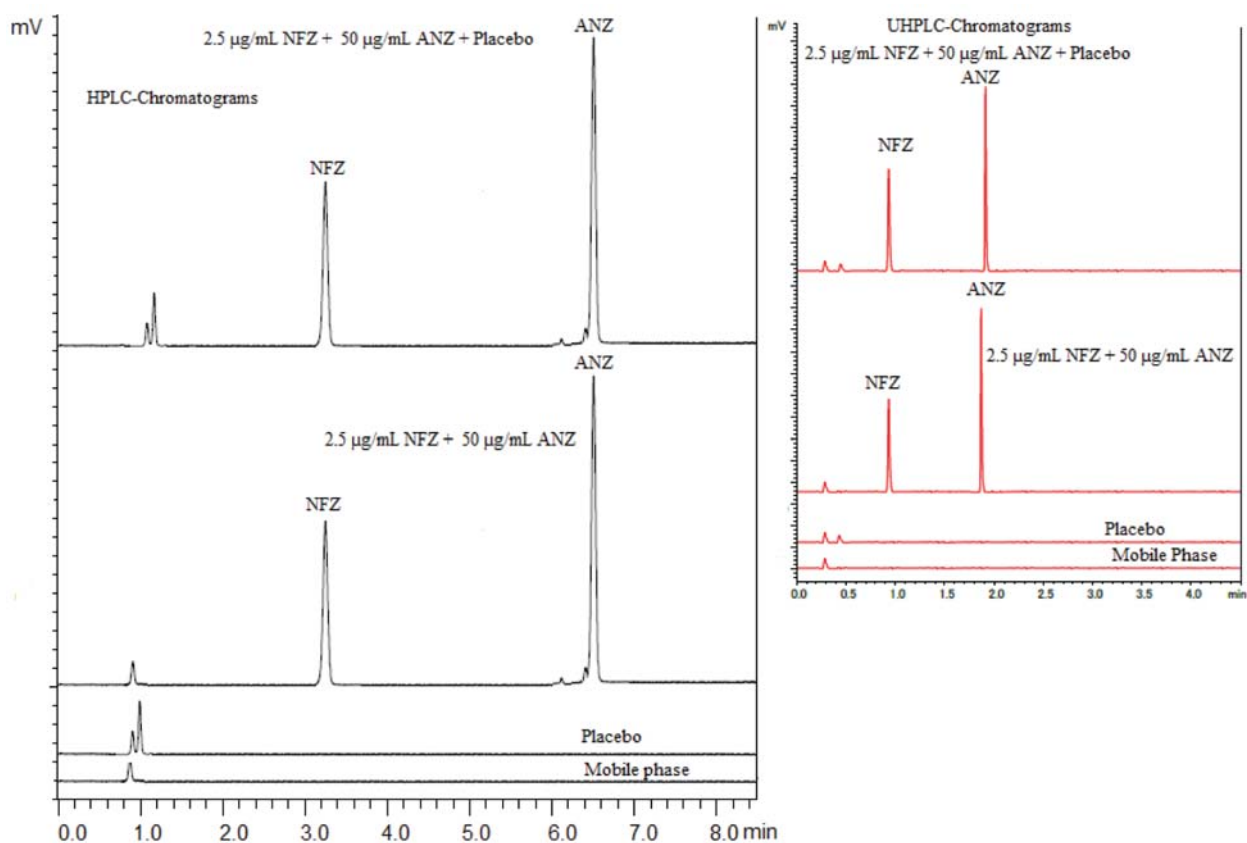


**Figure 2.** Typical HPLC and UHPLC Chromatograms of mobile phase, placebo, ANZ and NFZ

### 3. 2. Validation Studies

The specificity of the optimized UHPLC method was examined with NFZ and ANZ at 2.50 and 50.00  $\mu\text{g mL}^{-1}$ , respectively, relative to the blank mobile phase (Fig. 2).

The presence of placebo did not interfere during the determination of ANZ and NFZ as the components were baseline separated. For both chromatographic methods over a dynamic range of 0.5–100  $\mu\text{g mL}^{-1}$ , seven concen-

trations (0.5, 2.5, 12.5, 25, 50, 75, 100  $\mu\text{g mL}^{-1}$ ) were employed to construct a calibration graph for ANZ and NFZ. The calibration curves were linear for ANZ and NFZ with a coefficient of determination ( $r^2$ )  $\geq 0.9981$  regardless of the LC-based method (Table 3). Accuracy of methods by both the techniques under investigation was performed by evaluating the recovery studies after spiking the known amount of standard drugs in commercial products.

**Table 3.** Statistical evaluation of regression data of ANZ and NFZ by HPLC and UHPLC

Parameters	Analyte/Technique			
	HPLC		UHPLC	
	ANZ	NFZ	ANZ	NFZ
Linearity range ( $\mu\text{g/mL}$ )	0.5–100	0.5–100	0.5–100	0.5–100
Slope	6.0615	0.7585	0.5854	0.6854
Intercept	23.303	32.745	134.52	104.52
Standard error of slope	$1.01 \times 10^{-2}$	$5.41 \times 10^{-3}$	$3.1 \times 10^{-2}$	$4.21 \times 10^{-2}$
Standard error of intercept	0.163	0.087	1.132	1.932
Coefficient of determination ( $r^2$ )	0.9991	0.9989	0.9984	0.9981
Limit of detection ( $\mu\text{g mL}^{-1}$ )	0.078	0.041	0.052	0.029
Limit of quantification ( $\mu\text{g mL}^{-1}$ )	0.261	0.137	0.174	0.097

**Table 4.** Accuracy studies of ANZ and NFZ by HPLC and UHPLC

Drugs	Spiked concentration ( $\text{mg mL}^{-1}$ )	HPLC		UHPLC	
		<sup>a</sup> Concentration found ( $\text{mg mL}^{-1}$ ) $\pm$ SEM; RSD	Recovery (%)	<sup>a</sup> Concentration found ( $\text{mg mL}^{-1}$ ) $\pm$ SEM; RSD	Recovery (%)
ANZ	2.500	2.531 $\pm$ 0.021; 1.18	101.2	2.552 $\pm$ 0.022; 1.48	102.0
	5.000	5.071 $\pm$ 0.018; 0.71	101.4	5.081 $\pm$ 0.021; 0.71	101.6
	7.500	7.483 $\pm$ 0.017; 0.43	99.7	7.572 $\pm$ 0.014; 0.33	100.9
NFZ	0.125	0.127 $\pm$ 0.002; 2.08	101.6	0.126 $\pm$ 0.002; 2.55	100.8
	0.250	0.256 $\pm$ 0.001; 0.98	102.4	0.258 $\pm$ 0.002; 1.16	103.2
	0.375	0.379 $\pm$ 0.004; 1.98	101.1	0.379 $\pm$ 0.001; 0.40	101.1

<sup>a</sup> All measurements were made in triplicate SEM: Standard error mean RSD: Relative standard deviation

**Table 5.** Precision studies of ANZ and NFZ by HPLC and UHPLC

Technique: HPLC						
Drugs	Repeatability (n = 5)		Reproducibility (n = 5)			
	Concentration ( $\text{mg mL}^{-1}$ )	Concentration found ( $\text{mg mL}^{-1}$ ) $\pm$ SEM; RSD	Concentration found ( $\text{mg mL}^{-1}$ ) $\pm$ SEM; RSD			
			Day 1	Day 2	Day 3	
ANZ	4.0	3.941 $\pm$ 0.031; 1.45	3.922 $\pm$ 0.01; 0.61	3.931 $\pm$ 0.020; 1.41	4.013 $\pm$ 0.021; 1.03	
	5.0	4.910 $\pm$ 0.011; 0.42	4.951 $\pm$ 0.02; 0.84	4.991 $\pm$ 0.020; 1.00	5.021 $\pm$ 0.032; 1.19	
	6.0	5.982 $\pm$ 0.061; 1.70	5.992 $\pm$ 0.03; 1.20	5.992 $\pm$ 0.020; 0.80	6.041 $\pm$ 0.031; 1.01	
NFZ	0.20	0.192 $\pm$ 0.002; 1.88	0.198 $\pm$ 0.002; 2.30	0.205 $\pm$ 0.003; 2.23	0.204 $\pm$ 0.002; 1.98	
	0.25	0.246 $\pm$ 0.001; 1.02	0.258 $\pm$ 0.002; 1.72	0.253 $\pm$ 0.002; 1.97	0.252 $\pm$ 0.001; 1.29	
	0.30	0.291 $\pm$ 0.001; 0.72	0.299 $\pm$ 0.003; 2.49	0.306 $\pm$ 0.003; 1.88	0.301 $\pm$ 0.001; 0.98	
Technique: UHPLC						
ANZ	4.0	4.050 $\pm$ 0.021; 1.28	4.000 $\pm$ 0.021; 1.02	4.010 $\pm$ 0.021; 1.19	4.030 $\pm$ 0.011; 0.54	
	5.0	5.020 $\pm$ 0.020; 0.80	5.030 $\pm$ 0.022; 0.79	5.030 $\pm$ 0.012; 0.42	5.010 $\pm$ 0.012; 0.39	
	6.0	5.990 $\pm$ 0.022; 0.84	6.010 $\pm$ 0.021; 0.78	5.980 $\pm$ 0.011; 0.42	5.990 $\pm$ 0.022; 0.74	
NFZ	0.20	0.201 $\pm$ 0.001; 1.20	0.203 $\pm$ 0.002; 1.67	0.204 $\pm$ 0.001; 1.64	0.203 $\pm$ 0.002; 2.14	
	0.25	0.252 $\pm$ 0.001; 0.93	0.249 $\pm$ 0.001; 1.08	0.251 $\pm$ 0.001; 1.08	0.253 $\pm$ 0.001; 1.23	
	0.30	0.301 $\pm$ 0.001; 0.97	0.301 $\pm$ 0.001; 0.54	0.299 $\pm$ 0.001; 0.81	0.301 $\pm$ 0.002; 1.35	

The recovery results were obtained between the ranges 99.7–102.4% and 100.8–103.2% (Table 4) for HPLC and UHPLC respectively which justified the suitability of the techniques for their intended applications. For precision studies, the results of repeatability and reproducibility are presented in Table 5 by injecting three different concentrations (80, 100 and 120% level of analyte) of standard solutions of ANZ and NFZ ( $n = 5$ ) on same day and three consecutive days, respectively.

RSD values for repeatability and reproducibility were obtained less than 1.88 and 2.49, respectively, for HPLC while below than 1.28 for repeatability and 2.14 for reproducibility assays with UHPLC.

### 3. 3. Forced Degradation Studies

Forced degradation studies under mild and drastic conditions were performed to demonstrate the applicability of our UHPLC method to assess the stability of the drug. For each forced degradation experiment, the corresponding chromatograms are depicted in Figure 3 and 4, whereas the percentage of initial drug substance is shown in Table 6. The ANZ and NFZ stock solutions were diluted in separate measuring flasks with HCl (0.1 M and 1.0 M), NaOH (0.1 M and 1.0 M) and H<sub>2</sub>O<sub>2</sub> (3.0 and 30%) to a final concentration of 50.0  $\mu\text{g mL}^{-1}$  and incubated for 1 h and 10 h for mild and drastic stress, respectively. For both mild and drastic conditions, no degradations (Figs. 3 and 4) were observed for ANZ and NFZ under acidic stress and the extent of degradation was declared as none (Table 6).

In contrast, basic stress was found more effective than acidic one. Under mild conditions, there was only a slight extent of degradation and the remaining concentration of ANZ and NFZ compared to their initial values were 96.1% and 95.2%, respectively. Two impurity peaks at retention times  $t_R = 0.6$  min and  $t_R = 1.35$  min (FD1 and

FD2, Fig. 3b) were observed after basic degradation of NFZ, while one impurity peak at  $t_R = 2.25$  min (FD1, Fig. 4b) was observed for ANZ degradation under basic stress conditions. For drastic conditions, substantial amount of both ANZ and NFZ were degraded and remaining amount of 22.6% and 48.8% was found respectively under basic stress conditions. Two impurities peaks for each of ANZ and NFZ were observed at  $t_R = 0.9$  min,  $t_R = 2.35$  min (FD1 and FD2, Fig. 4g) and  $t_R = 1.08$  min,  $t_R = 1.35$  min (FD1 and FD2, Fig. 3g), respectively. The addition of 3% H<sub>2</sub>O<sub>2</sub> did not show any effect on ANZ but NFZ was degraded substantially and remaining amount obtained was 74.6% with impurities at  $t_R = 0.55$  min,  $t_R = 0.71$  min (FD1 and FD2, Fig. 3c). After treatment with 30% H<sub>2</sub>O<sub>2</sub>, slight degradation of ANZ (remaining amount 94.8%) and substantial degradation of NFZ (remaining amount 71.1%) were observed. Two peaks at  $t_R = 0.55$  min,  $t_R = 0.68$  min (FDD1 and FDD2, Fig. 3h) were obtained as degradation products of NFZ, while at  $t_R = 0.95$  min degradation product of ANZ was obtained (FDD1, Fig. 4h). Solid form of both analytes was kept at 100 °C in oven for thermal and under UV light at 254 nm for photolytic degradation.

NFZ degraded substantially under mild and drastic thermal stress conditions with two impurity peaks at  $t_R = 0.65$  min,  $t_R = 1.31$  min (Fig. 3d and 3i). In contrast, no ANZ degradation was observed under mild thermal stress, whereas substantial amount of ANZ degraded under drastic conditions (remaining amount 64.9%), indicated by an impurity at  $t_R = 0.95$  min (FDD1, Fig. 4i). No photolytic degradation resulted for ANZ and NFZ under mild conditions. However under drastic photolytic stress, substantial degradation of ANZ and NFZ resulted in an impurity peak at  $t_R = 0.95$  min and  $t_R = 0.60$  min, respectively (Fig 3j and 4j). As a result of these experiments, the proposed UHPLC method was found to be specific for the analysis of ANZ and NFZ including their degradation products.

**Table 6.** Forced degradation results of ANZ and NFZ by UHPLC

Stress conditions	Amount remaining <sup>a</sup> Mean $\pm$ SEM (%)		Extent of degradation		
	ANZ	NFZ	ANZ	NFZ	
Mild conditions	0.1M HCl (1 h)	99.9 $\pm$ 0.04	99.8 $\pm$ 0.04	None	None
	0.1M NaOH (1 h)	96.1 $\pm$ 0.09	95.2 $\pm$ 0.25	Slight	Slight
	3% H <sub>2</sub> O <sub>2</sub> (1 h)	98.6 $\pm$ 0.09	74.6 $\pm$ 0.05	None	Substantial
	6 h under 100 °C	99.6 $\pm$ 0.01	63.6 $\pm$ 0.02	None	Substantial
	6 h under UV-254	99.1 $\pm$ 0.01	99.0 $\pm$ 0.19	None	None
Drastic conditions	1.0 M HCl (10 h)	99.4 $\pm$ 0.04	99.7 $\pm$ 0.01	None	None
	1.0 M NaOH (10 h)	22.6 $\pm$ 0.16	48.8 $\pm$ 0.14	Substantial	Substantial
	30% H <sub>2</sub> O <sub>2</sub> (10 h)	94.8 $\pm$ 0.19	71.1 $\pm$ 0.09	Slight	Substantial
	24 h under 100 °C	64.9 $\pm$ 0.15	63.3 $\pm$ 0.18	Substantial	Substantial
	24 h under UV-254	89.1 $\pm$ 0.11	87.7 $\pm$ 0.05	Substantial	Substantial

<sup>a</sup> All measurements were made triplicate

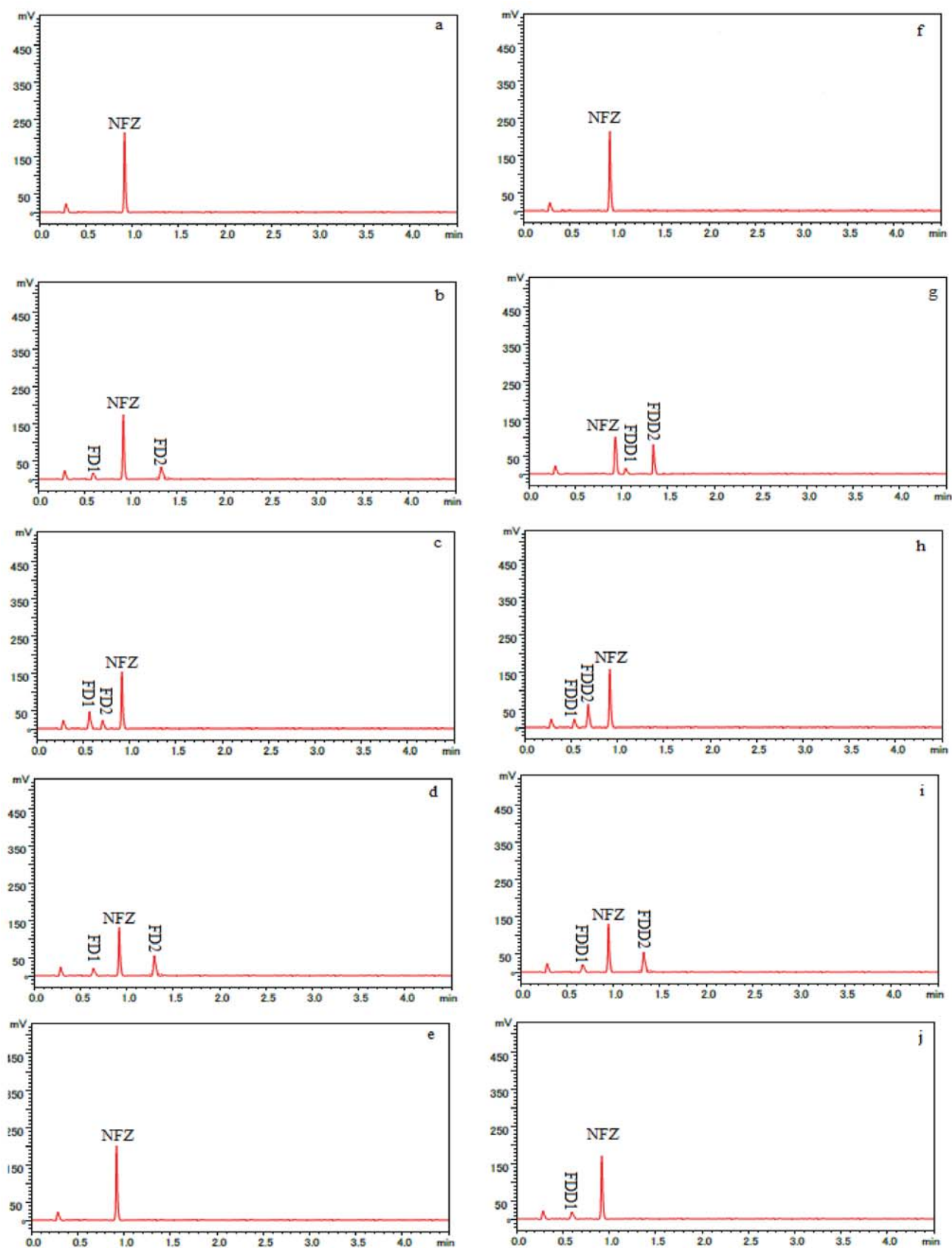


**Figure 3.** Typical UHPLC chromatograms of pure bulk sample of NFZ ( $50 \mu\text{g mL}^{-1}$ ) under stress conditions. Mild stress conditions: (a) acidic (b) basic (c) oxidative (d) thermal (e) photolytic. Drastic stress conditions: (f) acidic (g) basic (h) oxidative (i) thermal (j) photolytic.



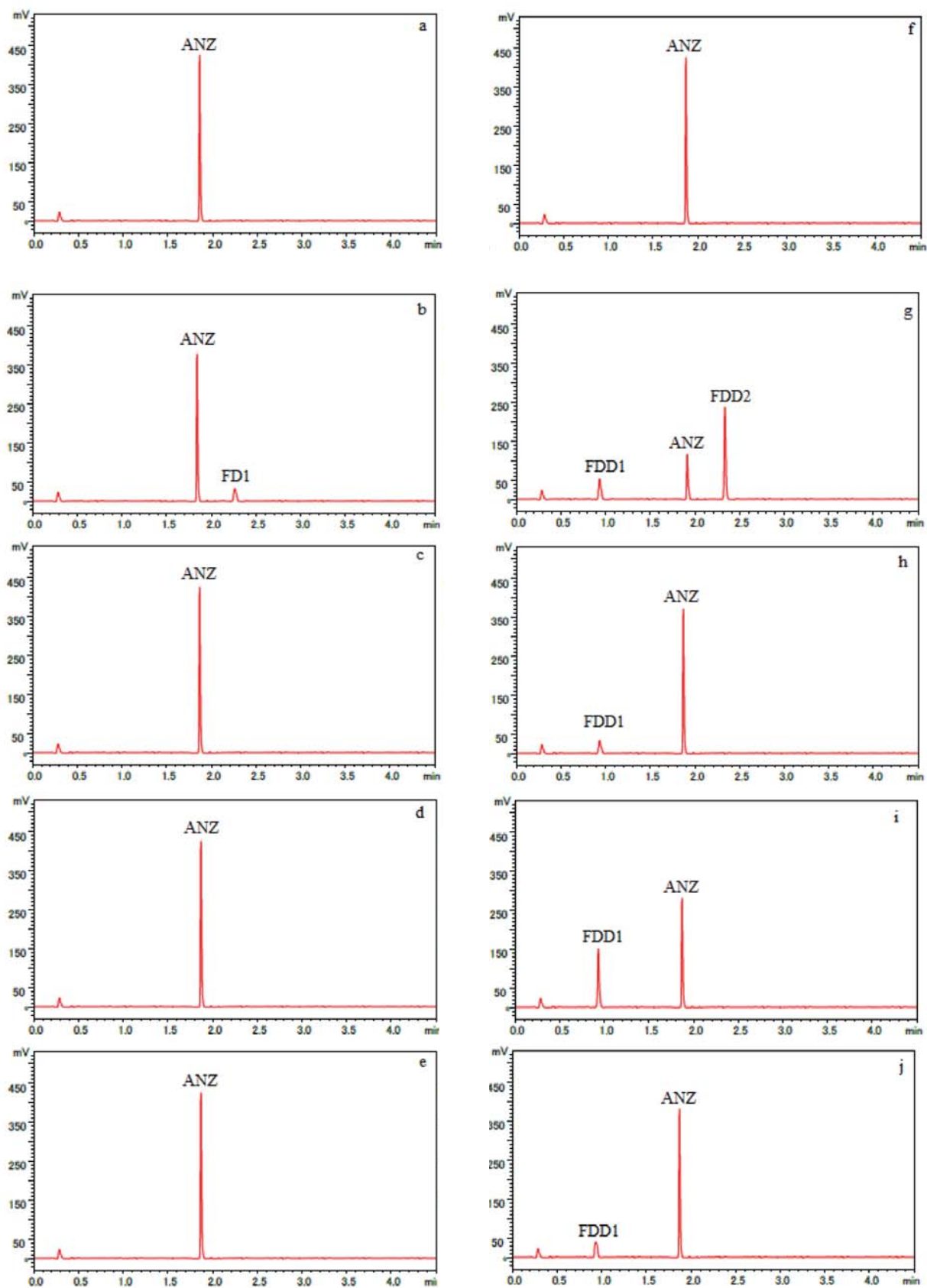


**Figure 4.** Typical UHPLC chromatograms of pure bulk sample of ANZ ( $50 \mu\text{g mL}^{-1}$ ) under stress conditions. Mild stress conditions: (a) acidic (b) basic (c) oxidative (d) thermal (e) photolytic. Drastic stress conditions: (f) acidic (g) basic (h) oxidative (i) thermal (j) photolytic.

### 3. 4. Method Robustness

The robustness of proposed the UHPLC method was evaluated by slight changes of the chromatographic parameters including the flow rate ( $\pm 0.1 \text{ mL min}^{-1}$ ), the mobile phase ratio ( $\pm 5.0 \text{ mL}$ ) including its pH ( $\pm 0.1$ ), the column temperature ( $\pm 5 \text{ }^\circ\text{C}$ ) and the detection wavelength ( $\pm 2 \text{ nm}$ ). Afterwards, the drug content besides chromatographic parameters like retention time, tailing factor, number of theoretical plates and resolution were determined. The results summarized in Table 7 demonstrated that the effects of the deliberate changes in chromatographic conditions are neglectable and that the proposed UHPLC method was robust for its intended applications.<sup>17</sup>

### 3. 5. Analysis of Commercial Ophthalmic Formulations

The applicability of proposed UHPLC method was evaluated by examining the commercial ophthalmic solutions (Curall-A<sup>®</sup> and Orbaclear<sup>®</sup>) with reported concentration of  $5.0 \text{ mg mL}^{-1}$  of ANZ and  $0.25 \text{ mg mL}^{-1}$  of NFZ. It was ensured that the removal of the excipients with an extraction step before analysis was unnecessary. It was concluded that the proposed UHPLC method was sufficiently accurate and precise (Table 8) with recovery and RSD ranges found between 99.6–100.4% and 1.03–1.20%, respectively.

## 4. Conclusion

In literature, UHPLC method for simultaneous determination of ANZ and NFZ in pharmaceutical formulations is not available. For this reason, stability indicating UHPLC method was fully validated according to ICH guidelines for determination of ANZ and NFZ in ophthalmic formulations. Remarkable advantages of UHPLC over HPLC were found, such as rapidity, ease of operation, minimum amount of solvents and high selectivity. Good recoveries, interference free and highly reproducible chromatograms were achieved. The proposed method was optimized and found suitable for quality control laboratories where time and economy are essentially required. Good recovery results showed that the proposed methods were free from interferences of commonly used excipients and additives in the formulations.

## 5. References

1. M. Gumustas, U. Alshana, N. Ertas, N. G. Goger, S. A. Ozkan, B. Uslu, *J. Pharm. Biomed. Anal.* **2016**, *124*, 390–398. <https://doi.org/10.1016/j.jpba.2016.02.032>
2. R. Wang, Y. Chu, X. Li, B. Wan, T. Yu, L. Wang, L. Hao, M. Guo, *Biomed. Chromatogr.* **2013**, *27*, 1595–1602. <https://doi.org/10.1002/bmc.2965>
3. S. C. Sweetman, *Martindale: the complete drug reference*.

Table 7. Robustness study of ANZ and NFZ by UHPLC

Chromatographic conditions	NFZ				ANZ				
	Assay (%)	$t_R$ (min)	N	TF	Assay (%)	$t_R$ (min)	N	TF	Rs
Flow rate:0.7	101.3	0.90	18540	0.95	101.2	1.85	17265	0.93	3.47
Flow rate:0.5	100.2	0.96	18351	0.99	99.8	1.88	17233	0.98	3.41
Mobile phase (65:35)	100.1	0.91	18040	0.93	99.1	1.87	17865	0.99	3.47
Mobile phase (55:45)	99.5	0.93	18259	0.98	99.8	1.87	17223	0.93	3.41
Column temp. (45 °C)	99.3	0.95	18390	0.97	101.3	1.89	17444	0.96	3.41
Column temp. (35 °C)	100.1	0.93	18287	0.96	100.1	1.81	17304	0.98	3.38
Wavelength (287 nm)	100.2	0.92	18289	0.99	100.2	1.87	17109	0.94	3.44
Wavelength (283 nm)	100.4	0.91	18401	0.96	100.3	1.86	17119	0.95	3.45
pH: 3.1	99.9	0.94	18540	0.96	100.4	1.88	17165	0.94	3.42
pH: 2.9	99.8	0.92	18387	0.93	100.3	1.89	17338	0.95	3.45

$t_R$ : Retention time, N: theoretical plates, TF: tailing factor, Rs: resolution

Table 8. Assay result of ANZ and NFZ by UHPLC in commercial ophthalmic formulations

Product	Contents (mg mL <sup>-1</sup> )	Label claim (mg mL <sup>-1</sup> ) $\pm$ SEM; RSD	<sup>a</sup> Concentration found	Recovery (%)
Curall-A <sup>®</sup>	ANZ	5.00	$5.010 \pm 0.02$ ; 1.20	100.2
	NFZ	0.25	$0.249 \pm 0.001$ ; 1.12	99.6
Orbaclear <sup>®</sup>	ANZ	5.00	$4.990 \pm 0.02$ ; 1.19	99.8
	NFZ	0.25	$0.251 \pm 0.001$ ; 1.03	100.4

<sup>a</sup>Results are expressed as average of ten measurements

- (Pharmaceutical press, 2009).
4. T. Huang, N. Chen, D. Wang, Y. Lai, Z. Cao, *Chem. Cent. J.* **2014**, *8*, 1. <https://doi.org/10.1155/2014/762954>
  5. R. Hajjan, N. Shams, I. Kaedi, *Journal of Chemistry* **2010**, *7*, 1530–1538.
  6. E. Sourji, M. Amanlou, H. Farsam, A. Afshari, *Chem. Pharm. Bull.* **2006**, *54*, 119–122. <https://doi.org/10.1248/cpb.54.119>
  7. A. Marchesini, M. Williner, V. Mantovani, J. Robles, H. Goicoechea, *J. Pharm. Biomed. Anal.* **2003**, *31*, 39–46. [https://doi.org/10.1016/S0731-7085\(02\)00600-3](https://doi.org/10.1016/S0731-7085(02)00600-3)
  8. M. Massaccesi, *Pharm. Acta Helv.* **1987**, *62*, 302–305.
  9. C. M. Peralta, R. A. Silva, L. P. Fernández, A. N. Masi, *Luminescence* **2011**, *26*, 689–695. <https://doi.org/10.1002/bio.1297>
  10. B. C. Díaz, S. C. Terrones, A. S. Carretero, J. M. C. Fernández, A. F. Gutiérrez, *Anal. Bioanal. Chem.* **2004**, *379*, 30–34. <https://doi.org/10.1007/s00216-004-2533-1>
  11. E. Y. Frag, G. G. Mohamed, F. N. El-Dien, M. E. Mohamed, *Analyst* **2011**, *136*, 332–339. <https://doi.org/10.1039/C0AN00343C>
  12. G. Santoni, A. Medica, P. Gratteri, S. Furlanetto, S. Pinzauti, *Farmaco (Societa chimica italiana: 1989)* **1994**, *40*, 751–754.
  13. A. Jonczyk, I. Wilczynska-Wojtulewicz, *Acta Pol. Pharm.* **1994**, *51*, 115–118.
  14. S. Noreen, M. Ahmed, M. A. Qadir, S. Shahzad, M. I. Shafiq, A. M. Mumtaz, A. Ali, *Lat. Amer. J. Pharm.* **2016**, *35*, 937–944.
  15. S. A. Ahmad, M. Ahmed, M. A. Qadir, M. I. Shafiq, Y. Safa, N. Awan, S. Shahzad, A. Ali, M. Feroz, Z. U. Khokhar, *Lat. Amer. J. Pharm.* **2016**, *35*, 1626–1633.
  16. M. A. Qadir, M. Ahmed, M. I. Shafiq, A. Ali, A. Sadiq, *J. AOAC Int.* **2016**, *99*, 1191–1196. <https://doi.org/10.5740/jaoacint.16-0026>
  17. M. A. Qadir, M. Ahmed, M. S. Tahir, A. Shakoore, M. I. Shafiq, S. Shahzad, A. Ali, *Lat. Amer. J. Pharm.* **2016**, *35*, 869–876.
  18. I. E. W. Group, presented at the Proceedings of the International Conference on Harmonisation of Technical Requirements for Registration of Pharmaceuticals for Human Use, 2005 (unpublished).
  19. I. H. T. Guideline, *QIA (R2), current step* **2003**, *4*.
  20. M. Gumustas, S. Kurbanoglu, B. Uslu, S. A. Ozkan, *Chromatographia* **2013**, *76*, 1365–1427. <https://doi.org/10.1007/s10337-013-2477-8>
  21. M. Gumustas, G. Coskun, S. A. Ozkan, *Rev. Roum. Chim* **2015**, *60*, 477–490.
  22. M. A. Qadir, M. Ahmed, S. Shahzad, M. I. Shafiq, S. S. Razaq, A. Gulzar, A. Ali, *Lat. Amer. J. Pharm.* **2016**, *35*, 912–920.
  23. M. Gumustas, B. Uslu, S. A. Ozkan, H. Y. Aboul-Enein, *Chromatographia* **2014**, *77*, 1721–1726. <https://doi.org/10.1007/s10337-014-2758-x>
  24. M. Gumustas, C. T. Sengel-Turk, C. Hascicek, S. A. Ozkan, *Biomed. Chromatogr.* **2014**, *28*, 1409–1417. <https://doi.org/10.1002/bmc.3183>
  25. A. Ali, M. Ahmed, T. Mahmud, M. Qadir, K. Nadeem, A. Saleem, *Indian J. Pharm. Sci.* **2015**, *77*, 515–521. <https://doi.org/10.4103/0250-474X.169042>
  26. M. A. Qadir, M. Ahmed, W. A. Hussain, M. S. Tahir, *Indian J. Pharm. Sci.* **2015**, *77*, 434–438. <https://doi.org/10.4103/0250-474X.164772>
  27. M. Ahmed, M. A. Qadir, S. Shahzad, R. Waseem, M. S. Tahir, *Int. J. Chem. Pharm. Sci.* **2013**, *2*, 536–540.
  28. M. Ahmed, S. K. Shahzadi, R. Waseem, S. Shahzad, W. Ahmad, *Inter. J. Chem Sci Res* **2013**, *3*, 1–6.
  29. A. Gasco-López, A. Santos-Montes, R. Izquierdo-Hornillos, *J. Chromatogr. Sci.* **1997**, *35*, 525–535. <https://doi.org/10.1093/chromsci/35.11.525>

## Povzetek

V predstavljeni študiji smo optimizirali novo metodo na osnovi ultravisokoločljivostne tekočinske kromatografije (UHPLC) za hkratno določanje antazolin hidroklorida (ANZ) in nafazolin hidroklorida (NFZ) v oftalmičnih pripravkih. Izkrajna ločba ANZ in NFZ je potekala pri 40 °C na ACE Excel 2 C18-PFP koloni (2 µm, 2,1 × 100 mm) pri pretoku 0,6 mL min<sup>-1</sup>, mobilna faza pa je bila sestavljena iz acetonitrila in fosfatnega pufru (60:40, v/v, pH 3,0), ki je vseboval 0,5 % trietilamina. Za oba analita je bila detekcija pri valovni dolžini 285 nm, volumen injiciranja pa je bil 1,0 µL. Skupni čas analize na vzorec je bil 4,5 min z retencijskim časom za NFZ 0,92 min in za ANZ 1,86 min. Kalibracijska krivulja je bila linearna od 0,500–100 µg mL<sup>-1</sup> za ANZ in NFZ s korelacijskim koeficientom ≥ 0,9981, medtem ko sta bili ponovljivost in obnovljivost (izraženi kot relativni standardni odmik) nižji od 1,28% za ANZ in od 2,14 % za NFZ. V primerjavi z visokoločljivostno tekočinsko kromatografijo (HPLC) ima razvita UHPLC metoda znatne prednosti, saj je bil čas analize bistveno krajši za 3,4-krat, poraba topil pa manjša za 5-krat. Pri študiju prisilnega razpada smo dobili popolno ločbo analitov v prisotnosti njihovih razpadnih produktov, kar pomeni visoko stopnjo specifičnosti metode. Predlagana UHPLC metoda se je izkazala kot preprosta in hitra za določanje ANZ in NFZ v komercialno dostopnih oftalmičnih pripravkih z izkoristki med 99,6 in 100,4%.

Scientific paper

# [M<sup>II</sup>(NCS)<sub>2</sub>(nia)<sub>2</sub>(OH<sub>2</sub>)<sub>2</sub>]: Preparation, Crystal Structure and Thermal Properties (M<sup>II</sup> = Mn, Fe; nia = nicotinamide)

Marta Počkaj,\* Nives Kitanovski, Boris Čeh and Romana Cerc-Korošec

Faculty of Chemistry and Chemical Technology, University of Ljubljana, Večna pot 113, SI-1000 Ljubljana, Slovenia.

\* Corresponding author: E-mail: E-mail: marta.pockaj@fkkt.uni-lj.si.

Received: 10-01-2017

## Abstract

Two novel isostructural coordination compounds of manganese(II) (**1**) and iron(II) (**2**) with common formulae [M<sup>II</sup>(NCS)<sub>2</sub>(nia)<sub>2</sub>(OH<sub>2</sub>)<sub>2</sub>] have been prepared from water solution of appropriate metal salt, nicotinamide and KSCN. Their crystal structures were determined by means of X-ray diffraction on single crystals. The mononuclear title compounds crystallize in a triclinic *P*-1 space group with six monodentate octahedrally arranged ligands around the metal centre. The coordination molecules are self-assembled with an extended network of hydrogen bonds into a three-dimensional structure. Additionally, **1** and **2** were characterized with infrared spectroscopy, magnetic measurements and thermal analysis.

**Keywords:** crystal structure; coordination chemistry; thiocyanate; nicotinamide; manganese(II); iron(II).

## 1. Introduction

The biological importance of transition metal ions such as manganese and iron cannot be denied:<sup>1,2</sup> manganese(II) ions act as cofactors in a variety of enzymes with a spectra of functions while the main roles of iron-containing species are electrons and oxygen transfer. Nicotinamide and thiocyanate also play an important role in biochemical processes. For example, in metabolism of thiocyanate several short-lived intermediates with antibacterial activity are formed and thus, significantly lowered levels of thiocyanate in the human body are damaging to the human host defense system.<sup>3,4</sup> On the other hand, nicotinamide is an amide of nicotinic acid (niacin, vitamin B<sub>3</sub>) and is a precursor to nicotinamide adenine dinucleotide phosphate (NADP), which is crucial for ATP synthesis, redox reactions and ADP-ribose transfer reactions.<sup>5</sup> In addition, manganese and iron coordination compounds have received significant attention also in the field of enzyme-mimicking compounds.<sup>6–9</sup> All aforementioned facts are driving force for research in coordination chemistry resembling biological systems.

Nicotinamide and its analogues (isonicotinamide, picolinamide) possess three potential coordinating sites: endocyclic nitrogen atom and amide nitrogen and oxygen

atom. Usually, the coordination takes place *via* ring N atom in a monodentate manner, though bridging also *via* amide O atom may follow as well. Similarly, the thiocyanate anion is typically bound monodentately, mostly *via* its N-end, following by additional bridging *via* its remaining S-end; the monodentate coordination *via* its S-end is the least common.<sup>10</sup> Combining both ligands, a variety of extended frameworks interconnected by hydrogen and/or coordination bonds leading to interesting physical properties, e.g. magnetism or catalytic activity, can be formed.<sup>11</sup> The Cambridge Structural Database contains only four structures of coordination compounds exclusively with thiocyanate and nicotinamide ligands at the same time:<sup>10</sup> with zinc(II) ([Zn(NCS)<sub>2</sub>(nia)<sub>2</sub>], refcode KITGAW),<sup>12</sup> copper(II) ([Cu(μ<sub>2</sub>-SCN)(nia)<sub>2</sub>]<sub>n</sub>, refcode UFAXII),<sup>13</sup> cadmium(II) ([Cd(μ<sub>2</sub>-SCN)<sub>2</sub>(nia)<sub>2</sub>]<sub>n</sub>·nH<sub>2</sub>O, refcode QIFMAT)<sup>14</sup> and mercury(II) ([Hg(μ<sub>2</sub>-SCN)(NCS)(nia)]<sub>n</sub>, refcode KITFUP).<sup>12</sup> Three additional crystal structures containing coordinated water are also known: with copper(II) ([Cu(NCS)<sub>2</sub>(nia)<sub>2</sub>(OH<sub>2</sub>)], refcode GISJAU)<sup>15</sup>, cobalt(II) ([Co(NCS)<sub>2</sub>(nia)<sub>2</sub>(OH<sub>2</sub>)<sub>2</sub>], refcode TCNICO)<sup>16,17</sup> and nickel(II) ([Ni(NCS)<sub>2</sub>(nia)<sub>2</sub>(OH<sub>2</sub>)<sub>2</sub>], refcode CIVRAC),<sup>18,19</sup> the latter two being isostructural with the title complexes. In this paper, we report on preparation, crystal structure, spectroscopic, magnetic and thermal properties of two

mononuclear coordination complexes with common formulae  $[M^{\text{II}}(\text{NCS})_2(\text{nia})_2(\text{OH})_2]$  ( $M = \text{Mn}, \text{Fe}$ ).

## 2. Experimental

### 2. 1. Reagents and Physical Measurements

All reagents and chemicals were purchased from commercial sources and used without further purification. CHN elemental analyses were performed with a Perkin-Elmer 2400 CHN Elemental Analyzer. The infrared spectra were measured on solid samples using a Perkin-Elmer Spectrum 100 series FT-IR spectrometer equipped with an ATR sampling accessory. Magnetic susceptibility of the substance was determined at room temperature by the Evans method using powdered samples and a Sherwood Scientific MSB-1 balance with  $\text{HgCo}(\text{NCS})_4$  as a calibrant. Diamagnetic corrections were estimated from Pascal's constants and the effective magnetic moments were calculated using the equation:  $\mu_{\text{eff}} = 2.828(\chi\text{MT})^{1/2}$ . Simultaneous thermogravimetric/dynamic scanning calorimetry (TG/DSC) measurements were performed on a Mettler Toledo TGA/DSC1 instrument under dynamic flow of air or argon, respectively. The flow rate of the gas was  $100 \text{ mL min}^{-1}$ . Around 5 mg of the sample was put into 150  $\mu\text{L}$  platinum crucible and heated in a temperature range from 25 to 800  $^\circ\text{C}$  with a heating rate of  $10 \text{ C min}^{-1}$ .

Empty crucible served as a reference. Blank curve was subtracted. Evolved gases were detected using a Balzers ThermoStar mass spectrometer. Evolved gases were introduced into mass spectrometer via 75 cm long heated capillary.

### 2. 2. Synthesis

**[Mn(NCS)<sub>2</sub>(nia)<sub>2</sub>(OH)<sub>2</sub>] (1).** To the mixture of  $\text{MnCl}_2 \cdot 4\text{H}_2\text{O}$  (792 mg, 4.0 mmol), KSCN (777 mg, 8.0 mmol) and nicotinamide (977 mg, 8.0 mmol), 5 mL of distilled water was added. The reaction mixture was heated under reflux at 60  $^\circ\text{C}$  until the clear solution was obtained. The reaction flask was sealed and stored in a refrigerator at  $\sim 8 \text{ }^\circ\text{C}$ . After several days, colourless crystals suitable for X-ray structural analysis were obtained. Yield: 433 mg (24%). Anal. Calcd. for  $\text{C}_{14}\text{H}_{16}\text{MnN}_6\text{O}_4\text{S}_2$ : C, 37.25%; H, 3.57%; N, 18.62%. Found: C, 37.50%; H, 3.31%; N, 18.43%.  $\mu_{\text{eff}} = 6.06 \text{ BM}$ .  $\bar{\nu}_{\text{max}}$ : 3400–3000 (O–H, N–H), 2096 (CN from SCN), 1668 (C=O), 1386 (CN from nia)  $\text{cm}^{-1}$ .

**[Fe(NCS)<sub>2</sub>(nia)<sub>2</sub>(OH)<sub>2</sub>] (2).** To the mixture of  $\text{FeSO}_4 \cdot 7\text{H}_2\text{O}$  (83.4 mg, 0.30 mmol), KSCN (116.6 mg, 1.20 mmol) and nicotinamide (73.3 mg, 0.60 mmol), 4 mL of distilled water was added. The reaction mixtures was stirred and slightly heated until all the solid reactants dissol-

Table 1. Crystal data, data collection and structure refinement.

Crystal data	1	2
Formula	$\text{C}_{14}\text{H}_{16}\text{MnN}_6\text{O}_4\text{S}_2$	$\text{C}_{14}\text{H}_{16}\text{FeN}_6\text{O}_4\text{S}_2$
$M_r$	451.39	452.30
Cell setting, space group	Triclinic, $P-1$	Triclinic, $P-1$
$a$ (Å)	7.5470(5)	7.5299(6)
$b$ (Å)	8.2535(5)	8.1847(7)
$c$ (Å)	9.1503(7)	9.0367(5)
$\alpha$ ( $^\circ$ )	73.196(6)	73.000(6)
$\beta$ ( $^\circ$ )	69.039(6)	69.536(6)
$\gamma$ ( $^\circ$ )	65.917(6)	66.518(8)
$V$ (Å <sup>3</sup> )	479.02(6)	470.92(7)
$Z$	1	1
$D_x$ (Mg m <sup>-3</sup> )	1.565	1.595
$\mu$ (mm <sup>-1</sup> )	0.940	1.056
$F(000)$	231	232
Data collection		
$T$ (K)	150(2)	150(2)
No. of measured, independent and observed reflections	4273, 2490, 2199	4111, 2432, 2055
$R_{\text{int}}$	0.0186	0.0221
Refinement		
Refinement method	full-matrix least-squares refinement on $F^2$	full-matrix least-squares refinement on $F^2$
$R$ (on $F_{\text{obs}}$ ), $wR$ (on $F_{\text{obs}}$ ), $S$	0.0290, 0.0674, 1.076	0.0330, 0.0699, 1.051
No. of contributing reflections	2490	2432
No. of parameters/restraints	140/0	140/0
$\Delta\rho_{\text{max}}, \Delta\rho_{\text{min}}$ (eÅ <sup>-3</sup> )	0.435, -0.320	0.448, -0.310

ved. The Erlenmeyer flask was then cooled down in a refrigerator and after 15 minutes, the yellowish crystals suitable for X-ray structural analysis were obtained. Yield: 37 mg (27%). Anal. Calcd. for  $C_{14}H_{16}FeN_6O_4S_2$ : C, 37.17%; H, 3.56%; N, 18.58%. Found: C, 37.30%; H, 3.24%; N, 18.34%.  $\mu_{\text{eff}} = 5.63$  BM.  $\bar{\nu}_{\text{max}}$ : 3400–3000 (O–H), 2101 (CN from SCN), 1663 (C=O), 1385 (CN from nia)  $\text{cm}^{-1}$ .

### 2. 3. Crystallography

For X-ray structure determination single crystals of both compounds were surrounded by silicon grease, mounted on the tip of glass fibres and transferred to the goniometer head in the stream of liquid nitrogen. Data were collected on a SuperNova diffractometer equipped with Atlas detector using CrysAlis software and monochromated Mo  $K\alpha$  radiation (0.71073 Å) at 150 K.<sup>20</sup> The initial structural model containing coordination molecule was obtained *via* direct methods using the *SIR97* structure solution program.<sup>21</sup> A full-matrix least-squares refinement on  $F^2$  magnitudes with anisotropic displacement parameters for all non-hydrogen atoms using *SHELXL2013* was employed.<sup>22</sup> All H atoms were initially located in difference Fourier maps and were further treated as riding on their parent atoms with C(aromatic)-H distance of 0.95 Å. The positions of water hydrogens as well as amide ones were obtained from a dif-

ference Fourier map and refined freely in iron complex while the N–H and O–H distances in manganese compound were restrained to 0.87(2) and 0.85(2) Å, respectively. Details on crystal data, data collection and structure refinement are given in Table 1. Figures depicting the structures were prepared with *ORTEP3* and *Mercury*.<sup>23,24</sup>

## 3. Results and Discussion

Both title compounds have been prepared by dissolving appropriate metal salt, KSCN and nicotinamide in water. If necessary the starting mixtures were heated mildly and after the clear solutions were obtained they were kept in a refrigerator at  $\sim 8$  °C until the crystals formed. The single crystals suitable for X-ray structural analysis were first tested by means of infrared spectroscopy. In IR spectra of both title compounds there is a broad band between 3400–3000  $\text{cm}^{-1}$  representing O–H and N–H stretching involved in extended hydrogen bond network. Considering stretching frequencies of N–C bond in a thiocyanate ion which appears at 2096  $\text{cm}^{-1}$  in **1** and 2101  $\text{cm}^{-1}$  in **2**, the N-end coordination of thiocyanate anion is also confirmed. The characteristic vibrations of nicotinamide bonds are in agreement with the theoretical study of Bakiler and coworkers, showing the usual coordination mode of nicotinamide *via* its endocyclic nitrogen atom.<sup>25</sup>

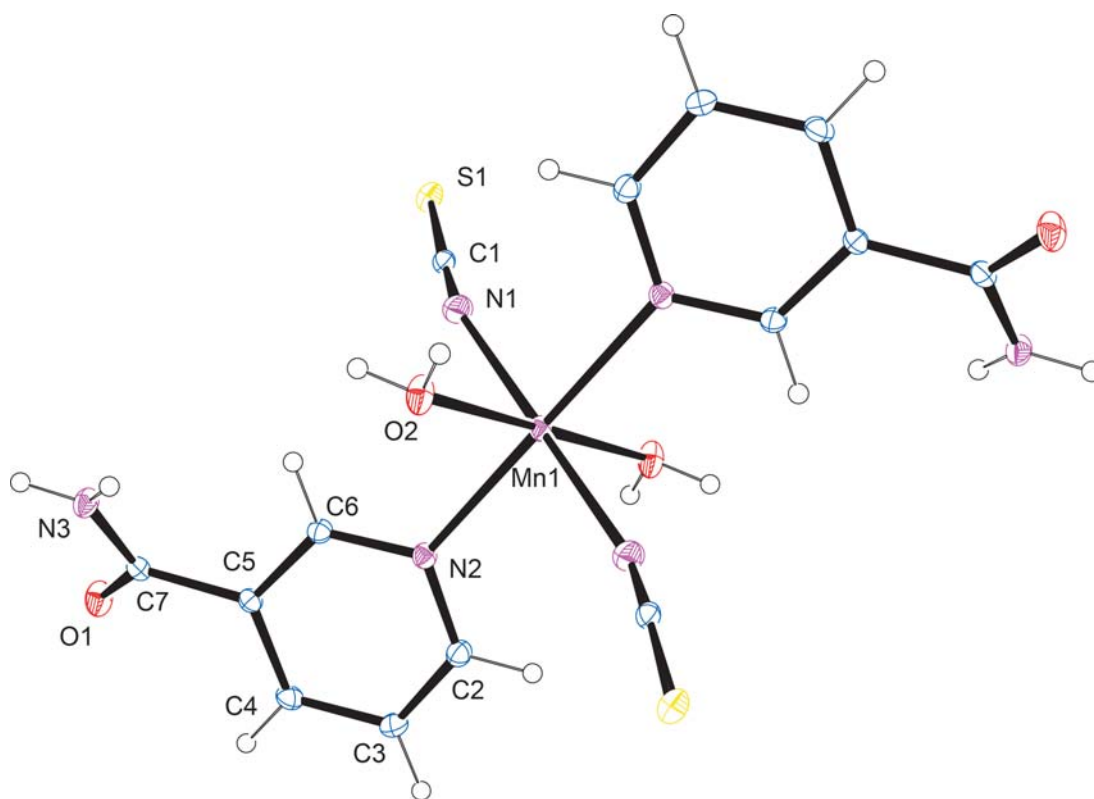


**Figure 1.** An ORTEP representation of coordination molecules in **1** with labels for atoms in asymmetric unit. Thermal ellipsoids are drawn at 30% probability level. Hydrogen atoms are represented as small spheres of arbitrary radii.

X-ray structural analysis has shown that both title coordination compounds are mononuclear (Fig. 1) with six-coordinated central metal ion in a shape of distorted octahedron. All three different ligands are bound in a monodentate mode: nicotinamide *via* endocyclic nitrogen and thiocyanate expectedly *via* its hard base *N*-end to both metals considered as hard acids according to Pearson principle.<sup>26</sup> The equatorial sites are occupied by two oxygens from water (distance M–O1 2.1775(12) Å in **1** and 2.1015(14) Å in **2**) and by two nitrogens from NCS<sup>−</sup> ligand (M–N1 distance of 2.1891(13) Å in **1** and 2.1398(17) Å in **2**). The bulkier and sterically more demanding nicotinamide ligand complements the first coordination sphere at axial positions (M–N2 distance of 2.2941(13) Å in **1** and 2.2225(14) Å in **2**). As observed, the bond distances in **2** are shorter than in **1** due to the smaller ionic radius of Fe<sup>2+</sup> ion in comparison with Mn<sup>2+</sup> (corresponding ionic radii for high-spin octahedral arrangements for Mn *d*<sup>5</sup> and Fe *d*<sup>6</sup> are 0.83 and 0.78 Å, respectively).<sup>27</sup> The pairs of equal ligands are *trans* to each other and due to symmetry restrictions (metal ion is located on an inversion centre) the angles *trans* ligand–M–*trans* ligand are constrained to 180°. The geometry of NCS<sup>−</sup> ligand deviates only slightly from linearity, with the N–C–S angle of 178.11(14)° in **1** and 178.25(17)° in **2**, respectively. However, it is not bound in a completely linear fashion as the C–N–M angles are 156.42(13)° in **1** and 157.97(15)° in **2**, respectively. Several other bond distances and angles are collected in Table 2. The pyridine ring of nia ligand is almost planar with maximum deviation from the meanplane of −0.011(2) Å for C4 (the values for **1** and **2** are the same) while the amide group is slightly out of pyridine-ring plane (torsion angles C6/C5/C7/N3 are 32.2(2)° in **1** and 31.9(3)° in **2**).

The coordination molecules are linked by extensive network of hydrogen bonds of O–H...O, O–H...S and N–H...S types forming a supramolecular structure (Fig. 2, Table 3). Hydrogen bonds donated by water oxygen link each coordination molecules with four adjacent and thus,

**Table 2.** Selected bond distances (Å) and angles (°) for complexes **1** and **2**.

	<b>1</b>	<b>2</b>
M–O2	2.1775(12)	2.1015(14)
M–N1	2.1891(13)	2.1398(17)
M–N2	2.2941(13)	2.2225(14)
N1–C1	1.159(2)	1.152(3)
C1–S1	1.6447(16)	1.651(2)
C7–O1	1.2353(18)	1.234(2)
C7–N3	1.329(2)	1.329(2)
O2–M–N1	90.65(5)	91.19(6)
O2–M–N2	91.17(5)	90.76(5)
N1–M–N2	87.05(5)	88.08(6)
N1–C1–S1	178.11(14)	178.25(17)
C1–N1–M	156.42(13)	157.97(15)

layers stacking in *ac* plane/normal to (010) direction with thickness around ~8 Å are formed. Two additional N–H...S short contacts are present forming *R*<sub>4</sub><sup>2</sup>(8) rings as usual in related compounds:<sup>28</sup> the shorter stabilizes the aforementioned two-dimensional layers while the longer connects two neighboring layers into a three-dimensional structure. Thus, the sulphur atom of thiocyanate ligand is involved in a trifurcated hydrogen bonding motif. Weak  $\pi$ – $\pi$  stacking is also observed between parallel pyridine rings of adjacent molecules with centroid-centroid distance of 3.8175(9) Å.

As already mentioned in the Introduction, several transition metal complexes with nia, SCN<sup>−</sup> and in some cases also water have been structurally characterized till now.<sup>12–19</sup> Surprisingly, their preparation is simple and similar for all of them. On the other hand, their structures differ significantly: from mononuclear [Zn(NCS)<sub>2</sub>(nia)<sub>2</sub>],<sup>12</sup> ([Cu(NCS)<sub>2</sub>(nia)<sub>2</sub>(OH<sub>2</sub>)<sub>2</sub>),<sup>15</sup> ([Co(NCS)<sub>2</sub>(nia)<sub>2</sub>(OH<sub>2</sub>)<sub>2</sub>),<sup>16,17</sup> [Ni(NCS)<sub>2</sub>(nia)<sub>2</sub>(OH<sub>2</sub>)<sub>2</sub>]<sup>18,19</sup> to polymeric ([Cu(μ<sub>2</sub>-SCN)(nia)<sub>2</sub>]<sub>*n*</sub>,<sup>13</sup> [Cd(μ<sub>2</sub>-SCN)<sub>2</sub>(nia)<sub>2</sub>]<sub>*n*</sub>·*n*H<sub>2</sub>O)<sup>14</sup> and [Hg(μ<sub>2</sub>-SCN)(NCS)(nia)]<sub>*n*</sub>.<sup>12</sup> In all cases, extensive hydrogen bonding is present. For mononuclear complexes the hydrogen

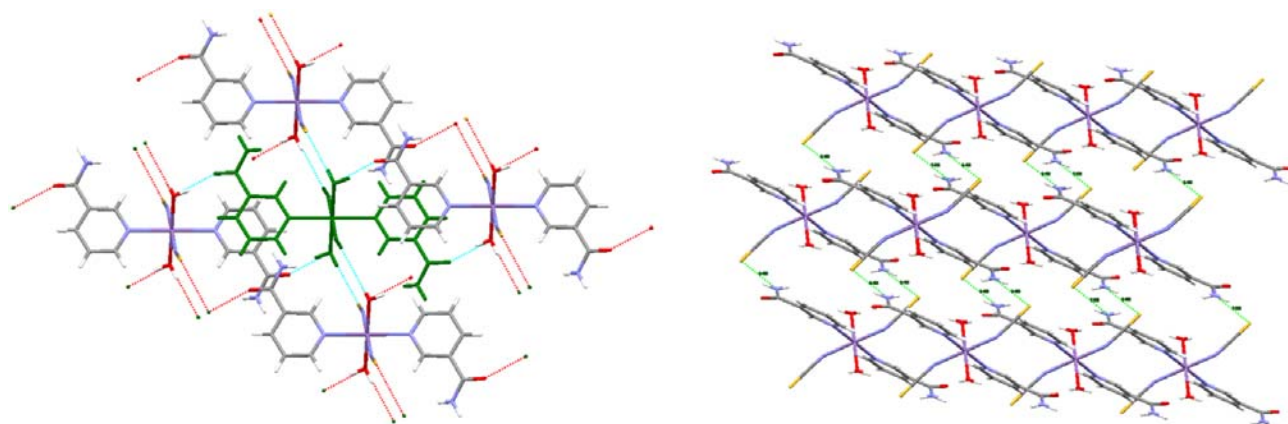


**Figure 2.** Hydrogen bond network/packing diagram in **1** leading to formation of layers (left) that get connected via N3–H3A...S1 hydrogen bond (right).

Table 3. Hydrogen bond geometry in **1** and **2**.

D–H···A	D–H (Å)	H···A (Å)	D···A (Å)	<D–H···A (°)
<b>1</b>				
O2–H2A···O1 <sup>i</sup>	0.84(3)	1.85(3)	2.6858(17)	170(2)
O2–H2B···S1 <sup>ii</sup>	0.81(3)	2.43(3)	3.2125(13)	163(2)
N3–H3B···S1 <sup>ii</sup>	0.83(2)	2.67(2)	3.4229(15)	151.0(18)
N3–H3A···S1 <sup>iii</sup>	0.88(2)	2.66(2)	3.4383(15)	147.9(16)
<b>2</b>				
O2–H2A···O1 <sup>i</sup>	0.816(15)	1.866(16)	2.6713(18)	169(2)
O2–H2B···S1 <sup>ii</sup>	0.825(16)	2.397(17)	3.2002(14)	164(2)
N3–H3B···S1 <sup>ii</sup>	0.848(15)	2.635(17)	3.4186(16)	154(2)
N3–H3A···S1 <sup>iii</sup>	0.872(15)	2.656(17)	3.4365(17)	149.6(18)

Symmetry codes: (i)  $x, y, z + 1$ ; (ii)  $-x, -y + 1, -z + 1$ ; (iii)  $x, y - 1, z$ .

bond scheme seems to be less uniform (N–H···O and N–H···S, usually not forming any ring motifs) but it always leads to 3D self-assembly of isolated coordination molecules. In polymeric complexes with four-coordinated metal, i.e.  $[\text{Hg}(\mu_2\text{-SCN})(\text{NCS})(\text{nia})]_n$ <sup>12</sup> and  $[\text{Cu}(\mu_2\text{-SCN})$

$(\text{nia})_2]_n$ <sup>13</sup> chains are formed, while in polymeric complex  $[\text{Cd}(\mu_2\text{-SCN})_2(\text{nia})_2]_n \cdot n\text{H}_2\text{O}$ <sup>14</sup> with six-coordinated Cd(II) layers are present. Chains or layers are further hydrogen bonded – in this case N–H···O hydrogen bonds are highly prevalent – resulting again in a formation of 3D structures.

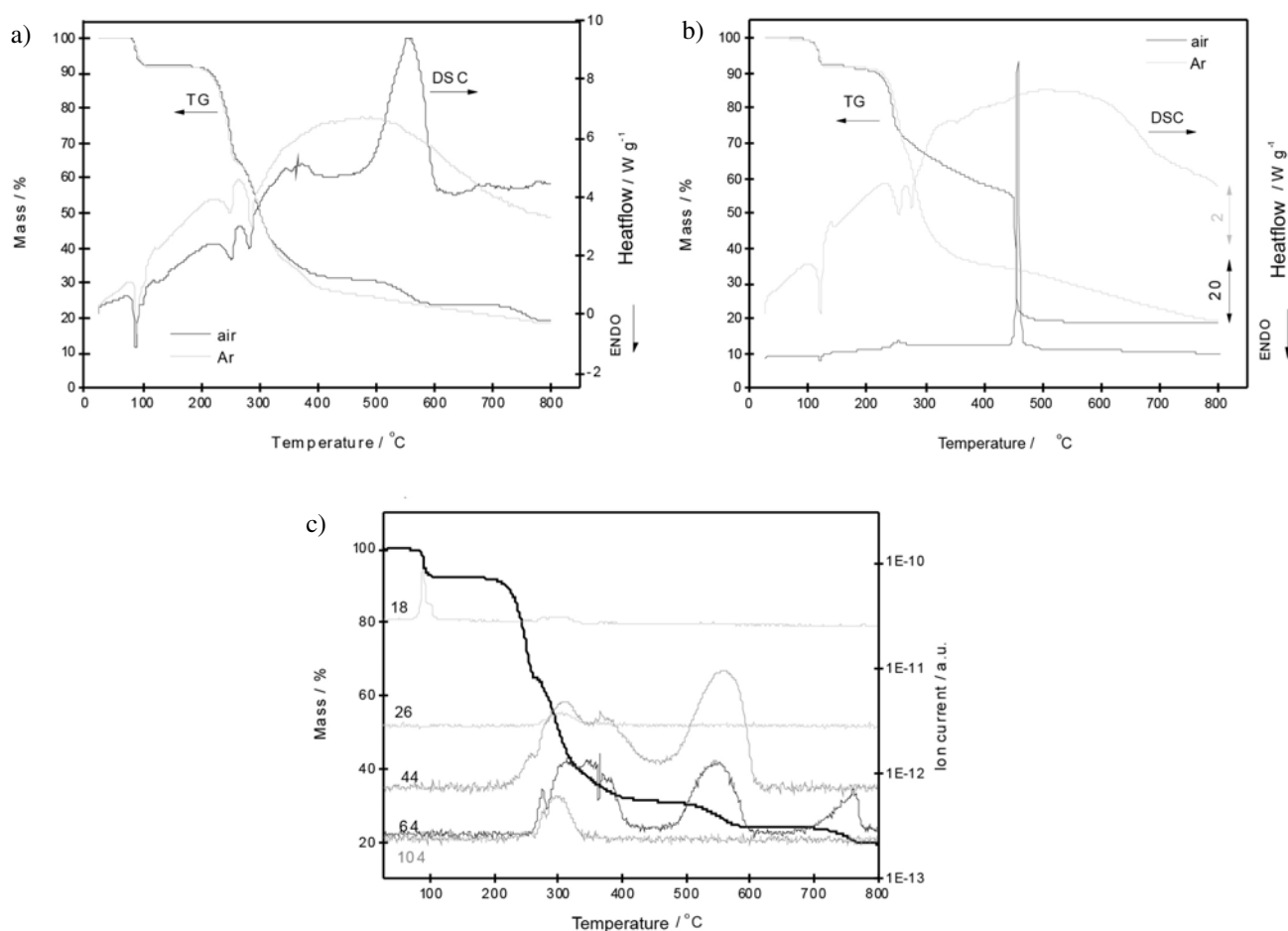


Figure 3. TG and DSC curves of a) Mn complex (**1**) and b) Fe-complex (**2**), and c) TG-MS curve of Mn complex (**1**) under air atmosphere. Note that in Fig. b two different scales on a DSC curve are presented, due to reducing the enthalpy signal under air atmosphere the first and the second DSC signals are not clearly seen.



In all cases D...A distances are comparable to those in the title compounds.

Thermal decomposition of both prepared complexes under air and argon atmosphere are shown in Figure 3. In the first step of thermal decomposition (70–110 °C for **1** and 85–130 °C for **2**) dehydration took place; evolution of water molecules is evident from a MS curve of Mn compound (see Figure 3c). Due to very similar molecular mass of both complexes, a theoretical mass loss for the dehydration process is the same for both complexes, 8.0 %, and that completely corresponds to the experimental value. At temperatures higher than 200 °C both complexes decompose further through several successive steps. Thermal decomposition of **1** is similar under air and argon atmosphere: from 200 to 270 °C sample lost 27 % and from 270 to 400 °C another 33.3 % under air and 37.5 % under argon atmosphere; overlapped reactions were endothermic. On MS curve evolution of CO<sub>2</sub> (*m/z* = 44) was observed at the beginning of the described decomposition reactions, followed by a multitude of other signals: water (*m/z* = 18), SO<sub>2</sub> (*m/z* = 64), CN<sup>-</sup> (*m/z* = 26); also *m/z* = 104, the signal most close to molecular peak of nicotinamide (*m/z* = 122). The high number of observed signals (22 altogether) indicates the complexity of the thermal decomposition of the described complex. After 300 °C the route of thermal decomposition became different; under air atmosphere there are two distinct steps between 400 and 800 °C, the first being exothermic while under argon atmosphere there is a continuous mass loss up to 800 °C. The total mass loss under air atmosphere is 80.4 % meaning that Mn complex most probably decomposed to MnO<sub>2</sub> (theoretical mass loss 80.7 %) and 81.5 % under argon atmosphere. Theoretical mass loss for decomposition to Mn<sub>2</sub>O<sub>3</sub> is 82.5 %, which most probably means that under argon atmosphere a final residue is a mixture of MnO<sub>2</sub> and Mn<sub>2</sub>O<sub>3</sub>.

The course of thermal decomposition of both Fe and Mn complex is very similar under argon atmosphere. The observed mass loss in a whole temperature range from 25 to 800 °C correspond to Fe<sub>2</sub>O<sub>3</sub> (measured value 81.4%, theoretical 82.3%). Under air atmosphere thermal decomposition from 270 °C onward differ much with regard to thermal decomposition under argon; the rate of decomposition became slower, but at 450 °C a sharp exothermic step with a mass loss of around 35 % took place, leading to the same residue as obtained in argon atmosphere.

## 4. Conclusions

Two novel, isostructural compounds, namely [Mn<sup>II</sup>(NCS)<sub>2</sub>(nia)<sub>2</sub>(OH<sub>2</sub>)<sub>2</sub>] (**1**) and [Fe<sup>II</sup>(NCS)<sub>2</sub>(nia)<sub>2</sub>(OH<sub>2</sub>)<sub>2</sub>] (**2**) have been isolated. Their crystal structures reveal *trans* octahedral slightly elongated MN<sub>2</sub>O<sub>2</sub>N<sub>2</sub> chromophores. Despite shorter M–O coordination bonds the water molecules are removed first at an elevated tempera-

ture, as expected. All three ligands enable H-bonds, thus building a 3D structure of mononuclear building blocks. Due to a lack of any coordination bridging weak magnetic interactions within solids among the metal centers are expected. On the other hand, strong intermolecular ability via H-bonding, especially in water, for the title manganese(II) and iron(II) compounds is noticed. Thermal decomposition of both complexes is similar losing water in first step of mass loss while in the remaining steps other ligands decompose yielding Fe<sub>2</sub>O<sub>3</sub> or a mixture of MnO<sub>2</sub> and Mn<sub>2</sub>O<sub>3</sub>, respectively.

## 5. Supplementary Information

CCDC 1498589 (**1**) and 1498590 (**2**) contain the supplementary crystallographic data. These data can be obtained free of charge from The Cambridge Crystallographic Data Centre via [www.ccdc.cam.ac.uk/data\\_request/cif](http://www.ccdc.cam.ac.uk/data_request/cif).

## 6. Acknowledgments

The authors thank Mateja Kožar and Silva Peternel for their assistance during synthesis. This work was financially supported by Slovenian research agency (grant P1-0175). The EN-FIST Centre of Excellence is also acknowledged for the use of SuperNova diffractometer.

## 7. References

1. C. A. Dlouhy, C. E. Outten, in: L. Banci (Ed.): *Metallomics and the Cell*. Springer Science+Business Media, Dordrecht, The Netherlands, **2013**, pp. 241–278. [https://doi.org/10.1007/978-94-007-5561-1\\_8](https://doi.org/10.1007/978-94-007-5561-1_8)
2. A. N. Jensen, L. T. Jensen, in: L. G. Costa, M. Aschner (Ed.): *Manganese in Health and Disease*. Royal Society of Chemistry, Cambridge, UK, **2015**, pp. 1–33.
3. K. M. Pruitt, J. Tenovuo, R. W. Andrews, T. McKane, *Biochemistry* **1982**, *21*, 562–567. <https://doi.org/10.1021/bi00532a023>
4. G. E. Conner, C. Wijkstrom-Frei, S. H. Randell, V. E. Fernandez, M. Salathe, *FEBS Lett.* **2007**, *581*, 271–278. <https://doi.org/10.1016/j.febslet.2006.12.025>
5. D. MacKay, J. Hathcock, E. Guarneri, *Nutr. Rev.* **2012**, *70*, 357–366. <https://doi.org/10.1111/j.1753-4887.2012.00479.x>
6. M. Počkaj, B. Kozlevčar, N. Kitanovski, *Acta Chim. Slov.* **2015**, *62*, 272–280. <https://doi.org/10.17344/acsi.2014.1048>
7. *Concepts and models in bioinorganic chemistry*, 3. ed., Eds., H.-B. Kraatz, N. Metzler-Nolte, Wiley-VCH, Weinheim, **2006**.
8. C. Pettinari, R. Pettinari, *Coord. Chem. Rev.* **2005**, *249*, 663–691. <https://doi.org/10.1016/j.ccr.2004.08.017>

9. N. Kitanovski, N. Borsan, M. Kasunič, V. Francetič, J. Popović, I. Djerdj, X. Rocquefelte, J. Reedijk, B. Kozlevčar, *Polyhedron* **2014**, *70*, 119–124. <https://doi.org/10.1016/j.poly.2013.12.029>
10. F. H. Allen, *Acta Crystallogr. B* **2002**, *58*, 380–388. <https://doi.org/10.1107/S0108768102003890>
11. C. B. Aakeröy, J. Desper, J. Valdés-Martínez, *CrystEngComm* **2004**, *6*, 413–418. <https://doi.org/10.1039/B410129B>
12. M. Đaković, Z. Popović, G. Giester, M. Rajić-Linarić, *Polyhedron* **2008**, *27*, 465–472. <https://doi.org/10.1016/j.poly.2007.09.036>
13. C. Näther, I. Jeß, *Acta Crystallogr. C* **2002**, *58*, m190–m192. <https://doi.org/10.1107/S0108270102001592>
14. G. Yang, H.-G. Zhu, B.-H. Liang, X.-M. Chen, *J. Chem. Soc., Dalton Trans.* **2001**, 580–585. <https://doi.org/10.1039/b009129o>
15. C. Li, W. Ding, C. Shao, *Acta Crystallogr. E* **2008**, *64*, m314–m314. <https://doi.org/10.1107/S1600536807068511>
16. R. E. Marsh, *Acta Crystallogr. B* **2005**, *61*, 359–359. <https://doi.org/10.1107/S0108768105009651>
17. D. Pandey, S. S. Narvi, S. Chaudhuri, *Acta Crystallogr. E* **2014**, *70*, m236–m236. <https://doi.org/10.1107/S1600536814011453>
18. D. Pandey, S. S. Narvi, G. K. Mehrotra, R. J. Butcher, *Acta Crystallogr. E* **2014**, *70*, m183–m183. <https://doi.org/10.1107/S1600536814006771>
19. D. Pandey, S. S. Narvi, G. K. Mehrotra, R. J. Butcher, *Chin. J. Struct. Chem.* **2015**, *34*, 777–785.
20. CrysAlis PRO, Oxford Diffraction Ltd, Yarnton, Oxfordshire, England, **2011**.
21. A. Altomare, M. C. Burla, M. Camalli, G. L. Casciarano, C. Giacovazzo, A. Guagliardi, A. G. G. Moliterni, G. Polidori, R. Spagna, *J. Appl. Cryst.* **1999**, *32*, 115–119. <https://doi.org/10.1107/S0021889898007717>
22. G. M. Sheldrick, *SHELXL2013*, University of Göttingen, Germany, **2013**.
23. L. J. Farrugia, *J. Appl. Crystallogr.* **1997**, *30*, 565–565. <https://doi.org/10.1107/S0021889897003117>
24. C. F. Macrae, P. R. Edgington, P. McCabe, E. Pidcock, G. P. Shields, R. Taylor, M. Towler, J. van de Streek, *J. Appl. Cryst.* **2006**, *39*, 453–457. <https://doi.org/10.1107/S002188980600731X>
25. M. Bakiler, O. Bolukbasi, A. Yilmaz, *J. Mol. Struct.* **2007**, *826*, 6–16. <https://doi.org/10.1016/j.molstruc.2006.04.021>
26. R. G. Pearson, *J. Am. Chem. Soc.* **1963**, *85*, 3533–3539. <https://doi.org/10.1021/ja00905a001>
27. R. D. Shannon, *Acta Crystallogr. A* **1976**, *32*, 751–767. <https://doi.org/10.1107/S0567739476001551>
28. M. Đaković, J. Jaźwiński, Z. Popović, *Acta Chim. Slov.* **2015**, *62*, 328–336. <https://doi.org/10.17344/acsi.2014.1128>

## Povzetek

Iz vodne raztopine, ki je vsebovala nikotinamid, KSCN in ustrezno sol kovine(II), smo pripravili dve novi, izostrukturalni, koordinacijski spojini mangana(II), **1**, in železa(II), **2**, s splošno formulo  $[M^{II}(NCS)_2(nia)_2(OH_2)_2]$ . Na osnovi difrakcije na monokristalu smo določili kristalni strukturi obeh spojin, ki kristalizirata v triklinski prostorski skupini  $P-1$ . Spojini sta enojedrni, centralni atom pa je v obeh koordiniran oktaedrično s šestimi ligandi. Koordinacijske molekule so povezane v tridimenzionalno strukturo s pomočjo vodikovih vezi. Spojini **1** in **2** smo okarakterizirali tudi z infrardečo spektroskopijo, magnetnimi meritvami in termično analizo.

Scientific paper

# Anti-inflammatory and Anti-ulcer Activities of New Fused Thiazole Derivatives Derived from 2-(2-Oxo-2*H*-chromen-3-yl)thiazol-4(5*H*)-one

Rafat M. Mohareb,<sup>1\*</sup> Fatima Al-Omran,<sup>2</sup> Mahmoud A. Abdelaziz<sup>3</sup> and Rehab A. Ibrahim<sup>4</sup>

<sup>1</sup> Department of Chemistry, Faculty of Science, Cairo University, Giza, A. R. Egypt

<sup>2</sup> Department of Chemistry, Faculty of Science, Kuwait University, P. O. Box 12613, Safat 13060, Kuwait

<sup>3</sup> Chemistry Department, Faculty of Science, Tabuk university, Tabuk 71491, P. O. Box 741, Kingdom of Saudi Arabia

<sup>4</sup> Higher Institute of Engineering and Technology, El-Tagammoe El-Khames, New Cairo, A. R. Egypt

\* Corresponding author: E-mail: raafat\_mohareb@yahoo.com

Received: 12-01-2017

## Abstract

The reaction of the 2-(4-oxo-4,5-dihydrothiazol-2-yl)acetonitrile (**1**) with salicylaldehyde (**2**) in 1,4-dioxane containing a catalytic amount of piperidine gave the coumarin derivative **3**. The latter reacted with different reagents to give pyrido[4,5-*b*]thiazole, pyrido[4,5-*b*]thiazole and thieno[5,4-*b*]thiazole derivatives. The anti-inflammatory and anti-ulcer activities of the newly synthesized products were evaluated and the results showed that compounds **7a**, **8a**, **10b**, **13b**, **15b**, **18a**, **19b**, **19c**, and **19d** showed higher activity compared to the rest of the compounds. In addition to this, toxicity of such active compounds was studied against shrimp larvae where compounds **10b**, **18a**, **19c** and **19d** showed to be non-toxic against the tested organisms.

**Keywords:** 4,5-dihydrothiazol, coumarin, pyrimidine, anti-inflammatory, anti-ulcer activity

## 1. Introduction

Thiazole is a core structural motif present in a variety of natural products, such as vitamin B1 (thiamine) and penicillin. Thiazole derivatives also exhibit a broad spectrum of medicinal and biological properties, such as antibacterial, antifungal,<sup>1</sup> anti-inflammatory,<sup>2</sup> antiviral,<sup>3</sup> antimalarial,<sup>4</sup> and anti-HIV activities.<sup>5</sup> Thiazole analogs have also been reported as ligands at estrogen receptors,<sup>6</sup>

neuropeptides,<sup>7</sup> Y5 adenosine receptors,<sup>8</sup> and act as inhibitors of human platelet aggregation factor,<sup>9</sup> urokinase,<sup>10</sup> and poly(ADP-ribose) polymerase-1.<sup>11</sup> Selenazoles have been reported to possess antibacterial properties,<sup>12</sup> superoxide-anion-scavenging activity,<sup>13</sup> and exhibit cytotoxicity and DNA fragmentation effects in human HT-1080 fibrosarcoma cells.<sup>14</sup> The structures of sulfathiazole, meloxicam, and selenazofurin and their pharmacological activities are given in Fig. 1.

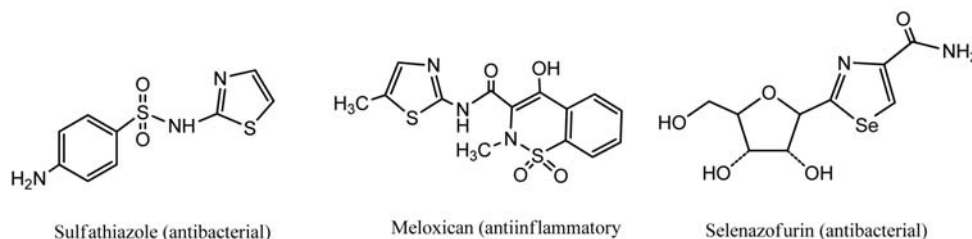
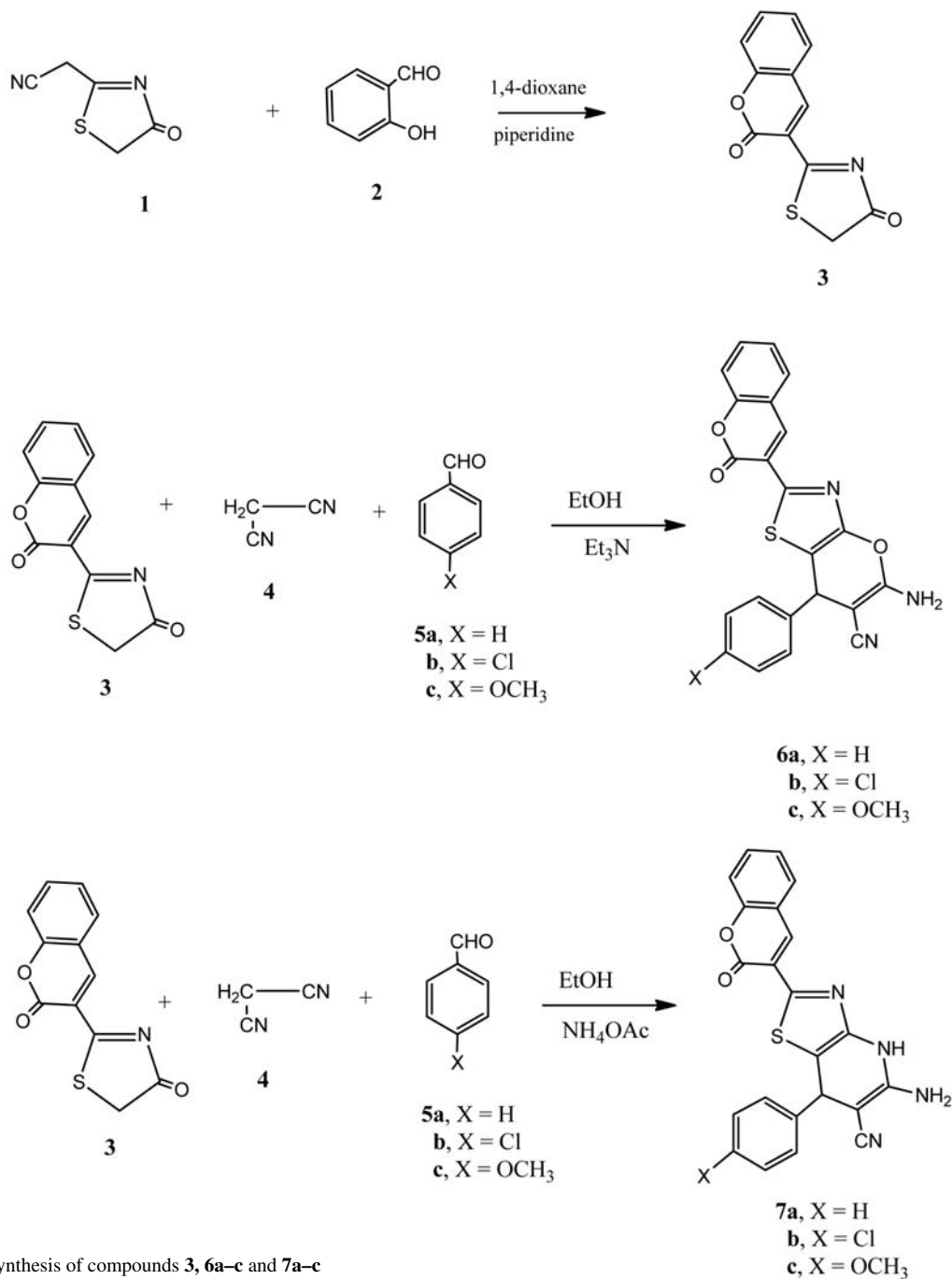


Fig 1. Biologically active thiazole and senazole drivatives

In many report structural modification of the heterocyclic rings through the construction of new heterocyclic nuclei enhances the pharmaceutical applications of the resulting molecules.<sup>15,16</sup> This encouraged our efforts in this work to modify 2-(4-oxo-4,5-dihydrothiazol-2-yl)acetonitrile through its reaction with salicylaldehyde to produce a chromen-3-yl)thiazol which was used as the key starting compound for many further heterocyclic transformations. The anti-inflammatory and anti-ulcer evaluations of the newly synthesized compounds were studied.

## 2. Results and Discussion

In the present work the 2-(4-oxo-4,5-dihydrothiazol-2-yl)acetonitrile (**1**) reacted with salicylaldehyde (**2**) in 1,4-dioxane containing a catalytic amount of piperidine to give the coumarin derivative **3**. The structure of **3** was based on its analytical and spectral data. Thus, the <sup>1</sup>H NMR spectrum showed a singlet at δ 4.28 ppm equivalent to the thiazole CH<sub>2</sub> group, a singlet at δ 6.52 ppm indicating the coumarin 4H, a multiplet at δ 7.28–7.38 ppm for the C<sub>6</sub>H<sub>4</sub> group. Moreover, the <sup>13</sup>C NMR spectrum sho-



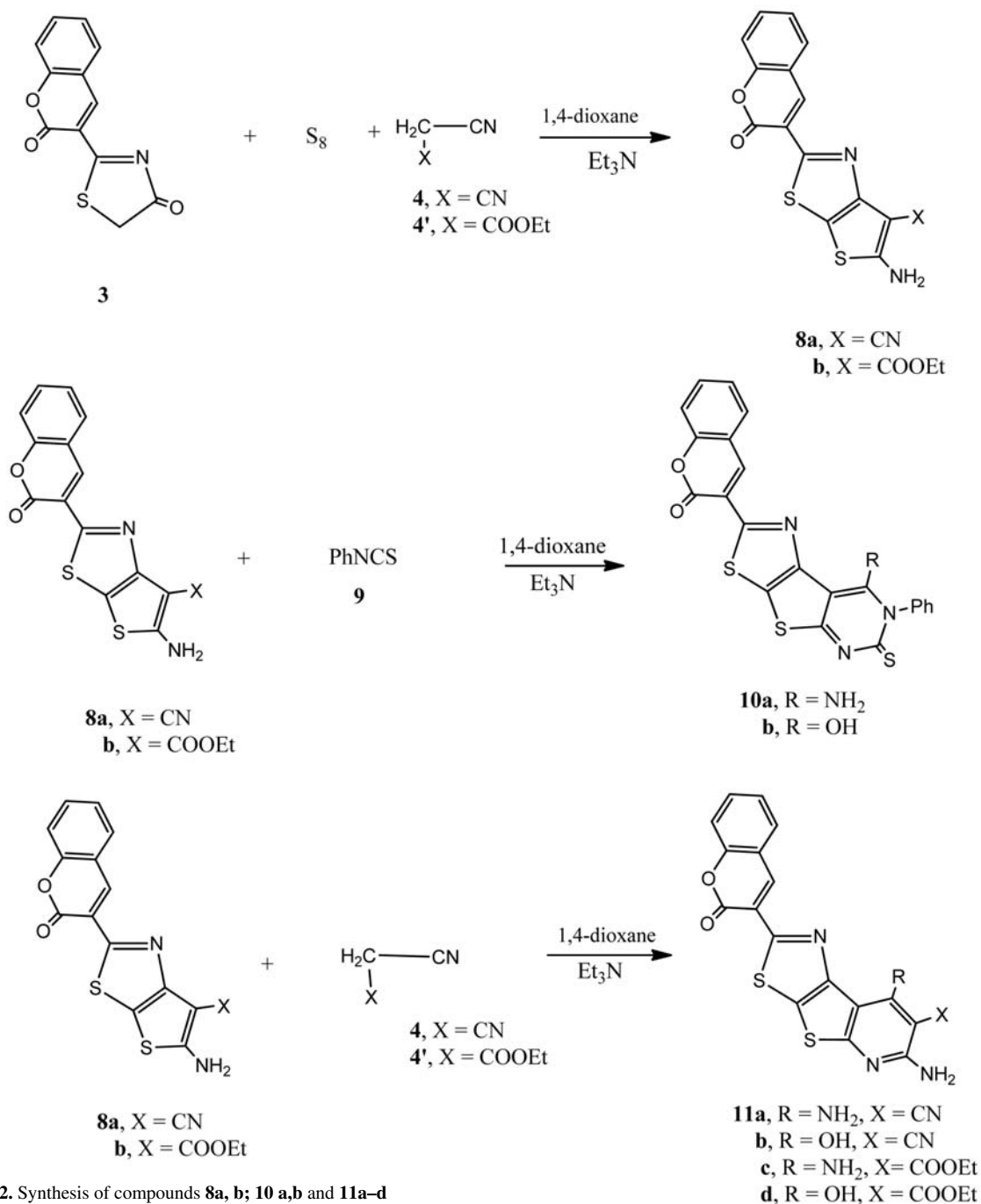
Scheme 1. Synthesis of compounds **3**, **6a–c** and **7a–c**

wed beside the expected signals,  $\delta$  58.6 ppm indicating the presence of the thiazole  $\text{CH}_2$ , two signals at  $\delta$  164.3, 168.6 ppm equivalent to the two CO groups and a signal at  $\delta$  170.3 ppm for the  $\text{C}=\text{N}$ .

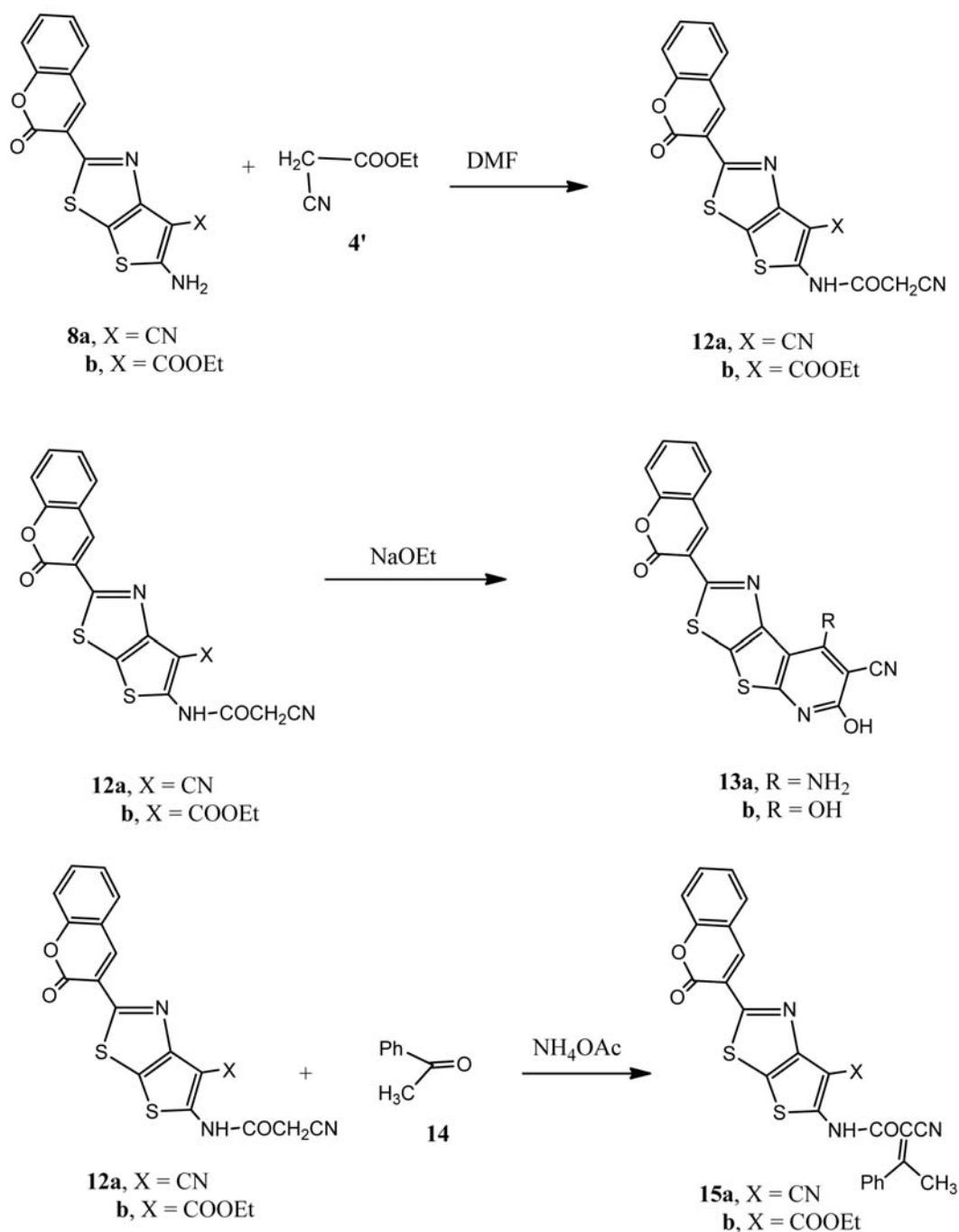
Compound **3** underwent multi-component reactions through its transformation with malonitrile (**4**) and any of benzaldehyde (**5a**), 4-chlorobenzaldehyde (**5b**) or 4-methoxybenzaldehyde (**5c**) to give the 5-amino-7*H*-pyrido[2,3-*d*]thiazole-6-carbonitrile derivatives **6a–c**, respectively. On the other hand, carrying out the same reaction, but using ammonium acetate instead of piperidine gave

the pyrido[2,3-*d*]thiazole derivatives **7a–c**, respectively (Scheme 1).

Compound **3** was ready for thiophene formation through the well known Gewald's thiophene synthesis.<sup>17,18</sup> Thus, the reaction of **3** with elemental sulfur and either malonitrile (**4**) or ethyl cyanoacetate (**4'**) gave the thieno[2,3-*d*]thiazole derivatives **8a** and **8b**, respectively. The analytical and spectral data of **8a,b** were the tools of their structural elucidation. Thus, the  $^1\text{H}$  NMR spectrum of **8a** showed a signal at  $\delta$  4.93 ppm equivalent to the  $\text{NH}_2$  group ( $\text{D}_2\text{O}$  exchangeable), a singlet at  $\delta$  6.62 ppm indica-



Scheme 2. Synthesis of compounds **8a, b**; **10 a,b** and **11a–d**

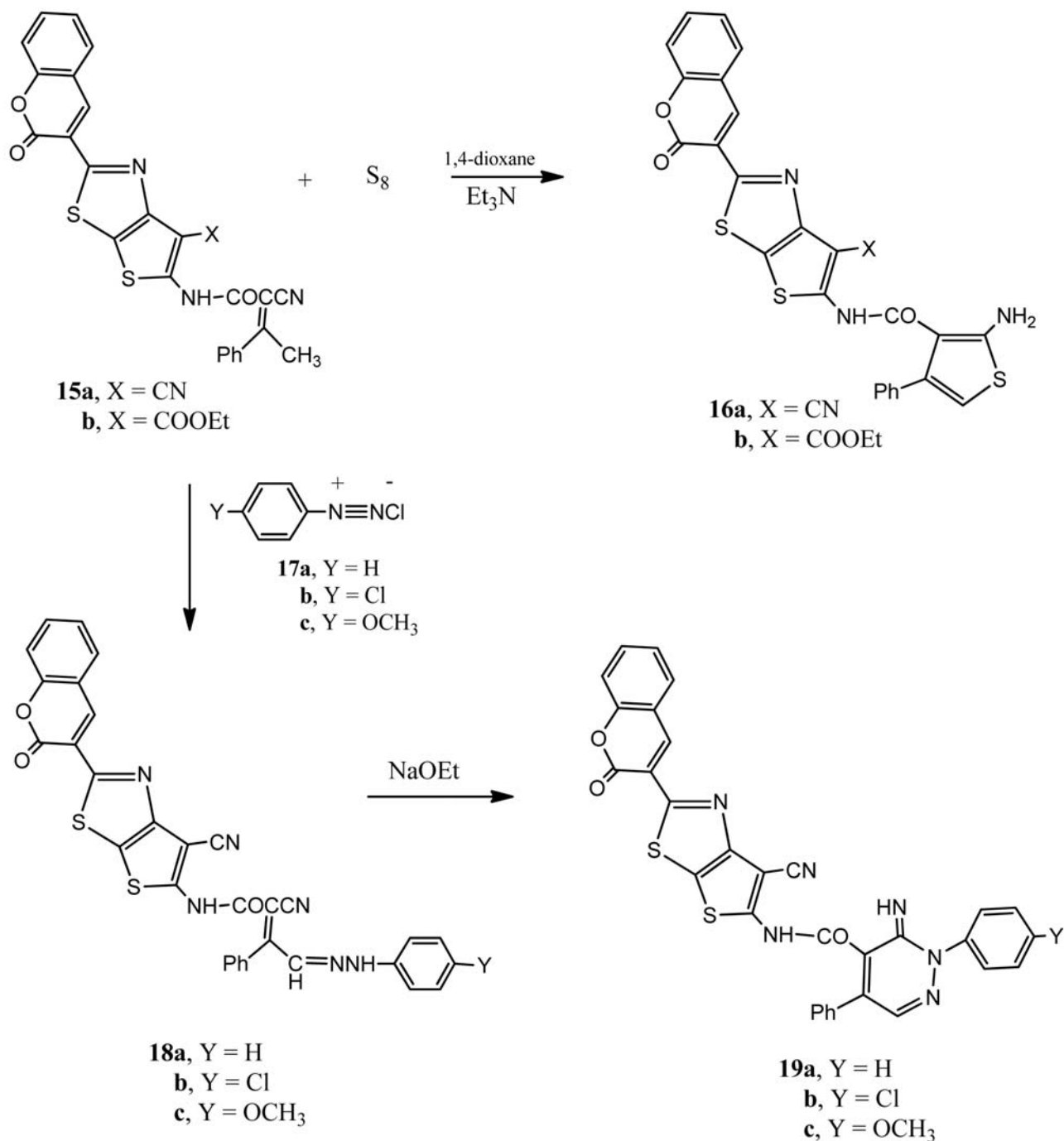


**Scheme 3.** Synthesis of compounds **12a, b**; **13 a, b** and **15a, b**

ting the coumarin H-4 and a multiplet at  $\delta$  7.26–7.40 ppm for the C<sub>6</sub>H<sub>4</sub> group. In addition, the <sup>13</sup>C NMR spectrum signals were consistent with the assigned structure. The reaction of either compound **8a** or **8b** with phenylisothiocyanate (**9**) gave the 7-phenylthiazolo[4',5':4,5]thieno[2,3-*d*]pyrimidin-6(7*H*)-thione derivatives **10a** and **10b**, respectively. On the other hand, the reaction of either compound **8a** or **8b** with either malononitrile (**4**) or ethyl cyanoacetate (**4'**) gave the 7-phenylthiazolo[4',5':4,5]thieno[2,3-*d*]pyridin-6(7*H*)-thione derivatives **11a–d**, res-

pectively (Scheme 2). The analytical and spectral data of the latter products were consistent with their respective structures (see experimental section).

The 2-amino group present in compounds **8a** and **8b** is capable for the amide group formation. Thus, the reaction of either **8a** or **8b** with ethyl cyanoacetate in refluxing dimethylformamide gave the amide derivatives **12a** and **12b**, respectively. The latter compounds readily underwent cyclization when heated in sodium ethoxide solution to give the 7-phenylthiazolo[4',5':4,5]thieno



**Scheme 4.** Synthesis of compounds **16a, b**; **18 a, c** and **19a–c**

[2,3-*d*]pyridine derivatives **13a** and **13b**, respectively. On the other hand, the reaction of either compound **12a** or **12b** with acetophenone (**14**) gave the Knoevenagel condensation products **15a** and **15b**, respectively (Scheme 3).

The presence of the but-2-enenitrile moiety in compounds **15a** and **15b** is suitable for thiophene synthesis. Thus, the reaction of either compound **15a** or **15b** with elemental sulfur gave the thiophene derivatives **16a** and **16b**, respectively. On the other hand, the reaction of either

her **15a** or **15b** with any of benzenediazonium chloride (**17a**), 4-chlorobenzenediazonium chloride (**17b**), or 4-methoxybenzenediazonium chloride (**17c**) gave the arylhydrazone derivatives **18a–c**, respectively (Scheme 4). The spectral and analytical data of compounds **18a–c** were in agreement with their respective structures (see experimental section). The latter compounds underwent cyclization when heated in sodium ethoxide solution to give corresponding pyridazine derivatives **19a–c**, respectively.

## 2. 1. Anti-inflammatory Evaluation Method

Carrageenin-induced rat hind paw oedema model was used. The method adopted resembles essentially that described by Winter.<sup>19</sup> The animals were studied for toxicity of DMSO up to 10% v/v in saline, and 5% DMSO was selected as a vehicle to suspend the standard drugs and the test compounds.

Albino rats weighing between 150 and 250 g of either sex were starved for 18 h prior to the experiment. The animals were weighed, marked for identification and divided into groups of six. The standard drugs, ibuprofen (20 mg/kg body weight), mefenamic acid (100 mg/kg body weight) and three graded doses (10, 20 and 40 mg/kg body weight) of the test compounds were given orally as a suspension using 5% DMSO as a vehicle.

One hour later foot paw oedema was induced by injecting 0.1 mL of 1% carrageenin subcutaneously into the planter portion of the right hind paw of each rat. Initial foot paw volume was measured immediately by mercury plethysmometer. Oedema was measured 3 h after carrageenin administration. The swelling in test group animals was used to calculate the % inhibition  $\pm$  SEM of oedema achieved by the compound at the test dose compared with the vehicle control group. The % protection of oedema was calculated according to the formula:

$$\% \text{ anti inflammatory activity} = 100 \left( \frac{1 - V_t}{V_c} \right) \quad (1)$$

where  $V_t$  and  $V_c$  are the volume of oedema in test compounds and control groups, respectively.

## 2. 2. Anti-ulcer Evaluation Method

Animals Wistar albino rats weighing 150–200 g of either sex maintained under standard husbandary conditions (temperature  $23 \pm 2$  °C, relative humidity  $55 \pm 10\%$  and 12 h light/dark cycle) were used for the screening. Animals were fed with standard laboratory food *ad libitum* during the study period.

Albino rats of either sex were divided into four groups of six animals each. Animals were fasted for 24 h before the study, but had free access to water. Animals in the control group received only distilled water. Each of the given compounds at 250 and 500 mg/kg, (p. o.) were given to the animals in the treatment group. Ranitidine (50 mg/kg) was used as a standard. After 1 h of drugs treatment, they were anaesthetized with the help of anesthetic ether; the abdomen was opened by a small midline incision below the xiphoid process. Pyloric portion of the stomach was slightly lifted out and ligated according to the method of Shay<sup>20</sup> avoiding traction to the pylorus or damage to its blood supply. The stomach was replaced carefully and the abdominal wall was closed by interrupted sutures. Rats were sacrificed by an over dose of anaesthetic ether after 4 h of pyloric ligation. The abdomen was

opened, cardiac end of the stomach was dissected out and the contents were drained into a glass tube. The volume of the gastric juice was measured and centrifuged at 2000 rpm for 10 min. From the supernatant, aliquots (1 mL each) were taken for the determination of pH, total and free acidity. Each stomach was examined for lesions in the fore stomach portion and indexed according to severity.

Determination of pH: an aliquot of 1 mL gastric juice was diluted with 1 mL of distilled water and pH of the solution was measured using pH meter.

## 2. 3. Toxicity Method on Shrimp Larvae

All toxicity tests were 96-h static renewal tests and water quality measurements (dissolved oxygen, pH, temperature, salinity) were taken in the control containers each day. Tests were run in a Revco's Environmental Chamber at 25 °C, 20% salinity, and a 16 h light/8 h dark cycle. A media change was made every 24 h. Larvae used for all tests were one to two days old and exposed in 600 mL glass beakers containing 400 mL of media with 10 larvae/beaker and three replicates/concentration. Larvae were fed newly hatched *Artemia* after daily media exchange. The concentration of each compound was taken in terms 10, 100 and 1000 mg/mL. Adult shrimp toxicity tests were also run to complete the grass shrimp toxicity profile. Adult shrimp (acclimated for two weeks before testing) were exposed in 4 L wide mouth glass jars containing 2 L of media and 10 shrimp/jar with two replicates/concentration, according to the modified method published by DeLorenzo<sup>21</sup> and were run under conditions as described above for larvae.

## 2. 4. Biological Evaluation

### 2. 4. 1. Anti-inflammatory Evaluations

From Table 1 it is clear that compounds **10b**, **13b**, **18a**, **19b** and **19c** showed high anti-inflammatory activity, but compounds **6b**, **6c**, **7a**, **8b**, **11a**, **11b**, **13a**, **16b** and **18c** showed low anti-inflammatory effect. Considering the 4,7-dihydrothiazolo[4,5-*b*]pyridine derivatives **7a–c**, compound **7b** with the 4-chlorophenyl moiety showed the highest anti-inflammatory activity among the three compounds. On the other hand, for the thieno[3,2-*d*]thiazole derivatives **8a,b**, compound **8a** with the 3-cyano group showed higher anti-inflammatory activity than compound **8b** with the COOEt moiety. For the thiazolo[4',5':4,5]thieno[2,3-*d*]pyrimidine derivatives **10a** and **10b**, it is obvious that compound **10b** with the hydroxyl group showed higher anti-inflammatory activity than compound **10a** with the amino group. Similarly for compounds **11a–d**, compound **11d** with the OH and COOEt moieties has the highest anti-inflammatory activity among the four compounds.

The reaction of either compound **8a** or **8b** with ethyl cyanoacetate gave the *N*-cyanoacetamido derivatives **12a**



or **12b**, respectively. Such change showed a remarkable decrease of anti-inflammatory activity in the case of **12a**. On the other hand, it showed an increase of anti-inflammatory activity of **12b**. For the thiazolo[4',5':4,5]thieno[2,3-*b*]pyridine derivatives **13a,b** the presence of the OH group in compound **13b** is responsible for its higher anti-inflammatory activity than compound **13a**. The reaction of either compound **12a** or **12b** with acetophenone gave the condensation products **15a** and **15b**, respectively, where compound **15b** with the COOEt had higher activity than compound **15a** with the CN group. However, the thiophene derivatives **16a,b** obtained from **15a,b** showed the reverse: compound **16a** with the CN group showed higher anti-inflammatory activity than compound **16b** with the COOEt moiety. Considering the arylhydrazone derivatives **18a–c**, it is clear from Table 1 that compound **18a** with the unsubstituted aryl moiety has the maximum anti-inflammatory activity among the three compounds. However, cyclization of compounds **18a–c** in sodium ethoxide solution gave the pyridazine derivatives **19a–c** where compound **19b** with 4-chloroaryl group showed the highest anti-inflammatory activity among the three compounds, followed by the compound **19c** with the 4-methoxyaryl group having the intermediate activity of the three compounds.

## 2. 5. Anti-ulcer Activity

From Table 2 it is clear that compounds **6a–c**, **7a–c**, **8b**, **10b**, **13a**, **16b**, **19b** and **19c** showed the maximum anti-ulcer activity. Moreover, these twelve compounds showed inhibition effect higher than the reference drug ranitidine. On the other hand, most of the newly synthesized products showed a moderate anti-ulcer activity at concentrations 250 and 500 mg/kg. Moreover, compounds **19b** and **19c** showed the maximum anti-ulcer activity among the tested compounds.

### 2. 5. 1. Macroscopic Evaluation of Stomach

The stomachs were opened along the greater curvature, rinsed with saline to remove gastric contents and blood clots and examined by a 10× magnifier lens to assess the formation of ulcers. The numbers of ulcers were counted. Scoring of ulcer was made as follows: (0) ... normal colored stomach; (0.5) ... red coloration; (1) ... spot ulcer; (1.5) ... hemorrhagic streak; (2) ... deep ulcers; (3) ... perforation. Mean ulcer score for each animal was expressed as ulcer index (UI). The percentage of ulcer protection was determined as follows. UI was measured by using the following formula:

$$UI = UN + US + (10^{-1}UP) \quad (2)$$

where UI is ulcer index; UN average number of ulcers per animal; US average number of severity score; UP percent-

age of animals with ulcers. Percentage inhibition of ulceration was calculated as below:

$$\begin{aligned} \% \text{ inhibition of ulceration} &= \quad (3) \\ &= [UI(\text{control}) - UI(\text{text})] \frac{100}{UI(\text{control})} \end{aligned}$$

## 2. 6. Toxicity

Bioactive compounds are often toxic to shrimp larvae. Thus, in order to monitor these chemicals *in vivo* lethality to shrimp larvae (*Artemia salina*), brine shrimp lethality assay was used. Results were analyzed with LC<sub>50</sub> program to determine LC<sub>50</sub> values and 95% confidence intervals.<sup>22</sup> Results are given in Table 4 for the compounds which exhibited optimal anti-inflammatory and anti-ulcer activity, that is the eleven compounds **7b**, **8a**, **10a**, **10b**, **13a**, **13b**, **15b**, **18a**, **19b**, **19c** and **19d**. The shrimp lethality assay is considered as a useful tool for preliminary assessment of toxicity, and it has been used for the detection of fungal toxins, plant extract toxicity, heavy metals, cyanobacteria toxins, pesticides, and cytotoxicity testing of dental materials,<sup>23</sup> natural and synthetic organic compounds.<sup>24</sup> It has also been shown that *A. salina* toxicity test results have a correlation with rodent and human acute oral toxicity data. Generally, a good correlation was obtained between *A. salina* toxicity test and the rodent data. Likewise, the predictive screening potential of the aquatic invertebrate tests for acute oral toxicity in humans, including *A. salina* toxicity test, was slightly better than the rat test for test compounds.<sup>25</sup>

In order to prevent the toxicity results from possible false effects originating from solubility of compounds and possible toxicity effect of DMSO, compounds were prepared by dissolving in DMSO in the suggested DMSO volume ranges. It is clear from Table 3 that compounds **10b**, **18a**, **19c** and **19d** showed no toxicity against the tested organisms. On the other hand, compound **7b**, **13b** and **15b** are very toxic compounds, while the rest of compounds are harmful.

## 3. Experimental

### 3. 1. General

All melting points were determined on an Electrothermal digital melting point apparatus and are uncorrected. IR spectra (KBr discs) were recorded on a FTIR plus 460 or Pye Unicam SP-1000 spectrophotometer (Pye Unicam, UK, Cambridge). <sup>1</sup>H NMR and <sup>13</sup>C NMR spectra were recorded with Varian Gemini-200 (200 MHz, Varian UK) and JEOL AS 500 MHz (JEOL, Japan) instruments in DMSO-*d*<sub>6</sub> as the solvent, using TMS as the internal standard, chemical shifts are expressed as δ ppm. The

Table 1. Anti-inflammatory evaluation of the newly synthesis products

Compound	Anti-inflammatory activity <sup>a</sup> carrageenin-induced rat hind paw oedema Mean value of Oedema volume (% protection)		
	10 mg/kg	20 mg/kg	40 mg/kg
<b>3</b>	0.60 ± 0.04 (74)	0.38 ± 0.06 (83)	0.19 ± 0.07 (92)
<b>6a</b>	0.55 ± 0.18 (76)	0.22 ± 0.02 (90)	0.23 ± 0.11 (90)
<b>6b</b>	0.99 ± 0.23 (57)	0.68 ± 0.08 (70)	1.13 ± 0.38 (51)
<b>6c</b>	0.98 ± 0.28 (57)	0.82 ± 0.03 (64)	0.63 ± 0.18 (72)
<b>7a</b>	0.82 ± 0.15 (64)	0.60 ± 0.13 (73)	0.92 ± 0.18 (58)
<b>7b</b>	0.38 ± 0.08 (83)	0.36 ± 0.07 (84)	0.29 ± 0.04 (87)
<b>7c</b>	0.80 ± 0.15 (65)	0.66 ± 0.12 (71)	0.52 ± 0.05 (77)
<b>8a</b>	0.44 ± 0.08 (81)	0.51 ± 0.09 (78)	0.05 ± 0.04 (98)
<b>8b</b>	0.93 ± 0.14 (59)	0.81 ± 0.20 (65)	1.22 ± 0.30 (48)
<b>10a</b>	1.30 ± 0.04 (43)	0.48 ± 0.06 (79)	0.93 ± 0.14 (59)
<b>10b</b>	0.09 ± 0.02 (96)	0.16 ± 0.08 (93)	0.19 ± 0.06 (92)
<b>11a</b>	1.22 ± 0.18 (47)	1.09 ± 0.23 (53)	1.19 ± 0.37 (48)
<b>11b</b>	1.08 ± 0.11 (53)	1.04 ± 0.18 (55)	1.09 ± 0.21 (53)
<b>11c</b>	0.83 ± 0.17 (64)	0.92 ± 0.20 (60)	0.69 ± 0.30 (70)
<b>11d</b>	0.68 ± 0.03 (70)	0.29 ± 0.04 (87)	0.59 ± 0.23 (74)
<b>12a</b>	0.83 ± 0.19 (64)	1.29 ± 0.36 (44)	1.33 ± 0.46 (42)
<b>12b</b>	0.60 ± 0.10 (74)	0.88 ± 0.08 (62)	0.49 ± 0.06 (79)
<b>13a</b>	1.54 ± 0.20 (33)	1.01 ± 0.23 (56)	0.51 ± 0.13 (78)
<b>13b</b>	0.39 ± 0.02 (83)	0.09 ± 0.01 (96)	0.39 ± 0.13 (83)
<b>15a</b>	0.63 ± 0.15 (73)	0.82 ± 0.21 (64)	0.65 ± 0.16 (72)
<b>15b</b>	0.33 ± 0.02 (86)	0.29 ± 0.07 (87)	0.40 ± 0.09 (83)
<b>16a</b>	0.75 ± 0.19 (67)	0.32 ± 0.04 (86)	0.22 ± 0.06 (90)
<b>16b</b>	1.39 ± 0.21 (39)	1.08 ± 0.25 (53)	1.19 ± 0.12 (48)
<b>18a</b>	0.13 ± 0.07(94)	0.24 ± 0.04 (89)	0.07 ± 0.03 (97)
<b>18b</b>	0.73 ± 0.18 (68)	0.52 ± 0.15 (77)	0.29 ± 0.02 (87)
<b>18c</b>	1.39 ± 0.26 (39)	1.52 ± 0.16 (34)	1.44 ± 0.29 (37)
<b>19a</b>	0.89 ± 0.17 (61)	0.62 ± 0.08 (73)	0.29 ± 0.01 (87)
<b>19b</b>	0.18 ± 0.03 (92)	0.18 ± 0.09 (92)	0.09 ± 0.01 (96)
<b>19c</b>	0.29 ± 0.11 (87)	0.37 ± 0.07(84)	0.49 ± 0.11 (79)
DMSO control	2.30	–	–
<b>Indomethacin</b>	<b>0.32 ± 0.09 (86)</b>	<b>0.31 ± 0.07 (88)</b>	<b>0.09 ± 0.29 (96)</b>

<sup>a</sup> Oral administration for all test compounds, P < 0.05, the standard drugs (dose and % protection) were ibuprofen (20 mg/kg, 33%) and mefenamic acid (100 mg/kg, 39%).

mass spectra were recorded with Hewlett Packard 5988 A GC/MS system (Hewlett Packard, Agilent, USA) and GCMS-QP 1000Ex Shimadzu (EI, 70 eV) (Shimadzu, Japan) instruments. Analytical data were obtained from Vario EL III Elemental CHNS analyzer (Germany).

### 3. 1. 1. 2-(2-Oxo-2H-chromen-3-yl)thiazol-4(5H)-one (3)

To a solution of compound **1** (1.40 g, 0.01 mol) in 1,4-dioxane (30 mL) containing piperidine (1.0 mL) salicylaldehyde (1.22 g, 0.01 mol) was added. The reaction mixture, in each case, was heated under reflux for 1 h, left to cool and the solid product formed, in each case, was collected by filtration and crystallized from ethanol.

Yellow crystals (ethanol), yield 82% (2.45 g), mp 166–168 °C; IR (KBr)  $\nu_{\max}$  3054, 2933, 1690, 1687, 1660, 1638  $\text{cm}^{-1}$ ; <sup>1</sup>H NMR (DMSO-*d*<sub>6</sub>, 200 MHz):  $\delta$

7.28–7.38 (4H, m, Bz), 6.52 (1H, s, H-4), 4.28 (2H, s, CH<sub>2</sub>); <sup>13</sup>C NMR (DMSO-*d*<sub>6</sub>, 75 MHz):  $\delta$  170.3 (C-2'), 168.6, 164.3 (C-2, C-4'), 58.6 (C-5'), 144.1, 139.5, 133.8, 130.1, 126.3, 123.6, 120.3 (C-3, C-4, C-5, C-6, C-7, C-8, C-9, C-10); EI-MS: *m/z* 245 [M]<sup>+</sup> (18); Analysis Calcd for C<sub>12</sub>H<sub>7</sub>NO<sub>3</sub>S (245.25): C, 58.77; H, 2.88; N, 5.71; S, 13.07%. Found: C, 58.85; H, 3.03; N, 5.92; S, 12.89%.

### 3. 1. 2. General Procedure for the Synthesis of the Pyrano[2,3-*d*]thiazole Derivatives 6a–c

To a solution of compound **3** (2.45 g, 0.01 mol) in ethanol (50 mL) containing triethylamine (0.50 mL) malononitrile (0.66 g, 0.01 mol) and any of benzaldehyde (1.06 g, 0.01 mol), 4-chlorobenzaldehyde (1.40 g, 0.01 mol) or 4-methoxybenzaldehyde (1.37 g, 0.01 mol) were added. The whole reaction mixture was heated under reflux for 4 h then left to cool. The formed solid product, in each case, was collected by filtration.

**Table 2.** Effect of DMSO solution of the given compounds on gastric ulcer induced by pylorus ligation in rats, pH, total and free acidity in pyloric ligation induced ulceration in rats

Treatment	Dose (mg/kg)	Ulcer index	% ulcer inhibition
Control (distilled water)	10	3.6 ± 0.45	–
<b>3</b>	250	1.91 ± 0.53	47
	500	0.98 ± 0.19	73
<b>6a</b>	250	0.43 ± 0.08	88
	500	0.18 ± 0.01	95
<b>6b</b>	250	0.32 ± 0.28	91
	500	0.82 ± 0.08	77
<b>6c</b>	250	0.77 ± 0.19	79
	500	0.59 ± 0.08	84
<b>7a</b>	250	0.66 ± 0.42	82
	500	0.49 ± 0.52	86
<b>7b</b>	250	0.88 ± 0.30	75
	500	0.38 ± 0.21	89
<b>7c</b>	250	0.58 ± 0.27	84
	500	0.32 ± 0.19	91
<b>8a</b>	250	1.29 ± 0.27	64
	500	1.38 ± 0.36	62
<b>8b</b>	250	0.13 ± 0.08	96
	500	0.19 ± 0.05	95
<b>10a</b>	250	1.86 ± 0.63	48
	500	0.82 ± 0.17	77
<b>10b</b>	250	0.80 ± 0.25	78
	500	0.32 ± 0.09	91
<b>11a</b>	250	1.77 ± 0.83	51
	500	1.20 ± 0.39	67
<b>11b</b>	250	1.83 ± 0.29	49
	500	0.66 ± 0.13	82
<b>11c</b>	250	1.73 ± 0.42	52
	500	1.39 ± 0.62	61
<b>11d</b>	250	1.23 ± 0.64	66
	500	0.88 ± 0.12	75
<b>12a</b>	250	1.93 ± 0.25	46
	500	0.83 ± 0.26	77
<b>12b</b>	250	1.82 ± 0.63	49
	500	1.94 ± 0.08	46
<b>13a</b>	250	0.63 ± 0.09	82
	500	1.19 ± 0.16	67
<b>13b</b>	250	1.09 ± 0.15	70
	500	0.86 ± 0.26	76
<b>15a</b>	250	1.73 ± 0.41	52
	500	1.63 ± 0.22	55
<b>15b</b>	250	1.87 ± 0.48	48
	500	1.29 ± 0.27	64
<b>16a</b>	250	1.53 ± 0.42	57
	500	0.89 ± 0.04	75
<b>16b</b>	250	0.63 ± 0.12	82
	500	0.58 ± 0.20	84
<b>18a</b>	250	0.92 ± 0.13	66
	500	0.62 ± 0.23	74
<b>18b</b>	250	2.88 ± 0.53	20
	500	2.21 ± 0.09	39
<b>18c</b>	250	1.42 ± 0.96	60
	500	0.89 ± 0.25	72

Treatment	Dose (mg/kg)	Ulcer index	% ulcer inhibition
<b>19a</b>	250	2.89 ± 0.68	20
	500	1.63 ± 0.71	55
<b>19b</b>	250	0.22 ± 0.05	94
	500	0.29 ± 0.09	92
<b>19c</b>	250	0.26 ± 0.06	93
	500	0.19 ± 0.01	95
<b>Ranitidine</b>	<b>50</b>	<b>1.65 ± 0.49</b>	<b>54</b>

Values are expressed as mean ± S.E.M.,  $n = 6$ ,  $*p < 0.05$  when compared with control group.

**Table 3.** Toxicity of the most potent compounds

Compound	Conc. (µg/mL)	Mortality <sup>a</sup>	Toxicity	LC <sub>50</sub>	Upper 95% lim.	Lower 95% lim.
<b>7b</b>	10	2	very toxic	120.29	–	–
	100	4				
	1000	10				
<b>8a</b>	10	1	harmful	210.55	197.22	
	148.38					
	100	4				
	1000	7				
<b>10b</b>	10	0	nontoxic	818.15	112.40	72.73
	100	2				
	1000	4				
<b>13b</b>	10	3	very toxic	112.49	276.40	66.30
	100	6				
	1000	10				
<b>15b</b>	10	2	very toxic	109.06	220.31	80.45
	100	5				
	1000	10				
<b>18a</b>	10	0	non toxic	909.28	–	–
	100	1				
	1000	4				
<b>19b</b>	10	1	harmful	133.40	236.50	93.28
	100	4				
	1000	10				
<b>19c</b>	10	0	non toxic	910.63	–	–
	100	3				
	1000	5				
<b>19d</b>	10	0	non toxic	890.63	–	–
	100	2				
	1000	6				

<sup>a</sup>Ten organisms (*A. salina*) tested for each concentration.

### 5-Amino-2-(2-oxo-2H-chromen-3-yl)-7-phenyl-7H-pyrano[2,3-d]thiazole-6-carbonitrile (6a)

Yellow crystals (ethanol), yield 80% (3.19 g), mp 188–191 °C; IR (KBr)  $\nu_{\max}$  3477, 3329, 3056, 2220, 1693, 1654, 1635  $\text{cm}^{-1}$ ;  $^1\text{H}$  NMR (DMSO- $d_6$ , 200 MHz):  $\delta$  7.42–7.25 (9H, m, 2Bz), 6.58 (1H, s, H-4'), 6.18 (1H, s, H-7), 4.82 (2H, s, D<sub>2</sub>O exchangeable, NH<sub>2</sub>);  $^{13}\text{C}$  NMR (DMSO- $d_6$ , 75 MHz):  $\delta$  86.4 (C-7), 116.8 (CN), 144.4, 143.1, 142.8, 138.8, 135.2, 130.3, 129.4, 128.9, 127.2,

126.3, 126.2, 125.4, 124.8, 122.8, 119.8 (Bz, C-8,C-9, C-5, C-6, C-1', C-2', C3', C-4', C-5', C-6'), 165.2 (C-7'), 173.2 (C-2); EI-MS:  $m/z$  399 [M]<sup>+</sup> (42%); Analysis Calcd for C<sub>22</sub>H<sub>13</sub>N<sub>3</sub>O<sub>3</sub>S (399.42): C, 66.15; H, 3.28; N, 10.52; S, 8.03. Found: C, 66.29; H, 3.41; N, 10.73; S, 7.92.

#### 5-Amino-7-(4-chlorophenyl)-2-(2-oxo-2H-chromen-3-yl)-7H-pyrano[2,3-d]thiazole-6-carbonitrile (6b)

Pale yellow crystals (ethanol), yield 73% (3.16 g), mp 166–169 °C; IR (KBr)  $\nu_{\max}$  3493, 3326, 3054, 2223, 1690, 1656, 1633 (C=C) cm<sup>-1</sup>; <sup>1</sup>H NMR (DMSO-*d*<sub>6</sub>, 200 MHz):  $\delta$  7.24–7.40 (8H, m, 2Bz), 6.61 (1H, s, H-4'), 6.15 (1H, s, H-7), 4.80 (s, 2H, D<sub>2</sub>O exchangeable, NH<sub>2</sub>); <sup>13</sup>C NMR (DMSO-*d*<sub>6</sub>, 75 MHz):  $\delta$  86.8 (C-7), 116.6 (CN), 120.4, 122.6, 123.9, 124.3, 124.9, 125.2, 125.7, 126.9, 129.2, 130.5, 133.9, 135.2, 138.1, 140.2, 142.9, 143.6 (Bz, C-8,C-9,C-5, C-6, C-1', C-2', C3', C-4', C-5', C-6'), 165.4 (C-7'), 173.0 (C-2); EI-MS:  $m/z$  433 [M]<sup>+</sup> (30%); Analysis Calcd for C<sub>22</sub>H<sub>12</sub>ClN<sub>3</sub>O<sub>3</sub>S (433.03): C, 60.90; H, 2.79; N, 9.69; S, 7.39%. Found: C, 61.28; H, 2.91; N, 9.49; S, 7.44%.

#### 5-Amino-7-(4-methoxyphenyl)-2-(2-oxo-2H-chromen-3-yl)-7H-pyrano[2,3-d]thiazole-6-carbonitrile (6c)

Orange crystals (ethanol), yield 88% (3.77 g), mp 211–213 °C; IR (KBr)  $\nu_{\max}$  3475, 3318, 3056, 2221, 1692, 1658, 1630 cm<sup>-1</sup>; <sup>1</sup>H NMR (DMSO-*d*<sub>6</sub>, 200 MHz):  $\delta$  7.29–7.41 (m, 8H, 2Bz), 6.63 (1H, s, H-4'), 6.18 (1H, s, H-7), 4.86 (2H, s, D<sub>2</sub>O exchangeable, NH<sub>2</sub>), 3.14 (3H, s, OCH<sub>3</sub>); <sup>13</sup>C NMR (DMSO-*d*<sub>6</sub>, 75 MHz):  $\delta$  173.3 (C-2), 165.4 (C-7'), 143.6, 143.0, 139.2, 138.7, 134.6, 133.7, 132.2, 131.8, 129.8, 127.4, 126.0, 125.7, 125.1, 124.6, 123.2, 120.7 (Bz, C-8,C-9,C-5, C-6, C-1', C-2', C3', C-4', C-5', C-6'), 116.8 (CN), 86.6 (C-7), 34.6 (C, OCH<sub>3</sub>); EI-MS:  $m/z$  429 [M]<sup>+</sup> (22%); Analysis Calcd for C<sub>23</sub>H<sub>15</sub>N<sub>3</sub>O<sub>4</sub>S (429.45): C, 64.33; H, 3.52; N, 9.78; S, 7.47%. Found: C, 64.40; H, 3.66; N, 9.83; S, 7.54%.

### 3. 1. 3. General procedure for the synthesis of the pyridino[2,3-d]thiazole derivatives 7a–c

To a solution of compound **3** (2.45 g, 0.01 mol) in ethanol (50 mL) containing ammonium acetate (0.50 mL) malononitrile (0.66 g, 0.01 mol) and any of benzaldehyde (1.06 g, 0.01 mol), 4-chlorobenzaldehyde (1.40 g, 0.01 mol) or 4-methoxybenzaldehyde (1.37 g, 0.01 mol) was added. The whole reaction mixture was heated under reflux for 4 h then left to cool. The solid product formed upon pouring onto ice/water containing a few drops of hydrochloric acid was collected by filtration.

#### 5-Amino-2-(2-oxo-2H-chromen-3-yl)-7-phenyl-4,7-dihydrothiazolo[4,5-*b*]pyridine-6-carbonitrile (7a)

Yellow crystals (ethanol), yield 77% (3.06 g), mp 201–203 °C; IR (KBr)  $\nu_{\max}$  3466–3380, 3059, 2222, 1688, 1652, 1633 cm<sup>-1</sup>; <sup>1</sup>H NMR (DMSO-*d*<sub>6</sub>, 200 MHz):

$\delta$  8.23 (s, 1H, D<sub>2</sub>O exchangeable, NH), 7.28–7.39 (m, 9H, 2Bz), 6.54 (1H, s, H-7), 6.16 (1H, s, H-4'), 4.80 (s, 2H, D<sub>2</sub>O exchangeable, NH<sub>2</sub>); <sup>13</sup>C NMR (DMSO-*d*<sub>6</sub>, 75 MHz):  $\delta$  173.0 (C-2), 165.8 (C-7'), 142.6, 141.3, 140.2, 139.4, 136.2, 134.9, 133.8, 128.7, 128.2, 126.8, 126.0, 125.3, 124.5, 121.5, 120.3 (Bz, C-8,C-9,C-5, C-6, C-1', C-2', C3', C-4', C-5', C-6'), 116.9 (CN), 86.2 (C-7); EI-MS:  $m/z$  398 [M]<sup>+</sup> (28%); Analysis Calcd for C<sub>22</sub>H<sub>14</sub>N<sub>4</sub>O<sub>2</sub>S (398.44): C, 66.32; H, 3.54; N, 14.06; S, 8.05%. Found: C, 66.59; H, 3.33; N, 14.18; S, 7.98%.

#### 5-Amino-7-(4-chlorophenyl)-2-(2-oxo-2H-chromen-3-yl)-4,7-dihydrothiazolo[4,5-*b*]pyridine-6-carbonitrile (7b)

Pale yellow crystals (ethanol), yield 73% (3.15 g), mp 241–243 °C; IR (KBr)  $\nu_{\max}$  3493–3327, 3056, 2220, 1688, 1653, 1630 cm<sup>-1</sup>; <sup>1</sup>H NMR (DMSO-*d*<sub>6</sub>, 200 MHz):  $\delta$  8.25 (s, 1H, D<sub>2</sub>O exchangeable, NH), 7.26–7.39 (m, 8H, 2Bz), 6.63 (1H, s, H-7), 6.18 (1H, s, H-4'), 4.83 (s, 2H, D<sub>2</sub>O exchangeable, NH<sub>2</sub>); <sup>13</sup>C NMR (DMSO-*d*<sub>6</sub>, 75 MHz):  $\delta$  173.2 (C-2), 165.6 (C-7'), 142.8, 141.4, 140.8, 137.2, 135.6, 134.3, 132.8, 128.7, 126.4, 126.0, 125.2, 123.9, 123.2, 122.4, 120.3 (Bz, C-8,C-9,C-5, C-6, C-1', C-2', C3', C-4', C-5', C-6'), 116.9 (CN), 86.2 (C-7); EI-MS:  $m/z$  432 [M]<sup>+</sup> (38%); Analysis Calcd for C<sub>22</sub>H<sub>13</sub>ClN<sub>4</sub>O<sub>2</sub>S (432.88): C, 61.04; H, 3.03; N, 12.94; S, 7.41%. Found: C, 61.29; H, 2.88; N, 12.72; S, 7.39%.

#### 5-Amino-7-(4-methoxyphenyl)-2-(2-oxo-2H-chromen-3-yl)-4,7-dihydrothiazolo[4,5-*b*]pyridine-6-carbonitrile (7c)

Orange crystals (ethanol), yield 79% (3.38 g), mp 255–258 °C; IR (KBr)  $\nu_{\max}$  3488–3359, 3052, 2220, 1689, 1654, 1632 cm<sup>-1</sup>; <sup>1</sup>H NMR (DMSO-*d*<sub>6</sub>, 200 MHz):  $\delta$  8.22 (s, 1H, D<sub>2</sub>O exchangeable, NH), 7.25–7.45 (8H, m, 2Bz), 6.62 (1H, s, H-7), 6.20 (1H, s, H-4'), 4.83 (s, 2H, D<sub>2</sub>O exchangeable, NH<sub>2</sub>), 3.70 (s, 3H, CH<sub>3</sub>); <sup>13</sup>C NMR (DMSO-*d*<sub>6</sub>, 75 MHz):  $\delta$  173.2 (C-2), 165.6 (C-7'), 142.9, 142.8, 139.9, 139.1, 136.0, 134.2, 132.8, 132.4, 130.2, 128.8, 126.2, 125.6, 125.2, 123.8, 122.0, 121.2 (Bz, C-8,C-9,C-5, C-6, C-1', C-2', C3', C-4', C-5', C-6'), 116.9 (CN), 86.6 (C-7), 34.8 (C, OCH<sub>3</sub>); EI-MS:  $m/z$  428 [M]<sup>+</sup> (20%); Analysis Calcd for C<sub>23</sub>H<sub>16</sub>N<sub>4</sub>O<sub>3</sub>S (428.46): C, 64.47; H, 3.76; N, 13.08; S, 7.48%. Found: C, 64.53; H, 3.80; N, 12.93; S, 7.62%.

### 3. 1. 4. General Procedure for the Synthesis of the Thieno[3,2-*d*]thiazole Derivatives 8a and 8b

To a solution of compound **3** (2.45 g, 0.01 mol) in 1,4-dioxane (40 mL) containing (0.01 mol) triethylamine, either malononitrile (0.66 g, 0.01 mol) or ethyl cyanoacetate (1.13 g, 0.01 mol) and elemental sulfur (0.32 g, 0.01 mol) were added. The whole reaction mixture was heated under reflux for 4 h then left to cool. The solid product

formed upon pouring onto ice/water containing a few drops of hydrochloric acid was collected by filtration.

### 5-Amino-2-(2-oxo-2H-chromen-3-yl)thieno[3,2-d]thiazole-6-carbonitrile (**8a**)

Orange crystals (1,4-dioxane), yield 82% (2.66 g), mp 189–193 °C; IR (KBr)  $\nu_{\text{max}}$  3488–3342, 3057, 2220, 1690, 1655, 1632  $\text{cm}^{-1}$ ;  $^1\text{H}$  NMR (DMSO- $d_6$ , 200 MHz):  $\delta$  7.40–7.26 (4H, m, Bz), 6.62 (1H, s, H-4'), 4.93 (2H, s, D<sub>2</sub>O exchangeable, NH<sub>2</sub>);  $^{13}\text{C}$  NMR (DMSO- $d_6$ , 75 MHz):  $\delta$  172.8 (C-2), 164.8 (C-2'), 142.3, 141.8, 138.1, 136.2, 133.2, 132.8, 130.5, 128.4, 126.2, 123.9, 122.0, 119.7 (Bz, C-4, C-5, C-7, C-8, C-3', C-4'), 117.3 (CN); EI-MS:  $m/z$  325 [M]<sup>+</sup> (15%); Analysis Calcd for C<sub>15</sub>H<sub>7</sub>N<sub>3</sub>O<sub>2</sub>S<sub>2</sub> (325.36): C, 55.37; H, 2.17; N, 12.91; S, 19.71%. Found: C, 55.52; H, 2.28; N, 13.18; S, 19.88%.

**Ethyl 5-amino-2-(2-oxo-2H-chromen-3-yl)thieno[3,2-d]thiazole-6-carboxylate (**8b**)** Yellow crystals (1,4-dioxane), yield 77% (3.86 g), mp 142–145 °C; IR (KBr)  $\nu_{\text{max}}$  3493–3338, 3055, 1688, 1653, 1630  $\text{cm}^{-1}$ ;  $^1\text{H}$  NMR (DMSO- $d_6$ , 200 MHz):  $\delta$  7.38–7.23 (4H, m, Bz), 6.64 (1H, s, H-4'), 4.96 (2H, s, D<sub>2</sub>O exchangeable, NH<sub>2</sub>), 4.20 (2H, q,  $J = 7.29$  Hz, OCH<sub>2</sub>CH<sub>3</sub>), 1.14 (3H, t,  $J = 7.29$  Hz, OCH<sub>2</sub>CH<sub>3</sub>);  $^{13}\text{C}$  NMR (DMSO- $d_6$ , 75 MHz):  $\delta$  172.9 (C-2), 164.8 (C-2'), 142.6, 141.2, 138.3, 136.0, 133.6, 132.5, 130.3, 128.3, 126.4, 123.7, 122.2, 119.3 (Bz, C-4, C-5, C-7, C-8, C-3', C-4'), 56.2 (C, CH<sub>2</sub>, OCH<sub>2</sub>CH<sub>3</sub>), 16.9 (C, CH<sub>3</sub>, OCH<sub>2</sub>CH<sub>3</sub>); EI-MS:  $m/z$  372 [M]<sup>+</sup> (30%); Analysis Calcd for C<sub>17</sub>H<sub>12</sub>N<sub>2</sub>O<sub>4</sub>S<sub>2</sub> (372.42): C, 54.83; H, 3.25; N, 7.52; S, 17.22%. Found: C, 54.76; H, 3.19; N, 7.73; S, 17.08%.

### 3. 1. 5. General Procedure for the Synthesis of 7-phenylthiazolo[4',5':4,5]-thieno[2,3-d]pyrimidine-6(7H)-thione Derivatives **10a** and **10b**

To a solution of either compound **8a** (3.25 g, 0.01 mol) or **8b** (3.72 g, 0.01 mol) in 1,4-dioxane (40 mL) containing triethylamine (0.50 mL), phenylisothiocyanate (1.30 g, 0.01 mol) was added. The whole reaction mixture was heated under reflux for 4 h then poured onto ice/water containing a few drops of hydrochloric acid and the formed solid product, in each case, was collected by filtration.

### 3-(8-Amino-7-phenyl-6-thioxo-6,7-dihydrothiazolo[4',5':4,5]thieno[2,3-d]pyrimidin-2-yl)-2H-chromen-2-one (**10a**)

Pale yellow crystals (1,4-dioxane), 74% (3.40 g), mp 222–225 °C; IR (KBr)  $\nu_{\text{max}}$  3459–3326, 3054, 2223, 1687, 1653, 1630, 1220  $\text{cm}^{-1}$ ;  $^1\text{H}$  NMR (DMSO- $d_6$ , 200 MHz):  $\delta$  7.25–7.42 (m, 9H, 2Bz), 6.62 (1H, s, H-4'), 4.92 (2H, s, D<sub>2</sub>O exchangeable, NH<sub>2</sub>);  $^{13}\text{C}$  NMR (DMSO- $d_6$ , 75 MHz):  $\delta$  178.2 (C-6), 170.8, 172.4 (C-2, C-10), 164.3

(C-2'), 142.6, 140.4, 139.2, 138.1, 136.2, 133.2, 132.8, 131.8, 130.2, 129.3, 128.6, 127.3, 125.8, 123.3, 121.8, 120.3 (2Bz, C-4, C-8, C-9, C-11, C-3', C-4'); EI-MS:  $m/z$  460 [M]<sup>+</sup> (35%); Analysis Calcd for C<sub>22</sub>H<sub>12</sub>N<sub>4</sub>O<sub>2</sub>S<sub>3</sub> (460.55): C, 57.37; H, 2.63; N, 12.17; S, 20.89%. Found: C, 57.50; H, 2.58; N, 12.22; S, 20.69%.

### 3-(8-Hydroxy-7-phenyl-6-thioxo-6,7-dihydrothiazolo[4',5':4,5]thieno[2,3-d]pyrimidin-2-yl)-2H-chromen-2-one (**10b**)

Yellow crystals (1,4-dioxane), yield 69% (3.18 g), mp 180–184 °C; IR (KBr)  $\nu_{\text{max}}$  3473–3340, 3052, 2220, 1689, 1652, 1632, 1223  $\text{cm}^{-1}$ ;  $^1\text{H}$  NMR (DMSO- $d_6$ , 200 MHz):  $\delta$  10.31 (1H, s, D<sub>2</sub>O exchangeable, OH), 7.46–7.28 (9H, m, 2Bz), 6.64 (1H, s, H-4');  $^{13}\text{C}$  NMR (DMSO- $d_6$ , 75 MHz):  $\delta$  178.2 (C-6), 170.5, 172.2 (C-2, C-10), 164.4 (C-2'), 143.1, 140.6, 138.0, 137.4, 136.1, 134.9, 132.6, 132.3, 130.6, 129.0, 126.1, 124.2, 123.6, 122.8, 120.5, 118.5 (2Bz, C-4, C-8, C-9, C-11, C-3', C-4'); EI-MS:  $m/z$  462 [M]<sup>+</sup> (18%); Analysis Calcd for C<sub>22</sub>H<sub>11</sub>N<sub>3</sub>O<sub>3</sub>S<sub>3</sub> (462.54): C, 57.25; H, 2.40; N, 9.10; S, 20.84%. Found: C, 57.39; H, 2.29; N, 9.28; S, 20.77%.

### 3. 1. 6. General Procedure for the Synthesis of the Thiazolo[4',5':4,5]thieno[2,3-b]pyridine Derivatives **11a–d**

To a solution of either compound **8a** (3.25 g, 0.01 mol) or **8b** (4.61 g, 0.01 mol) in 1,4-dioxane (30 mL) containing triethylamine (0.50 mL), either malononitrile (0.66 g, 0.01 mol) or ethyl cyanoacetate (1.13 g, 0.01 mol) was added. The reaction mixture was heated under reflux for 2 h then poured onto ice/water containing a few drops of hydrochloric acid and the solid product formed was collected by filtration.

### 6,8-Diamino-2-(2-oxo-2H-chromen-3-yl)thiazolo[4',5':4,5]thieno[2,3-b]pyridine-7-carbonitrile (**11a**)

Orange crystals (1,4-dioxane), yield 78% (4.83 g), mp 243–246 °C; IR (KBr)  $\nu_{\text{max}}$  3488–3336, 3056, 2221, 1689, 1653, 1632  $\text{cm}^{-1}$ ;  $^1\text{H}$  NMR (DMSO- $d_6$ , 200 MHz):  $\delta$  7.40–7.28 (4H, m, Bz), 6.65 (1H, s, H-4'), 5.21, 4.89 (4H, 2s, D<sub>2</sub>O exchangeable, 2NH<sub>2</sub>);  $^{13}\text{C}$  NMR (DMSO- $d_6$ , 75 MHz):  $\delta$  171.8, 170.3 (C-2, C-6), 164.6 (C-2'), 140.5, 138.2, 136.4, 135.2, 134.6, 132.7, 130.2, 129.7, 127.8, 125.0, 124.6, 122.7, 120.1, 119.2 (Bz, C-4, C-5, C-8, C-9, C-10, C-11, C-3', C-4'), 116.9 (CN); EI-MS:  $m/z$  391 [M]<sup>+</sup> (24%); Analysis Calcd for C<sub>18</sub>H<sub>9</sub>N<sub>5</sub>O<sub>2</sub>S<sub>2</sub> (391.43): C, 55.23; H, 2.32; N, 17.89; S, 16.38%. Found: C, 55.36; H, 2.41; N, 18.29; S, 16.29%.

### 6-Amino-8-hydroxy-2-(2-oxo-2H-chromen-3-yl)thiazolo[4',5':4,5]thieno[2,3-b]pyridine-7-carbonitrile (**11b**)

Pale yellow crystals (1,4-dioxane), yield 66% (2.58 g), mp 210–213 °C; IR (KBr)  $\nu_{\text{max}}$  3574–3332, 3054,

2222, 1686, 1651, 1631  $\text{cm}^{-1}$ ;  $^1\text{H}$  NMR (DMSO- $d_6$ , 200 MHz):  $\delta$  10.30 (1H, s,  $\text{D}_2\text{O}$  exchangeable, OH), 7.25–7.36 (4H, m, Bz), 6.63 (1H, s, H-4'), 4.87 (2H, s,  $\text{D}_2\text{O}$  exchangeable,  $\text{NH}_2$ );  $^{13}\text{C}$  NMR (DMSO- $d_6$ , 75 MHz):  $\delta$  171.5, 170.2 (C-2, C-6), 164.3 (C-2'), 141.8, 137.0, 136.4, 133.0, 132.8, 131.9, 130.2, 125.7, 125.1, 124.6, 123.4, 121.8, 120.6 (Bz, C-4, C-5, C-8, C-9, C-10, C-11, C-3', C-4'), 116.5 (CN); EI-MS:  $m/z$  392  $[\text{M}]^+$  (18%); Analysis Calcd for  $\text{C}_{18}\text{H}_8\text{N}_4\text{O}_3\text{S}_2$  (392.41): C, 55.09; H, 2.05; N, 14.28; S, 16.34%. Found: C, 55.18; H, 2.21; N, 14.50; S, 16.48%.

#### Ethyl 6,8-diamino-2-(2-oxo-2H-chromen-3-yl)thiazolo[4',5':4,5]thieno[2,3-b]pyridine-7-carboxylate (11c)

Yellowish white (1,4-dioxane), yield 73% (3.19 g), mp 188–192 °C; IR (KBr)  $\nu_{\text{max}}$  3464–3328, 3056, 1688, 1653, 1629  $\text{cm}^{-1}$ ;  $^1\text{H}$  NMR (DMSO- $d_6$ , 200 MHz):  $\delta$  7.37–7.27 (4H, m, Bz), 6.60 (1H, s, H-4'), 4.45, 5.28 (4H, 2s,  $\text{D}_2\text{O}$  exchangeable,  $2\text{NH}_2$ ), 4.20 (2H, q,  $J = 7.08$  Hz,  $\text{OCH}_2\text{CH}_3$ ), 1.14 (3H, t,  $J = 7.08$  Hz,  $\text{OCH}_2\text{CH}_3$ );  $^{13}\text{C}$  NMR (DMSO- $d_6$ , 75 MHz):  $\delta$  170.4, 171.4 (C-2, C-6), 164.2 (C-2'), 120.5, 121.8, 121.9, 122.8, 123.9, 124.2, 127.3, 127.8, 128.0, 129.3, 130.3, 131.3, 134.9, 139.2 (Bz, C-4, C-5, C-8, C-9, C-10, C-11, C-3', C-4'), 54.2 (C,  $\text{CH}_2$ ,  $\text{OCH}_2\text{CH}_3$ ), 16.8 (C,  $\text{CH}_3$ ,  $\text{OCH}_2\text{CH}_3$ ); EI-MS:  $m/z$  438  $[\text{M}]^+$  (23%); Analysis Calcd for  $\text{C}_{20}\text{H}_{14}\text{N}_4\text{O}_4\text{S}_2$  (438.48): C, 54.78; H, 3.22; N, 12.78; S, 14.63%. Found: C, 54.91; H, 3.40; N, 12.91; S, 14.80%.

#### Ethyl 6-amino-8-hydroxy-2-(2-oxo-2H-chromen-3-yl)thiazolo[4',5':4,5]thieno[2,3-b]pyridine-7-carboxylate (11d)

Yellow crystals (1,4-dioxane), yield 78% (3.42 g), mp 205–208 °C; IR (KBr)  $\nu_{\text{max}}$  3520–3336, 3058, 1689, 1651, 1632  $\text{cm}^{-1}$ ;  $^1\text{H}$  NMR (DMSO- $d_6$ , 200 MHz):  $\delta$  10.22 (1H, s,  $\text{D}_2\text{O}$  exchangeable, OH), 7.28–7.39 (4H, m, Bz), 6.62 (1H, s, H-4'), 4.48 (2H, s,  $\text{D}_2\text{O}$  exchangeable,  $\text{NH}_2$ ), 4.20 (2H, q,  $J = 7.22$  Hz,  $\text{OCH}_2\text{CH}_3$ ), 1.15 (3H, t,  $J = 7.22$  Hz,  $\text{OCH}_2\text{CH}_3$ );  $^{13}\text{C}$  NMR (DMSO- $d_6$ , 75 MHz):  $\delta$  171.6, 170.2 (C-2, C-6), 164.4, 164.2 (C-2'), 142.7, 134.9, 132.6, 131.8, 131.2, 129.7, 119.3, 126.7, 126.5, 124.8, 124.0, 123.6, 122.8, 121.6, (Bz, C-4, C-5, C-8, C-9, C-10, C-11, C-3', C-4'), 54.6 (C,  $\text{CH}_2$ ,  $\text{OCH}_2\text{CH}_3$ ), 16.7 (C,  $\text{CH}_3$ ,  $\text{OCH}_2\text{CH}_3$ ); EI-MS:  $m/z$  439  $[\text{M}]^+$  (18%); Analysis Calcd for  $\text{C}_{20}\text{H}_{13}\text{N}_3\text{O}_5\text{S}_2$  (439.46): C, 54.66; H, 2.98; N, 9.56; S, 14.59%. Found: C, 54.79; H, 3.17; N, 9.29; S, 14.63%.

### 3. 1. 7. General Procedure for the Synthesis of the 2-cyanoacetylthieno[3,2-d]thiazole Derivatives 12a and 12b

To a solution of either compound **8a** (3.25 g, 0.01 mol) or **8b** (4.61 g, 0.01 mol) in dimethylformamide (30 mL) ethyl cyanoacetate (1.13 g, 0.01 mol) was added. The reaction mixture was heated under reflux for 3 h then pou-

red onto ice/water containing a few drops of hydrochloric acid and the solid product formed was collected by filtration.

#### 2-Cyano-N-[6-cyano-2-(2-oxo-2H-chromen-3-yl)thieno[3,2-d]thiazol-5-yl]acetamide (12a)

Yellow crystals (1,4-dioxane), yield 83% (3.25 g), mp 188–191 °C; IR (KBr)  $\nu_{\text{max}}$  3468–3326, 3054, 2223, 2220, 1688, 1705, 1655, 1634  $\text{cm}^{-1}$ ;  $^1\text{H}$  NMR (DMSO- $d_6$ , 200 MHz):  $\delta$  8.20 (1H, s, NH,  $\text{D}_2\text{O}$  exchangeable), 7.26–7.36 (4H, m, Bz), 6.63 (1H, s, H-4'), 5.30 (2H, s,  $\text{CH}_2$ );  $^{13}\text{C}$  NMR (DMSO- $d_6$ , 75 MHz):  $\delta$  170.1 (C-2), 164.4, 165.2 (C-2', C, CO,  $\text{COCH}_2$ ), 141.2, 134.9, 134.8, 132.9, 131.9, 128.3, 126.9, 125.3, 124.7, 122.3, 121.9, 120.8 (Bz, C-4, C-5, C-7, C-8, C-3', C-4'), 116.6, 115.8 (2CN), 62.5 (C,  $\text{CH}_2$ ,  $\text{COCH}_2$ ); EI-MS:  $m/z$  392  $[\text{M}]^+$  (18%); Analysis Calcd for  $\text{C}_{18}\text{H}_8\text{N}_4\text{O}_3\text{S}_2$  (392.41): C, 55.09; H, 2.05; N, 14.28; S, 16.34%. Found: C, 55.28; H, 2.26; N, 14.25; S, 16.52%.

#### Ethyl 5-(2-cyanoacetamido)-2-(2-oxo-2H-chromen-3-yl)thieno[3,2-d]thiazole-6-carboxylate (12b)

Pale brown crystals (1,4-dioxane), yield 80% (3.51 g), mp 166–169 °C; IR (KBr)  $\nu_{\text{max}}$  3462–3329, 3057, 2222, 1689–1706, 1646, 1628  $\text{cm}^{-1}$ ;  $^1\text{H}$  NMR (DMSO- $d_6$ , 200 MHz):  $\delta$  8.31 (1H, s,  $\text{D}_2\text{O}$  exchangeable, NH), 7.39–7.26 (4H, m, Bz), 6.61 (1H, s, H-4'), 5.28 (2H, s,  $\text{CH}_2$ ), 4.22 (2H, q,  $J = 6.83$  Hz,  $\text{OCH}_2\text{CH}_3$ ), 1.38 (3H, t,  $J = 6.83$  Hz,  $\text{OCH}_2\text{CH}_3$ );  $^{13}\text{C}$  NMR (DMSO- $d_6$ , 75 MHz):  $\delta$  170.0 (C-2), 162.3, 163.0, 164.4 (C-2', COOEt, NHCO), 140.3, 134.8, 131.9, 128.4, 126.9, 126.0, 125.3, 124.1, 123.1, 122.2, 121.3, 120.8 (Bz, C-4, C-5, C-7, C-8, C-3', C-4'), 116.8 (CN), 62.8 (C,  $\text{CH}_2$ ,  $\text{COCH}_2$ ), 54.2 (C,  $\text{OCH}_2\text{CH}_3$ ), 16.5 (C,  $\text{OCH}_2\text{CH}_3$ ); EI-MS:  $m/z$  439  $[\text{M}]^+$  (37%); Analysis Calcd for  $\text{C}_{20}\text{H}_{13}\text{N}_3\text{O}_5\text{S}_2$  (439.46): C, 54.66; H, 2.98; N, 9.56; S, 14.59%. Found: C, 54.80; H, 3.11; N, 9.73; S, 14.79%.

### 3. 1. 8. General Procedure for the Synthesis of the Thiazolo[4',5':4,5]thieno[2,3-b]pyridine-7-carbonitrile Derivatives 13a and 13b

To a suspension of either compound **12a** (3.92 g, 0.01 mol) or **12b** (4.39 g, 0.01 mol) in sodium ethoxide solution [prepared by dissolving metallic sodium (0.46 g, 0.02 mol) in absolute ethanol (40 mL)] was heated in a boiling water bath for 3 h then poured onto ice/water containing a few drops of hydrochloric acid (till pH 6). The formed solid product, in each case, was collected by filtration.

#### 8-Amino-6-hydroxy-2-(2-oxo-2H-chromen-3-yl)thiazolo[4',5':4,5]thieno[2,3-b]pyridine-7-carbonitrile (13a)

Yellow crystals (1,4-dioxane), yield 73% (2.86 g), mp 245–247 °C; IR (KBr)  $\nu_{\text{max}}$  3533–3341, 3058, 2220,

1693, 1653, 1632  $\text{cm}^{-1}$ ;  $^1\text{H}$  NMR (DMSO- $d_6$ , 200 MHz):  $\delta$  10.19 (1H, s, OH,  $\text{D}_2\text{O}$  exchangeable), 7.39–7.28 (4H, m, Bz), 6.60 (1H, s, H-4'), 4.80 (2H, s,  $\text{D}_2\text{O}$  exchangeable,  $\text{NH}_2$ );  $^{13}\text{C}$  NMR (DMSO- $d_6$ , 75 MHz):  $\delta$  171.8, 170.5 (C-2, C-6), 164.2 (C-2'), 139.8, 137.9, 132.4, 131.9, 130.3, 129.7, 127.8, 127.1, 124.9, 124.2, 123.8, 122.3, 121.6, 120.2 (Bz, C-4, C-5, C-8, C-9, C-10, C-11, C-3', C-4'), 116.8 (CN); EI-MS:  $m/z$  392 [ $\text{M}$ ] $^+$  (32%); Analysis Calcd for  $\text{C}_{18}\text{H}_8\text{N}_4\text{O}_3\text{S}_2$  (392.41): C, 55.09; H, 2.05; N, 14.28; S, 16.34%. Found: C, 54.89; H, 2.31; N, 14.44; S, 16.41%.

### 6,8-Dihydroxy-2-(2-oxo-2H-chromen-3-yl)thiazolo [4',5':4,5]thieno[2,3-b]pyridine-7-carbonitrile (13b)

Yellow crystals (1,4-dioxane), yield 73% (2.86 g), mp 262–265  $^\circ\text{C}$ ; IR (KBr)  $\nu_{\text{max}}$  3542–3318, 3054, 1686, 1642, 1628  $\text{cm}^{-1}$ ;  $^1\text{H}$  NMR (DMSO- $d_6$ , 200 MHz):  $\delta$  10.32, 10.11 (2H, 2s,  $\text{D}_2\text{O}$  exchangeable, 2OH), 7.36–7.28 (4H, m,  $\text{C}_6\text{H}_4$ ), 6.64 (1H, s, H-4');  $^{13}\text{C}$  NMR (DMSO- $d_6$ , 75 MHz):  $\delta$  171.0, 170.2 (C-2, C-6), 164.2 (C-2'), 142.0, 138.3, 130.9, 130.6, 129.4, 128.3, 127.3, 126.3, 125.8, 125.4, 125.0, 123.9, 123.5, 122.6, 122.0, 120.2 (Bz, C-4, C-5, C-8, C-9, C-10, C-11, C-3', C-4'), 116.6 (CN); EI-MS:  $m/z$  393 [ $\text{M}$ ] $^+$  (44%); Analysis Calcd for  $\text{C}_{18}\text{H}_7\text{N}_3\text{O}_4\text{S}_2$  (393.40): C, 54.96; H, 1.79; N, 10.68; S, 16.30%. Found: C, 54.77; H, 2.01; N, 10.29; S, 16.42%.

### 3. 1. 9. General Procedure for the Synthesis of the Thieno[3,2-d]thiazole Derivatives 15a and 15b

To a dry solid of either **12a** (3.92 g, 0.01 mol) or **12b** (4.39 g, 0.01 mol) acetophenone (1.20 g, 0.01 mol) and ammonium acetate (0.50 g) was added. The whole reaction mixture was heated in an oil bath at 120  $^\circ\text{C}$  for 0.5 h and the solid product formed upon trituration with ethanol was collected by filtration.

### 2-Cyano-N-[6-cyano-2-(2-oxo-2H-chromen-3-yl)thieno[3,2-d]thiazol-5-yl]-3-phenylbut-2-enamide (15a)

Yellow crystals (1,4-dioxane), yield 73% (3.60 g), mp 221–223  $^\circ\text{C}$ ; IR (KBr)  $\nu_{\text{max}}$  3472–3318, 3057, 2222, 2220, 1689, 1690, 1642, 1627  $\text{cm}^{-1}$ ;  $^1\text{H}$  NMR (DMSO- $d_6$ , 200 MHz):  $\delta$  10.22 (1H, s,  $\text{D}_2\text{O}$  exchangeable, NH), 7.26–7.46 (9H, m, 2Bz), 6.59 (1H, s, H-4'), 2.88 (3H, s,  $\text{CH}_3$ );  $^{13}\text{C}$  NMR (DMSO- $d_6$ , 75 MHz):  $\delta$  170.2 (C-2), 164.5, 162.8 (C-2, NHCO), 140.5, 138.7, 136.2, 133.4, 132.6, 132.1, 130.8, 128.9, 127.8, 127.4, 126.1, 125.6, 124.2, 123.7, 122.1, 121.9, 120.9, 120.5 (2Bz, C-3, C-4, C-6, C-7, C-3', C-4'), 117.0, 116.4, (2CN), 90.6, 86.7 (C=C), 19.5 (C,  $\text{CH}_3$ ); EI-MS:  $m/z$  494 [ $\text{M}$ ] $^+$  (23%); Analysis Calcd for  $\text{C}_{26}\text{H}_{14}\text{N}_4\text{O}_3\text{S}_2$  (494.54): C, 63.14; H, 2.85; N, 11.33; S, 12.97%. Found: C, 62.98; H, 2.69; N, 11.41; S, 13.08%.

### Ethyl 2-[[6-cyano-2-(2-oxo-2H-chromen-3-yl)thieno[3,2-d]thiazol-5-yl]carbamoyl]-3-phenylbut-2-enoate (15b)

Yellow crystals (1,4-dioxane), yield 68% (3.67 g), mp 189–192  $^\circ\text{C}$ ; IR (KBr)  $\nu_{\text{max}}$  3488–3326, 3052, 2221, 1690, 1682, 1638, 1628  $\text{cm}^{-1}$ ;  $^1\text{H}$  NMR (DMSO- $d_6$ , 200 MHz):  $\delta$  8.31 (1H, s,  $\text{D}_2\text{O}$  exchangeable, NH), 7.39–7.26 (9H, m,  $\text{C}_6\text{H}_5$ ,  $\text{C}_6\text{H}_4$ ), 6.63 (1H, s, H-4'), 4.22 (q, 2H,  $J$  = 6.88 Hz,  $\text{OCH}_2\text{CH}_3$ ), 2.68 (3H, s,  $\text{CH}_3$ ), 1.13 (t, 3H,  $J$  = 6.88 Hz,  $\text{OCH}_2\text{CH}_3$ );  $^{13}\text{C}$  NMR (DMSO- $d_6$ , 75 MHz):  $\delta$  170.4 (C-2), 164.2 (C-2'), 163.9, 162.3 (C-2, NHCO), 141.2, 134.7, 132.6, 130.8, 129.2, 128.3, 127.1, 126.8, 125.8, 124.9, 124.2, 123.9, 123.5, 123.1, 122.2, 119.6 (2Bz, C-3, C-4, C-6, C-7, C-3', C-4'), 90.8, 86.3 (C=C), 52.3 (C,  $\text{OCH}_2\text{CH}_3$ ), 19.2 ( $\text{CH}_3$ ), 16.8 (C,  $\text{OCH}_2\text{CH}_3$ ); EI-MS:  $m/z$  541 [ $\text{M}$ ] $^+$  (28%); Analysis Calcd for  $\text{C}_{28}\text{H}_{19}\text{N}_3\text{O}_5\text{S}_2$  (541.60): C, 62.09; H, 3.54; N, 7.76; S, 11.84%. Found: C, 61.95; H, 3.72; N, 8.02; S, 12.03%.

### 3. 1. 10. General Procedure for the Synthesis of Thiophene Derivatives 16a and 16b

To a solution of either compound **15a** (4.94 g, 0.01 mol) or **15b** (5.41 g, 0.01 mol) in 1,4-dioxane (30 mL) containing triethylamine (0.50 mL) elemental sulfur (3.2 g, 0.01 mol) was added. The reaction mixture was heated under reflux for 2 h then poured onto ice/water containing a few drops of hydrochloric acid and the solid product formed, in each case, was collected by filtration.

### 2-Amino-N-[6-cyano-2-(2-oxo-2H-chromen-3-yl)thieno[3,2-d]thiazol-5-yl]-4-phenylthiophene-3-carboxamide (16a)

Yellow crystals (acetic acid), 82% (4.31 g), mp 187–190  $^\circ\text{C}$ ; IR (KBr)  $\nu_{\text{max}}$  3494–3326, 3053, 2224, 1687, 1694, 1646, 1629  $\text{cm}^{-1}$ ;  $^1\text{H}$  NMR (DMSO- $d_6$ , 200 MHz):  $\delta$  10.28 (1H, s,  $\text{D}_2\text{O}$  exchangeable, NH), 7.23–7.39 (9H, m, 2Bz), 6.61 (1H, s, H-4'), 6.24 (1H, s, H-5''), 4.68 (2H, s,  $\text{D}_2\text{O}$  exchangeable,  $\text{NH}_2$ );  $^{13}\text{C}$  NMR (DMSO- $d_6$ , 75 MHz):  $\delta$  170.3 (C-2), 162.5, 164.3 (C-2', CONH), 143.8, 142.6, 138.7, 133.4, 132.6, 132.4, 131.9, 130.6, 128.3, 127.4, 126.8, 125.9, 124.2, 123.9, 123.6, 122.3, 121.9, 120.9, 120.6, 119.6 (Bz, C-3, C-4, C-6, C-7, C-3', C-4', C-2'', C-3'', C-4'', C-5''), 116.8 (CN); EI-MS:  $m/z$  526 [ $\text{M}$ ] $^+$  (38%); Analysis Calcd for  $\text{C}_{26}\text{H}_{14}\text{N}_4\text{O}_3\text{S}_3$  (526.61): C, 59.30; H, 2.68; N, 10.64; S, 18.27%. Found: C, 59.52; H, 2.72; N, 10.39; S, 18.44%.

### Ethyl 5-(2-amino-4-phenylthiophene-3-carboxamido)-2-(2-oxo-2H-chromen-3-yl)thieno[3,2-d]thiazole-6-carboxylate (16b)

Yellow (1,4-dioxane), yield 73% (4.18 g), mp 203–207  $^\circ\text{C}$ ; IR (KBr)  $\nu_{\text{max}}$  3462–3346, 3056, 1689–1696, 1641, 1632  $\text{cm}^{-1}$ ;  $^1\text{H}$  NMR (DMSO- $d_6$ , 200 MHz):  $\delta$  8.33 (1H, s,  $\text{D}_2\text{O}$  exchangeable, NH), 7.23–7.37 (9H, m, 2Bz), 6.63 (1H, s, H-4'), 6.28 (1H, s, H-5''), 4.82 (2H, s,  $\text{D}_2\text{O}$  exchangeable,  $\text{NH}_2$ ), 4.20 (2H, q,  $J$  = 7.39 Hz,  $\text{OCH}_2\text{CH}_3$ ), 1.14 (3H, t,  $J$  = 7.39 Hz,  $\text{OCH}_2\text{CH}_3$ );  $^{13}\text{C}$  NMR (DMSO- $d_6$ , 75 MHz):  $\delta$  170.2 (C-2), 162.5, 164.0,

164.3 (C-2', CONH, COOEt), 143.1, 142.4, 136.1, 132.8, 131.6, 130.3, 129.6, 129.2, 128.4, 128.7, 126.7, 125.9, 125.3, 125.2, 124.9, 123.8, 123.8, 123.1, 122.9, 121.8 (Bz, C-3, C-4, C-6, C-7, C-3', C-4', C-2'', C-3'', C-4'', C-5''), 52.3 (C, OCH<sub>2</sub>CH<sub>3</sub>), 16.4 (C, OCH<sub>2</sub>CH<sub>3</sub>); EI-MS: *m/z* 573 [M]<sup>+</sup> (31%); Analysis Calcd for C<sub>28</sub>H<sub>19</sub>N<sub>3</sub>O<sub>5</sub>S<sub>3</sub> (573.66): C, 58.62; H, 3.34; N, 7.32; S, 16.77%. Found: C, 58.39; H, 3.51; N, 7.48; S, 16.91%.

### 3. 1. 11. General Procedure for the Synthesis of the Arylhydrazone Derivatives 18a–c

To a solution of compound **15a** (4.94 g, 0.01 mol) in ethanol (50 mL) containing sodium hydroxide (10 mL, 10%) any of benzenediazonium chloride, 4-chlorobenzenediazonium chloride or 4-methoxybenzenediazonium chloride [prepared through the addition of sodium nitrite solution (0.70 g, 0.01 mol) to a cold solution (0–5 °C) of the appropriate aromatic amine, namely aniline (0.93 g, 0.01 mol), 4-chloroaniline (1.27 g, 0.01 mol) or 4-methoxyaniline (1.24 g, 0.01 mol), dissolved in concentrated hydrochloric acid (10 mL, 18 mol) with continuous stirring] was added portion-wise with continuous stirring. The whole reaction mixture was stirred at room for 2 h and the solid product formed, in each case, was collected by filtration.

#### 2-Cyano-*N*-[6-cyano-2-(2-oxo-2*H*-chromen-3-yl)thieno[3,2-*d*]thiazol-5-yl]-3-phenyl-4-(2-phenylhydrazono)but-2-enamide (18a)

Yellow (1,4-dioxane), yield 76% (4.54 g) mp 133–137 °C; IR (KBr) *v*<sub>max</sub> 3469–3341, 3056, 2221, 2220, 1689, 1691, 1648, 1631 cm<sup>-1</sup>; <sup>1</sup>H NMR (DMSO-*d*<sub>6</sub>, 200 MHz): δ 10.23, 8.33 (2H, 2s, D<sub>2</sub>O exchangeable, 2NH), 7.48–7.25 (14H, m, 2Bz), 5.93 (1H, s, CH=N), 6.63 (1H, s, H-4'); <sup>13</sup>C NMR (DMSO-*d*<sub>6</sub>, 75 MHz): δ 173.1, 171.6 (C-2, C=N), 164.9, 162.8 (C-2', NHCO), 142.5, 141.3, 139.5, 138.2, 131.8, 131.2, 130.8, 127.6, 126.4, 125.2, 124.8, 124.6, 124.2, 123.3, 122.8, 122.0, 121.3, 120.8, 120.3, 119.8 (Bz, C-3, C-4, C-6, C-7, C-3', C-4', C-2'', C-3'', C-4'', C-5''), 116.8, 116.4 (2CN), 90.6, 88.3 (C=C); EI-MS: *m/z* 598 [M]<sup>+</sup> (28%); Analysis Calcd for C<sub>32</sub>H<sub>18</sub>N<sub>6</sub>O<sub>3</sub>S<sub>2</sub> (598.65): C, 64.20; H, 3.03; N, 14.04; S, 10.71%. Found: C, 64.49; H, 2.97; N, 14.22; S, 10.64%.

#### 4-[2-(4-Chlorophenyl)hydrazono]-2-cyano-*N*-[6-cyano-2-(2-oxo-2*H*-chromen-3-yl)thieno[3,2-*d*]thiazol-5-yl]-3-phenylbut-2-enamide (18b)

Yellow crystals (1,4-dioxane), 89% (5.63 g), mp 123–125 °C; IR (KBr) *v*<sub>max</sub> 3473–3341, 3058, 2223, 2220, 1688, 1696, 1642, 1635 cm<sup>-1</sup>; <sup>1</sup>H NMR (DMSO-*d*<sub>6</sub>, 200 MHz): δ 10.21, 8.36 (2H, 2s, 2NH, D<sub>2</sub>O exchangeable), 7.45–7.26 (13H, m, 3Bz), 6.62 (1H, s, H-4'), 5.90 (1H, s, CH=N); <sup>13</sup>C NMR (DMSO-*d*<sub>6</sub>, 75 MHz): δ 173.3, 171.8 (C-2, C=N), 164.6, 162.6 (C-2', NHCO), 142.2,

140.8, 132.3, 131.8, 130.8, 128.4, 127.9, 126.4, 125.9, 125.4, 124.9, 124.8, 124.2, 123.1, 122.9, 122.4, 121.3, 120.8, 120.1, 119.9 (Bz, C-3, C-4, C-6, C-7, C-3', C-4', C-2'', C-3'', C-4'', C-5''), 116.7, 115.8 (2CN); 88.4, 90.6 (C=C); EI-MS: *m/z* 633 [M]<sup>+</sup> (41%); Analysis Calcd for C<sub>32</sub>H<sub>17</sub>ClN<sub>6</sub>O<sub>3</sub>S<sub>2</sub> (633.10): C, 60.71; H, 2.71; N, 13.27; S, 10.13%. Found: C, 60.83; H, 2.83; N, 13.99; S, 10.28%.

#### 2-Cyano-*N*-[6-cyano-2-(2-oxo-2*H*-chromen-3-yl)thieno[3,2-*d*]thiazol-5-yl]-4-[2-(4-methoxyphenyl)hydrazono]-3-phenylbut-2-enamide (18c)

Yellow crystals (1,4-dioxane), yield 68%, (4.27 g), mp 203–207 °C; IR (KBr) *v*<sub>max</sub> 3489–3324, 3055, 2222, 2220, 1690, 1693, 1640, 1631 cm<sup>-1</sup>; <sup>1</sup>H NMR (DMSO-*d*<sub>6</sub>, 200 MHz): δ 10.25, 8.33 (2H, 2s, D<sub>2</sub>O exchangeable, 2NH), 7.48–7.28 (13H, m, 3Bz), 6.60 (1H, s, H-4'), 5.88 (1H, s, CH=N), 1.12 (3H, s, CH<sub>3</sub>); <sup>13</sup>C NMR (DMSO-*d*<sub>6</sub>, 75 MHz): δ 173.1, 171.9 (C-2, C=N), 162.8, 164.9 (C-2', NHCO), 141.6, 140.4, 132.8, 131.3, 130.9, 130.2, 129.4, 126.8, 126.0, 125.6, 125.3, 124.9, 124.4, 123.7, 123.0, 122.8, 121.4, 120.9, 120.3, 119.7 (Bz, C-3, C-4, C-6, C-7, C-3', C-4', C-2'', C-3'', C-4'', C-5''), 116.6, 116.3 (2CN), 90.3, 88.7 (C=C); EI-MS: *m/z* 628 [M]<sup>+</sup> (33%); Analysis Calcd for C<sub>33</sub>H<sub>20</sub>N<sub>6</sub>O<sub>4</sub>S<sub>2</sub> (628.68): C, 63.05; H, 3.21; N, 13.37; S, 10.20%. Found: C, 63.22; H, 3.51; N, 13.53; S, 10.42%.

### 3. 1. 12. General Procedure for the Synthesis of the Pyridazine Derivatives 19a–c

To a suspension of any of compound **18a** (5.98 g, 0.01 mol), **18b** (6.33 g, 0.01 mol) or **17c** (6.28 g, 0.01 mol) in sodium ethoxide solution [prepared via dissolving metallic sodium (0.46 g, 0.02 mol) in absolute ethanol (60 mL)] was heated in a boiling water bath for 3 h then poured onto ice/water containing a few drops of hydrochloric acid (till pH 6). The solid product formed was collected by filtration.

#### *N*-[6-Cyano-2-(2-oxo-2*H*-chromen-3-yl)thieno[3,2-*d*]thiazol-5-yl]-3-imino-2,5-diphenyl-2,3-dihydropyridazine-4-carboxamide (19a)

Yellow crystals (1,4-dioxane), yield 82% (4.90 g), mp 287–293 °C; IR (KBr) *v*<sub>max</sub> 3477–3321, 3053, 2220, 1689, 1691, 1648, (C=N), 1631 (C=C) cm<sup>-1</sup>; <sup>1</sup>H NMR (DMSO-*d*<sub>6</sub>, 200 MHz): δ 10.41, 8.31 (2H, 2s, D<sub>2</sub>O exchangeable, 2NH), 7.45–7.22 (14H, m, 3Bz), 6.60 (1H, s, H-4'), 6.02 (1H, s, H-3''); <sup>13</sup>C NMR (DMSO-*d*<sub>6</sub>, 75 MHz): δ 173.0, 170.3, 169.6 (C-3, C-3'', C-6''), 164.6, 162.6 (C-2', NHCO), 142.9, 140.2, 133.4, 132.6, 131.8, 131.2, 130.8, 128.2, 127.9, 126.7, 125.5, 124.8, 124.9, 123.0, 122.8, 122.3, 121.9, 120.9, 120.8, 119.2 (Bz, C-3, C-4, C-6, C-7, C-3', C-4', C-4'', C-5''), 116.2 (CN), EI-MS: *m/z* 598 [M]<sup>+</sup> (20%); Analysis Calcd for C<sub>32</sub>H<sub>18</sub>N<sub>6</sub>O<sub>3</sub>S<sub>2</sub> (598.65): C, 64.20; H, 3.03; N, 14.04; S, 10.71%. Found: C, 64.33; H, 3.19; N, 14.38; S, 10.54%.



### 2-(4-Chlorophenyl)-N-[6-cyano-2-(2-oxo-2H-chromen-3-yl)thieno[3,2-d]thiazol-5-yl]-3-imino-5-phenyl-2,3-dihydropyridazine-4-carboxamide (19b)

Pale yellow crystals (1,4-dioxane), yield 69% (4.12 g), mp 244–147 °C; IR (KBr)  $\nu_{\text{max}}$  3482–3329, 3057, 2221, 1689, 1696, 1640, 1632 (C=C)  $\text{cm}^{-1}$ ;  $^1\text{H}$  NMR (DMSO- $d_6$ , 200 MHz):  $\delta$  10.20, 8.38 (2H, 2s, D<sub>2</sub>O exchangeable, 2NH), 7.42–7.23 (13H, m, 3Bz), 7.03 (1H, s, H-3''), 6.64 (1H, s, H-4');  $^{13}\text{C}$  NMR (DMSO- $d_6$ , 75 MHz):  $\delta$  173.1, 170.2, 169.7 (C-3', C-3'', C-6''), 162.8, 164.3 (C-2', NHCO), 142.6, 140.2, 139.5, 138.6, 132.9, 131.8, 131.6, 130.8, 127.6, 126.4, 125.7, 125.6, 124.9, 124.8, 124.2, 123.1, 122.9, 122.4, 120.8, 120.1, 121.3, 119.9 (Bz, C-3, C-4, C-6, C-7, C-3', C-4', C-4'', C-5''), 116.6 (CN); EI-MS:  $m/z$  633 [M]<sup>+</sup> (23%); Analysis Calcd for C<sub>32</sub>H<sub>17</sub>ClN<sub>6</sub>O<sub>3</sub>S<sub>2</sub> (633.10): C, 60.71; H, 2.71; N, 13.27; S, 10.13%. Found: C, 60.92; H, 2.94; N, 13.40; S, 10.45%.

### N-[6-Cyano-2-(2-oxo-2H-chromen-3-yl)thieno[3,2-d]thiazol-5-yl]-3-imino-2-(4-methoxyphenyl)-5-phenyl-2,3-dihydropyridazine-4-carboxamide (19c)

Yellow crystals (1,4-dioxane), yield 73% (4.58 g), mp 192–196 °C; IR (KBr)  $\nu_{\text{max}}$  3479–3320, 3056, 2220, 1687, 1691, 1637, 1630  $\text{cm}^{-1}$ ;  $^1\text{H}$  NMR (DMSO- $d_6$ , 200 MHz):  $\delta$  10.26, 8.31 (2H, 2s, D<sub>2</sub>O exchangeable, 2NH), 7.23–7.45 (13H, m, 3Bz), 7.03 (1H, s, H-3''), 6.71 (1H, s, H-4'), 3.13 (3H, s, CH<sub>3</sub>);  $^{13}\text{C}$  NMR (DMSO- $d_6$ , 75 MHz):  $\delta$  173.5, 170.2, 169.6 (C-2', C-3'', C-6''), 164.3, 163.2 (C-2', NHCO), 141.3, 140.2, 130.3, 130.2, 128.6, 128.3, 127.1, 126.9, 126.2, 125.6, 125.2, 124.6, 124.4, 123.7, 123.0, 122.8, 121.7, 120.3, 120.3, 119.2 (Bz, C-3, C-4, C-6, C-7, C-3', C-4', C-4'', C-5''), 116.6 (CN), 32.6 (C, OCH<sub>3</sub>); EI-MS:  $m/z$  628 [M]<sup>+</sup> (33%); Analysis Calcd for C<sub>33</sub>H<sub>20</sub>N<sub>6</sub>O<sub>4</sub>S<sub>2</sub> (628.68): C, 63.05; H, 3.21; N, 13.37; S, 10.20%. Found: C, 63.31; H, 3.38; N, 13.42; S, 10.32%.

## 4. Conclusions

In summary, we have shown herein that our strategy is applicable for the synthesis of a wide range of thiazole derivatives and particularly of such which are incorporated into heterocyclic cores and for fused derivatives. Compounds **10b**, **13b**, **18a**, **19b** and **19c** showed the maximum anti-inflammatory activities while compounds **6–c**, **7a–c**, **8b**, **10b**, **13a**, **16b**, **19b** and **19c** showed high anti-ulcer activities among the synthesized compounds. The toxicity of selected compounds was studied against shrimp larvae where compounds **10b**, **18a**, **19c** and **19d** showed to be non toxic against the tested organisms.

## 5. Acknowledgement

R. M. Mohareb would like to thank the Alexander von Humboldt Foundation in Bonn, Germany for affor-

ding him regular fellowships in Germany for finance and completing his research work.

## 6. References

1. S. K. Bhatia, G. Nath, R. Tilah, S. K. Singh, *Eur. J. Med. Chem.* **2010**, *45*, 651–660.  
<http://dx.doi.org/10.1016/j.ejmech.2009.11.008>
2. B. V. Yang, D. S. Weinstein, L. M. Doweiko, H. Gong, W. Vaccaro, T. Huynh, H. Y. Xiao, A. M. Doweiko, L. Mckay, D. A. Holloway, J. E. Somerville, S. Habte, M. Cunningham, M. McMahon, R. Townsend, D. Shuster, J. H. Dodd, S. G. Nadler, J. C. Barrish, *J. Med. Chem.* **2010**, *53*, 8241–8251.  
<http://dx.doi.org/10.1021/jm100957a>
3. F. C. Spector, L. Liang, H. Giordano, M. Sivaraja, M. G. Peterson, *J. Virol.* **1998**, *72*, 6979–6987.  
<http://dx.doi.org/jvi.asm.org/content/72/9/6979>
4. G. C. Diego, F. Douelle, T. S. Feng, A. T. Nchinda, Y. Younis, K. L. White, Q. Wu, E. Ryan, J. N. Burrows, D. Waterson, M. J. Witty, S. Wittlin, S. A. Charman, K. Chibale, *J. Med. Chem.* **2011**, *54*, 7713–7719.  
<http://dx.doi.org/abs/10.1021/jm201108k>
5. F. W. Bell, A. S. Cantrell, M. Hoegberg, S. R. Jaskunas, N. G. Johansson, C. L. Jordan, M. D. Kinnick, P. Lind, J. M. Morin, *J. Med. Chem.* **1995**, *38*, 4929–4936.  
<http://dx.doi.org/10.1021/jm00025a010>
6. D. E. Fink, D. S. Mortensen, S. R. Stauffer, Z. D. Aron, *Chem. Biol.* **1999**, *6*, 205–219.  
[http://dx.doi.org/10.1016/S1074-5521\(99\)80037-4](http://dx.doi.org/10.1016/S1074-5521(99)80037-4)
7. M. Biagetti, C. P. Leslie, A. Mazzali, C. Seri, D. A. Pizzi, J. Bentley, T. Genski, R. Di Fabio, L. Zonzini, L. Caberlotto, *Bioorg. Med. Chem. Lett.* **2010**, *20*, 4741–4744.  
<http://dx.doi.org/10.1016/j.bmcl.2010.06.140>
8. E. W. Tilburg, P. A. M. Klein, M. D. Groote, M. W. Beukers, A. P. Jerman, *Bioorg. Med. Chem. Lett.* **2001**, *11*, 2017–2019.  
[http://dx.doi.org/10.1016/S0960-894X\(01\)00356-0](http://dx.doi.org/10.1016/S0960-894X(01)00356-0)
9. B. Umadevi, *Eur. J. Med. Chem.* **2007**, *42*, 1144–1150.  
<http://dx.doi.org/10.1016/j.ejmech.2007.01.016>
10. K. J. Wilson, C. R. Illig, N. Subasinghe, J. B. Hoffman, M. J. Rudolph, R. Soll, C. J. Molloy, R. Bone, D. Green, T. Randall, M. Zhang, F. A. Lewandowski, Z. Zhou, C. Sharp, D. Maguire, B. Grasberger, R. L. Jarlais, J. Spurlino, *Bioorg. Med. Chem. Lett.* **2001**, *11*, 915–918.  
[http://dx.doi.org/10.1016/S0960-894X\(01\)00102-0](http://dx.doi.org/10.1016/S0960-894X(01)00102-0)
11. W. T. Zhang, J. L. Ruan, P. F. Wu, F. C. Jiang, L. N. Zhang, W. Fang, X. L. Chen, Y. Wang, B. S. Cao, G. Y. Chen, Y. J. Zhu, J. Gu, J. G. Chen, *J. Med. Chem.* **2009**, *52*, 718–725  
<http://dx.doi.org/10.1021/jm800902t>
12. G. Gebeyehu, V. E. Marquez, A. V. Cott, D. A. Cooney, J. A. Kelley, H. N. Jayaram, G. S. Ahluwalia, R. L. Dion, Y. A. Wilson, D. G. Johns, *J. Med. Chem.* **1985**, *28*, 99–105.  
<http://dx.doi.org/10.1021/jm00379a018>
13. A. Sekiguchi, A. Nishina, H. Kimura, R. H. Fukumoto, K. Kanoh, H. A. Ishahara, M. Koketsu, *Chem. Pharm. Bull.*

- 2005, 53, 1439–1442.  
<http://dx.doi.org/10.1111/j.1742-4658.2007.06125.x>
14. M. Koketsu, H. Ishihara, W. Wu, K. Murakami, I. Saiki, *Eur. J. Pharm. Sci.* **1999**, 9, 157–161.  
[http://dx.doi.org/10.1016/S0928-0987\(99\)00058-5](http://dx.doi.org/10.1016/S0928-0987(99)00058-5)
15. A. I. Khalaf, Al-Kadhimi, A. A. H. Ahmed, J. H. Ali, *Acta Chim. Slov.* **2016**, 63, 689–704.  
<http://dx.doi.org/10.17344/acsi.2016.2775>
16. R. M. Mohareb, A. A. Mohamed, A. E. M. Abdallah, *Acta Chim. Slov.* **2016**, 63, 227–240.  
<http://dx.doi.org/10.17344/acsi.2015.1668>
17. M. I. I. Fakhr, M. A. A. Radwan, S. El-Batran, O. M. E. Abd El-Salam, S. M. El-Shenawy, *Eur. J. Med. Chem.* **2009**, 44, 1718–1725.  
<http://dx.doi.org/10.1016/j.ejmech.2008.02.034>
18. W. C. Shearouse, M. Z. Shumba, J. Mack, *Molecules* **2014**, 4, 171–179.  
<http://dx.doi.org/10.3390/app4020171>
19. C. A. Winter, E. A. Risley, G. W. Nuss, *Proc. Soc. Exp. Biol. Ther.* **1962**, 111, 544–547.
20. H. Shay, S. A. Komarov, S. S. Fels, D. Meranze, M. Grunstein, H. Sipler, *Gastroenterology* **1945**, 5, 43–61.
21. J. P. Overmyer, D. R. Rouse, J. K. Avants, A. W. Garrison, M. E. Delorenzo, K. W. Chung, P. B. Key, W. A. Wilson, M. C. Black, *J. Environ. Sci. Health* **2007**, 42, 471–480.  
<http://dx.doi.org/10.1080/10934520601187690>
22. R. Maltais, M. A. Fournier, D. Poirier, *Bioorg. Med. Chem.* **2011**, 19, 4652–68.  
<http://dx.doi.org/10.1016/j.bmc.2011.06.003>
23. S. Kanchithalaivan, R. R. Kumar, S. Perumal, *Steroids* **2013**, 78, 409–417.  
<http://dx.doi.org/10.1016/j.steroids.2012.12.017>
24. G. B. Djigoué, L. C. Kenmogne, J. Roy, D. Poirier, *Bioorg. Med. Chem. Lett.* **2013**, 23, 6360–6360.  
<http://dx.doi.org/10.1016/j.bmcl.2013.09.072>
25. M. G. Metcalf, *Clin. Biochem.* **1974**, 7, 119–130.  
[http://dx.doi.org/10.1016/S0009-9120\(74\)91218-1](http://dx.doi.org/10.1016/S0009-9120(74)91218-1)

## Povzetek

Reakcija 2-(4-okso-4,5-dihidrotiazol-2-il)acetonitrila (**1**) s salicilaldehidom (**2**) v 1,4-dioksanu ob dodatku katalitske množine piridina daje kumarinske derivate **3**. Ob reakciji le-teh z različnimi reagenti nastanejo pirano[4,5-*b*]tiazolni, pirido[4,5-*b*]tiazolni in tieno[5,4-*b*]tiazolni derivati. Za novo pripravljene spojine smo raziskali učinkovitost delovanja proti vnetjem in želodčnim razjedam ter ugotovili, da so spojine **7a**, **8a**, **10b**, **13b**, **15b**, **18a**, **19b**, **19c**, in **19d** pokazale bistveno večje aktivnosti kot ostale pripravljene spojine. Poleg tega smo raziskali tudi strupenost aktivnih spojin za ličinke morskih rakcev ter ugotovili, da spojine **10b**, **18a**, **19c** in **19d** ne kažejo strupenosti za testirane organizme.

Scientific paper

# Study on the Equilibria of the Complex Formation of the Ion-pair of Germanium(IV) with 4-Nitrocatechol and 1,4-Diphenyl-3-(phenylamino)-1*H*-1,2,4-triazole

Petya Racheva,<sup>1</sup> Kirila Stojnova,<sup>2</sup> Vidka Divarova<sup>1</sup> and Vanya Lekova<sup>2,\*</sup>

<sup>1</sup> Department of Chemical Sciences, Faculty of Pharmacy, Medical University-Plovdiv, 15A Vasil Aprilov Boulevard, Plovdiv 4002, Bulgaria

<sup>2</sup> Department of General and Inorganic Chemistry, Faculty of Chemistry, Plovdiv University "Paisii Hilendarski", 24 Tsar Assen Street, Plovdiv 4000, Bulgaria

\* Corresponding author: E-mail: vanlek@uni-plovdiv.bg;  
Tel.: +35932261420

Received: 18-01-2017

## Abstract

The complex formation of the ion-pair formed between the anionic chelate of Ge(IV)–4-nitrocatechol (4-NC) and the cation of 1,4-diphenyl-3-(phenylamino)-1*H*-1,2,4-triazole (Nitron, Nt) in the liquid-liquid extraction system Ge(IV)–4-NC–Nt–H<sub>2</sub>O–CHCl<sub>3</sub> was studied by spectrophotometry. The optimum extraction-spectrophotometric conditions for the complex formation were established. The validity of Beer's law was checked and some analytical characteristics of the system were calculated. The effect of co-existing ions and reagents on the process of complex formation was investigated. The association process in aqueous phase and the extraction equilibria were studied and quantitatively characterized. The following key constants of the processes were calculated: association constant, distribution constant, extraction constant and recovery factor. The molar ratio of the reagents was determined by independent methods. A reaction scheme and a general formula of the complex were suggested.

**Keywords:** Germanium(IV), nitron, ion-pair, chelate formation, extraction equilibriums

## 1. Introduction

The germanium and its compounds are widely used in various important areas of technology, science, and medicine. Germanium is present in all living plant and animal matter in micro-trace quantities and it is essential from a biochemical point of view. The germanium is relatively less toxic compared to many other metals. The accumulation of relatively high doses of germanium (milligram order of germanium per 1 g tissue) causes severe poisoning, including impairments in kidney, nerves, muscles. On the other hand, germanium deficiency can lead to seriously hematologic disorders and tumor formation. Pharmaceutical preparations, containing germanium are effectively applied in treatment of a wide range of serious afflictions, including cancer, arthritis, osteoporosis and acute renal failure.<sup>1–8</sup>

The germanium is a third row post-transition metal and its chemistry has developed considerably in the recent

years, indicated by the large number of publications in the scientific literature. Germanium(IV) forms complexes with various natural organic ligands containing O, N and S donor atoms such as polyphenols and their functional derivatives, polyhydroxycarboxylic acids, aminopolyhydroxycarboxylic acids, thiopolyhydroxycarboxylic acids, 8-hydroxyquinoline and its derivatives, aromatic derivatives of hydroxyaldehydes and hydroxyketones, hydroxyazodyes. The complexes of germanium with chelate ligands containing O, N and S donor atoms have diverse industrial, biological, pharmacological and medical applications.<sup>9–17</sup> Germanium(IV) gives colored chelates with aromatic compounds, containing two or more hydroxyl groups in *o*-position relative to each other. The colored anionic chelates of Ge(IV) form ion-associated complexes with bulky organic cations, like tetradecyl(trihexyl)phosphonium, methyltrioctylammonium, tetrazolium, cetylpyridinium, cetyltrimethylammonium, tetraphenylammonium, tetraphenylarsonium.<sup>18–25</sup>

Nitron (Nt) (1,4-diphenyl-3-(phenylamino)-1*H*-1,2,4-triazole) is an organic compound containing a quaternary nitrogen atom included in a five-membered ring.<sup>26</sup> The structure and properties of the nitron determine its ability to form ion-associated complexes with anionic chelates of metals. The bulky hydrophobic organic substituents in the molecule of the nitron increase the extractability of the ion-associated complexes. The presence of a quaternary nitrogen atom in the molecule of the nitron determines the ability to form ionic associates with chelates of metals in aqueous phase without protonation, as opposed to the amines.<sup>27–30</sup> Nitron is an important reagent for the determination of nitrates, perchlorates, borates, or traces of gold.<sup>31–34</sup>

The liquid-liquid extraction is a part of the chemistry of the solutions and the coordination compounds. It is applied to study the processes of complex formation and the extraction equilibria. The extraction spectrophotometry is a relatively simple, convenient, rapid to perform and inexpensive method for preparation and characterization of new complex compounds as well as for their application in the chemical analysis.<sup>35–38</sup>

The aim of this research was to study spectrophotometrically the extraction equilibria of the complex formation of the ion-pair formed between the anionic chelate of Ge(IV)–4-nitrocatechol (4-NC) and the cation of 1,4-diphenyl-3-(phenylamino)-1*H*-1,2,4-triazole (Nitron, Nt) in the liquid-liquid system Ge(IV)–4-NC–Nt–H<sub>2</sub>O–CHCl<sub>3</sub> as well as to evaluate the possible applications of the system for determination of traces of germanium(IV) in alloys, biological, medical and pharmaceutical samples.

## 2. Experimental

### 2.1. Reagents and Apparatus

GeO<sub>2</sub> (Sigma-Aldrich, Munich, Germany, p.a.): A  $2.0 \times 10^{-3}$  mol L<sup>-1</sup> aqueous solution of Ge(IV) was prepared by dissolving GeO<sub>2</sub> in water upon moderate heating. 4-Nitrocatechol (4-NC) (Sigma-Aldrich, p.a.): 4-NC was dissolved in distilled water to give a  $1.0 \times 10^{-2}$  mol L<sup>-1</sup> solution. 1,4-Diphenyl-3-(phenylamino)-1*H*-1,2,4-triazole (Nitron, Nt) (95%, Alfa Aesar GmbH & Co KG, Germany): A chloroform  $3.4 \times 10^{-4}$  mol L<sup>-1</sup> solution was prepared. The acidity of the aqueous medium was set using a buffer solution prepared by mixing 2.0 mol L<sup>-1</sup> aqueous solutions of CH<sub>3</sub>COOH and NH<sub>4</sub>OH. The organic solvent CHCl<sub>3</sub> was additionally distilled. The pH was checked by HI 83140 pH meter (Romania). A Camspec M508 spectrophotometer (United Kingdom), equipped with 10 mm path length cells, was employed for measurement of the absorbance.

### 2.2. Procedure for Establishment of the Optimum Extraction-Spectrophotometric Conditions

The required aliquots of the solutions of Ge(IV),

4-NC and buffer needed to adjust the pH of the aqueous phase were introduced into 250 cm<sup>3</sup> separatory funnels. The resulting solutions were diluted with distilled water to a total volume of 10 cm<sup>3</sup>. A required aliquot of a chloroform solution of Nitron was added and then the organic phase was brought up to 10 cm<sup>3</sup> with chloroform. The funnels were shaken for a defined time. A portion of the organic extract was filtered through a filter paper into a 1 cm cell and its absorbance was measured against a blank run in parallel.

### 2.3. Procedure for Determination of the Distribution Constant

The distribution constant ( $K_D$ ) was determined from the ratio  $K_D = A_1/(A_3 - A_1)$ , where  $A_1$  and  $A_3$  are the absorbance (measured against blanks) obtained after a single and triple extraction, respectively. The single extraction and the first stage of the triple extraction were performed under the optimum conditions for complex formation (Table 1, column 1). The organic layers were transferred into 25 cm<sup>3</sup> calibrated flasks and the flask from the single extraction was brought to volume with chloroform. The second stage of the triple extraction was performed by adding 7 cm<sup>3</sup> of chloroform to the aqueous phase that remained after the first stage. After extraction, the obtained extract was added to this first stage of the triple extraction. The third stage of the triple extraction was performed in the same manner as for the second stage and the extract was added to those of the first two stages. The volume of the flask was brought to the mark with chloroform. The calibrated flasks were shaken before the spectrophotometric measurements.<sup>30</sup>

## 3. Results and Discussion

### 3.1. Optimum Extraction-Spectrophotometric Conditions

The absorption spectrum of the extract of the studied ion-pair formed between the anionic chelate of Ge(IV) with 4-NC and nitronium cation in CHCl<sub>3</sub> was characterized by an absorption maximum in the visible range ( $\lambda_{\max} = 405$  nm) (Figure 1). The influence of the acidity of the aqueous phase on the extraction of the anionic chelate Ge(IV)–4-NC into the organic phase in the form of an ion-pair with the nitronium cation was investigated. The maximum and constant extraction of the ion-associated complex is achieved in the pH range from 3.0 to 4.5. Acetate buffer solution with pH = 4.0 was used in all further experiments. The results showed that the extraction equilibrium is achieved for shaking time of not less than 60 s. A longer shaking time did not affect the absorbance. The experiments were performed for 2 min. The concentrations of the reagents are the most important factor inf-

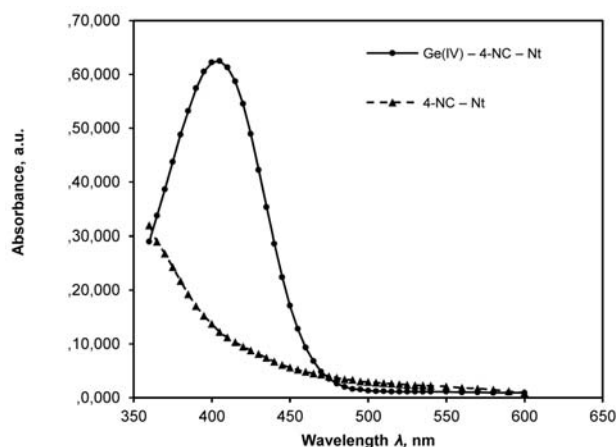


**Figure 1.** Absorption spectra of the complex Ge(IV)–4-NC–Nt and of the blank sample 4-NC–Nt in  $\text{CHCl}_3$ .  $C_{\text{Ge(IV)}} = 2.0 \times 10^{-5} \text{ mol L}^{-1}$ ;  $C_{4\text{-NC}} = 5.0 \times 10^{-4} \text{ mol L}^{-1}$ ;  $C_{\text{Nt}} = 1.7 \times 10^{-4} \text{ mol L}^{-1}$ ;  $\text{pH} = 4.0$ ;  $\lambda = 405 \text{ nm}$ ;  $\tau = 2 \text{ min}$

luencing the extraction equilibria. The chelate formation of Ge(IV)–4-NC requires 15.0-fold excess of 4-NC ( $C_{4\text{-NC}} \geq 3.0 \times 10^{-4} \text{ mol L}^{-1}$ ) and 5.1-fold excess of Nitron ( $C_{\text{Nt}} \geq 1.0 \times 10^{-4} \text{ mol L}^{-1}$ ) for maximum association and extraction. The optimum experimental conditions for the extraction of the ion-associated complex are summarized in Table 1, column 1.

### 3. 2. Beer's Law, Apparent Molar Absorptivity and Other Analytical Characteristics

The range of obedience to Beer's law, i.e. the linear relationship between the germanium(IV) concentration in the aqueous phase ( $C_{\text{Ge(IV)}}$ ,  $\mu\text{g mL}^{-1}$ ) and the absorbance of the ion-association complex in the organic phase after extraction was studied using regression analysis under the optimum conditions for complex formation. The equation of a straight line was found to be  $Y = 0.3807 X + 0.0483$  with a correlation coefficient squared 0.9982. Under the optimum conditions for complex formation, the linearity

is observed for concentrations up to  $5.81 \mu\text{g cm}^{-3}$  Ge(IV). Further analytical characteristics, such as apparent molar absorptivity  $\epsilon'$ , adherence to Beer's law, Sandell's sensitivity, limit of detection and limit of quantification, are shown in Table 1, column 2.

### 3. 3. Effect of Co-existing Ions and Reagents on the Complex Formation

The effect of various co-existing ions and reagents on the process of complex formation of the ion-pair formed between the anionic chelate Ge(IV)–4-NC and nitronium cation was studied under optimum extraction conditions (Table 1, column 1). The concentration of Ge(IV) in the presence of the co-existing ions and reagents was determined from the sequence of Beer's law. A deviation of  $\pm 3\%$  from the absorbance of the ion-associate in the absence of co-existing ions was accepted as an interfering effect. The results are presented in Table 2. From them, it can be concluded that most of the ions studied do not interfere, but some of them, like  $\text{Br}^-$ ,  $\text{F}^-$ ,  $\text{I}^-$ ,  $\text{C}_6\text{H}_5\text{O}_7^{2-}$ ,  $\text{NO}_3^-$ ,  $\text{C}_2\text{O}_4^{2-}$  and complexone III in concentrations higher than the indicated ones, hinder the extraction of Ge(IV) as an associated complex with 4-NC and Nitron. The extraction equilibrium is hindered by Al(III), Cr(III), Cr(VI), Fe(III), Mo(VI), W(VI) and V(V). The interfering ions can be masked or removed from the extraction system to avoid this. Our investigations as well as the studies published in the literature show that the some of the co-existing ions, like Al(III), Cr(III) and Fe(III) can be removed by their pre-precipitation with OH at  $\text{pH} = 11$ . The co-existing ions, like Mo(VI) and W(VI) can be masked with added L-ascorbic acid, Complexone III,  $\text{C}_6\text{H}_5\text{O}_7^{2-}$  or  $\text{C}_2\text{O}_4^{2-}$  in concentrations lower than the indicated.<sup>39</sup> Vanadium(V) can be co-precipitated with Fe(III) in alkali medium.<sup>40</sup>

### 3. 4. Molar Ratios of the Complex, Reaction Scheme and Suggested General Formula

The molar ratios of the complex were determined by three independent methods. The straight-line method of

**Table 1.** Optimum extraction-spectrophotometric conditions and analytical characteristics of the system Ge(IV)–4-NC–Nt– $\text{H}_2\text{O}$ – $\text{CHCl}_3$

Optimum Conditions	Analytical Characteristic
Absorption maximum ( $\lambda_{\text{max}}$ ) 405 nm ( $2.98 \pm 0.11$ ) $\times 10^4 \text{ L mol}^{-1} \text{ cm}^{-1}$	Apparent molar absorptivity ( $\epsilon'$ )
Volume of the aqueous phase $10 \text{ cm}^3$ ( $3.09 \pm 0.25$ ) $\times 10^4 \text{ L mol}^{-1} \text{ cm}^{-1}$	True molar absorptivity ( $\epsilon$ )
Volume of the organic phase $10 \text{ cm}^3$	Sandell's sensitivity (SS) $2.43 \text{ ng cm}^{-2}$
pH of the aqueous phase 3.0–4.5 up to $5.81 \mu\text{g cm}^{-3}$	Adherence to Beer's law
Shaking time ( $\tau$ ) 2 min	Relative standard deviation (RSD) 1.01%
Concentration of 4-NC $\geq 3.0 \times 10^{-4} \text{ mol L}^{-1}$	Limit of detection (LOD) $0.34 \mu\text{g cm}^{-3}$
Concentration of Nt $\geq 1.0 \times 10^{-4} \text{ mol L}^{-1}$	Limit of quantification (LOQ) $1.13 \mu\text{g cm}^{-3}$

**Table 2.** Effect of co-existing ions and reagents on the complex formation of the ion-associate Ge(IV)-4-NC-Nt for extraction in the presence of 14  $\mu\text{g}$  Ge(IV)

Co-existing ion and reagent	Co-existing ion and reagent, $\mu\text{g}/10\text{ cm}^3$ aqueous phase	Ge(IV) found, $\mu\text{g}$	R, %
Na <sup>+</sup>	10000	14.30	102.14
K <sup>+</sup>	10000	13.75	98.21
Cu <sup>2+</sup>	10000	14.23	101.64
Zn <sup>2+</sup>	10000	14.38	102.71
Cd <sup>2+</sup>	10000	13.92	99.43
Ni <sup>2+</sup>	10000	14.09	100.64
Mn <sup>2+</sup>	10000	14.19	101.36
Co <sup>2+</sup>	10000	13.66	97.57
Al <sup>3+</sup>	20		interference
Cr <sup>3+</sup>	20		interference
Fe <sup>3+</sup>	20		interference
V(V)	10		interference
Cr(VI)	30		interference
W(VI)	20		interference
Mo(VI)	30		interference
F <sup>-</sup>	100	14.31	102.21
Cl <sup>-</sup>	10000	14.18	101.29
Br <sup>-</sup>	3500	14.39	102.79
I <sup>-</sup>	5000	14.26	101.86
NO <sub>3</sub> <sup>-</sup>	2500	13.83	98.79
PO <sub>4</sub> <sup>3-</sup>	10000	13.97	99.79
C <sub>2</sub> O <sub>4</sub> <sup>2-</sup>	500	14.37	102.64
C <sub>6</sub> H <sub>5</sub> O <sub>7</sub> <sup>3-</sup>	400	13.72	98.00
Complexone <sup>222</sup>	3000	14.38	102.71
L-Ascorbic acid	10000	13.80	98.57

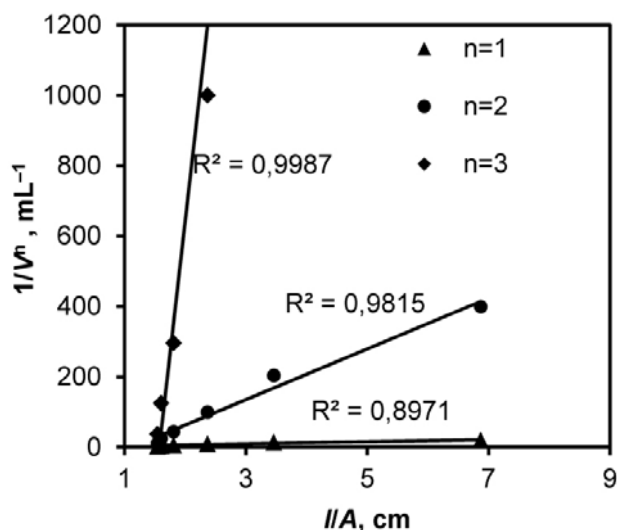


**Figure 2.** Determination of the molar ratio ( $n$ ) Ge(IV):4-NC by the method of Asmus.  $C_{\text{Ge(IV)}} = 2.0 \times 10^{-5} \text{ mol L}^{-1}$ ;  $C_{\text{Nt}} = 1.7 \times 10^{-4} \text{ mol L}^{-1}$ ; pH = 4.0;  $\lambda = 405 \text{ nm}$ ;  $\tau = 2 \text{ min}$

Asmus and the mobile equilibrium method were applied to prove the molar ratios Ge(IV):4-NC and Ge(IV):Nt.<sup>41</sup> The results from the application of these methods are shown in Figures 2–4, respectively. On the basis of the results it can be concluded that Ge(IV), 4-NC and Nitron in-

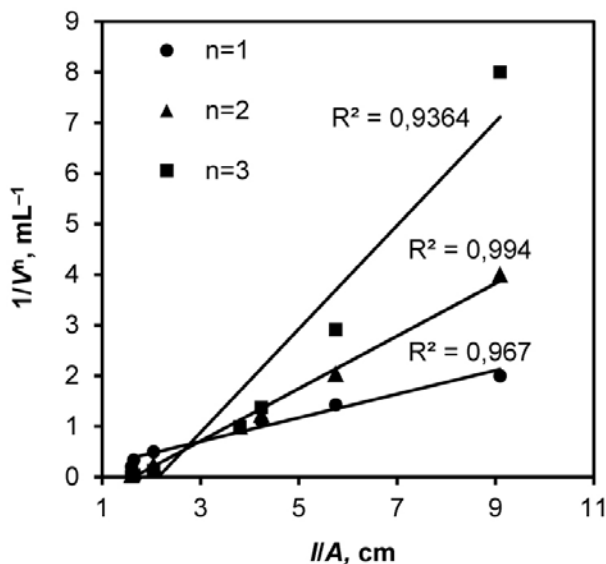


**Figure 3.** Determination of the molar ratio ( $n$ ) Ge(IV):Nt by the method of Asmus.  $C_{\text{Ge(IV)}} = 2.0 \times 10^{-5} \text{ mol L}^{-1}$ ;  $C_{4\text{-NC}} = 5.0 \times 10^{-4} \text{ mol L}^{-1}$ ; pH = 4.0;  $\lambda = 405 \text{ nm}$ ;  $\tau = 2 \text{ min}$

teract in molar ratio 1:3:2. The application of the method of continuous variations confirmed the molar ratio Ge(IV):Nt = 1:2 (Figure 5).<sup>41</sup>

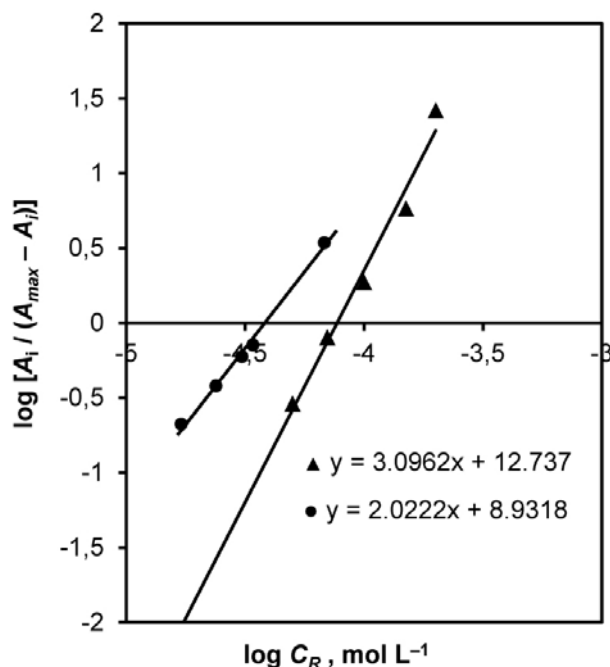


**Figure 4.** Straight lines by the mobile equilibrium method for determination of the molar ratios Ge(IV):4-NC and Ge(IV):Nt;  $C_{\text{Ge(IV)}} = 2.0 \times 10^{-5} \text{ mol L}^{-1}$ ; pH = 4.0;  $\lambda = 405 \text{ nm}$ ;  $\tau = 2 \text{ min}$  ▲ Ge(IV) : 4-NC,  $C_{\text{Nt}} = 1.7 \times 10^{-4} \text{ mol L}^{-1}$ ; ● Ge(IV) : Nt,  $C_{4\text{-NC}} = 5.0 \times 10^{-4} \text{ mol L}^{-1}$

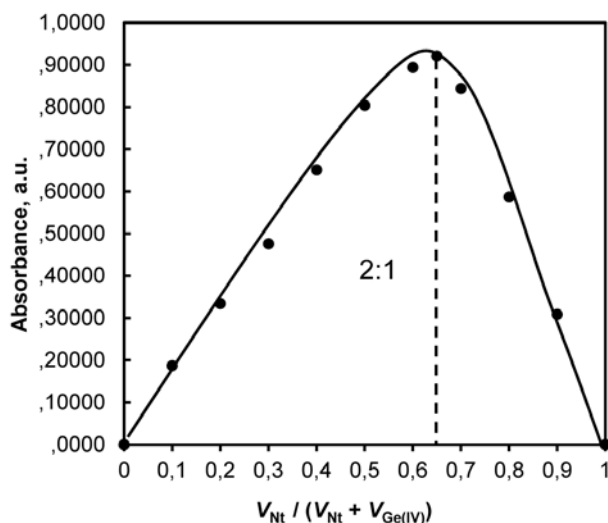
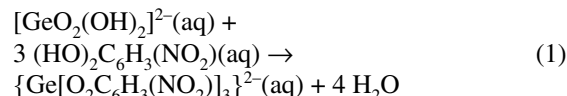


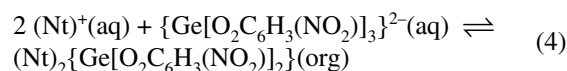
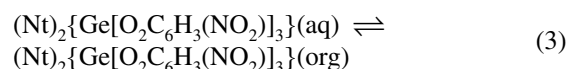
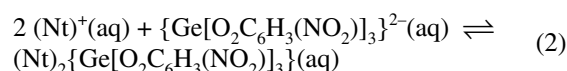
**Figure 5.** Determination of the molar ratio ( $n$ ) Ge(IV):Nt by the method of continuous variations.  $C_{\text{Ge(IV)}} + C_{\text{Nt}} = 1.0 \times 10^{-3} \text{ mol L}^{-1}$ ;  $C_{4\text{-NC}} = 5.0 \times 10^{-4} \text{ mol L}^{-1}$ ; pH = 4.0;  $\lambda = 405 \text{ nm}$ ;  $\tau = 2 \text{ min}$

Germanates containing  $[\text{Ge}(\text{OH})_6]^{2-}$  ions are already described in the literature although in dilute aqueous solutions the major determinate ions appear to be  $[\text{Ge}(\text{O}(\text{OH})_3)_3]^-$ ,  $[\text{GeO}_2(\text{OH})_2]^{2-}$  and  $\{[\text{Ge}(\text{OH})_4]_8(\text{OH})_3\}^{3-}$ .<sup>9</sup> The carried out experiments showed that the complex formation and the extraction of the ion-associated complex have occurred in dilute solutions and the molar ratio establis-

hed by the independent methods mentioned above was Ge(IV):4-NC:Nt = 1:3:2. Therefore, the complex formation of anionic chelate Ge(IV)–4-NC can be given by equation (1):



Having in mind the reaction of chelate formation of Ge(IV)–4-NC and molar ratio indicated above, it can be suggested that the formation of the ion-associate in the aqueous phase, its distribution between the aqueous and the organic phases and its extraction in chloroform can be given by the following equations (2–4).



Hence, the ion-pair formed between the anionic chelate of Ge(IV)–4-NC and the nitronium cation can be represented by the general formula  $(\text{Nt})_2\{\text{Ge}[\text{O}_2\text{C}_6\text{H}_3(\text{NO}_2)_3]\}$ .

### 3. 5. Extraction Equilibria, True Molar Absorptivity and Recovery Factor

The association process in aqueous phase and the extraction equilibria were investigated and quantitatively characterized with respect to the following key constants: association constant, distribution constant, extraction constant and recovery factor.

The association constant  $\beta$  was determined by the method of Komar-Tolmachev from equation (5).<sup>41</sup>

$$\beta = (l/n)^n / [\varepsilon (\text{tg } \alpha)^{n+1}] \quad (5)$$

where  $l$  is the cuvette thickness ( $l = 1 \text{ cm}$ );  $n$  is the molar ratio between the components independently determined (e.g. by the mobile equilibrium method, the straight-line method of Asmus or the method of continuous variations) ( $n = 2$ ),  $\varepsilon$  is the true molar absorptivity.

The true molar absorptivity  $\varepsilon$  was determined by the method of Komar-Tolmachev (Figure 6) from the equation of a straight line  $Y = 2.1644 X + 3.2386$  ( $\varepsilon = 1 / (b \times 10^{-5})$ ) and its value is given in Table 1, column 2.<sup>41</sup>

The distribution constant ( $K_D$ ) was determined by equation (6), where  $A_1$  and  $A_3$  are the absorbance (measured against blanks) obtained after a single and triple extraction, respectively.

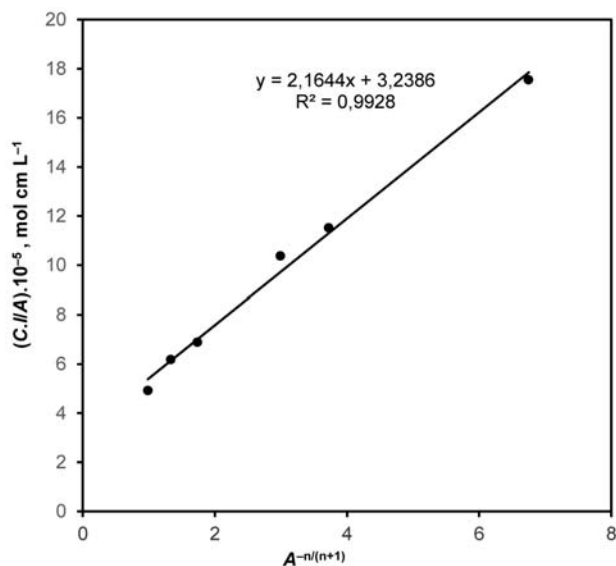


**Figure 6.** Dependency of  $(C./A)$  on  $A^{-n/(n+1)}$  (method of Komar-Tolmachev).  $C = C_{\text{Ge(IV)}} \text{ mol L}^{-1}$ ;  $C_{\text{Nt}} = 2 C_{\text{Ge(IV)}} \text{ mol L}^{-1}$ ;  $C_{4\text{-NC}} = 5.0 \times 10^{-4} \text{ mol L}^{-1}$ ;  $A$  – absorbance;  $l$  – cell thickness,  $l = 1 \text{ cm}$ ;  $n = 2$

$$K_D = \frac{\{(\text{Nt})_2\{\text{Ge}[\text{O}_2\text{C}_6\text{H}_3(\text{NO}_2)]_3\}\}(\text{org})}{\{(\text{Nt})_2\{\text{Ge}[\text{O}_2\text{C}_6\text{H}_3(\text{NO}_2)]_3\}\}(\text{aq})} = A_1 / (A_3 - A_1) \quad (6)$$

The recovery factor was determined from the equation (7):

$$R\% = 100 K_D / (K_D + 1) \quad (7)$$

The extraction constant  $K_{\text{ex}}$  was calculated by two independent methods:

$$(i) \log K_{\text{ex}} = \log K_D + \log \beta \quad (8)$$

where  $\beta$  was determined by the method of Komar-Tolmachev.

(ii) the method of Likussar-Boltz:<sup>42</sup>

The method of Likussar-Boltz uses the data from the method of continuous variations (Figure 5). The extraction constant  $K_{\text{ex}}$  was calculated by the equation of Likussar-Boltz for molar ratio 1:2 (equation 9):

$$\log K_{\text{ex}} = 0,3522 - 2 \log K + \log Y_{\text{max}} - 3 \log (1 - Y_{\text{max}}) \quad (9)$$

where  $K$  is the total concentration of reagents ( $K = C_{\text{Ge(IV)}} + C_{\text{Nt}} = 1.0 \times 10^{-3} \text{ mol L}^{-1}$ );  $Y_{\text{max}}$  and  $(1 - Y_{\text{max}})$  are determined from the additionally plotted normalized absorbance curve ( $Y_{\text{max}} = 0.933$ ;  $(1 - Y_{\text{max}}) = 0.067$ ).

The values of the equilibrium constants and the recovery factor are presented in Table 3. The results obtained by independent methods are statistically dissimilar and confirm the proposed scheme of the process of complex formation of the ion-pair in the aqueous phase, its distribution between the aqueous and the organic phases and its extraction in chloroform.

## 4. Conclusion

The extraction equilibria for complex formation of the ion-pair formed between the anionic chelate of Ge(IV)–4-nitrocatechol (4-NC) and the cation of 1,4-diphenyl-3-(phenylamino)-1*H*-1,2,4-triazole (Nitron, Nt) was studied by spectrophotometry. The processes of the chelate formation and extraction of the ion-associated complex Ge(IV)–4-NC–Nt into chloroform were investigated. The optimum conditions for the association in aqueous phase and extraction of the ion-associated complex were established. The validity of Beer's law was checked and a linear relationship between the germanium(IV) concentration in the aqueous phase and the absorbance of the ion-association complex in the organic phase extraction was observed for concentrations up to  $5.81 \mu\text{g mL}^{-1}$  Ge(IV). The presence of hydrophobic substituents, phenyl groups in the molecule of the triazole, increased the solu-

**Table 3.** Values of the Equilibrium Constants and the Recovery Factor

Equilibrium Constant and Recovery Factor	Value
Equilibrium (equation 3) - Association constant $\beta$	
$\beta = \frac{(\text{Nt})_2\{\text{Ge}[\text{O}_2\text{C}_6\text{H}_3(\text{NO}_2)]_3\}(\text{aq})}{\{[(\text{Nt})^+]^2(\text{aq})\}\{\{\text{Ge}[\text{O}_2\text{C}_6\text{H}_3(\text{NO}_2)]_3\}^2(\text{aq})\}}$	$\log \beta = (8.90 \pm 0.75)^a$ $\log \beta = (9.47 \pm 0.21)^b$
Equilibrium (equation 4) – Distribution constant $K_D$	
$K_D = \frac{\{(\text{Nt})_2\{\text{Ge}[\text{O}_2\text{C}_6\text{H}_3(\text{NO}_2)]_3\}\}(\text{org})}{\{(\text{Nt})_2\{\text{Ge}[\text{O}_2\text{C}_6\text{H}_3(\text{NO}_2)]_3\}\}(\text{aq})}$	$\log K_D = (1.30 \pm 0.01)^c$
Equilibrium (equation 5) - Extraction constant $K_{\text{ex}}$	
$K_{\text{ex}} = \frac{\{(\text{Nt})_2\{\text{Ge}[\text{O}_2\text{C}_6\text{H}_3(\text{NO}_2)]_2\}\}(\text{org})}{\{[(\text{Nt})^+]^2(\text{aq})\}\{\{\text{Ge}[\text{O}_2\text{C}_6\text{H}_3(\text{NO}_2)]_3\}^2(\text{aq})\}}$	$\log K_{\text{ex}} = (10.20 \pm 0.76)^d$ $\log K_{\text{ex}} = (9.85 \pm 0.45)^e$
Recovery factor $R\%$	$R = (95.21 \pm 0.03)\%^f$

<sup>a</sup> Calculated by Komar-Tolmachev method (equation (6)); <sup>b</sup> Calculated by Holme-Langmyhr method;<sup>42</sup> <sup>c</sup> Calculated by equation (6); <sup>d</sup> Calculated by equation (8), where  $\beta$  is determined by the Komar-Tolmachev method; <sup>e</sup> Calculated by Likussar-Boltz method (equation (9)); <sup>f</sup> Calculated by equation (7).



bility of the ion-associated complex in the organic solvent. The molar ratio of the components, determined by independent methods, shows that the ion-associated complex could be represented with the general formula  $(\text{Nt})_2\{\text{Ge}[\text{O}_2\text{C}_6\text{H}_3(\text{NO}_2)_3]\}_3$ . A corresponding reaction scheme of the complex was also suggested. The equilibrium constants and analytical characteristics needed for the quantitative assessment of the extraction equilibrium were calculated, i.e. the association constant ( $\beta$ ), the distribution constant ( $K_D$ ), the extraction constant ( $K_{ex}$ ), the recovery factor ( $R$ ), the apparent molar absorptivity ( $\epsilon'$ ), the true molar absorptivity ( $\epsilon$ ), the limit of detection ( $LOD$ ), the limit of quantification ( $LOQ$ ) and the Sandell's sensitivity ( $SS$ ). From the analytical characteristics of the extraction system  $\text{Ge(IV)}-4\text{-NC}-\text{Nt}-\text{H}_2\text{O}-\text{CHCl}_3$ , it can be concluded that the ion-pair formed between the anionic chelate of  $\text{Ge(IV)}-4\text{-NC}$  and the nitronium cation allows determinations of  $\text{Ge(IV)}$  with a high sensitivity.

## 5. Acknowledgements

The authors would like to thank the Research Fund of the University of Plovdiv for the financial support of the current research.

## 6. References

1. R. R. Moskalyk, *Miner. Eng.* **2004**, *17*, 393–402.  
<http://dx.doi.org/10.1016/j.mineng.2003.11.014>
2. L. Cao L, J. Park, P. Fan, B. Clemens, M. L. Brongersma, *NanoLett.* **2010**, *10*, 1229–1233.  
<http://dx.doi.org/10.1021/nl903727>
3. S. Goodman, *Med. Hypoth.* **1988**, *26*, 207–215.  
[http://dx.doi.org/10.1016/0306-9877\(88\)90101-6](http://dx.doi.org/10.1016/0306-9877(88)90101-6)
4. K. W. Yu, H. N. Murthy, C. S. Jeong, E. J. Hahn, K. Y. Paek, *Process Biochem.* **2005**, *40*, 2959–2961.  
<http://dx.doi.org/10.1016/j.procbio.2005.01.015>
5. T. Matsusaka, M. Fujii, T. Nakano, T. Terai, A. Kurata, M. Imaizumi, H. Abe, *Clin. Nephrol.* **1988**, *30*, 341–345.
6. S. H. Tao, P. M. Bolger, *Regul. Toxicol. Pharmacol.* **1997**, *25*, 211–219.
7. T. Sanai, S. Okuda, K. Onoyama, N. Oochi, Y. Oh, K. Kobayashi, K. Shimamatsu, S. Fujimi, M. Fujishima, *Nephron* **1990**, *54*, 53–60.  
<http://dx.doi.org/10.1159/000185810>
8. A. G. Shauss, *Ren. Fail.* **1991**, *13*, 1–4.  
<http://dx.doi.org/10.3109/08860229109022139>
9. F. A. Cotton, G. Wilkinson, C. A. Murillo, M. Bochmann: *Advanced Inorganic Chemistry*, Wiley Publishers, New Jersey, **1999**, pp. 392–394.
10. V. V. Skopenko, A. Y. Tsivadze, L. I. Sabranskiy, A. D. Garnovskiy: *Coordination Chemistry*, Akademkniga, Moscow, Russia, **2007**, pp. 78–81.
11. V. S. Sergienko, L. K. Minacheva, A. V. Churakov, *Rus. J. Inorg. Chem.* **2010**, *55*, 2001–2030.  
<http://dx.doi.org/10.1134/S0036023610130012>
12. W. Levason, G. Reid, W. Zhang, *Coordin. Chem. Rev.* **2011**, *255*, 1319–1341.  
<http://dx.doi.org/10.1016/j.ccr.2010.11.019>
13. M. F. Davis, W. Levason, G. Reid, M. Webster, *Dalt. Trans.* **2008**, *17*, 2261–2269.  
<http://dx.doi.org/10.1039/B716765B>
14. I. I. Seifullina, N. V. Shmatkova, E. E. Martsinko, *Russ. J. Coordin. Chem.* **2010**, *30*, 214–220.  
<http://dx.doi.org/10.1023/B:RUCC.0000022120.49644.5c>
15. F. Cheng, M. F. Davis, A. L. Hector, W. Levason, G. Reid, M. Webster, W. Zhang, *Eur. J. Inorg. Chem.* **2007**, *2007*, 2488–2495. <http://dx.doi.org/10.1002/ejic.200700233>
16. G. S. Pokrovski, F. Martin, J. L. Hazemann, J. Schott, *Chem. Geol.* **2000**, *163*, 151–165.  
[http://dx.doi.org/10.1016/S0009-2541\(99\)00102-3](http://dx.doi.org/10.1016/S0009-2541(99)00102-3)
17. D. Biller, C. Burschka, M. Penka, R. Tacke, *Inorg. Chem.* **2002**, *41*, 3901–3908.  
<http://dx.doi.org/10.1021/ic0255757>
18. V. A. Nazarenko: *Analytical Chemistry of Germanium*, Nauka, Moscow, Russia, **1973**, pp. 29–54.
19. I. I. Seifullina, A. G. Pesaroglo, L. K. Minacheva, E. E. Martsinko, V. S. Sergienko, *Russ. J. Inorg. Chem.* **2006**, *51*, 1892–1899.  
<http://dx.doi.org/10.1134/S0036023606120096>
20. L. Zaijun, P. Jiaomai, T. Jan, *Anal. Chim. Acta* **2001**, *445*, 153–159.  
[http://dx.doi.org/10.1016/S0003-2670\(01\)01259-4](http://dx.doi.org/10.1016/S0003-2670(01)01259-4)
21. F. N. Shi, L. C. Silva, M. J. Hardie, T. Trindade, F. A. Paz, J. Rocha, *Inorg. Chem.* **2007**, *46*, 6502–6515.  
<http://dx.doi.org/10.1021/ic700507j>
22. F. A. Torralvo, C. Fernandez-Pereira, M. C. Campanario, *Ind. Eng. Chem. Res.* **2010**, *49*, 4817–4823.  
<http://dx.doi.org/10.1021/ie901020f>
23. S. Jagatap, S. Kolekar, S. Han, M. Anuse, *Inter. J. Anal. Bioan. Chem.* **2012**, *2*, 235–240.
24. K. T. Mahmudov, R. A. Aliyeva, S. Z. Hamidov, F. M. Chyragov, S. R. Mardanova, M. N. Kopylovich, A. J. L. Pombeiro, *Am. J. Anal. Chem.* **2012**, *3*, 790–799.  
<http://dx.doi.org/10.4236/ajac.2012.312105>
25. K. Gavazov, A. Dimitrov, V. Lekova, *Russ. Chem. Rev.* **2007**, *76*, 169–179.  
<http://dx.doi.org/10.1070/RC2007v076n02ABEH003655>
26. C. Farber, M. Leibold, C. Bruhn, M. Maurer, U. Siemeling, *Chem. Commun.* **2012**, *48*, 227–229.  
<http://dx.doi.org/10.1039/C1CC16460K>
27. V. S. Archer, R. B. Twelves, *Talanta* **1968**, *15*, 47–54.  
[http://dx.doi.org/10.1016/0039-9140\(68\)80006-2](http://dx.doi.org/10.1016/0039-9140(68)80006-2)
28. Th. Koralewski, G. A. Parkar, *Anal. Chim. Acta* **1980**, *113*, 389–392.  
[http://dx.doi.org/10.1016/S0003-2670\(01\)93757-2](http://dx.doi.org/10.1016/S0003-2670(01)93757-2)
29. P. Racheva, K. Gavazov, V. Lekova, A. Dimitrov, *J. Materials* **2013**, *2013*, Article ID 897343, 7 pages.  
<http://dx.doi.org/10.1155/2013/897343>
30. K. Stojnova, V. Divarova, P. Racheva, G. Daskalov, V. Leko-

- va, *Monatsh. Chem.* **2015**, *146*, 867–873.  
<http://dx.doi.org/10.1007/s00706-014-1402-7>
31. M. J. Moorcroft, J. Davis, R. G. Compton, *Talanta* **2001**, *54*, 785–803.  
[http://dx.doi.org/10.1016/S0039-9140\(01\)00323-X](http://dx.doi.org/10.1016/S0039-9140(01)00323-X)
32. S. Shahine, I. Nazara, *Microchim. Acta* **1976**, *66*, 75–79.  
<http://dx.doi.org/10.1007/BF01257096>
33. S. Shahine, S. Khamis, *Microchem. J.* **1980**, *25*, 46–47.  
[http://dx.doi.org/10.1016/0026-265X\(80\)90240-4](http://dx.doi.org/10.1016/0026-265X(80)90240-4)
34. R. Koroda, N. Yoshikuni, *Microchim. Acta* **1974**, *62*, 653–662. <http://dx.doi.org/10.1007/BF01218202>
35. A. K. Babko, A. T. Pilipenko: *Photometric Analysis*, Khimiya, Moscow, Russia, **1968**, pp. 159–164.
36. V. A. Mikhaylov: *Extraction Chemistry*, Nauka, Novosibirsk, Russia, **1984**, pp. 194–249.
37. G. Kristian: *Analytical Chemistry*, BINOM, Moscow, Russia, **2009**, pp. 414–426.
38. U. A. Zolotov, V. A. Bodnya, A. N. Zagrusina, H. Freiser, *Anal. Chem.* **1982**, *14*, 93–174.  
<http://dx.doi.org/10.1080/10408348208542772>
39. K. Stojnova, P. Racheva, V. Divarova, K. Bozhinova, V. Lekova, *Acta Chim. Slov.* **2016**, *63*, 654–660.  
<http://dx.doi.org/10.17344/acsi.2016.2513>
40. V. Divarova, K. Stojnova, P. Racheva, V. Lekova, *Acta Chim. Slov.* **2016**, *63*, 97–103.  
<http://dx.doi.org/10.17344/acsi.2015.1987>
41. Z. Marczenko, M. Baltcerzak: *UV-Vis Spectrophotometric Methods Applied to the Inorganic Analysis*, BINOM, Moscow, Russia, **2009**, pp. 169–174.
42. B. F. Quin, R. R. Brooks, *Anal. Chim. Acta* **1975**, *74*, 75–84.  
[http://dx.doi.org/10.1016/S0003-2670\(01\)82781-1](http://dx.doi.org/10.1016/S0003-2670(01)82781-1)
43. M. I. Bulatov, I. P. Kalinkin: *Practical Handbook on Photometric Methods of Analysis*, Khimiya, Leningrad, Russia, **1986**, pp. 174–264.
44. W. Likussar, D. F. Boltz, *Anal. Chem.* **1971**, *43*, 1265–1272.  
<http://dx.doi.org/10.1021/ac60304a006>
45. A. Holme, F. J. Langmyhr, *Anal. Chim. Acta* **1966**, *36*, 383–391. [http://dx.doi.org/10.1016/0003-2670\(66\)80066-1](http://dx.doi.org/10.1016/0003-2670(66)80066-1)

## Povzetek

S pomočjo spektrofotometrije smo proučili tvorbo komplekso med anionskim kelatnim kompleksom Ge(IV)–4-nitrokatehol (4-NC) in kationom 1,4-difenil-3-(fenilamino)-1*H*-1,2,4-triazolom (Nitron, Nt) v tekočina–tekočina ekstrakcijskem sistemu Ge(IV)–4-NC–Nt–H<sub>2</sub>O–CHCl<sub>3</sub>. Določili smo optimalne ekstrakcijsko-spektrofotometrične pogoje za tvorbo kompleksov. Preverjena je bila veljavnost Beerovega zakona ter izračunane nekatere analizne karakteristike. Določen je bil tudi vpliv različnih ionov in reagentov na proces tvorbe kompleksov. Asociacijski proces v vodni fazi in ekstrakcijsko ravnotežje je bilo proučeno in kvantitativno okarakterizirano. Sledeče najpomembnejše konstante procesov so bile izračunane: asociacijska konstanta, distribucijska konstanta, ekstrakcijska konstanta in izkoristek ekstrakcije. Z neodvisnimi metodami smo določili molske deleže. Predlagana je reakcijska shema, splošna formula in struktura kompleksa.

Scientific paper

# A Natural Based Method for Hydrophobic Treatment of Natural Fiber Material

Thomas Kick, Thomas Grethe and Boris Mahltig\*

Hochschule Niederrhein, University of Applied Sciences, Faculty of Textile and Clothing Technology, Webschulstr. 31, 41065 Mönchengladbach, Germany

\* Corresponding author: E-mail: boris.mahltig@hs-niederrhein.de

Received: 30-01-2017

## Abstract

A treatment for hydrophobic functionalization of natural fiber materials is developed. This hydrophobic treatment is based mainly on natural products. As hydrophobic component the natural Tung Oil is used, which is originally a compound used for wood conservation purposes. The application on textile is done in a padding process under presence of an oxidative agent. For the current investigations a fiber felt from linen was used. The hydrophobic effect is determined by the concentration of Tung Oil and the duration of a thermal drying process. The hydrophobic effect is investigated by capillary rise tests and contact angle measurements. Scanning electron microscopy SEM is used to investigate the surface topography of the fiber material and the deposited hydrophobic material. Altogether, an interesting and promising method for hydrophobisation of natural fibers is developed, which could especially be used as part of a production process of a fiber reinforced composite material, mainly based on natural products.

**Keywords:** Tung Oil, contact angle measurements, natural fiber, fiber felt, non-woven

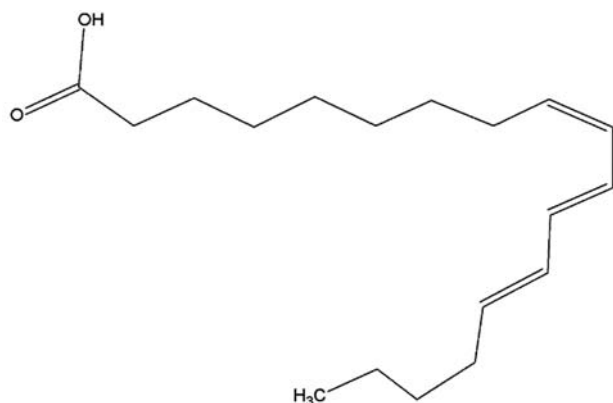
## 1. Introduction

Natural fiber materials are based on fibers from plants or animals.<sup>1,2</sup> They can be used as traditional textiles for clothes but also as non-woven materials for technical purposes. Natural fibers are also used as fiber component in fiber reinforced composite materials used for example in the automotive sector.<sup>3,4</sup> For composite applications natural fibers have to compete with composites containing glass or carbon fibers. The mechanical properties of these competing composite materials are excellent. However also natural fibers exhibit important advantages, if they are used in composites. These advantages are related to material properties, economic reasons and ecologic concerns. From the material point of view, natural fibers are of lower density compared to glass fibers, so composite materials of lower weight can be produced.<sup>4</sup> The use of low weight composite materials in automotive sector will reduce for the final product – the car – the fuel consumption.<sup>5</sup> From the economic point of view, natural fibers are low cost materials, if their price is compared to glass and carbon fibers.<sup>6,7</sup> From the ecologic point of view, the recycling of materials containing natural fibers is simple compared to the recycling of composite materials with

glass or carbon fibers.<sup>4,8</sup> One significant property of natural fibers is their hydrophilicity. Natural fibers are able to take up significant amounts of water.<sup>9–11</sup> For technical applications, this hydrophilicity is often disadvantageous, due to several reasons. The presence of water on a natural fiber can support the growth of fungi and bacteria, which can be the starting point of a bio corrosion. Also the up-take of water can lead to change in fiber volume, so crack formations in a composite material are promoted. Actually there are many excellent chemicals on the market, which are especially developed for a hydrophobic treatment of textile materials.<sup>12–14</sup> The main aim of those treatments is the realization of water- and soil-repellent textiles, usable as rain clothes or as home textiles.<sup>14,15</sup> The most effective chemicals in that field are based on fluorine-carbon compounds. Fluorine-carbon compounds are from the technical point of view excellent materials but in the last years significant concerns arise, due to potential environmental and health risks.<sup>16</sup> Other hydrophobic chemicals used in the textile field are polysiloxanes, which are also under discussion.<sup>17,18</sup>

With this background, there is a certain demand for a natural based hydrophobic agent usable for the hydrophobic treatment of natural fiber materials. This statement

is especially valid, if a fully “bio-based” product is wished. This product should be built up from natural fibers and a treatment which is as well gained from natural products. For this, in the current work a hydrophobic treatment for natural fibers based on a natural product is developed. As natural product the natural oil – Tung Oil – is used. Tung Oil is a natural product, sometimes named as China wood oil or China nut oil. It is produced from seeds of the Tung tree. This Tung tree is originated from China, there it is known and cultivated since centuries. Today Tung Oil is used for the surface treatment of wood.<sup>19</sup> The Tung Oil is used for wood conservation and protection in Europe in the 1920<sup>th</sup>.<sup>20,21</sup> Tung Oil-treatment on wood is used for protection against wood-decay fungi and to decrease water uptake of wood.<sup>22</sup> This decreased water uptake is reported for laboratory but also for long term field tests. The Tung Oil treatment is as well mentioned as an effective mean to replace traditional biocidal treatment for wood, which are under consideration, because of possible hazardous potential.<sup>22</sup> The use of Tung Oil for textile treatment is mentioned in some older patent references.<sup>23,24</sup> However, in those references the main focus for the Tung Oil is not to realize water-repellent textiles. The Tung Oil is reported for the improvement of crease and shrink resistance of textiles.<sup>23</sup> Also mentioned is the realization of high flex abrasion resistance of cotton textiles by Tung Oil.<sup>24</sup> Tung Oil is from chemical point of view a triglyceridic ester composed mainly from alpha-elaeostearic acid (*cis*-9, *trans*-11, *trans*-13-octadecatrienoic acid) (structure see Scheme 1).

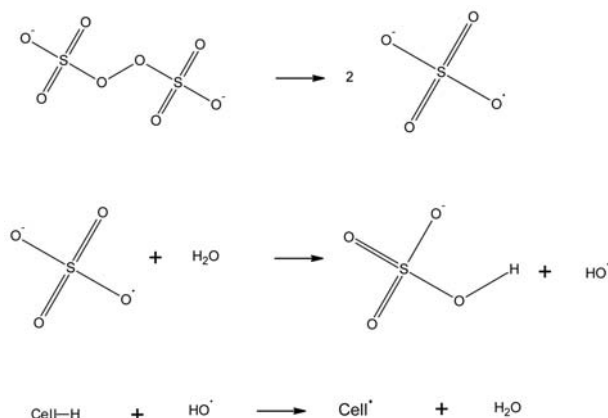


**Scheme 1:** Chemical structure of alpha-elaeostearic acid.

The content of this unsaturated organic acid is around 84% in the Tung Oil.<sup>25–27</sup> However other references reports lower content of only 64% alpha-elaeostearic acid in the Tung Oil.<sup>28</sup> It has to be kept in mind, Tung Oil is a natural product, and its composition can be influenced by the climate or other local conditions surrounding the originating plant.

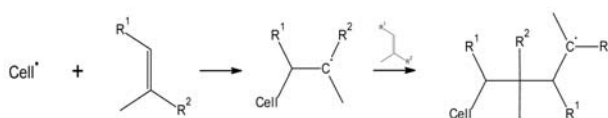
The appearance of multiple conjugated carbon/carbon double bonds makes the Tung Oil a monomer thermally

polymerizable at higher temperatures.<sup>25,29</sup> Such a thermal polymerization after application onto a fiber material can be part of a hydrophobic treatment process. However, due to the thermal sensitivity of natural fibers, the use of a temperature driven polymerization process could lead to partly fiber decomposition. Alternatively to the thermal polymerization, also oxidative processes are suitable for crosslinking of the unsaturated carbon-carbon double bonds.<sup>30</sup> By such a process also a crosslinking to the surface of a cellulosic based fiber is possible.<sup>31,32</sup> This connection to the fiber surface is especially necessary, if a long-term stability of the hydrophobic treatment onto the fiber material is wished. Persulfates are reported to initiate radical grafting reactions onto cotton fibers in aqueous media, however the formation of carbon or oxygen centered secondary radicals on the cellulose remains unclear.<sup>33</sup> However, using persulfate most authors imply a localization of the intermediate radical on the cellulosic oxygen (Scheme 2).<sup>31,34,35</sup>

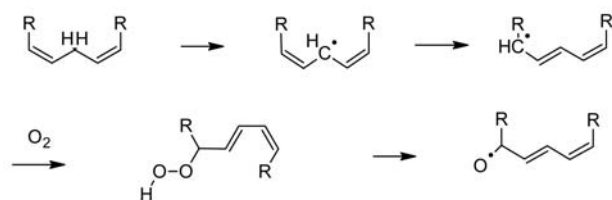


**Scheme 2:** Schematic drawing of persulfate reaction to form intermediate radicals on the cellulose.

Thakur et al. mention both options, but give no further evidence on the mechanism favoring one or the other.<sup>36</sup> The cellulosic radical can then undergo a grafting reaction with an unsaturated hydrocarbon, as described in Scheme 3. Natural oils like linseed oil or Tung Oil undergo a natural polymerization by atmospheric oxygen. The mechanism is proposed by Mallegol et al. and is summarized in Scheme 4.<sup>30</sup> The polymerization of these oils can consequently be enhanced by introducing an oxidizing agent. By using sodium persulfate the crosslinking can be accelerated combined with the option of a radical grafting reaction onto the cellulosic fiber.



**Scheme 3:** Drawing of cellulosic radical reacting with unsaturated hydrocarbon.



Scheme 4: Polymerisation step for unsaturated natural oil.

Based on this background, in the actual investigation a hydrophobic treatment based on Tung Oil and an oxidative agent is developed for application onto natural fibers. This demonstration is done on linen fiber felt. It is shown in a first approach that by this method natural oils can be used for hydrophobic modification of natural fiber materials.

## 2. Experimental Section

### 2.1. Materials

As textile material a nonwoven felt from linen fibers is chosen. This is a natural material and has to be cleaned before a further wet chemical treatment is performed. This cleaning is done with an enzymatic pretreatment, which is able to remove unwished substances and dirt from the fiber surface. This pretreatment is done in a dyeing machine (Then from Fong Europe GmbH, Schwäbisch Hall) usable for laboratory scale. For the pretreatment a water based recipe with following components is used – 30 liter water, 390 ml PERIZYM DBS from the company Dr. Petry GmbH, 60 ml PERIPLEX AHL from the company Dr. Petry GmbH and 60 ml KOLLASOL OCE from CHT.R. BEITLICH GmbH (Tübingen, Germany). PERIZYM DBS is a ready-made aqueous solution with enzymatic components of pectinase and amylase. PERIPLEX AHL is an aqueous yellow and transparent liquid. It contains complexing agents for heavy metal ions and ions from calcium and magnesium. KOLLASOL OCE is a clear transparent liquid containing wetting agents. It is used to improve the wetting of the aqueous recipe on the fiber material and to suppress the formation of foam during the application. The pH-value of the complete recipe is 7.2. With this recipe an amount of 569 g linen fibers is treated for 2 hours at 60 °C in the above mentioned dyeing machine. Afterwards the linen fibers are treated with 30 liter of water at 95 °C for 20 minutes, following by a washing step at 70 °C for 10 minutes. In the end the fiber felt is dried at room temperature. After the complete process a weight loss of 7% is determined for the fiber felt, probably related to the removed components from the fiber surface. For hydrophobic treatment of the linen fiber felt recipes containing following components are used. Tung Oil which is a yellow and viscose substance gained from Sigma-Aldrich, sodiumperoxodisulfate from VWR and sodiumoleate form Sigma-Aldrich.

### 2.2. Preparation

For hydrophobic functionalization, the linen fiber felt is treated with a recipe containing 45 mL water, 5 g sodiumperoxodisulfate, 0.5 g sodiumoleate and Tung Oil in an amount of 5 g, 10 g or 20 g. Before application on the fiber material all components are stirred together for a duration of 15 minutes. The application onto the fiber felt is done in a horizontal padder – 2-Walzen-Labor-Foulard supplied by the company Wichelhaus GmbH (Germany). During application the roller pressure is set to 0.3 MPa and the speed is set to 18 m/min. Each sample is treated twice. The wet pick-up of the fiber samples treated this way is 93 wt-%. Afterwards the samples are dried in an oven (from Memmert) at a temperature of 90 °C. The duration for this drying process is set in a range from 5 to 60 minutes.

### 2.3. Analytics

The hydrophobic properties of the prepared samples are determined by two methods, the capillary rise test and contact angle measurements. The capillary rise test is used to determine the capability of a textile sample to soak up water.<sup>37</sup> The actual measurements are performed according to DIN 53924. For this, the fiber felt samples are cut in strips of 30mm width and one end of the strip is placed vertically in contact with a testing liquid. This testing liquid is an aqueous solution of 0.5% of the blue dye C.I. Direct Blue 086. After the contact with the testing liquid, the textile sample soaks up the liquid and after 30 minutes the distance is measured as capillary rise. Each sample is tested twice and the average value is reported. Contact angle measurements are performed with a device Drop Shape Analyzer DSA25 supplied by KRÜSS GmbH (Hamburg, Germany). For measurement, a 30 µl drop of water is placed on the sample and after 10 seconds the contact angle is recorded. For each sample this measurement is repeated 5 times and the average value is reported. For testing the stability against rinsing, the textile samples are stirred into 250 mL water containing 1 mL of the surfactant Triton X. This procedure is done for 10 seconds at room temperature. To evaluate the mechanical properties of prepared textile samples, the elongation at break and the breaking strength are determined according to DIN EN 29 073. The measurements are performed with a device ZmartPro supplied by the company Zwick/Roell. The surface topography of the fiber materials is investigated by scanning electron microscopy, SEM. For this microscopic measurements a microscope Tabletop TM3000 supplied by Hitachi is used.

## 3. Results and Discussion

### 3.1. Material Properties

The morphology of the linen fiber felt is at first investigated by SEM (Figure 1). This morphology is recorded

before and afterwards of the enzymatic treatment for cleaning the linen felt. These measurements show that the enzymatic cleaning does not effected the arrangement and diameters of the linen fibers. However, by these SEM-investigations a more detailed statement concerning the structure and the surface topography of the fibers cannot be done. The hydrophobic treatments containing the Tung Oil are all applied onto the linen fiber felts after the enzymatic treatment is done.

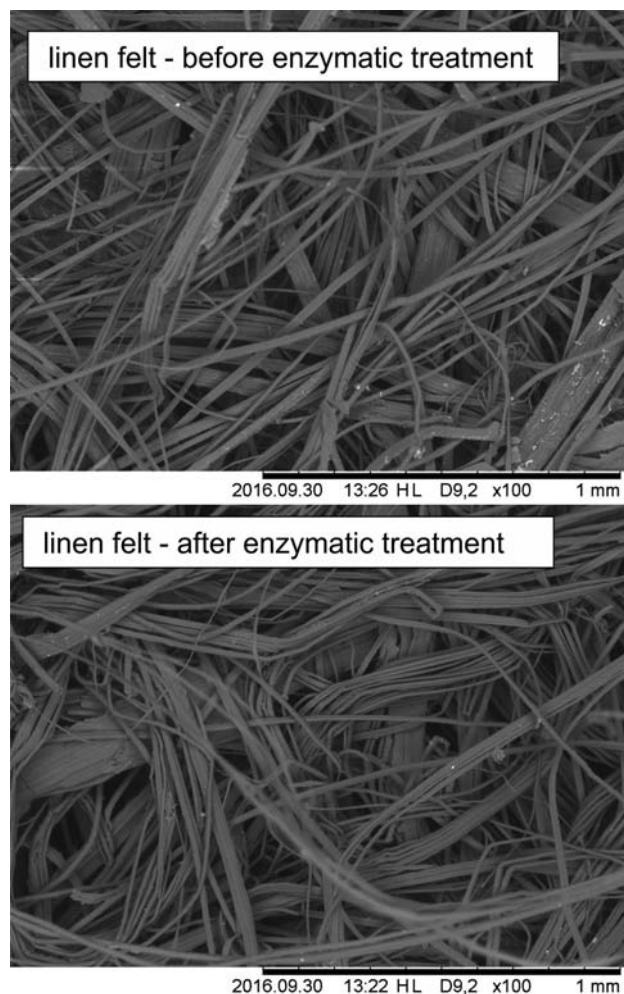


**Figure 1:** SEM-images of linen fiber felt before application of the hydrophobic recipe.

The mechanical properties of fiber samples after application of the hydrophobic recipes are investigated as function of the duration of thermal treatment after application of a hydrophobic recipe (Figure 2). This recipe contains with 20 g the highest amount of used Tung Oil. The thermal treatment is performed at 90 °C with a maximum duration of 60 minutes.

The determined elongation at break is drastically decreased after 30 minutes of thermal treatment. This result can be explained by the cross-linking reaction of the Tung

Oil by an oxidative process. The progress of the crosslinking reaction is indicated by the change in elongation at break as function of duration of thermal treatment. After 30 minutes the crosslinking is progressed in a way that the elongation of the treated linen fiber felt is drastically reduced. Similar to this, the crosslinking leads to a promotion of the hydrophobic effect of the Tung Oil application, as it is presented in the following sub-section.

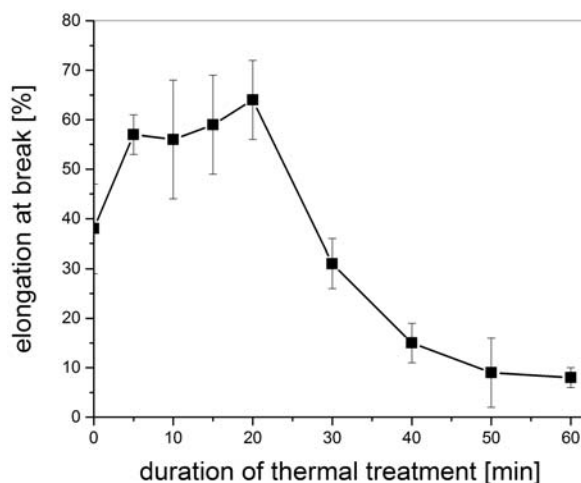


**Figure 2:** Mechanical properties as function of the duration of thermal treatment after application of a hydrophobic recipe containing 20 g Tung Oil. Shown is the elongation at break.

The breaking strength of fiber samples without the Tung Oil treatment is determined to be 60 N and can be significantly decreased by the Tung Oil treatment to values in the range of 20 N to 50 N (Figure 3). However compared to the determined elongation at break (Figure

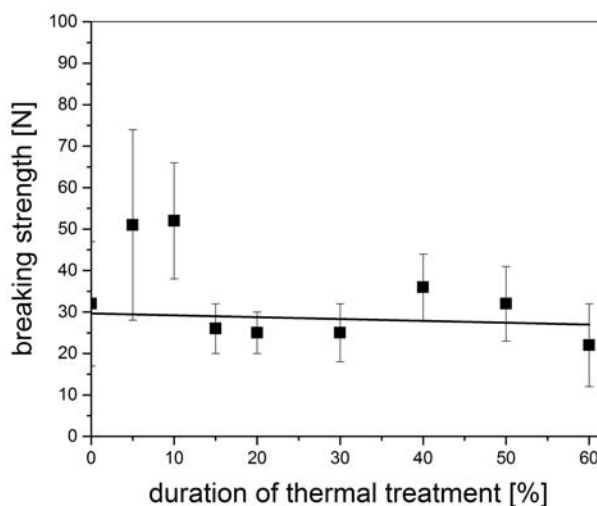


**Figure 3:** Mechanical properties as function of the duration of thermal treatment after application of a hydrophobic recipe containing 20 g Tung Oil. Shown is the breaking strength. The solid line is a guide for the eye based on a linear fit of measurement points.

2), it has to be remarked, that the duration of thermal treatment after the Tung Oil application has a less significant influence on the breaking strength (Figure 3). Evaluating the measurement data of breaking strength as function of duration of thermal treatment by using a linear fit, only a small decrease in the breaking strength can be estimated, if the duration of thermal treatment is expanded to 60 minutes. The oxidative crosslinking of the Tung Oil obviously glue the fibers together and decrease for this the elongation at break. However, the strength of this oil impregnation is less influenced by the progress of crosslinking driven by the thermal treatment.

The morphology of linen fiber felt after application of the Tung Oil recipe is presented in figure 4. By this SEM-images it can be clearly identified that the Tung Oil is especially up-taken by the interspace between the linen fibers. The change in the mechanical properties of the fiber samples could be also explained by a gluing together of the single linen fibers by the crosslinked Tung Oil.

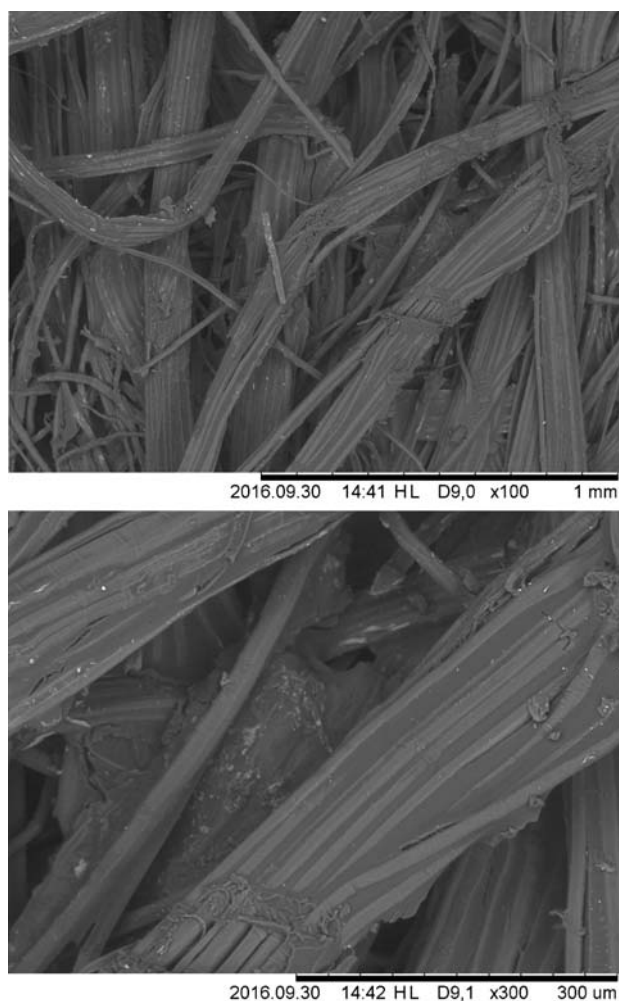


**Figure 4:** SEM-images of linen fiber after application of the hydrophobic recipe containing 20 g Tung Oil and dried for 30 minutes at 90 °C.

### 3. 2. Hydrophobic Properties

To optimize the hydrophobic treatment at first an investigation is performed as function of the duration of thermal treatment after application of the Tung Oil recipe, analogously to the investigation of mechanical properties presented in Figure 2.

This recipe contains with 20 g the highest amount of used Tung Oil. The thermal treatment is performed at 90 °C with a maximum duration of 60 minutes. The hydrophobic properties of the prepared linen samples is determined as capillary rise (Figure 5). The capillary rise of the linen fabric without the Tung Oil application is around 85 mm after 30 minutes measurement time. After Tung Oil application without further thermal treatment a capillary rise of around 10 mm is reached after 30 minutes, so a clear hydrophobic effect is gained even without a further drying procedure. This capillary rise is decreased, if the linen samples with the Tung Oil are thermal treated and this effect is stronger as function of the duration of thermal treatment. After 30 minutes of thermal treatment the capillary rise is nearly zero, so here strong hydrophobic properties are realized.

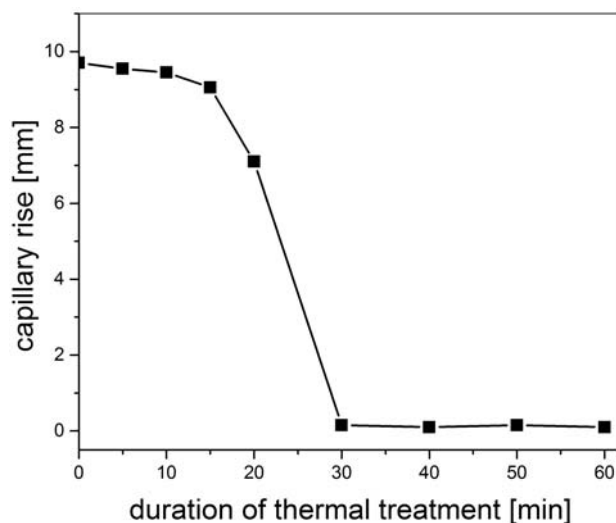


**Figure 5:** Hydrophobic properties as function of the duration of thermal treatment after application of a hydrophobic recipe containing 20 g Tung Oil. Shown is the capillary rise after 30 minutes testing time.

These results of determined capillary rise are in certain agreement with the determined mechanical properties of the investigated samples shown in Figure 2.

Additionally the reached hydrophobic effect is investigated as function of Tung Oil concentration in the applied recipe (Figures 6 and 7). Here it is of special interest, if also lower Tung Oil concentrations could lead to significant hydrophobic properties. The hydrophobic properties are determined by two methods, the capillary rise (Figure 6) and the contact angle measurement with water (Figure 7).

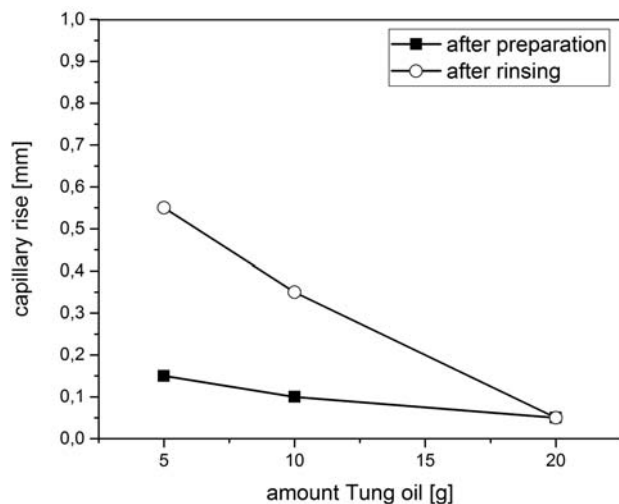


**Figure 6:** Hydrophobic properties as function of the content of Tung Oil in the hydrophobic recipe. After application of the hydrophobic recipe, the samples are dried for 30 minutes. Shown is the capillary rise after 30 minutes testing time.

Even with the lowest applied amount of Tung Oil with 5 g in the recipe a very low capillary rise can be reached, so significant hydrophobic effect is realized even if smaller amounts of Tung Oil are applied. However it can be also stated that this hydrophobic effect gained with smaller amounts of Tung Oil is less stable against a rinsing process. Probably, only small amounts of Tung Oil are needed to modify the surface of linen fibers with hydrophobic properties but larger amounts of this oil are necessary to support suitable crosslinking which is probably a necessary requirement for a certain rinsing stability. Similar results are gained with the contact angle measurements (Figure 7). The contact angle against water of the treated linen fiber samples increases as function of the amount of Tung Oil applied (Figure 7). All treated samples exhibit contact angles of more than  $100^\circ$  and are therefore clearly hydrophobic. Highest values are gained in the current investigation with highest amount – 20g recipe – of applied Tung Oil. However, also with the application of lower Tung Oil amounts of 5g hydrophobic fiber samples are realized. Determined contact angles are around  $115^\circ$ , which is similar to hydrophobic sol-gel agents supporting an intermediate hydrophobic effect on textiles.<sup>38,39</sup> However, with advanced hydrophobic sol-gel systems, containing long-chained alkylsilanes or even fluorinated additives, contact angles around  $140^\circ$  are reached.<sup>38</sup>

By wet chemical application on textile substrates with different perfluorinated recipes in different approaches even contact angles of water in the range of  $150^\circ$  to  $160^\circ$  are reported.<sup>40–42</sup> These applications are based on perfluorinated polysiloxanes, fluorinated acrylic lattices and perfluoroalkylacrylate compounds combined with silica nanoparticles.<sup>40–42</sup>

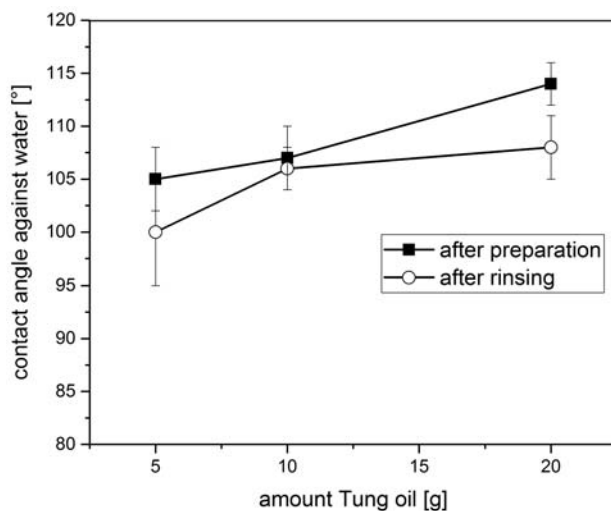


**Figure 7:** Hydrophobic properties as function of the content of Tung Oil in the hydrophobic recipe. After application of the hydrophobic recipe, the samples are dried for 30 minutes. Shown is the contact angle of water.

With different plasma deposition techniques also contact angles of water in the range of  $150^\circ$  to  $170^\circ$  are reached on textile substrates.<sup>43,44</sup> In this technique the type of monomer used for plasma deposition is significant for the gained hydrophobic effect. Suitable monomers are here hexamethyldisiloxane HMDSO and tetrafluoromethane  $\text{CF}_4$ .<sup>43,44</sup>

Such high contact angle values are often summarized under the terms superhydrophobic properties or superhydrophobic textiles.<sup>45–47</sup> Therefore, in relation to other hydrophobic recipes for textile treatment the actual developed Tung Oil recipe can be ranked in the range of moderate hydrophobic agents but not used for realization of superhydrophobic textiles. However, it should be kept in mind that for the application in fiber reinforced composites a moderate hydrophobic fiber functionalization could be advantageous, because it decreases the water up-take of the fiber material but contains still enough hydrophilic groups on the fiber surface necessary for the interaction with the polymer resin forming the matrix of a fiber-reinforced composite.

Altogether it was shown in a first proof of concept, that the natural Tung Oil can be successfully used as hydrophobic agent for natural fibers. This natural based method could be promising for future developments of fully bio based materials as for example fiber reinforced materials – so called bio composites.

## 4. Conclusions

A natural based method for hydrophobic treatment of natural fiber materials is realized by recipes of natural oil. As natural oil the Tung Oil originally used for protec-



tion of wood is used. By this natural recipe moderate hydrophobic properties can be introduced on natural fibers as linen. Suitable recipes contain beside the Tung Oil also sodiumperoxodisulfate to promote the crosslinking reaction of the Tung Oil and sodiumoleate to stabilize the recipe in a water based application recipe. The Tung Oil concentration is varied in a broad range and even with lower concentration a suitable hydrophobic effect is reached. However, it has to be remarked that even with the highest amounts of Tung Oil applied no superhydrophobic properties are reached for the treated fiber materials. Nevertheless, the realized materials are promising for future developments of fully bio based fiber and composite materials.

## 5. Acknowledgements

For funding of the electronmicroscopic equipment the authors acknowledge very gratefully the program FH-Basis of the German federal country North-Rhine-Westphalia NRW. All product and company names mentioned in this chapter may be trademarks of their respective owners, also without labeling. For many helpful discussions and technical help in the lab many thanks have to be acknowledged to Thomas Heistermann from Niederrhein University of Applied Sciences.

## 6. References

1. S. Tunger, F. Geringswald, D. Krügel, G. Steinak, *Faserstofflehre*, VEB Fachbuchverlag, Leipzig, **1974**.
2. V. K. Thakur, M.K. Thakur, R.K. Gupta, *International Journal of Polymer Anal. Charact.* **2004**, *19*, 256–271. <https://doi.org/10.1080/1023666X.2014.880016>
3. V. K. Thakur, M. K. Thakur, *Carbohydrate Polymers* **2014**, *109*, 102–117.
4. P. Wambua, J. Ivens, I. Verpoest, *Composites Sci. Technol.* **2003**, *63*, 1259–1264. [https://doi.org/10.1016/S0266-3538\(03\)00096-4](https://doi.org/10.1016/S0266-3538(03)00096-4)
5. H. Schürmann, *Konstruieren mit Faser-Kunststoff-Verbunden*, Springer-Verlag, Berlin, **2005**.
6. G. Bogoeva-Gaceva, M. Avella, M. Malinconico, A. Buza-rovskaja, A. Grozdanov, G. Gentile, M. E. Errico, *Polymer Composites* **2007**, *28*, 98–107. <https://doi.org/10.1002/pc.20270>
7. D. Pico, C. Wilms, G. Seide, T. Gries, *Chemical Fibers International* **2011**, *61*, 90–91.
8. K. Larsen, *Renewable Energy Focus* **2009**, *9*, 70–73. [https://doi.org/10.1016/S1755-0084\(09\)70045-6](https://doi.org/10.1016/S1755-0084(09)70045-6)
9. D. Behr, *Wirkerei und Strickereitechnik* **1991**, *41*, 7.
10. T. Textor, B. Mahltig, *Applied Surface Science* **2010**, *256*, 1668–1674. <https://doi.org/10.1016/j.apsusc.2009.09.091>
11. N. Erdumlu, B. Ozipek, *Fibres & Textiles in Eastern Europe* **2008**, *16*, 43–47.
12. A. Böhringer, *Textilveredlung* **2002**, *37*, 14–19.
13. G. Duschek, D. Sielemann, *Textilveredlung* **2008**, *43*, 4–7.
14. M. Türk, A. Ehrmann, B. Mahltig, *Journal of the Textile Institute* **2015**, *106*, 611–620. <https://doi.org/10.1080/00405000.2014.931108>
15. R. Haupt-Stephan, *Textilveredlung* **1997**, *32*, 161–165.
16. A. Geu, *Melliand Textilber.* **2010**, *91*, 182–183.
17. C. Dong, Z. Lu, F. Zhang, P. Zhu, L. Zhang, S. Sui, *Materials Letters* **2015**, *152*, 276–279. <https://doi.org/10.1016/j.matlet.2015.03.132>
18. F. Case, *Journal of Surfactants and Detergents* **2006**, *9*, 559–561.
19. S. Allen, *Oberflächenbehandlung von Holz. Klassische Techniken und Rezepte*, Vincentz Network GmbH, Hannover, **2011**.
20. A. Schöнемann, M. Eisbein, A. Unger, M. Dellmour, W. Frenzel, E. Kennidler, *Studies in Conservation* **2008**, *53*, 118–130. <https://doi.org/10.1179/sic.2008.53.2.118>
21. E. Fonrobert, *Das Holzöl*, Berliner Union, Stuttgart, **1951**.
22. M. Humar, B. Lesar, *International Biodeterioration & Biodegradation* **2013**, *85*, 223–227. <https://doi.org/10.1016/j.ibiod.2013.07.011>
23. F. E. Condo, C. W. Schroeder, US Patent Number 2886472A, date of patent April 27 **1956**.
24. J. J. C Arthur, J.A. Harris, US Patent Number 3926550A, date of patent November 26 **1974**.
25. F. Li, R.C. Larock, *Biomacromolecules* **2003**, *4*, 1018–1025. <https://doi.org/10.1021/bm034049j>
26. L. F. Trueb, *Pflanzliche Naturstoffe*, Borntraeger Verlagsbuchhandlung, Stuttgart, **2015**.
27. J. Mallegol, J. Lemaire, J. Gardette, *Journal of the American Oil Chemists Society* **1999**, *76*, 967–976. <https://doi.org/10.1007/s11746-999-0114-3>
28. J.-Y. Park, D.-K. Kim, Z.-M. Wang, P. Lu, S.-C. Park, J.-S. Lee, *Appl. Biochem. Biotechnol.* **2008**, *148*, 109–117. <https://doi.org/10.1007/s12010-007-8082-2>
29. C. Boelhouwer, J. T. Knegetel, M. Tels, *Fette, Seifen, Anstrichmittel* **1967**, *69*, 432–436. <https://doi.org/10.1002/lipi.19670690611>
30. J. Mallegol, J. Lemaire, J.-L. Gardette, *Progr. Org. Coat.* **2000**, *39*, 107–113. [https://doi.org/10.1016/S0300-9440\(00\)00126-0](https://doi.org/10.1016/S0300-9440(00)00126-0)
31. D. Roy, M. Semsarila, T. Guthrie, S. Perrier, *Chem. Soc. Rev.* **2009**, *38*, 2046–2064. <https://doi.org/10.1039/b808639g>
32. B. N. Misra, R. Dogra, I. Kaur, J. K. Jassel, *J. Polym. Sci.* **1979**, *17*, 1861–1863.
33. M. I. H. Mondal, Y. Uraki, M. Ubukata, K. Itoyama, *Cellulose* **2008**, *15*, 581–592. <https://doi.org/10.1007/s10570-008-9210-z>
34. A. Sand, M. Yadav, K. Behari, *Carbohydrate Polymers* **2010**, *81*, 97–103. <https://doi.org/10.1016/j.carbpol.2010.02.001>
35. V. K. Thakur, A.S. Singha, B. N. Misra, *J. Appl. Polym. Sci.* **2011**, *122*, 532–544. <https://doi.org/10.1002/app.34094>

36. V. K. Thakur, M. K. Thakur, R. K. Gupta, *Carbohydrate Polymers* **2013**, 98, 820–828.  
<https://doi.org/10.1016/j.carbpol.2013.06.072>
37. R.-D. Reumann, *Prüfverfahren in der Textil- und Bekleidungsindustrie*, Springer-Verlag, Berlin, **2000**.  
<https://doi.org/10.1007/978-3-642-57073-5>
38. B. Mahltig, H. Böttcher, *J. Sol-Gel Sci. Technol.* **2003**, 27, 43–52. <https://doi.org/10.1023/A:1022627926243>
39. B. Mahltig, T. Textor, *Nanosols and Textiles*, World Scientific, Singapore, **2008**. <https://doi.org/10.1142/6961>
40. B. Tomsic, B. Simoncic, B. Orel, L. Cerne, P.F. Tavcer, M. Zorko, I. Jerman, A. Vilcnik, J. Kovac, *J. Sol-Gel Sci. Technol.* **2008**, 47, 44–57.  
<https://doi.org/10.1007/s10971-008-1732-1>
41. G. Y. Bae, Y. G. Jeong, B. G. Min, *Fibers and Polymers*, **2010**, 11, 976–981.  
<https://doi.org/10.1007/s12221-010-0976-x>
42. V. Castelvetro, G. Francini, G. Ciardelli, M. Ceccato, *Textile Res. J.* **2001**, 71, 399–406.  
<https://doi.org/10.1177/004051750107100506>
43. D. Hegemann, A. Fischer, *Vakuum in Forschung und Praxis*, **2004**, 16, 240–244.  
<https://doi.org/10.1002/vipr.200400231>
44. S. H. Kim, J.-H. Kim, B.-K. Kang, H. S. Uhm, *Langmuir*, **2005**, 21, 12213–12217.  
<https://doi.org/10.1021/la0521948>
45. J. Zimmermann, F.A. Reifler, G. Fortunato, L.-C. Gerhardt, S. Seeger, *Adv. Functional Mater.* **2008**, 18, 3662–3669.  
<https://doi.org/10.1002/adfm.200800755>
46. W. A. Daoud, J.H. Xin, X. Tao, *J. Am. Ceram. Soc.* **2004**, 87, 1782–1784.  
<https://doi.org/10.1111/j.1551-2916.2004.01782.x>
47. H. Wang, J. Ding, Y. Xue, X. Wang, T. Lina, *J. Mater. Res.* **2010**, 25, 1336–1343.  
<https://doi.org/10.1557/JMR.2010.0169>

## Povzetek

Razvili smo postopek za hidrofobno funkcionalizacijo vlaken naravnih materialov, ki temelji na uporabi naravnih produktov. Za hidrofobno komponento smo uporabili tungovo olje, ki se sicer uporablja za zaščito lesa. Tungovo olje smo na tekstil nanašali v prisotnosti oksidanta. V raziskavi smo uporabili lanena vlakna. Hidrofobni učinek določa koncentracija tungovega olja in čas procesa tremičnega sušenja. Hidrofobnost smo preučevali s testom kapilarnega dviga in meritvami stičnega kota. Za preučevanje topografije površine vlaken in nanešenega hidrofobnega materiala smo uporabili vrstično elektronsko mikroskopijo (SEM). Razvili smo zanimivo in obetajočo metodo za hidrofobno funkcionalizacijo naravnih vlaken, ki jo lahko uporabimo že v procesu priprave vlaken in temelji na uporabi naravnih produktov.

Scientific paper

# Influence of Various Soluble Carbonates on the Hydration of Portland Cement studied by X-ray Diffraction

Simona Medvešček,<sup>1</sup> Venčeslav Kaučič<sup>2</sup> and Anton Meden<sup>1,\*</sup><sup>1</sup> Faculty of Chemistry and Chemical Technology, University of Ljubljana, Aškerčeva 5, SI-1000 Ljubljana, Slovenia<sup>2</sup> Laboratory for Inorganic Chemistry and Technology, National Institute of Chemistry, Hajdrihova 19, SI-1001 Ljubljana, Slovenia

\* Corresponding author: E-mail: simona.medvescek@fkt.uni-lj.si

Received: 02-02-2017

## Abstract

The effect of limestone on the hydration of Portland cement has been studied by many researchers. However, a possible influence of adding more soluble carbonates was not explained. Therefore we executed a qualitative and quantitative research on the influence of slightly soluble ( $\text{CaCO}_3$ ,  $\text{MgCO}_3$ , dolomite), medium soluble ( $\text{Li}_2\text{CO}_3$ ) and highly soluble ( $\text{K}_2\text{CO}_3$  and  $\text{KHCO}_3$ ) carbonates on the hydration.

Blending of Portland cement with differently soluble carbonates was found to influence the hydrate assemblage of the hydrated cement. With the help of the Rietveld analysis, the study indicated that the amount of reacted carbonate in cement hydration at a 15% addition of slightly or medium soluble carbonates does not exceed 5% and is not affected by their solubility; at a 15% addition of the highly soluble carbonate  $\text{K}_2\text{CO}_3$  the amount of reacted carbonate was around 6%.

An increase in temperature (25 to 40 °C) gradually affects the rate of hydration and the quantity of stable phase assemblage.

**Keywords:** Portland cement; Hydration; Carbonates; Solubility; Rietveld method; Quantitative phase analysis

## 1. Introduction

Over the last 20 years, the effects of using limestone in Portland cement (PC) have been well studied. The benefits of limestone as a partial replacement for PC are well established. Its economic and environmental advantages of reducing  $\text{CO}_2$  emissions are well known.

However, throughout the years, the general provisions which determine the amount of limestone permitted in cement, have remained unchanged. Most Portland cement specifications allow the use of limestone up to 5%. Beyond that, Portland limestone cements (PLC) are categorized on the basis of the percentage of limestone (6–35%) added to the cement. The European Standard (EN 197-1-2000) permits up to 5% limestone regarding it as a minor additional constituent. It also identifies four types of PLC containing 6–20% limestone (types II/A-L and II/A-LL) and 21–35% limestone (types II/B-L and II/B-LL), respectively.<sup>1</sup>

For a long time, the limestone has been considered as an inert filler. Recently it has been concluded that lime-

stone serves both as an inert filler and also reacts to a limited extent. The reactivity depends on its fineness (specific surface)<sup>2</sup> and content.<sup>3,4</sup>

Matschei et al found that at a low concentration, limestone (a molar ratio of  $\text{CO}_2/\text{Al}_2\text{O}_3 \sim 0.66$  with a fixed sulfate ratio  $\text{SO}_3/\text{Al}_2\text{O}_3 = 1$  and an excess of portlandite,  $T = 25$  °C) reacts completely to various forms of carboaluminate phases. The extension of limestone's reactivity is controlled by the amount of sulphate in the system. As the sulphate content increases, the likelihood of unreacted calcite increases.

It is agreed that limestone reacts primarily with the tricalcium aluminate ( $\text{C}_3\text{A}$ ) to form carboaluminates (hemicarboaluminate,  $\text{C}_4\text{A}\bar{\text{C}}_{0.5}\text{H}_{12}$  and monocarboaluminate,  $\text{C}_4\text{A}\bar{\text{C}}\text{H}_{11}$  are the most common) at the expense of hydrates.<sup>5,6</sup> On the other hand, the formation of ettringite ( $\text{C}_6\text{A}_3\bar{\text{S}}\text{H}_{32}$ ) in PLC, the hydration reaction of  $\text{C}_3\text{A}$  in the presence of gypsum, is still questionable. Some researchers found its formation delayed, while others found that ettringite (AFt) formation proceeded normally.<sup>5</sup>

Ramachandran and Zhang, for example, found that the formation of AFt accelerates.<sup>7,8</sup> The AFt conversion to monosulfate (Ms) will be delayed or stopped when a large amount of carbonate is present in the hydrated paste. This phenomenon occurs due to the fact that some sulfate ions can be interchanged by carbonate ions during the C<sub>3</sub>A hydration.<sup>9,10</sup> Thermodynamic calculations as well as experimental observations also indicate that in the presence of CaCO<sub>3</sub>, monocarboaluminate (Mc) and not Ms is stable. And even more, the stabilization of Mc in the presence of limestone caused AFt to stabilize.<sup>11</sup> In PLC, there is also an interaction between tricalcium silicate (C<sub>3</sub>S) and calcium carbonate (CaCO<sub>3</sub>); the latter accelerates the hydration of C<sub>3</sub>S and modifies the Ca/Si ratio of calcium silicate hydrate gel (C–S–H).<sup>12</sup>

It is worth noting that limestone does not show pozzolanic properties and, consequently, does not produce C–S–H.<sup>13</sup> It has been suggested that when large quantities of carbonate are present, some CaCO<sub>3</sub> can be incorporated into C–S–H to form calcium silicocarbonate hydrates.<sup>5,14</sup> The production of portlandite (CH) seems to be enhanced at early ages partly due to dissolution of limestone and also due to limestone's ability to act as nucleation sites.<sup>5</sup>

The important stable phases in hydrated calcite-containing cement are AFt, Mc and calcite.<sup>3</sup> They are calculated to be stable and present in comparable amounts in the temperature range of 25–40 °C.<sup>15,16</sup>

The Rietveld Method enables us to determine the amount of anhydrous and hydrous phases in PC to a high degree of precision.<sup>17</sup> This method employs a point-to-point adjustment of experimental intensities of the whole pattern to the calculated intensities based on the crystal structures (space groups, types of atoms, their coordinates in the unit cell and site occupancies) present in the mixture and it also provides the weight fractions for each crystalline phase.<sup>18,19</sup>

This paper examines the influence of differently soluble carbonates on the hydration of PC in the temperature range of 25–40 °C. The quantitative data obtained by using X-ray diffraction to study the hydration products of Portland cement upon addition of slightly soluble (CaCO<sub>3</sub>, MgCO<sub>3</sub>, dolomite), medium soluble (Li<sub>2</sub>CO<sub>3</sub>) and highly soluble (K<sub>2</sub>CO<sub>3</sub> and KHCO<sub>3</sub>) carbonates, are compared to similar data from a control sample, based on the same Portland cement paste.

## 2. The Experimental

### 2.1. Materials

Ordinary Portland cement, CEM I 52.2 R (Salonit Anhovo, Building Materials, Joint-Stock Co., Anhovo, Slovenia) was used. The cement consisted of clinker and chemically precipitated gypsum, both ground in the laboratory mill. Chemical and mineralogical compositions of cement are shown in Table 1.

**Table 1.** Chemical and mineralogical analysis of CEM I 52.2 R.

Chemical analysis		Mineralogical analysis	
Measured (wt%) <sup>†</sup>		Calculated (wt%) <sup>‡</sup>	
CaO	63.3		
SiO <sub>2</sub>	20.6	C <sub>3</sub> S	54.9
Al <sub>2</sub> O <sub>3</sub>	4.71	C <sub>2</sub> S	17.7
Fe <sub>2</sub> O <sub>3</sub>	3.50	C <sub>3</sub> A	6.6
SO <sub>3</sub>	3.37	C <sub>4</sub> AF	10.7
MgO	1.12		
K <sub>2</sub> O	0.87		
Na <sub>2</sub> O	0.21		
LOI	1.90		
Insoluble	0.37		

<sup>†</sup> By XRF. <sup>‡</sup>By Bogue equations.

\* Standard cement chemistry notation: S = SiO<sub>2</sub>, C = CaO,

A = Al<sub>2</sub>O<sub>3</sub>, F = Fe<sub>2</sub>O<sub>3</sub>.

Compressive strength: 36 MPa (2 days), 56.5 MPa (28 days).

The following carbonates were used:

- Calcium carbonate, CaCO<sub>3</sub>, laboratory reagent, precipitated, 99.1%, Kemika, Zagreb, Croatia. Specific surface area of 0.7 m<sup>2</sup>/g (micropore area: –), named C $\bar{C}$  hereafter.
- Natural, ground calcite, CaCO<sub>3</sub>, 99.6%, Magnesia 448, Magnesia GmbH, Lüneburg, Germany. Specific surface area of 2.1 m<sup>2</sup>/g (micropore area: 0.3 m<sup>2</sup>/g), named as calcite hereafter.
- Natural, ground magnesite, MgCO<sub>3</sub>, 98.1%, Magnesia 318, Magnesia GmbH, Lüneburg, Germany. Specific surface area of 4.6 m<sup>2</sup>/g (micropore area: 1.0 m<sup>2</sup>/g).
- Natural, ground dolomite, CaMg(CO<sub>3</sub>)<sub>2</sub>, 99.5%, Magnesia 4179, Magnesia GmbH, Lüneburg, Germany. Specific surface area of 1.7 m<sup>2</sup>/g (micropore area: 0.2 m<sup>2</sup>/g).
- Lithium carbonate (Li<sub>2</sub>CO<sub>3</sub>), potassium carbonate (K<sub>2</sub>CO<sub>3</sub>) and potassium hydrogen carbonate (KHCO<sub>3</sub>) were laboratory reagents of p. a. quality.

### 2.2. Sample Preparation

All the starting mixtures (10.00 g) contained 85 wt% of Portland cement and 15 wt% of carbonate to facilitate comparison (the amount of hydrating Portland cement was constant). Portland cement and the added carbonate were homogenized, and deionized water (w/s ratio of 0.5) was added. Suspensions were being homogenized with the VibraCell ultrasonic probe (Sonics & Materials, Inc., USA) for 30 seconds, placed in alkali-resistant flasks, capped airtight and hydrated at 25 °C or 40 °C for 3, 7, 28 and 90 days. For reference, Portland cement hydrated under the same conditions.

### 2.3. Characterization Techniques

X-ray powder diffraction data were collected on a PANalytical X'Pert PRO MPD diffractometer (PANalytical B.V., Almelo, the Netherlands) in CuK $\alpha$ <sub>1</sub> configuration from 3 to 70 2 $\theta$  in steps of 0.033 2 $\theta$ . Full

range of a linear PSD, having 128 channels, was used and the total counting time was 200 s per step (53 minutes of data collection per sample).

Identification of the phases, present in the samples, was performed by analyzing the patterns with X'Pert HighScore Plus Ver. 2.1.2 software and Crystallographica Search Match Ver. 3.0.0.5 with a database PDF-2, Release 2011 RDB (International Centre for Diffraction, Oxford Cryosystems).

The quantitative phase analyses of the phases with known structures were performed using the Rietveld method by using Topas Ver. 2.1 program (Bruker AXS, Karlsruhe, Germany). The method of internal standard addition was used to determine the absolute content of identified crystalline phases of the hydrated samples. For this purpose, 40% of  $\alpha$ - $\text{Al}_2\text{O}_3$ , MicroPolish II, 1- $\mu\text{m}$  deagglomerated alumina (Buehler Ltd., Lake Bluff, IL) was added to hydrated samples and thoroughly mixed in an agate mortar.

After the specified hydration time, samples were powdered in an agate mortar and analyzed. The XRD phase analyses of the data considered three replications of each treatment, adding up to 384 samples.

### 3. Results

#### 3. 1. Portland Cement (PC)

The following crystalline or partly crystalline phases were identified in the clear Portland cement and were included into the model for Rietveld refinement: CH (ICSD code 34241), Aft (ICSD code 16045), Mc (ICSD code 59327), partly crystalline C–S–H (ICSD code 87689),  $\text{CaCO}_3$  (CC) (ICSD code 73446), after 28 days of hydration also in vaterite modification (ICSD code 15879), calcium aluminium hydrate  $\text{C}_3\text{AH}_6$  (ICSD code 202316), unreacted clinker phases  $\text{C}_3\text{S}$  (ICSD code

81100),  $\text{C}_2\text{S}$  (ICSD code 39006),  $\text{C}_3\text{A}$  (ICSD code 6287),  $\text{C}_4\text{AF}$  (ICSD code 9197), and substances in traces (below 2%):  $\text{SiO}_2$  (S) (ICSD code 67117), gismondine  $\text{CAS}_2\text{H}_4$  (ICSD code 15838) and carbo-silicate tilleyite  $\text{C}_3\text{S}_2(\text{CC})_2$  (ICSD code 14256).

In Figure 1 a representative Rietveld plot is presented.

At a certain temperature (25 or 40 °C) and after the hydration process is finished (3, 7, 28, 90 days), parts of each individual phase are visible – presented in Figure 2. Each value of a given phase content presents an average of 3 measurements taken. There is also a minimum and a maximum value, so one can picture the discrepancy between the three values included in the calculated average.

In the PC samples most of CH (12–14%) is produced. Its amount is decreased after 90 days of the hydration process, which means that the hydration process is finished. This is also confirmed by the amount of crystalline C–S–H, which does not significantly change after 90 days of hydration and the minimal presence (2% and less) of  $\text{C}_3\text{S}$  and  $\text{C}_2\text{S}$ .

After 90 days, even Aft is no longer being produced; its amount is app. 3.7% at both temperatures. (Less Aft occurs at 40 °C after any days of hydration.) The occurrence of Ms is obviously hampered in the starting stages of hydration, as the amounts of Mc (app. 4 %) and  $\text{CaCO}_3$  (app. 1%) are too high and there is not enough  $\text{Al}_2\text{O}_3$ . The amount of  $\text{C}_3\text{A}$  is minimal after only 3 days of hydration (app. 0.15%), and after 28 days the substance is no longer present. Aft is stabilized in the presence of Mc and CC.

Hemicarboaluminate (Hc) was not identified even after the 3-day hydration, in spite of the fact that the samples were kept in airtight containers and were not dried with solvents, e.g. acetone or diethyl ether.<sup>6</sup> The reason might be the air carbonization, which can occur in the airtight containers. We presume that all of the Hc converted into the more stable Mc in the 3-day hydration. The in-

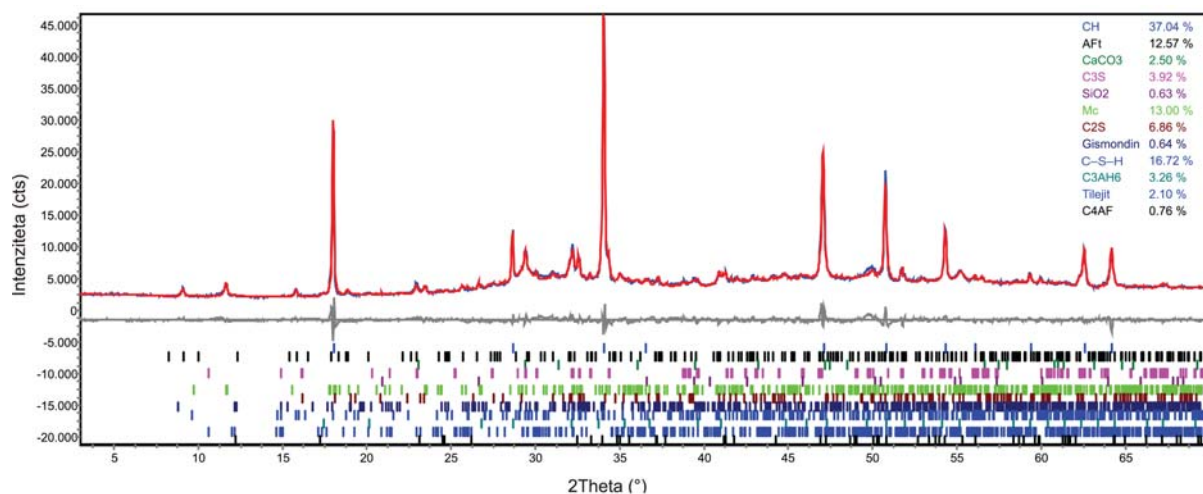


**Figure 1.** The Rietveld plot of PC, hydrated 90 days. Blue is the measured pattern, red is calculated and grey in the middle is the difference. The vertical bars below denote reflection positions of the included phases.

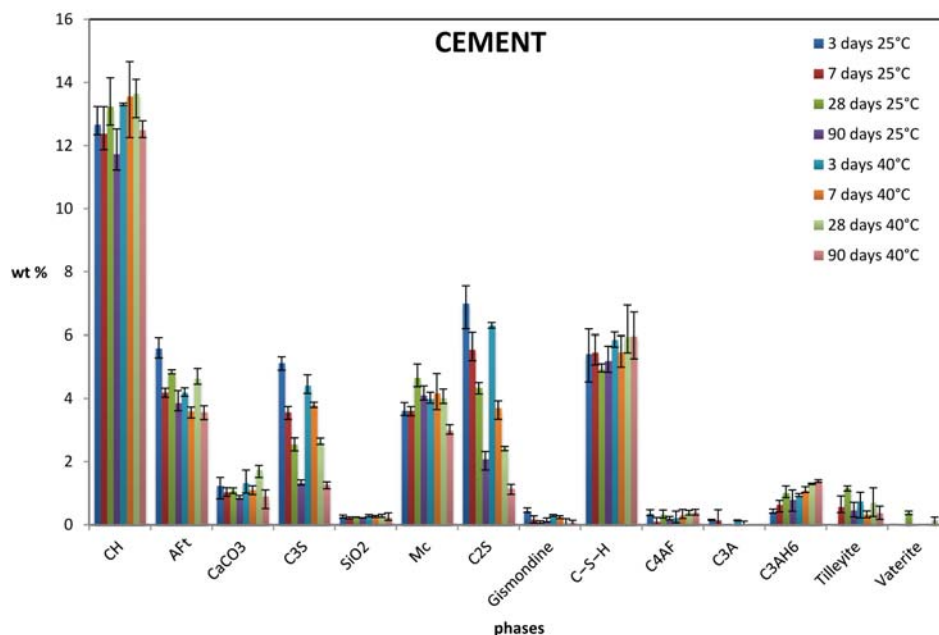


**Figure 2.** The quantitative analysis of cement hydration at 3, 7, 28 and 90 days of hydration and temperatures of 25 and 40 °C.

creased temperature (from 25 to 40 °C) does not influence hydration significantly – it accelerates it a bit. This can be seen in the results of the comparison of the unreacted phases of the cement clinker ( $C_3S$ ,  $C_2S$ ,  $C_3A$ ) after a certain number of hydration days and the increased amount of CH.

The crystallinity (mass fraction of all crystalline phases in a sample) of PC samples is app. 42% after 3 days of hydration and is decreased to app. 31% after 90 days of hydration at both temperatures. The exact values are shown in Table 2.

### 3. 2. Slightly soluble carbonates

#### 3. 2. 1. $CaCO_3$ , Synthetic and Natural (Solubility at 25 °C is $6.6 \cdot 10^{-3}g/100g$ Water<sup>22</sup>)

Natural  $CaCO_3$  (calcite) consists of much smaller particles than synthetic  $CaCO_3$  ( $CC\bar{}$ ), 14% of the specific surface of calcite consists of micro pores. Calcite has a higher kinetic reactivity and so a faster hydration is expected compared to  $CC\bar{}$ . In truth, the hydration of the  $C_3S$  is increased a bit in samples with calcite compared to those with  $CC\bar{}$  at any days of hydration at 25 °C and after the first three days of the hydration at 40 °C, while the reactivity of the calcite particles does not affect the hydration of  $C_2S$ , and after 90 days of hydration there was even more unreacted  $C_2S$  in the calcite samples at both temperatures. The amount of unreacted  $C_4AF$  is small in calcite-added samples and comparable to those with  $CC\bar{}$ . It is interesting, that despite the higher reactivity of calcite, after 90 days of hydration of calcite-added samples, there is more unreacted  $CaCO_3$  left, compared to samples with  $CC\bar{}$  at both temperatures. (Samples with  $CC\bar{}$ : 10.1% at 25 °C, 10.9% at 40 °C; Samples with calcite: 11. 6% at 25 °C,

**Table 2.** The crystallinity of samples in dependence on the level of hydration and the temperature.

sample	days of hydration	25 °C %	40 °C %
PC	3	42	42
	7	38	38
	28	42	38
	90	31	31
$CC\bar{}$	3	44	47
	7	43	44
	28	49	41
	90	41	39
Calcite	3	43	43
	7	44	43
	28	45	42
	90	43	41
$MgCO_3$	3	48	49
	7	45	43
	28	50	45
	90	40	41
Dolomite	3	52	49
	7	47	50
	28	46	48
	90	43	43
$Li_2CO_3$	3	53	52
	7	54	51
	28	53	48
	90	49	49
$KHCO_3$	3	50	50
	7	49	47
	28	49	48
	90	44	44
$K_2CO_3$	3	45	50
	7	47	46
	28	48	47
	90	45	45

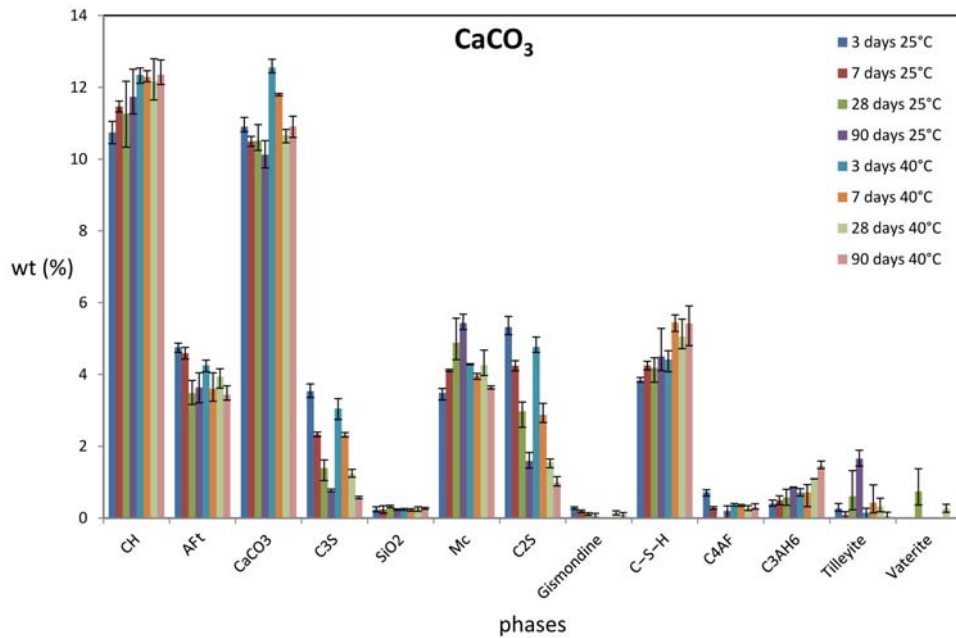


**Figure 3.** The quantitative analysis of hydration products in cement with added  $\text{CaCO}_3$  at 3, 7, 28 and 90 days of hydration and two temperatures, 25 and 40 °C.

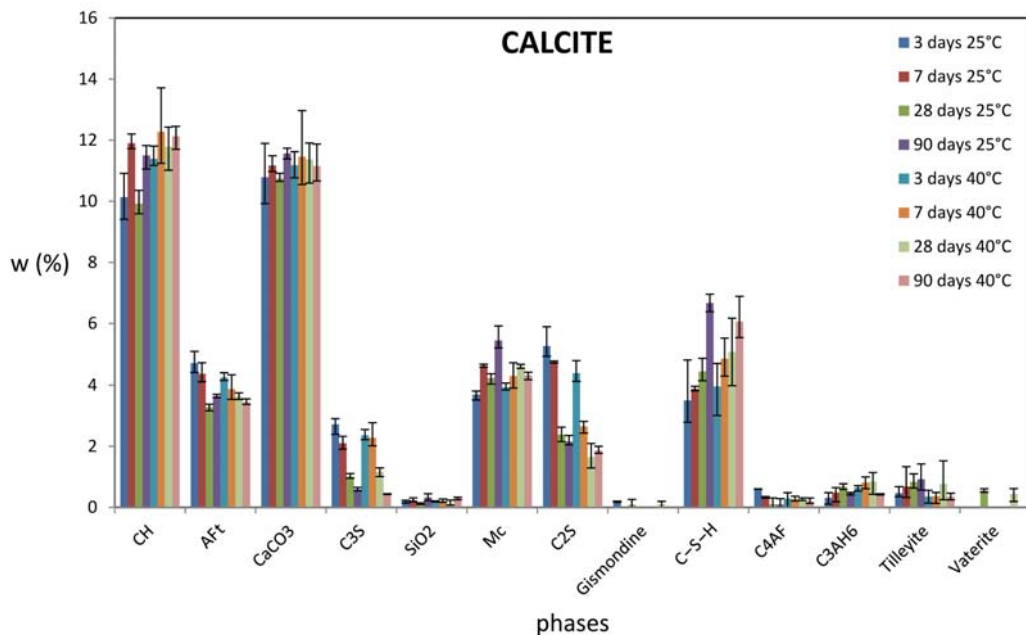


**Figure 4.** The quantitative analysis of hydration products in cement with added calcite at 3, 7, 28 and 90 days of hydration and two temperatures, 25 and 40 °C.

11.2% at 40 °C). The amount of the reacted  $\text{CaCO}_3$  is around 4%, while the rest serves as a filling. This value of the reactive carbonate matches with articles published in the past (up to 5%), or even a bit higher than suggested by T. Matschei and coworkers (approximately 2.9%) regarding the amount of  $\text{Al}_2\text{O}_3$  and relation to  $\text{SO}_3/\text{Al}_2\text{O}_3$  in PC.<sup>3</sup> The amount of AFt after 90 days of hydration in samples with calcite and  $\text{CaCO}_3$  is comparable. In fact, we got the same results: 3.6% at 25 °C, 3.4% at 40 °C. Something similar is true for Mc – samples with  $\text{CaCO}_3$ : 5.4% at 25 °C,

3.6% at 40 °C; samples with calcite: 5.5% at 25 °C, 4.3% at 40 °C. There are no considerable differences between  $\text{CaCO}_3$  – and calcite-added samples regarding the amounts of other hydration products, which is clearly seen by comparing Figures 3 and 4.

The increased temperature (from 25 to 40 °C) does not considerably affect hydration. It is just a bit accelerated, which is indicated by the comparison of the reactivity of the cement clinker phases ( $\text{C}_3\text{S}$ ,  $\text{C}_2\text{S}$ ) and thus the formation of an increased amount of CH and C–S–H. The

formation of AFt at 40 °C in the early stages of hydration is possibly somewhat hindered, the AFt contents after 90 days of hydration are comparable at both temperatures. The amount of Mc after 90 days is higher at 25 °C than at 40 °C in both samples, with added calcite or  $\text{CC}^-$ .

A 15% addition of carbonate dilutes the cement in the first stages of hydration, which can be seen on the smaller amount of CH formed in calcite- and  $\text{CC}^-$ -added samples. After 90 days the CH contents are comparable. The hydration of the clinker phases ( $\text{C}_3\text{S}$ ,  $\text{C}_2\text{S}$ ,  $\text{C}_3\text{A}$ ) is accelerated in samples with added carbonate. The amount of Mc after 90 days is higher in samples with added carbonate. The amount of AFt formed after 90 days of hydration is comparable to that in the samples without added carbonate. After 3 days of hydration at 25 °C less AFt is formed in samples with added carbonate, whereas at 40 °C there is no difference. After 7 days of hydration the contents of AFt in all samples (with or without the addition of carbonate) and both temperatures are comparable.

It would be difficult to conclude that the addition of carbonate has any significant influence on the formation of AFt (either impeding the formation or accelerating it).<sup>4</sup>

For a clearer demonstration and possible comparison all contents of the main hydration products (CH, AFt, Mc and  $\text{CaCO}_3$ ) are collected in Table 3 in relation to hydration time (3, 7, 28, 90 days) and temperature (25 and 40 °C). The minimum and maximum determined contents of the main hydration products are collected below, in Table 4 and Table 5.

C–S–H can include  $\text{CO}_3^{2-}$  anions in its structure, and consequently calcium silicocarbonate hydrates can be formed. We have not identified any with an XRD analysis, but we assume their formation. If the hydration of clinker phases in samples with added calcite or  $\text{CC}^-$  is accelerated, slightly more SCH should form in these samples than in clear PC samples. Actually we have identified less C–S–H during the hydration in samples with calcite compared to PC samples probably just due to formation of calcium silic-

**Table 3.** The average compositions of hydration products in relation to hydration time and temperature.

temperature sample	days of hydration	25 °C 40 °C		25 °C 40 °C		25 °C 40 °C		25 °C 40 °C	
		CH (wt%)		E (wt%)		$\text{CaCO}_3$ (wt%)		Mc (wt%)	
PC	3	12.7	13.3	5.6	4.2	1.3	1.3	3.6	4.0
	7	12.4	13.6	4.2	3.6	1.0	1.1	3.6	4.2
	28	13.3	13.7	4.8	4.7	1.1	1.8	4.7	4.0
	90	11.7	12.5	3.9	3.6	0.9	0.9	4.1	3.0
$\text{CC}^-$	3	10.7	12.4	4.8	4.3	10.9	12.6	3.5	4.3
	7	11.5	12.3	4.6	3.6	10.5	11.8	4.1	4.0
	28	11.3	12.2	3.5	3.9	10.5	10.7	4.9	4.3
	90	11.7	12.4	3.6	3.4	10.1	10.9	5.4	3.6
calcite	3	10.1	11.4	4.7	4.3	10.8	11.2	3.70	3.9
	7	11.9	12.3	4.4	3.8	11.2	11.5	4.64	4.3
	28	9.9	11.8	3.3	3.6	10.7	11.4	4.23	4.6
	90	11.5	12.1	3.6	3.4	11.6	11.2	5.47	4.3
$\text{MgCO}_3$	3	10.3	10.3	5.2	5.1	1.8	2.4	3.8	4.6
	7	10.5	9.5	4.6	4.1	2.0	2.4	4.3	4.3
	28	9.0	10.0	3.3	4.7	4.9	5.0	4.2	4.8
	90	9.0	8.8	3.5	4.5	4.6	9.6	4.6	3.7
dolomite	3	11.2	11.6	5.1	4.0	1.8	1.9	3.6	4.0
	7	11.1	12.7	4.6	3.9	1.6	1.9	4.1	4.7
	28	10.2	12.3	3.1	4.3	1.6	2.6	4.3	5.3
	90	11.6	12.2	3.6	3.9	1.7	2.5	5.4	4.6
$\text{Li}_2\text{CO}_3$	3	8.4	9.5	0.8	–	4.3	4.8	5.4	5.2
	7	10.2	10.1	0.7	–	4.5	5.3	5.6	5.6
	28	9.2	10.5	–	–	6.3	5.4	4.5	5.0
	90	11.6	12.0	–	–	4.8	5.5	5.4	4.6
$\text{KHCO}_3$	3	6.0	7.0	–	–	9.7	10.8	8.0	6.8
	7	7.5	8.5	–	–	10.1	10.5	6.7	4.9
	28	9.4	11.4	–	–	10.6	11.6	5.4	5.6
	90	10.4	11.3	–	–	10.9	12.6	6.5	5.6
$\text{K}_2\text{CO}_3$	3	9.5	11.5	–	–	4.7	6.2	5.3	5.0
	7	11.0	12.4	–	–	5.1	5.5	3.6	5.0
	28	9.0	14.1	–	–	9.1	5.8	2.7	4.3
	90	13.8	15.1	–	–	5.6	5.8	4.6	3.9



Table 4. The minimum and maximum contents of hydration products in relation to hydration time and 25 °C.

sample	days of hydration content/ 25 °C	CH (wt%)		E (wt%)		CaCO <sub>3</sub> (wt%)		Mc (wt%)	
		minimum	maximum	minimum	maximum	minimum	maximum	minimum	maximum
PC	3	12.34	13.23	5.29	5.93	0.82	1.50	3.47	3.87
	7	11.87	13.23	4.04	4.33	0.90	1.17	3.46	3.74
	28	12.65	14.15	4.78	4.91	0.99	1.17	4.37	5.09
	90	11.22	12.53	3.61	4.25	0.82	0.93	3.95	4.40
CC	3	10.43	11.05	4.61	4.87	10.76	11.16	3.29	3.61
	7	11.31	11.62	4.43	4.75	10.35	10.63	4.08	4.14
	28	10.33	12.17	3.17	3.83	10.24	10.96	4.41	5.57
	90	11.26	12.51	3.21	4.05	9.76	10.52	5.25	5.68
calcite	3	9.41	10.91	4.42	5.11	9.92	11.90	3.51	3.80
	7	11.72	12.20	4.11	4.73	10.98	11.49	4.59	4.68
	28	9.59	10.36	3.16	3.38	10.65	10.92	4.04	4.38
	90	11.05	11.83	3.59	3.70	11.38	11.74	5.22	5.92
MgCO <sub>3</sub>	3	9.23	11.24	4.85	5.49	1.38	2.07	3.51	4.07
	7	10.26	10.80	4.29	4.99	1.89	2.25	4.20	4.50
	28	8.46	9.45	2.80	3.63	4.67	5.16	3.99	4.42
	90	8.75	9.29	3.11	3.65	4.28	4.90	4.42	4.87
dolomite	3	10.79	11.36	4.93	5.50	1.40	2.37	3.42	3.79
	7	10.75	11.56	4.29	5.00	1.49	1.67	3.94	4.29
	28	10.00	10.40	2.83	3.32	1.61	1.67	4.20	4.33
	90	10.94	11.90	3.38	3.83	1.39	1.83	5.17	5.51
Li <sub>2</sub> CO <sub>3</sub>	3	8.04	8.70	0.66	1.12	4.14	4.61	5.08	5.83
	7	10.05	10.49	0.38	0.97	4.13	4.83	5.44	5.87
	28	8.82	9.56	–	–	6.06	6.59	4.30	4.68
	90	11.38	12.03	–	–	4.39	5.02	5.28	5.46
KHCO <sub>3</sub>	3	5.58	6.33	–	–	9.49	10.14	7.28	8.76
	7	7.23	7.70	–	–	9.17	10.61	6.40	6.90
	28	9.31	9.40	–	–	9.69	10.63	5.37	5.51
	90	10.29	10.61	–	–	10.11	11.99	5.63	7.37
K <sub>2</sub> CO <sub>3</sub>	3	9.34	9.70	–	–	4.42	5.02	5.14	5.52
	7	10.77	11.25	–	–	4.90	5.27	3.18	4.21
	28	8.42	9.82	–	–	6.49	11.54	2.48	2.86
	90	13.21	14.22	–	–	5.29	6.11	4.24	5.14

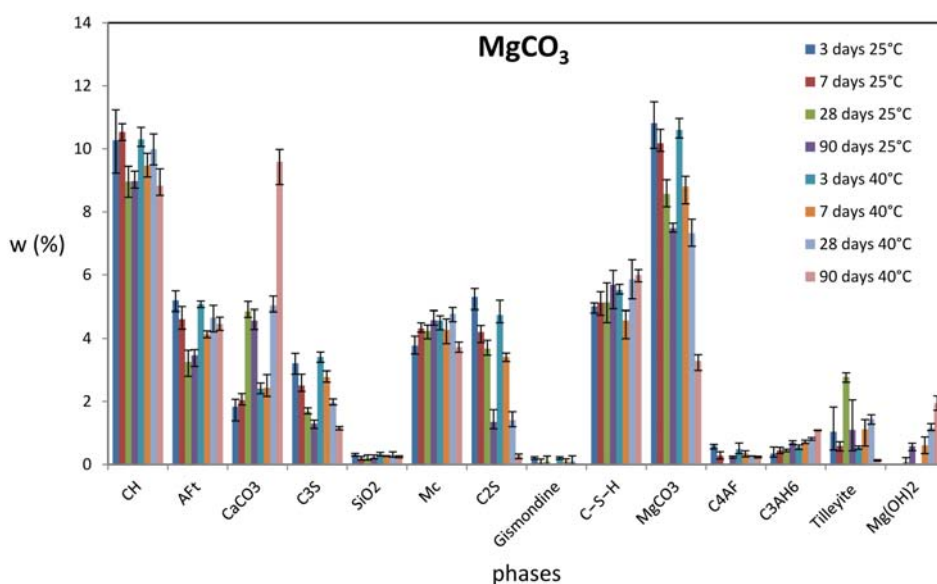
Figure 5. The quantitative determination of hydration products in cements with added MgCO<sub>3</sub> at 3, 7, 28 and 90 days of hydration and two temperatures, 25 and 40 °C.

Table 5. The minimum and maximum contents of hydration products in relation to hydration time and 40 °C.

sample	days of hydration content/ 40 °C	CH (wt%)		E (wt%)		CaCO <sub>3</sub> (wt%)		Mc (wt%)	
		minimum	maximum	minimum	maximum	minimum	maximum	minimum	maximum
PC	3	13.27	13.35	4.07	4.34	1.00	1.73	3.85	4.20
	7	12.25	14.66	3.38	3.73	0.96	1.23	3.65	4.79
	28	12.88	14.10	4.45	4.95	1.50	1.88	3.84	4.30
	90	12.25	12.79	3.33	3.77	0.51	1.10	2.87	3.17
CC	3	12.11	12.54	4.07	4.40	12.41	12.78	4.27	4.30
	7	12.15	12.46	3.26	4.05	11.77	11.83	3.86	4.03
	28	11.65	12.80	3.62	4.16	10.46	10.83	3.97	4.68
	90	12.08	12.76	3.29	3.69	10.60	11.20	3.60	3.68
calcite	3	11.17	11.81	4.15	4.41	10.76	11.62	3.84	4.07
	7	11.24	13.71	3.53	4.34	10.55	12.97	3.91	4.73
	28	11.02	12.43	3.53	3.75	10.60	11.91	4.55	4.68
	90	11.70	12.45	3.37	3.55	10.67	11.88	4.18	4.42
MgCO <sub>3</sub>	3	10.07	10.68	4.96	5.17	2.25	2.58	4.28	4.72
	7	9.11	9.86	4.02	4.24	2.16	2.85	3.84	4.62
	28	9.66	10.18	4.30	4.85	4.68	5.67	4.74	4.86
	90	8.52	9.37	4.26	4.67	8.87	9.98	3.56	3.88
dolomite	3	11.47	11.83	3.85	4.19	1.72	2.06	3.66	4.23
	7	12.33	13.12	3.81	3.98	1.81	1.97	4.47	4.80
	28	12.07	12.59	4.21	4.35	2.25	3.09	5.08	5.44
	90	11.72	12.42	3.73	4.02	1.82	3.09	4.16	4.86
Li <sub>2</sub> CO <sub>3</sub>	3	8.90	9.89	–	–	4.44	5.02	4.67	5.58
	7	9.59	10.59	–	–	4.97	5.69	5.28	5.77
	28	10.31	10.75	–	–	5.10	5.75	4.91	5.04
	90	11.57	12.77	–	–	5.33	5.79	4.32	5.07
KHCO <sub>3</sub>	3	6.60	7.29	–	–	10.53	11.06	6.64	6.88
	7	8.14	8.92	–	–	9.91	11.13	3.21	6.63
	28	10.91	11.63	–	–	11.43	11.94	5.55	5.66
	90	11.00	11.69	–	–	12.27	13.00	5.15	6.35
K <sub>2</sub> CO <sub>3</sub>	3	10.66	11.91	–	–	6.00	6.38	3.86	6.39
	7	11.96	12.65	–	–	5.11	5.94	4.62	5.34
	28	13.95	14.42	–	–	5.51	6.03	4.06	4.59
	90	14.64	15.56	–	–	5.62	5.99	3.53	4.52

ocarbonate hydrates. After 90 days of hydration the C–S–H contents in the samples with added calcite are comparable to those in the samples of clear PC, whereas the C–S–H contents in the samples with added CC were still lower compared to samples of clear PC, especially at 25 °C.

The crystallinity of samples with added carbonate does not depend on temperature, after 3 days of hydration it is around 44% and after 90 days of hydration it is around 41%. Exact values are collected in Table 2. After 3 days of hydration the crystallinity in samples with added carbonate and samples with PC is comparable, whereas after 90 days of hydration the crystallinity of samples with added carbonate is higher than that of PC samples (around 10%).

### 3. 2. 2. MgCO<sub>3</sub> (Solubility at 25 °C is 0.18g/100g Water<sup>20</sup>)

The hydration products in samples with added MgCO<sub>3</sub> are the same as the hydration products in PC sam-

ples, with the difference that due to the dissolution of MgCO<sub>3</sub> in the presence of CH, the additional formation of Mg(OH)<sub>2</sub> occurs after 28 days of hydration at 25 °C or after 7 days of hydration at 40 °C. (The reaction: MgCO<sub>3</sub> + Ca(OH)<sub>2</sub> → CaCO<sub>3</sub> + Mg(OH)<sub>2</sub>) After 28 days no vaterite forms at 25 °C as well as at 40 °C. Hydration products and their contents at 3, 7, 28 and 90 days of hydration and both temperatures are demonstrated in Figure 5.

Figure 5 and the above reaction clearly explain that the amount of reacted MgCO<sub>3</sub> increases with temperature (after 90 days of hydration: 25 °C 7.52%, 40 °C 11.71%). Consequently, at a higher temperature Mg(OH)<sub>2</sub> is formed earlier (after 7 days) and in larger amount (90 days hydration: 25 °C 0.58%, 40 °C 1.95%). The same holds for CaCO<sub>3</sub> and more CH is being used (see Table 3). The hydration of the clinker phases (C<sub>3</sub>S, C<sub>2</sub>S, C<sub>3</sub>A) is accelerated. The increased temperature (from 25 to 40 °C) accelerates the hydration of C<sub>2</sub>S after 3 days, whereas the amount of reacted C<sub>3</sub>S is larger after 90 days of hydration. In sam-

ples with added  $\text{MgCO}_3$  after 90 days of hydration  $\text{C}_3\text{S}$ : 25 °C 1.30%, 40 °C 1.17% and  $\text{C}_2\text{S}$ : 25 °C 1.35%, 40 °C 0.27% remains. Because CH is being used for the dissolution reaction, there is less of it in samples with added  $\text{MgCO}_3$  than in samples of clear PC (see Figure 3). More of it is used up during the hydration time at both temperatures (25 °C at 28 days, 40 °C at 7 days) for the dilution reaction than is formed during the hydration of calcium di-/tri-silicates. The formation of semi-crystalline C–S–H is unhindered by the addition of  $\text{MgCO}_3$  and is quantitatively comparable with clear PC samples at both temperatures and all hydration stages (after 90 days of hydration: samples with  $\text{MgCO}_3$  25 °C 5.68%, 40 °C 5.99%; PC samples 25 °C 5.19%, 40 °C 5.99%). We could not identify partial formation of calcium silicocarbonate hydrates, but predict them. After 90 days of hydration the AFt contents at both temperatures are comparable to both samples without and with added  $\text{MgCO}_3$  (see Figure 3). After 90 days of hydration there is a slightly higher amount of formed Mc at both temperatures in samples with added  $\text{MgCO}_3$  compared to samples of clear PC (Table 3). We can thus conclude that a 15% addition of  $\text{MgCO}_3$  at both temperatures does not significantly affect the formation of AFt and Mc, but it does accelerate the hydration of the clinker phases ( $\text{C}_3\text{S}$ ,  $\text{C}_2\text{S}$  in  $\text{C}_3\text{A}$ ). In samples with  $\text{MgCO}_3$  after 90 days of hydration there is a lot of slightly soluble calcium carbonate ( $\text{CaCO}_3 + \text{MgCO}_3$ ) present (25 °C 12.05%, 40 °C 12.88%), for which we gather that it is unreacted (that is, it serves as a filling) and together with Mc it only stabilizes the AFt. The amount of reacted calcium carbonate after 90 days of hydration is around 3.7%, which is even slightly less than in samples with added  $\text{CC}$  or calcite. For all samples with the addition of different soluble carbonates are considered that the part of reactive carbonate depends on the molecular weight of added carbonate so it can be calculated from the following equation:

$$W_{(\text{reactive carbonate})} = 15\% \text{ (or initial carbonate content added in the sample) -}$$

$$\left( \frac{M_{\text{added carbonate}}}{M_{\text{CaCO}_3}} \cdot W_{\text{CaCO}_3} + W_{\text{rest of added carbonate}} \right) \quad (1)$$

The added carbonate which is converted into inert  $\text{CaCO}_3$  is considered to be unreactive.

The  $\text{SiO}_2$ , gismondine,  $\text{C}_4\text{AF}$ ,  $\text{C}_3\text{AH}_6$  and tilleyite portion are small and comparable to samples of clear PC.

The crystallinity of samples with added  $\text{MgCO}_3$  does not depend on temperature and after 3 days of hydration it is approximately at 49% and after 90 days of hydration it is around 41%. The exact values are collected in Table 2. The crystallinity in the samples with added  $\text{MgCO}_3$  is always higher than in PC samples and after 90 days of hydration the values are around 10% higher than in samples of clear PC.

### 3. 2. 3. Dolomite

Hydration products in samples with added dolomite are the same as hydration products in PC samples, with the difference, due to the dilution of dolomite in water, that besides crystallizing  $\text{CaCO}_3$  on the surface of the dolomite grains  $\text{MgCO}_3$  crystallizes as well (after 3 and 7 days of hydration at both temperatures). We predict that a small quantity of  $\text{MgCO}_3$  then reacts with CH (as in the samples with  $\text{MgCO}_3$ ), although after 28 as well as 90 days of hydration via the Rietveld method we did not identify the formed  $\text{Mg}(\text{OH})_2$ , due to insufficient quantities. Moreover, we confirmed that there was no dedolomitisation reaction, no expansion reaction between the dolomite and the base (CH):  $\text{CaMg}(\text{CO}_3)_2 + \text{Ca}(\text{OH})_2 = \text{Mg}(\text{OH})_2 + 2\text{CaCO}_3$  even after 90 days of hydration at an increased temperature, 40 °C.<sup>21</sup> After 28 days vaterite is not formed both at 25 °C and 40 °C. Hydration products and their contents at 3, 7, 28, 90 days of hydration and both temperatures is clearly visible on Figure 6. Figure 6 clearly shows the amount of diluted dolomite, which after 90 days of hydration is around 5% (25 °C 4.74%, 40 °C 5.68%). Thus, after 90 days of hydration in samples with added dolomite there was a lot of unreacted carbonate present (unreacted dolomite +  $\text{CaCO}_3$ : 25 °C 11.93%; 40 °C 11.79%). We anticipate that it acts like a filling and at the same time, together with Mc, stabilizes AFt, the portions of which, in samples with or without the added slightly soluble carbonate, are comparable after 90 days of hydration at both temperatures and are around 3.5% (see Table 3). The amount of reacted carbonate after 90 days of hydration is thus around 1.4% at both temperatures, which is even lower comparable to samples with added  $\text{MgCO}_3$  or samples with added  $\text{CC}$ / calcite.

The amounts of formed Mc after 90 days of hydration in all samples with added slightly soluble carbonate are comparable (see Table 3). As with other samples with added slightly soluble carbonate the hydration of the clinker phases is accelerated ( $\text{C}_3\text{S}$ ,  $\text{C}_2\text{S}$ ,  $\text{C}_3\text{A}$ ) and after 90 days the amounts of unreacted di-/tri-silicates are small ( $\text{C}_3\text{S}$ : 25 °C 0.69%, 40 °C 0.66% and  $\text{C}_2\text{S}$ : 25 °C 2.05%, 40 °C 1.24%). The amount of the formed CH is around 12%, after 90 days of hydration, its contents are comparable to those in the samples with added calcium carbonate or  $\text{CC}$  (see Table 3), because CH is not being used up like in samples with added  $\text{MgCO}_3$ . Furthermore, in samples with added dolomite the formation of partly crystalline C–S–H is unhindered and is after 90 days of hydration at both temperatures quantitatively slightly higher than in samples of clear PC or other slightly soluble carbonates (25 °C 6.74%, 40 °C 7.16%). However we assume partial formation of calcium silicocarbonate hydrates but we could not identify them. The amount of  $\text{SiO}_2$ , gismondine,  $\text{C}_4\text{AF}$ ,  $\text{C}_3\text{AH}_6$  and tilleyite are small, their contents do not exceed 1%. The increased temperature (from 25 to 40 °C) somewhat accelerates the hydration speed and increases

the degree of reactivity of the clinker phases  $C_3S$  and  $C_2S$ . The amount of stable hydration products (CH, Mc,  $\overline{CC}$ ) is changed slightly during the hydration process, the differences being minor (see Table 3).

The crystallinity of the samples with added dolomite does not depend on temperature. After 3 days of hydration it is around 50%, after 90 days it is around 43%. The exact values are collected in Table 2. The crystallinity is in the samples with added dolomite always higher than in PC samples and after 90 days of hydration the values exceed the samples with clear PC by 12%.

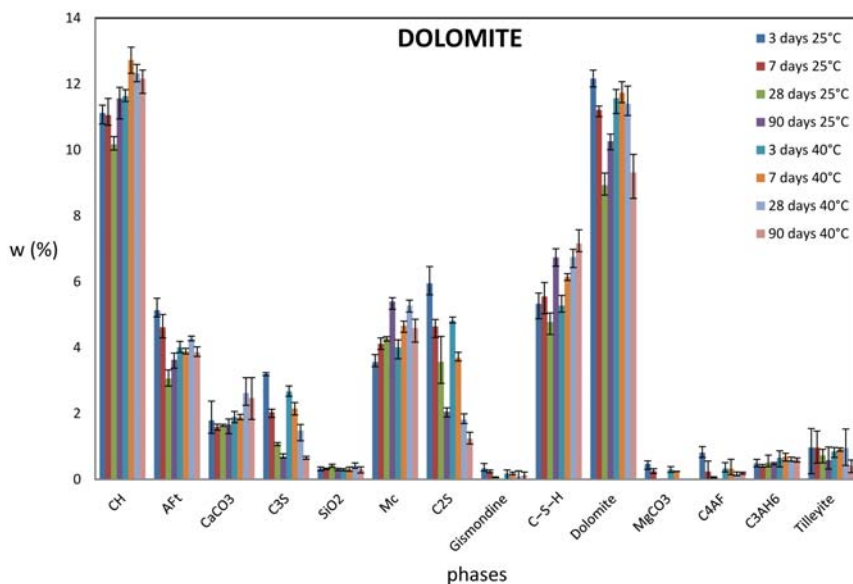


**Figure 6.** The quantitative analysis of hydration products in cements with added dolomite at 3, 7, 28 and 90 days of hydration and two temperatures, 25 and 40 °C.

### 3. 3. Medium Soluble Carbonate

$Li_2CO_3$  (solubility at 25 °C is 1.30g/100g water<sup>20</sup>)

A 15% addition of the moderately soluble carbonate  $Li_2CO_3$  affects the cement hydration. With the applied Rietveld method the following phases were identified: CH, AFt (3 and 7 days hydration at 25 °C) Mc, partly crystalline C–S–H,  $CaCO_3$ ,  $Li_2CO_3$ , calcium aluminum hydrate  $C_3AH_6$ , unreacted clinker phases  $C_3S$ ,  $C_2S$ ,  $C_4AF$  and compounds in traces (under 2%): stratlingite  $C_2ASH_8$ , lithium sulfate hydrate  $Li_2SO_4(H_2O)$ ,  $SiO_2$ , gismondine  $CAS_2H_4$  and carbosilicate tilleyite  $3CaO \cdot SiO_2 \cdot 2CaCO_3$ . The hydration of the clinker phases of  $C_3A$  and  $C_2S$ <sup>22</sup> is accelerated, whilst the hydration of  $C_3S$  at both temperatures is decelerated (see Figure 7). What remains after 90 days of hydration in samples with added  $Li_2CO_3$  is 2.44% of  $C_3S$  at 25 °C and 1.78% of  $C_3S$  at 40 °C. ( $C_3S$  in PC after 90 days: 25 °C 1.33%; 40 °C 1.28%.) Consequently, the amount of formed C–S–H is increased and the differences between samples with and without the added  $Li_2CO_3$  increase with the level of hydration. After 90 days of hydration in samples with  $Li_2CO_3$  at 25 °C there is 8.58% and at 40 °C there is 8.22% C–S–H. (PC 25 °C 5.19%; 40 °C

5.99%.) After 90 days of hydration around 4%  $Li_2CO_3$  is reacted (25 °C 4.07%, 40 °C 3.8%). Lithium with sulfate ions forms the lithium sulfate hydrate  $Li_2SO_4(H_2O)$ . At both temperatures the contents during the hydration remain low, under 1%, but apparently high enough to not allow the formation of AFt or Ms, probably due to the lack of availability of sulfate ions. AFt only occurs in small amounts (under 1%) at 25 °C during the beginning stages of hydration (after 3 and 7 days), whereas at 40 °C it does not even occur. The amount of the formed Mc increased, the exact values are collected in Table 3. A part of the alu-

minum is used for the formation of stratlingite  $C_2ASH_8$  (the contents during the 90 days of hydration at both temperatures do not exceed 1%). We propose that a part of  $Li_2CO_3$  dilutes in CH, through which  $CaCO_3$  precipitates (its contents increase with hydration levels and increased temperature and are collected in Table 3), as the contents of CH after 3, 7 and 28 days of hydration are too low with regard to the high amounts of formed C–S–H or the reactivity of di-/tri-silicates. After 90 days, the amount of formed CH at both temperatures (around 12%, the exact values are collected in Table 3) is comparable to samples with added slightly soluble calcium carbonate and  $\overline{CC}$ . In samples with  $Li_2CO_3$  after 90 days of hydration there is a lot of carbonate present ( $Li_2CO_3 + CaCO_3$ ; 25 °C 15.72%; 40 °C 16.74%), for which we propose that its role in the later stages of cement hydration is predominantly an inert filling. After 90 days of hydration there is no reactive carbonate present in the samples with added  $Li_2CO_3$ , which means that all dissolved  $Li_2CO_3$  (about 4%) is transformed into stable/ inert  $CaCO_3$ .

The portions of  $SiO_2$ , gismondine,  $C_4AF$ ,  $C_3AH_6$  and tilleyite are relatively minor, not exceeding 2%. The

increased temperature (from 25 to 40 °C) somewhat accelerates the hydration speed and increases the degree of reactivity of the clinker phases. The amount of stable hydration products (CH, Mc,  $\text{C}\bar{\text{C}}$ ) is changed slightly during the hydration process, the differences being minor, around 1% or less (see Table 3).

The crystallinity of the samples with added  $\text{Li}_2\text{CO}_3$  does not depend on temperature. After 3 days of hydration it is around 53% and after 90 days of hydration it is 49%. The exact values are collected in Table 2. The crystallinity in the samples with added medium soluble carbonates is

after 90 days of hydration there is some more reacted  $\text{C}_3\text{S}$  than in PC. (90 days hydration:  $\text{KHCO}_3$  25 °C 1.52%, 40 °C 0.40%; PC 25 °C 1.33%, 40 °C 1.28%.) The amount of formed C–S–H is increased and the differences compared with clear PC only increase with hydration stages. The amounts of the formed C–S–H are at both temperatures comparable and are slightly higher at 40 °C (See Figure 8). After 90 days of hydration in the samples with  $\text{KHCO}_3$  there is 7.56% C–S–H at 25 °C and 7.76% at 40 °C. (PC 25 °C 5.19%; 40 °C 5.99%.) Already after 3 days of hydration at both temperatures no  $\text{KHCO}_3$  is visible. The hy-

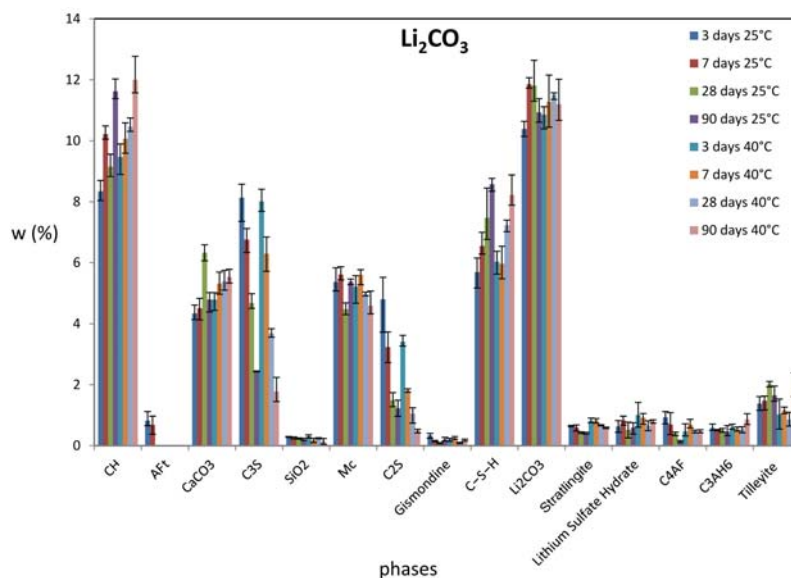


**Figure 7.** The quantitative analysis of hydration products in cements with added  $\text{Li}_2\text{CO}_3$  at 3, 7, 28 and 90 days of hydration and two temperatures, 25 and 40 °C.

always higher than in PC samples. After 90 days of hydration the values are 18% higher compared to samples with clear PC. This is attributed to the high amounts of the present carbonate ( $\text{Li}_2\text{CO}_3 + \text{CaCO}_3$ ) in samples with added  $\text{Li}_2\text{CO}_3$ .

### 3. 4. Highly Soluble Carbonates

#### 3. 4. 1. $\text{KHCO}_3$

A 15% addition of the highly soluble carbonate  $\text{KHCO}_3$  significantly affects the cement hydration due to the high solubility and its important role in changing the pH-value (towards making it less basic). With the applied Rietveld method the following phases were identified: CH, Mc, partly crystalline C–S–H,  $\text{CaCO}_3$ ,  $\text{K}_2\text{SO}_4$ , calcium aluminum hydrate  $\text{C}_3\text{AH}_6$ , unreacted clinker phases  $\text{C}_3\text{S}$ ,  $\text{C}_2\text{S}$ ,  $\text{C}_4\text{AF}$  and compounds in traces (under 2%):  $\text{SiO}_2$ , gismondine  $\text{CAS}_2\text{H}_4$  and carbo-silicate tilleyite  $3\text{CaO}\cdot\text{SiO}_2\cdot 2\text{CaCO}_3$ . The hydration of the clinker phases ( $\text{C}_3\text{A}$  in  $\text{C}_2\text{S}$ ) is accelerated, whereas the hydration of  $\text{C}_3\text{S}$  is decelerated. It reaches contents comparable with those in PC only after 90 days of hydration at 25 °C and at 40 °C

hydration products make it clear that part of  $\text{KHCO}_3$  reacts with gypsum ( $\text{CaSO}_4\cdot 2\text{H}_2\text{O}$ ) at both temperatures, during which  $\text{K}_2\text{SO}_4$  and  $\text{CaCO}_3$  is formed. Apparently the entire available sulfate in gypsum is used for the formation of  $\text{K}_2\text{SO}_4$  during the reaction, thus we predict that the formation of AFt or Ms is hindered. After 90 days at 25 °C in samples with  $\text{KHCO}_3$  there is 3.40%  $\text{K}_2\text{SO}_4$  present and at 40 °C there is 3.31%  $\text{K}_2\text{SO}_4$  present. The amount of formed Mc increased, the values are collected in Table 3. The CH contents are low at both temperatures during the hydration process (see Table 3) compared to the high amounts of formed C–S–H or the reactivity di-/tri-silicates. We anticipate the  $\text{KHCO}_3$  dissolving in CH and furthermore the CH reacting with dissolved  $\text{CO}_2$  during which  $\text{CaCO}_3$  is formed (the contents are collected in Table 3). Thus, in samples with  $\text{KHCO}_3$  after 90 days of hydration there is 25 °C 10.92%  $\text{CaCO}_3$  present and 12.57% at 40 °C. The amount of reactive carbonate is around 3%.

The amounts of  $\text{SiO}_2$ , gismondine,  $\text{C}_4\text{AF}$ ,  $\text{C}_3\text{AH}_6$  and tilleyite are small, not exceeding 2%. At a higher temperature (from 25 to 40 °C) the amount of the reacted

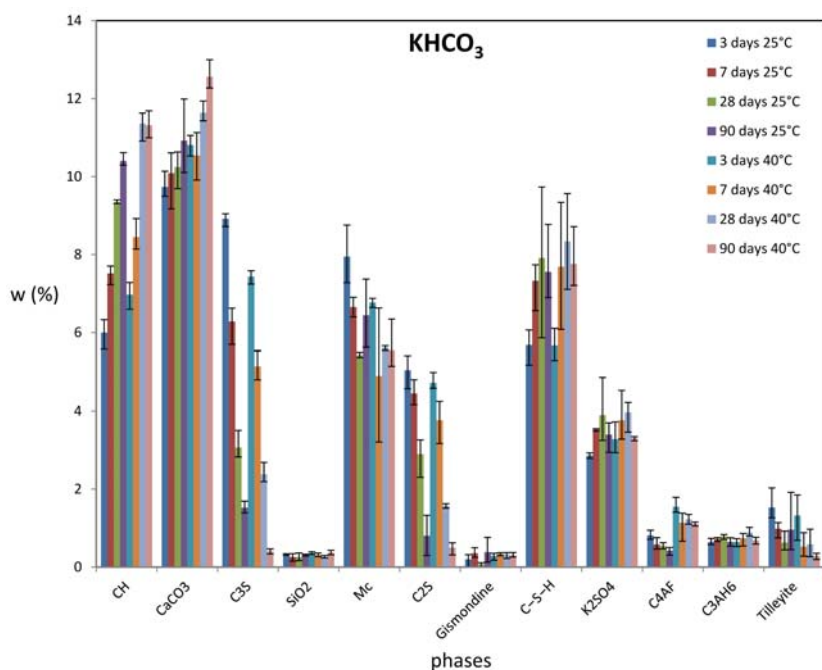


**Figure 8.** The quantitative analysis of hydration products in cements with added  $\text{KHCO}_3$  at 3, 7, 28 and 90 days of hydration and two temperatures, 25 and 40 °C.

clinker phases  $\text{C}_3\text{S}$  and  $\text{C}_2\text{S}$  is higher, which is consequently shown on a higher amount of hydration products (CH, C–S–H) – Figure 8. At 40 °C the amount of  $\text{CaCO}_3$  is slightly higher during the hydration process as there was more CH available, which could then react with dissolved  $\text{CO}_2$ .

The crystallinity of samples with added  $\text{KHCO}_3$  does not depend on temperature. After 3 days of hydration it is 50% and after 90 days of hydration it is 44%. The exact values are collected in Table 2. The crystallinity in samples with added  $\text{KHCO}_3$  is always higher compared to PC samples and after 90 days of hydration the values exceed those of clear PC samples by 13%.

### 3. 4. 2. $\text{K}_2\text{CO}_3$

A 15% addition of the highly soluble carbonate  $\text{K}_2\text{CO}_3$  significantly affects the cement hydration. With the applied Rietveld method the following phases were identified: CH, Mc, partly crystalline C–S–H,  $\text{CaCO}_3$ ,  $\text{K}_2\text{SO}_4$ ,  $\text{K}_2\text{CO}_3$ , calcium aluminum hydrate  $\text{C}_3\text{AH}_6$ , unreacted clinker phases  $\text{C}_3\text{S}$ ,  $\text{C}_2\text{S}$ ,  $\text{C}_4\text{AF}$  and compounds in traces (under 2%):  $\text{SiO}_2$ , gismondine  $\text{CAS}_2\text{H}_4$  and carboxylic tilleyite  $3\text{CaO}\cdot\text{SiO}_2\cdot 2\text{CaCO}_3$ . The hydration of the clinker phases ( $\text{C}_3\text{A}$  and  $\text{C}_2\text{S}$ ) is accelerated, whereas the hydration of  $\text{C}_3\text{S}$  is decelerated in the first stages of the hydration (3 and 7 days), but after 28 in 90 days of hydration it is accelerated at both temperatures. (90 days hydration:  $\text{K}_2\text{CO}_3$  25 °C 0.88%, 40 °C 0.37%; PC 25 °C 1.33%, 40 °C 1.28%.) The amount of the formed C–S–H is increased and the difference after 90 days of hydration is 5

% higher compared to clear PC samples. ( $\text{K}_2\text{CO}_3$ : 25 °C 10.63%, 40 °C 10.47%; PC: 25 °C 5.19%, 40 °C 5.99%.) The hydration products make it clear (see Figure 9) that  $\text{K}_2\text{CO}_3$  at both temperatures reacts with gypsum ( $\text{CaSO}_4\cdot 2\text{H}_2\text{O}$ ), at which point  $\text{K}_2\text{SO}_4$  is formed. The entire available sulfate is apparently used for the formation of  $\text{K}_2\text{SO}_4$  and thus the formation of AFt or Ms is indirectly hindered. After 90 days at 25 °C in samples with  $\text{K}_2\text{CO}_3$  there is 5.03% of  $\text{K}_2\text{SO}_4$  present and 4.82% at 40 °C. A part of  $\text{K}_2\text{CO}_3$  remains unreacted, but the amount after 90 days of hydration at both temperatures is small, not exceeding 1.5% (25 °C 1.29%, 40 °C 1.22%). The amount of formed Mc is minimally increased after 90 days of hydration at both temperatures, the values are collected in Table 3. The CH amounts in the beginning stages of hydration (3 and 7 days at 25 °C and 3 days at 40 °C) are low compared to the high amounts of formed C–S–H or reactivity of di-/trisilicates. Thus we predict that a part of  $\text{K}_2\text{CO}_3$  dilutes in CH during the beginning phases of hydration, during which  $\text{CaCO}_3$  is formed. After 90 days of hydration at 25 °C and 28 days of hydration at 40 °C the CH is not being used up anymore and so the contents of CH exceed those in clear PC (see Table 3). In samples with  $\text{K}_2\text{CO}_3$  after 90 days of hydration there is around 7% calcium ( $\text{K}_2\text{CO}_3 + \text{CaCO}_3$ : 25 °C 6.91%; 40 °C 7%) present for which we predict that it serves as an inert filling during the later stages of the cement hydration process. The amount of reactive carbonate is after 90 days of hydration and the both temperatures around 6%.

The amounts of  $\text{SiO}_2$ , gismondine,  $\text{C}_4\text{AF}$ ,  $\text{C}_3\text{AH}_6$  and tilleyite are small, not exceeding 2%. At an increased

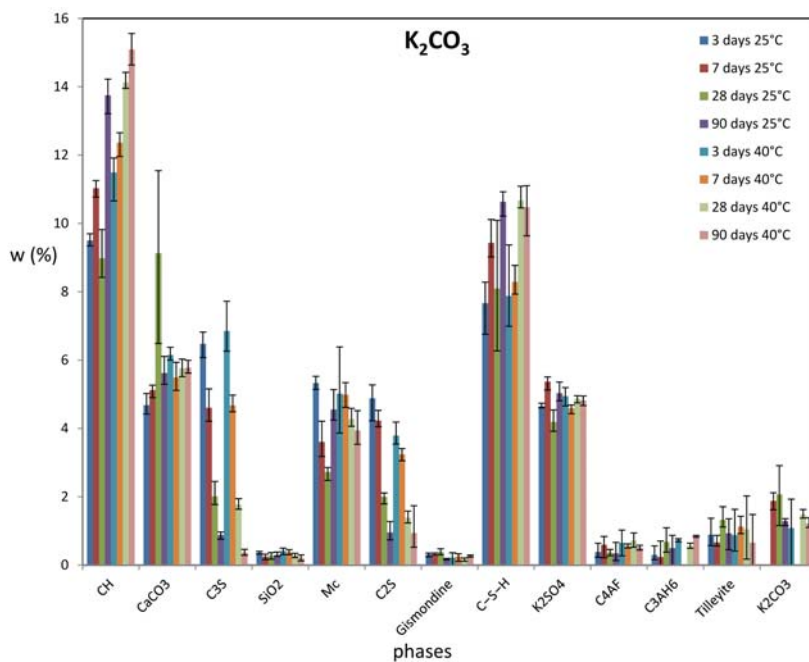


**Figure 9.** The quantitative analysis of hydration products in cements with added  $K_2CO_3$  at 3, 7, 28 and 90 days of hydration and two temperatures, 25 and 40 °C.

temperature (from 25 to 40 °C) the reactivity of the clinker phase  $C_2S$  is slightly higher, whereas the majority of the reacted  $C_3S$  is only visible after 28 days of hydration (see Figure 9).

The crystallinity of the samples with added  $K_2CO_3$  does not depend on temperature. After 3 days it is between 45 and 50% and after 90 days of hydration it is 45%. The exact values are collected in Table 2. The crystallinity in samples with added  $K_2CO_3$  is always higher compared to PC samples and after 90 days of hydration the values exceed those of clear PC samples by 14%.

## 4. Discussion

Results presented above show that the addition of differently soluble carbonates does have an influence on cement hydration, the higher the solubility the more obvious the differences are (see Figure 10).

Hydration process and the contents of stable hydration products do not change significantly in the temperature range 25 to 40 °C. The hydration of the clinker phases ( $C_3A$ ,  $C_3S$  and  $C_2S$ ) is at 40 °C somewhat accelerated and the amount of stable phases (E in slightly soluble carbonates, Mc, CH, calcite and C–S–H) of cement hydration is slightly changed. Presence of stable phases in our samples confirm T. Matschei calculations.<sup>3</sup>

Slightly soluble carbonates ( $CC\bar{}$ , calcite,  $MgCO_3$ , dolomite) accelerate the hydration of the clinker phases  $C_3A$ ,  $C_3S$  and  $C_2S$ . Medium soluble ( $Li_2CO_3$ ) and highly soluble ( $KHCO_3$ ,  $K_2CO_3$ ) carbonates accelerate the hydra-

tion of  $C_3A$  and  $C_2S$ , whereas the hydration of  $C_3S$  is decelerated:

- in samples with added  $Li_2CO_3$  even after 90 days of hydration;
- in samples with added  $KHCO_3$  at 25 °C even after 90 days of hydration, at 40 °C in the first stages of the hydration (3, 7 days), after 28 and 90 days the amount of unreacted  $C_3S$  is smaller than in PC samples;
- in samples with  $K_2CO_3$  in the first stages of the hydration (3, 7 days), after 28 and 90 days the amount of unreacted  $C_3S$  is smaller than in PC samples.

The amount of reacted carbonate in cement hydration at a 15% addition of slightly or moderately soluble carbonates does not exceed 5% and is not affected by their solubility. At a 15% addition of the highly soluble carbonate  $K_2CO_3$  a higher amount of carbonate is used up during the hydration process and after 90 days it is around 6%. At the addition of the highly soluble carbonate  $KHCO_3$  the change in the pH value also plays a role in addition to the solubility and great amounts of  $CaCO_3$  are formed in samples due to the reaction between dissolved  $CO_2$  and CH (after 90 days they exceed 10%). The rest of the carbonate serves predominantly as an inert filling.

In PC samples as well as samples with differently soluble carbonates the stable hydration products are Mc, AFt (at the addition of slightly soluble carbonates),  $CC\bar{}$ , C–S–H and CH. While the samples were prepared with PC which had a molar ratio  $SO_3/Al_2O_3 = 0.9$  and even after 3 days of hydration in all samples Mc and Hc were not identified, we conclude, that the molar ratio  $CO_2/Al_2O_3$  is equal or higher from 1. That means that all our samples

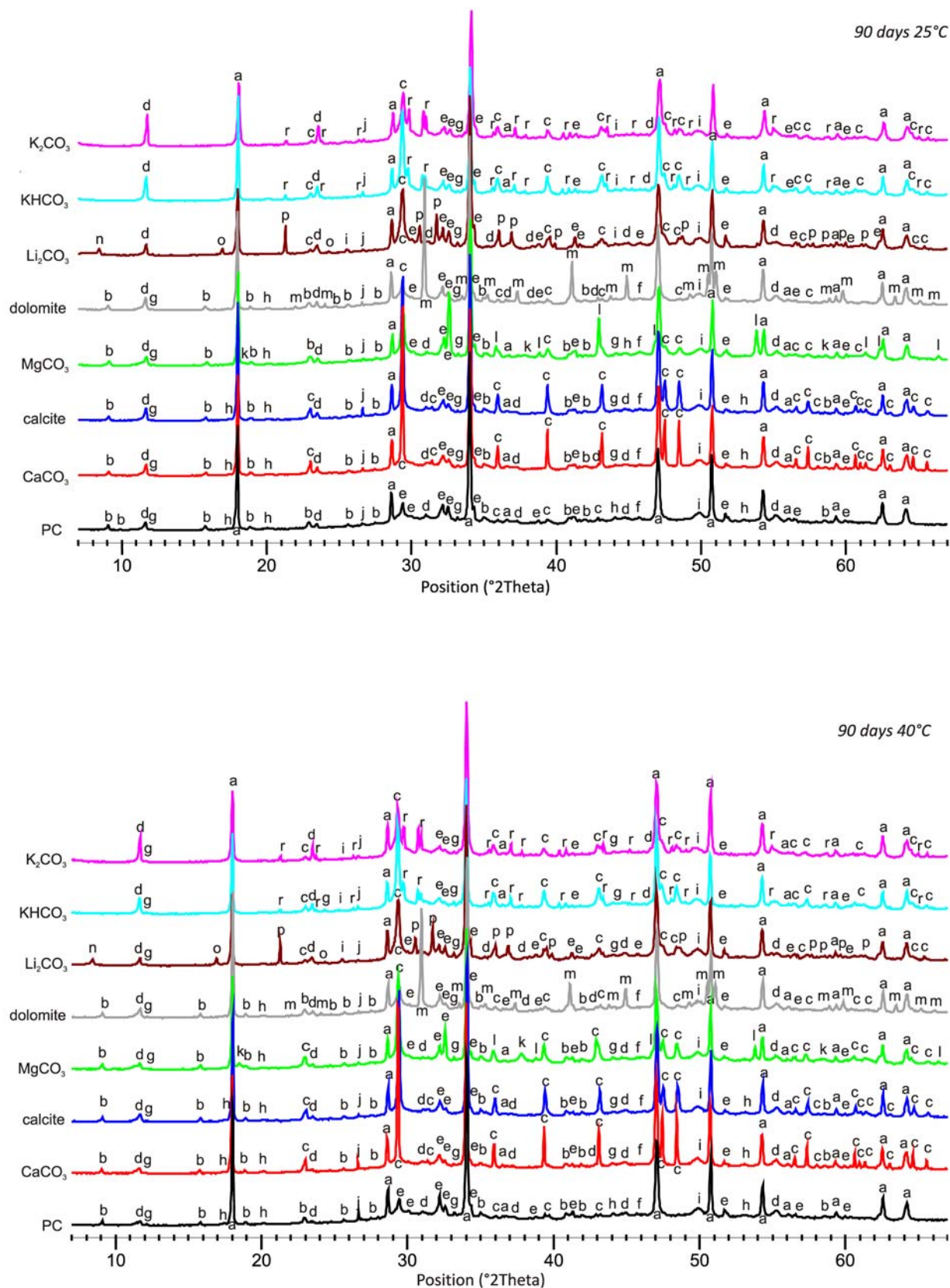


**Figure 10.** X-ray diffraction patterns of 90-day hydrated samples at 25 °C/40 °C and phases identified: a-CH; b-E; c-Calcite; d-Mc; e-C<sub>3</sub>S; f-C<sub>2</sub>S; g-C<sub>4</sub>A<sub>F</sub>; h-C<sub>3</sub>A<sub>H<sub>6</sub></sub>; i-4-C-S-H; j-SiO<sub>2</sub>; k-Mg(OH)<sub>2</sub>; l-MgCO<sub>3</sub>; m-Dolomite; n-Stratlingite; o-Lithium Sulfate Hydrate; p-Li<sub>2</sub>CO<sub>3</sub>; r-K<sub>2</sub>SO<sub>4</sub>.



(also include samples of pure PC) had excess of reactive carbonate after 3 days of hydration already.

The amount of Mc after 90 days of hydration at the addition of any kind of carbonates is slightly higher than in PC samples. With the presence of differently soluble carbonates Mc is stabilized and in turn causes AFt to be stabilized in slightly soluble carbonates, whereas the formation of AFt in moderately and highly soluble carbonates is hindered. The amount of AFt in samples with or without the added slightly soluble carbonates is comparable and after 90% days of hydration the content is around 4%. It is well known that the addition of carbonate affects the change of the Ca/Si ratio in C–S–H, but it cannot cause the formation of new C–S–H gel, as it has no pozzolanic qualities. Scientific writings show us that a part of the carbonate is incorporated in the C–S–H, at which point calcium silicocarbonate hydrates are formed but we could not identify any with Rietveld method. We do, however, predict their formation, as with the addition of slightly soluble carbonates ( $\text{CCl}_2$ , calcite,  $\text{MgCO}_3$ ) we can identify comparable C–S–H contents only after 90 days of hydration compared to clear PC samples, even if the hydration of di-/tri- silicates is accelerated. The amount of identified C–S–H increases with the solubility of the added carbonates and after 90 days of hydration with the addition of the slightly soluble carbonate dolomite the C–S–H contents exceed those of PC samples by 1%, with the addition of the medium soluble carbonate  $\text{Li}_2\text{CO}_3$  and the highly soluble carbonate  $\text{KHCO}_3$  it is even higher for about 2%, with the addition of  $\text{K}_2\text{CO}_3$  the C–S–H contents are higher for about 5%. Even though the quantification of C–S–H with XRD analysis is more difficult and harder to determine due to its semi amorphous nature, we can conclude based on the gathered data that the addition of carbonates affects its formation during the hydration – in the way of changing the Ca/Si relation and/or partial inclusion of  $\text{CO}_3^{2-}$  into its structure.

The crystallinity of the samples does not depend on temperature and after 90 days of hydration is always lower than after 3 days of hydration both in PC samples as well as at the addition of differently soluble carbonates. After 90 days of hydration the crystallinity in PC samples is 31%, after the addition of slightly soluble carbonates the crystallinity is higher for about 10%, after the addition of moderately soluble carbonates for about 18% and after the addition of highly soluble carbonates for about 14% (when compared to clear samples of PC).

## 5. Conclusions

We can conclude that blending of PC with differently soluble carbonates was found to influence the hydrate assemblage of the hydrated cement. With the help of the Rietveld analysis the study indicated that Mc and not Ms were stable in the presence of any carbonate. Even more,

the Mc was stabilized in the presence of slightly soluble carbonates, consequently causing the stabilization of AFt. The amount of Mc after 90 days of hydration at the addition of any kind of carbonates is slightly higher than in PC. In the presence of either medium or highly soluble carbonates AFt is not formed or its formation is delayed. Their amount is comparable in samples with or without slightly soluble carbonates. Carbonates accelerate the hydration of the clinker phases  $\text{C}_2\text{S}$  and  $\text{C}_3\text{A}$ , whereas the hydration of  $\text{C}_3\text{S}$  is accelerated in slightly soluble carbonates and decelerated in moderately and highly soluble carbonates. The amount of reacted carbonate in cement hydration at a 15% addition of slightly or medium soluble carbonates does not exceed 5% and is not affected by their solubility; at a 15% addition of the highly soluble carbonate  $\text{K}_2\text{CO}_3$  it is around 6%. An increase in temperature (25 to 40 °C) gradually effects one, the rate of hydration and two, the quantity of stable phase assemblage (E in slightly soluble carbonate-blended cements, monocarboaluminate, calcite and portlandite).

The crystallinity of the samples is independent on the temperatures (25 to 40 °C) and is after the 90 days of hydration always lower than after 3 days of hydration in the samples of clear PC and in the samples to which carbonate was added.

## 6. References

1. EN 197-1, European Standard, Cement – Part 1, Composition, specifications and conformity criteria for common cements, CEN, Brussels, 2000.
2. I. Soroka, N. Setter, *Cem. Concr. Res.* **1977**, *7*, 449–456. [https://doi.org/10.1016/0008-8846\(77\)90073-4](https://doi.org/10.1016/0008-8846(77)90073-4)
3. T. Matschei, B. Lothenbach, F. P. Glasser, *Cem. Concr. Res.* **2007**, *37*, 551–558. <https://doi.org/10.1016/j.cemconres.2006.10.013>
4. T. Matschei, B. Lothenbach, F. P. Glasser, *Cem. Concr. Res.* **2007**, *37*, 118–130. <https://doi.org/10.1016/j.cemconres.2006.10.010>
5. R. D. Hooten, M. Nokken, M. D. A. Thomas, Portland-Limestone Cement: State-of-the-Art Report and Gap Analysis for CSA A 3000, Cement Association of Canada, Toronto, 2007, 59 pp.
6. Vuk, V. Kaučič, J. Maček, A. Meden, *J. Am. Ceram. Soc.* **2011**, *94*, 1238–1242.
7. V. S. Ramachandran, *Thermochim. Acta* **1988**, *127*, 385–394. [https://doi.org/10.1016/0040-6031\(88\)87515-4](https://doi.org/10.1016/0040-6031(88)87515-4)
8. V. S. Ramachandran, C. Zhang, *Mater. Constr.* **1986**, *19*, 437–444. <https://doi.org/10.1007/BF02472147>
9. C. Vernet, G. Noworyta, Proc. Int. Congr. Chem. Cem., 9th, New Delhi, India IV, 1992, pp. 430–436.
10. V. L. Bonavetti, V. F. Rahhal, E. F. Irassar, *Cem. Concr. Res.* **2001**, *31*, 853–859. [https://doi.org/10.1016/S0008-8846\(01\)00491-4](https://doi.org/10.1016/S0008-8846(01)00491-4)
11. B. Lothenbach, G. Le Saout, E. Gallucci, K. Scrivener, *Cem.*

- Concr. Res.* **2008**, *38*, 848–860.  
<https://doi.org/10.1016/j.cemconres.2008.01.002>
12. J. Pera, S. Husson, B. Guilhot, *Cem. Concr. Comp.* **1999**, *21*, 99–105. [https://doi.org/10.1016/S0958-9465\(98\)00020-1](https://doi.org/10.1016/S0958-9465(98)00020-1)
13. K. Sersale, Proc. Int. Congr. Chem. Cem., 9th, New Delhi, India I, **1992**, pp. 277–279.
14. S. Husson, B. Guilhot, J. Pera, Proc. Int. Congr. Chem. Cem., 9th, New Delhi, India IV, **1992**, pp. 83–89.
15. B. Lothenbach, T. Matschei, G. Moeschner, F. P. Glasser, *Cem. Concr. Res.* **2008**, *38*, 1–18.  
<https://doi.org/10.1016/j.cemconres.2007.08.017>
16. T. Matschei, F. P. Glasser, *Cem. Concr. Res.* **2010**, *40*, 763–777. <https://doi.org/10.1016/j.cemconres.2009.11.010>
17. K. L. Scrivener, T. Fuellmann, E. Gallucci, G. Walenta, E. Bermejo, *Cem. Concr. Res.* **2004**, *34*, 1541–1547.  
<https://doi.org/10.1016/j.cemconres.2004.04.014>
18. V. S. Ramachandran, J. J. Beaudoin (Ed.): Handbook of analytical techniques in concrete science and technology, Principles, Techniques and Applications, Noyes Publications, Norwich, **2001**, pp. 275–333.
19. R. A. Young (Ed.), The Rietveld Method, Oxford Science Publications, Oxford University Press, **1995**, 308 pp.
20. D. R. Lide (Ed.), CRC Handbook of Chemistry and Physics, 90<sup>th</sup> Edition, CD-ROM version **2010**.
21. S. Gali, C. Ayora, P. Alfonso, E. Tauler, M. Labrador, *Cem. Concr. Res.* **2001**, *31*, 933–939.  
[https://doi.org/10.1016/S0008-8846\(01\)00499-9](https://doi.org/10.1016/S0008-8846(01)00499-9)
22. P. Gu, J. J. Beaudoin, *J. Mater. Sci. Lett.* **1997**, *16*, 696–698.  
<https://doi.org/10.1023/A:1018504324894>

## Povzetek

Učinek apnenca na hidratacijo Portland cementa so študirali mnogi raziskovalci, učinek bolj topnih karbonatov pa doslej ni bil pojasnjen. Zato smo izvedli kvalitativno in kvantitativno študijo vpliva slabo topnih ( $\text{CaCO}_3$ ,  $\text{MgCO}_3$ , dolomit), srednje topnih ( $\text{Li}_2\text{CO}_3$ ) in dobro topnih ( $\text{K}_2\text{CO}_3$  in  $\text{KHCO}_3$ ) karbonatov na hidratacijo.

Ugotovili smo, da dodatek različno topnih karbonatov Portland cementu vpliva na fazno sestavo hidratiranega cementa. Rietveldova analiza je pokazala, da pri 15 % dodatku slabo in srednje topnih karbonatov ne reagira več kot 5 % karbonata, medtem ko je pri 15 % dodatku dobro topnega  $\text{K}_2\text{CO}_3$  količina reagiranega karbonata dosegla približno 6 %.

Povišana temperatura (s 25 na 40 °C) vpliva tako na hitrost hidratacije kot na končno fazno sestavo hidratiranega cementa.

Scientific paper

# New Bioactive Heteroleptic Copper(II) Carboxylates: Structure, Enzymatic and DNA-Binding Studies

Afifa Mushtaq,<sup>1</sup> Saqib Ali,<sup>1,\*</sup> Muhammad Nawaz Tahir,<sup>2</sup> Hammad Ismail,<sup>3</sup>  
Bushra Mirza,<sup>3</sup> Muhammad Saadiq,<sup>4</sup> Muhammad Abdul Haleem<sup>4</sup>  
and Muhammad Iqbal<sup>4,\*</sup>

<sup>1</sup> Department of Chemistry, Quaid-i-Azam University, Islamabad 45320, Pakistan

<sup>2</sup> Department of Physics, University of Sargodha, Sargodha, Pakistan

<sup>3</sup> Department of Biochemistry, Quaid-i-Azam University, Islamabad 45320, Pakistan

<sup>4</sup> Department of Chemistry, Bacha Khan University, Charsadda 24420, KPK, Pakistan

\* Corresponding author: E-mail: drsa54@hotmail.com, saqibali@qau.edu.pk

Tel.: +92 51 90642130; fax: +92 51 90642241

iqbalmo@yahoo.com, iqbalmo@bkuc.edu.pk

Tel.: Tel.: +92 91 6002934; fax: +92 91 6540060

Received: 03-02-2017

## Abstract

Two new binuclear O-bridged copper(II) carboxylates with chemical formulas  $[\text{Cu}_2(3\text{-ClC}_6\text{H}_4\text{CH}_2\text{COO})_4(\text{phen})_2]$  (**1**) and  $[\text{Cu}_2(3\text{-ClC}_6\text{H}_4\text{CH}_2\text{COO})_4(\text{bipy})_2]$  (**2**) where phen = 1,10-phenanthroline and bipy = 2,2'-bipyridine have been synthesized and characterized by FT-IR, UV-Visible spectroscopy, CHN analysis and single crystal XRD. The results revealed distorted square pyramidal geometry around each copper atom of **1** and **2**. The DNA interaction studies showed strong binding with  $K_b = 5.07 \times 10^3$  and  $4.62 \times 10^3 \text{ M}^{-1}$  for **1** and **2**, respectively. Both complexes showed strong enzyme inhibition, i.e., 70% and 90% for  $\alpha$ -glucosidase with  $\text{IC}_{50} = 34.6$  and  $30.1 \mu\text{M}$  for **1** and **2**, respectively, where acarbose was employed as control. However, both the complexes were found inactive against  $\alpha$ -amylase. Using galantamine hydrobromide as control, **1** showed moderate inhibition activity (47%) with  $\text{IC}_{50} = 179.4 \mu\text{M}$  for acetylcholine esterase whereas **2** showed strong inhibition activity (76%) with  $\text{IC}_{50} = 95.8 \mu\text{M}$  for butyrylcholine esterase. The data reflects active anti-diabetic and anti-Alzheimer's nature of the synthesized complexes.

**Keywords:** Copper(II) Carboxylates, Structure, Enzymatic study, DNA-Binding Study

## 1. Introduction

Despite decades research work in the field of metal carboxylates, these fascinating materials with diverse structures and applications have still kept interest of scientists alive in them. Since their discovery they have been serving mankind in one way or the other. The striking application of metal carboxylates is that they act as accelerators for a number of industrially and biologically important chemical reactions such as oxidations, reductions, couplings, C–H insertions, transformations, and charge transfers.<sup>1–4</sup> A number of bioactive metal carboxylates have also been reported to date.<sup>5,6</sup> Inevitable relationship

between chemical reactions naturally carried out within the human body, pharmacology and medicine has lead the scientists to design new bioactive materials in the form of potent drugs for therapeutic intervention in treatment of many life threatening diseases. Metal charge, interactions with ligands, structure and bonding, Lewis acid character, partially filled *d*-shell and its redox activity defines its suitability for biological systems.<sup>7–10</sup>

Copper is one of essential metals with multifaceted role in human life. It has been used as medicine for healing purposes since ancient civilizations.<sup>11–13</sup> In case of exogenous administration in the form of synthetic compounds, it interacts with various biomolecules mainly pro-

teins and nucleic acid.<sup>14,15</sup> Cytochrome c oxidase, superoxide dismutase, ferroxidases, monoamine oxidase, and dopamine  $\beta$ -monooxygenase are copper dependent enzymes within the human body.<sup>16,17</sup> Recently, greater interest in copper carboxylates has emerged because of their potential use as antimicrobial, antiviral, anti-inflammatory and antitumor agents due to their ability to interact with DNA through Fenton type reaction and they offer reduced side effects attributed to their superoxide dismutase (SOD) mimetic activity.<sup>18,19</sup> In this regard casiopeinas, generic name of heteroleptic copper(II) complexes with good antineoplastic activity have set a foundation for synthesis of therapeutically potent agents based on mix ligand copper(II) complexes.<sup>20,21</sup> Moreover, copper complexes can act as enzyme inhibitors by blocking the active sites on enzyme surface as copper has ability to bind to various proteins in biological system. However, a very few copper carboxylates have been reported so far with alpha glucosidase, acetylcholine and butyrylcholine esterases inhibition activity.<sup>22–25</sup>

Since enzyme targeting is potential therapy in modern era of medicinal research therefore combining an essential metal and two different organic ligands together in

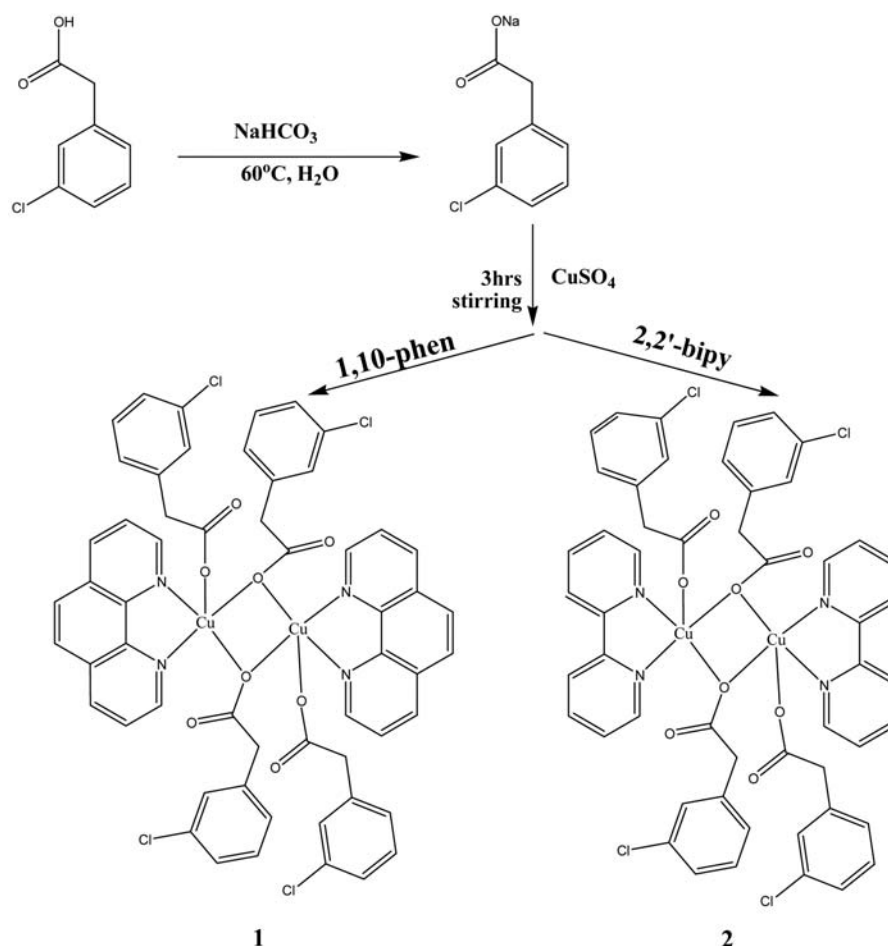
a single molecule to develop lifesaving drugs could be attractive solution. Organic ligands in these complexes affect and regulate their activity by neutralizing the charge on copper ion and facilitating the transport across the cell membranes.<sup>26,27</sup>

Therefore, keeping in view all these facts, as well as in continuation of our previous work,<sup>28–30</sup> the present study is designed with aim to synthesize biologically active heteroleptic copper(II) complexes with substituted phenylacetic acids and 1,10-phenanthroline and 2,2'-bipyridine. DNA binding ability of synthesized complexes was evaluated through UV-Visible spectroscopy which exhibited good results and their strong enzyme inhibition capacity revealed their therapeutic applications as well.

## 2. Results and Discussion

### 2.1. Synthesis, UV-Visible and FT-IR spectroscopy

The complexes were synthesized in aqueous medium using mild reaction conditions as depicted in Sche-



Scheme 1. Synthetic procedure and proposed structures of the complexes.

me 1. These were obtained in good yield followed by their purification and recrystallization. The crystalline samples were subjected to characterization techniques such as UV-Visible, FT-IR and single-crystal X-ray crystallographic studies. UV-Visible and FT-IR spectra clearly indicated the essential peaks that helped in characterization of the complexes. The bands observed at 673 nm and 663 nm in visible region for complexes **1** and **2**, respectively, were assigned to d–d electronic transition of copper metal ion. These band positions are typical of those observed for other copper complexes having square pyramidal geometry. Two bands were observed in region below 400 nm for complex **1**. An intense band at 272 nm was assigned to intra-ligand  $\pi \rightarrow \pi^*$  and  $n \rightarrow \pi^*$  electronic transitions for aromatic rings and carbonyl group of the ligands. Second broad band at 315 correspond to ligand to metal charge transfer transition. Similarly, for complex **2** intense band at 270 nm corresponds to intra-ligand  $\pi \rightarrow \pi^*$  and  $n \rightarrow \pi^*$  electronic transitions while band at 305 nm is assigned to ligand to metal charge transfer transition. Values of  $\epsilon$  for complexes **1** and **2** are  $93.4 \text{ L mol}^{-1} \text{ cm}^{-1}$  at  $\lambda_{\text{max}}$  272 nm and  $92.2 \text{ L mol}^{-1} \text{ cm}^{-1}$  at  $\lambda_{\text{max}}$  270 nm, respectively.

Both complexes were characterized by FT-IR spectroscopy. All the characteristic bands were observed in the spectrum. Absorption bands at  $2980 \text{ cm}^{-1}$  and  $3080 \text{ cm}^{-1}$  were due to aromatic C–H stretching for complex **1** and **2**, respectively. While absorption bands at  $1625 \text{ cm}^{-1}$  and  $1427 \text{ cm}^{-1}$  represented asymmetric and symmetric O–C=O stretching modes of fully deprotonated carboxylate group in complex **1** and at  $1633 \text{ cm}^{-1}$  and  $1444 \text{ cm}^{-1}$  in complex **2**.<sup>31</sup> Absorption bands at  $1519$ ,  $1562 \text{ cm}^{-1}$  and  $1604$ ,  $1566 \text{ cm}^{-1}$  were assigned to aromatic C=C stretching for complexes **1** and **2**. While Ar–Cl stretch was observed at  $723$  and  $769 \text{ cm}^{-1}$  for two complexes. Bonding of Cu(II) with O-atom of carboxylate moiety and N-atom of pyridine was depicted by absorption bands at  $611$ ,  $605 \text{ cm}^{-1}$  and  $482$ ,  $479 \text{ cm}^{-1}$  for complexes **1** and **2**, respectively.

Binding mode of carboxylate moiety either monodentate or bidentate in both complexes was defined by calculating the value of  $\Delta\nu \{ \nu(\text{OCO})_{\text{asym}} - \nu(\text{OCO})_{\text{sym}} \}$  which is 198 for complex **1** and 189 for **2** supporting monodentate and bridging coordinate binding mode in both the complexes. This fact was also confirmed by X-ray single-crystal analysis.<sup>32</sup>

## 2. 2. Crystal Structure Description

The ORTEP and close packing diagrams of both complexes with the atomic numbering scheme and mode of coordination of ligands is shown in Figs. 1 and 3 and 2 and 4, respectively. The crystal data and structure refinement parameters are given in Table 1 while the selected bond lengths and angles are listed in Table 2. The crystals remained stable throughout the data collection

and both the crystals were comprised of Cu(II) dimeric units in which each copper atom is penta-coordinated giving rise to a distorted square pyramidal geometry around each copper atom with small distortion as reflected by value of distortion factor  $\tau (= \beta - \alpha/60^\circ)$  which is found to be 0.172 and 0.002 for complexes **1** and **2**, respectively.<sup>33</sup>

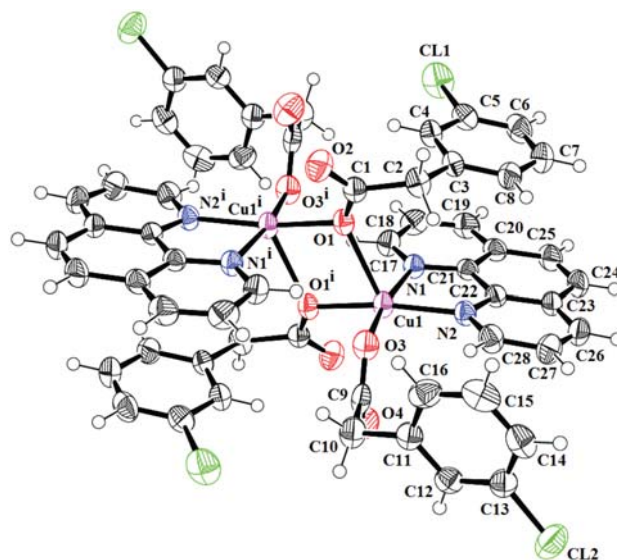


**Figure 1.** ORTEP diagram of complex **1** with thermal ellipsoids drawn at 50% probability level. The H-atoms are shown as small circles of arbitrary radii. Symmetry code  $i = 2 - x, -y, -z$ .

In both crystals each copper atom of a dimeric unit is surrounded by two nitrogen atoms from phen or bipy moiety and three oxygen atoms from three phenylacetate acids. Two nitrogen atoms and two oxygen occupy the four corners of a square plane while third bridging oxygen atom occupies the apical position giving rise to a square pyramidal geometry around each metal atom of a discrete dimer. The Cu–N<sub>phen</sub> and Cu–N<sub>bipy</sub> distances in complexes **1** and **2** are 2.0284(18), 2.0392(19) Å and 2.0094(19), 2.023(2) Å, respectively.

The Cu–O apical and equatorial plane distances are different from each other. In complex **1** Cu–O equatorial plane distances are 1.9629(15), 1.9350(16) Å and in complex **2** 1.9662(16), 1.9514(17) Å. The apical Cu–O distance is significantly longer than equatorial ones and is 2.3678(16) Å for complex **1** while 2.4053(16) Å for complex **2**. This lengthening of apical bond is not Jahn-Teller elongation and is attributed to the double electron occupancy of the antibonding  $a_1 (d_x^2 - y^2)$  orbital and single occupancy of  $b_1 (d_x^2 - y^2)$  leading to increased antibonding electron density along the apical Cu–Ligand accompanied with weak Cu–Ligand interaction along this axis. The angle between a Cu atom and two nitrogen atoms of dimer i.e., N–Cu–N is  $80.58(8)^\circ$  and  $80.26(8)^\circ$  for **1** and **2**, res-

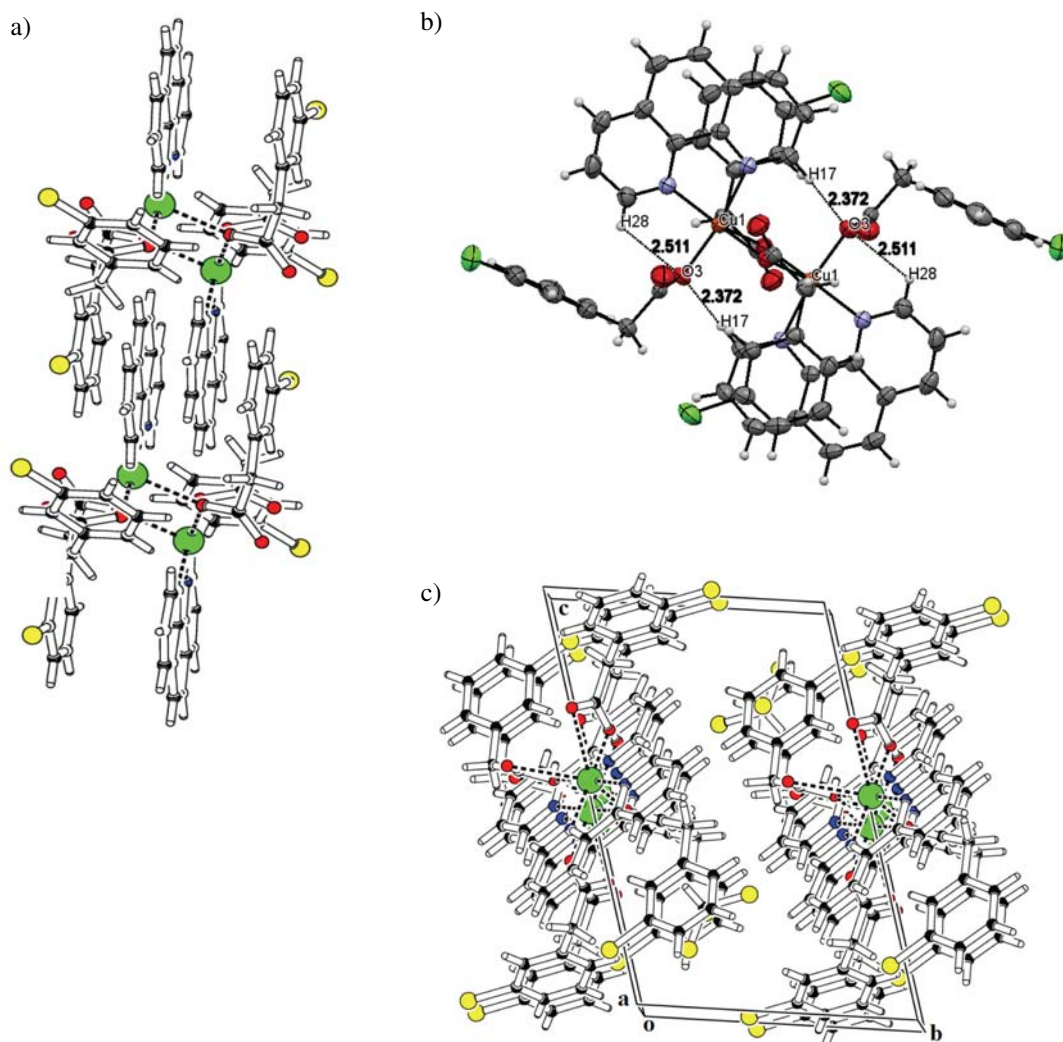


**Figure 2.** (a) intermolecular and intramolecular  $\pi$ - $\pi$  interactions, (b) intramolecular hydrogen bonding, (c) 3D close packing diagram of complex **1** and intermolecular hydrogen bonding.

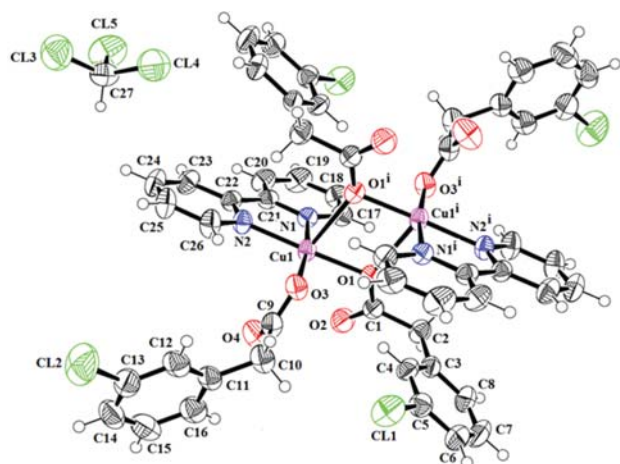


**Figure 3.** ORTEP diagram of complex **2** with thermal ellipsoids drawn at 50% probability level. The H-atoms are shown as small circles of arbitrary radii. One solvent molecule ( $\text{CHCl}_3$ ) has not been shown. Symmetry code  $i = -x, 2 - y, 1 - z$ .

pectively.<sup>32,34</sup> Smallest angle is observed between equatorial bridging oxygen atoms and a copper atom i.e.,  $\text{O1}-\text{Cu1}-\text{O1}^i$  of a dimeric unit and is equal to  $76.52(6)^\circ$  and  $77.68(7)^\circ$  for **1** and **2**, respectively. All the data of bond lengths and angles are comparable with previously reported similar  $\text{Cu}(\text{II})$  complexes with O- and N-donor ligands.<sup>35,36</sup>

Supramolecular interactions in complexes are different from one another owing to different dihedral planes and the presence of  $\text{CHCl}_3$  in **2**. In complex **1** two molecules of 3-chlorophenylacetate form different dihedral angles around copper which enable them to take part in  $\text{C}-\text{H}\cdots\text{O}$  interactions with 1,10-phenanthroline moiety of the neighboring molecule. Thus, the bridging carboxylate moiety is involved in intramolecular  $\pi$ - $\pi$  interactions with aromatic rings of 1,10-phenanthroline. Intramolecular hydrogen bonding is present between H17 and H18 atoms of 1,10-phenanthroline and O3 atoms of adjacent carboxylates ligand which is coordinated to metal atom with

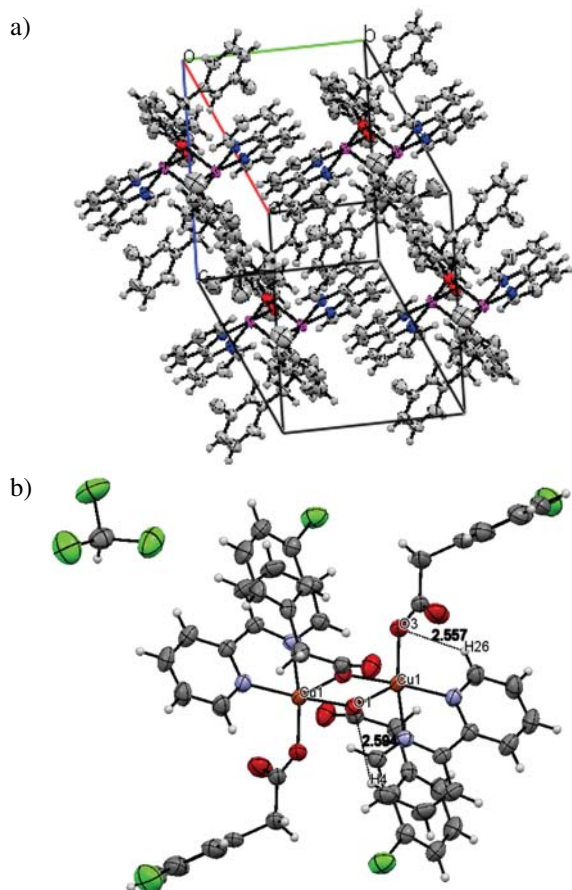


**Figure 4.** (a) 3D close packing diagram of complex **2**, (b) intramolecular hydrogen bonding.

**Table 2.** Selected bond lengths and angles of the complexes

Distances, Å		
	Complex 1	Complex 2
N1–Cu1	2.0284(18)	2.0094(19)
N2–Cu1	2.0392(19)	2.023(2)
O1–Cu1	1.9629(15)	1.9662(16)
O1–Cu1 <sup>i</sup>	2.3678(16)	2.4053(16)
O3–Cu1	1.9350(16)	1.9514(17)
Angles, °		
Cu1–O1–Cu1 <sup>i</sup>	103.48(6)	102.32(7)
O3–Cu1–O1	90.32(7)	91.07(7)
O3–Cu1–N1	169.94(8)	171.26(8)
O3–Cu1–N2	89.37(7)	93.32(8)
O1–Cu1–N1	96.46(7)	95.29(7)
O1–Cu1–N2	169.58(7)	175.53(7)
N1–Cu1–N2	80.58(8)	80.26(8)
O3–Cu1–O1 <sup>i</sup>	93.39(7)	91.79(7)
O1–Cu1–O1 <sup>i</sup>	76.52(6)	77.68(7)
N1–Cu1–O1 <sup>i</sup>	93.91(7)	95.41(7)
N2–Cu1–O1 <sup>i</sup>	113.54(7)	102.99(7)

Symmetry codes:  $i = 2 - x, -y, -z$  for **1**;  $i = -x, 2 - y, 1 - z$  for **2**.

H···A distance of 2.37 and 2.51 Å, respectively as shown in Fig. 2. Each monomer in crystal lattice is linked to another monomer through hydrogen bonds which arises between uncoordinated O2 and O4 atoms of carboxylate moiety and hydrogen atoms of phenanthroline rings with distance of 2.57 Å. In addition to this, Cl atoms also participate in intermolecular hydrogen bonding with near-

**Table 1.** Crystal data and structure refinement parameters for the complexes

	<b>1</b>	<b>2</b>
Empirical Formula	C <sub>56</sub> H <sub>40</sub> Cl <sub>4</sub> Cu <sub>2</sub> N <sub>4</sub> O <sub>8</sub>	C <sub>54</sub> H <sub>42</sub> Cl <sub>10</sub> Cu <sub>2</sub> N <sub>4</sub> O <sub>8</sub>
Formula weight (g mol <sup>-1</sup> )	1165.80	1356.49
Crystal system	Triclinic	Triclinic
Space group	<i>P</i> -1	<i>P</i> -1
Unit cell dimensions		
<i>a</i> (Å)	8.8156(4)	9.8539(4)
<i>b</i> (Å)	11.0165(6)	10.3186(4)
<i>c</i> (Å)	13.0297(7)	15.4092(7)
$\alpha$ (°)	72.853(3)	73.331(2)
$\beta$ (°)	83.183(3)	73.4550(10)
$\gamma$ (°)	89.275(3)	83.481(2)
<i>V</i> (Å <sup>3</sup> )	1200.28(11)	1437.93(11)
<i>Z</i>	1	1
$\rho_{\text{calc}}$ (g cm <sup>-3</sup> )	1.613	1.566
$\mu$ (mm <sup>-1</sup> )	1.173	1.261
<i>F</i> (000)	594	686
Reflections collected	18408	20560
Independent Reflections	5187	5608
Data/Restraints/Parameters	5187/0/334	5608/0/352
Goodness-of-fit on <i>F</i> <sup>2</sup>	1.016	1.032
<i>R</i> <sub>1</sub> , <i>wR</i> <sub>2</sub> indices [ <i>I</i> > 2σ( <i>I</i> )]	0.0373, 0.0871	0.0481, 0.1026
<i>R</i> <sub>1</sub> , <i>wR</i> <sub>2</sub> indices (all data)	0.0503, 0.0945	0.0375, 0.0953

by H atoms of phenyl rings. While intermolecular  $\pi$ - $\pi$  stacking interactions between two adjacent phenanthroline rings with centroid-to-centroid distance of 3.526–3.851 Å give rise to strong intermolecular interaction thus providing overall stability to the crystal lattice. This stacking effect present in the complex is comparable with stacking effect present in DNA strands and enables the complex to interact with DNA through intercalation.<sup>37,38</sup>

Similar intramolecular forces as well as intermolecular forces are present in complex **2** where two solvent molecules are integral part of the unit cell and further extend the intermolecular interactions. In this complex two carboxylate ligands i.e. 3-chlorophenylacetic acid also behave differently. One carboxylate moiety around one Cu atom of dimer (O1/O2/C11/C1–C8), in plane A (O1/C1/O2) is oriented at dihedral angle of 70.40(18)° with respect to plane B (C2–C8/C11). While second non-bridging carboxylate moiety (O3/O4/C12/C9–C16) in plane C (O3/C9/O4) makes dihedral angle of 56.85(24)° with plane D (C10–C16/C12). The 2,2'-bipyridine moiety in plane E (N1/N2/C17–C28) is planar with r.m.s. deviation of 0.0500. The dihedral angle between B/E is 23(11)°. This shows that bridging carboxylate moiety is involved in intramolecular  $\pi$ - $\pi$  interactions with aromatic rings of

2,2'-bipyridine. The intermolecular  $\pi$ - $\pi$  interactions arise between two adjacent bipyridine rings with centroid-to-centroid distance of 3.42–3.94 Å and give rise to stack effect thus enabling this complex to interact with DNA through intercalation.<sup>39,40</sup> Intramolecular hydrogen bonding in complex **2** is furnished by bridging oxygen atoms O1 and non-bridging oxygen atoms O3 with hydrogen atoms of phenyl rings of bipyridine as well as adjacent carboxylate ligand as shown in Fig. 4. Moreover, solvent molecules participate in intermolecular hydrogen bonding giving overall strength to the lattice.

### 2. 3. DNA Binding Studies Through UV-Visible Spectroscopy

UV-Visible spectroscopy has been employed to check the binding ability, extent of binding as well as mode of interaction of two complexes with DNA as shift in  $\lambda_{\max}$  and decrease in absorbance clearly indicates the mode and extent of binding of substance with DNA. A blue shift indicates electrostatic while red shift indicates intercalative binding mode. However, smaller red shift indicates groove binding mode of interactions. Both complexes showed small red shifts of 1–2 nm accompanied by strong

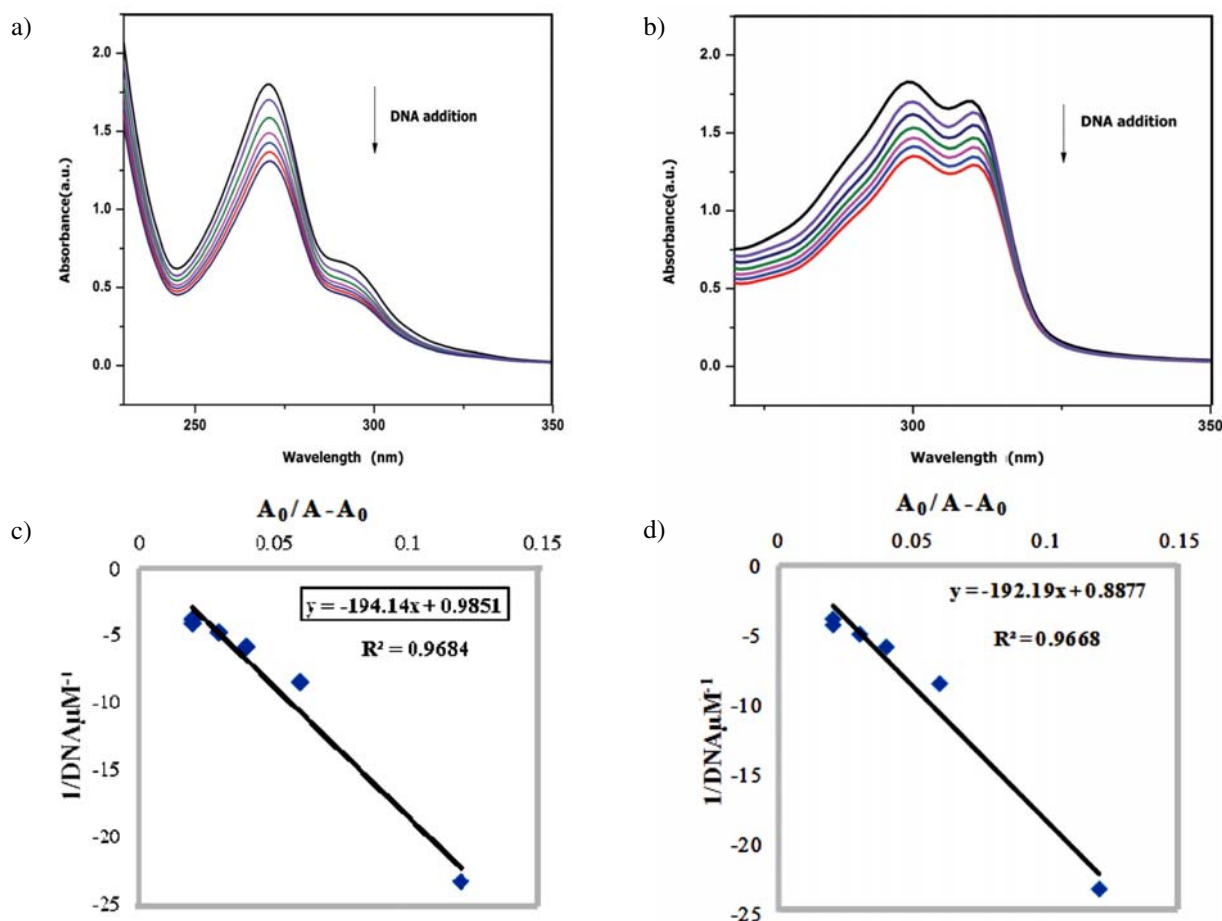


Figure 5. (a), (b) UV spectra of complexes **1** and **2**. (c), (d) plots of  $1/[DNA]$  along abscissa and  $A_0/A - A_0$  along ordinate for **1** and **2**, respectively.



hypochromism (decrease in absorbance) with subsequent addition of SSDNA solution. All these observations suggest partial intercalative and groove binding mode of interaction for complexes **1** and **2** with SSDNA.

Extent of interaction of complexes with SSDNA was judged by calculating binding parameter such as  $K_b$  which is binding constant and tells how strongly a chemical substance interacts with SSDNA during specific study.  $K_b$  for both complexes was calculated by using famous Benesi-Hildebrand equation<sup>41,42</sup> which is given below

$$\frac{A_o}{A - A_o} = \frac{\epsilon_G}{\epsilon_{H-G} - \epsilon_G} + \frac{\epsilon_G}{\epsilon_{H-G} - \epsilon_G} \frac{1}{K[DNA]} \quad (1)$$

Where  $K_b$  is binding constant,  $A$  and  $A_o$  are absorbance of complex-DNA adduct and pure complex solution.  $[DNA]$  represents the concentration of SSDNA in mol/L and  $\epsilon_{H-G}$ ,  $\epsilon_G$  are molar absorption co-efficients of complex-DNA adduct and pure complex, respectively. The value of  $K_b$  was calculated from intercept to slope ratio of the plot of  $1/[DNA]$  along abscissa and  $A_o/A - A_o$  along ordinate as shown in the Fig. 5.  $K_b$  value thus calculated was found to be  $5.07 \times 10^3 \text{ M}^{-1}$  for complex **1** with  $\Delta G = -21 \text{ kJ}$ , and  $4.62 \times 10^3 \text{ M}^{-1}$  for complex **2** with  $\Delta G = -20 \text{ kJ}$ . These values of binding constants are comparable with previously reported complexes of copper which bind with DNA.<sup>43,44</sup> Intercalative interaction of both complexes with SSDNA is attributed to  $\pi$ - $\pi$  stacking effect present in synthesized complexes which is comparable with stack effect present in DNA strand. Moreover negative  $\Delta G$  values reflect the spontaneity of these interactions.<sup>45,46</sup>

A 24 hrs absorption spectroscopic study of 0.2 mM/MeOH solutions of these complexes in visible region was carried in order to elucidate the structural stability of synthesized complexes in solution. It was observed that no shift in  $\lambda_{\text{max}}$  occurred during 24 hrs (Fig. 6a, b) confirming that square pyramidal geometry around copper atom

remains intact. On the basis of this observation it was proposed that both complexes might remain in dimeric form within the solution. However, a little increase in absorbance was noted which was attributed to local temperature variations during 24 hrs.

## 2. 4. Enzyme Inhibition Study of Complexes

### 2. 4. 1. $\alpha$ -Glucosidase Inhibition Assay

$\alpha$ -Glucosidase is an enzyme present in brush border of small intestine consisting of 952 amino acids with complex structure. It breaks down starch and disaccharides to glucose. Active sites of this enzyme consist of both electrophilic and nucleophilic centers. Blocking these active sites through suitable chemical agents can lead to its inactivity. Although copper ions have been found to lower the blood glucose level in diabetic patients yet, only few copper(II) complexes with amino acids and Schiff bases have been reported to date having  $\alpha$ -glucosidase inhibitory activity.<sup>47,48</sup> No structurally similar complexes like those described here have been reported to date having  $\alpha$ -glucosidase inhibitory activity. Keeping in view all these facts, *in vitro* anti-diabetic activity of synthesized complexes was investigated against pure  $\alpha$ -glucosidase enzyme using PNG as a substrate and was compared with acarbose. Acarbose is a standard drug for  $\alpha$ -glucosidase inhibitor which showed an  $IC_{50}$  value of 13.10  $\mu\text{M}$  (Table 3). Acarbose binds reversibly with active sites of  $\alpha$ -glucosidase enzyme and inhibits its activity through competitive mode. Both synthesized complexes showed good  $\alpha$ -glucosidase inhibitory activity in a dose dependent manner. The highest inhibitory activity was recorded for the compound **2** which exhibited 94% activity with  $IC_{50}$  30.1  $\mu\text{M}$  while compound **1** showed 78% inhibition with  $IC_{50}$  value of 34.6  $\mu\text{M}$  at the same concentration. It is interesting to note that  $IC_{50}$  values (Table 3) of both compounds are comparable representing their active anti-diabetic nature. This

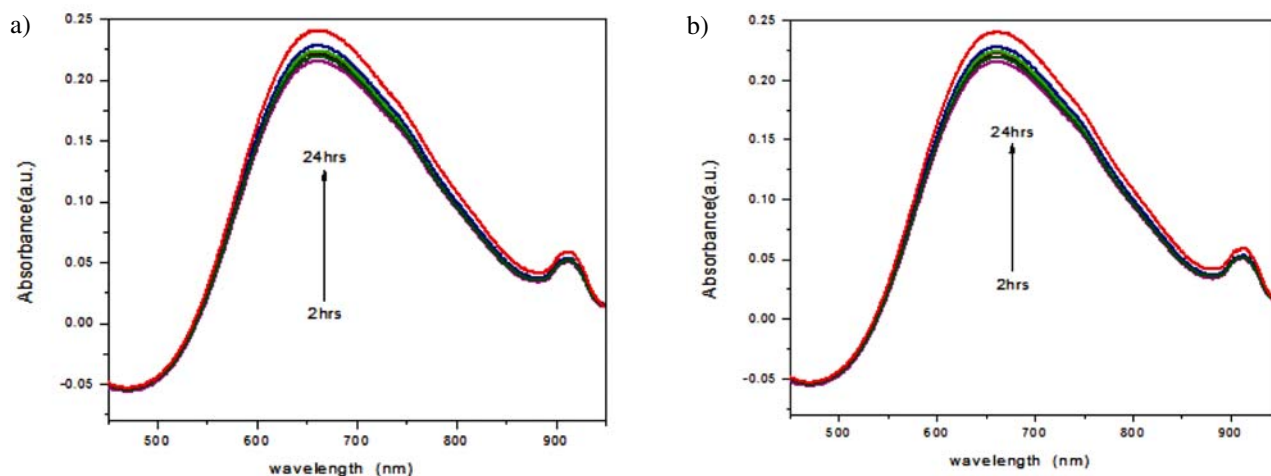
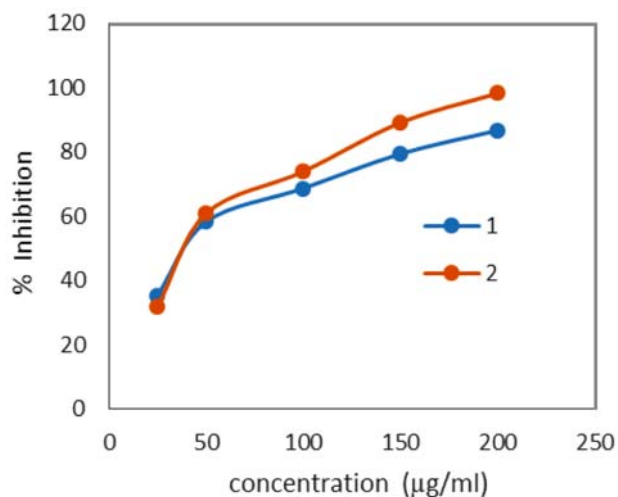


Figure 6. 24 hrs visible spectra of 0.2 mM/MeOH solutions of (a) **1** and (b) **2**.

percentage inhibition exhibited by synthesized complexes is found to be greater than previously reported Cu(II) complexes with nitrogen donor ligands like ethylenediamine.<sup>49</sup> A graph was plotted by taking % inhibition along y-axis and concentration of inhibitor along x-axis to check the mode of inhibition of complexes **1** and **2** as shown in Fig. 7. Both complexes exhibited enzyme inhibition activity in dose dependent manner.



**Figure 7.** Plot of concentration of **1** and **2** against % inhibition of enzyme.

It is proposed that in synthesized copper complexes the presence of fused pyridines and carboxylate ligands facilitates the transport of these complexes across the cell membrane and structural flexibility provided by carboxylate ligand enhances the chances of binding metal center of the complex with electron donors such as nitrogen present on the active site of enzyme and eventually inhibiting its activity. Moreover, from the literature it is evident that higher the capacity of inhibitor to establish hydrogen bonds with hydrogen donor and acceptors centers present on active site of an enzyme higher will be the inhibitory activity. Non-coordinated oxygen atoms of carboxylate ligands in these complexes provide opportunity to complexes to develop hydrogen bonds with amino-acids Thr-215

(H-bond acceptor) and Ser-244 (H-bond donor) present on active site of  $\alpha$ -glucosidase enzyme. This arrangement thus partially blocks the active sites for incoming substrate and finally partially inhibits its activity. The results of the assay reflected that these complexes have potential to inhibit this enzyme and can be suggested that such complexes incorporating copper as metal center and easily available ligands can provide a foundation in drug designing to cure type-II diabetes mellitus in future.<sup>50,51</sup>

#### 2. 4. 2. Anticholinesterase Assays

Acetylcholinesterases are critically important CNS and PNS enzymes that hydrolyze the neurotransmitter acetylcholine. The anticholinesterase activity of these new complexes was investigated *in vitro* using purified AChE and BChE enzymes and the results are summarized in Table 3. Galantamine hydrobromide is used as standard drug for AChE and BChE enzyme inhibitor which showed an  $IC_{50}$  value of 2.97 and 4.69  $\mu$ M, respectively (Table 3). This drug is successfully employed for the treatment of Alzheimer disease. It is reversible competitive inhibitor of acetylcholinesterase. As copper complexes have ability to bind with various proteins and because of encouraging results of  $\alpha$ -glucosidase enzyme inhibition assay, the synthesized complexes were further tested for their anticholinesterase capacity. The results of our assay showed that compound **1** showed moderate activity only against AChE with  $IC_{50}$  value of 179.4  $\mu$ M. On the other hand compound **2** showed good inhibitory activity against BChE with 76.3% inhibition at 200  $\mu$ g/mL with  $IC_{50}$  value 95.8  $\mu$ M. This moderate enzyme inhibition capacity of complexes is attributed to their ability of blocking the active sites on enzyme surface because of presence of electrophile and nucleophile acceptor centers present in the synthesized complexes.<sup>52,53</sup> Some copper complexes with curcumin and bis(thiosemicarbazones) have been reported which exhibit anti-Alzheimer activity through different routes, while other copper complexes with 2-(diphenylmethylene)hydrazinocarbothioamide, Schiff bases and flavanone have shown good anticholinesterase activity, yet no heteroleptic copper(II) complexes with phenyl acetic acid and N-donor ligands have been

**Table 3.** Enzyme inhibition activity of the newly synthesized compounds

Sr. No.	Complexes	$\alpha$ -glucosidase inhibition	$IC_{50}$ ( $\mu$ M)	
			Acetylcholinesterase inhibition	Butyrylcholinesterase inhibition
1	I	34.6	179.4	–
2	II	30.1	–	95.8
3	Acarbose	13.10	N.A	N.A
4	Galantamine hydrobromide	N.A	2.97	4.69

Where “N.A” means not applicable and “–” represents no activity

reported so far having anti-Alzheimer activity. So, all these findings can help in future drug designing for Alzheimer disease.<sup>54,55</sup>

### 3. Experimental

#### 3.1. Materials and Methods

All the analytical grade chemicals used in the study were purchased from Fluka, Switzerland, and used as received. Analytical grade methanol and chloroform were obtained from Merck, Germany, and were used without further purification. Doubly distilled water was used for synthesis. Melting points of both complexes were obtained in a capillary tube using Gallenkamp, serial number C040281, U.K, electrothermal melting point apparatus. CHN analysis was carried out with a Perkin-Elmer 2400 series-II instrument. FT-IR spectra were recorded on a Nicolet-6700 FT-IR spectrophotometer, Thermoscientific, USA, in the range of 4000 to 400  $\text{cm}^{-1}$ . UV-Visible spectra of **1** and **2** were recorded by employing UV-1800 Shimadzu spectrometer within wavelength range of 190–800 nm where lower cut off region was found to be 220 nm. For UV-visible measurements 0.2 mM solutions of **1** and **2** were prepared in methanol at room temperature.

#### 3.2. Synthesis of **1** and **2**

One-pot synthesis scheme was employed for synthesis of both complexes by subsequent addition of  $\text{NaHCO}_3$  (0.42 g, 5.0 mmol) to 3-chlorophenylacetic acid (0.85 g, 5.0 mmol) in distilled water at 60 °C with continuous stirring. When effervescence was stopped in the reaction mixture aqueous solution of copper sulphate (0.72 g, 2.5 mmol) was added drop wise and mixture was stirred for next three hours. After that, 1,10-phenanthroline (0.49 g, 2.5 mmol) for complex **1** and 2,2'-bipyridine (0.40 g, 2.5 mmol) for complex **2** was added in reaction mixture and stirring was continued for next three hours. Precipitates of both complexes were separated from the reaction mixture by filtration and washed thoroughly with distilled water and air dried. Later on both complexes were recrystallized from chloroform and analyzed by FT-IR and X-ray single crystal analyses.

Dark blue crystals (**1**); yield (75%). Anal. Calcd. for  $\text{C}_{56}\text{H}_{40}\text{Cl}_4\text{Cu}_2\text{N}_4\text{O}_8$  (%): calc. C, 57.64%; H, 3.43%; N, 4.80%; found: C, 56.45%; H, 3.23%; N, 4.54%; m.p. 171–172 °C; FT-IR ( $\text{cm}^{-1}$ ): 1625  $\nu(\text{OCO})_{\text{asym}}$ , 1427  $\nu(\text{OCO})_{\text{sym}}$ ,  $\Delta\nu = 198$ , 2980  $\nu(\text{Ar-H})$ , 1519, 1562  $\nu(\text{Ar}(\text{C}=\text{C}))_{\text{sym}}$ , 723  $\nu(\text{Ar-Cl})$ , 611  $\nu(\text{Cu-O})$ , 482  $\nu(\text{Cu-N})$ ;  $\epsilon = 93.4 \text{ L mol}^{-1} \text{ cm}^{-1}$ .

Light blue crystals (**2**); yield (70%) Anal. Calcd. for  $\text{C}_{54}\text{H}_{42}\text{Cl}_{10}\text{Cu}_2\text{N}_4\text{O}_8$  (%): calc. C, 47.77%; H, 3.09%; N, 4.13%; found: C, 46.87%; H, 2.93%; N, 4.05%; m.p. 164–165 °C; FT-IR ( $\text{cm}^{-1}$ ): 1633  $\nu(\text{OCO})_{\text{asym}}$ , 1444  $\nu(\text{OCO})_{\text{sym}}$ ,  $\Delta\nu = 189$ , 3080  $\nu(\text{Ar-H})$ , 1604, 1566

$\nu(\text{Ar}(\text{C}=\text{C}))$ , 769  $\nu(\text{Ar-Cl})$ , 605  $\nu(\text{Cu-O})$ , 479  $\nu(\text{Cu-N})$ ;  $\epsilon = 92.2 \text{ L mol}^{-1} \text{ cm}^{-1}$ .

#### 3.3. X-ray Crystallographic Study

Crystallographic data were collected at 296 K using an Oxford Gemini Ultra S CCD diffractometer using graphite monochromatic Mo-K $\alpha$  radiations ( $\lambda = 0.71073 \text{ \AA}$ ). Data reduction and empirical absorption corrections were accomplished using CrysAlisPro. Structures were solved by direct methods using SHELXS-86 and refined by full matrix least-squares analysis against  $F^2$  with SHELXL-2014/7 within the WinGX package. The drawings of the complexes were produced using ORTEP3.<sup>56–58</sup>

#### 3.4. DNA Interaction Studies by Absorption Spectroscopy

Suitable amount of salmon sperm DNA (SSDNA) was dissolved in distilled water and stirred for overnight before use. The nucleotide to protein (N/P) ratio of ~ 1.7 was obtained from the ratio of absorbance at 260 nm and 280 nm ( $A_{260}/A_{280} = 1.7$ ), for prepared DNA solution which indicated that solution is free of proteins. The SSDNA concentration was determined by absorption spectroscopy using molar absorption coefficient of 6600  $\text{M}^{-1} \text{ cm}^{-1}$  (260 nm) for SSDNA. Solutions of both complexes for UV-Visible spectrophotometric analysis were prepared in methanol at a concentration of 0.2 mM. The absorption titrations were performed by keeping complexes concentration constant with change of SSDNA at the rate of 150  $\mu\text{L}$  to aliquots to eliminate the absorbance of SSDNA itself. The solutions were allowed to incubate for 30 mins at room temperature before the measurements were made. Absorption spectra were recorded using cuvettes of 1 cm path length at room temperature.

#### 3.4. Enzyme Inhibition Assays

##### 3.4.1. $\alpha$ -Glucosidase and Amylase Inhibition

Anti-diabetic property of synthesized complexes was evaluated by previously reported  $\alpha$ -glucosidase enzyme inhibition assay with modifications.<sup>59</sup>  $\alpha$ -glucosidase from *Saccharomyces cerevisiae* (Sigma-Aldrich) was dissolved in 50 mM potassium phosphate buffer (pH 6.8) to make enzyme stock solution (1 unit/mL) and *p*-nitrophenyl- $\alpha$ -D-glucopyranoside (PNG) prepared in same buffer at 20 mM was used as substrate. Assay was performed in triplicate in 96-well plates and samples were prepared in DMSO with 200, 100 and 50 ppm final concentration. For experiment, in each well 25  $\mu\text{L}$  of PNG, 65  $\mu\text{L}$  of phosphate buffer (50 mM, pH 6.8), 5  $\mu\text{L}$  of test sample and 5  $\mu\text{L}$  of  $\alpha$ -glucosidase enzyme (0.05 U/mL) were used. Acarbose and DMSO were used as positive and negative controls, respectively. Plates were incubated

at 37 °C for 30 min, followed by addition of 0.5 mM sodium bicarbonate (100  $\mu$ L) as stopping agent. Percentage activity was measured by the following formula after taking absorbance ( $A$ ) at 405 nm using microplate reader (BioTek Elx-800, USA).  $IC_{50}$  was calculated by using Graph pad Prism 5 according to the equation:

$$\% \text{ Inhibition} = [(A_{\text{control}} - A_{\text{sample}}) / A_{\text{control}}] \times 100$$

### 3. 4. 2. Anticholinesterase Assays

The anticholinesterase potential of newly synthesized complexes was determined by the previously reported colorimetric method with modifications.<sup>60</sup> In this study, acetylcholinesterase (AChE) and butyrylcholinesterase (BChE) activity assay was performed by using acetylthiocholine iodide (AChI) and butyrylthiocholine iodide (BChI) as substrates, respectively. Assay was performed in triplicate in 96-well plates and samples were prepared in DMSO with 200, 100 and 50 ppm final concentration. 5  $\mu$ L of sample, 20  $\mu$ L of 0.1 mM sodium phosphate buffer (pH 8.0) and 5  $\mu$ L enzyme preparation (0.05 U/mL) of AChE and BChE, respectively. Then 10  $\mu$ L substrate solution was added with final concentrations of 15 mM for AChI and 4 mM for BChI followed by the addition of 60  $\mu$ L DTNB-phosphate-ethanol reagent (3 mM). The reaction mixtures were then incubated for 30 min at 37 °C. Galantamine hydrobromide (Sigma) and DMSO were used as positive and negative controls, respectively. Percentage activity was measured by the following formula after taking absorbance ( $A$ ) at 405 nm using microplate reader (BioTek Elx-800, USA).  $IC_{50}$  was calculated by using Graphpad Prism 5 according to the equation:<sup>61</sup>

$$\% \text{ Inhibition} = [(A_{\text{control}} - A_{\text{sample}}) / A_{\text{control}}] \times 100$$

## 4. Conclusion

Two isostructural dimeric heteroleptic Cu(II) complexes have been synthesized and characterized by UV-Visible, FTIR and XRD techniques. The data revealed slightly distorted square pyramidal geometry around each Cu atom and monodentate coordination mode of carboxylate ligands with metal atom in both complexes. DNA binding ability is checked through UV-Visible spectroscopy which revealed strong binding tendency of both complexes with SSDNA with  $K_b = 5.07 \times 10^3 \text{ M}^{-1}$  for complex **1** with  $\Delta G = -21 \text{ kJ}$ , and  $K_b = 4.62 \times 10^3 \text{ M}^{-1}$  for complex **2** with  $\Delta G = -20 \text{ kJ}$ . Enzyme inhibition assay of both complexes disclosed their potential therapeutic applications as anti-diabetic as well as anti-Alzheimer's disease in dose dependent manner with  $IC_{50}$  ( $\mu$ M) values of 34.6 and 30.1 for  $\alpha$ -glucosidase for complexes **1** and **2**, respectively.  $IC_{50}$  values for acetylcholinesterase and butyrylcholinesterase were found to be 179.4 and 95.8  $\mu$ M for complexes **1** and **2**, respectively. On the basis of this data we proposed that both synthesized complexes are biologically active

and in future could provide a solid foundation in drug designing.

## 5. Acknowledgements

We would like to thank Higher Education Commission of Pakistan for providing financial support for the research work. We are also thankful for single-crystal analysis undertaken at Department of Physics, University of Sargodha, Pakistan.

## 6. Appendix A. Supplementary data

Crystallographic data for the structures reported in this paper has been deposited with the Cambridge Crystallographic Data Centre, CCDC #1473940 and 1473941 for **1** and **2** respectively. Copies of this information may be obtained free of charge from The Director, CCDC, 12, Union Road Cambridge CB2 1EZ [Fax: +44 (1223)336 033] or e.mail: deposit @ccdc.cam.ac.uk.

## 7. References

1. S. Kannan, G. Venkatachalam, H. J. Lee, B. K. Min, W. Kim, E. Koo, Y. R. Do, S. Yoon, *Polyhedron* **2011**, *30*, 340–346. <https://doi.org/10.1016/j.poly.2010.10.019>
2. L. N. Jin, Q. Liu, W. Y. Sun, *Cryst. Eng. Comm.* **2014**, *16*, 3816–3828. <https://doi.org/10.1039/c3ce41962b>
3. J. Hansen, B. Li, E. Dikarev, J. Autschbach, H. M. L. Davies, *J. Org. Chem.* **2009**, *17*, 6564–6571. <https://doi.org/10.1021/jo900998s>
4. J. C. Zhong, F. Wan, Y. Q. Sun, Y. P. Chen, *J. Solid State Chem.* **2015**, *221*, 14–20. <https://doi.org/10.1016/j.jssc.2014.08.037>
5. R. Jayakumar, M. Rajkumar, R. Nagendran, S. Nanjundan, *J. Appl. Polym. Sci.* **2002**, *85*, 1194–1206. <https://doi.org/10.1002/app.10694>
6. M. V. Marinho, M. I. Yoshida, K. J. Guedes, K. Krambrock, A. J. Bortoluzzi, M. Horner, F. C. Machado, W. M. Teles, *Inorg. Chem.* **2004**, *43*, 1539–1544. <https://doi.org/10.1021/ic035251y>
7. L. You, W. Zong, G. Xiong, F. Ding, S. Wang, B. Ren, I. Dragutan, V. Dragutan, Y. Sun, *Appl. Catal., A* **2016**, *511*, 1–10.
8. K. L. Haas, K. J. Franz, *Chem. Rev.* **2009**, *109*, 4921–4960. <https://doi.org/10.1021/cr900134a>
9. T. K. Sawyer, *Chem. Biol. Drug. Des.* **2006**, *67*, 196–200. <https://doi.org/10.1111/j.1747-0285.2006.00371.x>
10. R. Vafazadeh, N. Hasanzade, M. M. Heidari, A. C. Willis, *Acta Chim. Slov.* **2015**, *62*, 122–129. <https://doi.org/10.17344/acsi.2014.797>
11. S. P. Fricker, *Dalton Trans.* **2007**, *43*, 4903–4917. <https://doi.org/10.1039/b705551j>
12. S. J. Lippard, J. M. Berg, Principles of Bioinorganic Chemi-

- stry, University Science Books, Mill Valley, **1994**, 411–412.
13. R. H. Holm, P. Kennepohl, E. I. Solomon, *Chem. Rev.* **1996**, *96*, 2239–2314. <https://doi.org/10.1021/cr9500390>
14. S. Mandal, R. Sadhukhan, U. Ghosh, S. Mandal, M. Saha, R. J. Butcherd, N. C. Saha, *J. Coord. Chem.* **2016**, *69*, 1618–1634. <https://doi.org/10.1080/00958972.2016.1174773>
15. R. Vafazadeh, F. Jafari, M. M. Heidari, A. C. Willis, *J. Coord. Chem.* **2016**, *69*, 1313–1325. <https://doi.org/10.1080/00958972.2016.1163547>
16. G. J. Brewer, *J. Am. Coll. Nutr.* **2009**, *28*, 238–242. <https://doi.org/10.1080/07315724.2009.10719777>
17. K. Balamurugan, W. Schaffner, *BBA Mol. Cell. Res.* **2006**, *1763*, 737–746.
18. R. Vafazadeh, Z. Moghadas, A. C. Willis, *J. Coord. Chem.* **2015**, *68*, 4255–4271. <https://doi.org/10.1080/00958972.2015.1096349>
19. N. Shahabadi, S. M. Fili, M. Shahlaei, *J. Coord. Chem.* **2015**, *68*, 3667–3684. <https://doi.org/10.1080/00958972.2015.1078897>
20. O. O. E. Onawumi, O. O. P. Faboya, O. A. Odunola, T. K. Prasad, M. V. Rajasekharan, *Polyhedron* **2008**, *27*, 113–117. <https://doi.org/10.1016/j.poly.2007.08.041>
21. F. Tisato, C. Marzano, M. Porchia, M. Pellei, C. Santini, *Med. Res. Rev.* **2010**, *30*, 708–749.
22. J. O. Noyce, H. Michels, C. W. Keevil, *Appl. Environ. Microb.* **2007**, *73*, 2748–2750. <https://doi.org/10.1128/AEM.01139-06>
23. G. Borkow, *J. Gabbay, FASEB J.* **2004**, *18*, 1728–1730.
24. Z.-J. Chen, C.-N. Xu, J.-L. Zhu, D.-D. Yang, S.-S. Zhao, Y.-N. Chen, S.-S. Qian, *Acta Chim. Slov.* **2016**, *63*, 165–172. <https://doi.org/10.17344/acs.2015.2109>
25. Y. Wang, X. Zhang, Q. Zhang, Z. Yang, *BioMetals.* **2016**, *23*, 265–273. <https://doi.org/10.1007/s10534-009-9284-6>
26. T. Suksrichavalit, S. Prachayasittikul, C. N. Chartchalerm, I. N. Ayudhya, V. Prachayasittikul, *Eur. J. Med. Chem.* **2009**, *44*, 3259–3265. <https://doi.org/10.1016/j.ejmech.2009.03.033>
27. M. Hazra, T. Dolai, A. Pandey, S. Kumar Dey, A. Patra, *Bioinorg. Chem. Appl.* **2014**, *2014*, 1–13.
28. N. Ali, M. N. Tahir, S. Ali, M. Iqbal, K. S. Munawar, S. Perveen, *J. Coord. Chem.* **2014**, *67*, 1290–1308. <https://doi.org/10.1080/00958972.2014.910653>
29. S. T. Hafeez, S. Ali, M. N. Tahir, M. Iqbal, K. S. Munawar, *J. Coord. Chem.* **2014**, *67*, 2479–2495. <https://doi.org/10.1080/00958972.2014.940922>
30. S. T. Hafeez, M. N. Tahir, S. Ali, M. Iqbal, H. Gulab, K. S. Munawar, *J. Coord. Chem.* **2015**, *68*, 3636–3650. <https://doi.org/10.1080/00958972.2015.1073269>
31. Saeed-Ur-Rehman, S. Rehman, M. Ikram, F. Ullah, *J. Saudi Chem. Soc.* **2013**, *17*, 353–359. <https://doi.org/10.1016/j.jscs.2011.04.012>
32. M. A. Halcrow, *Chem. Soc. Rev.* **2013**, *42*, 1784–795. <https://doi.org/10.1039/C2CS35253B>
33. A. W. Addison, T. N. Rao, J. Reedijk, J. van Rijn, G. C. Verschoor, *J. Chem. Soc., Dalton Trans.*, **1984**, 1349–1356. <https://doi.org/10.1039/DT9840001349>
34. N. Alarcón-Payer, T. Pivetta, D. Choquesillo-Lazarte, J. M. González-Pérez, G. Crisponi, A. Castineiras, J. Niclos-Gutiérrez, *Inorg. Chim. Acta.* **2005**, *358*, 1918–1926. <https://doi.org/10.1016/j.ica.2004.12.056>
35. L. J. Daumann, P. Comba, J. A. Larrabee, G. Schenk, R. Stranger, G. Cavigliasso, L. R. Gahan, *Inorg. Chem.* **2013**, *52*, 2029–2043. <https://doi.org/10.1021/ic302418x>
36. M. Iqbal, S. Ali, Z. Rehman, N. Muhammad, M. Sohail, V. Pandarinathan, *J. Coord. Chem.* **2014**, *67*, 1731–1745. <https://doi.org/10.1080/00958972.2014.926337>
37. Y. Sikdar, R. Modak, D. Bose, S. Banerjee, D. Bienko, W. Zierkiewicz, A. Bienko, K. D. Saha, S. Goswami, *Dalton Trans.* **2015**, *44*, 8876–8888. <https://doi.org/10.1039/C5DT00752F>
38. S. H. Sun, Z. G. Sun, Y. Y. Zhu, D. P. Dong, C. Q. Jiao, J. Zhu, J. Li, W. Chu, H. Tian, M. J. Zheng, W. Y. Shao, Y. F. Lu, *Cryst. Growth. Des.* **2012**, *13*, 226–238. <https://doi.org/10.1021/cg301392p>
39. T. R. Cook, Y. R. Zheng, P. J. Stang, *Chem. Rev.* **2012**, *113*, 734–777. <https://doi.org/10.1021/cr3002824>
40. J. Sun, H. Xu, *Molecules* **2010**, *15*, 8349–8359. <https://doi.org/10.3390/molecules15118349>
41. R. R. Pulimamidi, R. Nomula, R. Pallepogu, H. Shaik, *Eur. J. Med. Chem.* **2014**, *79*, 117–127. <https://doi.org/10.1016/j.ejmech.2014.03.084>
42. N. Sohrabi, *J. Pharm. Sci. Res.* **2015**, *7*, 533–537.
43. D. Tiwari, A. K. Mishra, S. B. Mishra, B. B. Mamba, B. Maji, S. Bhattacharya, *Spectrochim. Acta Part A* **2011**, *79*, 1050–1056. <https://doi.org/10.1016/j.saa.2011.04.018>
44. R. Gomathi, A. Ramu, A. Murugan, *Bioinorg. Chem. Appl.* **2014**, *2014*, 215–230.
45. J. Borowska, M. Sierant, E. Sochacka, D. Sanna, E. L. Chruscinaska, *J. Bio. Inorg. Chem.* **2015**, *20*, 989–1004. <https://doi.org/10.1007/s00775-015-1282-2>
46. R. Miyazaki, H. Yasui, Y. Yoshikawa, *Open J. Inorg. Chem.* **2016**, *6*, 114–124. <https://doi.org/10.4236/ojic.2016.62007>
47. Y. Yoshikawa, R. Hirata, H. Yasui, H. Sakurai, *Biochimie* **2009**, *91*, 1339–1341. <https://doi.org/10.1016/j.biochi.2009.06.005>
48. P. Tripathi, M. M. Kumar, M. Chinmayi, T. Ruchita, S. L. Kant, P. K. Bihari, K. Arti, *Res. J. Chem. Sci.* **2013**, *3*, 54–59.
49. M. Qazzaz, R. A. Ghani, M. Metani, R. Husein, A. L. Abu-Hijleh, A. S. A. Ghani, *Biol. Trace Elem. Res.* **2013**, *154*, 88–96. <https://doi.org/10.1007/s12011-013-9697-5>
50. M. Zhou, J. H. Zhou, Y. Meng, M. B. Chen, *J. Chem. Theory Comput.* **2006**, *2*, 157–165. <https://doi.org/10.1021/ct050168g>
51. H. Park, K. Y. Hwang, Y. H. Kim, K. H. Oh, J. Y. Lee, K. Kim, *Bioorg. Med. Chem. Lett.* **2008**, *18*, 3711–3715. <https://doi.org/10.1016/j.bmcl.2008.05.056>
52. Y. M. Cui, X. W. Dong, W. Chen, W. J. Wang, Y. G. Li, H. L. Zhu, *J. Enzym. Inhibit. Med. Chem.* **2012**, *27*, 528–532. <https://doi.org/10.3109/14756366.2011.599065>
53. S. Wanninger, V. Lorenz, A. Subhan, F. T. Edelman, *Chem. Soc. Rev.* **2015**, *44*, 4986–5002.

- <https://doi.org/10.1039/C5CS00088B>
54. B. M. Paterson, P. S. Donnelly, *Chem. Soc. Rev.* **2011**, *40*, 3005–3018. <https://doi.org/10.1039/c0cs00215a>
55. Y. C. Chan, A. S. M. Ali, M. Khairuddean, K. Y. Khaw, V. Murugaiyah, A. Basiri, *Chinese Chem. Lett.* **2013**, *24*, 609–612. <https://doi.org/10.1016/j.ccllet.2013.04.013>
56. G. M. Sheldrick, SHELX Release 97.2 ed., University of Göttingen, Göttingen, **1997**.
57. L. J. Farrugia, *J. Appl. Crystallogr.* **1999**, *32*, 837–838. <https://doi.org/10.1107/S0021889899006020>
58. L. J. Farrugia, *J. Appl. Crystallogr.* **1997**, *30*, 565–566. <https://doi.org/10.1107/S0021889897003117>
59. G. L. Ellman, K. D. Courtney, V. Andres, R. M. Featherstone, *Biochem. Pharmacol.* **1977**, *7*, 88–95. [https://doi.org/10.1016/0006-2952\(61\)90145-9](https://doi.org/10.1016/0006-2952(61)90145-9)
60. F. S. Aziz-ur-Rehman, N. Afza, A. Malik, L. Iqbal, M. A. Rasool, M. I. Ali, R. B. Tareen, *J. Enzym. Inhibit. Med. Chem.* **2009**, *24*, 1128–1132.
61. V. Gorun, I. Proinov, V. Baltescu, G. Balaban, O. Barzu, *Anal. Biochem.* **1978**, *86*, 324–326. [https://doi.org/10.1016/0003-2697\(78\)90350-0](https://doi.org/10.1016/0003-2697(78)90350-0)

## Povzetek

Sintetizirali smo dva nova dvojedrna bakrova(II) karboksilata z O-mostom s kemijsko formulo  $[\text{Cu}_2(3\text{-Cl-C}_6\text{H}_4\text{CH}_2\text{COO})_4(\text{phen})_2]$  (**1**) in  $[\text{Cu}_2(3\text{-Cl-C}_6\text{H}_4\text{CH}_2\text{COO})_4(\text{bipy})_2]$  (**2**), kjer je phen = 1,10-fenantrolin in bipy = 2,2'-bipiridin, ter ju okarakterizirali z FT-IR in UV-vidno spektroskopijo, CHN analizo in monokristalno rentgensko difrakcijo. Strukturna analiza razkriva popačeno kvadratno-piramidalno geometrijo okoli vsakega bakrovega centra v **1** in **2**. Študij interakcij z DNA kaže na močno vezavo s  $K_b = 5.07 \times 10^3$  in  $4.62 \times 10^3 \text{ M}^{-1}$  za **1** in **2**. Oba kompleksa izkazujeta močno inhibicijo encimov in sicer 70% in 90% inhibicijo  $\alpha$ -glukozidaze z  $\text{IC}_{50} = 34.6$  in  $30.1 \mu\text{M}$  za **1** in **2**, pri čemer smo uporabili akarbozo kot kontrolo. Oba kompleksa pa sta neaktivna proti  $\alpha$ -amilazi. Ob uporabi galantamin hidrobromida kot kontrole, **1** izraža delno inhibitorno aktivnost (47%) z  $\text{IC}_{50} = 179.4 \mu\text{M}$  proti acetilholin esterazi, medtem ko **2** izraža močno inhibitorno aktivnost (76%) z  $\text{IC}_{50} = 95.8 \mu\text{M}$  proti butirilholin esterazi. Rezultati kažejo anti-diabetično in anti-Alzheimerjevo delovanje obeh sintetiziranih kompleksov.

Scientific paper

# Synthesis and Structural Characterization of a Double Helical Dinuclear Copper(II) Complex With Tetradentate Biacetyl Bis(benzoylhydrazone)

Rasoul Vafazadeh,<sup>1,\*</sup> Najmeh Abdollahi<sup>1</sup> and Anthony C. Willis<sup>2</sup><sup>1</sup> Department of Chemistry, Yazd University, Yazd, Iran.<sup>2</sup> Research School of Chemistry, Australian National University, Canberra, ACT 2601, Australia.\* Corresponding author: E-mail: (RasoulVafazadeh) rvafazadeh@yazd.ac.ir and rvafazadeh@gmail.com  
Tel: +98 3538214778 Fax: +98 3537250110

Received: 06-02-2017

## Abstract

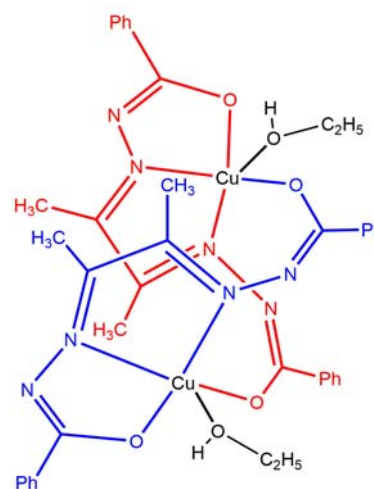
The reaction of tetradentate hydrazone ligand H<sub>2</sub>babh with Cu(CH<sub>3</sub>COO)<sub>2</sub> in methanol solvent leads to the formation of the mono-nuclear complex [Cu(babh)]. However, on being dissolved in dichloromethane solvent and on addition of ethanol solvent, a dinuclear complex of [Cu<sub>2</sub>(μ<sub>1,3</sub>-babh)<sub>2</sub>(C<sub>2</sub>H<sub>5</sub>OH)<sub>2</sub>] is obtained. The X-ray crystallography indicates that the dinuclear helical complex formation is caused due to the unsymmetrical twisting of the H<sub>2</sub>babh ligand. One oxygen and two nitrogen atoms from the ligand and one oxygen atom from the other ligand coordinate to each copper(II) center. Both the copper(II) centers in a dinuclear unit are penta-coordinate with a slightly distorted square pyramidal geometry. The IR spectra of mono- and dinuclear copper(II) complexes have different bands. The absorption spectra of mono- and di-nuclear complexes are quite similar in methanol solvent. However, the electronic absorption spectra of the two complexes are basically different in the solid state.

**Keyword:** Copper(II) complex; Hydrazone ligand; Dinuclear; Helical complex; Unsymmetrical twisting

## 1. Introduction

The design and construction of multinuclear transition metal complexes have attracted great interest in recent years because of the role that these metal systems play in a large number of biological processes, molecular magnetic materials, and their variety of structures and interesting properties.<sup>1–8</sup> Among them, the synthesis and study of multinuclear copper(II) complexes has attracted considerable interest due to exploration of their structures, and also because the function of copper(II) centers in many important biological process.<sup>8–12</sup>

There are a variety of strategies for synthesizing homo- and hetero-multinuclear complexes. The bridging ligands such as halides, pseudo-halides, oxalate, sulfate, etc. have been widely used in the synthesis of multinuclear complexes.<sup>13–16</sup> In the self-assembly process, the constituent ligands play important roles in the synthesis of polynuclear copper(II) compounds. The most common ligands used for the construction of these complexes are especially Schiff base ligands, which contain potentially



Scheme 1. Structure of dinuclear copper(II) complex

bridging phenoxo or hydroxo oxygen donor atoms.<sup>11,17,18</sup> The other strategy for the formation of these complexes

are helicity processes. Helical structures are often formed via a self-assembly process by ligands that connect two or more bidentate coordinating units with appropriate spacers and two or more metal ions.<sup>19–21</sup>

Herein, we have described the synthesis and crystal structures of a dinuclear copper(II) complex double helicates with the tetradentate N<sub>2</sub>O<sub>2</sub>-donor ligand biacetyl bis(benzoylhydrazone), H<sub>2</sub>babh (Scheme 1). Also, the structure of the complex is compared with mono- and dinuclear copper(II) complexes that have been previously reported with the H<sub>2</sub>babh ligand.<sup>21,22</sup>

## 2. Experimental

### 2.1. Materials

The tetradentate hydrazone ligand, H<sub>2</sub>babh, and the mononuclear complex [Cu(babh)] were prepared as previously reported elsewhere by others.<sup>21</sup> All chemicals were used as supplied by Merck and Fluka without further purification.

### 2.2. Physical Measurements

Infrared spectra were taken with an Equinox 55 Bruker FT-IR spectrometer using KBr pellets in the 400–4000 cm<sup>-1</sup> range. Absorption spectra were determined in the solvent methanol using a GBC UV-Visible Cintra 101 spectrophotometer with 1 cm quartz, in the range of 200–800 nm at 25 °C. The electronic spectra in the solid state were recorded on a Jasco V-670 UV-VIS spectrophotometer in the range of 200–800 nm. Elemental analyses (C, H, N) were performed using a CHNS-O 2400II PERKIN-ELMER elemental analyzer.

### 2.3. X-ray Crystallography

Diffraction images were measured at 150 K on a Nonius Kappa CCD diffractometer using Cu K $\alpha$  with graphite monochromator ( $\lambda = 1.54184$  Å). Data was extracted using the *CrysAlis PRO* Agilent Technologies. The structures were solved by direct methods with the use of SIR92 and refined on  $F^2$  by full matrix least-squares techniques using the CRYSTALS program package.<sup>23,24</sup> Crystallographic details are summarized in Table 1.

### 2.4 Synthesis of the

#### [Cu<sub>2</sub>( $\mu_{1,3}$ -babh)<sub>2</sub>(C<sub>2</sub>H<sub>5</sub>OH)<sub>2</sub>] Complex

The [Cu<sub>2</sub>( $\mu_{1,3}$ -babh)<sub>2</sub>(C<sub>2</sub>H<sub>5</sub>OH)<sub>2</sub>] complex was prepared by first adding the [Cu(babh)] (0.192 g, 0.500 mmol) complex in dichloromethane solvent (30 mL). The solution was stirred at room temperature for 2 h. The resulting brown solution was filtered and ethanol (15 mL) was added to the solution. After two days, crystals of brown needles were obtained by slow evaporation of the

**Table 1.** Crystallographic data of [Cu<sub>2</sub>( $\mu_{1,3}$ -babh)<sub>2</sub>(C<sub>2</sub>H<sub>5</sub>OH)<sub>2</sub>] complex

Compound	[Cu <sub>2</sub> ( $\mu_{1,3}$ -babh) <sub>2</sub> (C <sub>2</sub> H <sub>5</sub> OH) <sub>2</sub> ]
Chemical formula	C <sub>40</sub> H <sub>44</sub> Cu <sub>2</sub> N <sub>8</sub> O <sub>6</sub>
Formula weight	859.93
Temperature (K)	150
Space group	Triclinic, $P\bar{1}$
Z	2
Unit cell dimensions	
<i>a</i> (Å)	8.4016(4)
<i>b</i> (Å)	15.5626(5)
<i>c</i> (Å)	16.3803(7)
$\alpha$ (°)	101.944(3)
$\beta$ (°)	104.296(4)
$\gamma$ (°)	102.394(3)
<i>V</i> (Å <sup>3</sup> )	1949.09(15)
<i>F</i> (000)	892
<i>D</i> <sub>calc</sub> (g cm <sup>-3</sup> )	1.465
$\mu$ (mm <sup>-1</sup> )	1.82
Measured reflections	21666
Independent reflections	7466
<i>R</i> (int)	0.032
Observed reflections	6388
<i>R</i> [ $F^2 > 2\sigma(F^2)$ ]	0.035
<i>wR</i> ( $F^2$ ) (all data)	0.089*

$$* w = 1/[\sigma^2(F^2) + (0.04P)^2 + 1.32P], \text{ where } P = (\max(F_o^2, 0) + 2F_c^2)/3$$

solvent. They were isolated by filtration, washed with cold ethanol and dried in air. One of the needle crystals was used for X-ray data collection. The yield was 53%. Anal. Calc. for C<sub>40</sub>H<sub>44</sub>Cu<sub>2</sub>N<sub>8</sub>O<sub>6</sub>: C, 50.11; H, 3.74; N, 12.99. Found: C, 50.32; H, 3.81; N, 12.74. IR (KBr, cm<sup>-1</sup>):  $\nu$ C=N = 1619,  $\nu$ C=C (aromatic) = 1476,  $\nu$ C–N = 1368 and  $\nu$ C–O = 1206.

## 3. Results and Discussion

### 3.1. Characterization of the Complex

A comparison of the IR spectra of the free ligand and mononuclear, Cu(babh), and dinuclear, [Cu<sub>2</sub>( $\mu_{1,3}$ -babh)<sub>2</sub>(C<sub>2</sub>H<sub>5</sub>OH)<sub>2</sub>], complexes indicates that the ligand is coordinated to the copper(II) center. The IR spectrum of the H<sub>2</sub>babh ligand, shows bands at 1600 and 1651 cm<sup>-1</sup>, which are assigned as  $\nu$ C=N and  $\nu$ C=O, respectively. In the IR spectra mono- and di-nuclear, the strong bands at 1613 and 1619 cm<sup>-1</sup> are assigned to  $\nu$ C=N, respectively. The IR spectra of mono- and di-nuclear copper(II) complexes have different bands at the range of 1000–1600 cm<sup>-1</sup>.

The electronic absorption spectra were recorded for copper(II) complexes in various solvents, methanol, ethanol, dichloromethane and *N,N'*-dimethylformamide (DMF) in the visible and UV regions. The absorption spectra of mono- and dinuclear Cu(II) complexes are qui-



te similar in studied solvents. The spectra exhibit one maximum at 642 nm which can be attributed to the d–d transition. Two bands at 446 and 274 nm are due to intraligand  $\pi$ – $\pi^*$  and  $n$ – $\pi^*$  transition, respectively.<sup>11–13,25</sup> Therefore, we can conclude that the dinuclear copper(II) complex in the solvent is converted to mononuclear complex.

The electronic spectra of the complexes were recorded also in the solid state. The electronic absorption spectra of the two complexes are basically different in the solid state (Fig. 1). Both complexes exhibit a band in the region 265 nm due to intraligand transition. The broad band is centered at 410 nm for the dinuclear complex and two bands at 547 and 423 nm for the mononuclear complex are attributed to LMCT transitions.<sup>21</sup> The bands at 628 and 661 nm are assigned to d–d transition for di- and mononuclear complexes, respectively. This shift in position of d–d transition may be explained in terms of the change in the coordination number and the presence of different coordination environments for the copper(II) ions in the two complexes.

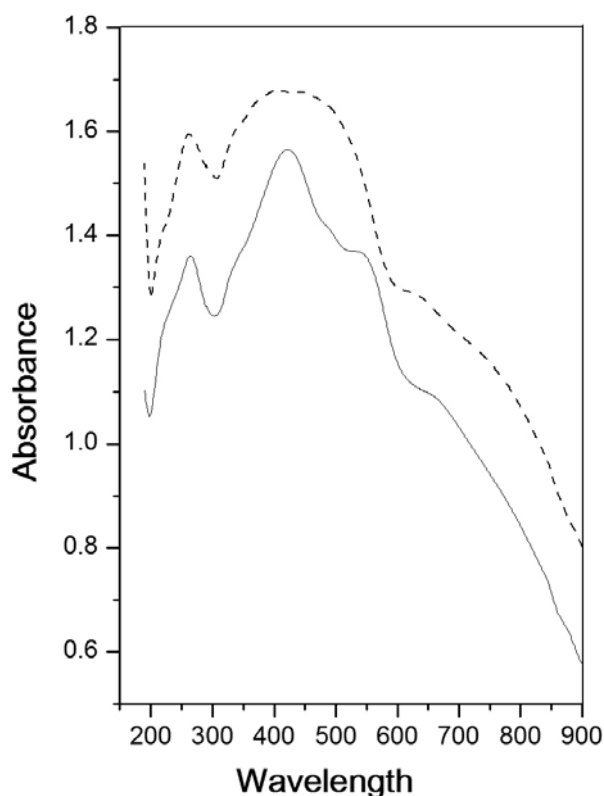


**Fig. 1.** The solid state electronic spectra of [Cu(babh)] (—) and [Cu<sub>2</sub>( $\mu_{1,3}$ -babh)<sub>2</sub>(C<sub>2</sub>H<sub>5</sub>OH)<sub>2</sub>] (---)

### 3. 2. Description of Crystal Structure of the Complex

The single crystal X-ray diffraction data for the complex is listed in Table 1. A structural representation

and selected interatomic distances and angles of the complex are presented in Fig. 2 and Table 2. The complex crystallizes in the triclinic space group  $P\bar{1}$ . The asymmetric unit consists of two Cu(II) ions, two babh<sup>2-</sup> ligands, and two coordinated ethanol molecules (Fig. 2). There is disorder in the packing of one of the ethanol species over two positions with relative occupancies which refined to 57%:43%.

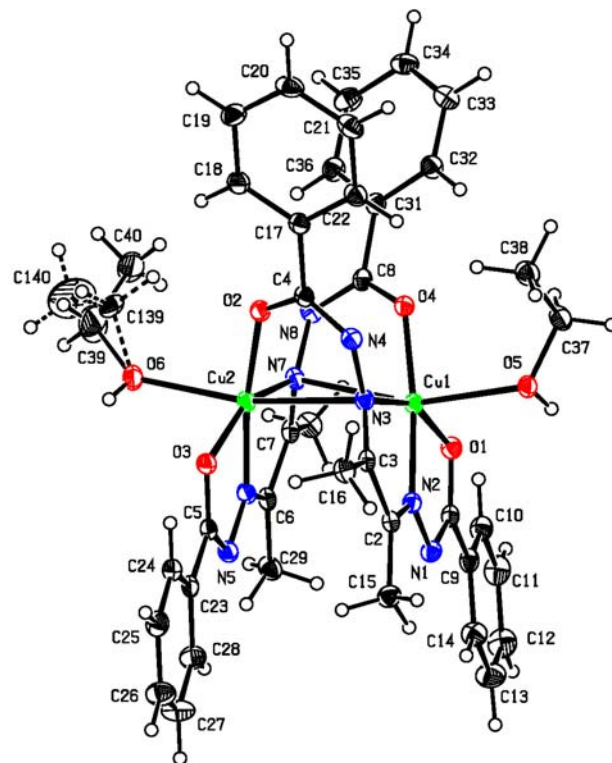


**Fig. 2.** The structure of the [Cu<sub>2</sub>( $\mu_{1,3}$ -babh)<sub>2</sub>(C<sub>2</sub>H<sub>5</sub>OH)<sub>2</sub>] complex, with labelling of selected atoms. Anisotropic displacement ellipsoids exhibit 30% probability levels. Hydrogen atoms are drawn as circles with small radii

**Table 2.** Selected bond lengths (Å) and angles (°) in [Cu<sub>2</sub>( $\mu_{1,3}$ -babh)<sub>2</sub>(C<sub>2</sub>H<sub>5</sub>OH)<sub>2</sub>] complex

Cu1–O1	2.0402(15)	O1–Cu1–O5	90.41(6)
Cu1–O4	1.9062(15)	O1–Cu1–O4	101.83(6)
Cu1–O5	2.2883(16)	O4–Cu1–O5	92.04(6)
Cu1–N2	1.9212(18)	O1–Cu1–N2	78.78(7)
Cu1–N3	2.0604(18)	O4–Cu1–N2	173.64(7)
Cu2–O2	1.9041(15)	O5–Cu1–N2	94.29(7)
Cu2–O3	2.0568(15)	O1–Cu1–N3	157.40(7)
Cu2–O6	2.2644(17)	O3–Cu2–O6	87.98(6)
Cu2–N6	1.6213(18)	O2–Cu2–O3	104.25(6)
Cu2–N7	2.0658(19)	O2–Cu2–O6	93.94(7)
Cu1N7	2.7494(18)	O3–Cu2–N7	156.91(7)
Cu2N3	2.7254(19)	O2–Cu2–N6	172.20(7)
C1–O1	1.289(3)	O6–Cu2–N7	98.26(7)
C1–N1	1.331(3)	N2–N1–C1	108.21(18)
C2–N2	1.290(3)	N2–C2–C3	113.09(19)

From the crystal structure and based on the bond lengths between the copper and coordinating atoms, it has been found that in the complex, two copper(II) centers are penta-coordinate with a  $N_2O_3$  donor. Coordination geometry about each copper(II) ion is essentially a distorted square pyramid with one oxygen atom and two nitrogen atoms from the ligand, one oxygen atom from ethanol molecule and one oxygen atom from the other ligand of the dinuclear complex. The four equatorial positions are occupied by two nitrogen atoms (N2 and N3), one oxygen atom (O1) from one hydrazone ligand and the fourth position is occupied by the oxygen atom (O4) of the other ligand of the dinuclear complex. The axial position is occupied by one oxygen atom (O5) of the ethanol molecule. The axial Cu–O5 bond is 2.2883(16) Å which is longer than the equatorial Cu–O ones [1.9062(15) and 2.0402(15) Å], and consistent with analogous systems observed in the literature.<sup>27–30</sup> The coordination spheres of the copper(II) ions in the complex are best described as a distorted square pyramidal according to the Addison parameter  $\tau$  values of 0.27 (for Cu1) and 0.25 (for Cu2). The parameter  $\tau$  is defined as  $\tau = (\alpha - \beta)/60$ ,  $\alpha > \beta$ , where  $\alpha$  and  $\beta$  are the largest angles; with  $\tau = 1$  for a regular trigonal bipyramid and  $\tau = 0$  for a regular square pyramid.<sup>31</sup> The copper(II) ion is displaced from the basal plane of  $N_2O_2$  by 0.116 Å towards the apical oxygen atom. The Cu...Cu distance is 3.149 Å.

The comparison of C–O and C–N bond lengths of the hydrazone ligand is a useful techniques in identifying the mode of bonding of the ligand (keto or enol) to the metal ion.<sup>32</sup> The C1–O1 and C8–O4 bond lengths of complex (1.289(3) and 1.283(3) Å, respectively) and C1–N1 and C8–N8 (1.331(3) and 1.314(3) Å, respectively) are si-

milar and are in good agreement with analogous Cu(II) complexes observed in the literature where a hydrazone ligand coordinates to the Cu(II) center in its iminolate form.<sup>2,13,14,25,33</sup>

The average of Cu–O bond lengths in the dinuclear complex (1.978 Å) is very similar to the corresponding distances in previously reported mononuclear copper(II) complex (1.978 Å).<sup>22</sup> However, the average of Cu–N bond lengths in the dinuclear complex (1.992 Å) is longer than the corresponding bonds in mononuclear copper(II) complex (1.918 Å).<sup>22</sup> The differences are perhaps due to the difference in the coordination modes and the twisting of ligand *babh*<sup>2-</sup> along the –C=N–N=C– single bond for the coordination of the ligand to the copper(II) ions in the formation of  $[Cu_2(\mu_{1,3}\text{-babh})_2(C_2H_5OH)_2]$ .

The dinuclear helical complex formation is caused by the unsymmetrical twisting along the –C=N–N=C– single bond and two nitrogen atoms and one oxygen from each ligand are coordinated to each copper(II) center. In the dinuclear complex reported by Pal<sup>21</sup> the complex was formed by symmetrical twisting around the central C–C single bond in fragment of  $=(CH_3)C-C(CH_3)=$ . One nitrogen atom and one oxygen from each ligand of *babh* was coordinated to each copper(II) center.

The single crystal X-ray analyses indicate the presence of non-covalent interactions between the nitrogen atom of the imine group of the ligand and the other copper(II) center in the dinuclear complex. The distance between Cu1 and Cu2 centers and the N atoms of the imine group is 2.750(1) Å for Cu1–N7 and 2.725(1) Å for Cu2–N3, respectively, which suggests a weak non-covalent interaction.

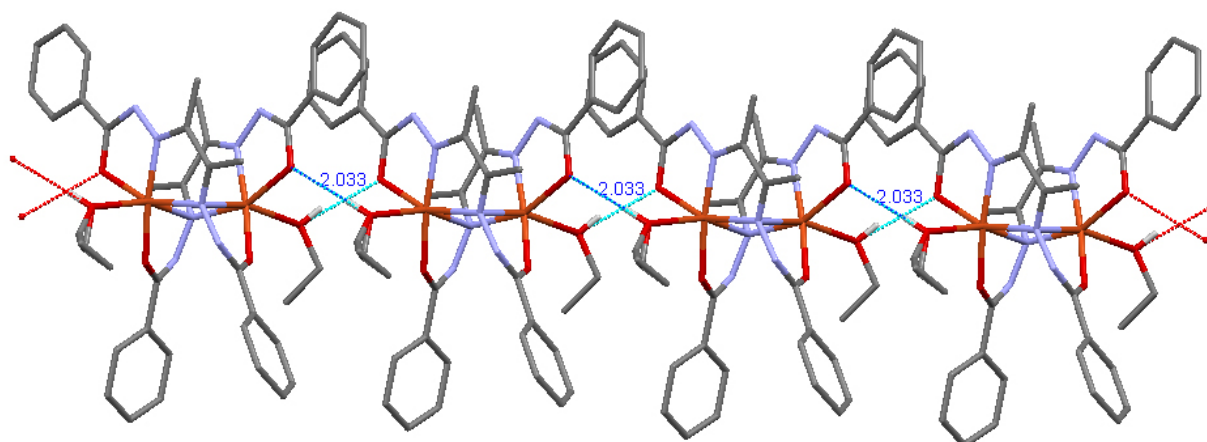


Fig. 3. Various hydrogen bonding interactions, O–H...O in  $[Cu_2(\mu_{1,3}\text{-babh})_2(C_2H_5OH)_2]$  complex, other hydrogen atoms are omitted for clarity.

Table 3. Hydrogen bonding (Å) and angles (°) for  $[Cu_2(\mu_{1,3}\text{-babh})_2(C_2H_5OH)_2]$  complex

D–H...A	D–H	H...A	D...A	D–H...A	Symmetry code
O5–H1...O3	0.76(3)	2.03(3)	2.776(5)	166(3)	$x + 1, y, z$
O6–H2...O1	0.71(4)	2.13(4)	2.841(5)	171(4)	$x - 1, y, z$

Dinuclear complexes are involved in intermolecular O5–H1...O3( $x - 1, y, z$ ) and O6–H2...O1( $x + 1, y, z$ ) hydrogen bonding interactions between coordinated ethanol molecules and the oxygen atoms of a neighboring babb<sup>2-</sup> ligands (Fig. 3). The details of the hydrogen bonding are given in Table 3.

## 4. Conclusion

The new homo-dinuclear complex [Cu<sub>2</sub>(μ<sub>1,3</sub>-babb)<sub>2</sub>(C<sub>2</sub>H<sub>5</sub>OH)<sub>2</sub>] has been synthesized and the crystal structure of the complex has been determined. Single crystal X-ray diffraction indicate that the dinuclear helical complex formation was caused due to the unsymmetrical twisting of the ligand, N<sub>2</sub>O<sub>2</sub> along the –C=N–N=C– single bond. Two nitrogen atoms and one oxygen from each ligand are coordinated to each copper(II) center. Two copper(II) centers are penta-coordinate with a N<sub>2</sub>O<sub>3</sub> donor. Coordination geometry about each copper (II) ion is essentially a square pyramid with one oxygen atom and two nitrogen atoms from the ligand, one oxygen atom from an ethanol molecule, and one oxygen atom from the other ligand of the dinuclear complex. The absorption spectra of mono- and di-nuclear complexes are quite similar in solvent. However, the electronic absorption spectra of two the complexes are basically different in the solid state.

## 5. Supplementary Material

The deposition numbers of the studied dinuclear complex is CCDC 1527221. These data can be obtained free-of-charge via [www.ccdc.cam.ac.uk/data\\_request/cif](http://www.ccdc.cam.ac.uk/data_request/cif), by emailing [data-request@ccdc.cam.ac.uk](mailto:data-request@ccdc.cam.ac.uk), or by contacting The Cambridge Crystallographic Data Centre, 12 Union Road, Cambridge CB2 1EZ, UK; fax +44 1223 336033.

## 6. Acknowledgments

The authors are grateful to the Yazd University (YU) and the Australian National University (ANU) for partial support of this work.

## 7. References

1. E. I. Solomon, D. E. Heppner, E. M. Johnston, J. W. Ginsbach, J. Cirera, M. Qayyum, M. T. Kieber-Emmons, C. H. Kjaergaard, R. G. Hadt, L. Tian, *Chem. Rev.* **2014**, *114*, 3659–3853. <https://doi.org/10.1021/cr400327t>
2. R. Vafazadeh, B. Khaledi, A. C. Willis, M. Namazian, *Polyhedron* **2011**, *30*, 1815–1819. <https://doi.org/10.1016/j.poly.2011.04.026>
3. R. Vafazadeh, A. C. Willis, *Acta Chim. Slov.* **2016**, *63*, 186–192. <https://doi.org/10.17344/acsi.2016.2263>
4. R. Vafazadeh, B. Khaledi, A. C. Willis, *Acta Chim. Slov.* **2012**, *59*, 954–958.
5. X. Z. Zhang, Y. Gu, Y. Li, A. Liu, F. Liu, Z. You, H. L. Zhu, *Acta Chim. Slov.* **2016**, *63*, 721–725. <https://doi.org/10.17344/acsi.2016.2421>
6. B. Ardan, Y. Slyvka, E. Goreshnik, M. Mys'kiv, *Acta Chim. Slov.* **2013**, *60*, 484–490.
7. B. Dojer, A. Pevec, F. Belaj, M. Kristl, *Acta Chim. Slov.* **2015**, *62*, 312–318. <https://doi.org/10.17344/acsi.2014.1111>
8. Z. Li- Hua, W. Wei-Na, W. Yuan, S. Guang, *J. Coord. Chem.* **2013**, *66*, 227–242.
9. A. Galani, E. K. Efthimiadou, G. Mitrikas, Y. Sanakis, V. Psycharis, C. Raptopoulou, G. Kordas, A. Karaliota, *Inorg. Chim. Acta*, **2014**, *423*, 207–218. <https://doi.org/10.1016/j.ica.2014.08.005>
10. G. Y. Li, K. J. Du, J. Q. Wang, J. W. Liang, J. F. Kou, X. J. Hou, L. N. Ji, H. Chao, *J. Inorg. Biochem.* **2013**, *119*, 43–53. <https://doi.org/10.1016/j.jinorgbio.2012.09.019>
11. R. Vafazadeh, F. Jafari, M. M. Heidari, A.C. Willis, *J. Coord. Chem.* **2016**, *69*, 1313–1325. <https://doi.org/10.1080/00958972.2016.1163547>
12. R. Vafazadeh, N. Hasanzade, M. M. Heidari, A.C. Willis, *Acta Chim. Slov.* **2015**, *62*, 122–129. <https://doi.org/10.17344/acsi.2014.797>
13. R. Vafazadeh, Z. Moghadas, A. C. Willis, *J. Coord. Chem.* **2015**, *68*, 4255–4271.
14. R. Vafazadeh, R. Esteghamat-Panah, A. C. Willis, A. F. Hill, *Polyhedron* **2012**, *48*, 51–57. <https://doi.org/10.1016/j.poly.2012.08.057>
15. J.R. Zimmerman, A. Bettencourt-Dias, *Inorg. Chem. Commun.* **2011**, *14*, 753–758. <https://doi.org/10.1016/j.inoche.2011.02.028>
16. R. Pedrido, M.J. Romero, M.R. Bermejo, M. Martinez-Calvo, A.M. Gonzalez-Noyab, G. Zaragoza, *Dalton Trans.* **2009**, 8329–8340. <https://doi.org/10.1039/b908782f>
17. R. Vafazadeh, A. C. Willis, *J. Coord. Chem.* **2015**, *68*, 2240–2252. <https://doi.org/10.1080/00958972.2015.1048688>
18. D. Venegas-Yazigi, D. Aravena, E. Spodine, E. Ruiz, S. Alvarez, *Coord. Chem. Rev.* **2010**, *254*, 2086–2095. <https://doi.org/10.1016/j.ccr.2010.04.003>
19. M. A. Sharif, G. R. Najafi, *Acta Chim. Slov.* **2013**, *60*, 138–143.
20. Y. Lan, G. Novitchi, R. Clerac, J. K. Tang, N. T. Madhu, I. J. Hewitt, C. E. Anson, S. Brooker, A. K. Powell, *Dalton Trans.* **2009**, 1721–1727. <https://doi.org/10.1039/b818113f>
21. T. Ghosh, S. Pal, *Inorg. Chim. Acta* **2010**, *363*, 3632–3636. <https://doi.org/10.1016/j.ica.2010.07.007>
22. T. Ghosh, A. Mukhopadhyay, K. S. C. Dargaiah, S. Pal, *Struct. Chem.* **2010**, *21*, 147–152. <https://doi.org/10.1007/s11224-009-9557-2>
23. A. Altomare, G. Casciarano, G. Giacovazzo, A. Guagliardi, M. C. Burla, G. Polidori, M. Camalli, *J. Appl. Cryst.* **1994**, *27*, 435–436.

24. P. W. Betteridge, J. R. Carruthers, R. I. Cooper, K. Prout, D.J. Watkin, *J. Appl. Cryst.* **2003**, *36*, 1487–1487. <https://doi.org/10.1107/S0021889803021800>
25. R. Vafazadeh, M. Alinaghi, A. C. Willis, A. Benvidi, *Acta Chim. Slov.* **2014**, *61*, 121–125.
26. R. Vafazadeh, V. Hayeri, A. C. Willis, *Polyhedron* **2010**, *29*, 1810–1814. <https://doi.org/10.1016/j.poly.2010.02.030>
27. X.-J. Li, K. Zheng, Y.-T. Li, C.-W. Yan, Z.-Y. Wu, S.-Y. Xuan, *J. Coord. Chem.* **2015**, *68*, 928–948. <https://doi.org/10.1080/00958972.2015.1009452>
28. D. Barut, N. Korkmaz, S. T. Astley, M. Aygün, *Acta Chim. Slov.* **2015**, *62*, 88–94. <https://doi.org/10.17344/acsi.2014.734>
29. A. Ray, C. Rizzoli, G. Pilet, C. Desplanches, E. Garribba, E. Rentschler and S. Mitra, *Eur. J. Inorg. Chem.* **2009**, 2915–2928. <https://doi.org/10.1002/ejic.200900188>
30. A. Biswas, M. G. B. Drew, J. Ribas, C. Diaz, A. Ghosh, *Eur. J. Inorg. Chem.* **2011**, 2405–2412. <https://doi.org/10.1002/ejic.201100067>
31. A. W. Addison, N. Rao, J. Reedijk, J.V. Rijn, G.C. Verschoor, *J. Chem. Soc. Dalton Trans.* **1984**, 1349–1356. <https://doi.org/10.1039/DT9840001349>
32. T. Ghosh, S. Pal, *J. Chem. Sci.* **2015**, *127*, 1201–1209. <https://doi.org/10.1007/s12039-015-0887-x>
33. M. Nandy, D. L. Hughes, G. M. Rosair, R. K. B. Singh, S. Mitra, *J. Coord. Chem.* **2014**, *67*, 3335–3353. <https://doi.org/10.1080/00958972.2014.964697>

## Povzetek

Reakcija štiriveznega hidrazonskega liganda  $H_2babh$  z  $Cu(CH_3COO)_2$  v metanolu vodi do nastanka enojedrnega kompleksa  $[Cu(babh)]$ . Po raztapljanju v diklorometanu in ob dodatku etanola nastane dvojedrni kompleks  $[Cu_2(\mu_{1,3}-babh)_2(C_2H_5OH)_2]$ . Rentgenska kristalografija razkrije, da zaradi nesimetričnega zvitja  $H_2babh$  liganda nastane dvojedrni kompleks z vijačno strukturo. En kisikov in dva dušikova atoma z liganda in en kisik z drugega liganda se koordinirajo na posamezen bakrov(II) center. Oba bakrova(II) centra v dvojedrni enoti sta pentakoordinirana z delno popačeno kvadratno-piramidalno geometrijo. IR spektra eno- in dvojedrnega bakrovega(II) kompleksa imata različne trakove. Absorpcijska spektra eno- in dvojedrnega kompleksa v metanolu sta zelo podobna, medtem ko se elektronska absorpcijska spektra obeh kompleksov v trdnem stanju delno razlikujeta.

Scientific paper

# Electroanalytical Determination of Escitalopram Oxalate Using Nickel Nanoparticles Modified Carbon Paste Sensor

Ali Kamal Attia,<sup>1,\*</sup> Mona A. Mohamed<sup>1</sup> and Amany M. Fekry<sup>2</sup><sup>1</sup> National Organization for Drug Control and Research, P.O. Box 29, Cairo, Egypt<sup>2</sup> Chemistry Department, Faculty of Science, Cairo University, Giza-12613, Egypt

\* Corresponding author: E-mail: alikamal1978@hotmail.com

Tel.: 002 0235851278; Fax: 002 0235855582

Received: 10-01-2017

## Abstract

A sensitive voltammetric method was described for the determination of escitalopram oxalate based on electrocatalytic oxidation at nickel nanoparticles modified chloranil carbon paste sensor in Britton-Robinson buffer (pH range from 2 to 10). The modified electrode was characterized by scanning electron microscopy, electrochemical impedance and cyclic voltammetry. The investigation of electrochemical behavior of escitalopram oxalate was performed using cyclic voltammetry and differential pulse voltammetry. The anodic peak current showed a linear range from  $1.0 \times 10^{-6}$  to  $7.0 \times 10^{-5}$  mol L<sup>-1</sup>. The detection limit is below  $2.0 \times 10^{-7}$  mol L<sup>-1</sup>. The proposed method is rapid, economical, simple, precise and sensitive voltammetric method for the determination of escitalopram oxalate in bulk, dosage form and urine.

**Keywords:** Escitalopram oxalate, voltammetry, nickel nanoparticles, modified electrode, urine

## 1. Introduction

Escitalopram oxalate (ESC) has high effectivity for the treatment of major depressive episodes and generalized anxiety disorders explaining its pharmacological and clinical applications.<sup>1–3</sup>

Various reported methods have been employed for determination of ESC, including chromatography,<sup>4–16</sup> fluorimetry,<sup>14</sup> spectrophotometry,<sup>15–21</sup> chemiluminescence,<sup>22</sup> capillary electrophoresis,<sup>23,24</sup> potentiometry,<sup>25,26</sup> and voltammetry.<sup>27</sup>

Some electron acceptor reagents such as 2,3-dichloro-5,6-dicyano-1,4-benzoquinone (DDQ), 7,7,8,8-tetracyano-quinodimethane (TCNQ), tetracyanoethylene (TCNE) and chloranil (CA) can be used in electroanalytical field as mediators or electrode modifiers.<sup>28–36</sup>

The development of nanoscale materials has been extensively used, particularly with respect to metallic nanoparticles. Interests have focused on their use in analytical chemistry because of their specific physico-chemical properties. The modified electrodes increase the selectivity and the sensitivity of electro-

analytical processes more than the bare electrodes leading to increase in their analytical applicability.<sup>37–45</sup> On the other hand, nanoparticles have excellent electronic and electrocatalytic properties, which accelerate the rate of heterogeneous electron exchange between the electrode surface and some species in solution and increase the effective surface area of the working electrode.<sup>46–54</sup>

The aim of this work is the study of the electrochemical behavior of ESC utilizing cyclic voltammetry (CV), differential pulse voltammetry (DPV) and electrochemical impedance spectroscopy (EIS) for the analysis of ESC in bulk powder, tablets and urine at nickel nanoparticles modified chloranil carbon paste sensor (NiCACP).

## 2. Experimental

### 2.1. Materials and Reagents

ESC was supplied by Hikma Pharmaceuticals, Egypt, and Cipralax tablets (10 mg ESC per tablet) were purchased from Multi Pharma/Lundbeck.

DDQ, TCNQ and TCNE were obtained from Merck. CA, nickel nitrate, graphite powder and paraffin oil were supplied by Sigma-Aldrich.

Stock solution of ESC ( $1.0 \times 10^{-3}$  mol L<sup>-1</sup>) was prepared by dissolving an appropriate amount in methanol. Britton-Robinson (BR) buffer was prepared by mixing phosphoric acid (0.04 mol L<sup>-1</sup>), acetic acid (0.04 mol L<sup>-1</sup>) and boric acid (0.04 mol L<sup>-1</sup>). The pH values were adjusted using 0.2 mol L<sup>-1</sup> NaOH.

## 2. 2. Preparation of Working Electrodes

1. Chloranil modified carbon paste electrode (CACP) was made by dissolving CA (10 mg) in ethyl ether, then mixing with graphite powder (990 mg) in a mortar. After evaporation of solvent, paraffin oil was added and mixed until a uniformly wetted paste was obtained. The paste was packed into the hole of the electrode and smoothed on a filter paper until it had a shiny appearance.
2. Bare carbon paste electrode (CP) was prepared according to the above procedures without addition of CA.
3. Different modified electrodes (DDQCP, TCNECP and TCNQCP) were prepared by adding DDQ, TCNQ and TCNE instead of CA.
4. Nickel nanoparticles modified chloranil carbon paste sensor (NiCACP) was prepared by electro-deposition of nickel nanoparticles on CACP immersed in an aqueous solution of 0.1 mol L<sup>-1</sup> acetate buffer solution of pH 4.0 containing  $1.0 \times 10^{-3}$  mol L<sup>-1</sup> Ni(NO<sub>3</sub>)<sub>2</sub> at -1.0 V vs. Ag/AgCl/3 mol L<sup>-1</sup> NaCl reference electrode for 240 s.<sup>55</sup>

## 2. 3. Apparatus

AEW2 electrochemical workstation with ECProg3 electrochemistry software (Sycopel, England) was used in this study. A platinum wire (BASi model MW-1032) and an Ag/AgCl/3 mol L<sup>-1</sup> NaCl (BASi model MF-2063) were used as a counter electrode and reference electrode, respectively. The pH measurements were carried out utilizing a cyberscan 500 pH meter (EUTECH Instruments, USA).

EIS was performed using IM6e electrochemical workstation (Zahner-electrik GmbH, Germany). All diagrams were recorded by applying 10 mV sinusoidal potential within a frequency range from 100 kHz to 100 mHz.

Scanning electron microscopy (SEM) measurements were achieved by a JSM-6700F scanning electron microscope (Japan Electro Company, Japan).

## 2. 4. Determination of ESC in Bulk Powder

The working, counter and reference electrodes were submerged in electrolytic cell containing 5 mL of BR buf-

fer (pH 7.0). Aliquots of ESC ( $1.0 \times 10^{-3}$  mol L<sup>-1</sup>) were added, and then voltammetric analyses were carried out by using DPV method and the voltammograms were recorded at scan rate of rate of 20 mV s<sup>-1</sup>, pulse amplitude of 50 mV and accumulation time of 100 s.

## 2. 5. Determination of ESC in Tablets

Ten tablets were weighed and crushed to a fine powder using mortar and pestle, and then sufficient amount to prepare  $1.0 \times 10^{-3}$  mol L<sup>-1</sup> ESC was transferred into 100 mL volumetric flask already containing 60 mL of methanol. The flask was sonicated for about 15 min and completed to the volume with methanol. The solution was filtered to remove the insoluble excipients. ESC was determined by standard addition method.

## 2. 6. Analysis of ESC in Urine

Urine sample obtained from a healthy person (50 mL) was stored in a refrigerator at 8.0 °C for one week. 10 mL from urine sample was centrifuged for 10 min at 2000 rpm. The supernatant was filtered using 0.45 μm filter paper, and then diluted ten times with BR buffer of pH 7.0. Successive additions of ESC ( $1.0 \times 10^{-3}$  mol L<sup>-1</sup>) were added to the voltammetric cell containing diluted urine (5.0 mL) and DPV voltammograms were listed. The experiments were performed in compliance with the Helsinki Declaration of 1975, as revised in 2008. The institutional committees (NODCAR, Egypt) have approved these experiments. Informed consent was obtained from all participants.

## 3. Results and Discussion

### 3. 1. Electrochemical Behavior of ESC

The pharmaceutical and biomedical analysis is among the most important branches of applied analytical chemistry. Analytical measurement procedures should have a critical role in drug analysis as well as in biological samples. DPV method has been developed for determination of ESC in the bulk, tablets and urine using nickel nanoparticles modified chloranil carbon paste sensor.

Fig. 1a presents the cyclic voltammograms of ESC ( $1.0 \times 10^{-4}$  mol L<sup>-1</sup>) in BR buffer of pH 7.0 at different working electrodes: CP, DDQCP, TCNQCP, TCNECP and CACP, exhibiting one well defined anodic peak with no peak on the reverse scan, suggesting the irreversibility of the electrode reaction. This anodic peak may be attributed to the oxidation of tertiary amine group which agree with the reported method<sup>27</sup> (Fig 1c).

Fig. 1b describes the effect of mediator type on the anodic current of ESC in BR buffer of pH 7.0. The anodic peak current values are in the following order: CACP (15.16 μA) < DDQCP (13.02 μA) < TCNECP (10.08 μA)

< TCNQCP (9.29  $\mu\text{A}$ ) < CP (6.09  $\mu\text{A}$ ). CA increases the anodic peak current from 6.09  $\mu\text{A}$  at CP to 15.16  $\mu\text{A}$  at CACP and lowers the oxidation potential from 1.147 V at CP to 1.095 V at CACP, thus CA acts as an electrocatalytic mediator.

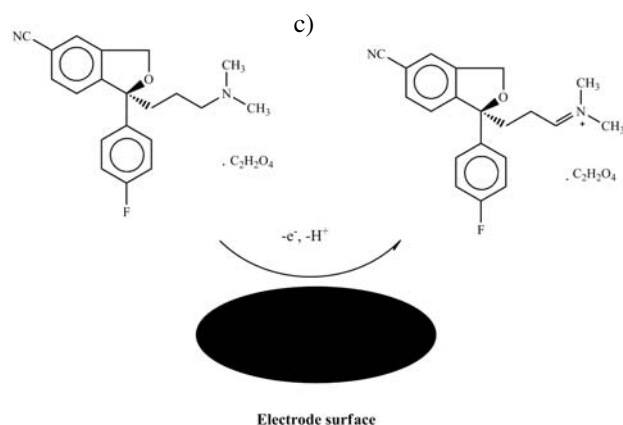
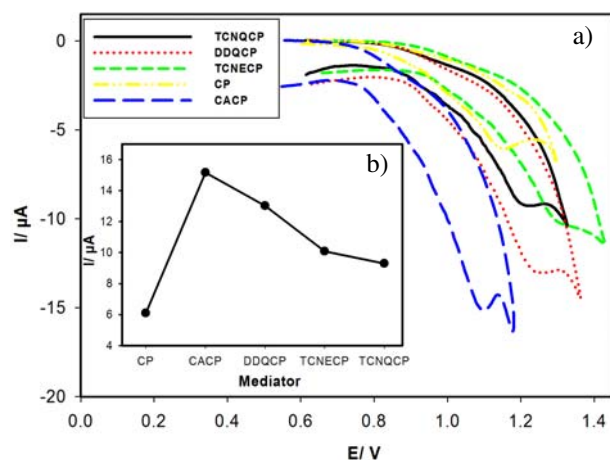


**Figure 1:** Cyclic voltammograms of  $1.0 \times 10^{-4}$  mol L $^{-1}$  ESC in BR buffer of pH 7.0 in case of CACP, DDQCP, TCNECP, TCNQCP and CP, scan rate 100 mV s $^{-1}$  (a). The inset: the plot of anodic current as a function of mediator type (b). The oxidation mechanism of ESC (c).

### 3. 2. Effect of pH

Voltammetric behavior of ESC was studied in BR buffer over the pH range from 2 to 10 at CACP as shown in Fig. 2a. The peak current increases as the pH increases up to pH 7.0, after pH 7.0 the peak current decreases as the pH increases (Fig. 2b). Therefore, pH 7.0 was selected as a suitable supporting electrolyte because the peak current reaches its maximum value at this pH value.

Fig. 2c demonstrates that the peak potential varies linearly with pH over the pH values (2–10) with the linear regression equation of  $E(\text{V}) = 1.451 - 0.054 \text{ pH}$ , with a correlation coefficient (R) of 0.9937. The slope was found

to be  $-54$  mV/pH units, which is close to the theoretical value of  $-59$  mV suggesting that the number of protons and transferred electrons involved in the oxidation mechanism is equal.<sup>56</sup>

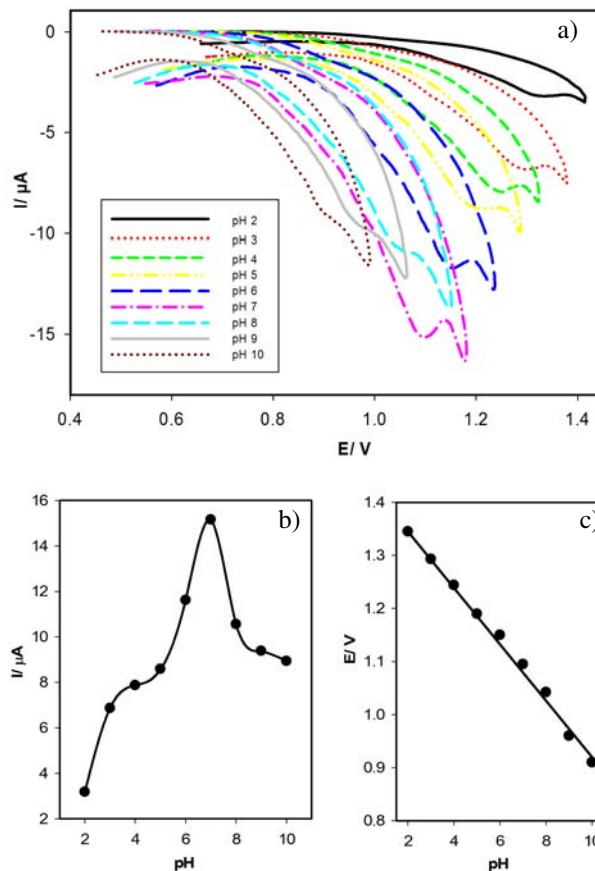


**Figure 2:** Cyclic voltammograms of  $1.0 \times 10^{-4}$  mol L $^{-1}$  ESC in BR buffer over the pH range of 2–10 at CACP, scan rate of 100 mV s $^{-1}$  (a). Plots of anodic peak current (b) and peak potential (c) as a function of pH.

### 3. 3. Effect of Ni(NO<sub>3</sub>)<sub>2</sub> Concentration

The influence of Ni(NO<sub>3</sub>)<sub>2</sub> concentration on response of fabricated sensor was investigated using different concentrations of Ni(NO<sub>3</sub>)<sub>2</sub> (1.0, 2.0 and 3.0  $\times 10^{-3}$  mol L $^{-1}$ ) which were deposited at CACP at  $-1.0$  V for different times (120, 180, 240 and 300 s). It was found that  $1.0 \times 10^{-3}$  mol L $^{-1}$  Ni(NO<sub>3</sub>)<sub>2</sub> and 240 s are the optimum concentration and deposition time used to prepare the modified sensor (NiCACP) to give the best results for the determination of ESC.

### 3. 4. Morphologies of Different Electrodes

Electronic Supplementary Information 1 (ESI 1) displays the significant differences in the surface structure

of CP, CACP and NiCACP. The surface of CP was predominated by irregular shaped graphite flaks and separate layers (ESI 1A). The SEM of CACP illustrates irregular ice shaped surface (ESI 1B). The SEM of NiCACP shows a tree shaped structure, the nanoparticles appear randomly and space among them produce large surface area (ESI 1C).

### 3. 5. Electrochemical Behavior of ESC at NiCACP

ESI 2A presents the cyclic voltammograms of ESC ( $1.0 \times 10^{-4} \text{ mol L}^{-1}$ ) at CP, CACP and NiCACP in BR buffer of pH 7.0. We note that the anodic oxidation peak has the highest current and the lowest potential values (25.03  $\mu\text{A}$ , 0.980 V) in case of NiCACP in comparison with these values in case of CACP (15.16  $\mu\text{A}$ , 1.095 V) and CP (6.09  $\mu\text{A}$ , 1.147 V). NiCACP shows catalytic effect in the anodic oxidation of ESC. Therefore, it was selected to determine ESC in bulk, tablets and urine.

Scan rate ( $\nu$ ) effect on the the peak current ( $I$ ) of ESC ( $1.0 \times 10^{-4} \text{ mol L}^{-1}$ ) was carried out by immersing NiCACP in BR buffer of pH 7.0, and the cyclic voltammograms were recorded over the scan range of 10–250  $\text{mV s}^{-1}$ . ESI 2B shows a linear relationship between  $\log I$  and  $\log \nu$  as given by the following equation:  $\log I = 0.28 + 0.56 \log \nu$ . The slope of 0.56 indicates a diffusion controlled process with some adsorption character.<sup>57</sup>

Accumulation time ( $T_{\text{acc}}$ ) effect on the peak current was studied at open circuit condition at NiCACP in BR buffer of pH 7.0 containing  $1.0 \times 10^{-4} \text{ mol L}^{-1}$  ESC. It was found that the peak current increases as the accumulation time increases up to 100 s and then it decreases as  $T_{\text{acc}}$  increases. 100 s was selected as the optimum accumulation time in the determination of ESC (ESI 2C).

The electron transfer coefficient ( $\alpha$ ) can be calculated using the following equation:  $\alpha = 47.7/(E_p - E_{p/2}) \text{ mV}$ ,<sup>58</sup> where  $E_p$  is the peak potential and  $E_{p/2}$  is the potential where the current is at half peak value.  $\alpha$  was calculated to be 0.48.

The standard rate constant of ESC ( $K^\circ$ ) =  $1.0 \times 10^{-3} \text{ s}^{-1}$  was obtained utilizing Laviron equation:  $E_p = E^\circ + 2.303 RT/\alpha nF [\log RTK^\circ/\alpha nF + \log \nu]$ , where  $n$  is number of electrons,  $T$  is the temperature (298 K),  $R$  the gas constant (8.314  $\text{J K}^{-1} \text{ mol}^{-1}$ ),  $F$  the Faraday constant (96,485  $\text{C mol}^{-1}$ ) and  $E^\circ$  is the formal potential obtained by plotting the relation between  $E_p$  and  $\nu$  (extrapolating the line to  $\nu = 0$ ),<sup>59</sup>  $E^\circ = 0.908 \text{ V}$ ,  $\alpha n = 0.537$ , hence  $n$  was calculated to be 1.12 ( $n \approx 1$ ).

The electroactive area of NiCACP was obtained by applying Randles-Sevcik equation,<sup>60</sup> using  $1.0 \times 10^{-3} \text{ mol L}^{-1} \text{ K}_3\text{Fe}(\text{CN})_6$  at different scan rates, the diffusion coefficient of  $\text{K}_3\text{Fe}(\text{CN})_6$  is  $7.6 \times 10^{-6} \text{ cm}^2 \text{ s}^{-1}$ ,<sup>61</sup> the electroactive area ( $A$ ) was calculated to be  $0.128 \text{ cm}^2$ . The surface concentration of ESC ( $\Gamma$ ) at NiCACP was calculated employing the following equation:  $I = n^2 F^2 A \Gamma \nu / 4RT$ ,  $n = 1$ ,  $\Gamma$  was found to be  $1.215 \times 10^{-6} \text{ mol cm}^{-2}$ .<sup>62</sup>

### 3. 6. Electrochemical Impedance Spectroscopy Study

Nyquist plots of ESC using NiCACP and CACP exhibit the difference in the presence of metallic nickel nanoparticles as shown in Fig. 3a.

A simple equivalent circuit model (Fig. 3b) was used to fit the results.  $R_s$  is the solution resistance and  $R_p$  is the polarization resistance.  $Q$  represents the constant phase element (CPE) of capacitance for the film,  $n$  is its corresponding empirical exponents,  $C_f$  is the capacitance of the double layer and  $W$  is the Warburg impedance due to diffusion (Table 1). The capacitance value for NiCACP is relatively higher than CACP in terms of  $C_f$  and  $Q$  denoting the increase of ionic adsorption at the electrode/electrolyte interface for NiCACP. Moreover, the decrease in the  $R_p$  is attributed to the selective interaction between nickel nanoparticles and ESC that resulted in the increase of the current in the electro-oxidation process.

NiCACP stability was studied in BR buffer of pH 7.0 containing  $1.0 \times 10^{-4} \text{ mol L}^{-1}$  ESC as a function of immersion time (Fig. 3c). The results show good stability till 12 h, thus NiCACP works well.

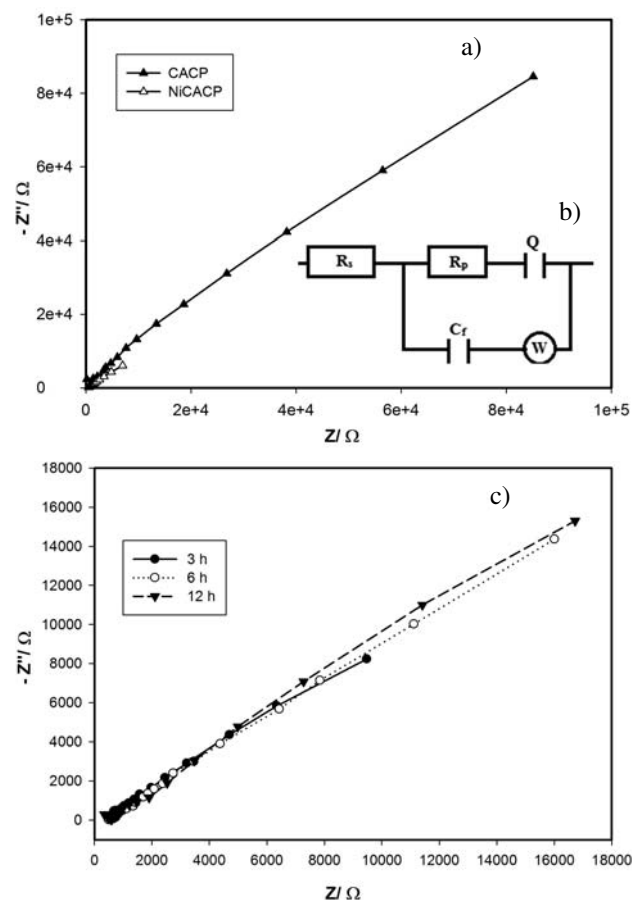


**Figure 3:** Nyquist plots of NiCACP and CACP in BR buffer pH 7.0 containing  $1.0 \times 10^{-4} \text{ mol L}^{-1}$  ESC solution (a). Equivalent circuit for Nyquist plot (b). Nyquist plot of NiCACP in BR buffer pH 7.0 containing  $1.0 \times 10^{-4} \text{ mol L}^{-1}$  ESC solution as a function of immersion time (c).



**Table 1:** Fitting data of electrochemical impedance spectroscopy.

Electrode	$R_s / k\Omega \text{ cm}^2$	$R_p / k\Omega \text{ cm}^2$	$Q / \mu\text{F cm}^2$	n	$C_f / \mu\text{F cm}^2$	$W / K\Omega \text{ s}^{-1}$
NiCACP	0.35	312	27	0.81	15	43
CACP	0.35	4587	10.1	0.85	3.5	415

### 3. 7. Determination of ESC in Bulk Powder

DPV method was applied for quantitative analysis of ESC in 5.0 mL of BR buffer (pH 7.0) at NiCACP. Successive additions from ESC solution ( $1.0 \times 10^{-3} \text{ mol L}^{-1}$ ) were introduced into the electrolytic cell and the voltammograms were recorded, giving linearity over the concentration range of  $1.0 \times 10^{-6} - 7.0 \times 10^{-5} \text{ mol L}^{-1}$  ( $0.414 - 29.01 \mu\text{g mL}^{-1}$ ) as shown in Fig. 4.

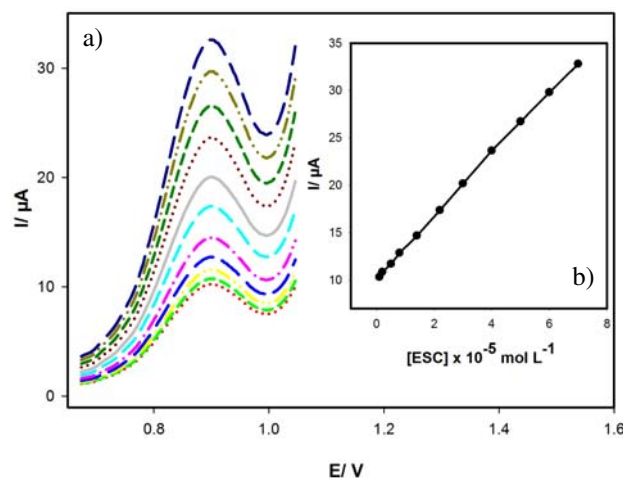


**Figure 4:** Calibration curve of ESC at NiCACP, pulse amplitude = 50 mV,  $T_{acc} = 100 \text{ s}$  and scan rate =  $20 \text{ mV s}^{-1}$  (a). Plot of anodic current as a function of ESC concentration (b).

The validation of the method was performed according to the International Conference on Harmonization (ICH) guideline,<sup>63</sup> through the evaluation of limit of detection (LOD), limit of quantification (LOQ), precision, accuracy, ruggedness and robustness. The LOD and LOQ were found to be  $1.98 \times 10^{-7} \text{ mol L}^{-1}$  and  $6.60 \times 10^{-7} \text{ mol L}^{-1}$ , respectively. The relative standard deviation (RSD) and the percentage recovery values were found in the following ranges: 0.33–0.77% and 99.91–101.35%, respectively.

The proposed method is more sensitive than some reported methods such as chromatographic methods:  $20-120 \mu\text{g mL}^{-1}$ ,<sup>10</sup>  $50-300 \mu\text{g mL}^{-1}$ ,<sup>11</sup>  $80-120 \mu\text{g mL}^{-1}$ ,<sup>12</sup>  $2-20 \mu\text{g mL}^{-1}$ ,<sup>13</sup>  $10-60 \mu\text{g mL}^{-1}$ ,<sup>15</sup> and  $10-50 \mu\text{g mL}^{-1}$ ,<sup>16</sup> spectrophotometric methods:  $10-50 \mu\text{g mL}^{-1}$ ,<sup>16</sup>  $2-20 \mu\text{g mL}^{-1}$ ,<sup>17</sup>  $2-10 \mu\text{g mL}^{-1}$ ,<sup>18</sup>  $5-100 \mu\text{g mL}^{-1}$ ,<sup>19</sup>  $0.50-8.00 \mu\text{g mL}^{-1}$ ,<sup>20</sup> and  $20-120 \mu\text{g mL}^{-1}$ ,<sup>21</sup> and electrochemical method:  $150-400 \mu\text{g mL}^{-1}$ .<sup>27</sup>

The ruggedness of the method was done through the analysis of  $1.0 \times 10^{-5} \text{ mol L}^{-1}$  ESC by two different analysts with the percentage recovery values of 99.94% and

100.30% for the first and the second analyst, respectively. Hence, the results show good agreement.

The robustness of the method was examined by testing the influence of small variations from the optimum conditions: pH ( $7.00 \pm 0.20$ ), scan rate ( $20 \pm 2.00$ ) and accumulation time ( $100 \pm 5.00$ ) on the peak current of ESC ( $1.00 \times 10^{-5} \text{ mol L}^{-1}$ ). The RSD values were 0.35%, 0.58% and 0.42% for pH, scan rate and accumulation time, respectively, indicating the robustness of the proposed method.

### 3. 8. Interference Study

Some interfering species ( $1.00 \times 10^{-3} \text{ mol L}^{-1}$ ) such as inorganic cations ( $\text{Na}^+$ ,  $\text{K}^+$ , and  $\text{Ca}^{2+}$ ), sugars (glucose and dextrose) and amino acid (valine and alanine) were used to study their interference with ESC ( $1.00 \times 10^{-3} \text{ mol L}^{-1}$ ). There is no interference between these species and ESC; NiCACP shows good selectivity for the determination of ESC.

### 3. 9. Analysis of ESC in Tablets

Standard addition method was successfully applied to determine ESC in Ciprex tablets at NiCACP without any pretreatment or time consuming extraction steps prior to analysis. The mean recovery and mean RSD values for five replicate measurements were 100.58% and 1.18%, respectively. The results listed in Table 2 show there is no interference between ESC and the excipients suggesting the selectivity and the sensitivity of the proposed method in the determination of ESC in dosage forms.

**Table 2:** Determination of ESC in Ciprex tablets by applying standard addition technique.

Dosage form	ESC ( $\text{mol L}^{-1}$ )	ESC ( $\text{mol L}^{-1}$ )		Recovery (%)
	Taken	Added	Found	
Ciprex tablets	$8.00 \times 10^{-6}$	$4.00 \times 10^{-6}$	$12.15 \times 10^{-6}$	101.25
		$8.00 \times 10^{-6}$	$15.96 \times 10^{-6}$	99.75
		$12.00 \times 10^{-6}$	$20.11 \times 10^{-6}$	100.55
		$16.00 \times 10^{-6}$	$24.18 \times 10^{-6}$	100.75
Mean recovery $\pm$ RSD*%				100.58 $\pm$ 1.18

\* Number of replicates (n) = 5.

### 3. 10. Analysis of ESC in Urine

The proposed method was used to determine ESC in urine samples (ESI3) in concentration range of  $4.00 \times$

$10^{-6}$ – $6.00 \times 10^{-5}$  mol L<sup>-1</sup> with correlation coefficient of 0.9998, the LOD and LOQ were  $7.57 \times 10^{-7}$  mol L<sup>-1</sup> and  $2.52 \times 10^{-6}$  mol L<sup>-1</sup>, respectively. Four different concentrations ( $8.00 \times 10^{-6}$ ,  $2.20 \times 10^{-5}$ ,  $3.60 \times 10^{-5}$ , and  $4.40 \times 10^{-5}$  mol L<sup>-1</sup>) were chosen to be repeated five times to evaluate the accuracy and precision of the method. The RSD and the percentage recovery values were in the following ranges: 0.41–0.89% and 99.38–101.94%, respectively.

The proposed method is more sensitive than chromatographic method used to determine ESC in urine ( $22.80 \times 10^{-5}$  mol L<sup>-1</sup>).<sup>64</sup> The proposed method is less sensitive than capillary electrophoresis method ( $1.496 \times 10^{-9}$ – $1.61 \times 10^{-6}$  mol L<sup>-1</sup>) but our method is more simple, cheap and it is used to determine ESC in urine without any extraction steps or pretreatment.<sup>24</sup>

## 4. Conclusion

It is important to determine drugs at higher sensitivity than in the reported methods, therefore it was our intention to develop a precise and sensitive electroanalytical voltammetric method for the determination of ESC. The use of chloranil as modifier and Ni nanoparticles increases the active sites at the electrode surface which increases the sensitivity toward ESC. The proposed method is more sensitive than some reported methods as mentioned before in the text, thus it is an excellent means for determination of ESC in quality control because of its low cost, accuracy, selectivity and enforcement. The proposed method can be applied in clinical laboratories and pharmacokinetic studies.

## 5. Acknowledgment

The authors would like to express their gratitude to the National Organization for Drug Control and Research (NODCAR, Egypt) for providing instruments and the means necessary to accomplish this work.

## 6. References

1. W. J. Burke, *Expert Opin. Investig. Drugs*, **2002**, *11*, 1477–1486. <https://doi.org/10.1517/13543784.11.10.1477>
2. C. Sanchez, K. P. Bogeso, B. Elbert, E. H. Reines, and C. Braestrup, *Psychopharmacology (Berl.)*, **2014**, *174*, 163–176.
3. M. A. Margoob, D. Mushtaq, I. Murtaza, H. Mushtaq, and A. Ali, *Indian J. Psychiatry*, **2008**, *50*, 47–50. <https://doi.org/10.4103/0019-5545.39759>
4. M. V. Mahadik, S. R. Dhaneshwar, and M. J. Kulkarni, *Eurasian J. Anal. Chem.*, **2007**, *2*, 101–117.
5. N. Dhavale, S. Gandhi, S. Sabnis, and K. Bothara, *Chromatographia*, **2008**, *67*, 487–490. <https://doi.org/10.1365/s10337-008-0524-7>
6. C. Greiner, C. Hiemke, W. Bader, and E. Haen, *J. Chromatogr. B*, **2007**, *848*, 391–394. <https://doi.org/10.1016/j.jchromb.2006.10.058>
7. S. B. Syama, and A. Suneetha, *Int. J. Pharm. Bio. Sci.*, **2011**, *2*, 140–146.
8. B. Raman, B. A. Sharma, P. D. Ghugare, S. Nandavadekar, D. Singh, P. K. Karmuse, and A. Kumar, *J. Pharm. Biomed. Anal.*, **2010**, *53*, 895–901.
9. M. S. Charde, *Int. J. Pharm. Chem.*, **2012**, *2*, 23–26.
10. C. N. Bhimanadhuni, D. R. Garikapati, and P. Usha, *Int. Curr. Pharm. J.*, **2012**, *1*, 193–198.
11. T. Samanta, S. Dey, H. B. Samal, D. B. Kumar, D. L. M. Mohanty, and K. Bhar, *Int. J. Chem. Res.*, **2011**, *2*, 11–15.
12. A. Chanda, N. Ramalakshmi, C. N. Nalini, S. Arunkumar, and S. Mahabubi, *IAJPR*, **2016**, *6*, 5622–5629.
13. N. Rahul, G. Vaibhavi, and D. K. Vilasrao, *IAJPR*, **2015**, *5*, 2497–2502.
14. E. A. Taha, N. N. Salama, and S. Wang, *Anal. Chem. Insights*, **2009**, *4*, 1–9. <https://doi.org/10.4137/ACI.S2274>
15. S. V. Gandhi, N. D. Dhavale, V. Y. Jadhav, and S. S. Sabnis, *J. AOAC Int.*, **2008**, *91*, 33–38.
16. S. C. Patel, and D. G. Maheshwari, *AJPTI*, **2016**, *4*, 59–70.
17. S. Sharma, H. Rajpurohit, C. Sonwal, A. Bhandari, V. R. Choudhary, and T. Jain, *J. Young Pharm.*, **2010**, *2*, 420–423. <https://doi.org/10.4103/0975-1483.71626>
18. T. Vetrichelvan, K. Arul, M. Sumithra, and B. Umadevi, *Indian J. Pharm. Sci.*, **2010**, *72*, 269–271. <https://doi.org/10.4103/0250-474X.65011>
19. R. B. Kakde, and D. D. Satone, **2009**, *71*, 702–705. <https://doi.org/10.4103/0250-474X.59559>
20. K. M. Al-Ahmary, *Int. J. Pharm. Chem.*, **2012**, *2*, 121–125.
21. S. Pinki, D. Patel, D. Meshram, and S. Desai, *IAJPR*, **2016**, *6*, 4544–4553.
22. N. A. Alarfaj, F. A. Aly, and A. A. Al-Qahtany, *Luminescence*, **2013**, *28*, 84–92. <https://doi.org/10.1002/bio.2372>
23. B. Sungthong, P. Jac, and G. K. E. Scriba, *J. Pharm. Biomed. Anal.*, **2008**, *46*, 959–965. <https://doi.org/10.1016/j.jpba.2007.05.029>
24. N. Johannesson, and J. Bergquist, **2007**, *43*, 1045–1048. <https://doi.org/10.1016/j.jpba.2006.09.008>
25. F. M. G. Al-Amri, N. A. Alarfaj, and F. A. Aly, *Int. J. Electrochem. Sci.*, **2013**, *8*, 10044–10058.
26. A. F. Khorshid, *UKJPB*, **2014**, *2*, 9–21.
27. R. Jain, Dhanjai, and S. Sharma, *Colloids Surf. A*, **2013**, *133*, 178–184. <https://doi.org/10.1016/j.colsurfa.2013.06.007>
28. O. R. Luca, T. Wang, S. J. Konezny, V. S. Batista, and R. H. Crabtree, *New J. Chem.*, **2011**, *35*, 998–999. <https://doi.org/10.1039/c0nj01011a>
29. S. A. M. Refaey, A. A. Hassan, and H. S. Shehata, *Int. J. Electrochem. Sci.*, **2008**, *3*, 325–337.
30. Y. Hanyu, and I. Honma, *J. Mater. Chem.*, **2011**, *21*, 9154–9159. <https://doi.org/10.1039/c1jm00026h>
31. R. Ojani, J. B. Raoof, and S. Zamani, *Electroanalysis*, **2005**, *17*, 1740–1745. <https://doi.org/10.1002/elan.200503277>
32. A. A. Ensafi, M. Dadkhah, and H. K. Maleh, **2011**, *84*,

- 148–154. <https://doi.org/10.1016/j.colsurfb.2010.12.028>
33. A. K. Attia, and M. A. Elshal, *Anal. Bioanal. Electrochem.*, **2012**, *4*, 213–224.
34. A. A. Ensafi, A. Arabzadeh, and H. K. Maleh, *J. Braz. Chem. Soc.*, **2010**, *21*, 1572–1580. <https://doi.org/10.1590/S0103-50532010000800024>
35. H. K. Maleh, M. A. Khalilzadeh, Z. Ranjbarha, H. Beitollahi, A. A. Ensafi, and D. Zareyee, *Anal. Methods*, **2012**, *4*, 2088–2094. <https://doi.org/10.1039/c2ay05865k>
36. H. Yaghoobian, V. S. Nejad, and S. Roodsaz, *Int. J. Electrochem. Sci.*, **2010**, *5*, 1411–1421.
37. M. A. Mohamed, N. S. Abdelwahab, and C. E. Banks, *Anal. Methods*, **2016**, *8*, 4345–4353. <https://doi.org/10.1039/C6AY00454G>
38. N. N. Salama, S. M. Azab, M. A. Mohamed, and A. M. Fekry, *RSC Adv.*, **2015**, *5*, 14187–14195.
39. H. M. Ahmed, M. A. Mohamed, and W. M. Salem, *Anal. Methods*, **2015**, *7*, 581–589. <https://doi.org/10.1039/C4AY02450H>
40. D. Yang, L. Wang, Z. Chen, M. Megharaj, and R. Naidu, *Electrochim Acta*, **2014**, *132*, 223–229. <https://doi.org/10.1016/j.electacta.2014.03.147>
41. S. Tajik, M. A. Taher, and H. Beitollahi, *Sens. Actuators B*, **2014**, *197*, 228–236. <https://doi.org/10.1016/j.snb.2014.02.096>
42. A. K. Attia, W. M. Salem, and M. A. Mohamed, *Acta Chim. Slov.*, **2015**, *62*, 588–594. <https://doi.org/10.17344/acsi.2014.950>
43. B. Nigovic, M. Sadikovic, and M. Sertic, *Talanta*, **2014**, *122*, 187–194. <https://doi.org/10.1016/j.talanta.2014.01.026>
44. Y. Liu, G. Su, B. Zhang, G. Jiang, and B. Yan, *Analyst*, **2011**, *136*, 872–877. <https://doi.org/10.1039/c0an00905a>
45. Y. Oztekin, A. Ramanaviciene, and A. Ramanavicius, *Electroanalysis*, **2011**, *23*, 701–709. <https://doi.org/10.1002/elan.201100121>
46. A. K. Attia, A. M. Badawy, and S. G. Abd-Elhamid, *RSC Adv.*, **2016**, *6*, 39605–39617.
47. M. A. Sultan, A. K. Attia, M. M. Abou El-Alamin, and M. A. Atia, *WJPPS*, **2016**, *5*, 93–108.
48. R. A. Ahmed, and A. M. Fekry, *Int. J. Electrochem. Sci.*, **2013**, *8*, 6692–6708.
49. M. H. Mashhadizadeh, and E. Afshar, *Electrochim Acta*, **2013**, *87*, 816–823. <https://doi.org/10.1016/j.electacta.2012.09.004>
50. J. Tashkhourian, M. R. H. Nezhad, J. Khodavesi, and S. Javadi, *J. Electroanal. Chem.*, **2009**, *633*, 85–91. <https://doi.org/10.1016/j.jelechem.2009.04.028>
51. H. Heli, M. Hajjizadeh, A. Jabbari, and A. A. M. Movahedi, *Anal. Biochem.*, **2009**, *388*, 81–90. <https://doi.org/10.1016/j.ab.2009.02.021>
52. C. M. Welch, and R. G. Compton, *Anal. Bioanal. Chem.*, **2006**, *384*, 601–619. <https://doi.org/10.1007/s00216-005-0230-3>
53. H. Ibrahim, and Y. Temerk, *Sens. Actuators B*, **2015**, *206*, 744–752. <https://doi.org/10.1016/j.snb.2014.09.011>
54. M. A. Mohamed, A. K. Attia, and H. M. Elwy, *Electroanalysis*, **2017**, *29*, 506–513. <https://doi.org/10.1002/elan.201600311>
55. A. M. Fundo, and L. M. Abrantes, *J. Electroanal. Chem.*, **2007**, *600*, 63–79. <https://doi.org/10.1016/j.jelechem.2006.03.023>
56. I. G. David, D. E. Popa, A. A. Calin, M. Buleandra, and E. E. Iorgulescu, *Turk. J. Chem.*, **2016**, *40*, 125–135. <https://doi.org/10.3906/kim-1504-42>
57. D. K. Gosser: *Cyclic Voltammetry Simulation and Analysis of Reaction Mechanism*, New York, USA: VCH, **1993**.
58. A. J. Bard, L. R. Faulkner, J. Leddy, and C. G. Zoski. *Electrochemical methods: Fundamentals and Applications*, Wiley, New York, **1980**.
59. E. Laviron, *J. Electroanal. Chem. Interfacial Electrochem.*, **1979**, *101*, 19–28. [https://doi.org/10.1016/S0022-0728\(79\)80075-3](https://doi.org/10.1016/S0022-0728(79)80075-3)
60. B. R. Eggins., *Chemical Sensors and Biosensors*, John Wiley & Sons, Ltd, UK, **2003**.
61. J. Xia, Z. Wang, F. Cai, F. Zhang, M. Yang, W. Xiang, S. Bi, and R. Gui, **2015**, *5*, 39131–39137.
62. L. Fotouhi, M. Fatollahzadeh, M. M. Heravi, *Int. J. Electrochem. Sci.*, **2012**, *7*, 3919–3928.
63. ICH, *Stability Testing of New Drug Substances and Products*. International Conference on Harmonization, IFPMA, Geneva, **1993**.
64. A. Salomone, D. Di Corcia, E. Gerace, and M. Vincenti, *J. Anal. Tox.*, **2011**, *35*, 519–523. <https://doi.org/10.1093/anatox/35.7.519>

## Povzetek

Opisujemo občutljivo voltametrično metodo za določanje escitalopram oksalata, ki temelji na elektrokatalitski oksidaciji v Britton-Robinsonovem pufru (pH območje 2 do 10) na senzoru iz ogljikove paste s kloramilom, modificirane z nikljevimi nanodelci. Modificirano elektrodo smo okarakterizirali z vrstično elektronsko mikroskopijo, elektrokemijsko impedanco in ciklično voltametrijo. Raziskavo elektrokemijskega obnašanja escitalopram oksalata smo izvedli s ciklično voltametrijo in diferencialno pulzno voltametrijo. Maksimalni anodni tok je imel linearno območje od  $1,0 \times 10^{-6}$  do  $7,0 \times 10^{-5}$  mol L<sup>-1</sup>. Meja zaznave je pod  $2,0 \times 10^{-7}$  mol L<sup>-1</sup>. Predlagana metoda je hitra, ekonomična, preprosta, točna in občutljiva voltametrična metoda za določanje escitalopram oksalata v farmacevtskem produktu, farmacevtskih oblikah in v urinu.

Scientific paper

# Peach and Cherry Agroindustrial Wastes: New and Economic Sources for the Production of Lignocellulolytic Enzymes

Merve Akpinar<sup>1</sup> and Raziye Ozturk Urek<sup>2,\*</sup><sup>1</sup> Chemistry Department, Graduate School of Natural and Applied Sciences, Dokuz Eylül University, 35160 Buca, Izmir, Turkey.<sup>2</sup> Chemistry Department, Biochemistry Division, Faculty of Science, Dokuz Eylül University, 35160 Buca, Izmir, Turkey

\* Corresponding author: E-mail: raziye.urek@deu.edu.tr

Tel: +90 232 301 8689; Fax: +90 232 453 4188

Received: 06-02-2017

## Abstract

*Pleurotus eryngii* was incubated on both peach and cherry agroindustrial wastes by solid state fermentation for 30 days without/with pretreatment conditions. The lignocellulosic substrates were pretreated with dilute acid and alkaline solutions, hot water before incubation. The maximum carboxymethyl cellulase and xylanase activities peaked on 3<sup>rd</sup> and 5<sup>th</sup> days under control conditions of both wastes, respectively. The highest laccase and manganese peroxidase activities reached to their maximum on 17<sup>th</sup> day as  $2193.06 \pm 50.4 \text{ UL}^{-1}$  and  $732.73 \pm 19.8 \text{ UL}^{-1}$ , respectively. The highest aryl alcohol oxidase activity was obtained as  $239.25 \pm 7.3 \text{ UL}^{-1}$  in control condition of peach cultures. The used pretreatment methods had generally negative effects on lignocellulolytic enzyme production. The highest lignocellulolytic activities were detected using peach wastes. To results, these wastes could be used as alternative, new and economic energy sources to produce high amounts of lignocellulolytic enzymes.

**Keywords:** Agroindustrial wastes, lignocellulolytic enzymes, *Pleurotus eryngii*, pretreatment, solid state fermentation.

## 1. Introduction

Lignocellulosic substrate from forestry, agricultural and agroindustrial wastes is abundant, renewable and inexpensive energy sources for the production of various value added products, such as ethanol, food additives, organic acids, enzymes, and others due to their chemical composition based on sugars and other compounds of interest.<sup>1</sup> Also, the accumulation of lignocellulosic wastes in large quantities causes environmental problems when they could not be used for the production of these products.<sup>1,2</sup>

Bioconversion of lignocellulosic substrate to value added products is so difficult to its tertiary architecture consisting of primarily cellulose, hemicelluloses and lignin that are strongly intermeshed and chemically bonded by non-covalent forces and by covalent crosslinkages. Selective organisms, especially white rot fungi (WRF), can efficiently degrade lignocelluloses.<sup>2</sup> This degradative ability of WRF is due to their extracellular hydrolytic and ligninolytic enzyme systems. For lignocellulose bioconversion, the hydrolytic

enzyme systems are divided into two groups: cellulolytic and hemicellulolytic, which contain carboxymethyl cellulase (endo-1,4- $\beta$ -glucanase; CMCase), exo-1,4- $\beta$ -glucanase, 1,4- $\beta$ -glucanase and xylanases. Another enzyme system is ligninolytic group, which includes laccase (Lac), manganese peroxidase (MnP), lignin peroxidase (LiP) and aryl alcohol oxidase (AAO). The highly specific hydrolytic enzyme systems convert cellulose and hemicellulose carbohydrates into fermentable sugars; hexoses and pentoses. The non-specific oxidative ligninolytic enzymes catalyze phenolic and non-phenolic compounds in lignin structure.<sup>3</sup>

The lignocellulose-based biotechnological applications such as biopulping, biobleaching, decolorization, degradation of environmental contaminants, etc. require low cost and large scale enzymes due to increasing demand for markets.<sup>4</sup> Solid state fermentation (SSF) stands out in the production of lignocellulolytic and other industrially important enzymes. Examples of enzymes produced by different organisms such as *Bacillus* sp., *Pleurotus* sp., *Aspergillus* sp., *Trametes* spp., etc. under SSF using different sub-

strates, wheat bran, wheat straw, apple pomace, rice straw, sugarcane bagasse, include laccase, cellulose, lipase, pectinase, protease, xylanase, amylase, etc.<sup>5</sup> SSF, an alternative culture method, has several advantages over the conventional submerged ones, like higher yields of enzymes. Generally, this process was carried out by using lignocellulosic wastes used as substrates and support material for microbial growth and production of several value added products.<sup>4,6</sup> The effective utilization of lignocellulosic components would play a significant role in economic enzyme production. For this reason, lignocellulosic substrate sometimes requires pretreatment to improve enzymatic hydrolysis by fungi. The purpose of the pretreatment is to remove lignin and hemicelluloses, reduce cellulose crystallinity, and increase the porosity of the materials.<sup>7</sup> Pretreatment should ideally involve requirement of low energy with no recycling or environmental costs.<sup>8</sup> A wide range of thermal, mechanical and chemical pretreatment methods and their combinations could be used for efficiently conversion of lignocelluloses. The pretreatment methods may vary depending on the raw material selected, but they could be eco-friendly and not increase the total economy of the bioconversion of the lignocellulosic substrate.<sup>8,9</sup>

The present study evaluated peach and cherry wastes as substrates for production of lignocellulolytic enzymes by *Pleurotus eryngii* in SSF, and is the first study in this regard. Different agroindustrial wastes were screened for lignocellulolytic enzyme production under SSF,<sup>1</sup> however peach and cherry wastes have not been reported in production of various industrially important enzymes including lignocellulolytic enzymes by fungi as per the published literature so far. Namely, these wastes were firstly investigated for the production of lignocellulolytic enzymes by *P.eryngii*, and also the use of them for SSF as substrates with or without any pretreatment conditions. These agro-industrial wastes (with and without pretreatment) were used as major nutritional sources for production of cellulases (carboxymethylcellulase (CMCase), exo-1,4- $\beta$ -glucanase, 1,4- $\beta$ -glucosidase), xylanase and ligninolytic (laccase (Lac), manganese peroxidase (MnP), lignin peroxidase (LiP), aryl alcohol oxidase (AAO)) enzymes by the fungus. Three chemical pretreatment processes including neutral, dilute acid and alkaline, utilized for improving the production of lignocellulolytic enzymes. The study has showed that peach and cherry agroindustrial wastes can serve as important alternative cheap substrates for economic production of lignocellulolytic enzymes by *P.eryngii*.

## 2. Experimental

### 2. 1. Lignocellulosic Substrates and Their Chemical Compositions

Peach and cherry agroindustrial wastes from Dimes fruit juice factory, Izmir, Turkey, were collected and used

as the solid substrate for the SSF. According to knowledge from Dimes fruit juice factory, the peach and cherry fruits cultivated in the Aegean region of Turkey were harvested at optimum technological maturity. Their wastes came for two or three pressing to make fruit juice. The chemical compositions of both wastes were analyzed before and after all pretreatment methods. The total carbohydrate, protein and lignin contents of them were colorimetrically determined by the phenol-sulfuric acid method,<sup>10</sup> Bradford dye-binding assay,<sup>11</sup> and thioglycolic acid method,<sup>12</sup> respectively. In addition, cellulose levels after acid hydrolysis in these wastes were determined gravimetrically.<sup>13</sup>

### 2. 2. Media Preparation

The white rot fungus *P. eryngii* (DC.) Gillet (MCC58) was used in this study and obtained from Agro-ma Mushroom Cultivation (Denizli, Turkey). This strain was selected as a suitable organism for bioprocessing of SSF for its potential for higher lignocellulolytic enzyme production.<sup>14</sup> *P.eryngii* cultures were maintained on malt-peptone-agar medium at  $4 \pm 1$  °C and transferred every month to fresh medium, and then incubated at  $25 \pm 1$  °C during 12 day. For enzyme production, untreated peach and cherry agroindustrial wastes and pretreated wastes were used as substrates for growth media. They were stored at  $-20 \pm 1$  °C prior to use. SSF was carried out in 100 mL Erlenmeyer flasks containing 5.0 g of these wastes as major nutritional sources and 10 mL of basal culture medium of the following composition per liter:  $\text{NH}_4\text{NO}_3$ , 2.0 g;  $\text{KH}_2\text{PO}_4$ , 0.8 g;  $\text{K}_2\text{HPO}_4 \times 7\text{H}_2\text{O}$ , 0.75 g;  $\text{MgSO}_4 \times 7\text{H}_2\text{O}$ , 0.5 g; yeast extract, 2.0 g;  $\text{ZnSO}_4 \times 7\text{H}_2\text{O}$ , 0.002 g;  $\text{FeSO}_4 \times 7\text{H}_2\text{O}$ , 0.005 g;  $\text{CaCl}_2 \times 2\text{H}_2\text{O}$ , 0.06 g,  $\text{CuSO}_4 \times 7\text{H}_2\text{O}$ , 0.02 g;  $\text{MnSO}_4 \times \text{H}_2\text{O}$ , 0.05 g.<sup>15</sup> The ratio between amount of solid waste and volume of basal medium was adjusted at 1:2.<sup>16</sup> The moisture levels of peach and cherry wastes after adding the basal culture medium in this study were  $18.41 \pm 1.6$  and  $39.73 \pm 3.5\%$ , respectively. Also, the final pH of the medium was adjusted to 6.0 after sterilization. Three agar plugs (1 cm<sup>2</sup> disks) cut from actively growing culture (12 day old), were used as inoculums. The fermentation was carried out in a controlled environment with temperature at  $28 \pm 0.5$  °C for 30 days under stationary condition in complete darkness. Under control conditions, the agroindustrial wastes were directly used without any pretreatment methods. Samples from flasks were harvested after 3, 5, 7, 10, 12, 15, 17, 20, 26 and 30 days of cultivation. Experiments were done triplicate and samples were analyzed in triplicate.

### 2. 3. Pretreatment of Agroindustrial Wastes

The both peach and cherry wastes, lignocellulosic substrates, were pretreated with dilute acid (sulfuric acid 1.0%, w/v) and alkaline (sodium hydroxide 1.0%, w/v) solutions, hot water. The hot water treatment was named

as neutral pretreatment, while alkaline treatments could be named as base pretreatments. At all pretreatment methods, the substrate at a solid loading of 10% (w/w) was mixed with pretreatment agents and pretreated at 100 °C with 60 minutes. And also, the substrate was washed until the pH adjusted to initial pH value at dilute acid and alkaline pretreatments for getting the same pH levels. After pretreatment, the substrate was separated by filtration at room temperature, and then it was ready for the utilization in SSF bioprocess.

## 2. 4. Enzyme Extraction

The samples in SSF were mixed with 25 mL of 50 mM sodium-acetate buffer (pH 5.0) two times and stirred at 180 rpm for 1 hour on ice bath to extract the samples. Solids were separated by centrifugation ( $4 \pm 1$  °C, 15000 rpm, 10 minutes).<sup>16</sup> The lignocellulosic substrate was completely removed after centrifugation and the clear supernatant was obtained. The all supernatants were used for measurements of the extracellular lignocellulolytic enzyme activities and analysis's of protein, reducing sugar and nitrogen amounts.

## 2. 5. Assay of Enzyme Activities

CMCase and xylanase activities were estimated by the dinitrosalicylic acid method (DNS) using 2% carboxymethyl cellulose and xylan from beechwood in the sodium citrate buffer (50 mM, pH 4.8) as the substrates with glucose and xylose as the standards, respectively.<sup>17,18</sup> Exoglucanase and  $\beta$ -glucosidase activities were monitored using 2.0 mM p-nitrophenyl- $\beta$ -cellobioside and p-nitrophenyl- $\beta$ -glucopyranoside in the sodium acetate buffer (50 mM, pH 5.0) as the substrates, respectively.<sup>17</sup> Lac activity was assayed by measuring the oxidation of 2, 2-amino-bis(3-ethyl benzothiazoline-6-(sulfonate) according to Johannes & Majcherczyk with minor modifications using 5.0 mM 2,2'-azino-bis(3-ethylbenzothiazoline-6-sulphonic acid) as a substrate and sodium acetate buffer (100 mM, pH 4.5).<sup>19</sup> MnP activity was measured by 2, 6-dimethoxyphenol oxidation, 20 mM, with minor modifications

in the presence of hydrogen peroxide (4 mM) and manganese sulfate (30 mM).<sup>20</sup> LiP activity was determined by the oxidation of veratryl alcohol to veratraldehyde in the presence of hydrogen peroxide using sodium tartarate buffer (125 mM, pH 2.5).<sup>21</sup> AAO activity was assayed spectrophotometrically using veratryl alcohol as a substrate with no adding hydrogen peroxide.<sup>22</sup> The all enzymatic activity of 1 U was defined as the amount of enzyme that transforms 1  $\mu$ mol substrate/minute in terms of volumetric activity.

## 2. 6. Estimation of Protein, Reducing Sugar and Nitrogen Contents

Protein concentrations were measured using the Bradford dye-binding assay with bovine serum albumin as standard.<sup>11</sup> Reducing sugars levels were measured by the DNS method using D-glucose as standard, according to Miller.<sup>23</sup> Ammonium nitrogen content was assayed by the phenol-hypochlorite method using  $(\text{NH}_4)_2\text{SO}_4$  as standard.<sup>24</sup>

## 2. 7. Statistical Analysis

All statistical analyses were performed with the program SPSS 15.0 for Windows. The all values were the mean of three separate experiments.

## 3. Results and Discussion

Selection of appropriate lignocellulolytic organisms for SSF is one of the important factors via useful agricultural solid substrates. In this study, *P.eryngii* was used for enzyme producer due to its lignocellulolytic ability.<sup>16,25</sup> The chemical compositions of untreated and pretreated peach and cherry wastes are demonstrated in Table 1. According to the obtained results, the lignin and protein concentrations for untreated peach waste were higher than that of untreated waste cherry. The lignin concentrations in both wastes were higher when compared to other lignocellulosic wastes; while the cellulose concentrations in

**Table 1.** The changes of main components of peach and cherry wastes after all pretreatments.

		Protein Concentration (%)	Cellulose Concentration (%)	Lignin Concentration (%)	Total Carbohydrate Concentration (%)
Peach	Untreated	0.08 $\pm$ 0.005	4.63 $\pm$ 0.3	40.56 $\pm$ 3.1	18.59 $\pm$ 1.1
	Neutral-pretreated	0.08 $\pm$ 0.006	4.72 $\pm$ 0.4	38.45 $\pm$ 3.3	23.46 $\pm$ 1.8
	Acid-pretreated	0.072 $\pm$ 0.006	4.44 $\pm$ 0.3	34.07 $\pm$ 2.6	28.46 $\pm$ 1.9
	Alkaline-pretreated	0.074 $\pm$ 0.005	4.12 $\pm$ 0.3	31.23 $\pm$ 2.2	36.06 $\pm$ 2.8
Cherry	Untreated	0.05 $\pm$ 0.002	14.04 $\pm$ 1.0	38.8 $\pm$ 2.6	19 $\pm$ 1.1
	Neutral-pretreated	0.05 $\pm$ 0.004	14.46 $\pm$ 1.1	37.24 $\pm$ 3.4	24.12 $\pm$ 1.7
	Acid-pretreated	0.044 $\pm$ 0.003	13.34 $\pm$ 0.9	33.59 $\pm$ 2.7	29.74 $\pm$ 1.8
	Alkaline-pretreated	0.047 $\pm$ 0.002	12.56 $\pm$ 0.9	30.65 $\pm$ 2.4	36.86 $\pm$ 2.7

peach and cherry wastes were lower.<sup>1</sup> Also, the total carbohydrate concentrations with all pretreatments in both wastes increased, while lignin concentrations in those were reduced by them. This may be due to the different structural properties of peach and cherry waste. In other words, peach wastes have softer fiber when compared to intact fiber of cherry wastes.

The reducing sugar and nitrogen levels in all growth media decreased rapidly up to 3<sup>rd</sup> day of cultivation, but not depleted fully by *P.eryngii*, so that the cultivation was reached to carbon and nitrogen-limited conditions. In addition, good colonization on these wastes with control and pretreated conditions was achieved with *P.eryngii*, fungal growth being observed from the second day of the fermentation, and complete colonization of fungus was observed within 30 days of cultivation. Also, the protein production in *P.eryngii* enzyme supernatant were changed up to  $187.78 \pm 8.6$  ppm for cherry wastes with and without pretreatment conditions, and this value was 1.26-fold higher than that of control ( $p < 0.05$ ). The highest protein production was obtained in acid pretreated condition followed by alkaline, neutral pretreatment and control conditions, respectively. On the other hand, the highest protein production in control conditions of peach cultures was determined as  $303.49 \pm 10.2$  ppm on 20<sup>th</sup> day following alkaline, neutral and acid conditions, respectively. According to obtained results, the observation of the consumption of glucose and nitrogen by *P.eryngii*, fungal growth and protein production could be proofs that these peach and cherry wastes generated by food processing industries were good substrates for producing lignocellulolytic enzymes. Also, the use of peach and cherry wastes for economically production of these enzymes in this research has an importance and novel with regards to literature, most agro-industrial wastes used to produce lignocellulolytic enzymes by WRF have not been published since to date.

Lignocellulosic materials are recalcitrant to fungal hydrolysis due to their composite structure.<sup>3</sup> Effective pretreatments should improve the lignocellulolytic enzyme

production, but selection of these methods is great importance for economic SSF process. According to the literature, there is no study about lignocellulolytic enzyme production by *P.eryngii* using peach and cherry wastes with and/or without any pretreatment conditions. The activities of CMCase and xylanase showed similar trends under control and neutral-treatment condition of peach cultures. The both cellulolytic enzyme activities under control conditions of peach cultures were increased up to 5<sup>th</sup> day of incubation, and then decreased. The highest levels of these enzymes were determined as  $3.64 \pm 0.02$  U mL<sup>-1</sup> and  $3.08 \pm 0.02$  U mL<sup>-1</sup>, respectively. Similarly, the maximum values of CMCase and xylanase enzymes were detected as  $1.30 \pm 0.01$  and  $1.16 \pm 0.01$  U mL<sup>-1</sup> on the 3<sup>rd</sup> day of incubation under control condition of cherry cultures. The decrements in both enzymes were observed after all treatments in peach and cherry cultures as can be seen in Figures. 1 and 2. That is, the CMCases in both cultures were produced simultaneously with xylanases by the *P.eryngii* during the cultivation period. Dias et al. have noted that during the SSF period the very low CMCase activities were detected in both *Irpex lacteus* and Euc-1 strains compared to our maximum CMCase activities of peach and cherry cultures by *P.eryngii*.<sup>26</sup> In that study, *I. lacteus* and Euc-1 showed a peak of xylanase activity ( $0.08$  U mL<sup>-1</sup>) after 10 days of incubation. On the other hand, Sharma and Arora researched which supplements were enhanced the lignocellulolytic enzyme activities of *Phlebia floridensis* by using paddy straw of SSF.<sup>27</sup> According to their results, the maximum CMCase and xylanase activities were respectively recorded as 3.27 and 1.83 U mL<sup>-1</sup> on supplemented conditions, namely control values were below them. Naraian et al. subtracted lignocellulolytic enzyme profiles of *Pleurotus* spp.; *Pleurotus florida*, *Pleurotus sajor-caju* and *P.eryngii*.<sup>28</sup> The CMCase and xylanase activities separately ranged from 198 to 317 U L<sup>-1</sup> and from 178 to 269 U L<sup>-1</sup> as well as they attained very low Lac and MnP activities by these strains. Moreover, Saritha et al. illustrated that *Trametes hirsuta* used

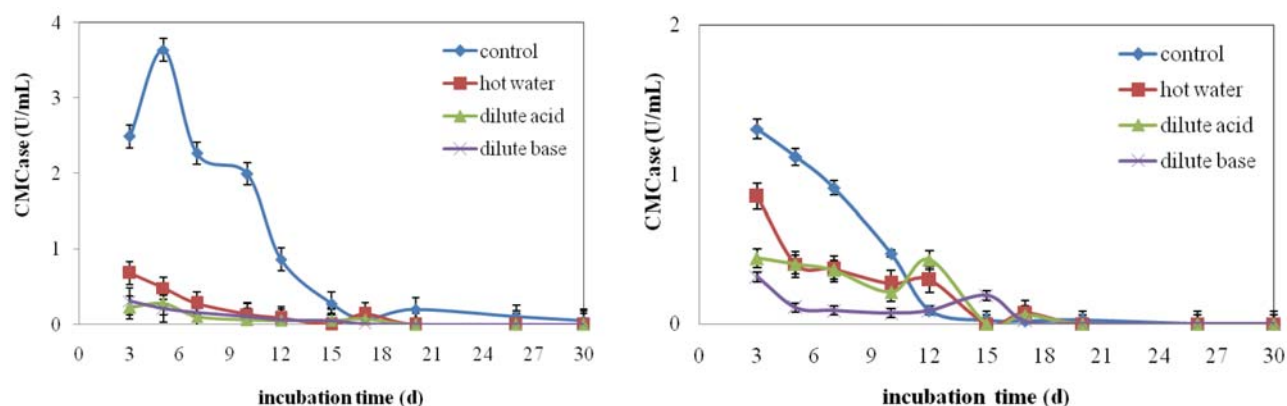


**Figure 1.** Variations of CMCase activities depending on peach (left side) and cherry (right side) cultures. The values are the mean  $\pm$  SD for experiments of three separate experiments.

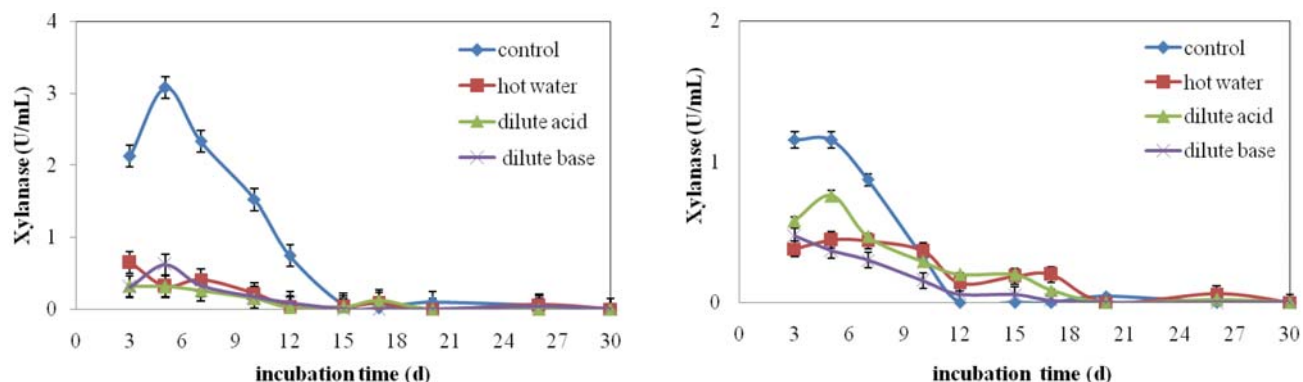


**Figure 2.** Variations of xylanase activities depending on peach (left side) and cherry (right side) cultures. The values are the mean  $\pm$  SD for experiments of three separate experiments.

paddy straw as a carbon source and produced the highest CMCase activity  $0.71 \text{ U mL}^{-1}$  on the 15<sup>th</sup> day of incubation and this value was 5.13-fold lower than that of our result in obtained peach culture.<sup>29</sup>

The  $\beta$ -glucosidase activities were increased up to 20<sup>th</sup> day of incubation, then decreased on both peach and cherry cultures. In peach cultures, the maximum  $\beta$ -glucosidase activity was attained in alkaline-treated cultures followed neutral, control and acid conditions. The maximum activity was found as  $29.96 \pm 0.9 \text{ U L}^{-1}$ , which was 2.35-fold higher than that of control ( $p < 0.05$ ). Similar to peach culture, the highest  $\beta$ -glucosidase activity was obtained as  $35.67 \pm 1.1 \text{ U L}^{-1}$  in alkaline-treated of cherry cultures, which was 1.52-fold higher than that of control ( $p < 0.05$ ). In addition, when the cherry wastes were pretreated with dilute acid solution and hot water, this enzyme activity decreased approximately 50% ( $p < 0.05$ ). The very low exoglucanase activities were detected in all conditions of peach and cherry cultures. The exoglucanase activities in *Peryngii* enzyme supernatant were changed up to  $42.57 \pm 1.2 \text{ U L}^{-1}$  for substrates peach and cherry wastes with and without pretreatment conditions during 30 days of cultivation. The highest exoglucanase activity was detected as  $42.57 \pm 1.2 \text{ U L}^{-1}$  (3<sup>rd</sup> day) in control condition of peach cultures, while  $13.15 \pm 0.2 \text{ U L}^{-1}$  (20<sup>th</sup>

day) in alkaline pretreatment of cherry cultures. There were a few studies about exoglucanase and  $\beta$ -glucosidase production by *Pleurotus* spp.<sup>30</sup> Similar to our activity values,  $\beta$ -glucosidase activities of *Pleurotus* spp. were extremely low.<sup>28</sup> According to literature, fungi generally have not produced all of cellulolytic enzymes. Thus, the consortium cultures have stood out in fungal cellulolytic system and *Pleurotus* spp. secrete dominantly CMCCase of them in peach and cherry cultures of SSF.<sup>31</sup>

The maximum Lac activities in *Peryngii* enzyme supernatant ranged from  $337.29 \pm 11.2$  to  $2193.06 \pm 50.4 \text{ U L}^{-1}$  for peach and cherry wastes with and without pretreatment conditions during 30 days of cultivation as shown in Figure 3. The maximum Lac activities in control conditions of both cultures were attained, and also they were decreased slightly under all pretreatment conditions. Also, the highest Lac activities in peach and cherry cultures were respectively determined as  $2193.06 \pm 50.4 \text{ U L}^{-1}$  (17<sup>th</sup> day) and  $1297.22 \pm 34.6 \text{ U L}^{-1}$  (10<sup>th</sup> day). There were insignificant differences among Lac activities in control conditions of cherry cultures on 7, 10 and 12<sup>th</sup> day of incubation ( $p > 0.05$ ). Stajic et al. showed that the maximum Lac activity by *Pleurotus ostreatus* was attained as  $746.1 \text{ U L}^{-1}$  on the 10 day of incubation using grapevine sawdust as a substrate.<sup>32</sup> When compared to other research of

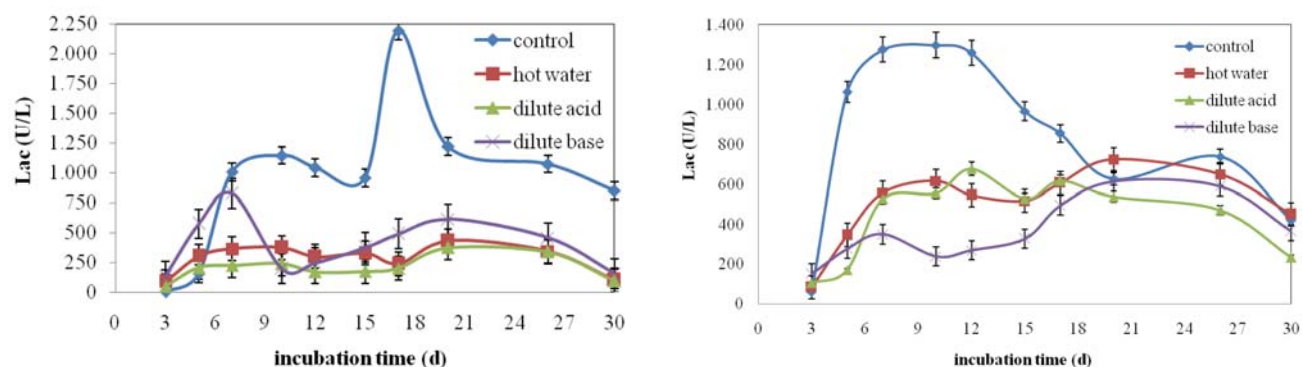


**Figure 3.** Variations of Lac activities depending on peach (left side) and cherry (right side) cultures. The values are the mean  $\pm$  SD for experiments of three separate experiments.



Dias et al.,<sup>26</sup> four white rot fungi screened for Lac production during 46 days and only Euc-1 produced this enzyme (the highest activity of 100 U L<sup>-1</sup>; at the end of the incubation period) using wheat straw. There were insignificantly differences between the highest Lac activity obtained from grape culture with the same strain<sup>16</sup> and peach culture in this study.

As depicted in Figure 4, the highest MnP activity was obtained under control condition followed by alkaline, neutral and acid pretreatments of peach cultures. Concurrently, the highest activity in this culture was detected on 17<sup>th</sup> day as similar to activity of Lac. On the other hand, the maximum MnP activity was obtained under control condition of cherry cultures followed alkaline pretreatment. Also, they were approximately same in acid and neutral pretreatments of cherry cultures, while their levels were lower in activity of alkaline pretreatment. The highest MnP activity in peach cultures was found as 732.73 ± 19.8 U L<sup>-1</sup> on the 17<sup>th</sup> day of incubation. Stajic et al. showed that the maximum MnP activity by *P. ostreatus* was attained as 10.3 U L<sup>-1</sup> (10<sup>th</sup> day) using grapevine sawdust as a substrate and the highest activity obtained was 71.14-fold higher than that of their results,<sup>32</sup> while Isikhuemhen et al. researched the lignocellulolytic enzymes activities from corn stalks under SSF by white rot fungus, *Lentinus squarrosulus* Mnt. during 30 days of incubation, and they determined the highest MnP activity as 13 U L<sup>-1</sup> on the 6<sup>th</sup> day.<sup>33</sup> Also, the highest MnP activity in this study was 2.68-fold higher than the activity determined with Euc-1 strain.<sup>26</sup> Additionally, the effects of lignocellulosic apricot and pomegranate wastes on ligninolytic enzymes by *Peryngii* under SSF conditions were investigated. The highest Lac and MnP activities in this study were 1.36- and 1.26-fold higher than obtained in that study.<sup>34</sup>

Generally, there were little LiP activities in *Pleurotus* sp. according to literature.<sup>16,35</sup> Insignificant levels of LiP activities were detected in all untreated and pretreated of both cultures with similar trends in this study. The highest value was detected as 94.09 ± 4.1 U L<sup>-1</sup> in peach cul-

tures was 2.50-fold higher than that of cherry culture under control conditions ( $p < 0.05$ ). The declines in LiP activities were observed after pretreatment of peach and cherry cultures. Comparing peach and cherry cultures in all conditions for AAO activities, the highest value was achieved as 239.25 ± 7.3 U L<sup>-1</sup> in control condition of peach cultures as shown in Figure 5. The activities in control condition of peach cultures were continuously increased up to 17<sup>th</sup> day of incubation, and then decreased. After pretreatment of peach cultures, the very important decreases in AAO activities were observed, approximately 9.2-fold ( $p < 0.05$ ). Similar to peach cultures, the maximum AAO activity was obtained as 91.4 ± 3.8 U L<sup>-1</sup> in control condition of cherry cultures. The AAO activities under control condition of cherry cultures were increased up to 15<sup>th</sup> day, then decreased. After pretreatment of cherry cultures, the activities were significantly decreased (nearly 4.33-fold, especially alkaline pretreatment) ( $p < 0.05$ ). The maximum activities in acid and neutral pretreated cherry cultures were respectively determined on 30<sup>th</sup> and 17<sup>th</sup> day of incubation. In addition, *I. lacteus* and Euc-1 strains showed their maximum LiP activities as 60 and 80 U L<sup>-1</sup> after 23 and 35 days of incubation during SSF,<sup>26</sup> these results were lower than our highest LiP activity value. When these results were compared to the results of Akpinar and Ozturk Urek, the highest LiP and AAO activities in this study were 1.82 and 1.52-fold higher than that of these attained in optimal conditions, separately.<sup>16</sup> Moreover, Guillén et al. detected very low AAO activities by *Peryngii*.<sup>36</sup> According to literature, most WRF secrete at least two ligninolytic enzymes, whereas *Peryngii* secretes three of them during SSF conditions in this study. Ruqayyah et al. studied that the ligninolytic enzyme activity of two *Panus tigrinus* strains on the substrates; rice straw, rice husk and cassava peel.<sup>37</sup> According to their results, rice husk stimulated maximum Lac (2556 U L<sup>-1</sup>) and LiP (24 U L<sup>-1</sup>) activities by the strains M109RQY and M609RQY, respectively. Moreover, cassava peel stimulated maximum MnP (141 U L<sup>-1</sup>) activity by the strain M109RQY.

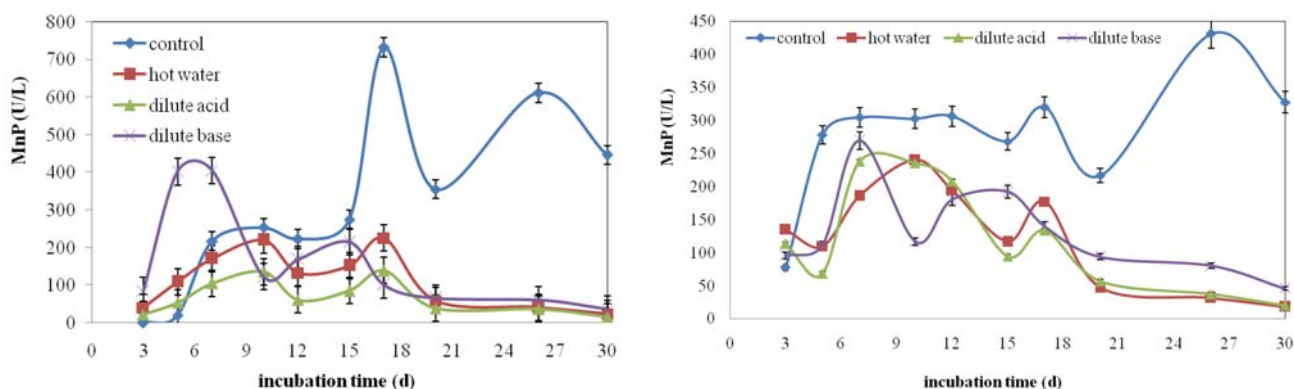


**Figure 4.** Variations of MnP activities depending on peach (left side) and cherry (right side) cultures. The values are the mean ± SD for experiments of three separate experiments.

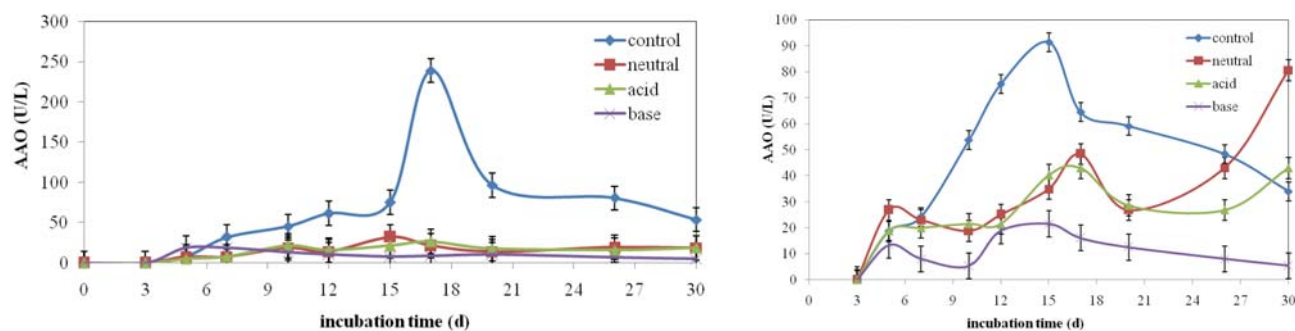


**Figure 5.** Variations of AAO activities depending on peach (left side) and cherry (right side) cultures. The values are the mean  $\pm$  SD for experiments of three separate experiments.

There were few studies about lignocellulolytic enzymes especially hydrolytic enzymes produced by *Pleurotus* species using lignocellulosic wastes according to literature.<sup>30</sup> Namely, this study presented that *P. eryngii* could have the ability to degrade cellulose, hemicellulose and lignin in peach and cherry agroindustrial wastes due to its enzymatic complex. According to the results, there could be a relationship between secretion times of hydrolytic and ligninolytic enzymes. Firstly, the hydrolytic enzymes were produced by *P. eryngii* and then the ligninolytic enzyme secretion was started when other enzyme activities were lowered at the beginning time of incubation. Thus, it could be originated from the lignocellulosic structure of agroindustrial wastes.<sup>2,3</sup> The lignocellulolytic activities were generally decreased with pretreatments methods in the presence of peach and cherry wastes as substrates.  $\beta$ -glucosidase and exoglucanase activities in cherry cultures were increased at alkaline pretreated conditions, while the  $\beta$ -glucosidase activity in peach cultures only was increased at the same conditions. On the both cultures, the CMCase and xylanase reached their highest activity at the initial days of incubation, while the highest ligninolytic enzyme activities occurred after 7<sup>th</sup> day of incubation due to their synergistic interactions among each other. On the other hand, the maximum  $\beta$ -glucosidase activities were attained after the CMCase and xylanase activities were decreased. Thus, it could be held model for the synergism between CMCases, xylanases and  $\beta$ -glucosidases.<sup>38</sup> In addition, the findings of higher lignocellulolytic enzyme activities under control condition of both cultures could be associated with the industrial fruit juice process steps.

In this study, the main components of these wastes were analyzed to investigate their changes during all pretreatments and the effects of the changes on lignocellulolytic enzymes production by *P. eryngii*. After all pretreatments, the chemical compositions of the wastes changed. Generally, the lignin contents decreased, while the total carbohydrate contents increased. Also, the protein contents in all conditions were approximately same with each other. The highest decreases in cellulose contents of both wastes with alkaline-pretreated were obser-

ved followed by acid-pretreated. Likewise, the decreasing in most lignocellulolytic activity could be brought by the treatment of wastes and mainly depend on reducing cellulose contents after treatments. Also, it could be explained by the release of furfural and hydroxymethylfurfural derivatives from hexoses and pentoses in the lignocellulosic wastes following the pretreatment. The excess of these substances could affect the microbial growth and the production of enzymes.<sup>39</sup> On the other hand; the efficiency of pretreatment methods depends on different factors such as composition of lignocellulosic wastes, chemicals, processing time, etc.<sup>40,41</sup> These parameters should be optimized in subsequent experiments for higher lignocellulolytic enzyme yields.

The purpose of this study was to reveal the potentials of peach and cherry wastes as nutrient and carbon-energy sources in economic production of lignocellulolytic enzymes which are practiced on the many biotechnological applications. The fact that these cheap and easily available wastes were firstly utilized in the lignocellulolytic enzymes production having biotechnological importance plays roles in both providing economic efficiency of the process and bringing about the disposal of them. On the other hand, the *P. eryngii* grew on these wastes and produced high amount of lignocellulolytic enzymes when compared to literature. *Pleurotus* sp. appear to play a role in the production of ligninolytic enzyme rather than hydrolytic enzymes. For this reason, it is observed that peach and cherry wastes were highly potential when the efficiency of the used wastes in enzyme production is evaluated. In our another study, apricot and pomegranate agro-industrial wastes contained high lignocellulosic contents, but the enzyme productions were lower than those in this study.<sup>34</sup> Especially, the carbon sources constituted extremely large amounts of the process costs.<sup>42,43</sup> and thus the utilization of these wastes by *P. eryngii* notably reduced the product costs of these enzymes. In addition, there could be unimportant effects on lignocellulolytic enzymes production using these pretreated wastes as some pretreatments methods were performed in order to ensure the availability of them by it. According to our results, the first utilization of these peach and cherry wastes by

*Peryngii* to produce lignocellulolytic enzymes with and without pretreatment reflected the significance of this study.

## 4. Conclusions

This report showed that *Peryngii* can be successfully cultivated on peach and cherry lignocellulosic wastes due to its ability to produce enzymes which are essential for lignocellulose degradation, firstly. A search for newer sources of agroindustrial wastes are of great importance for the economic lignocellulolytic enzyme productions by SSF. According to the obtained results, peach and cherry wastes had high lignocellulosic contents in their composition. The pretreatment methods generally could improve the enzyme productions, however better results were obtained with untreated peach and cherry wastes except exoglucanase and  $\beta$ -glucosidases. Moreover, the peach wastes were more appropriate than cherry wastes for producing lignocellulolytic enzymes by *Peryngii* under SSF conditions. Thus, the lignocellulolytic enzyme production cost of SSF bio-processing was reduced using the untreated peach and cherry wastes. And also, the energy to be given to the system during the pretreatment process would also be another parameter that increases the production cost. The production cost was reduced in this way, referring to the results obtained without the pretreatment. In addition, this study proved that they can be good choice as cheap agroindustrial wastes for the economic and eco-friendly production of lignocellulolytic enzymes by *Peryngii*.

## 5. Acknowledgements

We are thankful to Scientific Research Project of Dokuz Eylül University (project number: 2012.KB.FEN.078). We also are thankful to Dimes, Izmir for providing lignocellulosic substrates for research.

## 6. References

1. S. I. Mussatto, J. A. Teixeira, in: A. Méndez-Vílas, (Ed.), Lignocellulose as Raw Material in Fermentation Processes: Current Research, Technology and Education Topics Applied Microbiology and Microbial Biotechnology, Badajoz, 2010, pp. 897–907.
2. C. Sánchez, *Biotech. Adv.* **2009**, *27*, 185–194. <https://doi.org/10.1016/j.biotechadv.2008.11.001>
3. M. Dashtban, H. Schraft, W. Qin, *Int. J. Biol. Sci.* **2009**, *5*, 578–595. <https://doi.org/10.7150/ijbs.5.578>
4. M. J. Maciel, A. C. Silva, H. C. T. Ribeiro, *Electron. J. Biotechnol.* **2010**, *13*, 1–12.
5. C. R. Soccol, E. S. F. Costa, L. A. J. Letti, S. G. Karp, A. L. Woiciechowski, L. P. Souza Vandenberghe, *Biotechnol. Res. Innov.* 2017, in press, <https://doi.org/10.1016/j.biori.2017.01.002>.
6. J. Barrios-González, *Process. Biochem.* **2012**, *47*, 175–185. <https://doi.org/10.1016/j.procbio.2011.11.016>
7. R. Samuel, M. Foston, N. Jiang, L. Allison, A. J. Ragauskas *Polym. Degrad. Stabil.* **2011**, *96*, 2002–2009. <https://doi.org/10.1016/j.polymdegradstab.2011.08.015>
8. C. H. , C. K. , *Bioresour. Technol.* **2009**, *100*, 866–871. <https://doi.org/10.1016/j.biortech.2008.07.001>
9. G. Y. S. Mtui, *Afr. J. Biotechnol.* **2009**, *8*, 1398–1415.
10. S. K. Saha, C. F. Brewer, *Carbohydr. Res.* **1994**, *254*, 157–167. [https://doi.org/10.1016/0008-6215\(94\)84249-3](https://doi.org/10.1016/0008-6215(94)84249-3)
11. M. Bradford, *Anal. Biochem.* **1976**, *72*, 248–254. [https://doi.org/10.1016/0003-2697\(76\)90527-3](https://doi.org/10.1016/0003-2697(76)90527-3)
12. R. J. Bruce, C. A. West, *Plant. Physiol.* **1989**, *91*, 889–897. <https://doi.org/10.1104/pp.91.3.889>
13. I. Romero, E. Ruiz, E. Castro, M. Moya, *Chem. Eng. Res. Des.* **2010**, *88*, 633–640. <https://doi.org/10.1016/j.cherd.2009.10.007>
14. J. M. R. Luz, M. D. Nunes, S. A. Paes, D. P. Torres, M. C. S. Silva, M. C. M. Kasuya, *Braz. J. Microbiol.* **2012**, *43*, 1508–1515. <https://doi.org/10.1590/S1517-83822012000400035>
15. M. Stajić, L. Persky, D. Friesem, Y. Hadar, S. P. Wasser, E. Nevo, J. Vukojević, *Enzyme. Microb. Tech.* **2006**, *38*, 65–73. <https://doi.org/10.1016/j.enzmictec.2005.03.026>
16. M. Akpınar, R. Ozturk Urek, *Prep. Biochem. Biotech.* **2012**, *42*, 582–597. <https://doi.org/10.1080/10826068.2012.673528>
17. P. Baldrian, V. Valaskova, V. Merhautova, J. Gabriel, *Res. Microbiol.* **2005**, *156*, 670–676. <https://doi.org/10.1016/j.resmic.2005.03.007>
18. S. Kumaran, C. A. Sastry, S. Vikineswary, *World. J. Microb. Biot.* **1997**, *13*, 43–49. <https://doi.org/10.1007/BF02770806>
19. C. Johannes, A. Majcherczyk, *J. Biotechnol.* **2000**, *78*, 193–199. [https://doi.org/10.1016/S0168-1656\(00\)00208-X](https://doi.org/10.1016/S0168-1656(00)00208-X)
20. H. Kamitsuji, Y. Honda, T. Watanabe, M. Kuwahara, *Appl. Microbiol. Biot.* **2004**, *65*, 287–294. <https://doi.org/10.1007/s00253-003-1543-9>
21. M. Tien, T. K. Kirk, *Methods Enzymol.* **1988**, *161*, 238–249. [https://doi.org/10.1016/0076-6879\(88\)61025-1](https://doi.org/10.1016/0076-6879(88)61025-1)
22. K. Okamoto, H. Yanase, *Mycoscience.* **2002**, *43*, 391–395. <https://doi.org/10.1007/S102670200057>
23. G. L. Miller, *Anal. Chem.* **1956**, *31*, 426–428. <https://doi.org/10.1021/ac60147a030>
24. M. W. Weatherburn, *Anal. Chem.* **1967**, *39*, 971–974. <https://doi.org/10.1021/ac60252a045>
25. X. Q. Dong, J. S. Yang, N. Zhu, E. T. Wang, H. L. Yuan, *Bioresour. Technol.* **2013**, *131*, 443–451. <https://doi.org/10.1016/j.biortech.2012.12.182>
26. A. A. Dias, G. S. Freitas, G. S. M. Marques, A. Sampaio, I. S. Fraga, M. A. M. Rodrigues, D. V. Evtuguin, R. M. F. Bezerra, *Bioresour. Technol.* **2010**, *101*, 6045–6050. <https://doi.org/10.1016/j.biortech.2010.02.110>
27. R. K. Sharma, D. S. Arora, *Int. Biodeter. Biodegr.* **2011**, *65*, 990–996. <https://doi.org/10.1016/j.ibiod.2011.07.007>

28. R. Naraiian, D. Singh, A. Verma, S. K. Garg, *J. Environ. Biol.* **2010**, *31*, 945–951.
29. M. Saritha, A. Arora, L. Nain, *Bioresour. Technol.* **2012**, *104*, 459–465. <https://doi.org/10.1016/j.biortech.2011.10.043>
30. M. Téllez-Téllez, R. Díaz, C. Sánchez, G. Díaz-Godínez, *Afr. J. Microbiol. Res.* **2013**, *7*, 276–281. <https://doi.org/10.5897/AJMR12x.016>
31. Y. Chi, A. Hatakka, P. Majjala, *Int. Biodeter. Biodegr.* **2007**, *59*, 32–39. <https://doi.org/10.1016/j.ibiod.2006.06.025>
32. M. Stajčić, J. Vukojević, A. Knežević, I. Milovanović, *Biore-sources.* **2013**, *8*, 3027–3037. <https://doi.org/10.15376/biores.8.2.3027-3037>
33. O. S. Isikhuemhen, N.A. Mikiashvili, C.O. Adenipekun, E.I. Ohimain, G. Shahbazi, *World. J. Microbiol. Biotechnol.* **2012**, *28*, 1961–1966. <https://doi.org/10.1007/s11274-011-0998-6>
34. M. Akpinar, R. Ozturk Urek, *Prep. Biochem. Biotech.* **2014**, *44*, 772–781. <https://doi.org/10.1080/10826068.2013.867870>
35. Y. Fukushima, T. Kirk, *Appl. Environ. Microb.* **1995**, *61*, 872–876.
36. F. Guillén, A. T. Martínez, M. J. Martínez, C. S. Evans, *Appl. Microbiol. Biotechnol.* **1994**, *41*, 465–470.
37. T. I. D. Ruqayyah, P. Jamal, Z. Alam, E. S. Mirghani, *J. Environ. Manage.* **2013**, *118*, 115–121. <https://doi.org/10.1016/j.jenvman.2013.01.003>
38. L. R. Lynd, P. J. Weimer, W. H. Zyl, I. S. Pretorius, *Microbiol. Mol. Biol. R.* **2002**, *66*, 506–577. <https://doi.org/10.1128/MMBR.66.3.506-577.2002>
39. A. M. J. Kootstra, H. H. Beeftink, E. L. Scott, J. P. M. Sanders, *Biotechnol. Biofuels.* **2009**, *2*, 1–14. <https://doi.org/10.1186/1754-6834-2-31>
40. Y. C. Dong, Y. N. Dai, T. Y. Xu, J. Cai, Q. H. Chen, *Bioprocess. Biosyst. Eng.* **2014**, *37*, 755–64. <https://doi.org/10.1007/s00449-013-1045-9>
41. T. López-Arenas, P. Rathi, E. Ramírez-Jiménez, M. Sales-Cruz, *Comput. Aided. Chem. Eng.* **2010**, *28*, 979–984.
42. Z. Velioglu, R. Ozturk Urek, *Appl. Biochem. Biotechnol.* **2014**, *174*, 1354–1364. <https://doi.org/10.1007/s12010-014-1136-3>
43. H. Li, R. Zhang, L. Tang, J. Zhang, Z. Mao, *Chin. J. Chem. Eng.* **2015**, *23*, 227–233. <https://doi.org/10.1016/j.cjche.2014.11.001>

## Povzetek

Gliva *Pleurotus eryngii* je bila inkubirana na agroindustrijskih trdnih odpadkih breskve in češnje. Potekala je 30-dnevna fermentacija brez oziroma z predobdelavo substrata z razredčeno kislino, lugom in vročo vodo pred inkubacijo. Maksimalni aktivnosti karboksimetil celulaz in ksilanaz sta se pojavili tretji in peti dan pri obeh substratih, maksimalni aktivnosti lakaz in mangan peroksidaz pa sta bili doseženi sedemnajsti dan. Predobdelava je v glavnem imela negativen učinek na sintezo ligninolitičnih encimov. Najvišje encimske aktivnosti so bile dosežene na odpadkih breskve. Rezultati kažejo, da ti odpadki lahko služijo kot alternativni in ekonomičen vir energije za produkcijo velikih količin ligninolitičnih encimov.

Scientific paper

# 2D Frameworks Self-assembled From a Hydrazone Ligand and Azide Salts: Synthesis, Structures, and Luminescent Property

Peng Wang,<sup>†</sup> Yu-Shan Wu,<sup>†</sup> Xiao-Meng Han, Shan-Shan Zhao and Jie Qin\*

School of Life Sciences, Shandong University of Technology, Zibo 255049, P. R. China

\* Corresponding author: E-mail: qinjietutu@163.com  
Tel.: 0086-533-2780271; Fax: 0086-533-2781329

Received: 08-02-2017

<sup>†</sup> These authors contributed equally to this work.

## Abstract

Three metal-organic coordination polymers  $\{[\text{Cu}(\text{L})(\text{N}_3)] \cdot (\text{H}_2\text{O})_{0.25}\}_n$  (**1**),  $\{[\text{Zn}(\text{L})(\text{N}_3)] \cdot (\text{H}_2\text{O})_{0.5}\}_n$  (**2**) and  $[\text{Cd}_2(\text{L})_2(\text{N}_3)_2(\text{H}_2\text{O})]_n$  (**3**) have been synthesized from hydrazone ligand *N*'-(1-(pyrazin-2-yl)ethylidene)isonicotinohydrazide (**HL**),  $\text{NaN}_3$  and corresponding metal nitrates. Complexes were characterized by elemental analysis, IR spectroscopy and single-crystal X-ray diffraction. All three complexes feature 2D coordination network in which  $\text{L}^{1-}$  acts as *NNON* tetradentate ligand and azide acts as end-on bridging ligand. In complexes **1** and **2**, only intra-sheet hydrogen bonding interactions are found, while the hydrogen bonding interactions between water molecules and host framework result in 3D network for **3**. In addition, complexes **2** and **3** exhibited intense fluorescent emissions in the solid state at room temperature.

**Keywords:** Hydrazone; azide; crystal structure; luminescence property

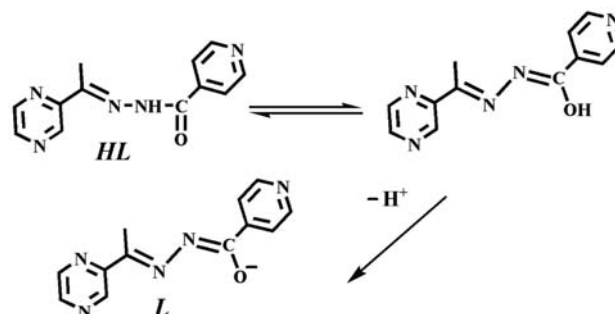
## 1. Introduction

Metal compounds have attracted considerable interest because of their fascinating structures,<sup>1</sup> and functional applications in many research fields such as adsorption,<sup>2</sup> gas storage and separation,<sup>3,4</sup> photoluminescence,<sup>5</sup> and ion exchange.<sup>6,7</sup> The organic ligands are considered to be the most important factor that affects the structures and properties of the coordination polymers.<sup>8</sup>

Hydrazone ligands obtained from condensation reaction of aldehydes (or ketones) and hydrazide are an important class of Schiff bases.<sup>9</sup> We have been interested in coordination compounds involving hydrazone ligands owing to their facile keto-enol tautomerization, the versatile coordination modes, and the strong hydrogen-bonding capability. In previous studies, we synthesized a series of complexes derived from Schiff bases with metal chloride, acetate or nitrate. These complexes showed mononuclear, 1D chain or 3D network.<sup>10–12</sup>

Azide has been demonstrated as the most common used linear ligand.<sup>13</sup> In the azide complexes, the mono-

coordinated, the bidentate including end-on ( $\mu_{1,1}\text{-N}_3^-$ ) and the end-to-end ( $\mu_{1,3}\text{-N}_3^-$ ) bridging modes are frequently observed.<sup>13–15</sup> While the azide group may also function in triply or quadruply bridging modes.<sup>16,17</sup> So, the complexes derived from hydrazone ligands and azide are good candidates allowing the access to intriguing architectures.



Scheme 1. Tautomerization and deprotonation of **HL**.

Recently Shaabani and coworkers reported Cr(III), Mn(II) and Fe(III) complexes with 4-hydroxy-*N'*-(pyridin-2-yl)-methylene)benzohydrazide and azide as bridging ligands. These three complexes showed mononuclear or dinuclear structure with moderate antimicrobial activity.<sup>18</sup> Xu and coworkers reported a series of copper complexes showing antitumor activities based on *N'*-(1-(pyrazin-2-yl)ethylidene)isonicotinohydrazide (**HL**) (Scheme 1).<sup>19</sup> In this paper, we were prompted to study the coordination chemistry of **HL** in the presence of azide. Herein three complexes namely  $\{[\text{Cu}(\text{L})(\text{N}_3)](\text{H}_2\text{O})_{0.25}\}_n$  (**1**),  $\{[\text{Zn}(\text{L})(\text{N}_3)] \cdot (\text{H}_2\text{O})_{0.25}\}_n$  (**2**) and  $[\text{Cd}_2(\text{L})_2(\text{N}_3)_2(\text{H}_2\text{O})]_n$  (**3**) were synthesized, their crystal structure and luminescence properties were also studied.

## 2. Experimental

### 2.1. Materials and Measurements

The chemicals utilized in this investigation such as 2-acetylpyrazine, isoniazid,  $\text{Cu}(\text{NO}_3)_2 \cdot 3\text{H}_2\text{O}$ ,  $\text{Zn}(\text{NO}_3)_2 \cdot 6\text{H}_2\text{O}$  and  $\text{Cd}(\text{NO}_3)_2 \cdot 4\text{H}_2\text{O}$  were commercially available and purchased from Aladdin Industrial Corporation (China).  $\text{NaN}_3$  was purchased from Xiya Reagent (China). *N'*-(1-(pyrazin-2-yl)ethylidene)isonicotinohydrazide (**HL**) was prepared according to the literature.<sup>12</sup> Elemental analyses (C, H and N) were performed using a Perkin Elmer 240 elemental analyzer. IR spectra were recorded on a FT-IR Nicolet 5700 spectrometer from 4000 to 400  $\text{cm}^{-1}$  with KBr pellets. Fluorescence spectra were obtained using Cary Eclipse spectrofluorimeter at room temperature.

**Caution!** Azide compounds of metal ions are potentially explosive. Only a small amount of material should be prepared and it must be handled with care.

### 2.2. Synthesis of $\{[\text{Cu}(\text{L})(\text{N}_3)] \cdot (\text{H}_2\text{O})_{0.25}\}_n$ (**1**)

The methanol solution (4 mL) of the ligand (9.64 mg, 0.040 mmol) was carefully layered on the top of the (4 mL) of  $\text{Cu}(\text{NO}_3)_2 \cdot 3\text{H}_2\text{O}$  (9.66 mg, 0.040 mmol). The (0.20 mol/L, 0.4 mL) of  $\text{NaN}_3$  was gently added as the third layer. The solutions were left for 5 days at room temperature, and complex **1** (7.43 mg) was obtained. Yield: 53%. IR (KBr,  $\text{cm}^{-1}$ ): 3434, 3058, 3008, 2047, 1616, 1562, 1498, 1457, 1408, 1378, 1345, 1326, 1311, 1229, 1194, 1175, 1153, 1140, 1069, 1038, 1008, 868, 848, 797, 760, 709, 696, 656, 607, 581, 520, 456, 423. Anal. Calcd. For  $\text{C}_{12}\text{H}_{10.50}\text{CuN}_8\text{O}_{1.25}$ (%): C, 41.14; H, 3.02; N, 31.99. Found: C, 41.26; H, 3.01; N, 32.12.

### 2.3. Synthesis of $\{[\text{Zn}(\text{L})(\text{N}_3)] \cdot (\text{H}_2\text{O})_{0.5}\}_n$ (**2**)

Complex **2** (5.78 mg) was obtained by similar procedure as **1** by using  $\text{Zn}(\text{NO}_3)_2 \cdot 6\text{H}_2\text{O}$  (11.90 mg, 0.040 mmol) instead of  $\text{Cu}(\text{NO}_3)_2 \cdot 3\text{H}_2\text{O}$ . Yield: 41%. IR (KBr,  $\text{cm}^{-1}$ ): 3411, 3060, 3011, 2056, 1610, 1564, 1460, 1416, 1404, 1364, 1323, 1307, 1234, 1188, 1173, 1154, 1142, 1089, 1067, 1033, 1022, 1008, 914, 866, 854, 793, 765, 716, 702, 660, 612, 578, 558, 519, 457. Anal. Calcd. For  $\text{C}_{12}\text{H}_{11}\text{N}_8\text{O}_{1.5}\text{Zn}$ (%): C, 40.41; H, 3.11; N, 31.42. Found: C, 40.57; H, 3.09; N, 31.51.

Table 1. Crystallographic data for 1–3.

Empirical formula	<b>1</b> $\text{C}_{12}\text{H}_{10.50}\text{CuN}_8\text{O}_{1.25}$	<b>2</b> $\text{C}_{12}\text{H}_{11}\text{N}_8\text{O}_{1.5}\text{Zn}$	<b>3</b> $\text{C}_{24}\text{H}_{22}\text{Cd}_2\text{N}_{16}\text{O}_3$
$M_r$	350.32	356.66	807.38
Crystal system	monoclinic	monoclinic	Triclinic
Space group	$P2_1/n$	$P2_1/n$	$P\bar{1}$
$a$ (Å)	10.1082(6)	10.247(3)	10.3084(18)
$b$ (Å)	14.1898(10)	14.165(4)	11.1749(19)
$c$ (Å)	10.7272(7)	10.703(3)	14.372(2)
$\alpha$ (°)	90.00	90.00	88.687(5)
$\beta$ (°)	116.467(2)	115.063(8)	89.140(5)
$\gamma$ (°)	90.00	90.00	68.924(5)
$V$ (Å <sup>3</sup> )	1377.37(16)	1407.3(7)	1544.4(5)
$Z$	4	4	2
$\rho_c$ (g cm <sup>-3</sup> )	1.689	1.683	1.736
$F(000)$	710	724	796
Data / param. / restr.	2708 / 215 / 11	2760 / 215 / 10	6045 / 421 / 4
$T$ / K	298	298	298
$\mu$ (Mo-K $\alpha$ )/ mm <sup>-1</sup>	1.604	1.765	1.432
GOF ( $F_2$ )	1.051	1.059	1.052
$R1_a, wR2_b$ ( $I > 2\sigma(I)$ )	0.0275, 0.0704	0.0281, 0.0706	0.0330, 0.0936

<sup>a</sup>  $R_1 = \sum \|F_o\| - |F_c| / \sum \|F_o\|$ . <sup>b</sup>  $wR_2 = [\sum w(F_o^2 - F_c^2)^2 / \sum w(F_o^2)]^{1/2}$

## 2. 4. Synthesis of $[\text{Cd}_2(\text{L})_2(\text{N}_3)_2(\text{H}_2\text{O})]_n$ (**3**)

Complex **3** (7.76 mg) was obtained by similar procedure as **1** by using  $\text{Cd}(\text{NO}_3)_2 \cdot 4\text{H}_2\text{O}$  (12.34 mg, 0.040 mmol) instead of  $\text{Cu}(\text{NO}_3)_2 \cdot 3\text{H}_2\text{O}$ . Yield: 48%. IR (KBr,  $\text{cm}^{-1}$ ): 3330, 3079, 2054, 1613, 1568, 1510, 1462, 1404, 1358, 1303, 1233, 1180, 1152, 1137, 1061, 1037, 996, 915, 853, 789, 763, 696, 656, 558, 510, 452. Anal. Calcd. For  $\text{C}_{24}\text{H}_{22}\text{Cd}_2\text{N}_{16}\text{O}_3$ (%): C, 35.70 ; H, 2.75; N, 27.76. Found: C, 35.81; H, 2.74; N, 27.87.

## 2. 5. X-ray crystallography

The data were collected at 298 K on a computer-controlled Bruker D8 venture diffractometer equipped with graphite monochromated Mo-K $\alpha$  radiation ( $\lambda =$

0.71073 Å). The collected diffraction data were reduced using the SAINT program,<sup>20</sup> and multi-scan absorption corrections were performed *via* the SADABS program.<sup>21</sup> The structures were solved by direct methods and refined against  $F^2$  by full-matrix least-squares methods applying the SHELXL program package.<sup>22</sup> All of the non-hydrogen atoms were refined anisotropically. In complexes **1** and **2**, the ADPs of N6 and N7 atoms were restrained to be same within a standard deviation of 0.005 Å. In total 11 geometric restraints were used in modeling this structure. In complex **3**, the atoms O3 were constrained to have the same ADPs as atoms Cd1. Total 4 restraints were used in modeling the structure. The azide ion N13 was disordered over two positions in refined ratio 0.50(4):0.50(4). All the hydrogen atoms bonded to C atoms were generated geo-

**Table 2.** Selected bond distances (Å) and angles (°) for complex **1** and **2**.

<b>1</b>			
Cu1–N1	2.0526(17)	Cu1–N3	1.9310(17)
Cu1–N5 <sup>i</sup>	2.2876(17)	Cu1–N6	1.9468(18)
Cu1–N6 <sup>ii</sup>	2.7755(19)	Cu1–O1	2.0059(14)
O1–C7	1.278(2)	N4–C7	1.322(3)
N3–Cu1–N1	79.43(7)	N3–Cu1–O1	79.31(6)
N6–Cu1–O1	100.78(7)	N6–Cu1–N1	98.57(7)
N6 <sup>ii</sup> –Cu1–N5 <sup>i</sup>	172.18(6)	C7–N4–N3	107.39(16)
<b>2</b>			
Zn1–N1	2.1939(17)	Zn1–N3	2.0521(17)
Zn1–N5 <sup>i</sup>	2.1277(17)	Zn1–N6	2.0009(19)
Zn1–N6 <sup>ii</sup>	2.618(2)	Zn1–O1	2.1176(15)
O1–C7	1.271(3)	N4–C7	1.329(3)
N3–Zn1–N1	75.41(7)	N3–Zn1–O1	75.60(6)
N6–Zn1–O1	100.67(7)	N6–Zn1–N1	105.03(7)
N6 <sup>ii</sup> –Zn1–N5 <sup>i</sup>	170.70(6)	C7–N4–N3	108.47(16)

Symmetry codes: (i)  $-x + 1/2, y - 1/2, -z + 3/2$ ; (ii)  $-x + 1, -y + 1, -z + 1$ .

**Table 3.** Selected bond distances (Å) and angles (°) for complex **3**.

Cd1–N1	2.575(3)	Cd1–N3	2.364(3)
Cd1–O1	2.359(3)	Cd1–N11	2.278(3)
Cd1–O3	2.445(3)	Cd1–N11 <sup>i</sup>	2.552(4)
Cd1–N10 <sup>iii</sup>	2.309(3)	Cd2–N5	2.311(3)
Cd2–N7	2.408(3)	Cd2–N8	2.312(3)
Cd2–O2	2.268(3)	Cd2–N14	2.265(4)
Cd2–N14 <sup>ii</sup>	2.402(4)	C7–O1	1.265(5)
C7–N4	1.309(5)	C19–O2	1.265(5)
C19–N9	1.326(5)		
O1–Cd1–N3	67.62(10)	N3–Cd1–N1	65.28(11)
N1–Cd1–O3	72.61(11)	N11 <sup>i</sup> –Cd1–O3	77.81(11)
N11 <sup>i</sup> –Cd1–O1	76.57(11)	N11–Cd1–N10 <sup>iii</sup>	164.72(12)
O2–Cd2–N8	68.93(11)	N14–Cd2–O2	100.41(14)
N8–Cd2–N7	68.20(11)	N14–Cd2–N7	122.34(14)
N5–Cd2–N14 <sup>iii</sup>	159.97(15)	C7–N4–N3	111.7(3)
C19–N9–N8	109.5(3)		

Symmetry codes: (i)  $-x, 1 - y, 1 - z$ ; (ii)  $1 - x, 2 - y, -z$ ; (iii)  $x, y, 1 + z$ .

metrically and refined isotropically using the riding model. The H atoms attached to water molecules were fixed by difference Fourier maps with  $O-H = 0.85(2)$  Å,  $H\cdots H = 1.44(2)$  Å and  $U_{iso}(H) = 1.5U_{eq}(O)$ . The occupancy factors for water molecules in **1** and **2** were obtained by refinement of occupancy number. Details of data collection and refinements of complexes **1–3** are summarized in Table 1, selected bond distance and angles are given in Tables 2 and 3.

## 3. Results and Discussion

### 3.1. IR Spectroscopy

The IR spectra of complexes **1–3** (Figure S1) display broad band at about  $3300\text{--}3400\text{ cm}^{-1}$  due to the stretching band of water molecules.<sup>23</sup> The absence of typical  $\nu(C=O)$  band of **HL** ( $1662\text{ cm}^{-1}$ ) and the appearance of  $\nu(C-O)$  absorption bands ( $1616\text{ cm}^{-1}$  for **1**,  $1610\text{ cm}^{-1}$  for **2**, and  $1613\text{ cm}^{-1}$  for **3**) support the coordination of **HL** in the enol form.<sup>24</sup> The stretching vibration of the azomethine bands for complexes **1–3** are found at  $1562$ ,  $1564$ , and  $1568\text{ cm}^{-1}$ , respectively. Whereas the same band in the free ligand **HL** was observed at  $1632\text{ cm}^{-1}$ . On complexation the shifts of azomethine  $C=N$  band towards lower wavenumbers indicates coordination of the azomethine to the metal center.<sup>12,25</sup> The sharp band of the azide ions are found at  $2047\text{ cm}^{-1}$  for **1**,  $2056\text{ cm}^{-1}$  for **2**, and  $2054\text{ cm}^{-1}$  for **3**.

### 3.2. Structural Analysis

On the self-assembly process, ligand **HL** featured keto-enol tautomerism. The structural transformation can be supported by changes of the bond lengths and angles as follows (Tables 2 and 3).<sup>12,26,27</sup> The bond distances of carbonyl group  $C=O$  are elongated to  $1.278(2)$  Å in **1**,

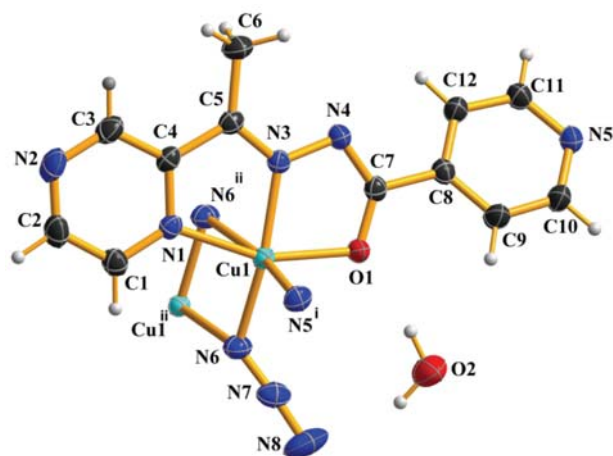


**Figure 1.** Coordination environment of  $Cu^{II}$  in **1**. Symmetry codes: (i)  $-x + \frac{1}{2}, y - \frac{1}{2}, -z + \frac{3}{2}$ ; (ii)  $-x + 1, -y + 1, -z + 1$ .

$1.272(3)$  Å in **2**, and  $1.265(5)$  Å in **3**, which is the typical  $C-O$  single bond length; meanwhile the  $C-N$  bond lengths are shortened to  $1.322(3)$  Å in **1**,  $1.329(3)$  Å in **2**, and  $1.309(5)$ ,  $1.326(5)$  Å in **3**, corresponding to the increasing  $\pi$ -bond order. These bond distance changes are accompanied by shrunk angle of  $C-N-N$  being  $107.40(16)^\circ$  in **1**,  $108.47(17)^\circ$  in **2**,  $111.7(3)^\circ$  and  $109.5(3)^\circ$  in **3**.

Complexes **1** and **2** crystallize in the monoclinic system, space group  $P2_1/n$ . As shown in Figures 1 and S2, the two complexes possess very similar coordination environment; so only the structure of **1** is described in detail herein.

The asymmetric unit of compound **1** is composed of one  $Cu^{II}$  ion, one deprotonated ligand  $L^{-}$ , one azide anion  $N_3^-$ , and one lattice water molecule. As presented in Figure 1, the coordination polyhedron around the  $Cu(II)$  center is distorted octahedral. The equatorial plane is surrounded by one nitrogen donor N1 from pyrazine ring, one nitrogen donor N3 from azomethine, one enolate oxygen donor O1 and one nitrogen donor N6 from azide ion. The sum of the four equatorial angles ( $\approx 358.09^\circ$ ) is very close to the ideal value ( $360.00^\circ$ ), which ensures the planarity of equatorial plane. The copper ion is only  $0.0984$  Å out of the basal plane. The axial positions are occupied by the pyridyl nitrogen donor  $N5^i$  from another ligand and azide nitrogen  $N6^{ii}$  (symmetry codes: (i)  $-x + \frac{1}{2}, y - \frac{1}{2}, -z + \frac{3}{2}$ ; (ii)  $-x + 1, -y + 1, -z + 1$ ). The average bond length of the equatorial plane is  $1.9839(17)$  Å, while the average axial bond length is  $2.5313(18)$  Å, thus the coordination sphere for  $Cu$  in complex **1** is a stretched octahedron.

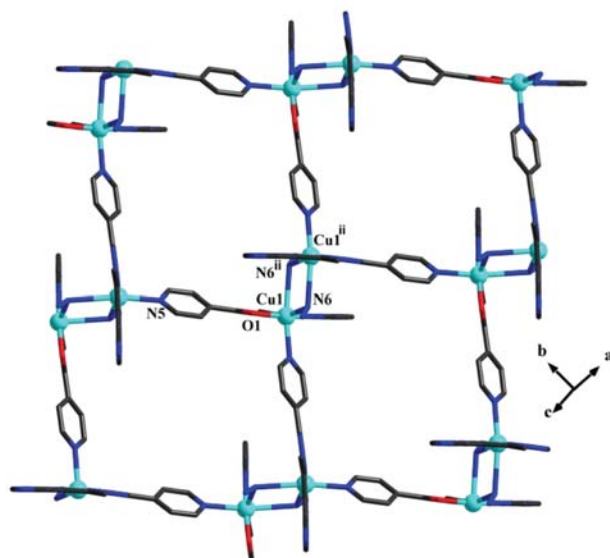


**Figure 2.** View of the 2D structure of **1**.

In complex **1**, the azide group adopts the asymmetric end-on bridging mode. The  $Cu-N_{azide}$  bond length, especially the bond length of  $Cu1-N6^{ii}$  ( $2.7748(19)$  Å), is



somewhat longer than those reported in Cu-hydrazone-azide analogues,<sup>25,28</sup> while it is shorter than that in Cu-bipyridine-(N<sub>3</sub>)<sub>2</sub> being 2.849(4) Å.<sup>29</sup> The Cu(II) centers are bridged by two  $\mu_{1,1}$ -N<sub>3</sub> to form a planar Cu-( $\mu_{1,1}$ -N<sub>3</sub>)<sub>2</sub>-Cu ring. The Cu...Cu distance within the four-membered cyclic units is 3.5837(5) Å. The adjacent (CuL)<sub>2</sub>( $\mu_{1,1}$ -N<sub>3</sub>)<sub>2</sub> units are connected with each other *via* the pyridine N5 atoms forming the 2D sheet structure of **1** (Figure 2). In earlier work, Xu et al. have reported a series of mono-, bi-, tetra-nuclear and 1D chain Cu(II) complexes derived from **HL** and copper salts.<sup>19</sup> **HL** was also in enolic form in those complexes, and acts as *NNO* donor in mono-, bi-, and tetranuclear complexes. While in the 1D chain complex  $[\text{Cu}_2(\text{L})_2(\text{NO}_3)(\text{H}_2\text{O})_2] \cdot (\text{NO}_3)_n$ , **L** acts as *NNON* donor as that in complex **1**, however the monodentate coordination mode of the nitrate anion limits the further extension of the structure. Therefore the counter anions influence the structures of the complexes efficiently.<sup>19</sup>

In complex **1**, the free water molecules are linked to the sheet *via* hydrogen-bonding interactions O2–H2A...N7, O2–H2A...N8, and O2–H2B...O1 (Figure S3).

Crystal structure study reveals that **3** crystallizes in triclinic system, space group *P* $\bar{1}$ . The asymmetric unit of **3** consists of two crystallographically independent Cd<sup>2+</sup>, two deprotonated ligands L<sup>1-</sup>, two counter anion N<sub>3</sub><sup>-</sup>, and one coordinated water molecule.

As shown in Figure 3, Cd1 center adopts a pentagonal bipyramid coordination geometry. The deprotonated ligand acts as pincer-type ligand, occupying three of the five equatorial coordination sites through pyrazine atom N1, azomethine atom N3 and enolate atom O1. The remaining two sites are held by azide atom N11<sup>i</sup> and water molecule O3 (symmetry code: (i)  $-x, 1 - y, 1 - z$ ). The sum of the five equatorial angles ( $\approx 359.89^\circ$ ) is very close to the ideal value ( $360^\circ$ ). The nitrogen donors N11 from

another azide ion and N10<sup>iii</sup> from another pyridyl ring occupy the axial positions (symmetry code: (iii)  $x, y, 1 + z$ ). The bond angle of N11–Cd1–N10<sup>iii</sup> being  $164.72(12)^\circ$  suggests a distorted coordination core. Meanwhile the average axial bond length (2.293(3) Å) is shorter than the equatorial bond length (2.459(3) Å) showing a compressed pentagonal bipyramid structure. The Cd2 center possesses a distorted octahedral coordination environment. The ligand L<sup>1-</sup> still serves as pincer ligand occupying the basal plane through N7, N8, and O2. Azide atom N14 takes up the remaining site. The azide donor N14<sup>ii</sup> (symmetry code: (ii)  $1 - x, 2 - y, -z$ ) and pyridyl donor N5 occupy the axial positions. The angle of N5–Cd2–N14<sup>ii</sup> being  $159.97(15)^\circ$  also deviates markedly from linearity.

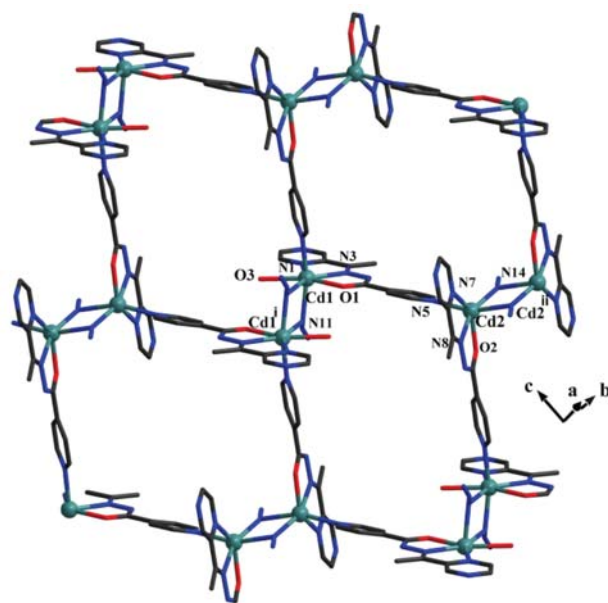


Figure 4. The 2D sheet structure of **3**.

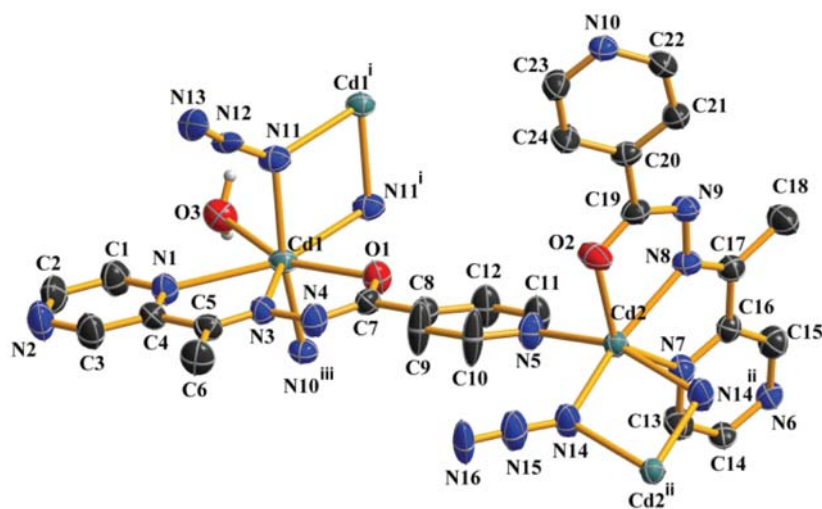
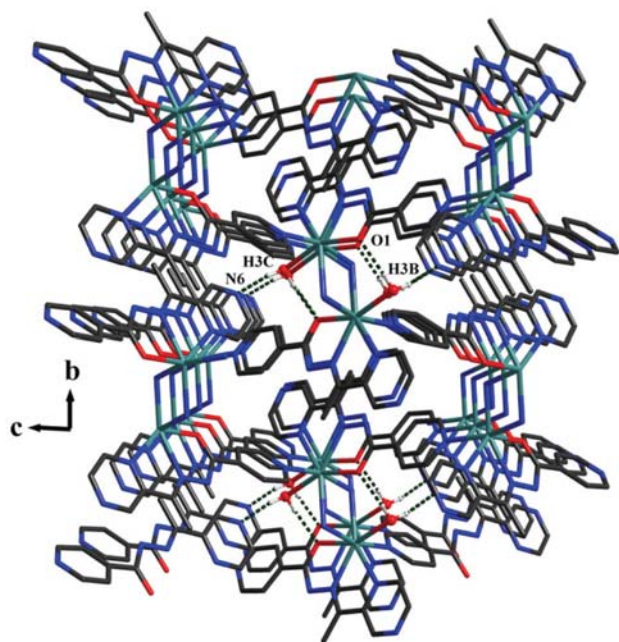


Figure 3. Coordination environment of Cd<sup>II</sup> in **3** (H atoms are omitted for clarity). Symmetry codes: (i)  $-x, 1 - y, 1 - z$ ; (ii)  $1 - x, 2 - y, -z$ ; (iii)  $x, y, 1 + z$ .

The azide ions in **3** are more bent than those in **1** and **2** with average N–N–N angle of  $168.6(3)^\circ$ . The azide ligands also bridge in an end-on fashion in complex **3**, which is similar with complexes **1** and **2**. The Cd(II) centers are bridged by two  $\mu_{1,1}$ -N<sub>3</sub> with Cd···Cd separation of 3.71(1) Å. The Cd1–N11–Cd1<sup>ii</sup> and Cd2–N14–Cd2<sup>iii</sup> bridging angles are  $100.07(13)$  and  $105.06(14)^\circ$ , respectively. The adjacent Cd<sub>2</sub>( $\mu_{1,1}$ -N<sub>3</sub>)<sub>2</sub> units are connected with each other *via* the pyridine N atoms (N5 and N10) forming the 2D sheet structure of **3** (Figure 4). In **3**, the coordinated water molecules are hydrogen bond donors and link these 2D sheets into 3D network *via* O3–H3B···O1<sup>i</sup> and O3–H3C···N6<sup>iv</sup> (symmetry code: (iv)  $-x + 1, -y + 1, -z + 1$ ). (Figure 5).



**Figure 5.** The 3D framework connected by H-bonding interactions in complex **3**.

### 3. 3. Luminescence Study

The d<sup>10</sup> transition metal based complexes with no d–d transition have intrinsic electronic properties. They are potential candidates for photoactive materials. Here the luminescent properties of **HL**, **2** and **3** were investigated in the solid state at room temperature.

As shown in Figure 7 upon excitation at 402 nm the free ligand **HL** exhibits fluorescent emission centered at 468 nm, which can be attributed to the intra-ligand  $\pi^*$ – $\pi$  and  $\pi^*$ –n transitions. Complexes **2** and **3** exhibit a little less intense photoluminescence, with emissions around 541 and 551 nm, respectively. As Zn<sup>2+</sup> or Cd<sup>2+</sup> ions are difficult to oxidize or reduce owing to their closed shell structure,<sup>30,31</sup> thus the luminescent emissions of the corresponding complexes **2** and **3** can be ascribed to the intra-ligand transitions. The red shifts of their emission spectra may be due to

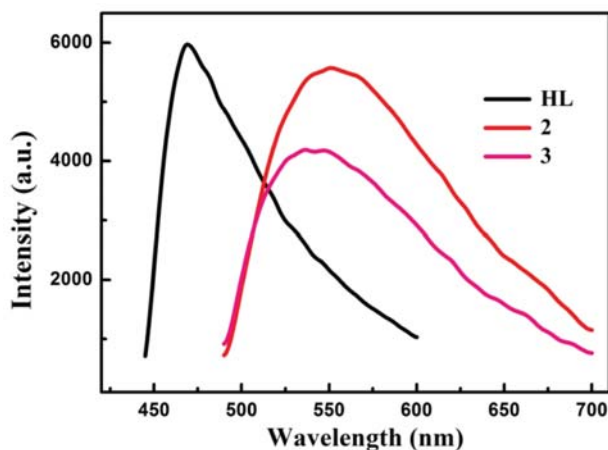


**Figure 6.** Fluorescence emission properties of the **HL** and complexes **2**, **3** in the solid state.

the coordination and hydrogen bonding effect, which can effectively enhance the coplanar arrangement of **HL**.<sup>32</sup>

## 4. Conclusions

In this paper, three complexes with 2D layered structures based on multidentate hydrazone ligand **HL** and azide salts have been isolated. The asymmetric end-on bridging mode of N<sub>3</sub><sup>−</sup> was found in complexes **1**–**3**. The monoanionic ligand L<sup>1−</sup> coordinated to the metal centers in an enolic form and served as tetradentate *NNON* type bridging ligand. In complexes **1** and **2** only intra-sheet hydrogen bonds were observed. The hydrogen bonding interactions between the water molecules and host framework construct a 3D supramolecular network for **3**. In addition, complexes **2** and **3** exhibit green emission fluorescence behaviors owing to the rigidity of structure.

## 5. Supplementary Material

Crystallographic data (excluding structure factors) for the structural analysis have been deposited with the Cambridge Crystallographic Data Center as supplementary publication Nos. CCDC 1530937 (**1**), 1530938 (**2**), and 1530939 (**3**). Copies of the data can be obtained free of charge *via* [www.ccdc.ac.uk/conts/retrieving.html](http://www.ccdc.ac.uk/conts/retrieving.html) (or from The Director, CCDC, 12 Union Road, Cambridge CB2 1EZ, UK, Fax: +44-1223-336-033. E-mail: deposit@ccdc.cam.ac.uk).

## 6. Acknowledgment

This work was supported by the National College Students' Innovative and Entrepreneurial Training Plan of China (201610433115 and 201610433157).

## 7. References

- S. Das, H. Kim, K. Kim, *J. Am. Chem. Soc.* **2009**, *131*, 3814–3815. <https://doi.org/10.1021/ja808995d>
- T. K. Maji, K. Uemura, H. C. Chang, R. Matsuda, S. Kitagawa, *Angew. Chem.* **2004**, *116*, 3331–3334. <https://doi.org/10.1002/ange.200453923>
- R. Banerjee, H. Furukawa, D. Britt, C. Knobler, M. O'Keefe, O. M. Yaghi, *J. Am. Chem. Soc.* **2009**, *131*, 3875–3877. <https://doi.org/10.1021/ja809459e>
- C. Wang, D. Liu, W. Lin, *J. Am. Chem. Soc.* **2013**, *135*, 13222–13234. <https://doi.org/10.1021/ja308229p>
- P. Wang, J. P. Ma, Y. B. Dong, *J. Am. Chem. Soc.* **2009**, *15*, 10432–10445.
- M. O'Keefe, O. M. Yaghi, *Chem. Rev.* **2012**, *112*, 675–702. <https://doi.org/10.1021/cr200205j>
- S. Hou, Q. K. Liu, J. P. Ma, Y. B. Dong, *Inorg. Chem.* **2013**, *52*, 3225–3235. <https://doi.org/10.1021/ic302716n>
- Y. Bai, J. L. Wang, D. B. Dang, M. M. Li, J. Y. Niu, *Cryst-Eng Comm.* **2012**, *14*, 1575–1581. <https://doi.org/10.1039/C1CE06030A>
- S. Mondal, S. Naskar, A. K. Dey, E. Sinn, C. Eribal, S. R. Herron, S. K. Chattopadhyay, *Inorg. Chim. Acta* **2013**, *398*, 98–105. <https://doi.org/10.1016/j.ica.2012.12.018>
- Y. F. Liu, Y. P. Liu, K. K. Zhang, Q. L. Ren, J. Qin, *Acta Cryst.* **2015**, *C71*, 116–121.
- J. Qin, Q. Yin, S. S. Zhao, J. Z. Wang, S. S. Qian, *Acta Chim. Slov.* **2016**, *63*, 55–61. <https://doi.org/10.17344/acsi.2015.1918>
- Q. L. Ren, S. S. Zhao, L. X. Song, S. S. Qian, J. Qin, *J. Coord. Chem.* **2016**, *69*, 227–237. <https://doi.org/10.1080/00958972.2015.1110240>
- Z. Dori, R. F. Ziolo, *Chem. Rev.* **1973**, *73*, 247–254. <https://doi.org/10.1021/cr60283a003>
- F. A. Mautner, C. Berger, E. Domian, R. C. Fischer, S. S. Massoud, *J. Mol. Struct.* **2016**, *1122*, 234–238. <https://doi.org/10.1016/j.molstruc.2016.06.004>
- M. Shyamal, A. Panja, A. Saha, *Polyhedron* **2014**, *69*, 141–148. <https://doi.org/10.1016/j.poly.2013.11.035>
- A. Laachir, S. Guesmi, M. Saadi, L. E. Ammari, O. Mentré, H. Vezin, S. Colis, F. Bentiss, *J. Mol. Struct.* **2016**, *1123*, 400–406. <https://doi.org/10.1016/j.molstruc.2016.07.053>
- F. Meyer, P. Kircher, H. Pritzkow, *Chem. Comm.* **2003**, *6*, 774–775. <https://doi.org/10.1039/b211486k>
- B. Shaabani, A. A. Khandar, N. Ramazani, M. Fleck, H. Mobaïyen, L. Cunha-Silva, *J. Coord. Chem.* **2017**, *70*, 696–708. <https://doi.org/10.1080/00958972.2016.1274028>
- J. Xu, T. Zhou, Z. Q. Xu, X. N. Gu, W. N. Wu, H. Chen, Y. Wang, L. Jia, T. F. Zhu, R. H. Chen, *J. Mol. Struct.* **2017**, *1128*, 448–454. <https://doi.org/10.1016/j.molstruc.2016.09.016>
- Bruker, SMART and SAINT. Bruker AXS Inc., Madison, Wisconsin, USA, **2002**.
- G. M. Sheldrick, SADABS. Program for Empirical Absorption Correction of Area Detector, University of Göttingen, Germany, **1996**.
- G. M. Sheldrick, *Acta Cryst.* **2008**, *A64*, 112–122. <https://doi.org/10.1107/S0108767307043930>
- J. Qin, N. Lei, H. L. Zhu, *J. Coord. Chem.* **2014**, *67*, 1279–1289. <https://doi.org/10.1080/00958972.2014.909591>
- J. Qin, S. S. Zhao, Y. P. Liu, Z. W. Man, P. Wang, L. N. Wang, Y. Xu, H. L. Zhu, *Bioorg. Med. Chem. Lett.* **2016**, *26*, 4925–4929. <https://doi.org/10.1016/j.bmcl.2016.09.015>
- S. Banerjee, S. Mondal, W. Chakraborty, S. Sen, R. Gachhui, R. J. Butcher, A. M. Z. Slawin, C. Mandal, S. Mitra, *Polyhedron* **2009**, *28*, 2785–2793. <https://doi.org/10.1016/j.poly.2009.05.071>
- M. M. Đorđević, D. A. Jeremić, M. V. Rodić, V. S. Simić, I. D. Brčeski, V. M. Leovac, *Polyhedron* **2014**, *68*, 234–240. <https://doi.org/10.1016/j.poly.2013.10.029>
- S. P. Xu, F. L. Yang, G. Z. Zhu, H. L. Shi, X. L. Li, *Polyhedron* **2014**, *68*, 1–9. <https://doi.org/10.1016/j.poly.2013.10.013>
- S. Sen, S. Mitra, D. L. Hughes, G. Rosair, C. Desplanches, *Polyhedron* **2007**, *26*, 1740–1744. <https://doi.org/10.1016/j.poly.2006.12.015>
- G. De Munno, M. G. Lombardi, M. Julve, F. Lloret, J. Faus, *Inorg. Chim. Acta* **1984**, *282*, 82–89. [https://doi.org/10.1016/S0020-1693\(98\)00193-5](https://doi.org/10.1016/S0020-1693(98)00193-5)
- A. Thirumurugan, S. Natarajan, *Dalton Trans.* **2004**, *18*, 2923–2928. <https://doi.org/10.1039/b408403a>
- L. Zhang, Z. W. Man, Y. Zhang, J. Hong, M. R. Guo, J. Qin, *Acta Chim. Slov.* **2016**, *63*, 891–898. <https://doi.org/10.17344/acsi.2016.2895>
- J. F. Fang, J. X. Cheng, S. T. Huang, J. Zhang, C. Q. Ni, Y. J. Xiong, Q. Chen, F. F. Zhu, Y. Li, S. T. Yue, *Z. Anorg. Allg. Chem.* **2015**, *641*, 2657–2663. <https://doi.org/10.1002/zaac.201500613>

## Povzetek

Sintetizirali smo tri kovinsko-organske koordinacijske polimere  $\{[\text{Cu}(\text{L})(\text{N}_3)] \cdot (\text{H}_2\text{O})_{0,25}\}_n$  (**1**),  $\{[\text{Zn}(\text{L})(\text{N}_3)] \cdot (\text{H}_2\text{O})_{0,5}\}_n$  (**2**) in  $[\text{Cd}_2(\text{L})_2(\text{N}_3)_2(\text{H}_2\text{O})]_n$  (**3**) z uporabo hidrazonskega liganda  $N'$ -(1-(pirazin-2-il)etiliden)izonikotinohidrazida (**HL**),  $\text{NaN}_3$  in ustreznega kovinskega nitrata. Komplekse smo okarakterizirali z elementno analizo, IR spektroskopijo in monokristalno rentgensko difrakcijo. Vsi trije kompleksi imajo 2D koordinacijsko mrežo, kjer ima  $\text{L}^{1-}$  vloga  $\text{NVON}$  štiritveznega liganda, azidni anion pa je mostovni ligand. V kompleksih **1** in **2** so prisotne samo vodikove vezi znotraj plasti, medtem ko v kompleksu **3** vodikove vezi med vodo in gostiteljsko mrežo tvorijo 3D mrežo. Kompleksa **2** in **3** intenzivno fluorescirata v trdnem stanju pri sobni temperaturi.

*Scientific paper*

# Synthesis of MnO<sub>2</sub> on Activated Carbon and its Potential Application in the Adsorption of As(V) and Pb(II) in Aqueous Solutions

Roberto Contreras-Bustos,<sup>1</sup> E. Manríquez-Reza,<sup>1</sup> Jaime Jiménez-Becerril,<sup>2,\*</sup> Melania Jiménez-Reyes<sup>2</sup> and Bibiana Cercado-Quezada<sup>1</sup>

<sup>1</sup> Centro de Investigación y Desarrollo Tecnológico en Electroquímica S. C., Parque Tecnológico Querétaro, Sanfandila, Pedro Escobedo, C. P. 76703, Querétaro. México.

<sup>2</sup> Departamento de Química, Instituto Nacional de Investigaciones Nucleares, Apartado Postal 18-1027. C. P. 11801, Distrito Federal, México.

\* Corresponding author: E-mail: jaime.jimenez@inin.gob.mx  
Telephone: + (55) 53297200

Received: 08-02-2017

## Abstract

The conditions for the synthesis of a material with MnO<sub>2</sub> (OMD) on activated carbon (AC) were studied. These conditions were: reaction time, temperature, stirring speed, concentrations of AC, H<sub>2</sub>SO<sub>4</sub>, and O<sub>3</sub> in solution, and particle size. Agglomerates on AC were observed by means of scanning electron microscopy (SEM) and microanalysis by energy dispersive spectroscopy (EDS) and revealed the presence of OMD deposited on the surface. The activation energy and the factor of frequency for the reaction were determined as  $E_a = 1.2$  kcal/mol and  $A = 2.2$ . The value of  $E_a$  indicates that the precipitation of OMD on the AC was controlled by mass transfer in aqueous solution and the order of reaction was zero. The adsorption capacities of AC were  $q = 14$  mg Pb(II)/g AC and  $q = 9.1$  mg As(V)/g AC. Whereas, for the OMD/AC obtained in the following conditions: [AC] 1 or 2 g/L, particle size of AC of +0.59 mm, [H<sub>2</sub>SO<sub>4</sub>] 1 or 2 mol/L, 25 °C, stirring speed 600 rpm, and [O<sub>3</sub>] 1.35 mol/L, the adsorption capacities were  $q = 90.5$  mg Pb(II)/g OMD/AC and 25.4 mg As(V)/g OMD/AC. Therefore, the fixing of OMD on the surface of the AC greatly improved the removal of both Pb(II) and As(V) from aqueous solutions.

**Keywords:** MnO<sub>2</sub>, Activated carbon, Lead, Arsenic, Adsorption

## 1. Introduction

Studies on absorbent materials for natural and anthropogenic contaminant ions, in both surface water and groundwater, remain of interest. Arsenic and lead ions have notable deleterious effects on human health. In Mexico, their presence has been detected in aquifers, especially in the north of the country.<sup>1</sup> They cause various diseases including skin diseases, bone diseases and diseases in other vital organs. Moreover, they can lead to death when high-dose exposure is continuous. Thus, it is important to find efficient alternatives for the removal of these ions from water and to reduce the risks to human health.

Arsenic is present in the atmosphere, soil, rocks, natural water and organisms. Most environmental problems

related to arsenic contamination are due to mobilization under natural conditions. For human beings, arsenic has an important impact in the form of mining, burning fossil fuels and use of arsenic-containing pesticides, herbicides and livestock feed.<sup>2</sup> The presence of arsenic in water usually indicates nearby mines or metallurgical industries in operation or agricultural areas where materials with arsenic are used.<sup>3</sup> The average levels of arsenic in groundwater are between 0.001 and 0.002 mg/L; however, in areas with volcanic rocks and sulfide ore deposits, these levels are > 3 mg/L. The World Health Organization (WHO) established that the arsenic in water for human consumption should not exceed 0.01 mg/L.<sup>4</sup> This is a provisional value given the uncertainty of the risks associated with a lower concentration of arsenic; in 1984, the WHO had set limit

value of 0.05 mg/L. The U.S. Environmental Protection Agency (EPA) indicates a maximum permissible limit concentration of arsenic of 0.01 mg/L for drinking water.<sup>5</sup> The Mexican official standard is a maximum permissible limit concentration of 0.025 mg/L.<sup>6</sup>

Lead is present in the environment, including in the air, dust, soil and water. This element and its compounds are widely used for batteries, pigments, ammunitions, weldings, pipes, coated cables and bearings. Other sources of contamination are mining and smelting waste, petrol and paintings.<sup>7</sup> The maximum permissible limit concentration of lead in drinking water established by the WHO for water is 0.01 mg/L. Per the U.S. EPA, the limit is 0.015 mg/L, though it is also 0.01 mg/L according to the Mexican official standard.<sup>4–6</sup>

There are several technologies for the treatment of contaminated water with arsenic and lead ions such as coagulation-filtration, chemical precipitation, ion exchange and lime softening, among others.<sup>7–15</sup> In recent years, research has been conducted on low-cost and easily obtainable materials that may be useful for absorbing heavy metals. Among these materials are: activated charcoal, zeolites, chitosan, clays, biocarbon, and sand.<sup>16–19</sup> To increase the adsorption capacity of these natural adsorbents materials, changes to their surfaces have been proposed. For lead removal, several possibilities have been tested, including: manganese dioxide onto zeolites, sand or resins, cellulose, carbon nanotubes, pre-treated clinoptilolite, and graphene.<sup>20–25</sup> Regarding arsenic removal, the deposition of MnO<sub>2</sub> (OMD) onto polystyrene resins, zeolites and MCM-41 has been proposed.<sup>10,11,26–30</sup>

Oxidation of manganese ions by ozone in an aqueous solution has been widely studied, and it is a feasible alternative for the production of OMD.<sup>31</sup> Ozone is one of the strongest oxidants and offers the advantage of not introducing unwanted specimen into the system; therefore, its use guarantees the purity of the product obtained. OMD obtained *via* this method has better characteristics than if it was produced *via* other methods. Moreover, this type of OMD exhibits good behavior for ion exchange.<sup>32–34</sup> Preferentially, OMD exchanges with other ions in the order Pb(II) > Zn(II) > Cd(II) > Tl(I).<sup>35</sup>

Activated carbon (AC) is a low-cost adsorbent that, depending on the conditions of the adsorbate, can be used in a wide pH range. Its adsorption capacity stems not only from its surface area but also its physicochemical nature, i.e. properties obtained during the activation process.<sup>36–38</sup> Manganese dioxide obtained by specific conditions of ozonation (OMD) has better adsorption capabilities than if it was obtained by electrolytic or chemical methods. The size of the OMD obtained by direct precipitation is relatively small. An interesting option is the use of a supporting material such as AC to obtain a larger material useful in traditional adsorption columns. The synthesis of OMD consumes electricity for the for-

mation of ozone; however, with the use of alternate energy sources (i.e., solar), costs could be mitigated. Manganese sulfate can be obtained during the acid leaching of manganese ore, whose oxidation with ozone can be directly applied in the presence of AC. The cost of obtaining OMD from manganese ore is comparable to that of obtaining it by the electrolytic method. In addition, OMD/AC provides the features for adsorption of Pb(II) or As(V); furthermore, the reversibility of adsorption has been proved for cadmium(II) and zinc(II) with an acid solution at pH 1–2.<sup>35</sup>

The present investigation proposes the synthesis of an adsorbent material, which consists of OMD supported by AC to examine whether its physical and chemical characteristics are suitable for the adsorption columns used in water purification. The specific aims of this research are: 1) to establish the best conditions for the synthesis of OMD/AC, 2) to characterize the material, and 3) to determine the adsorption capacity of the material for Pb(II) and As(V) ions.

## 2. Experimental

### 2.1. Synthesis of MnO<sub>2</sub>/AC

For the synthesis of the OMD, MnSO<sub>4</sub> (Karl S. A. de C. V., reagent grade) and H<sub>2</sub>SO<sub>4</sub> (Baker, reagent grade) were used. Granular AC type CAGR 8 × 30 (Clarimex), certified by the National Science Foundation and previously characterized was used.<sup>39</sup> The AC is of lignite origin, is activated by vapor steam, has an average pore diameter of 3.5 nm and has a surface area of 664 m<sup>2</sup>/g. The determinations using the inductively coupled plasma (ICP-OES) spectrometry (Perkin Elmer, Optima 3300 DV) gave the following data: Al: 256 mg/kg, Si: 143 mg/kg, Na: 1085 mg/kg, K: 300 mg/kg, Ca: 872 mg/kg, Sr: 756 mg/kg and V: 14 mg/kg.

OMD synthesis was performed *via* the oxidation by ozonation of Mn(II) in aqueous solution. A solution of 1 g/L of MnSO<sub>4</sub> and 1 mol/L H<sub>2</sub>SO<sub>4</sub> was prepared with deionized water and was deposited in a glass reactor with 2 g of AC. The system was stirred to 600 rpm for 2 h, and the temperature was controlled at 25 °C. A gaseous mixture of O<sub>2</sub>/O<sub>3</sub>, produced in an ozone generator (PCI Ozone & Control Systems, mod. GL-1) supplied with oxygen was introduced into the reactor. Samples were taken at 0, 30, 60, 90 and 120 min of reaction. The samples were filtered and the solid was washed with 100 mL of deionized water. These samples were identified as OMD/AC. Finally, the samples were stored in a desiccator. Liquid samples were analyzed by ICP-OES.

The base conditions for the synthesis were: temperature, 25 °C; stirring, 600 rpm; concentration of AC, 2 g/L; [H<sub>2</sub>SO<sub>4</sub>], 1 mol/L; [O<sub>3</sub>] in solution, 1.32 mol/L; and particle size of AC, +0.59 mm. Each parameter was independently varied in order to find out the best adsorption capa-

city of the material for Pb(II) and As(V) ions. The temperature ranged from 25 to 70 °C; the concentration of AC from 0.5 to 5 g/L; the ozone concentration in solution from 0.35 to 1.65 mol/L; the concentration of H<sub>2</sub>SO<sub>4</sub> from 1 to 3 mol/L; the stirring speed from 200 to 800 rpm; and the particle size from AC of +0.59 to +1.6 mm.

The resulting solid material was characterized using scanning electron microscopy (SEM) and microanalysis by Energy Dispersive Spectroscopy (EDS) (Jeol, mod. JSM35CFLV) to corroborate the presence of manganese deposits on the surface of the AC and to identify other elements in the samples.

## 2. 2. Adsorption of Lead and Arsenic

The solutions used for the experiment were one of lead and one of arsenic, each with a concentration of 1 g of the element per liter. They were prepared with Pb(NO<sub>3</sub>)<sub>2</sub> (Baker, reactive grade) and Na<sub>2</sub>HAsO<sub>4</sub> · 7H<sub>2</sub>O (Mallinckrodt Chemical Works, reagent grade) in deionized water. These solutions were stored in polyethylene containers. The stock solutions were diluted up to a concentration of 100 mg/L for the adsorption experiments. 0.1 g of OMD/AC prepared in specific conditions was put in contact with 100 mL of these solutions. For lead, the adsorption experiments were carried out at pH = 4.7 to avoid the precipitation of lead as hydroxide. According to the chemical species diagram at pH = 4.7 lead is present only as Pb(II).<sup>40</sup> Arsenic experiments were done at pH 8.8, when As(V) can be found as the anionic species 30% (H<sub>2</sub>AsO<sub>4</sub>)<sup>-</sup>. Contact was done in an isothermal bath with stirring at 300 rpm at 25 °C for 24 h.

After the contact the solutions were filtered and a nitric acid solution added to maintain the pH < 2, the samples were stored in polyethylene bottles. Lead was then present as Pb(II) and As(V) was ca. 70% as H<sub>3</sub>AsO<sub>4</sub> and ca. 30% H<sub>2</sub>AsO<sub>2</sub><sup>4-</sup> all of which are water soluble.<sup>40</sup> These samples were analyzed for Pb(II) or As(V) using ICP-OES. The OMD/AC was flushed with 100 mL of deionized water, dried at temperatures up to 35 °C for 12 h and stored in a desiccator with silica gel.

To determine the influence of each individual condition on the synthesis of OMD/AC, the adsorption capacity of the material for Pb(II) and As(V) was tested using the

material obtained under different stirring speed, ozone concentration, acidity, AC concentration, temperatures, and AC particle sizes.

The equation used for the calculation of the adsorption capacity was:

$$q = \frac{(C_i - C_f) \cdot V}{m} \quad (1)$$

where  $q$  is the adsorption capacity (mg ion/g adsorbent),  $m$  is the mass of the adsorbent (g),  $C_i$  is the initial concentration of ions in solution (mg/L),  $C_f$  is the final concentration of ions in solution (mg/L) and  $V$  is the volume of the solution (L).<sup>41</sup> The adsorption capacity of AC for Pb(II) and As(V) was measured as well.

## 3. Results and Discussion

### 3. 1. OMD/AC Synthesis

#### 3. 1. 1. Stirring Speed

The values of Mn(II) when remaining in solution for the same amount of time are very similar (Table 1); this means that the parameter does not significantly alter the oxidation rate reaction. It can be deduced that the mass-transfer phenomenon in that range of stirring speed is not important. A slight increase of Mn(II) deposition was observed, however, at a stirring speed of 800 rpm at 120 minutes of reaction. Mn(II) probably spreads in the AC by means of electrostatic attraction with the electrically charged sites of the surface, and then, when ions are already deposited, oxidation occurs to form OMD.

#### 3. 1. 2. Ozone Concentration

Table 1 shows the influence of the concentration of ozone on the oxidation rate reaction of Mn(II) in the presence of AC. The oxidation rate increases in relation to the concentration of ozone in solution. The best conditions for attaining the lowest concentration of Mn(II) in solution are 1.35 mol/L and 120 min of reaction.

With  $t > 90$  min of ozonation and a concentration of O<sub>3</sub> of 1.65 mol/L, a re-dissolution of manganese ions was

**Table 1.** Manganese concentration (mg/L, in italics) remaining in solution, with respect to stirring speed (rpm), ozone concentration (mol/L) and reaction time (min).

t (min)	Stirring (rpm)				[O <sub>3</sub> ] (mol/L)			
	200	400	600	800	0.35	1.32	1.35	1.65
0	1000	1000	1000	1000	1000	1000	1000	1000
30	920	826	834	816	890	834	790	680
60	770	705	711	642	780	670	590	360
90	608	550	508	410	670	508	388	38
120	423	380	377	184	565	340	180	299

observed due to the oxidation of the ions Mn(IV) up to Mn(VII), revealed by the characteristic violet color. In accordance with the Pourbaix diagram at the experimental pH, Mn(II) can be oxidized to MnO<sub>2</sub> and subsequently to MnO<sub>4</sub><sup>-</sup>.<sup>42</sup> The calculation of the order of reaction was performed with the following equation:

$$\log(-r_A) = \log k + n \log C_A \quad (2)$$

where  $r_A$  expresses the variation of the concentration of a species (Mn(II)) with respect to time,  $C_A$  is the concentration of ozone,  $k$  is the rate constant and  $n$  is the order of reaction.

The graphics (not included) corresponding to 30, 60 and 90 min of stirring and ozone concentrations of 0.35 to 1.35 mol/L have slopes  $\approx 0.5$ ; this is considered a zero-order reaction. The value of  $\log(-r_A)$  tended to be higher, indicating a change in slope, only in the case of 90 min and 1.35 mol/L ozone. For the lowest concentrations of ozone in solution the mass-transfer phenomena have more influence in the process than the chemical reaction itself during oxidation of Mn(II). However, as the concentration of dissociated ozone increases, the chemical reaction becomes more important.<sup>43</sup>

### 3. 1. 3. Sulfuric-acid Concentration

The oxidation rate reaction of Mn(II) decreases with the increase in sulfuric-acid concentration (Table 2). For the range of acidity used, the best condition was 1 mol/L H<sub>2</sub>SO<sub>4</sub>. Moreover, the start-up time for reaction increases when the acid concentration increases. The low rate of oxidation with high concentrations of H<sub>2</sub>SO<sub>4</sub> may be due

to a competition between protons and Mn(II) ions for the active sites of AC. Another explanation is that the low rate of oxidation is due to the high viscosity observed with a high concentration of acid.

### 3. 1. 4. AC Concentration

As can be seen in Table 2, the values corresponding to the change of Mn(II) for the oxidation reaction without AC have tendency very similar to that of the tests carried out with the presence of AC. Rodríguez-Santillan et al. mention that the AC favors the decomposition of O<sub>3</sub> in solution even at low pH;<sup>44</sup> however, in the conditions of the present work, this was not observed.

According to the calculations done in accordance with Equation 2, the oxidation reaction is of zero-order with respect to this variable. This means that, in the interval of the AC used, this parameter does not have a significant influence on the rate of oxidation of Mn(II) by ozone.

### 3. 1. 5. AC Particle Size

The rate reaction is quite similar for the three particle sizes, namely 0.59, 1.19 and 1.6 mm (Table 3). Thus, it can be deduced that this variable does not influence the process of oxidation of Mn(II).

### 3. 1. 6. Temperature

Increasing temperature to 70 °C and reaction times to greater than 60 min favors oxidation; for lower temperatures, there was no noticeable difference (Table

**Table 2.** Manganese concentration (mg/L, in italics) remaining in solution, with respect to initial sulfuric-acid concentration (mol/L), quantity of activated carbon (g) and reaction time (min).

t (min)	[H <sub>2</sub> SO <sub>4</sub> ] (mol/L)					AC (g)				
	1	2	3	0	0.5	1	2	3	5	
0	1000	1000	1000	1000	1000	1000	1000	1000	1000	
30	834	959	992	743	723	761	834	787	742	
60	711	852	925	592	549	629	711	651	657	
90	508	654	848	439	351	392	508	489	448	
120	377	452	805	255	143	269	377	246	276	

**Table 3.** Manganese concentration (mg/L, in italics) remaining in solution, with respect to the particle size of activated carbon (mm), temperature (°C) and reaction time (min).

t (min)	Particle size (mm)				Temperature (°C)			
	0.59	1.19	1.6	25	40	60	70	
0	1000	1000	1000	1000	1000	1000	1000	
30	834	751	793	834	840	876	876	
60	711	589	618	711	666	643	647	
90	508	404	412	508	469	419	417	
120	377	242	251	377	251	221	60	

3). Similar observations have been reported previously.<sup>35</sup>

The  $k$  values for temperatures of 25, 40, 60, and 70 °C were calculated considering the slopes of the graphs of Figure 1A. These values were used to determine the activation energy by the Arrhenius linear equation:

$$\ln k = \ln A - E_a / RT \quad (3)$$

where  $k$  is the rate constant,  $A$  is the factor of frequency,  $E_a$  is the activation energy (kcal/mol),  $R$  is the universal constant of the gases, and  $T$  is temperature (K).

Figure 1B shows a graph in which the activation energy and the factor of frequency are the slope and the intercept of the line, respectively. These values are  $E_a = 1.2$  kcal/mol and  $A = 2.2$ . According to Peters and Bolton,  $E_a$  values under 4.7 kcal/mol and occasionally under 2.3 kcal/mol correspond to mechanisms controlled by mass-transfer in an aqueous solution;<sup>45</sup> therefore, deposition of  $MnO_2$  on AC can be considered as such. Thus, temperature does not influence the process of  $MnO_2$  precipitation.

### 3. 2. Characterization by SEM

Figure 2 shows typical images obtained by SEM. In the micrograph taken to the scale of 150× and 100 μm (a), fine particles were observed on the AC. Yet, in the micrograph taken to the scale of 2000× and 10 μm (b), agglomerates of OMD were deposited on the surface of the AC. The EDS (c) revealed the presence of manganese and silicon, which were located on the AC surface.

When low ozone concentrations were used for synthesis, the images showed less deposits of manganese on the AC than on samples synthesized with high concen-

trations of ozone; thus, the increase of ozone can be said to favors precipitation.

### 3. 3. Adsorption of Pb(II) in OMD/AC

Table 4 shows the influence of different conditions on the synthesis of OMD/AC in terms of the composite's adsorption capacity for lead. This adsorption capacity increases with the stirring speed, probably due stirring speed's creation of more homogeneous deposits of OMD. However, the OMD/AC formed at 800 rpm does not present the best features for removing Pb(II), because the dissemination processes do not favor the solid-liquid interface or because the contact time between the particles of OMD and AC was reduced. Moreover, this condition of synthesis could also create fractures of AC particles; hence, the OMD deposited on them may become detached.

The adsorption capacity of lead in the OMD/AC increased when the concentration of ozone used in the synthesis of the material was changed from 0.35 to 1.32 mol/L (Table 4); however, with higher concentrations, this adsorption capacity decreased. This can be explained by a partial re-dissolution of manganese as  $MnO_4^-$  during synthesis, and resulting decrease of manganese as an oxide on the surface of the AC, which is the chemical species that allows for efficient adsorption.

Table 4 also shows the influence of sulfuric-acid concentration. When the concentration of the acid reaches 2 M, the formation of  $\gamma$ - $MnO_2$  is promoted, thereby increasing adsorption capacity. A higher concentration of sulfuric acid (3 mol/L) favors the formation of Mn(III), an intermediate species between Mn(II) and  $MnO_2$ .<sup>35</sup> In addition, in this case, the decrease of manganese as an oxide on the surface of the AC reduces the lead adsorption capacity of the material.

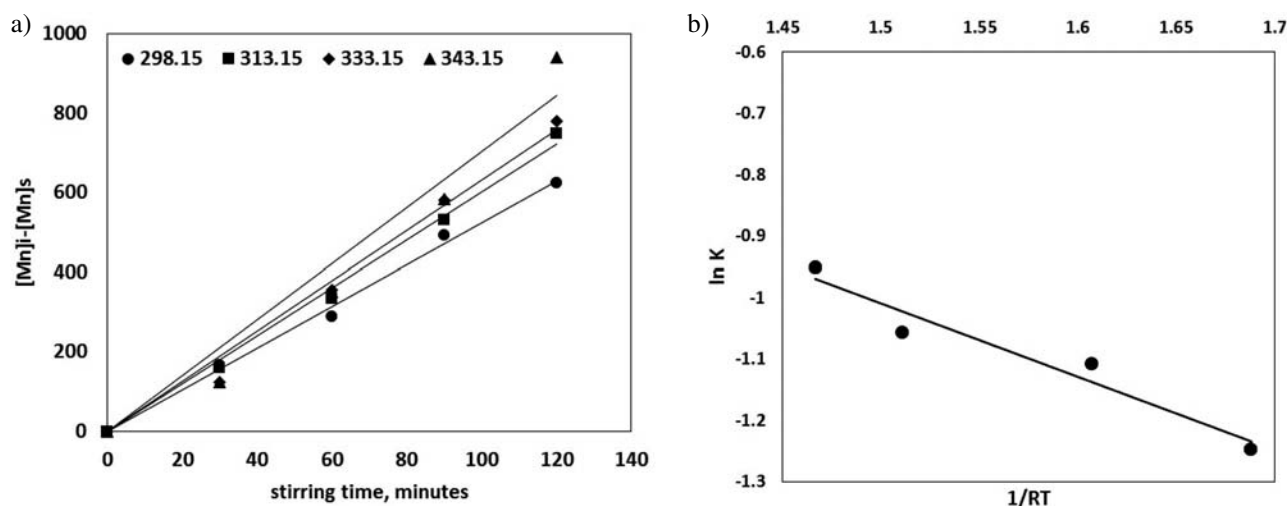


**Figure 1.** a: Initial manganese (mg/L) minus manganese remaining in solution as a function of stirring time. The slopes are: 5.24, 6.02, 6.33, and 7.04 for 298.15, 313.15, 333.15, and 343.15 K, respectively. b: Estimation of activation energy by means of the Arrhenius equation.  $\ln K = -1.2*(1/RT) + 0.797$  ( $R^2 = 0.94$ )



The adsorption capacity of Pb(II) by OMD/AC decreases when the concentration of AC used in the synthesis of the material increases (Table 4), for the amount of OMD present in the adsorbent material is proportionally smaller.

The best adsorption capacity with respect to the temperature of the formation of the OMD/AC was 82.7 mg Pb(II)/g in the material prepared at 40 °C. The adsorption capacity of the material is reduced at higher temperatures during synthesis. Umetsu et al. reported a similar behavior; they observed that OMD does not present adsorption for a synthesis at 70 °C.<sup>46</sup> Although there are significant deposits of OMD in the synthesized material at that temperature, the results indicate that the main factor responsible for the removal of Pb(II) is AC.

Regarding particle size, the best adsorption capacity (85.8 mg Pb(II)/g OMD/AC) was obtained using the synthesized material with the largest AC particle, because it presents more deposits of OMD on the surface. In the intermediate-sized synthesized material with AC, the removal of Pb(II) was reduced because of small amount OMD deposits, which was observed in the micrographs for particles sizes of 0.59 and 1.6 mm. Finally, when using the smallest AC particles, the Pb(II) removal was also high (71.7 mg Pb(II)/g OMD/AC); the presence of few OMD deposits, the adsorption capacity increased if the size of the AC was reduced.

The conditions of synthesis of OMD/AC with the maximum adsorption capacity of Pb(II) are: 2 mol/L of sulfuric acid, temperature at 25 °C, stirring at 600 rpm, AC par-

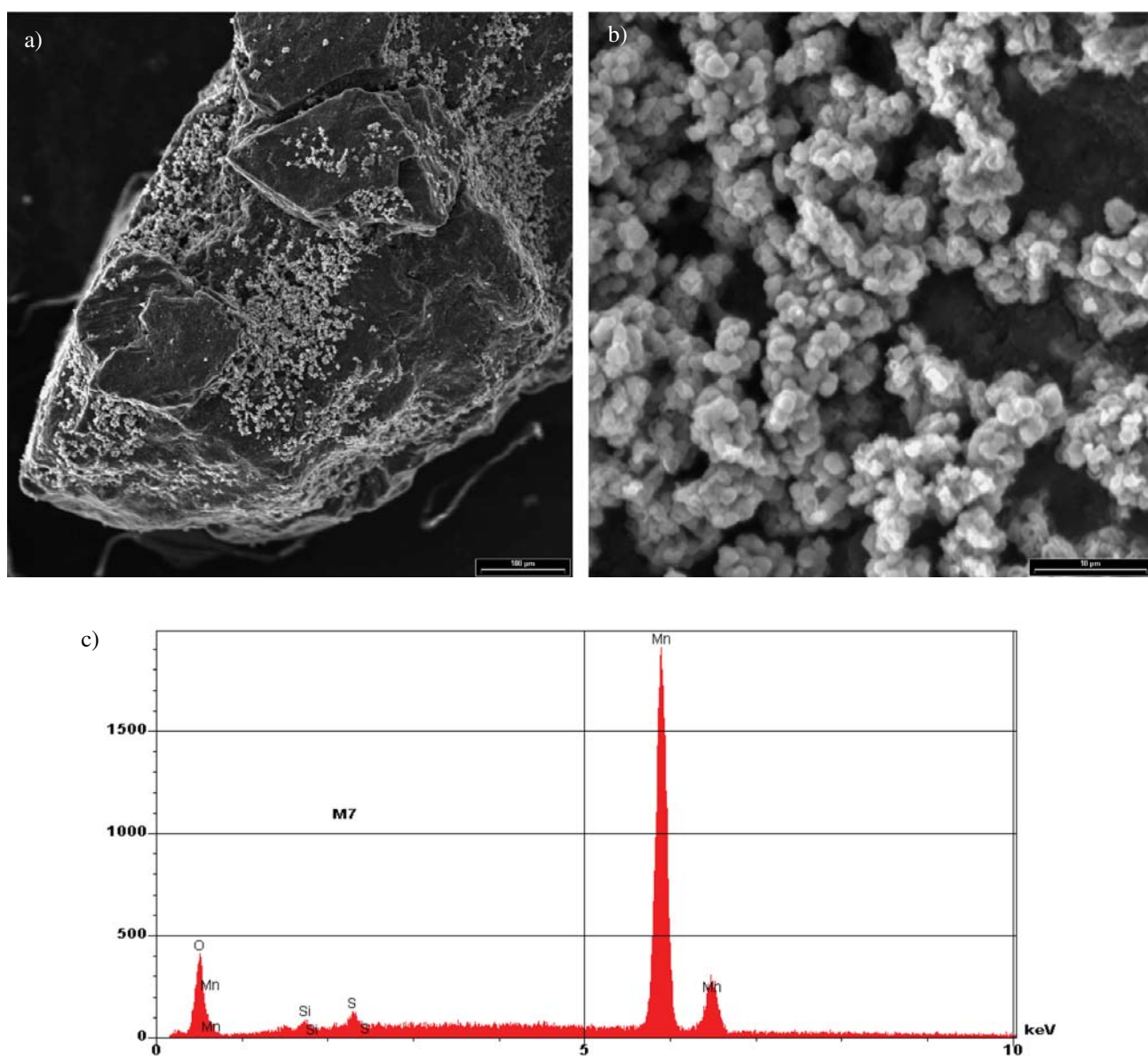


**Figure 2.** Typical microographies of the synthesized materials. (a) 150 $\times$ , (b) 2000 $\times$ , (c) EDS obtained in micrography.

**Table 4.** Adsorption capacities of OMD/AC for Pb(II) and As(V) with respect to different synthesis parameters for OMD/AC. Initial concentrations = 100 mg/L. Without OMD,  $q_0 = 14.0$  mg Pb(II)/g AC and  $q_0 = 9.1$  mg As(V)/g AC.

Synthesis parameters for OMD/AC	Condition	$q$ (mg Pb(II)/g OMD/AC)	$q$ (mg As(V)/g OMD/AC)
Temperature (°C)	25	71.7	4.3
	40	82.7	19.0
	60	70.7	18.8
	70	71.0	8.0
Stirring (rpm)	200	54.6	17.3
	400	60.9	18.5
	600	71.7	4.3
	800	39.3	4.7
[O <sub>3</sub> ] (mol/L)	0.35	40.0	5.6
	1.32	71.7	4.3
	1.35	56.6	1.0
	1.65	76.8	4.5
[AC] (g/L)	0.5	84.6	17.6
	1.0	81.4	25.1
	2.0	72.0	4.3
	3.0	20.3	1.8
	5.0	44.0	7.3
[H <sub>2</sub> SO <sub>4</sub> ] (mol/L)	1.0	71.7	4.3
	2.0	90.6	16.5
	3.0	34.7	19.5
Particle size of AC (mm)	0.59	71.7	4.3
	1.19	49.5	19.7
	1.60	85.8	10.1

ticle size at +0.59 mm, [O<sub>3</sub>] 1.35 mol/L, and [AC] 2 g/L. The adsorption-capacity value in these conditions is 90.5 mg Pb(II)/g OMD/AC; for AC, however, it is 14 mg Pb(II)/g AC. Therefore, the fixing of MnO<sub>2</sub> on the surface of the AC greatly improves the removal of ions Pb(II) of aqueous solutions.

### 3. 4. Adsorption of As(V) in OMD/AC

The results of the experiments carried out to determine the adsorption capacity of As(V) on the material in each of the conditions of synthesis was calculated in the same way as described for lead, following Equation 1 and determining the influence of each individual parameter. The values obtained are shown in Table 4.

At the experimental pH (8.8), As(V) can be found as an anionic species H<sub>2</sub>AsO<sub>4</sub><sup>2-</sup>.<sup>40</sup> Even if the OMD is considered a cation exchanger, the use of this material to remove As(V) has been reported in the literature.<sup>47–49</sup>

Table 4 shows that the adsorption capacity was better with a slow stirring speed during synthesis (200 and 400 rpm); the highest value obtained was for 400 rpm (18.5 mg As(V)/g OMD/AC). The increased stirring speed resulted in a drastic decrease in the adsorption capacity because of fewer deposits of manganese oxide, which is responsible for adsorption.

The ozone concentration used for the synthesis of OMD/AC does not have a significant influence on the adsorption capacity for arsenic ions. The maximum adsorption capacity is less than 6 mg As(V)/g OMD/AC for a concentration of O<sub>3</sub> = 1.65 mol/L. This behavior is different from that observed with the adsorption of Pb(II) for the same parameter because the mechanism of ion exchange of the OMD is different for cations and anions.

The adsorption capacity of As(V) in OMD/AC depends on H<sub>2</sub>SO<sub>4</sub> concentration; it increased when that concentration increased from 1 to 3 M. The best adsorption capacity was 19.5 mg As(V)/g OMD/AC for 3 mol/L of H<sub>2</sub>SO<sub>4</sub>. The increase of the anion exchange of the OMD is given by the presence of sulfate ions on the surface, which allowed for a greater exchange of anions. However, the variation of the adsorption capacity between 2 and 3 mol/L did not produce noticeable changes. The amount of OMD deposited on the AC decreased when the concentration of the acid increased; therefore, the adsorption of As(V) also decreased.

An adsorption capacity of 25.1 mg As(V)/g OMD/AC was obtained when the concentration of AC was 1 g/L; with higher concentrations, smaller values were obtained. This behavior is similar to that observed for Pb(II), and similarly related to the amount of OMD pre-

sent in the adsorbent material, which is proportionally smaller.

With respect to the temperature of the synthesis of OMD/AC, the tendency is the same for the As(V) as for the Pb(II). At low synthesis temperatures the adsorption capacity was higher showing the best results at 40 °C, although it remained virtually constant up to 60 °C, with 19.0 and 18.5 mg As(V)/g OMD/AC, respectively. At 70 °C a significant decrease in the adsorption capacity was observed. The reduction of the ion-exchange capacity of OMD/AC meant that the capacity for retention of the material decreased when more deposits of manganese were present in the adsorbent material.

The adsorption of As(V) with respect to particle size displayed the opposite behavior as the adsorption of Pb(II). In this case, with the smallest particle size, the adsorption capacity was the lowest. The sample used for this experiment probably had few OMD deposits, so the main adsorbent was AC. For other particle size, OMD deposits were confirmed; however, no high adsorption capacity was observed. The highest adsorption capacity was 19.7 mg As(V)/g, for a particle size of AC = +1.19 mm. The removal of As(V) does not present a clear tendency with regard to the particle size used for the synthesis of OMD/AC in the present work.

The best adsorption capacity obtained was 25.4 mg As(V)/g OMD/AC with a material prepared as follows: AC concentration 1 g/L, temperature at 25 °C, stirring speed at 600 rpm, AC particle size at +0.59 mm, [O<sub>3</sub>] 1.35 mol/L, and [H<sub>2</sub>SO<sub>4</sub>] 1 mol/L. The adsorption capacity of As(V) in AC is 9.1 mg As(V) /g AC; therefore, it can be seen that the presence of OMD greatly improves the adsorption of As(V).

The mechanism of removing the As(V) in anionic form from water by the OMD/AC is complicated. The first stage is probably the formation of complexes on the surface of the AC, which is followed by ion exchange. The adsorption of anions has been related to reactions of complex formations on protonated sites or the presence of electrophilic sites. The As(V) is quite basic, suggesting that its adsorption in AC has a close relationship with the concentration of functional strong acid groups.

### 3. 5. Comparison of the Adsorption Data for Pb(II) and As(V)

One published review focused on adsorbents for the removal of arsenic, cadmium, and lead from contaminated waters.<sup>50</sup> Table 5 shows a comparison of the present work's data and some data from the literature for the same kind of adsorbent material. The adsorption capacity of OMD/CA is similar to that of Al<sub>2</sub>O<sub>3</sub>-pillared layered MnO<sub>2</sub> and Al-pillared montmorillonite (A, B) and better than that of other materials. Regarding the adsorption capacity of OMD/CA for As(V), the result obtained is not too low; though there are other materials with higher values of *q*.

## 4. Conclusions

The conditions for the synthesis of a material with MnO<sub>2</sub> (OMD) on activated carbon (AC) were studied. It can be deduced that mass-transfer phenomena in the range of the stirring speed (200–800 rpm) are not important. The oxidation rate increases according to the concentration of ozone in solution and the best conditions for attaining the lowest concentration of Mn(II) in solution which results in more deposits of manganese dioxide are 1.35 mol/L and 120 min of reaction. The rate of reaction of Mn(II) oxidation decreases with increased in sulfuric-acid concentration. Neither the concentration nor the particle size of AC influences the process of oxidation of Mn(II). Increasing temperature to 70 °C and a reaction time to greater than 60 min favors oxidation; for lower temperatures, oxidation is not significantly different.

For all experimental conditions agglomerates on AC were observed by means of SEM and EDS and the presence of manganese dioxide deposited on the surface of the AC was identified. The activation energy and the factor of frequency for the reaction were determined as  $E_a = 1.2$  kcal/mol and  $A = 2.2$ , respectively. The value of  $E_a$  indicates that the precipitation of manganese dioxide in the AC is controlled by mass transfer in aqueous solution. The order of this reaction is zero.

The best conditions for the synthesis of OMD/AC to ensure maximum adsorption capacity for Pb(II) and

**Table 5.** Comparison of the adsorption capacities (*q*) of the materials in the present work and those of previously studied materials.

Material	<i>q</i> (mg Pb(II)/g)	Ref.	Material	<i>q</i> (mg As(V) /g)	Ref.
CA	14	This work	CA	9.1	This work
OMD/AC	90.5	51	OMD/AC	25.4	47
δ-MnO <sub>2</sub>	27.81	52	Calcite/α-MnO <sub>2</sub>	10.36	48
Al <sub>2</sub> O <sub>3</sub> -pillared layered MnO <sub>2</sub>	80.22	53	Calcite/goethite/α-MnO <sub>2</sub>	41.94	49
Montmorillonite-K10	95–97	54	MnO <sub>2</sub> nanowires/diatomite	108.2	50
Al-pillared clay					
α-MnO <sub>2</sub>	99.8%	55	Functionalized-nanoporous C/MnO <sub>2</sub>	9.43	56
MnO <sub>2</sub> /carbon nanotubes	6.7	57			
Silica/4-amino-2-mercaptopyridine	2.45 μmol/g	58			

As(V) were established. These values are 90.5 mg Pb(II)/g OMD/AC and 25.4 mg As(V)/g OMD/AC. When only AC is used, these values are: 14 mg Pb(II)/g AC and 9.1 mg As(V)/g AC. Therefore, the fixing of MnO<sub>2</sub> on the surface of the AC greatly improves the removal of Pb(II) and As(V) from aqueous solutions.

## 5. Acknowledgement

The authors would like to recognize the financing provided by CONACYT-Mexico in the form of Project No. 59989 and the scholarship awarded to E. Manríquez-Reza.

## 6. References

1. M. Fuentes, Arsénico en las Incrustaciones en las Redes de Distribución de Agua Potable en el Norte de México y su Desprendimiento, Agua Latinoamérica, Marzo/abril, 15, **2005**. <http://www.bvsde.paho.org/bvsAIDIS/PuertoRico29/fuentes.pdf> (assessed: January 27, 2017)
2. WHO, Air Quality Guidelines - Second Edition. Chapter 6.7 Lead, World Health Organization, Regional Office for Europe, Copenhagen, Denmark, **2001**. [http://www.euro.who.int/\\_data/assets/pdf\\_file/0020/123077/AQG2ndEd\\_6\\_7Lead.pdf](http://www.euro.who.int/_data/assets/pdf_file/0020/123077/AQG2ndEd_6_7Lead.pdf) (assessed: January 27, 2017)
3. F. N. Kemmer and J. McCallion, Manual del agua. Su naturaleza, tratamiento y aplicaciones. Tomo I, II. 1ra. ed. McGraw - Hill. México, **1989**. ISBN 9684225156
4. WHO. Guidelines for drinking-water quality [electronic resource]: incorporating first addendum. Vol. 1, Recommendations. – 3<sup>rd</sup> ed., World Health Organization, ISBN 92 4 154696 4, NML classification: WA 675, **2006**. [http://www.who.int/water\\_sanitation\\_health/dwq/gdwq0506.pdf](http://www.who.int/water_sanitation_health/dwq/gdwq0506.pdf) (assessed: January 27, 2017).
5. US-EPA, National Primary Drinking Water Regulations EPA 816-F-03-016 U.S. Environmental Protection Agency, **2003**. <https://www.epa.gov/ground-water-and-drinking-water/table-regulated-drinking-water-contaminants> (assessed: January 27, 2017)
6. Secretaria de Salud, Norma Oficial Mexicana NOM-127-SSA1-1994, Salud ambiental. Agua para uso y consumo humano. Límites permisibles de calidad y tratamientos a que debe someterse el agua para su potabilización, **2000**. [http://www.gob.mx/cms/uploads/attachment/file/110534/NOM\\_127\\_SSA1\\_1994.pdf](http://www.gob.mx/cms/uploads/attachment/file/110534/NOM_127_SSA1_1994.pdf) (assessed: January 27, 2017)
7. J. R. Conner, Chemical fixation and solidification of hazardous wastes, Springer Netherlands, **1990**. ISBN 978-0-442-20511-9
8. P. C. Hayes, Process Selection in extractive metallurgy, Hayes Publishing Co. **1985**. ISBN 0958919712
9. V. Lenoble, C. Laclautre, B. Serpaud, V. Deluchat and J. C. Bollinger, *Sci. Total Environ.*, **2004** 326(1-3), 197–207. <http://dx.doi.org/10.1016/j.scitotenv.2003.12.012>
10. V. Petkova, M. de L. Rivera, M. Piña, M. Avilés, and S. Pérez, Evaluación de diversos minerales para la remoción de arsénico de agua para consumo humano, Memorias técnicas. XI Congreso Nacional de Ingeniería Sanitaria y Ambiental. Zacatecas, 1 **1997**. <http://www.zeocat.es/docs/aguaarsenico.pdf> (assessed: January 31 2017)
11. M. L. Rivera and M. Piña, Tratamiento de agua para remoción de arsénico mediante adsorción sobre zeolita natural acondicionada, **2005**. <http://www.zeocat.es/docs/aguaarsenico2.pdf> (assessed: January 27, 2017)
12. US EPA, Technologies and Costs for Removal of Arsenic from Drinking Water, EPA 815R00028, Prepared by Malcolm Pirnie, Inc. under contract 68C60039 for EPA ORD, December **2000**. <https://nepis.epa.gov/Exe/ZyPDF.cgi/P1004WDI.PDF?Dockey=P1004WDI.PDF> (assessed: January 27, 2017)
13. US-EPA, Arsenic Treatment Technologies for soil, waste and water, U.S. Environmental Protection Agency, EPA-542-R-02-004, **2002**. [https://www.epa.gov/sites/production/files/2015-04/documents/arsenic\\_report.pdf](https://www.epa.gov/sites/production/files/2015-04/documents/arsenic_report.pdf) (assessed: January 31, 2017)
14. J. G. Parsons, M. L. Lopez, J. R. Peralta-Videa and J. L. Gardea-Torresdey, *Microchem. J.* **2009**, 91, 100–106. <http://dx.doi.org/10.1016/j.microc.2008.08.012>
15. R. Contreras-Bustos, F. Espejel-Ayala, B. Cercado-Quezada, J. Jiménez-Becerril and M. Jiménez-Reyes, *Pol. J. Chem. Technol.* **2016**, 18, 46–50. <https://doi.org/10.1515/pjct-2016-0008>
16. V. López-Ramón, C. Moreno-Castilla, J. Rivera-Utrilla and L.R. Radovic, *Carbon* **2002**, 41, 2020–2022. [http://dx.doi.org/10.1016/S0008-6223\(03\)00184-2](http://dx.doi.org/10.1016/S0008-6223(03)00184-2)
17. M. M. Rao, A. Ramesh, G. P. C. Rao and K. Seshiah, *J. Hazard. Mater.* **2006**, 129, 123–129. <http://dx.doi.org/10.1016/j.jhazmat.2005.08.018>
18. L. Beesley and M. Marmiroli, *Environ. Pollut.* **2011**, 159, 474–480. <http://dx.doi.org/10.1016/j.envpol.2010.10.016>
19. A. Bogusz, P. Oleszczuk and R. Dobrowolski, *Bioresource Technol.* **2015**, 196, 540–549. <http://dx.doi.org/10.1016/j.biortech.2015.08.006>
20. D. Dong, L. Liu, X. Hua and Y. Lu, *Microchem. J.* **2007**, 85, 270–275. <http://dx.doi.org/10.1016/j.microc.2006.06.015>
21. L. Dong, Z. Zhu, H. Ma, Y. Qiu and J. Zhao, *J. Environ. Sci.* **2010**, 22, 225–229. [http://dx.doi.org/10.1016/S1001-0742\(09\)60097-8](http://dx.doi.org/10.1016/S1001-0742(09)60097-8)
22. A. Günay, E. Arslankaya and I. Tosun, *J. Hazard. Mater.* **2007**, 146, 362–371. <http://dx.doi.org/10.1016/j.jhazmat.2006.12.034>
23. Z. Song, F. Lian, Z. Yu, L. Zhu, B. Xing and W. Qiu, *Chem. Eng. J.* **2014**, 242, 36–42. <http://dx.doi.org/10.1016/j.cej.2013.12.061>
24. Y. Ren, N. Yan, J. Feng, J. Ma, Q. Wen, N. Li and Q. Dong, *Mater. Chem. Phys.* **2012**, 136, 538–544. <http://dx.doi.org/10.1016/j.matchemphys.2012.07.023>
25. S. Wang, B. Gao, Y. Li, A. Meuse, A. R. Zimmerman, L. Q.

- Ma, W. G. Harris and K. W. Migliaccio, *Bioresour. Technol.* **2015**, *181*, 13–17.  
<http://dx.doi.org/10.1016/j.biortech.2015.01.044>
26. L. M. Camacho, R. R. Parra and S. Deng, *J. Hazard. Mater.* **2011**, *189*, 286–293.  
<http://dx.doi.org/10.1016/j.jhazmat.2011.02.035>
27. R. Han, W. Zou, Z. Zhang, J. Shi and J. Yang, *J. Hazard. Mater.* **2006**, *137*, 384–395.  
<http://dx.doi.org/10.1016/j.jhazmat.2006.02.021>
28. S. Wang, W. Gong, X. Liu, Y. Yao, B. Gao and Q. Yue, *Sep. Purif. Technol.* **2017**, *58*, 17–23.  
<http://dx.doi.org/10.1016/j.seppur.2007.07.006>
29. Y. Wu, S. Yang, M. Zhang, A. Aierken and Y. Wu, *Korean J. Chem. Eng.* **2015**, *32*, 1667–1677.  
<http://dx.doi.org/10.1007/s11814-014-0352-4>
30. T. M. Albayati, G. M. Alwan and O. S. Mahdy, *Korean J. Chem. Eng.* **2017**, *34*, 259–265.  
<http://dx.doi.org/10.1007/s11814-016-0231-2>
31. N. Kijima, H. Yasuda, T. Sato and Y. Yoshimura, *J. Solid State Chem.* **2001**, *159*, 94–102.  
<http://dx.doi.org/10.1006/jssc.2001.9136>
32. R. Contreras and G. T. Lapidus, *J. Colloid Interf. Sci.* **1999**, *213*, 251–257. <http://dx.doi.org/10.1006/jcis.1999.6114>
33. C. Bigliocca, F. Girardi, J. Pauly, E. Sabbioni, S. Meloni and A. Provasoli, *Anal. Chem.* **1967**, *39*, 1634–1639.  
<http://dx.doi.org/10.1021/ac50156a040>
34. D. Glover, B. Schumm and A. Kozawa, Handbook of Manganese Dioxides Battery grade, International Battery Material Association (IBA Inc.), USA, **1989**.
35. R. Contreras, Producción de dióxido de manganeso por ozonización y estudio de sus propiedades de intercambio iónico, Doctoral dissertation, Universidad Autónoma Metropolitana, campus Iztapalapa, Mexico, **1999**.  
<http://tesiuami.izt.uam.mx/uam/aspum/presentatesis.php?recno=468&docs=UAM0468.PDF>
36. K. Schaeffer, *Agua Latinoam.* **2003**, *3*, 1–5.  
<http://www.agualatinoamerica.com/docs/pdf/Intermedio.pdf> (assessed: January 31, 2017)
37. R. Leyva, L. G. Velázquez, J. Mendoza and R. M. Guerrero, *J. Mex. Chem. Soc.* **2002**, *46*, 159–166.  
<http://www.redalyc.org/pdf/475/47546214.pdf>
38. A. J. Rubin and D. L. Mercer, In: Adsorption of Inorganics at Solid-Liquid Interfaces; Anderson, M. A.; Rubin, A. J. Ed.; Ann Arbor Science Publishers Inc.: **1981**; p. 300.
39. H. Pérez, Modificación termoquímica y caracterización de un carbón activado lignítico, Bachelor dissertation, Universidad Veracruzana, **2006**.
40. I. Puigdomenech, **2010**. Program MEDUSA (Make Equilibrium Diagrams Using Sophisticated Algorithms). Royal Institute of Technology, Inorganic Chemistry, Stockholm, swedenignasi@inorg.kth.se.
41. M. Al-Anber and Z. A. Al-Anber, *Desalination* **2008**, *225*, 70–81. <http://dx.doi.org/10.1016/j.desal.2007.07.006>
42. M. Pourbaix, Atlas d'équilibres électrochimiques, Gauthier-Villars, Paris, **1963**.
43. C. Gottschalk, J. A. Libra and A. Saupe, Ozonation of water and waste water: A practical guide to understanding ozone and its applications, 2nd Ed., Wiley-VCH, Germany, **2010**. ISBN: 978-3-527-31962-6
44. J. L. Rodríguez-Santillán, T. Poznyak and J. L. Mayorga, Efecto del pH y Carbón Activado Sobre la Descomposición de Ozono en Solución Acuosa, In: XXVII Encuentro Nacional de la AMIDIQ, 2006.  
<https://www.dropbox.com/s/57sdrecsy8amha3/2006.rar> (assessed: January 31, 2017)
45. E. Peters and G. Bolton, *Hydrometallurgy: Theory and Practice*, Center for metallurgical and Process Engineering Department and Metallurgical Engineering, Chapter I, UBC. Vancouver, B. C. **1999**. ISBN-13: 978-0444896568
46. T. Nishimura and Y. Umetsu, *Shigen-to-Sozai* **1992**, *108*, 373–377. <https://doi.org/10.2473/shigentosozai.108.373>
47. Y. Umetsu, T. Nishimura and R. C. Bustos, M. Tokuda, *Shigen-to-Sozai* **2000**, *116*, 999–1004.  
<https://doi.org/10.2473/shigentosozai.116.999>
48. J. S. Markovski, V. Dokić, M. Milosavljević, M. Mitrić, A. A. Perić-Grujić, A. A., A. E. Onjia, A. D. Marinković, *Ultrason. Sonochem.* **2014**, *21*, 790–801.  
<https://doi.org/10.1016/j.ultsonch.2013.10.006>
49. Y. Du, G. Zheng, J. Wang, L. Wang, J. Wu, H. Dai, *Micropor. Mesopor. Mat.* **2014**, *200*, 27–34.  
<https://doi.org/10.1016/j.micromeso.2014.07.043>
50. S. Pathan, N. Pandita, N. Kishore, *Arabian J. Chem.* **2016** Available online 31 December 2016.  
<http://doi.org/10.1016/j.arabjc.2016.12.011>
51. S. K. R. Yadanaparthi, D. Graybill, R. von Wandruszka, *J. Hazard. Mater.* **2009**, *171*, 1–15.  
<https://doi.org/10.1016/j.jhazmat.2009.05.103>
52. H. Zhang, L. Gu, L. Zhang, S. Zheng, H. Wan, J. Sun, D. Zhu, Z. Xu, *Appl. Surf. Sci.* **2017**, *406*, 330–338.
53. D. Humelnicu, M. Ignat, M. Suche, *Acta Chim. Slov.* **2015**, *62*, 947–957. <https://doi.org/10.17344/acsi.2014.1825>
54. S. T. El-Wakeel, R. S. El-Tawil, H. A. M. Abuzeid, A. E. Abdel-Ghany, A. M. Hashem, *J. Taiwan Inst. Chem. Eng.* **2017**, *72*, 95–103.
55. B. Yang, Q. Gong, L. Zhao, H. Sun, N. Ren, J. Qin, J. Xu, H. Yang, *Desalination* **2011**, *278*, 65–69.  
<https://doi.org/10.1016/j.desal.2011.05.010>

## Povzetek

Proučili smo pogoje za pripravo materialov z  $\text{MnO}_2$  (OMD) na aktivnem oglju (AC) in sicer reakcijski čas, temperaturo, hitrost mešanja, koncentracije AC,  $\text{H}_2\text{SO}_4$  in  $\text{O}_3$  v raztopinah ter velikost delcev. Aglomerate na AC smo spremljali z vrstičnim elektronskim mikroskopom (SEM) in z mikroanalizo z energijsko disperzijsko spektroskopijo (EDS) potrdili prisotnost OMD depozitov na površini. Izračunali smo aktivacijsko energijo in frekvenčni faktor reakcije  $E_a = 1.2$  kcal/mol in  $A = 2.2$ . Vrednost  $E_a$  kaže, da je nalaganje OMD na AC kontroliran z masnim prenosom v vodnih raztopinah, reakcija je ničtega reda.

Adsorpcijska kapaciteta AC je  $q = 14$  mg Pb(II)/g AC in  $q = 9.1$  mg As(V)/g AC. Adsorpcijska kapaciteta na sistemu OMD/AC pri sledečih pogojih: [AC] 1 ali 2 g/L, velikost delcev AC +0.59 mm,  $[\text{H}_2\text{SO}_4]$  1 ali 2 mol/L, 25 °C, hitrost mešanja 600 rpm, in  $[\text{O}_3]$  1.35 mol/L je  $q = 90.5$  mg Pb(II)/g OMD/AC in 25.4 mg As(V)/g OMD/AC. Vezava OMD na površino AC torej izredno izboljša odstranjevanje Pb(II) in As(V) iz vodnih raztopin.

*Scientific paper*

# Adsorption Kinetics of Malachite Green and Methylene Blue from Aqueous Solutions Using Surfactant-modified Organoclays

Haseeb Ullah,<sup>1</sup> Muhammad Nafees,<sup>2</sup> Farhat Iqbal,<sup>3</sup> Muhammad Saifullah Awan,<sup>4</sup> Afzal Shah<sup>1</sup> and Amir Waseem<sup>1,\*</sup>

<sup>1</sup> Department of Chemistry, Quaid-i-Azam University, Islamabad- 45320, Pakistan

<sup>2</sup> State Key Laboratory of Coordination Chemistry, School of Chemistry and Chemical Engineering, Nanjing University, Nanjing-210093, China

<sup>3</sup> Department of Statistics, University of Balochistan, Quetta-Pakistan

<sup>4</sup> Ibn-i-Sina Institute of Technology, H-11/4, Islamabad, Pakistan

\* Corresponding author: E-mail: waseemq2000@hotmail.com

Received: 14-02-2017

## Abstract

The main objective of this research is to study the adsorption behaviour of malachite green and methylene blue dyes onto the surfactant modified natural clays. The results of SEM, XRD, IR, and thermal analysis confirms the intercalation of organic moiety in to the clay. The adsorption results show that pseudo-first order kinetics best fitted for both the dyes adsorbed on organo-clay. The data also reveals that both dyes are in a good agreement with Langmuir isotherm in both types of modified clays. The value of separation factor,  $R_L$ , from Langmuir equation and Freundlich constant,  $n$ , give an indication of favourable adsorption. The maximum adsorption capacity  $q_m$  based on Langmuir model was found to be 294-303 mg/g at 25 °C, is in good agreement with the experimental values.

**Keywords:** Environmental remediation, montmorillonite, dyes, cationic surfactants, isotherm models.

## 1. Introduction:

Ecological issues have turned into a worldwide concern in the light of their effect on public health.<sup>1,2</sup> Almost 25% of the sicknesses confronting people today is because of their long-term exposure to environmental pollutants.<sup>3</sup> Dye-bearing effluents are one of the most significant contributors from the textile field and such effluents have a wide detrimental impact on the human health.<sup>4,5</sup> It has been estimated that annually  $7 \times 10^5$  metric ton of different commercial dyes and pigments are being produced globally, and of which 5–10% are being lost and discharged into the wastewater in the form of industrial effluents.<sup>6,7</sup> Among them azo dyes are the one most widely used and accounts 65–70% of the total dyes produced.<sup>8</sup> A great deal of dyes exists and exhibit structural variations and can be classified in several ways. These can be classified due to their structural similarity or application to the fiber type.<sup>9,10</sup>

Dyes, such as malachite green (MG) and methylene blue (MB) have been used extensively as model dyes for adsorption studies onto various low cost adsorbents.<sup>8</sup> In addition, MG is largely being utilized as a food colouring agent, food additive, and a therapeutic disinfectant and anthelmintic as well as a dye in a vast majority of industries,<sup>11</sup> On the other hand, MB is generally being utilized as a colouring agent in the biomedical field such as in microbiology, surgery, and diagnostics.<sup>12</sup> Beside their greater use, they have now turned into an exceedingly questionable compounds because of the risks it (MG) poses to the consumers of treated fish including its effects on the immune and reproductive system,<sup>13,14</sup> similarly, intense exposure to MB can bring about numerous health risks such as fast pulse, skin disease, jaundice, and tetraplegia and tissue necrosis.<sup>6</sup>

In response to concerns regarding the health risks associated with the utilization of dyes, adsorption is prob-

ably the most adaptable and versatile approach for the expulsion of dyes from aqueous solutions.<sup>15</sup> Sometimes, it is conceivable to recoup the adsorbed dye through desorption and also to reuse the huge amount of water utilized by textile sector. Adsorption has been observed to be one of the very most effective physicochemical techniques, better than numerous different approaches for water reuse in terms of the simplicity of operation. The design of adsorption system play a crucial role in order to generate high quality treated effluent.<sup>16,17</sup> Activated carbon has been generally utilized for this reason in view of its high adsorption capacity; however, its high cost tends to limit its use. In the past few decades, much research has been focused on the development of adsorbents from natural sources, for example, naturally occurring clays, zeolites, and other cheap and accessible solid materials to remove dyes from wastewater.<sup>18</sup> Clay minerals are appropriate for adsorption process because of their specific surface area and nanometer-scale size.<sup>19</sup> Recent progress in the synthesis of nanostructured materials offers a broader spectrum to change surface properties of naturally occurring clays in order to increase their adsorption properties. The organoclays (OCs) are set up by introducing cationic surfactant molecules (e.g. hexadecyltrimethylammonium, HDTMA, trimethylammonium TMA etc) into the interlamellar space of a clay (e.g. smectite) through ion exchange which consequently change the surface properties of natural clay from hydrophilic to hydrophobic.<sup>20</sup> The OCs have long been used for the adsorption of a range of organic compounds from water and wastewater.<sup>18,21–23</sup>

Adsorption process is a surface phenomenon, where substance of interest is concentrated on the surface of solid adsorbent material. Liquid and gaseous substances can be adsorbed in suitable adsorbent and is widely used in isolation and purification processes in the chemical industries including biotechnology and environmental technology.<sup>24–26</sup> Adsorption is very reasonably superior technique because of simplicity of design availability, ability to treat dyes more concentrated from other techniques.<sup>27,28</sup> Being a dynamic process, the rate of adsorption in adsorption equilibrium is controlled by mass transfer processes. The amount of adsorbate (analyte) adsorbed per unit mass is determined through equilibrium, where data is represented in the form of adsorption isotherms.<sup>24</sup> Literature review shows the number of models which govern adsorption equilibrium, out of them the Langmuir and the Freundlich isotherm models are the most commonly used, others include modified Freundlich, Sips, Redlich–Peterson, Dubnin–Radushkevich constants, Tempkin constants etc.<sup>24,29</sup> Several steps can be used to study the controlling mechanism of adsorption process such as chemical reaction, diffusion control, and mass transfer; kinetic models are used to the experimental data from the adsorption process.<sup>28</sup> The kinetic parameters are useful for the prediction of adsorption rate, and gives valuable information for designing and modelling the adsorption processes.

Various structural and non-structural models have been described in the literature with variable degree of success.<sup>24,30</sup> Some of them are: pseudo first and second-order rate expressions; which are most often used, other includes intraparticle diffusion model, Bangham's equation etc.<sup>24,30,31</sup>

The aim of this study was to examine the adsorption capability of natural clay (Pakistan based montmorillonite) for removal of malachite green (MG) and methylene blue (MB) as a model dyes from aqueous solutions. The peculiar montmorillonite was gotten from Khyber Pakhtunkhwa region of Pakistan, and emended with a cationic surfactant, Hexadecyl trimethylammonium bromide (HDTMA) and Hexadecylpyridinium chloride (HDPy), in order to assess the changes in the clays and its adsorption capacity. The structures of natural and organoclay were assessed by utilizing, Powdered X-ray diffraction (XRD), X-ray Fluorescence microscopy (XRF) Fourier Transform infrared (FT-IR) spectroscopy, Scanning electron microscopy (SEM) and Thermogravimetric analysis (TGA). The impacts of various parameters, for example, pH, contact time, dye concentration and adsorbent dosage were also studied. The adsorption systems of dyes (MG & MB) onto organoclay were assessed in terms of adsorption isotherms which were portrayed by utilizing Langmuir and Freundlich isotherm models.

## 2. Materials and Methods

### 2.1. Materials

Both quaternary ammonium salts, hexadecylpyridinium chloride (HDPy) and hexadecyltrimethylammonium bromide (HDTMA) were purchased from Sigma-Aldrich and used without any purification. The cationic dyes methylene blue (MB)  $C_{16}H_{18}ClN_3S \cdot 3H_2O$  (98%) and malachite green (MG)  $C_{23}H_{25}ClN_2$  (96%) were used as the adsorbate in this study and obtained from Sigma-Aldrich. All the chemicals used were of analytical reagents grade being purchased from Merck and were used without further purification.

### 2.2. Preparation of Organoclays

The organoclays were synthesized according to the general procedure described as under. The clay impurities were removed by sedimentation method, followed by oven drying at 110 °C for 3h and pulverized through 200  $\mu$ m sieve. Briefly, thirty millilitres of the quaternary ammonium salt solution (1:1 CEC) was placed in a beaker and 1g of pre-dried clay was added into it. The mixture was stirred with the magnetic stirrers for about 16 h at room temperature, followed by centrifugation and washing several times with deionized water until no halides ions were detected from the supernatant. The modified clays were oven dried



at 60 °C for 5 hours, ground to 74 µm sizes and finally stored in a desiccator for later use.

## 2. 3. Characterization Methods

Characteristics of the adsorbent materials are imperative in evaluating the mechanism of adsorbate binding onto the surface of the adsorbent. The chemical analysis of the natural clay was determined using X-ray fluorescence (XRF) spectrometer (Phillips PW 1404 X-ray spectrometer). The basal spacing patterns of the clay mineral were analysed through X-ray diffraction (XRD). The data are recorded on a Philips PANalytical X'pert PRO diffractometer using CuK $\alpha$  radiation ( $\lambda = 1.540598$  Å). The diffractometer was operated at accelerating voltage of 40kV and the emission current of 30mA, and scan range ( $2\theta =$  from 2 to 10) at a step size of 0.015°. The Fourier Transform Infrared (FT-IR) spectra of natural and organoclay were recorded to examine the surface functional group using Nicolet Nexus 870 FT-IR spectrometer in the region 500–4000  $\text{cm}^{-1}$  with resolution of 4  $\text{cm}^{-1}$  and ten interferograms recorded for each sample. An FEI Quanta 450 scanning electron microscope (SEM) was used to define the change in surface morphology of natural and organoclay. The thermogravimetric analyses (TGA) were performed using PerkinElmer Thermogravimetric analyser instrument in an atmosphere of nitrogen (90  $\text{cm}^3/\text{min}$ ) at a heating rate of 10 °C/min in a temperature range of 25–800 °C. The BET surface area and average pore size of the samples were performed by (Micromeritics, ASAP 2020) System. The cation exchange capacity (CEC) of the clay was measured using a simple BaCl $_2$  method.<sup>32</sup>

## 2. 4. Adsorption Studies Method

The adsorption study of dyes on modified MMt was carried out by batch equilibrium experiment of known amount of the adsorbent with 50 ml of aqueous dye solutions of known concentration in a series of 100 ml stoppered flasks. The solution mixtures were kept under isothermal conditions in a shaking water bath at 150 rpm at the desired temperature. At predefined time, the solution mixtures were removed from the shaker, and centrifuged. The residual dye concentration in the reaction mixture were analyzed by UV/Vis spectrophotometer (Shimadzu UV1700 Japan) using calibration curve. The effect of various experimental factors such as pH, adsorbent dose, initial dye concentration and contact time were investigated employing the univariate approach. After each adsorption experiment, the suspensions were centrifuged, filtered through 0.45 µm of nitrocellulose membrane (Sartorius Stedim Biotech. GmbH), to remove the solid organoclays particles and the supernatant were subsequently analysed by spectrophotometer for the residual concentration of the MB and MG. The sorption efficiency

(S%) and adsorption capacity at equilibrium ( $q_e$ ) were calculated by using the following equations:

$$\text{Sorption Efficiency (S\%)} = \frac{(C_o - C_e)}{C_o} \times 100 \quad (1)$$

$$q_e = \frac{(C_o - C_e) \times V}{m}$$

Where  $C_i$  (mg/L) represents is the initial dye concentration,  $C_e$  (mg/L) is the equilibrium concentration of dye, V is the volume of solution (L), and m is the mass of adsorbent (g).

## 3. Results and Discussion

### 3. 1. Material Characterization

#### 3. 1. 1. XRF, CEC & BET

The host clay utilized was a montmorillonite (MMt) (Smectite clay) from Khyber-Pakhtunkhwa (KPK) region of Pakistan. There are many MMt deposits available in Pakistan, but most of them including KPK are Ca bentonites. The chemical compositions of MMt was found to be (weight %) 57.38  $\pm$  0.11% SiO $_2$ , 2.33  $\pm$  0.05% MgO, 15.20  $\pm$  0.10% Al $_2$ O $_3$ , 1.10  $\pm$  0.03% K $_2$ O, 4.07  $\pm$  0.06% CaO, 2.72  $\pm$  0.03% Na $_2$ O, 0.1  $\pm$  0.02% SO $_3$ , 6.49  $\pm$  0.07% (FeO + Fe $_2$ O $_3$ ) as determined by XRF. Results of XRF declare that predominant exchangeable cation was calcium along with sodium and potassium. The cation exchange capacity (CEC) of MMt clay was found to be 68.3 meq/100g and a BET surface area of 58 m $^2$ /g.

#### 3. 1. 2. FT-IR

To understand the presence of functional groups onto the surfaces of the adsorbent with and without modification, the FT-IR spectral analysis was performed within the range of 400–4000  $\text{cm}^{-1}$ . The FT-IR spectra of natural clay, HDP-clay and HDTMA-clay are shown in Figure 2. The IR region between 3700–3000  $\text{cm}^{-1}$  shows the region of OH stretching and is observed by two key bands and is observed in almost all the natural hydrous silicate (Fig. 1).

Different stretching vibrations of OH are present in this region. A peak at 3621  $\text{cm}^{-1}$  for MMt is assigned to OH stretching vibrations for the structural hydroxyl group attached to the octahedral magnesium and the tetrahedral silicon. The bands at 3404, and 3243  $\text{cm}^{-1}$  can be ascribed to water molecules, within the interlayer of the clay which are hydrogen bonded adsorbed. The bands between 3500–3000  $\text{cm}^{-1}$  are relatively dependent on the concentration of surfactant loaded on clay and becomes broad upon loading. The conformational changes of the surfactant loading on clay can be monitored through the sensitive CH stretching bands. The CH stretching region (2700 and 2900  $\text{cm}^{-1}$ ) for the clay loaded with surfactant mole-

cule shows asymmetric  $\nu_{as}(\text{CH}_2)$  and symmetric  $\nu_s(\text{CH}_2)$  stretching modes of  $2920\text{ cm}^{-1}$  and  $2853\text{ cm}^{-1}$ . The region between  $1700\text{--}1600\text{ cm}^{-1}$  shows the HOH bending of adsorbed water molecules in both clay and organoclays (Fig. 2. peak observed at  $1641\text{ cm}^{-1}$ ). The strong band between  $1100\text{--}900\text{ cm}^{-1}$  for natural clay and organoclays were assigned to the Si–O–Si and Si–O–Al stretching. The peak between  $910\text{--}800\text{ cm}^{-1}$  corresponds for the OH deformation linked to the Mg and Al. The peaks between  $800\text{--}600$  were assigned to the Si–O quartz vibrations.

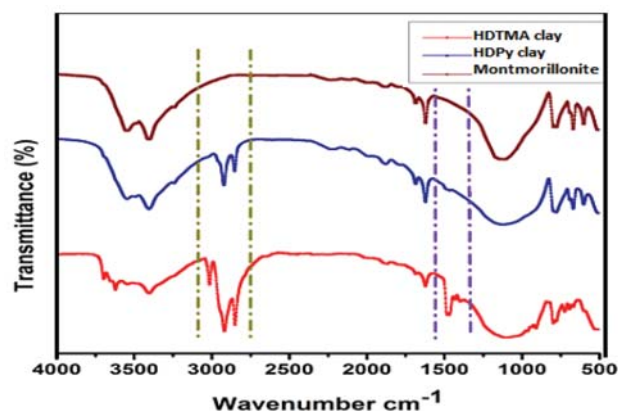


Figure 1. FT-IR spectra of (a) pure clay, (b) HDP-clay, (c) HDTMA-clay

### 3. 1. 3. XRD

The potential arrangements of intercalated organic molecules (surfactants) were proposed according to the obtained basal spacing of organoclays and the size of organic cations.<sup>15,29,33–35</sup> In the current work, the unmodified MMt has a d-spacing of  $1.23\text{ nm}$ , which expanded when the intercalated ions were exchanged with surfactants

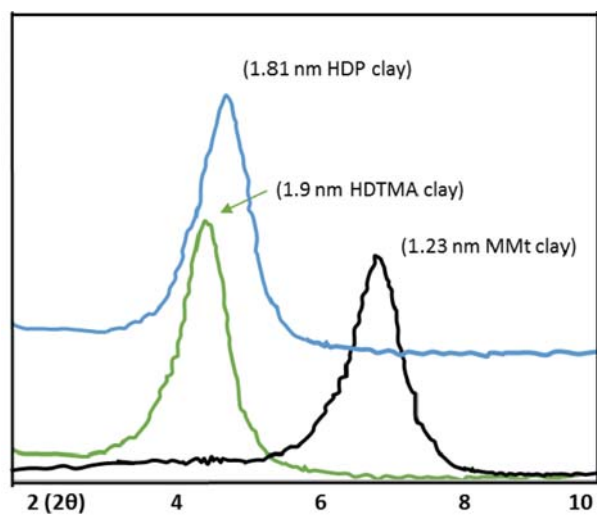


Figure 2. Powder XRD patterns of MMt modified and unmodified clay

(HDTMA or HDP). Upon increasing the HDTMA and HDP loading, the peak at  $1.23\text{ nm}$  disappears due to the increase in interlayer basal spacing and new peaks appeared at  $1.81$  and  $1.90\text{ nm}$  respectively (Fig. 2). The observed interlayer spacing of MMt and organoclays is used to observe the structural configuration of modified molecule, in the present study lateral-monolayer arrangement was observed with CEC of 1:1.<sup>20,33,36,37</sup>

### 3. 1. 4 SEM

The resulted SEM photomicrographs of natural clay and organoclays are shown in Figure 4. It is observed that (Fig. 3a), that natural clay has agglomerated structure with

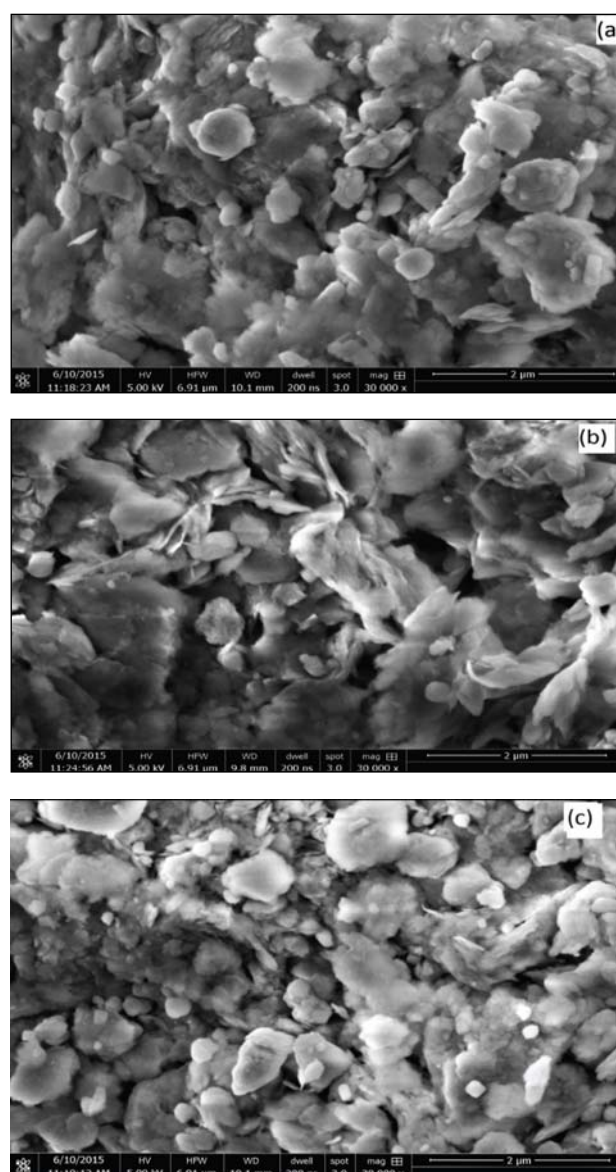


Figure 3. SEM micrograph of (a) pure clay, (b) HDP-clay, (c) HDTMA-clay

small particle size, smooth and micro-porous surface with fluffy appearance due to the closely packed flakes. The BET surface area of unmodified MMT clay was found to be 58 m<sup>2</sup>/g, whereas the modified MMT clay shows the decrease of surface area to 18.5 m<sup>2</sup>/g & 16.5 m<sup>2</sup>/g for HDTMA and HDPy surfactant respectively. These results are attributed to the fact that the most of the exchange sites of MMT clay is occupied by organic surfactants molecules with large molecular size and the inaccessibility of the internal surface to nitrogen gas.<sup>38</sup> However, larger average pore size (12.2 nm) was observed in modified clay than the precursor clay (5.2nm). After the modification of clay with HDMA and HDPy surfactant, the surface morphology slightly changed from foliated structure to non-agglomerated and crumpled structure containing heterogeneous pores with large particles as depicted in Figure 3. MMT have massive and curved plates (Fig. 3a) generally as a heterogeneous surface morphology.<sup>33</sup> However, the clay modified with organic surfactants shows significant changes in the morphology. Compared with the morphology of the MMT, there are many small and aggregated particles and the plates become relatively flat in while the introduction of organic moiety leads to large particles and coarse porous surface, which may be due to the penetration of organic molecules into the galleries of MMT, resulting in an increase in the adsorption capacity of modified clay.<sup>37</sup>

### 3. 1. 5. TGA

Thermogravimetric analysis has been performed to study the arrangement and packing of surfactant molecules within the organoclays and the thermal decomposition behaviour of the organoclay. Thermogravimetric analysis curve for the natural clay and organoclays are shown in Figure 4. TGA pattern of the unmodified natural clay reveals that mass loss occurs mainly at two stages; a) the initial mass loss due to desorption of water occurs at

30–120 °C temperature range; b) the second mass loss due to the loss of structural hydroxyl group occurs at 400–540 °C and 580–690 °C temperature range respectively.<sup>39</sup> While there are three stages of mass loss with the increase in temperature are occurred for the HDTMA and HDPy modified clay. The first weight loss corresponds to the dehydration of water from organoclays that occur at 30 °C–180 °C, the weight loss in both the organoclays are lower than the unmodified clay because in organoclays the surfactant molecules replaced some of the water molecules present in clay structure. The second mass loss that is only present in both organoclays is attributed to the removal of surfactant molecules from the organoclays that occurs at 220 °C–350 °C temperature range. This is consistent with the previously reported studies.<sup>34,40</sup> This corresponds to 7 to 8% mass loss for both clays, which indicates the surfactant loading to the clays is not very efficient. The last stage shows that besides degradation of Al, Si-polyoxy cations, dehydroxylation of structural hydroxyl unit in clay in the octahedral layer of montmorillonite also takes place.<sup>39,40</sup>

## 3. 2. Adsorption Optimization Experiments

Effect of various parameters i.e, the effect of pH, time, adsorbate, and adsorbent concentrations respectively were investigated in univariate design at room temperature (25 °C).

### 3. 2. 1. Effect of pH

To investigate the impact of pH on the adsorption capacity of HDTMA- and HDPy-organoclays for the MG and MB, adsorption tests were performed with an initial dye concentration of 150 mg/L and organoclay concentration was 0.1g and contact time of 30 minutes by varying the pH of solutions over a range of 3–10. It is clear from the Figure 5 that increasing pH of a solution, the adsorp-

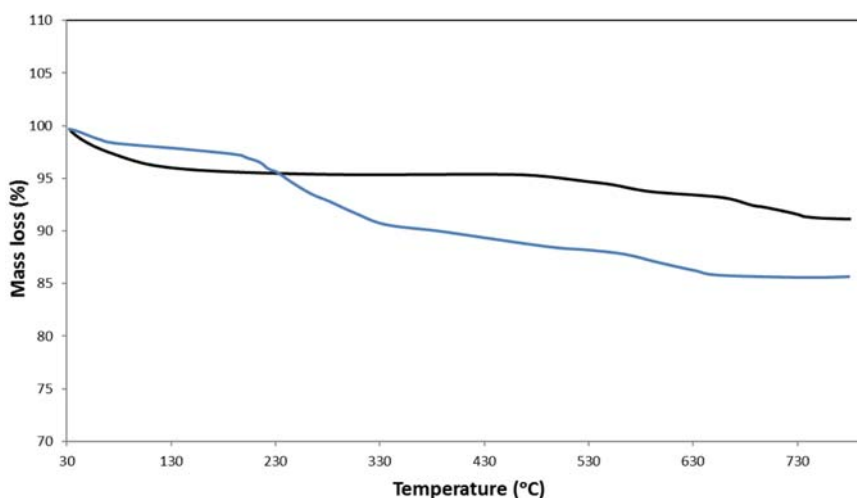
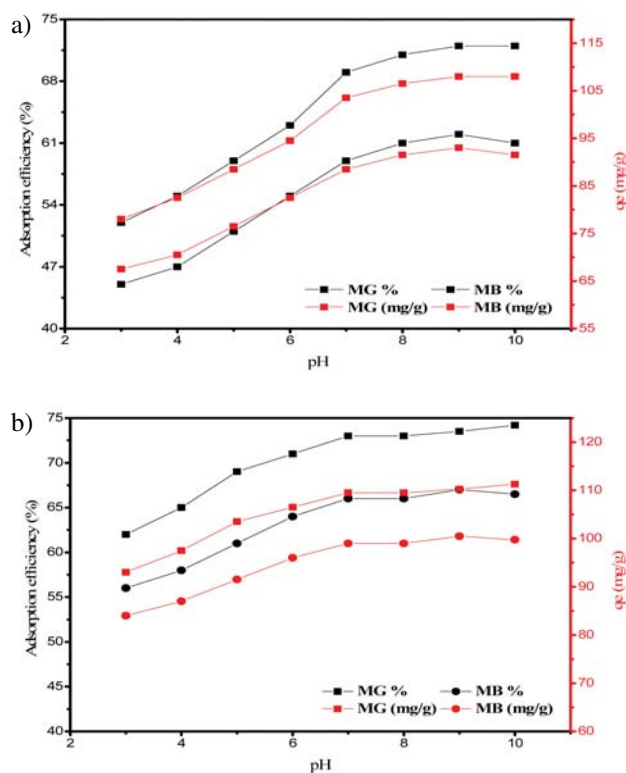


Figure 4. Thermogram of (a) pure clay, (b) organoclay

tion of cationic dyes also increases. Basically, cationic dyes produces molecular cations ( $C^+$ ) and reduced ions ( $CH^+$ ) on dissolution in water<sup>31</sup> and depends on the water pH. At lower pH, the surface of the adsorbent become protonated results in lower adsorption of the protonated dyes.<sup>41</sup> Increase in adsorption of dyes with the increase of pH from 3 to 10; is because of the way that the overall positive charge in aqueous solution diminishes and at neutral pH, it shows a balanced surface charge that is required for the adsorption.<sup>22,42–44</sup> It was observed that both dyes show little increase in sorption after pH 7, it is therefore pH 7 was selected to investigate the effects of other parameters.



**Figure 5.** Effect of pH on the adsorption of MB and MG dyes on (a) HDPy-clay (b) HDTMA-clay

### 3. 2. 2. Effect of Time

The effect of contact time on the adsorption of MG and MB dyes at various time points onto HDTMA- and HDPy-clays were examined using a fixed adsorbent dose of 0.1g and dye concentration was 150 mg/L at pH 7. As depicted by the Figure 6 that adsorption of both dyes onto the organoclays increases with the increase of contact time, which is consistent with the previous studies.<sup>14,29,34</sup> At first, the adsorption of dyes occurs through boundary layer adsorption and the adsorptions rates were high because of the accessibility of the higher surface area for the rapid attachment of these dyes to the external exposed surfaces of the organoclays and backs off step by step in the

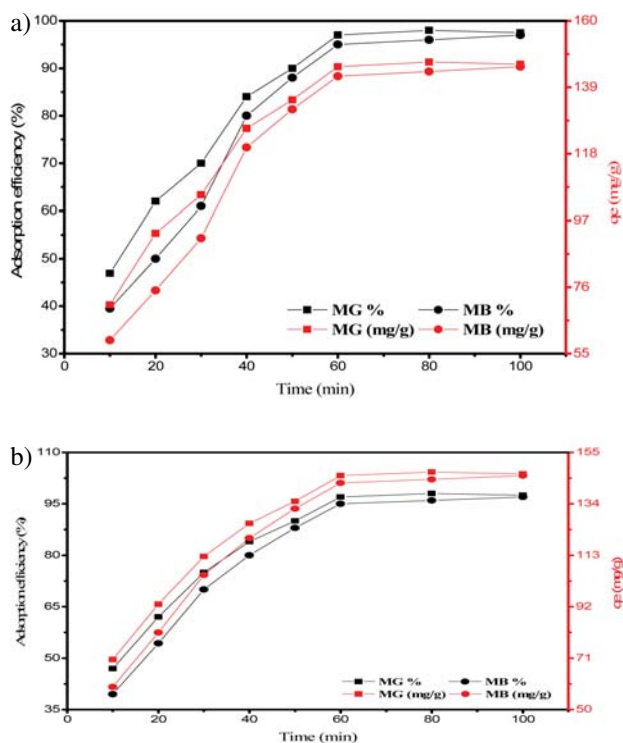


**Figure 6.** Effect of time on the adsorption of MB and MG dyes on (a) HDPy-clay (b) HDTMA-clay

wake of achieving the equilibrium. After the initial rapid adsorption of dyes, the adsorbent surface gets saturated enough that opposed further adsorption due to the repulsive forces presents between the cationic dye molecules on solid surface and cationic dye molecules present in the bulk phases.

Hence, the adsorption happens because of the diffusion of dyes into the pores of organoclays or might be because of the surface reaction of dyes with the adsorbent clay.<sup>45,46</sup> There is little increase in dyes adsorption after 60 minutes of equilibrium time, hence 60 minutes selected for further studies.

### 3. 2. 3. Effect of Initial Dye Concentration

The initial concentration of adsorbate (dyes) plays important role in adsorption capacity of organoclays.<sup>34,47</sup> The influence of initial dye concentrations was examined using 0.1g of the HDPy and HDTMA-organoclays at pH 7 with equilibrium time of 60 minutes. Figure 7 shows that adsorption of dyes onto organoclays increases with the increase in the concentration of dyes in a solution up to a certain value after which it levelled off. This is because of the fact that an increase in the concentration of dye solution results to produce the high mass gradient pressure between the dye solution and organoclay, this pressure gradient than acts as a driving force for the transfer of dye molecules into the particle surface of the organoclays.<sup>48–50</sup> The results also indicate that percent removal and adsorption capacity of

dye onto the organoclay shows opposite trends by varying the concentration of dye solution. Several researchers also found the same adsorption results as function of MB and MG dye concentration.<sup>28,34,45,47,51</sup> The inverse patterns for the adsorption capacity and percent removal can be clarified with the way that: there are fixed number of binding sites on the organoclay surface. At the point when the dyes are available in little concentration, the adsorption will be fast and the percent removal of dyes will be high because of the higher number of accessible sites on the surface of organoclays. The quantity of accessible sites for adsorption is higher at lower dyes concentration and decreased with the increase in the concentration of dyes because of the saturation of adsorbed dye molecule. The dye molecules at high concentration compete with each other for the fixed number of binding sites, thus, some of the dye molecules did not get adsorbed and remains in solution, causing lower percent removal of dyes.<sup>37,49,52</sup>

### 3. 2. 4. Effect of Adsorbent Dose

The effects of organoclay concentration on the removal of dyes from aqueous solutions were investigated

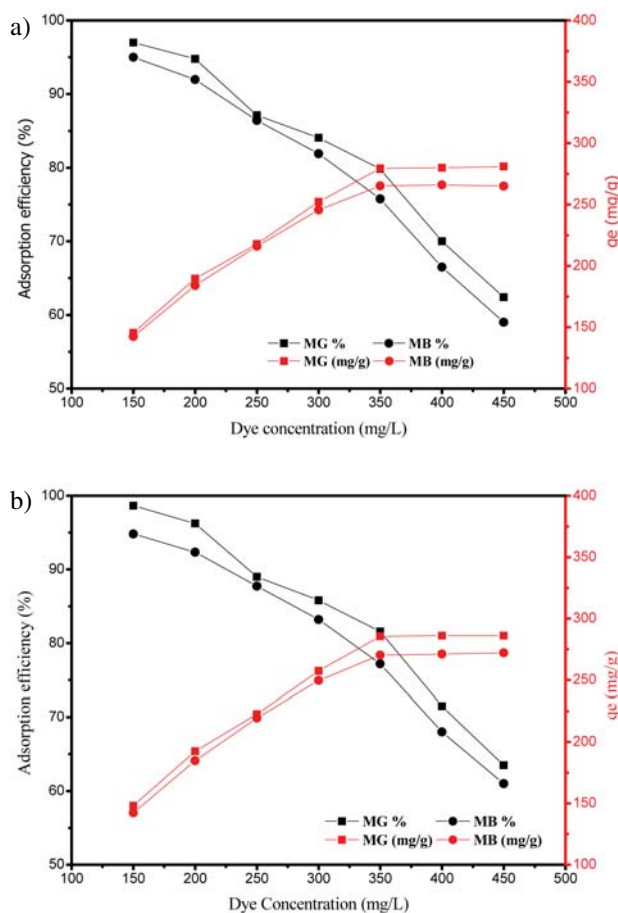


**Figure 7.** Effect of initial dye concentrations on the adsorption of MB and MG dyes on (a) HDP-clay (b) HDTMA-clay.

by using different concentrations of organoclays in the range of 0.1–0.3 grams and initial dye concentration of 150 mg L<sup>-1</sup> at pH 7.0 and equilibrium time of 60 minutes. The results indicate (Fig. 8) that the adsorption efficiency (%) increases with the increase of adsorbent dosage but show opposite trend for the adsorption capacity, i.e., lesser amount of dye is adsorbed per gram of organoclay. Increase in adsorption efficiency is attributed due to the higher surface area of adsorbent and number of available binding sites for adsorption at a high adsorbent dose.<sup>42,45</sup> While the decrease in adsorption capacity are attributed due to the fact that total number of dye molecules are fixed ( $C_e = 150$  mg/L) against the increasing organoclay dose (0.1 g to 0.3), at higher adsorbent dose some of the adsorption site remains uncovered and thus causing the decrease in the adsorption capacity of the adsorbent.<sup>34,53–55</sup>

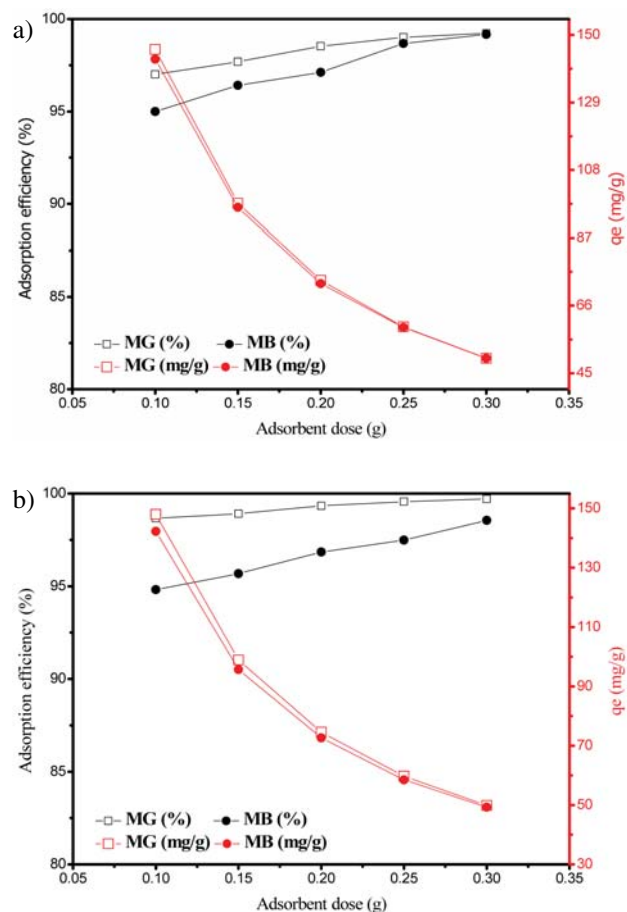


**Figure 8.** Effect of adsorbent dose on the adsorption of MB and MG dye on (a) HDP-clay (b) HDTMA-clay.

### 3. 3. Kinetic Study

The kinetic study is important to understanding the mechanism of the adsorption process. During the process of adsorption of dyes onto the organoclay, the adsorbate

molecules undergo various stages while moving from the bulk solution to the organoclay surface. Usually to understand the adsorption mechanism, pseudo first-order and pseudo second-order kinetics model were applied. The pseudo first-order model proposed by Lagergren is widely applied for the adsorption of an adsorbate from an aqueous solution. According to this model, the change in rate of the solute uptake with time is directly proportional to the difference in saturation concentration and the solute uptake with time.<sup>20,56</sup> The linearized integral form of the pseudo first-order model can be expressed as follows:

$$\log(q_e - q_t) = \log q_e - \frac{k_1}{2.303} t \quad (2)$$

Where  $q_e$  (mg/g) and  $q_t$  (mg/g) are the amounts of dyes adsorbed by organoclay at equilibrium and time  $t$  (min) respectively.  $k_1$  ( $\text{min}^{-1}$ ) is the equilibrium rate constant of pseudo first-order adsorption. The values of  $q_e$  and adsorption rate constant ( $k_1$ ) can be calculated from the intercept and the slope of the linear plot of  $\log(q_e - q_t)$  versus  $t$ , respectively. The plot should give a straight line with slope of  $-k_1/2.303$  and intercept  $\log q_e$  which allows calculation of adsorption rate constant  $k_1$  and equilibrium adsorption capacity  $q_e$  (cal).

The pseudo second-order proposed by Ho and McKay,<sup>57</sup> based on the assumption that “the rate limiting step are chemisorption involves forces by sharing or exchanging electrons between the adsorbent and the adsorbate”<sup>20,38,56</sup> and is given as:

$$\frac{dq_t}{dt} = k_2 (q_e - q_t)^2 \quad (3)$$

Integrating with the boundary conditions at  $t = 0$ ,  $q_t = 0$ , and  $t = t$ ,  $q_t = q_t$  and rearranging, we received.

$$\frac{t}{q_t} = \frac{1}{(k_2 q_e^2)} + \frac{t}{q_e}$$

Where  $k_2$  (g/mg min) is the rate constant of pseudo second-order adsorption. Ideally the plot of  $t/q_t$  versus  $t$  is a straight line with slope of  $1/q_e$  and intercept  $1/k_2 q_e^2$ . The values of  $k_2$  and  $q_e$  were calculated from the intercept and slope of the plot respectively. Figure 9, represents the plots of the pseudo-first-order and pseudo-second-order kinetic models of MG and MB onto the organoclays. The optimized condition used for the kinetic studies includes

the concentrations of organoclays as 0.1 grams and initial dye concentration of  $150 \text{ mg L}^{-1}$  at pH 7.0 at room temperature ( $25 \text{ }^\circ\text{C}$ ) with varying time. The calculated kinetic parameters of pseudo-first order and pseudo-second order are given in Table 1. The regression coefficients ( $R^2$ ) values of pseudo-first order kinetic model are better than those for the pseudo-second order for both types of organoclays. Moreover, the calculated values of equilibrium adsorption capacity are found close to the experimental adsorption capacity onto the organoclays also confirms further the feasibility of the pseudo-first order kinetic model.

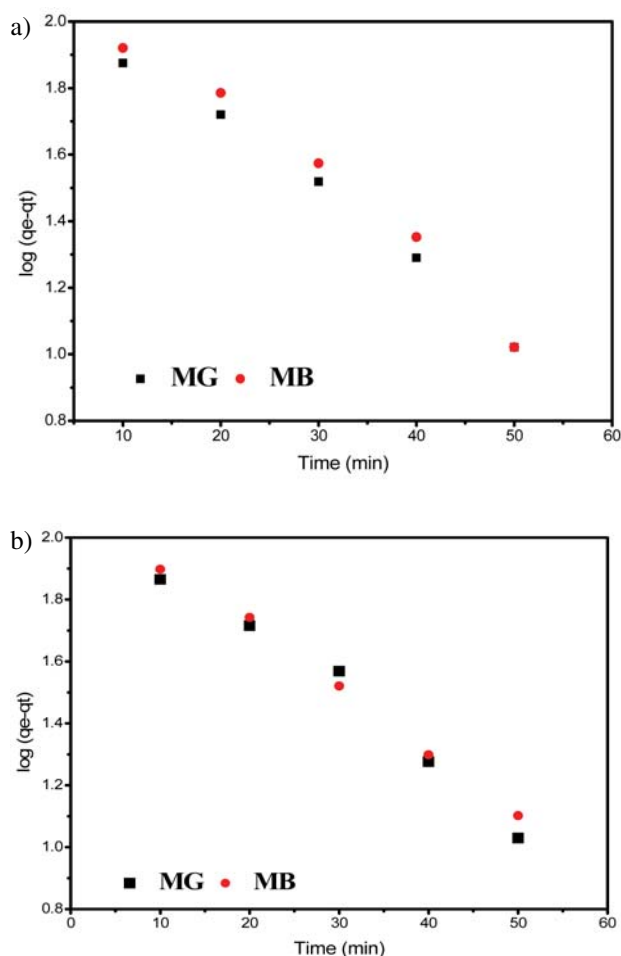


Figure 9. Pseudo-first-order-kinetic model for the adsorption of MB and MG dye on (a) HDP-clay (b) HDTMA-clay.

Table 1. The Pseudo-first and Pseudo-second order kinetic parameters for adsorption of MG and MB on organoclays.

Adsorbent	Dye	$q_{(\text{exp})}$ (mg/g)	Pseudo-first order				Pseudo-second order		
			$q_{e(\text{calc})}$ (g/mg)	$k_1$ ( $\text{min}^{-1}$ )	$R^2$	$q_{e(\text{calc})}$ (mg/g)	$k_2$ (mg/g)	$R^2$	
HDTMA-clay	MG	147.99	145.85	0.0532	0.9778	181.82	$3.3 \times 10^{-4}$	0.9848	
HDTMA-clay	MB	142.22	135.67	0.0444	0.9967	175.44	$2.8 \times 10^{-4}$	0.9847	
HDP-clay	MG	145.5	133	0.0493	0.9900	178.57	$3.31 \times 10^{-4}$	0.9843	
HDP-clay	MB	142.5	158.52	0.0514	0.9763	196.07	$2.0 \times 10^{-4}$	0.9856	

### 3. 4. Adsorption Isotherm Models

Different isotherm models can be used to analyse the equilibrium adsorption data.<sup>25,26,29</sup> In this work, the Langmuir and Freundlich isotherm models were used to showing the relationship between the amount of adsorbed MG and MB dyes and their concentration in solution at constant pH at room temperature. Langmuir isotherm model suggests that the adsorption of adsorbate molecules by the adsorbent materials takes place on a homogenous surface by monolayer without any interaction with adjacent adsorbed molecules.<sup>58</sup> The linear form of the Langmuir isotherm equation can be represented as follows:

$$\frac{C_e}{q_e} = \frac{C_e}{q_m} + \frac{1}{K_L q_m} \quad (4)$$

Where  $q_m$  (mg/g) represents the maximum adsorption capacity and  $K_L$  (L/mg) is Langmuir adsorption equilibrium constant related to the free energy of adsorption. The adsorption isotherm can be plotted by  $C_e/q_e$  vs  $C_e$ , best fit data should give a straight line, and shows the suitability of the model, where slope of the curve equals to  $1/q_m$  and intercepts  $1/K_L q_m$ .

Freundlich adsorption isotherm is applicable for a reaction where the multilayer formation occurs due to the heterogeneous adsorption reactions.<sup>59</sup> The linear form of

the Freundlich adsorption isotherm equation can be expressed as:

$$\ln q_e = \ln K_F + \frac{1}{n_F} \ln C_e \quad (5)$$

Where  $q_e$  (mg/g) represent the amount of adsorbate adsorbed per unit mass of the adsorbent at equilibrium,  $C_e$  (mg/L) is the equilibrium adsorbate concentration in solution,  $K_F$  (mg/g) is the Freundlich constants related to the adsorption capacity and  $1/n_F$  is the heterogeneity factor, the value of “ $n_F$ ” is large than 1 indicates the favourable adsorption. These values can be obtained from the linear plot of the  $\ln q_e$  vs  $\ln C_e$  where slope =  $1/n_F$  and intercept =  $\ln K_F$ .

The results in Table 2, shows that the experimental data fits well for both the isotherm models, however, the regression coefficient ( $R^2$ ) values of Langmuir isotherm for both of the dyes are better than that of the Freundlich isotherm, which indicates that adsorption of both dyes takes place as a monolayer on the surface of the modified clay. Further the experimental maximum adsorption capacity is well matched with the  $q_m$  calculated from the Langmuir isotherm model. Based on the Langmuir equation, a dimensionless separation factor,  $R_L$  an important parameter indicating the favourability of the adsorption can be calculated using equation given as follows.<sup>7,14,29,34</sup>

**Table 2.** The Langmuir and Freundlich adsorption isotherm parameters.

Adsorbent	Dye	Exp. $q_m$ (mg/g)	Langmuir			Freundlich			
			$q_m$ (mg/g)	$K_L$ (L/mg)	$R^2$	$R_L$	$n$	$K_F$ (mg/g)	$R^2$
HDTMA-clay	MG	285.5	294.12	0.22	0.9871	0.03	5.57	130.61	0.9786
HDTMA-clay	MB	270.13	303.03	0.10	0.9987	0.06	3.65	84.26	0.9825
HDP-clay	MG	279.4	294.12	0.145	0.9876	0.04	4.51	106.64	0.9732
HDP-clay	MB	265.2	294.12	0.158	0.9974	0.04	3.93	87.67	0.989

**Table 3.** Adsorption efficiency of different adsorbents for MB and MG.

Adsorbent	MG (mg/g)/Temp.	MB (mg/g)/Temp.	Reference
HDTMA-clay	285.71 (298K)	303.03 (298K)	This study
HDPy-clay	277.77 (298K)	285.71 (298K)	This study
Carbon nanotubes	11.73 (328K)	–	14
Algerian halloysite heat/acid treated	192.6 (298K)	–	60
Diatomite	23.64 (298K)	–	61
Montmorillonite clay	262.5	–	62
Activated carbon loaded with ZnO nanoparticles	322.58	–	63
Halloysite nanotubes	99.6	–	64
Clayey soil	78.57 (303K)	–	65
Chitosan coated bentonite	435	–	43
Fe <sub>3</sub> O <sub>4</sub> /activated montmorillonite nanocomposite	–	106.38 (293K)	66
kaolinite clay-water interface electrolyte enhanced adsorption	–	15.6	23
Chitosan/bentonite composite	–	142.86 (313K)	7
Montmorillonite clay modified with iron oxide	–	71.12 (333K)	67
Dodecyl sulfobetaine modified montmorillonite clay	–	254 (298K)	68
Acid/Al(OH) <sub>3</sub> modified clay	–	223.19 (303K)	52

Where  $K_L$  is the Langmuir constant and  $C_0$  is the highest initial dye concentration. The value of  $R_L$  indicates the type of the isotherm to be either favourable ( $0 < R_L < 1$ ), unfavourable ( $R_L > 1$ ), linear ( $R_L = 1$ ) or irreversible ( $R_L = 0$ ). The results in Table 2 further indicate that the  $R_L$  values lies between 0 and 1, which shows the favourable Langmuir adsorption process. Comparison of the maximum adsorption capacities and optimized temperature of the removal of MG and MB using proposed organoclays with that of the other similar adsorbent previously reported has been made and presented in Table 3. It shows that most of the recent studies for MG and MB removal possess less Langmuir maximum adsorption capacities comparatively than the low cost proposed organoclays.

## 4. Conclusions

The performance of hexadecyltrimethylammonium/Hexadecylpyridinium-intercalated montmorillonite clay for the removal of malachite green/methylene blue from aqueous solutions has been evaluated in this study. The surface and physical properties of clay and organoclay were evaluate using SEM, XRD, IR, thermal analysis and the results indicated the successful intercalation of these surfactants onto clay. Kinetic characteristic constants of sorption were determined using a pseudo-first/second order equation of Lagergren based solid capacity and pseudo-first order was found suitable. The experimental data were applied to the Langmuir and Freundlich isotherm equations. The results indicate that the experimental data fits well for both the isotherm models, however, the regression coefficient ( $R^2$ ) values of Langmuir isotherm for both dyes are better than that of the Freundlich isotherm, which indicates that adsorption of both dyes takes place as a monolayer on the surface of the modified clay. Further the experimental maximum adsorption capacity is well matched with the  $q_m$  calculated from the Langmuir isotherm model.

## 5. Acknowledgement

The authors are grateful to Higher Education Commission, Pakistan for providing financial assistance under NRPU project no. 6172.

## 6. References

1. A. Waseem, J. Arshad, F. Iqbal, A. Sajjad, Z. Mehmood and G. Murtaza, *Biomed Research International* **2014**, vol. 2014, 29 pages. <http://dx.doi.org/10.1155/2014/813206>.
2. N. Faheem, A. Sajjad, Z. Mehmood, F. Iqbal, Q. Mahmood, S. Munsif and A. Waseem, *Fresenius Environ. Bull.* **2015**, 24, 4555–4566.

3. Li Zhou, Chao Gao and W. Xu, *ACS Appl. Mater. Interfaces* **2010**, 2, 1483–1491. <https://doi.org/10.1021/am100114f>
4. R. S. Blackburn, *Environ. Sci. Technol.* **2004**, 38, 4905–4909. <https://doi.org/10.1021/es049972n>
5. H. I. Chieng, L. B. Lim and N. Priyantha, *Environ. Technol.* **2015**, 36, 86–97. <https://doi.org/10.1080/09593330.2014.938124>
6. T. K. Sen, S. Afroze and H. M. Ang, *Water, Air, Soil Pollut.* **2011**, 218, 499–515. <https://doi.org/10.1007/s11270-010-0663-y>
7. Y. Bulut and H. Karaer, *J. Dispersion Sci. Technol.* **2014**, 36, 61–67. <https://doi.org/10.1080/01932691.2014.888004>
8. V. K. Gupta and Suhas, *J Environ Manage* **2009**, 90, 2313–42. <https://doi.org/10.1016/j.jenvman.2008.11.017>
9. K. Hunger, P. Gregory, P. Miederer, H. Berneth, C. Heid and W. Mennicke: *Industrial Dyes*, Wiley-VCH Verlag GmbH & Co. KGaA, **2004**, pp. 13–112.
10. K. Hunger, R. Hamprecht, P. Miederer, C. Heid, A. Engel, K. Kunde, W. Mennicke and J. Griffiths: *Industrial Dyes*, Wiley-VCH Verlag GmbH & Co. KGaA, **2004**, pp. 113–338.
11. Sandra J. Culp and F. A. Beland, *International Journal of Toxicology* **1996**, 15, 219–238. <https://doi.org/10.3109/10915819609008715>
12. S. Afroze, T. K. Sen, M. Ang and H. Nishioka, *Desalin Water Treat* **2015**, 57, 5858–5878. <https://doi.org/10.1080/19443994.2015.1004115>
13. D. J. Alderman and R. S. Clifton-Hadley, *J. Fish Dis.* **1993**, 16, 297–311. <https://doi.org/10.1111/j.1365-2761.1993.tb00864.x>
14. M. Rajabi, B. Mirza, K. Mahanpoor, M. Mirjalili, F. Najafi, O. Moradi, H. Sadegh, R. Shahryari-ghoshekandi, M. Asif, I. Tyagi, S. Agarwal and V. K. Gupta, *J. Ind. Eng. Chem.* **2016**, 34, 130–138. <https://doi.org/10.1016/j.jiec.2015.11.001>
15. B. Mu and A. Wang, *J. Environ. Chem. Eng.* **2016**, 4, 1274–1294. <https://doi.org/10.1016/j.jece.2016.01.036>
16. P. Wu, T. Wu, W. He, L. Sun, Y. Li and D. Sun, *Colloids Surf., A* **2013**, 436, 726–731. <https://doi.org/10.1016/j.colsurfa.2013.08.015>
17. S. Elemen, E. P. Akçakoca Kumbasar and S. Yapar, *Dyes Pigm.* **2012**, 95, 102–111. <https://doi.org/10.1016/j.dyepig.2012.03.001>
18. M. Nafees, A. Waseem and A. R. Khan, *The Scientific World Journal*, **2013**, vol. 2013, 6 pages. <http://dx.doi.org/10.1155/2013/681769>
19. B. Schampera, R. Solc, S. K. Woche, R. Mikutta, S. Dultz, G. Guggenberger and D. Tunega, *Clay Miner.* **2015**, 50, 353–367. <https://doi.org/10.1180/claymin.2015.050.3.08>
20. Y. Park, G. A. Ayoko, E. Horvath, R. Kurdi, J. Kristof and R. L. Frost, *J. Colloid Interface Sci.* **2013**, 393, 319–34. <https://doi.org/10.1016/j.jcis.2012.10.067>
21. M. Nafees and A. Waseem, *CLEAN* **2014**, 42, 1500–1508.
22. M. D. Mullassery, N. B. Fernandez and T. S. Anirudhan, *Desalin Water Treat* **2015**, 56, 1929–1939. <https://doi.org/10.1080/19443994.2014.958110>
23. K. Mukherjee, A. Kedia, K. Jagajjanani Rao, S. Dhir and S.



- Paria, *RSC Advances* **2015**, *5*, 30654–30659.  
<https://doi.org/10.1039/C5RA03534A>
24. B. Likozar, D. Senica and A. Pavko, *AIChE J.* **2012**, *58*, 99–106. <https://doi.org/10.1002/aic.12559>
25. B. Likozar, D. Senica and A. Pavko, *Brazilian Journal of Chemical Engineering* **2012**, *29*, 635–652.  
<https://doi.org/10.1590/S0104-66322012000300020>
26. B. Likozar, D. Senica and A. Pavko, *Ind. Eng. Chem. Res.* **2013**, *52*, 9247–9258.  
<https://doi.org/10.1021/ie400832p>
27. M. T. Yagub, T. K. Sen, S. Afroz and H. M. Ang, *Adv. Colloid Interface Sci.* **2014**, *209*, 172–84.  
<https://doi.org/10.1016/j.cis.2014.04.002>
28. M. T. Yagub, T. K. Sen and H. Ang, *Water, Air, Soil Pollut.* **2012**, *223*, 5267–5282.  
<https://doi.org/10.1007/s11270-012-1277-3>
29. A. S. Bhatt, P. L. Sakaria, M. Vasudevan, R. R. Pawar, N. Sudheesh, H. C. Bajaj and H. M. Mody, *RSC Advances* **2012**, *2*, 8663. <https://doi.org/10.1039/c2ra20347b>
30. M. Zabka, M. Minceva and A. E. Rodrigues, *Chemical Engineering and Processing: Process Intensification* **2006**, *45*, 150–160. <https://doi.org/10.1016/j.cep.2005.07.002>
31. D. Kavitha and C. Namasivayam, *Bioresour. Technol.* **2007**, *98*, 14–21. <https://doi.org/10.1016/j.biortech.2005.12.008>
32. William H. Hendershot and M. Duquette, *Soil Sci. Soc. Am. J.* **1986**, *50*, 605–608.  
<https://doi.org/10.2136/sssaj1986.03615995005000030013x>
33. H. He, R. L. Frost, T. Bostrom, P. Yuan, L. Duong, D. Yang, Y. Xi and J. T. Kloprogge, *Appl. Clay Sci.* **2006**, *31*, 262–271. <https://doi.org/10.1016/j.clay.2005.10.011>
34. E. Orucoglu and S. Haciyakupoglu, *Journal of Environmental Management* **2015**, *160*, 30–38.  
<https://doi.org/10.1016/j.jenvman.2015.06.005>
35. M. Önal and Y. Sarikaya, *Colloids Surf., A* **2007**, *296*, 216–221. <https://doi.org/10.1016/j.colsurfa.2006.09.046>
36. R. Zhu, Q. Chen, H. Liu, F. Ge, L. Zhu, J. Zhu and H. He, *Appl. Clay Sci.* **2014**, *88–89*, 33–38.  
<https://doi.org/10.1016/j.clay.2013.12.010>
37. M. Kiranşan, R. D. C. Soltani, A. Hassani, S. Karaca and A. Khataee, *J. Taiwan Inst. Chem. Eng.* **2014**, *45*, 2565–2577.
38. L. Wang and A. Wang, *J Hazard Mater* **2008**, *160*, 173–180.  
<https://doi.org/10.1016/j.jhazmat.2008.02.104>
39. H. Pálková, J. Madejová and P. Komadel, *Open Chemistry* **2009**, *7*.
40. Z. Qin, P. Yuan, J. Zhu, H. He, D. Liu and S. Yang, *Appl. Clay Sci.* **2010**, *50*, 546–553.  
<https://doi.org/10.1016/j.clay.2010.10.011>
41. Z. Sun, C. Li and D. Wu, *J. Chem. Technol. Biotechnol.* **2010**, *85*, 845–850. <https://doi.org/10.1002/jctb.2377>
42. P. Baskaralingam, M. Pulikesi, D. Elango, V. Ramamurthi and S. Sivanesan, *J Hazard Mater* **2006**, *128*, 138–144.  
<https://doi.org/10.1016/j.jhazmat.2005.07.049>
43. W. Ngah, W. Saime, N. F. M. Ariff, A. Hashim and M. A. K. M. Hanafiah, *CLEAN* **2010**, *38*, 394–400.
44. C. Leodopoulos, D. Doulia and K. Gimouhopoulos, *Separation & Purification Reviews* **2015**, *44*, 74–107.  
<https://doi.org/10.1080/15422119.2013.823622>
45. B. Nandi, A. Goswami and M. Purkait, *J Hazard Mater* **2009**, *161*, 387–395.  
<https://doi.org/10.1016/j.jhazmat.2008.03.110>
46. V. S. Mane and P. V. Babu, *Desalination* **2011**, *273*, 321–329. <https://doi.org/10.1016/j.desal.2011.01.049>
47. A. Gürses, Ç. Doğar, M. Yalçın, M. Açıkyıldız, R. Bayrak and S. Karaca, *J Hazard Mater* **2006**, *131*, 217–228.  
<https://doi.org/10.1016/j.jhazmat.2005.09.036>
48. B. Karagozoglu, M. Tasdemir, E. Demirbas and M. Kobya, *J Hazard Mater* **2007**, *147*, 297–306.  
<https://doi.org/10.1016/j.jhazmat.2007.01.003>
49. M. Auta and B. Hameed, *Chem. Eng. J. (Lausanne)* **2012**, *198*, 219–227. <https://doi.org/10.1016/j.cej.2012.05.075>
50. M. Doğan, M. Alkan, Ö. Demirbaş, Y. Özdemir and C. Özmetin, *Chem. Eng. J. (Lausanne)* **2006**, *124*, 89–101.  
<https://doi.org/10.1016/j.cej.2006.08.016>
51. Y. Safa and H. N. Bhatti, *Desalination* **2011**, *272*, 313–322.  
<https://doi.org/10.1016/j.desal.2011.01.040>
52. M. Auta and B. Hameed, *J. Ind. Eng. Chem.* **2013**, *19*, 1153–1161. <https://doi.org/10.1016/j.jiec.2012.12.012>
53. M. S. U. Rehman, M. Munir, M. Ashfaq, N. Rashid, M. F. Nazar, M. Danish and J.-I. Han, *Chem. Eng. J. (Lausanne)* **2013**, *228*, 54–62.  
<https://doi.org/10.1016/j.cej.2013.04.094>
54. W.-T. Tsai, H.-C. Hsu, T.-Y. Su, K.-Y. Lin, C.-M. Lin and T.-H. Dai, *J Hazard Mater* **2007**, *147*, 1056–1062.  
<https://doi.org/10.1016/j.jhazmat.2007.01.141>
55. V. Gupta, A. Mittal and V. Gajbe, *J. Colloid Interface Sci.* **2005**, *284*, 89–98. <https://doi.org/10.1016/j.jcis.2004.09.055>
56. B. Nandi, A. Goswami and M. Purkait, *Appl. Clay Sci.* **2009**, *42*, 583–590. <https://doi.org/10.1016/j.clay.2008.03.015>
57. Y.-S. Ho and G. McKay, *Process Biochem. (Amsterdam, Neth.)* **1999**, *34*, 451–465.
58. I. Langmuir, *J. Am. Chem. Soc.* **1918**, *40*, 1361–1403.  
<https://doi.org/10.1021/ja02242a004>
59. U. Freundlich, *Z. Phys. Chem.* **1906**, *57*, 385–470.
60. F. Bessaha, K. Marouf-Khelifa, I. Batonneau-Gener and A. Khelifa, *Desalin Water Treat* **2016**, *57*, 14609–14621.  
<https://doi.org/10.1080/19443994.2015.1063090>
61. L. Tian, J. Zhang, H. Shi, N. Li and Q. Ping, *J. Dispersion Sci. Technol.* **2016**, *37*, 1059–1066.  
<https://doi.org/10.1080/01932691.2015.1080610>
62. B. A. Fil, *Part. Sci. Technol.* **2016**, *34*, 118–126.  
<https://doi.org/10.1080/02726351.2015.1052122>
63. M. Ghaedi, A. Ansari, M. H. Habibi and A. R. Asghari, *J. Ind. Eng. Chem.* **2014**, *20*, 17–28.  
<https://doi.org/10.1016/j.jiec.2013.04.031>
64. G. Kiani, M. Dostali, A. Rostami and A. R. Khataee, *Appl. Clay Sci.* **2011**, *54*, 34–39.
65. P. Saha, S. Chowdhury, S. Gupta and I. Kumar, *Chem. Eng. J. (Lausanne)* **2010**, *165*, 874–882.  
<https://doi.org/10.1016/j.cej.2010.10.048>
66. J. Chang, J. Ma, Q. Ma, D. Zhang, N. Qiao, M. Hu and H. Ma, *Appl. Clay Sci.* **2016**, *119, Part 1*, 132–140.  
<https://doi.org/10.1016/j.clay.2015.06.038>

67. L. Cottet, C. Almeida, N. Naidek, M. Viante, M. Lopes and N. Debacher, *Appl. Clay Sci.* **2014**, *95*, 25–31.  
<https://doi.org/10.1016/j.clay.2014.03.023>

68. H. Fan, L. Zhou, X. Jiang, Q. Huang and W. Lang, *Appl. Clay Sci.* **2014**, *95*, 150–158.  
<https://doi.org/10.1016/j.clay.2014.04.001>

## Povzetek

Glavni namen raziskav je študij adsorpcije barvil malahitno zeleno in metilensko modro na dve vrsti naravne glin, obdelane s površinsko aktivnimi snovmi. Rezultati SEM, XRD, IR in termične analize potrjujejo vezavo organskega dela na glino. Rezultati kažejo najboljše ujemanje s kinetiko psevdoprvega reda na organo-glino za obe barvili. Ravnotežji za obe vrsti barvil lahko opišemo z Langmuirjevo izotermo za obe vrsti modificirane glin. Vrednosti parametrov Langmuirjeve in Freundlichove izoterme kažejo na ugodno adsorpcijo. Maksimalna adsorpcijska kapaciteta  $q_m$  po Langmuirjevem modelu pri 25 °C je 294–303 mg/g in se dobro ujema z eksperimentalnimi podatki.

Scientific paper

# First Direct Isolation of Stable $\alpha$ -Form Crystals of Mirabegron, a Selective $\beta_3$ -Adrenoceptor Agonist

Dattatray G. Deshmukh,<sup>1,2</sup> Mukund N. Bangal,<sup>1</sup> Anil C. Mali,<sup>1</sup>  
Vijay J. Medhane<sup>2</sup> and Vijayavithal T. Mathad<sup>1,\*</sup>

<sup>1</sup> Department of Process Research and Development, Megafine Pharma (P) Ltd., 201, Lakhmapur, Dindori, Nashik-422 202, Maharashtra, India.

<sup>2</sup> Organic Chemistry Research Center, Department of Chemistry, K. T. H. M College, Nashik-422 002, Maharashtra, India.

\* Corresponding author: E-mail: vt.mathad@megafine.in, drvtmathad@yahoo.co.in

#Megafine Publication Number: MF/026/2016

Received: 17-02-2017

## Abstract

An efficient and scalable method for the direct isolation of stable  $\alpha$ -form crystals of Mirabegron (**1**) is developed. The developed method negates transformation of metastable  $\beta$ -form crystals into  $\alpha$ -form crystals thereby overcoming the limitations of reported methods and avoids additional processing steps during its manufacture. The developed method directly provides stable  $\alpha$ -form crystals of Mirabegron (**1**) with yield of around 84% and purity of >99.77% by HPLC in a single step.

**Keywords:**  $\beta_3$ -adrenoceptor agonist, Mirabegron, polymorphism, polymorphic transformation.

## 1. Introduction

Crystallization operation is often critical in pharmaceutical industries as it solely determines product properties such as the polymorphism, crystal size distribution, and crystal habit.<sup>1</sup> Change in polymorphic form may alter product characteristics such as dissolution, hardness, color, optical properties, melting point or chemical reactivity. As regulatory perspective, developing the process which provides exclusively pure polymorph of a drug substance that should be stable enough to maintain the polymorph integrity during formulation of the drug product and storage throughout its life cycle is very necessary. The driving force in crystal formation is super saturation and when a super saturation of crystallizing compound is created by chemical reaction, the operation is known as reactive crystallization. In reactive crystallization, reactions can be very fast compared to the mass transfer rates and growth rates to the crystals thus reactive crystallizations can lead to the exclusive formation of the metastable polymorph of a system.<sup>2</sup> This article is aimed to provide a case study wherein systematic crystallization of stable  $\alpha$ -form

crystals of Mirabegron (**1**) is achieved by circumventing the following limitations of the known processes; (a) reactive crystallization of metastable  $\beta$ -form crystals of **1** and (b) transformation of metastable  $\beta$ -form crystals into  $\alpha$ -form crystals using a seed.

## 2. Background

Mirabegron (**1**), chemically known as 2-(2-amino-1,3-thiazol-4-yl)-N-[4-(2-[(2R)-2-hydroxy-2-phenylethyl]amino)ethyl]phenyl]acetamide is a selective agonist for the human beta 3-adrenoceptor<sup>3</sup> ( $\beta_3$ -AR) approved for the symptomatic treatment of urinary urgency, increased micturition frequency and/or urgency incontinence in patients with overactive bladder (OAB) syndrome.<sup>4-5</sup> Mirabegron has distinct and novel mechanism of action compared to antimuscarinics<sup>6</sup> as it improves the storage capacity of the bladder without inhibiting bladder voiding thereby prolonging the time between trips to the toilet for the patient.<sup>5</sup> Mirabegron (**1**), developed by Astellas Pharma was approved by the USFDA in 2012 and EMA in 2013

and is currently available in the market under the trade name Myrbetriq® in the US and Betmiga® in Europe.<sup>8</sup>

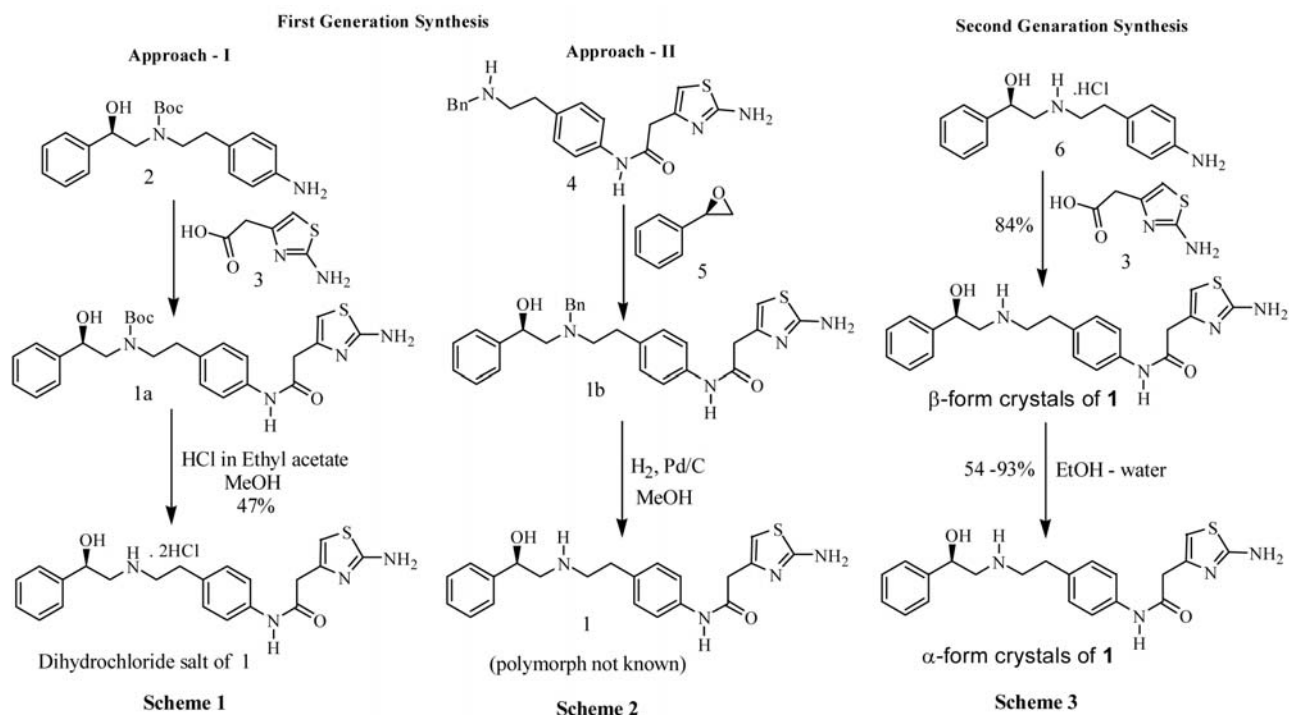
According to the literature reports Mirabegron free base exhibits polymorphism and is known to possess two crystalline forms, namely  $\alpha$ -form and  $\beta$ -form crystals. The  $\beta$ -form crystals of mirabegron are hygroscopic and tend to gain water content up to 3% under the relative humidity of about 20%, whereas  $\alpha$ -form crystals did not show any increase in the water content over the entire range of relative humidity from 5% to 95% concluding that  $\alpha$ -crystal form is stable and suitable for use as a medicine.<sup>9</sup> According to EMA assessment report, Betmiga formulation is known to contain  $\alpha$ -crystalline form of mirabegron free base.<sup>5</sup>

The first generation syntheses<sup>10</sup> disclose two synthetic approaches for **1** (Schemes 1 and 2). The first approach (Scheme 1) involves condensation of Boc-protected aniline **2** with thiazole acid **3** to obtain Boc-protected intermediate **1a**. The Boc group was de-protected in **1a** using HCl to furnish di-hydrochloride salt of **1** with an overall yield of about 26% over two stages. However, this report does not exemplify the isolation of free base of mirabegron (**1**).

The second approach (Scheme 2) mentioned in the report is shuffling of synthetic steps of Scheme 1. In the second approach, benzyl (Bn) protected secondary amine **4** was reacted with (*R*)-styrene oxide (**5**) to provide Bn-protected intermediate **1b**. However, detailed synthetic procedure is not provided in the report for this approach. Neither of these approaches have provided procedure for preparing mirabegron free base (**1**) which has been used

to formulate drug product and clarify on polymorphic forms associated with free base.

Second generation synthesis<sup>9</sup> (Scheme 3) reported for **1** involves coupling of **6** with **3** followed by addition of aqueous sodium hydroxide solution to provide  $\beta$ -crystal form directly from the reaction mass through reactive crystallization.  $\beta$ -Form crystals were then re-crystallized in subsequent stage in aqueous ethanol using seeds of  $\alpha$ -crystals to provide  $\alpha$ -crystal form with 74–78% yield over two stages. Though second generation synthesis is improved over first generation but has a limitation to perform additional manufacturing step of converting  $\beta$ -form crystals into  $\alpha$ -form crystals using seeds of  $\alpha$ -crystals. This additional step to achieve  $\alpha$ -form decreases the efficiency in terms of yield loss and productivity. However, reported transformation of  $\beta$ -form crystals to  $\alpha$ -form crystals lack consistency in providing pure  $\alpha$ -form crystals at our end. Several other known methods for the preparation of  $\alpha$ -form involve additional crystallization of the isolated material using various solvent systems.<sup>11</sup> Most importantly the desired crystals achieved via polymorphic transformation generally pose increased risk of polymorph contamination (polymorphic purity) during the manufacturing process as well as during its stability studies. Thus, it may be difficult to maintain the integrity of the polymorphs which are achieved via transformation of metastable form / pseudo form. This triggered us to aim for the process which could directly produce  $\alpha$ -form crystals selectively and directly through a proper solvent-mediated crystallization process. The details of process optimization work carried out in providing a single stage met-



Schemes 1–3. Reported syntheses of mirabegron (**1**).

hod for direct isolation of  $\alpha$ -form crystals which is suitable for industrial scale are discussed herein.

### 3. Results and Discussion

Our initial approach to achieve  $\alpha$ -form crystals obviating the polymorphic transformations was to replace the reported reaction medium (water) with a suitable organic solvent. The purpose of replacing the water with organic solvent before neutralizing the reaction mass was to avoid the reactive crystallization and to retain the product in solution phase. Among the several solvents explored for the reaction, methanol showed moderately good conversion of **6** to **1** in solution state. The reaction mixture was then neutralized with aqueous solution of sodium hydroxide as base and obtained clear solution was concentrated to provide crude residue, which was dissolved in organic solvent, filtered to remove the insoluble inorganic material and crystallization of **1** was explored using various solvents and anti-solvents, but the approach was unsuccessful as it provided impure and hygroscopic solids.

In our next approach, water was retained as a reaction solvent and water immiscible organic solvent was added to the reaction mass prior to basification to extract the product into the organic phase to arrest reactive crystallization of  $\beta$ -form. The organic phase containing the product was then separated and crystallization was attempted using anti-solvent(s) preferentially to achieve pure  $\alpha$ -form crystals of **1**. Among several solvents explored for extraction, ethyl acetate as a solvent and *n*-heptane, toluene, MIBK, DIPE as anti-solvents exclusively provided pure  $\alpha$ -crystalline form. However, this combination of solvent and anti-solvents failed to provide chemical purity as per ICH<sup>12</sup> requirement. Additionally, poor solubility of **1** in ethyl acetate necessitated huge volume of ethyl acetate (around 25 volumes/g of **6**) for complete extraction of **1** even at the elevated temperature. The yields obtained with this approach were also not satisfactory. Attempts to achieve yield and ICH quality material by judicious choice of anti-solvents were not successful. The results of the various combinations of solvent(s) and anti-solvent explored in this approach are provided in Table 1.

**Table 1.** Screening of solvents and anti-solvents for isolation of  $\alpha$ -form crystals of **1**.

Entry	Solvent <sup>1</sup> (vol <sup>#</sup> )	Co-solvent <sup>2</sup> (vol <sup>#</sup> )	Anti-solvent (vol <sup>#</sup> )	Anti-solvent addition temp(°C)	Yield (%)	Purity by HPLC (area %)				Crystal form
						<b>1</b>	<b>6</b>	<b>3</b>	SMI*	
1	2-MeTHF (30)	–	<i>n</i> -heptane (80)	25–30	21.6	99.37	ND	0.01	0.13	$\alpha$ + $\beta$
2	DCM (20)	–	<i>n</i> -heptane (10)	25–30	59.7	97.63	0.05	0.04	1.02	$\alpha$
3	EA (25)	–	<i>n</i> -heptane (20)	55–60	78.3	97.42	0.16	ND	1.02	$\alpha$
4	EA (25)	–	PhMe (20)	60–65	60.1	99.61	0.06	ND	0.07	$\alpha$
5	EA (25)	EtOH (5)	<i>n</i> -heptane (15)	70–75	77.4	99.32	0.17	ND	0.17	$\alpha$
6	EA (25)	IPA (10)	<i>n</i> -heptane (25)	55–60	71.1	99.40	0.07	ND	0.16	$\alpha$
7	EA (25)	MeCN (5)	<i>n</i> -heptane (20)	55–60	53.5	99.65	0.06	ND	0.04	$\alpha$
8	EA (25)	Me <sub>2</sub> CO (10)	<i>n</i> -heptane (30)	45–50	70.9	99.75	0.04	ND	0.10	$\alpha$
9	EA (25)	Me <sub>2</sub> CO (5)	PhMe (30)	45–50	68.3	99.56	ND	ND	0.17	$\alpha$
10	EA (25)	Me <sub>2</sub> CO (5)	DIPE (30)	45–50	70.2	99.58	ND	ND	0.18	$\alpha$
11	EA (25)	Me <sub>2</sub> CO (5)	MIBK (30)	45–50	46.4	99.69	ND	ND	0.11	$\alpha$

2-MeTHF = 2-methyltetrahydrofuran, DCM = dichloromethane, EA = ethyl acetate, EtOH = ethanol, IPA = isopropyl alcohol, MeCN = acetonitrile, Me<sub>2</sub>CO = acetone, PhMe = toluene, DIPE = diisopropyl ether, MIBK = methyl isobutyl ketone; <sup>#</sup>volumes of solvent and anti-solvent are with respect to quantity of **6**; solvent<sup>1</sup>: solvent used for extraction; co-solvent<sup>2</sup>: solvent added after extraction of product to enhance the HPLC purity of **1**; \*SMI: single maximum impurity; isolation of **1** in entry 1 to 11 is carried out by filtration at 25–30 °C.

**Table 2.** Optimization results of anti-solvents with *n*-butanol with respect to their volumes, impurity profile and yields of  $\alpha$ -form crystals.

Entry	Solvent (vol <sup>#</sup> )	Anti-solvent (vol <sup>#</sup> )	Anti-solvent addition temp (°C)	Purity by HPLC (area %)					<b>9</b> (ppm)	<b>10</b> (%)	Yield (%)	Crystal form
				<b>1</b>	<b>6</b>	<b>7</b>	<b>8</b>	SMUI				
1	<i>n</i> -butanol (10)	<i>n</i> -heptane (20)	75–80	96.87	0.13	0.27	ND	1.53	NA	NA	69.7	$\alpha$
2	<i>n</i> -butanol (12)	toluene (12)	65–70	99.79	0.02	0.05	ND	0.06	NA	0.01	71.9	$\alpha$
3	<i>n</i> -butanol (6)	toluene (14)	65–70	99.77	0.02	0.05	ND	0.07	NA	0.01	84.9	$\alpha$
4	<i>n</i> -butanol (6)	toluene (14)	65–70	99.78	0.01	0.07	ND	0.07	NA	0.04	84.6	$\alpha$
5	<i>n</i> -butanol (6)	toluene (14)	65–70	99.77	0.01	0.10	ND	0.04	ND	ND	81.1	$\alpha$
6	<i>n</i> -butanol (6)	toluene (14)	65–70	99.86	0.02	0.03	ND	0.02	16	ND	83.9	$\alpha$

Note: Entries 3 to 6 are carried out under the same process conditions; ND: Not detected; NA: Not analyzed; <sup>#</sup>volumes of solvent and anti-solvent are with respect to quantity of **6**; Isolation of  $\alpha$ -form crystals of **1** in entry 1 to 6 is carried out by filtration at 25–30 °C; SMUI: single maximum unknown impurity.

To overcome the issues associated with ethyl acetate, extraction of **1** was attempted with an amphiphilic solvent that was polar enough to solubilize the molecule but had enough hydrophobicity to have very limited miscibility with water. *n*-Butanol has all the attributes that we were looking in a solvent to be used for extraction of **1**. The exploratory reactions using *n*-butanol (Table 2; entries 1 and 2) furnished **1** with comparable yields and purity to those obtained with ethyl acetate. More importantly, only 10–12 volumes of *n*-butanol were sufficient to extract as opposed to 25 volumes of ethyl acetate. In addition to this, the extraction of **1** could be carried out at room temperature. This made *n*-butanol the perfect choice since it hit the ‘trifecta’ for all that was desired in the solvent of choice. Among the two preferred anti solvents (*n*-heptane and toluene), toluene furnished extremely promising results with *n*-butanol with respect to chemical purity and yield as shown in Table 2.

Further, to improve the yield of **1**, around half of the volume of *n*-butanol used for the extraction was concentrated *in vacuo* below 70 °C before the toluene was added as anti-solvent. The mixture was gradually cooled to 25–30 °C, precipitated solid was filtered and dried under vacuum at 55–60 °C to get **1** with 84% yield and 99.86% purity by HPLC. Around 10% yield was increased without compromising on stringent quality requirements with this

modification. The trend data of yield, purity and polymorphic form for kilogram-scale batches is provided in Table 2 (entries 5 and 6).

The schematic representation of single step process for achieving the  $\alpha$ -form crystals is provided in Scheme 4 and structure of impurities controlled during the crystallization process are provided in Figure 1.

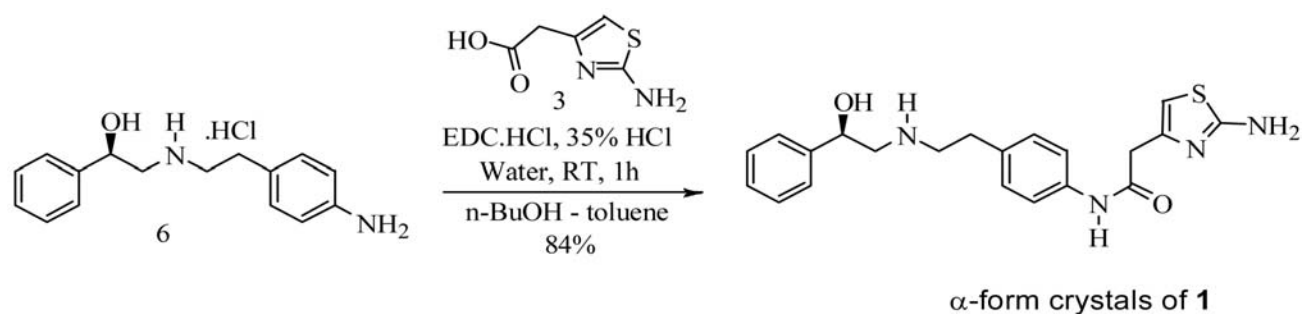
## 4. Conclusion

In conclusion, an efficient and robust method for direct isolation of the  $\alpha$ -form crystals of mirabegron (**1**) has been developed using *n*-butanol mediated work-up. The developed process provided  $\alpha$ -form crystals obviating the subsequent recrystallization step necessitated by earlier methods with an overall yield of around 84% and purity of around 99.77% by HPLC.

## 5. Experimental Section

### 5.1 General

All reagents, solvents, and processing aids are commercial products and were used as received. For reactions



**Scheme 4.** Direct isolation of  $\alpha$ - form crystals of Mirabegron (**1**).

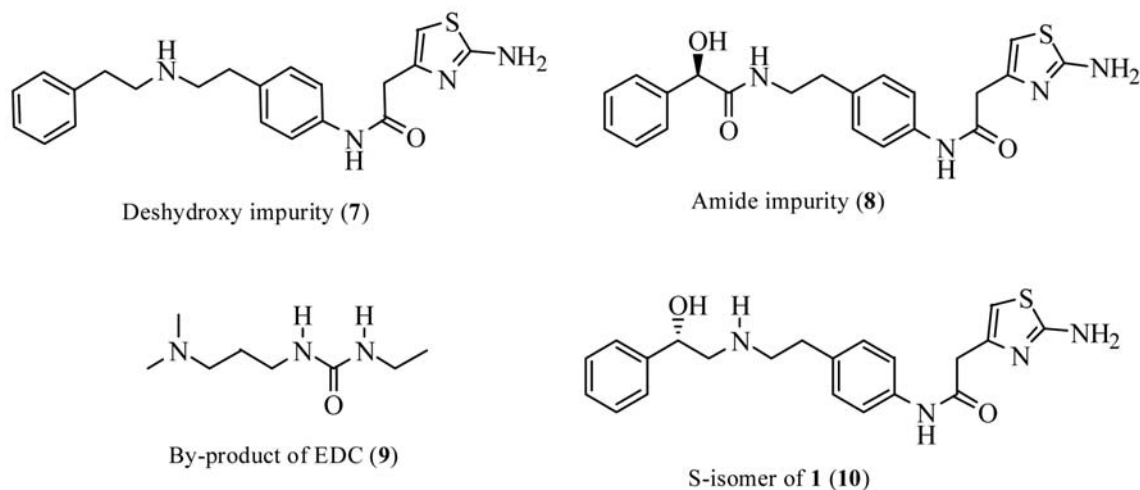


**Figure 1.** Process related impurities.

run of pilot scale, glass line reactors having variable rate agitation, with  $-10$  to  $150$  °C jacket temperature range were used for the reaction.  $^1\text{H}$  NMR spectra was recorded in DMSO- $d_6$  using Varian Gemini 400 MHz FT NMR spectrometer; the chemical shifts are reported in  $\delta$  ppm relative to TMS. ESI mass spectra were performed on the Shimadzu LCMS-2020 spectrometer. Related substance purity was monitored by high performance liquid chromatography (HPLC) on Agilent Technologies 1200 series. The gas chromatography on Agilent Technologies 7683B with head space was used for analyzing the residual solvents.

## 5. 2. HPLC Method for Calculating the Chemical, Assay and Chiral Purity

Related substances, assay and chiral purity of Mirabegron (**1**) were estimated by a gradient HPLC analysis method developed at Megafine.

- (a) Related substances and assay of Mirabegron (**1**) were estimated by using Zorbax SB-C8, ( $150 \times 4.6$  mm ID),  $3.5\mu$  column; mobile phase-A comprising a mixture of phosphate buffer (3.4 g potassium dihydrogenorthophosphate, in 1000 mL of HPLC grade water sonicate to dissolve, adjust the pH 6.8 with triethylamine and filter through  $0.45\mu$  nylon filter and degas. Mobile phase-B comprising a mixture of acetonitrile/methanol/water in the ratio 45:45:10 (v/v/v); gradient elution: time (min)/A (v/v): B (v/v),  $T_{0.0}/85:15$ ,  $T_{8.0}/85:15$ ,  $T_{35.0}/70:30$ ,  $T_{45.0}/70:30$ ,  $T_{48.0}/85:15$ ,  $T_{55.0}/85:15$ ; flow rate 1.0 mL/min column temperature  $35$  °C, wavelength 245 nm. The observed retention time of Mirabegron under these chromatographic conditions is about 17.5 min.
- (b) Chiral purity was estimated using Chiralpak IA ( $250 \times 4.6$  mm ID),  $5\mu$  column; mobile phase comprising a mixture of *n*-hexane, 2-propanol, methanol, THF and ethanolamine in the ratio of 183:67:67:17:1 (v/v/v/v/v) respectively; flow rate 1.0 mL/min.; column temperature  $25$  °C; wavelength 245 nm. The observed retention time of (*S*)-isomer is about 14.4 min and (*R*)-isomer (**1**) is about 16.8 min.
- (c) Samples generated as described in the solid form were typically analyzed by X-ray powder diffractogram (XRPD). XRPD was conducted on a Bruker D8 advance X-ray powder diffractometer using Cu  $K\alpha$  radiation at 1.54. The instrument was equipped with a fine focus X-ray tube. The voltage and amperage of X-ray generator were set at 40 kV and 80 mA, respectively. The divergence slices were set at  $0.3^\circ$ . The diffracted radiation was detected by a Lynx Eye detector. Typically, a theta-two theta continuous scan at  $4.95^\circ/\text{min}$  ( $0.4\text{ sec}/0.033^\circ$  step) from  $2^\circ 2\theta$  to  $50^\circ 2\theta$  was used. A corundum probe standard was used to check the peak position. In general, positions of XRPD peaks are expected to individually vary on a measurement-by-measurement basis by about  $\pm 0.2^\circ 2\theta$ .

## 5. 3 Scale-up procedure for the synthesis of 2-(2-amino-1,3-thiazol-4-yl)-N-[4-(2-[(2*R*)-2-hydroxy-2-phenylethyl]amino}ethyl)phenyl]acetamide (**1**)

Water (17.25 L), aniline **6** (1.15 kg, 3.93 mol) and acid **3** (0.63 kg, 4.01 mol) was added to the reactor. To the reaction mixture 37% HCl (0.409 kg, 3.93 mol) was added at  $25$ – $30$  °C and stirred for 10–15 min. EDCI (0.828 kg, 4.32 mol) was added to the reaction mixture at  $25$ – $30$ °C and stirred for 2 h, completion of the reaction was monitored by HPLC. Upon completion of the reaction, *n*-butanol (11.5 L) and 20% ammonium hydroxide solution (0.92 L) was added to reaction mass and stirred for  $25$ – $30$  min. Organic layer was preserved and aqueous layer was extracted with *n*-butanol (2.3 L). Combined organic layer was washed with 5% ammonium hydroxide solution ( $2 \times 11.5$  L) to eliminate acid **3**. Organic layer was then washed with 0.3% ( $4 \times 17.2$  L) brine solution. Organic layer was concentrated to about 40% of its initial volume to obtain turbid mass. To the concentrated mass, toluene (16.1 L) was added at  $65$ – $70$  °C, cooled to  $20$  °C to obtain thick slurry and stirred at  $20$  °C for 2–3 h. Solid was filtered, washed with toluene (1.15 L) and dried in a vacuum tray dryer at  $50 \pm 5$  °C for 2–3 h to provide 1.28 kg of **1** (84% yield). Purity by HPLC: 99.79%;  $m/z$   $[\text{M}+\text{H}]^+$  calcd for  $\text{C}_{21}\text{H}_{24}\text{N}_4\text{O}_2\text{S}$ : 396.51; found: 397.  $^1\text{H}$  NMR (DMSO- $d_6$ ):  $\delta$  1.60 (br s, 1H), 2.61–2.68 (m, 4H), 2.69–2.77 (m, 2H), 3.44 (s, 2H), 4.57–4.61 (m, 1H), 5.21–5.22 (d, 1H), 6.29 (s, 1H), 6.90 (br s, 2H), 7.10–7.12 (d, 2H), 7.19–7.23 (m, 1H), 7.27–7.32 (m, 4H), 7.48–7.50 (d, 2H), 9.99 (s, 1H);  $^{13}\text{C}$  NMR (DMSO- $d_6$ ):  $\delta$  168.29, 167.82, 145.87, 144.59, 137.17, 135.13, 128.77, 127.90, 126.74, 125.86, 119.04, 102.61, 71.51, 57.56, 50.77, 39.90, 35.40. Anal. Calcd (%) for  $\text{C}_{21}\text{H}_{24}\text{N}_4\text{O}_2\text{S}$  (396.51): C, 63.5; H, 6.1; N, 14.1; S, 8.1. Found (%): C, 63.6; H, 5.82; N, 14.28; S, 7.96.

## 6. Acknowledgment

Authors thank the management of Megafine Pharma (P) Ltd. for permission to publish this work. Authors also thank colleagues of the Analytical Research and Development team for valuable inputs and support for this work.

## 7. References

1. M. R. Abu Bakar, Z. K. Nagy, A. N. Saleemi, C. D. Rielly, *Crystal Growth and Design* **2009**, *9*, 1378–1384. <https://doi.org/10.1021/cg800595v>
2. D. Z. Shende, Reactive crystallization in pharma industry International conference and exhibition on Pharmacognosy, Phytochemistry and Natural Products, October 21-23, 2013, Hyderabad, India.

- <https://www.omicsonline.org/proceedings/reactive-crystallization-in-pharma-industry-13978.html>, (assessed: Dec 01, 2016)
- J. Gras, *Drugs Today* **2012**, 48 (1), 25–32.  
<https://doi.org/10.1358/dot.2012.48.1.1738056>
  - T. Yamanishi, C. R. Chapple, K. Yasuda, K. Yoshida, R. Chess-Williams, *Neurourology and urodynamics* **2003**, 22, 338–342. <https://doi.org/10.1002/nau.10130>
  - European Medicines Agency, assessment report (EMA/706651/2012), Assessed on Oct, 18, **2012**.
  - V. Khullar, G. Amarenco, J. C. Angulo, J. Cambroner, K. Hoye, I. Milsom, P. Radziszewski, T. Rechberger, P. Boerrigter, T. Drogendijk, EAU 2012 Poster AM12-2389.
  - P. Tyagi, V. Tyagi, M. Chancellor, *Expert Opin. On Drug Safety*, **2011**, 10.2, 287–294.  
<https://doi.org/10.1517/14740338.2011.542146>
  - New Class of Treatment for Overactive Bladder Approved in Europe, Astellas Pharma Europe Ltd., Chertsey, UK, 11<sup>th</sup> January 2013. [https://www.astellas.com/en/corporate/news/pdf/131111\\_eg.pdf](https://www.astellas.com/en/corporate/news/pdf/131111_eg.pdf)
  - S. Kawazoe, K. Sakamoto, Y. Awamura, T. Maruyama, T. Suzuki, K. Onda, T. Takasu, US Patent Number 7,342,117, date of patent Mar 11, **2008**.
  - T. Maruyama, T. Suzuki, K. Onda, M. Hayakawa, H. Moritomo, T. Kimizuka, T. Matsui, US Patent Number 6,346,532, date of patent Feb 12, **2002**.
  - V. Peddy, R. Boge, PCT Int. Appl. 0156998, US Patent Number 9,283,210, date of patent Mar 15, **2016**.
  - ICH Quality Guideline, <http://www.ich.org/products/guidelines/quality/article/quality-guidelines.html> (assessed: November 18, 2016)

## Povzetek

Razvili smo učinkovito metodo za neposredno izolacijo stabilne  $\alpha$ -oblike kristalov mirabegrona (**1**), ki jo je mogoče uporabiti tudi z večjimi količinami. Razvita metoda zanika pretvorbo metastabilne  $\beta$ -oblike kristalov v  $\alpha$ -obliko in s tem presega omejitve doslej objavljenih metod ter se s tem izogne dodatnim procesnim stopnjam med pripravo mirabegrona (**1**). Opisana metoda v eni stopnji neposredno daje stabilno  $\alpha$ -obliko kristalov mirabegrona (**1**) z izkoristki okoli 84% in čistoto >99.77% (določene s HPLC).



*Scientific paper*

# AB Initio Prediction of Stable Conformer Polymorphs of Benzocaine Molecule- a Local Anaesthetic Molecule

Pallipurath Veleelath Nidhin,<sup>1</sup> Arputharaj David Stephen<sup>2,\*</sup>  
and Charles Selvaraj Arun Paul<sup>3</sup>

<sup>1</sup> Department of Physics, Sri Shakthi Institute of Engineering and Technology, Coimbatore, India 641062

<sup>2\*</sup> Assistant Professor of Physics, Department of Physics, Sri Shakthi Institute of Engineering and Technology, Coimbatore, India 641062, Telephone: +91995227392

<sup>3</sup> Department of Science and Humanities, Sri Krishna Institute of Engineering and Technology, Coimbatore, India-641008

\* Corresponding author: E-mail: davidstephen\_dav@yahoo.co.in

Received: 21-02-2017

## Abstract

An ab initio methodology to predict the crystal structures of thermodynamically stable polymorphs of benzocaine within the least energy region of energy landscape by analyzing the local minima from the initial gas phase optimization initiated through the flexible torsion using MP2/6-31G(d,p) method. The global search for the hypothetical dense packing for the structures within the energy penalty region of the local minima have revealed the possible stable conformers under a repulsion alone potential field. The generated hypothetical dense packings from the global search were selected for lattice minimization using the repulsion – dispersion potential field to authenticate the stability. The stability and the characteristics of the generated structures were analyzed from the comparative hydrogen bond analysis and second derivative properties with the known experimental polymorphs. The morphological studies of the global minima of benzocaine molecule from the valid lattice energy landscape was studied in detail to find the morphological important lattice.

**Keywords:** Polymorphism, Ab initio crystal structure prediction, PES scan, Lattice minimization, 2D Finger print plot, Morphology.

## 1. Introduction

Polymorphism is the ability of a flexible molecule to crystallize in different crystal lattice. As the physiochemical properties of the molecule depends on the crystalline parameters of a molecule, the prediction of different polymorphic structures of a molecule in a crystal phase gains its importance.<sup>1</sup> Effect of polymorphs may alter the pharmaceutical nature of flexible drug molecules which indeed exposed the search of polymorphs as commercially and academically vital methodology. As the experimental methods to predict, the polymorphs have been considered to be tough to analyse, theoretical ab initio prediction methodology paved the way in easy procedure with more accuracy. Recent reports have been justified the accuracy of Ab initio methodology in predicting the polymorphs of molecular solids.<sup>2</sup>

The prior aim of the current research was to analyze the possible conformer polymorphs of a local anesthetic

molecule of Benzocaine. The reported analysis of the flexible benzocaine with a ester group attached to the aromatic ring, and the amino group attached in the para position to the ester group revealed the presence of three polymorphic forms. The reports suggested that the structures were found to be stabilized through the hydrogen bond interaction between the carbonyl and amino group. The polymorphism exhibited by benzocaine showed the three forms, mainly Form I, Form II and Form III in crystal structure database. The needle like morphological crystals of Form I showed the deviation of the terminal ethyl and carbonyl functional groups from the plane of the phenyl ring, which have justified as the conformational changes in the alkyl ring, thereby increasing the possibility of existence of conformational polymorphism. The Form II crystals are found to be in orthorhombic morphology implementing the  $P2_1/c$  space group. The low temperature phase transition of form II molecule resulted the forma-

tion of a twinned monoclinic structure with space group  $P112_1$ . The structures were found to be stabilized by the interaction through carbonyl and amine functional groups of the molecule.<sup>3,4,5</sup> As the possibility of conformational polymorphism prevailed in the molecules with stability achieved from the position of terminal carbonyl and amine group, *ab initio* prediction methodology can be initialized for accurate prediction.

## 2. Computational Methodology

The prior aim of the research was the identification of local minima, for the possible crystal structures of the concerned parent molecule which may exhibit conformational polymorphisms. A potential energy surface scan with MP2 level theory using polarized basis set through the selected flexible torsion have been executed. As the central aromatic ring was found to be rigid with  $\pi$ - $\pi$  interactions, the terminal torsions C(7)-C(6)-C(16)-O(1) and C(17)-O(2)-C(16)-C(6) were taken as  $\theta_1$  and  $\theta_2$  (Fig. 1) to execute the Potential Energy Surface scan. Accuracy of the *ab initio* prediction methodology in identifying the stable polymorphs which satisfies the principle relation of

$$E_{\text{total}} = U_{\text{lattice}} + \Delta E_{\text{intra}} \quad (1)$$

solely depends on the exhibition of the local minima associated with the flexible benzocaine molecule. The conformers at local minima and the those which are likely to overcome the energy penalty raised from the torsion distortions are validated by analyzing the energy associated with the distorted conformers.

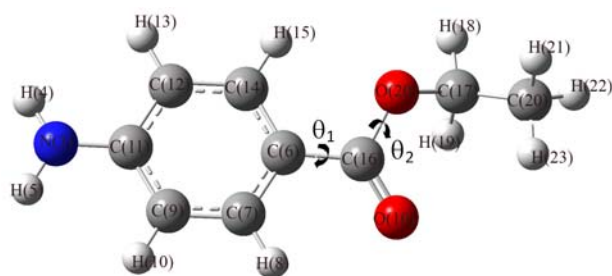


Fig. 1. Benzocaine molecule with selected flexible torsion

The PES scan executed through the flexible torsions ( $\theta_1$  and  $\theta_2$ ) commence the partial gas phase optimizations of each step ranging from  $-180^\circ$  to  $180^\circ$  of the flexible torsions through MP2 level 6-31G(d,p) basis set using the Gaussian 09 package.<sup>6</sup> The promising stable conformers are selected for lattice minimization from the troughs of the plot generated using the torsion angles and corresponding energy of each conformers. (Fig. 2), remaining structures were discarded as they were improbable to overthrow the energy penalty of distortion to achieve local minimum.

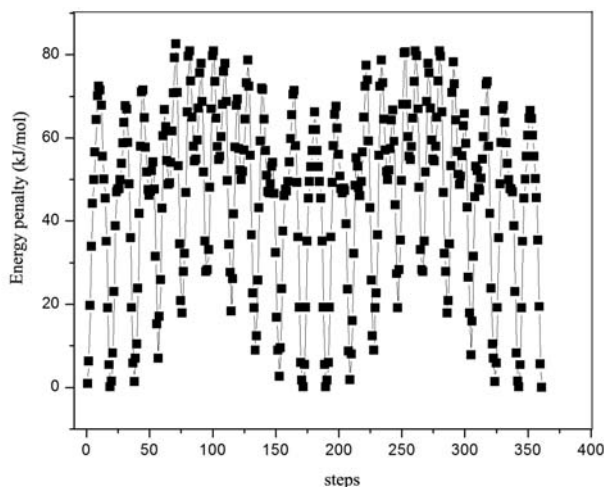


Fig. 2. 2D PES scan plot of the benzocaine molecule with energy penalty associated with each step

The selected within the range of  $\sim 5$  KJ/mol of energy penalty of torsion angle distortions with respect to the local minimum were selected and subjected for global search.

### 2. 1. Global Search

The global search for the plausible conformers of the benzocaine molecule was executed using the MOLPAK<sup>7</sup> algorithm to generate the candidate structure in the space group where it belongs; within the most common space groups occurred in the Cambridge structural database (CSD) with the minimum volume of the unit cell.<sup>8</sup> The MOLPAK global search investigates the unique orientations of the central molecule and constructs approximate coordination patterns of the concerned molecule. Global search algorithm was designed to search for the densest packing patterns of the minimum volume for molecules with fixed conformers. The algorithm initiates the search for the possible dense crystal packings encountering in the common space groups of P1, P-1, P2, Pm, Pc, P2<sub>1</sub>, P2/c, P2<sub>1</sub>/m, P2/m, P2<sub>1</sub>/c, Cc, C2, C2/c, Pnn2, Pba2, Pnc2, P22<sub>1</sub>, Pmn2<sub>1</sub>, Pma2, P2<sub>1</sub>2<sub>1</sub>2<sub>1</sub>, P2<sub>1</sub>2<sub>1</sub>2, Pca2<sub>1</sub>, Pna2<sub>1</sub>, Pnma and Pbca from the 3D orientation and repetition of the central molecule in  $10^\circ$  steps, ranging from  $-90^\circ$  to  $+90^\circ$  specified by the Eulerian angles in a 3Dimensional grid. Each orientations satisfying the threshold interaction with neighboring unit cells have been subjected for the PMIN<sup>9</sup> using the repulsion alone UMD potential<sup>10</sup> to create a possible crystal phase with minimum cell volume initiated through a DFT level theory<sup>11</sup> using becke 3-Parameter exchange basis set (B3LYP) operation.<sup>12</sup> The 500 hypothetical crystal structures of benzocaine for each space groups, generated with dense packing were ranked on the basis of minimum cell volume were subjected to the lattice minimization implementing the repulsion dispersion potential field of form 2

$$U = \sum_{i \in 1, k \in 2} [(A_{ii} A_{kk})^{1/2}] \exp [-(B_{ii} + B_{kk}) R_{ik} / 2] - (C_{ii} C_{kk})^{1/2} / R_{ik}^6 \quad (2)$$

## 2. 2. DMACRYS Minimization

Lattice minimization of the generated conformers from the MOLPAK global search were executed by implementing the repulsion dispersion potential using the DMACRYS<sup>13</sup> algorithm, rectifying the effect of repulsion alone UMD potential in the global search. The minimization was initiated with the candidate structure with space group constraints by analyzing the distributed multipole associated with the system through GDMA<sup>14</sup> algorithm. The algorithm imposes the FIT potential field of the form (2), parameterized by Williams and Cox<sup>15</sup> with additional terms for the hydrogen atoms bound to nitrogen later fitted by Coombes *et al.*<sup>16</sup> The promising densest hypothetical benzocaine crystals at 0K were refined from the analysis of the Ewald summed charge-charge, charge-dipole, dipole-dipole interactions of the molecules. The second derivative properties of the rigid conformers were calculated by the algorithm to justify the thermodynamic and mechanical stability of the benzocaine polymorphs. The stability of the lattice minimized benzocaine conformers were authenticated from the born criterion<sup>17</sup> achieved by

the conformers and those conformers which get minimized with negative eigen values where re minimized by removing the negative representation of the symmetric constraints.

The candidate structures preferred from the lattice minimizations were compared with the experimental polymorphs of benzocaine through COMPACT<sup>18</sup> comparison. The algorithm determines the similarity of the optimized structures with experimental from the least RMS deviation in the crystal packing. The optimized rigid conformers of benzocaine with RMSD less than 0.4 with 20 molecules in common for a coordination sphere of 20 molecules within 40% of tolerance were selected as duplicates and discarded from the studies. The unique structures of benzocaine with valid minimization were ranked on the basis of the energy (Table 1) associated and selected to generate the energy landscape.<sup>19</sup>

## 3. Results and Discussion

### 3. 1. Energy Landscape Validation

The generated energy landscape (Fig. 4) was authenticated by exploiting the presence of experimental known polymorphs of benzocaine molecule in the gene-

**Table 1.** List of Lowest energy conformers of benzocaine with the reproduced experimentally observed polymorphs of Benzocaine.

Structures	E <sub>total</sub> (KJ/mol)	Density	Space Group	a(Å)	b(Å)	c(Å)	α(°)	β(°)	γ(°)
benz1	-99.676	1.191	P2 <sub>1</sub> 2 <sub>1</sub> 2 <sub>1</sub>	4.713	8.363	23.373	90.00	90.00	90.00
benz2	-98.293	1.172	P2 <sub>1</sub> /c	8.235	6.069	18.746	90.00	92.45	90.00
benz4	-98.278	1.172	P2 <sub>1</sub> /c	8.235	6.069	18.747	90.00	92.52	90.00
benz5	-99.710	1.191	P2 <sub>1</sub> 2 <sub>1</sub> 2 <sub>1</sub>	8.364	4.706	23.397	90.00	90.00	90.00
str 1	-122.126	1.263	P2 <sub>1</sub> /c	9.052	6.630	15.550	90.00	111.46	90.00
str 2	-121.348	1.258	P2 <sub>1</sub>	9.053	14.583	6.607	90.00	90.64	90.00
str 3	-121.275	1.260	P2 <sub>1</sub>	9.053	14.560	6.609	90.00	89.93	90.00
str 4	-120.007	1.280	P1	6.785	12.070	16.185	26.09	130.59	131.89
str 5	-119.749	1.254	Cc	10.731	12.817	16.555	90.00	157.40	90.00
str 6	-119.100	1.238	P-1	6.905	9.041	7.333	77.47	90.06	82.91
str 7	-118.557	1.272	P21/n	10.409	7.399	11.568	90.00	104.52	90.00
str 8	-118.285	1.256	P2 <sub>1</sub>	9.120	6.783	15.188	90.00	111.58	90.00
str 9	-117.972	1.247	P-1	6.845	9.134	7.430	107.54	96.03	85.36
str 10	-117.547	1.242	P2 <sub>1</sub>	9.096	14.398	6.762	90.00	94.07	90.00
str 11	-117.545	1.261	P2 <sub>1</sub> 2 <sub>1</sub> 2 <sub>1</sub>	14.213	6.733	9.094	90.00	90.00	90.00
str 12	-117.475	1.259	P2111	14.232	6.730	9.097	89.46	90.00	90.00
str 13	-117.389	1.245	P-1	10.837	6.889	10.264	132.40	98.10	56.86
str 14	-117.134	1.282	P2 <sub>1</sub> 2 <sub>1</sub> 2 <sub>1</sub>	11.716	8.562	8.531	90.00	90.00	90.00
str 15	-116.953	1.221	P2 <sub>1</sub>	9.061	6.695	8.007	90.00	112.29	90.00
str 16	-116.941	1.252	P2 <sub>1</sub>	7.660	6.824	18.108	90.00	67.82	90.00
str 17	-116.739	1.196	P21/n	9.940	8.650	10.674	90.00	88.19	90.00
str 18	-116.480	1.247	Pc	6.851	18.144	14.157	90.00	88.40	90.00
str 19	-116.426	1.251	Cc	12.138	11.325	9.373	90.00	137.09	90.00
str 20	-116.260	1.256	Pc	9.105	7.391	13.055	90.00	96.26	90.00
str 158	-111.055	1.201	P2 <sub>1</sub> 2 <sub>1</sub> 2 <sub>1</sub>	24.080	4.541	8.353	90.00	90.00	90.00
str 210	-109.865	1.213	P2 <sub>1</sub> 2 <sub>1</sub> 2 <sub>1</sub>	5.010	21.792	8.282	90.00	90.00	90.00
str 302	-108.555	1.215	P2 <sub>1</sub> /c	8.320	5.117	21.235	90.00	92.33	90.00
str 362	-107.766	1.185	P2 <sub>1</sub> /c	8.399	4.521	24.384	90.00	90.34	90.00

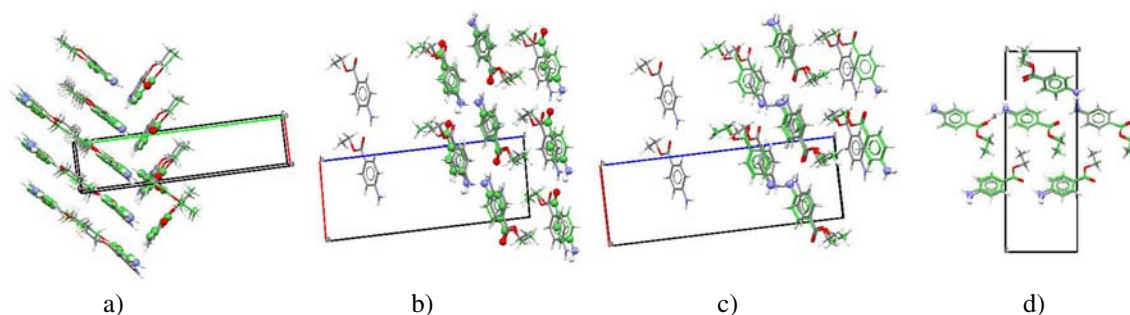


**Fig. 3.** Crystal packing similarity between a) Str210(blue) and Form II (green) b) Str 302 (blue) and Form I (green) c) Str 362 (blue) and Form I (green) d) Str 158(blue) and Form II (green) with 20 molecules in common in a coordination sphere. [Str 210, Str 302, Str 362 and Str 158 are theoretically predicted conformers, Form I and II are experimental known polymorphs.]

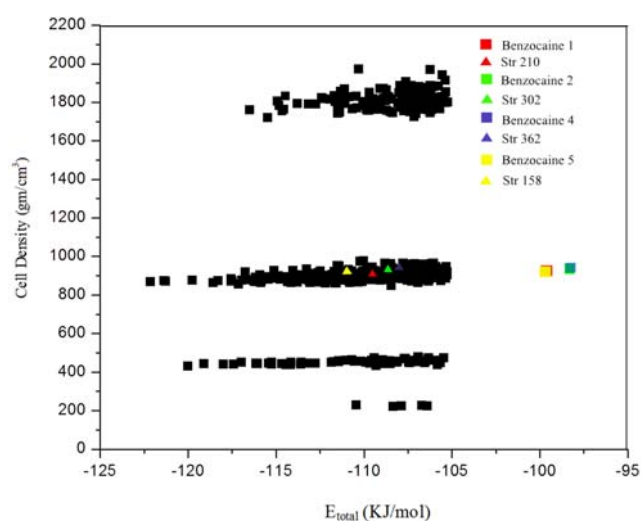


**Fig. 4.** Energy landscape consisting the possible conformers of benzocaine associating the  $E_{total}$

rated landscape. The COMPACT comparison of the unique structures with experimental forms of benzocaine employing the criterion of 20 molecules in common for the coordination sphere with least RMSD in crystal packing similarity revealed that the str 158, str 210, str 302 and str 362 (optimized conformers generated at the 158, 210, 302 and 362 position in the energy rank with  $E_{total}$   $-111.055$  KJ/mol,  $-109.865$  KJ/mol,  $-108.555$  KJ/mol and  $-107.766$  KJ/mol respectively) resembles to the experimental benzocaine Form I ( $E_{total}$   $-99.710$  KJ/mol and  $E_{total}$   $-99.676$  KJ/mol) and II ( $E_{total}$   $-98.293$  KJ/mol and  $E_{total}$   $-98.278$  KJ/mol) [Str 158 and Str 210 resembled FORM II and Str 302 and Str 362 resembled Form I] Fig 3.

The equivalent nature of the optimized conformers with the experimental forms were analyzed from the comparative analysis of the lattice parameters (Table 2), intermolecular short contacts and the mechanical stability of the structures at 0K.

**Table 2.** Regeneration of the crystal structures of Benzocaine molecule using the experimental data, minimized experimental conformation (Expminexp) and the matching structures (20 molecules in common) found during the search of conformers.

Structures	$a(\text{\AA})$	$b(\text{\AA})$	$c(\text{\AA})$	$\alpha(^{\circ})$	$\beta(^{\circ})$	$\gamma(^{\circ})$	Volume	Density	$E_{total}$ (KJ/mol)	rmsd
<b>Benz1 (Form II)</b>										
Observed	5.302	8.217	20.87	90	90	90	909.234			
Expminexp	4.713	8.363	23.373	90.00	90.00	90.00	921.118	1.191	$-99.676$	
Expminopt (Str 210)	5.010	21.792	8.282	90.00	90.00	90.00	904.230	1.213	$-109.865$	0.46
<b>Benz2 (Form I)</b>										
Observed	8.198	5.43	19.592	90	91.35	90	871.899			
Expminexp	8.235	6.069	18.746	90.00	92.45	90.00	935.981	1.172	$-98.293$	
Expminopt (Str 302)	8.320	5.117	21.235	90.00	92.33	90.00	903.256	1.215	$-108.555$	0.9
<b>Benz4 (Form I)</b>										
Observed	8.257	5.5009	19.956	90	91.699	90	906.022			
Expminexp	8.235	6.069	18.747	90.00	92.52	90.00	936.081	1.172	$-98.278$	
Expminopt (Str 362)	8.399	4.521	24.384	90.00	90.34	90.00	925.940	1.185	$-107.766$	1.97
<b>Benz5 (Form II)</b>										
Observed	8.2424	5.3111	20.9044	90	90	90	915.115			
Expminexp	8.364	4.706	23.397	90.00	90.00	90.00	920.981	1.191	$-99.710$	
Expminopt (Str 158)	24.080	4.541	8.353	90.00	90.00	90.00	913.272	1.201	$-111.055$	0.29

The table exposed the equivalent nature of the optimized conformers with the known experimental forms with similar lattice parameters. The deviation of the energy associated with the structures might be due to the temperature dependence of the molecule as it were regenerated at 0K. The equivalence of crystal phase between experimentally determined and predicted structures were authenticated from the peaks generated at the simulated XRD patterns of the structures (Fig. 5–Fig. 8).

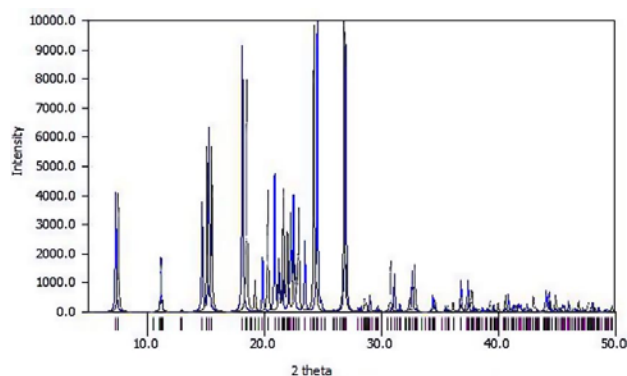


**Fig. 5.** Comparison of the XRD spectrum of Str 158 (black) and Form II (benz5) (blue)

their corresponding equivalent experimental form of II and I were found to be stabilized by the C—H—O interaction through the aromatic carbon atoms beside to the aromatic nitrogen and the carbonyl oxygen atom along with the interaction of Carbon atom at the terminal ethyl group with the carbonyl oxygen. The notable result were observed for the str158 in which the carbon atom of the terminal methyl group interacts with the oxygen atom of the carbonyl functional group. The common hydrogen

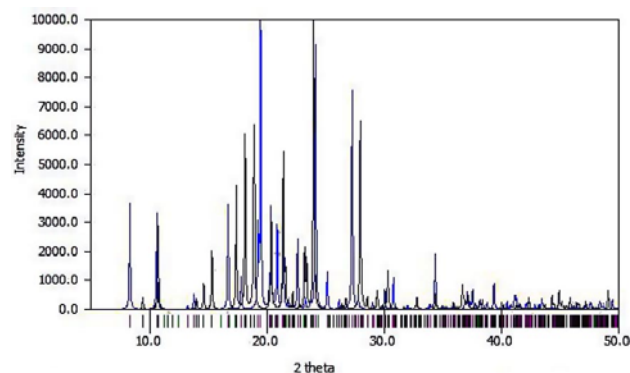


**Fig. 7.** Comparison of the XRD spectrum of Str 302 (black) and Form I (benz2) (blue)

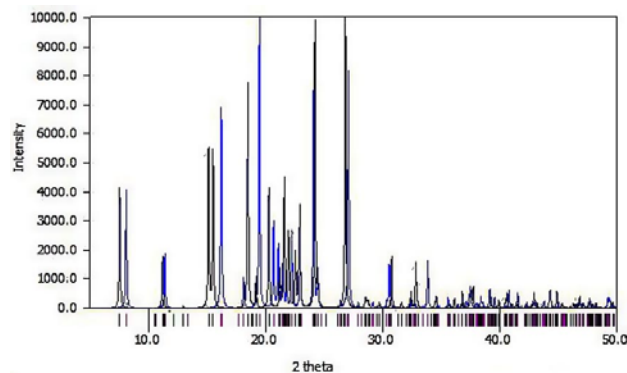


**Fig. 6.** Comparison of the XRD spectrum of Str 210 (black) and Form II (benz1)(blue)

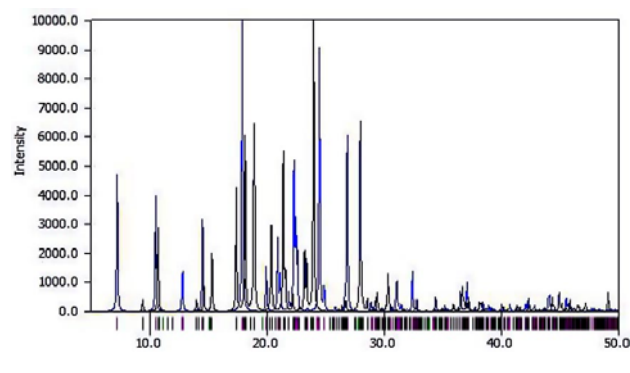


**Fig. 8.** Comparison of XRD spectrum of Str 362 (black) and Form I (benz4)(blue)

The studies indicated that the predicted structures were stable from the presence of the highest peaks. The shift in the XRD pattern were due to the shear factor associated with the molecules at 0K. The analysis have also exposed the str 158 and str 302 were exhibiting more perfect match in the XRD. The hydrogen bonds prevails in the predicted and experimental polymorphs of benzocaine were studied in detail and tabulated. The hydrogen bond analysis revealed the experimental polymorphs and predicted equivalent were stabilized from the N—H—O interactions between the carbonyl oxygen attached to the terminal with the amide group attached to the aromatic ring of the molecule contributing to the chain type graph set of  $C_1^18$  and. In addition to the carbonyl -amide interaction, the predicted structures (str 210, str 302 and str 362) and

bond interactions that are likely to crystallize the conformers were listed in Table 3.

**Table 3.** Common intermolecular H-Bonds between the experimental and Predicted conformers.

Predicted conformers	Common H-bonds		Experimental forms	
str 158	N—H—O	C—H—O	N—H—N	Form II benz5
str 210	N—H—O	C—H—O	—	Form II benz1
str 302	N—H—O	C—H—O	—	Form I benz2
str 362	N—H—O	C—H—O	—	Form I benz4

The in match nature of the hydrogen bonds for the predicted structures and the experimental equivalent justi-

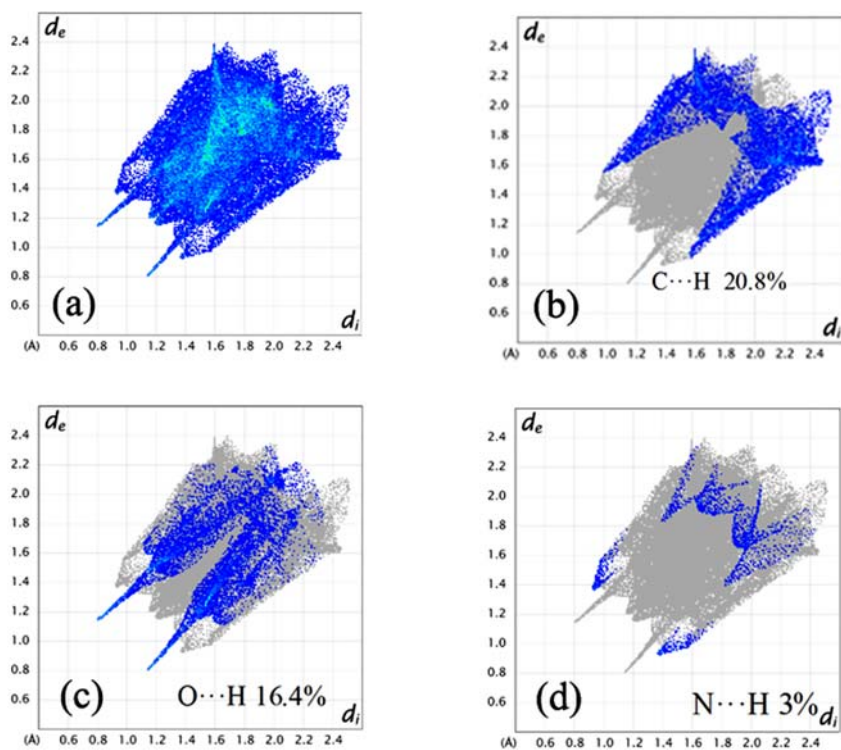


**Fig. 9.** 2D Finger print plot of experimental Form II with a) 100% contribution of all elements b) 20.8% of C...H/H...C interaction c) 16.4% O...H/H...O interaction d) 3% of N...H/H...N interaction.

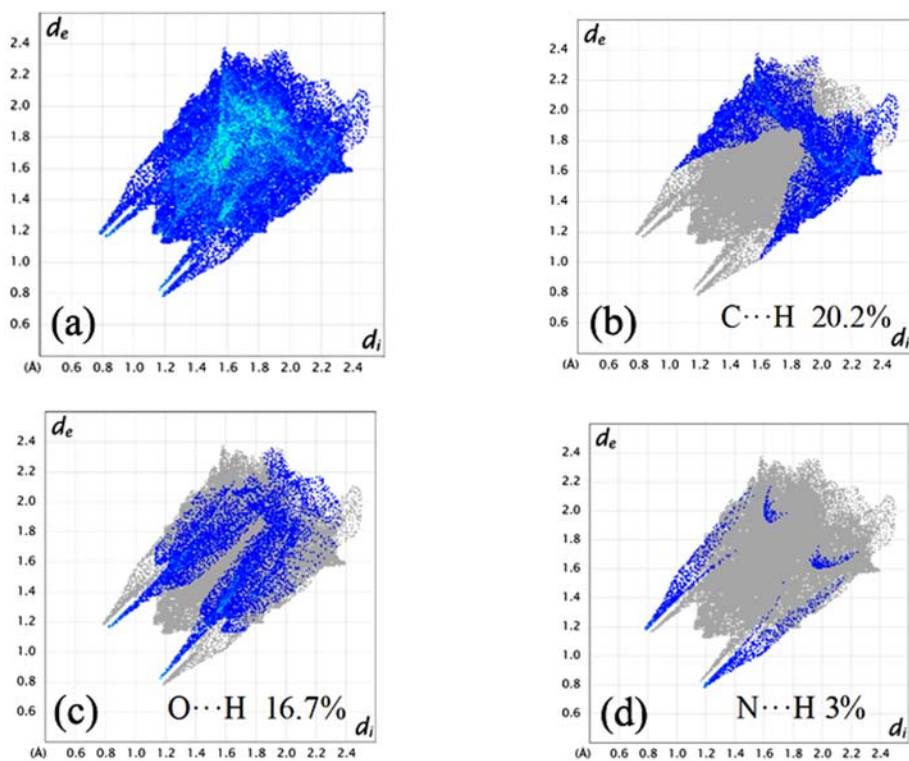


**Fig. 10.** 2D Finger print plot of Str 158 with a) 100% contribution of all elements b) 20.2% of C...H/H...C interaction c) 16.7% O...H/H...O interaction d) 3% of N...H/H...N interaction.

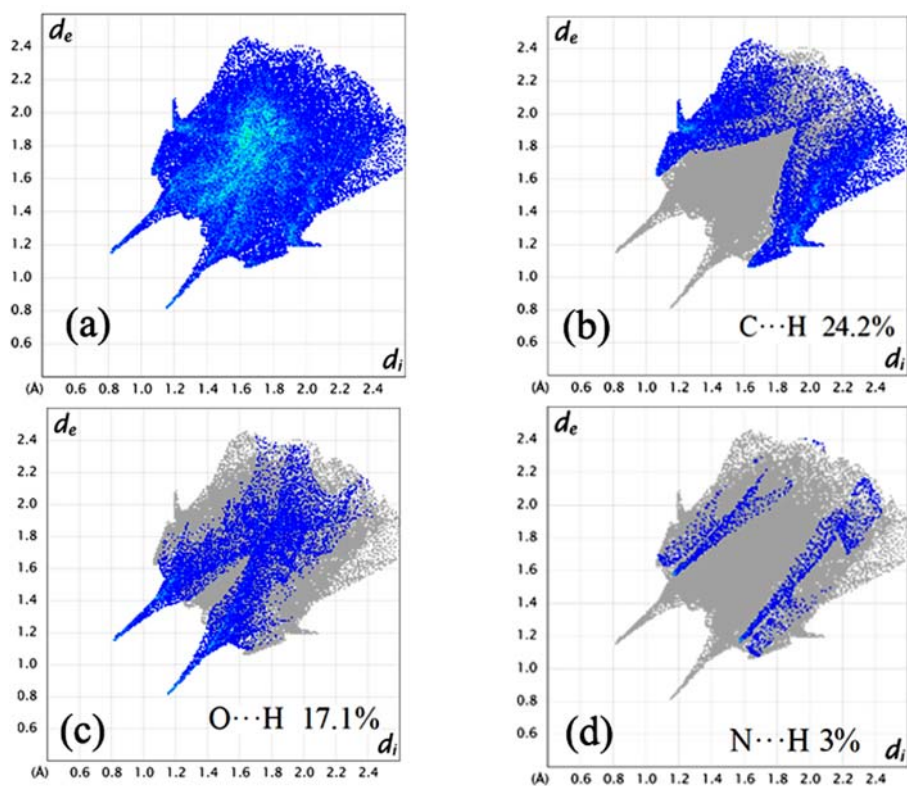


**Fig. 11.** 2D Finger print plot of experimental Form II with a) 100% contribution of all elements b) 24.2% of C...H/H...C interaction c) 17.1% O...H/H...O interaction d) 3% of N...H/H...N interaction.

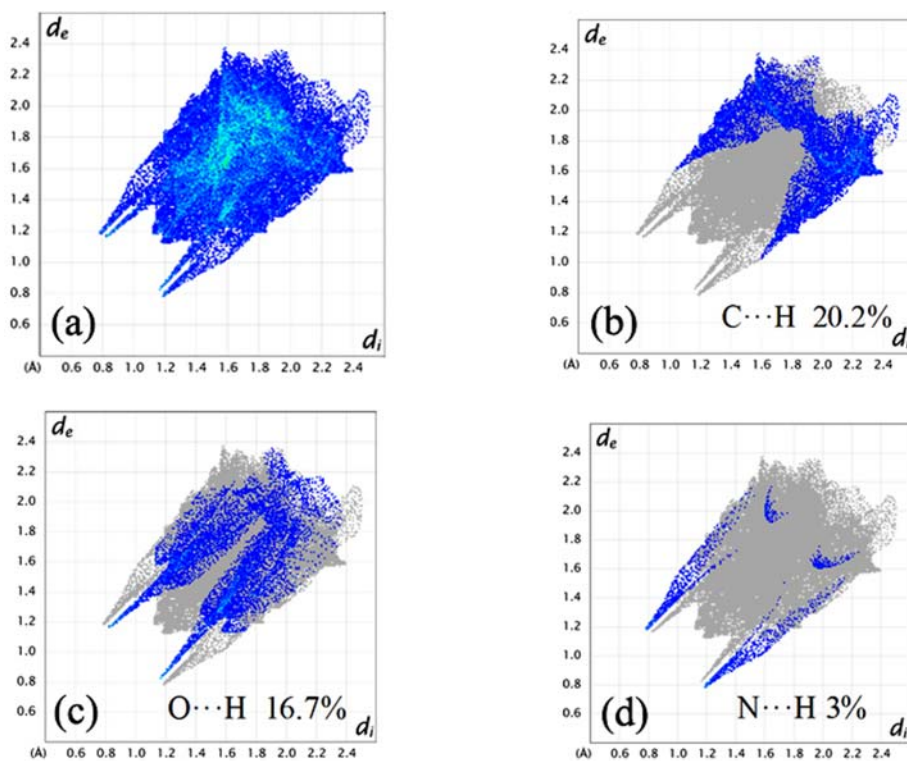


**Fig. 12.** 2D Finger print plot of Str 302 with a) 100% contribution of all elements b) 25.7% of C...H/H...C interaction c) 17.5% O...H/H...O interaction d) 3% of N...H/H...N interaction.

fies the accuracy of the prediction methodology and energy landscape. The detailed analysis and comparative studies of the hydrogen bonds and the peaks of the simulated XRD exhibited the perfect match of str 158 and str 302 with the polymorphic form of benzocaine II and I with least RMSD of 0.294 and 0.9 in crystal packing similarity; were selected for further studies. The percentage of contribution of the key intermolecular interactions to the crystal stability were studied from the Hirshfeld surface.

### 3. 2. Hirshfeld Finger Print Plot Analysis

The contribution of the vital interatomic interaction in the crystal stability and crystallization of the benzocaine molecule have been studied thoroughly from the Hirshfeld surface and 2D contour plots generated using the Crystal Explorer software package.<sup>20</sup>

The Hirshfeld analysis of the experimental benzocaine molecule of form I and Form II with the predicted equivalent structures, str 302 and str 158 emphasized the perfect match. The crystal were found to be stabilized N–H–O and C–H–O interactions, were the latter interaction providing average of 22.5% percentage of the overall contribution to the stability of the conformers. The pointed nature of the O–H/H–O interactions towards the lower points of the *di/de* region indicates the vital importance of the interaction in the stability. The 2D contour plot of the N–H/H–N interaction also shows its importance from the pointed nature with a percentage of contribution of 3%. The in match and perfect similarity of the predicted conformers and the experimental equivalents authenticates str 158 and str 302 as known experimental forms of Form II and Form I of benzocaine, thereby validating the energy landscape. As the mechanical properties are closely related to several material parameters which are within reach of theoretical calculations.<sup>21</sup> Studies have been made to analyze the mechanical strength of the experimental polymorphs and the equipotential predicted structure from the elastic components of the  $C_{ij}$  matrix.<sup>22</sup>

henticated the energy landscape. The structures generated at the lowest energy region of the energy landscape are the possible polymorphs of the benzocaine.

### 3. 3. Analysis of the Predicted Lowest Energy Polymorph of Benzocaine (Str 1)

The authenticity of the lattice minimized energy landscape generated from the hypothetical unique structures of benzocaine conformers justified the existence of possible stable polymorphs at the lowest energy region. The optimized monoclinic crystal structure of the benzocaine polymorph ( Fig. 13) generated with  $E_{\text{total}} -122.126\text{KJ/mol}$  and space group  $P2_1/c$  was analyzed in detail to expose the mechanical stability and the morphological importance.

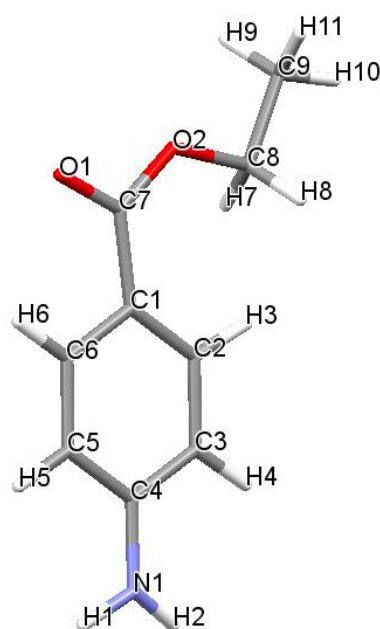


Fig. 13. The optimized crystal structure of benzocaine polymorph generated as Str 1.

Table 4: Comparison of the mechanical properties of the ab initio predicted benzocaine crystal structure and experimental polymorphs of Benzocaine at 0K.

Structures	$C_{11}$	$C_{22}$	$C_{33}$	$C_{44}$	$C_{55}$	$C_{66}$	Young's modulus (GPa)
Form II	44.633	14.617	26.010	9.705	13.306	8.962	24.038
Str158	34.230	18.098	50.619	11.086	21.688	13.444	31.231
Form I	47.385	17.706	19.711	9.459	6.316	10.053	21.440
Str302	51.709	20.661	26.242	10.797	15.312	8.607	26.883

The diagonal elements of the Hessian matrix are found to be positive and definite; revealed that the structures have met born criteria and are mechanically stable at 0K.<sup>23</sup> The perfect match of the parameters between the experimental and predicted polymorphs of benzocaine aut-

The benzocaine conformer generated at the global minima was found to be mechanically stable at 0 K by achieving born criteria of stability with elastic sensitivity of 29.89GPa. The thermodynamic stability of the global minimum (explained as Str 1 henceforward) were justified



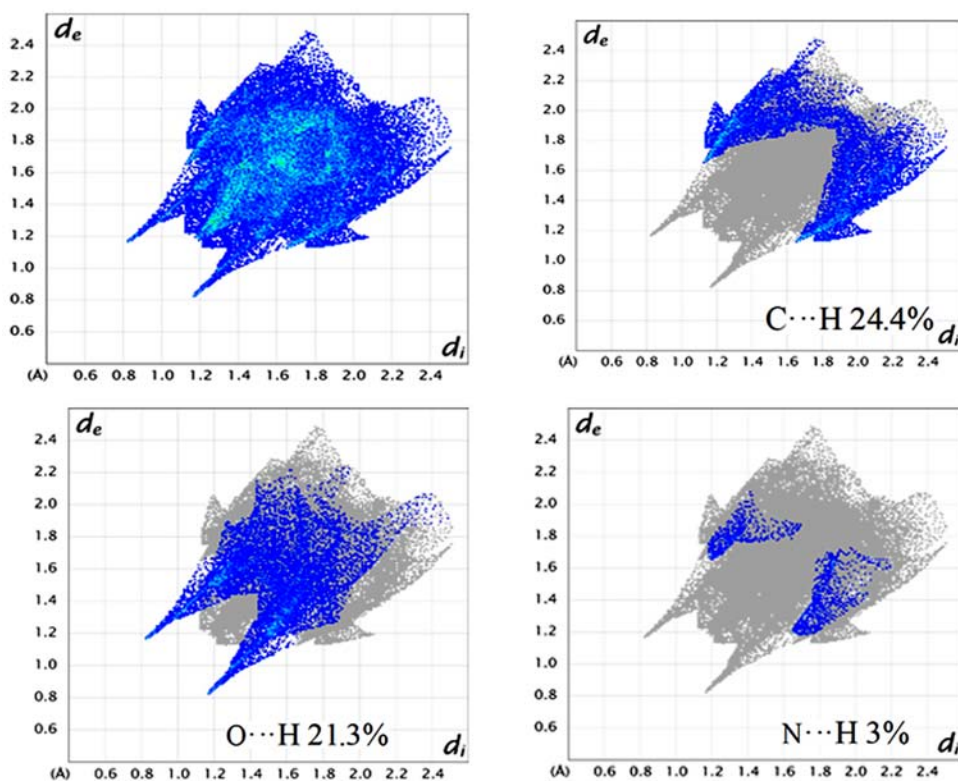


**Fig. 14:** 2D Finger print plot of predicted Str 1 with a) 100 % contribution of all elements b) 24.4% of C...H/H...C interaction c) 21.3% O...H/H...O interaction d) 3% of N...H/H...N interaction.

from the Intermolecular attraction prevailed on the system. The H-bond analysis of Str 1 reveals that the structure were found to be stable by establishing the intermolecular interaction among the Nitrogen atom of the amide group N(1) attached to the ring and O(2), generating C11(8) graph set through N(1)–H(2)–O(2) linkage. The detailed analysis have also revealed the Carbon atoms of the terminal ethyl group interacts with the carbonyl oxygen making a bond length of 3.401 Å with an angle of 122° through C(8)–H(7)–O(1). The identification studies of the possible hydrogen bonds prevailed in the Str 1 also exposed a key interaction via H(7) between C(8) and O(1)[C(8)–H(7)–O(1)] making an angle of 122.5° with bond length 3.401 Å, in addition the methyl carbon atom C(9) also found to be bonded with the amide nitrogen (N(1)) with bond angle 155.5° and bond length 3.865 Å.

The Hirshfeld analysis and the 2D contour plots of str1 detailed the percentage of contribution of each interaction towards the crystal stability.

The percentage of contribution of the key interactions exhibit the dominant nature of the O–H interaction Oxygen being the acceptor, from the pointed nature of the 2D contour plot towards the lower region of  $d_i/d_e$ . The interaction contributes to the 21.3% of the hirshfeld surface, where as the C–H interaction contributes 24.4% of the surface. The hirshfeld surface reflected the stability of the crystal structure from the N–H–O bonding, justifying the

thermodynamical satbility of Str 1 from the pointed nature of the fingerprint plot .

The simulated XRD patterns were generated for the global minimum structure of benzocaine at 0K. The XRD graphs was found to be exhibiting high peaks at different 2 values. The diffraction patterns are represented in fig. 15

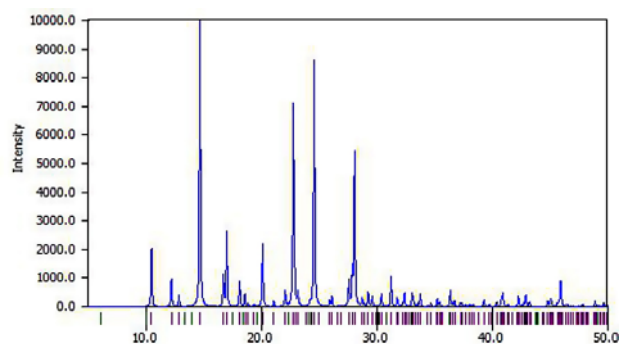


**Fig. 15:** Simulated XRD pattern of the Predicted polymorph (Str 1)

As the morphological importance of crystal structure depends on the growth rate and surface area of the crystal phases , studies have been carried out to interpret the morphology and the growth rate of str1 by calculating the interplanar d spacing through the formula (3)

$$1/d_{hkl}^2 = (1/\sin\beta)(h^2/a^2 + k^2\sin^2\beta/b^2 + l^2/c^2 - 2lh\cos\beta/ac) \quad (3)$$

The morphological analysis of the structure have been carries out by using the BFDH theory<sup>24,25,26</sup> incorporating the interplanar spacing ( $d_{hkl}$ ) and the crystal symmetry which provide a good insight to the morphology of the polymorphs (fig. 16).

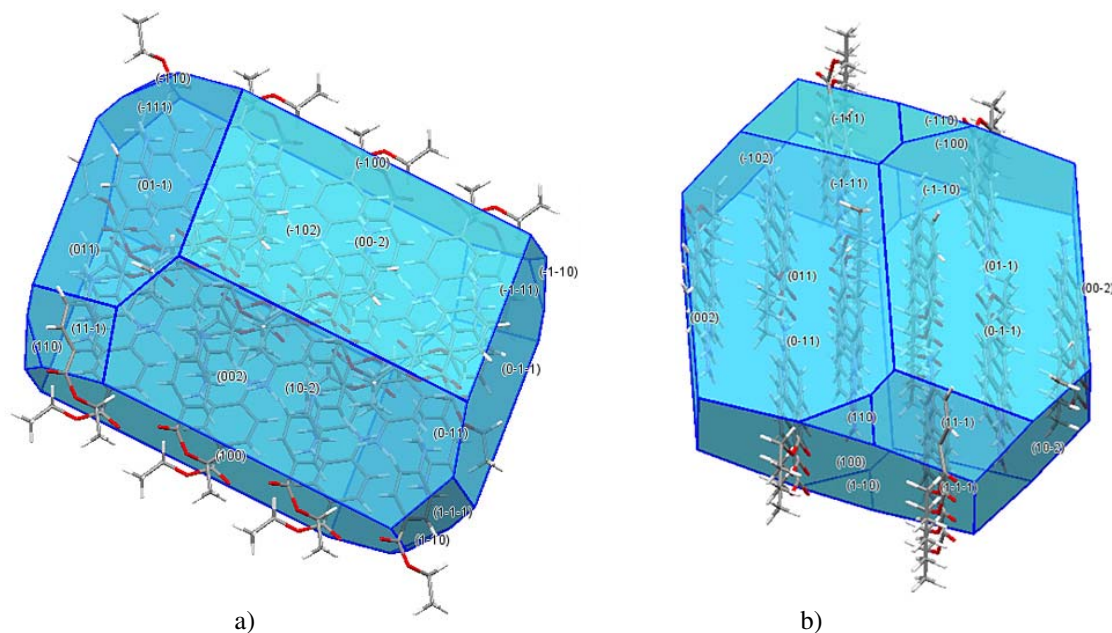


**Fig. 16:** Predicted morphology of Str 1 with a) longitudinal view b) Transverse view.

The growth rate of the each miller indices have been noted and tabulated to expose the morphologically important of the structure (Table 5). The studies have revealed

miller indices of  $(-1\ 0\ 0)$  and  $(1\ 0\ 0)$  are morphologically important due to their comparatively less growth rate by exhibiting the higher  $d_{spacing}$ .<sup>27</sup>

The theoretical analysis of the Str 1 revealed that the structure is a thermodynamically possible stable monoclinic polymorph of Benzocaine, which have the ability to crystallize by attaining intermolecular short contacts with stabilized dense packing.

## 4. Conclusion

Ab initio prediction of the possible stable polymorph of benzocaine molecule, a flexible local anesthetic

**Table 5:** List of the predicted miller indices of Str 1 with interplanar d spacing.

$h$	$k$	$L$	$a$	$B$	$C$	$a$	$B$	$\gamma$	$D$
-1	1	1	9.056	6.6302	15.5501	90	111.4606	90	5.12
-1	1	0	9.056	6.6302	15.5501	90	111.4606	90	5.35
0	1	-1	9.056	6.6302	15.5501	90	111.4606	90	6.10
0	1	1	9.056	6.6302	15.5501	90	111.4606	90	6.10
1	1	0	9.056	6.6302	15.5501	90	111.4606	90	5.35
1	1	-1	9.056	6.6302	15.5501	90	111.4606	90	5.12
0	0	2	9.056	6.6302	15.5501	90	111.4606	90	7.76
1	0	0	9.056	6.6302	15.5501	90	111.4606	90	9.04
-1	0	2	9.056	6.6302	15.5501	90	111.4606	90	6.09
1	0	-2	9.056	6.6302	15.5501	90	111.4606	90	6.09
-1	0	0	9.056	6.6302	15.5501	90	111.4606	90	9.04
0	0	-2	9.056	6.6302	15.5501	90	111.4606	90	7.76
0	-1	1	9.056	6.6302	15.5501	90	111.4606	90	6.10
0	-1	1	9.056	6.6302	15.5501	90	111.4606	90	6.10
-1	-1	1	9.056	6.6302	15.5501	90	111.4606	90	5.12
-1	-1	0	9.056	6.6302	15.5501	90	111.4606	90	5.35
1	-1	0	9.056	6.6302	15.5501	90	111.4606	90	5.35
-1	-1	-1	9.056	6.6302	15.5501	90	111.4606	90	4.99

molecule via generating the energy landscape; by analyzing the energy associated for each different conformers showed good accuracy in generating the possible crystal structures of benzocaine. The conformers with compromising energy penalty of torsional distortions were successfully generated the hypothetical structures, owing to the global search through the repulsion alone potential field. The lattice minimization using the distributed multipole analysis associated with the hypothetical structures authenticated the methodology from the generation of experimental equivalent polymorph of benzocaine. The comparison analysis of the experimental known polymorph of benzocaine with predicted hypothetical conformers revealed that Str 158 and Str 302 were equivalent to the experimental known polymorphs of Form II and Form I, with packing rmsd of 0.294 and 0.9 respectively. The thermodynamic stability crystal nature of the predicted conformers was proved from the simulated XRD patterns, with perfect match of Str 158 and Str 302 with Form II and Form I respectively. The Hirshfeld analysis indicated that the predicted and experimental polymorphs of benzocaine were stabilized through N-H-O and C-H-O interactions with dominant interaction through the carbonyl Oxygen atom. As the landscape was authenticated from the presence of experimental known polymorphs of benzocaine, the conformers generated at the lowest energy region can be considered as the possible polymorphs of benzocaine which are yet to be resolved. The Hirshfeld analysis and XRD patterns revealed the thermodynamic stability of the polymorph at lowest energy region along with the morphological studies exposed useful insight to the crystal morphology.

## 5. Acknowledgement

The authors were grateful to the DST-SERB for providing financial assistance to the research under the fast track scheme and Dr L S price for the support in DMACRYS usage. The authors also thankful to the garuda clustering service for the computational aid provided for the proper completion of this research .

## 6. References

1. K. Raza, P.Kumar, S. Ratan, R. Malik, S. Arora, *SOJ Pharma Pharma Sci.* **2014**, 1(2), 10.  
<https://doi.org/10.15226/2374-6866/1/1/00111>
2. A. M. Reilly, R. I. Cooper, C. S. Adjiman, S. Bhattacharya, A. D. Boese, J. G. Brandenburg, P. J. Bygrave, R. Bylsma, J. E. Campbell, R. Car, D. H. Case, R. Chadha, J. C. Cole, K. Cosburn, H. M. Cuppen, F. Curtis, G. M. Day, R. A. DiStasio Jr, A. Dzyabchenko, B. P. van Eijck, D. M. Elking, J. A. van den Ende, J.C. Facelli, M.B. Ferraro, L. Fusti-Molnar, C.-A. Gatsiou, T.S. Gee, R. de Gelder, L.M. Ghiringhelli, H. Goto, S. Grimme, R. Guo, D.W.M. Hofmann, J. Hoja, R.K. Hylton, L. Iuzzolino, W. Jankiewicz, D. T. de Jong, J. Kendrick, N. J. J. de Klerk, H.-Y. Ko, L. N. Kuleshova, X. Li, S. Lohani, F. J. J. Leusen, A. M. Lund, J. Lv, Y. Ma, N. Marom, A. E. Masunov, P. McCabe, D. P. McMahon, H. Meekes, M. P. Metz, A. J. Misquitta, S. Mohamed, B. Monserrat, R. J. Needs, M. A. Neumann, J. Nyman, S. Obata, H. Oberhofer, A. R. Oganov, A. M. Orendt, G. I. Pagola, C. C. Pantelides, C. J. Pickard, R. Podszwa, L. S. Price, S. L. Price, A. Pulido, M. G. Read, K. Reuter, E. Schneider, C. Schober, G. P. Shields, P. Singh, I. J. Sugden, K. Szalewicz, C. R. Taylor, A. Tkatchenko, M. E. Tuckerman, F. Vacarro, M. Vasileiadis, A. Vazquez-Mayagoitia, L. Vogt, Y. Wang, R. E. Watson, G. A. de Wijs, J. Yang, Q. Zhu, C. R. Groom, *Acta Crystallographica Section B*, **2016**, 72, 439–459.  
<https://doi.org/10.1107/S2052520616007447>
3. B. K. Sinha, Vasantha pattabhi, *proc indian acad sci (chem sci)*. **1987**, 98, no3, 229–234.
4. D. E. Lynch and I. McClenaghan, *Acta Crystallographica Section E* **2002**, 58, o708–o709.  
<https://doi.org/10.1107/S1600536802009674>
5. E. J. Chan, A. D. Rae and T. R. Welberry, *Acta Crystallographica Section B* **2009**, 65, 509–515.  
<https://doi.org/10.1107/S0108768109018898>
6. M. J. Frisch, G. W. Trucks, H. B. Schlegel, G. E. Scuseria, M. A. Robb, J. R. Cheeseman, G. Scalmani, V. Barone, B. Mennucci, G. A. Petersson, H. Nakatsuji, M. Caricato, X. Li, H. P. Hratchian, A. F. Izmaylov, J. Bloino, G. Zheng, J. L. Sonnenberg, M. Hada, M. Ehara, K. Toyota, R. Fukuda, J. Hasegawa, M. Ishida, T. Nakajima, Y. Honda, O. Kitao, H. Nakai, T. Vreven, J. A. Montgomery Jr., J. E. Peralta, F. Ogliaro, M. J. Bearpark, J. Heyd, E. N. Brothers, K. N. Kudin, V. N. Staroverov, R. Kobayashi, J. Normand, K. Raghavachari, A. P. Rendell, J. C. Burant, S. S. Iyengar, J. Tomasi, M. Cossi, N. Rega, N. J. Millam, M. Klene, J. E. Knox, J. B. Cross, V. Bakken, C. Adamo, J. Jaramillo, R. Gomperts, R. E. Stratmann, O. Yazyev, A. J. Austin, R. Cammi, C. Pomelli, J. W. Ochterski, R. L. Martin, K. Morokuma, V. G. Zakrzewski, G. A. Voth, P. Salvador, J. J. Dannenberg, S. Dapprich, A. D. Daniels, Ö. Farkas, J. B. Foresman, J. V. Ortiz, J. Cioslowski and D. J. Fox, Gaussian, Inc., Wallingford, CT, USA, 2009.
7. J. R. Holden, Z. Du, H. L. Ammon, *Journal of Computational Chemistry*. **1993**, 14, 422–437.  
<https://doi.org/10.1002/jcc.540140406>
8. P. G. Karamertzanis and C. C. Pantelides, *Journal of Computational Chemistry* **2005**, 26, 304–324.  
<https://doi.org/10.1002/jcc.20165>
9. W. R. Busing, *Report ORNL-5747*. Oak Ridge National Laboratory, Oak Ridge **1981**.
10. S. M. Prasad, Z. Du, N. Albu, H. L. Ammon, University of Maryland, College Park MD **2004**
11. J. P. Perdew, *Physical Review B* **1986**, 33, 8822–8824.  
<https://doi.org/10.1103/PhysRevB.33.8822>
12. C. Lee, W. Yang and R. G. Parr, *Physical Review B* **1988**, 37, 785–789. <https://doi.org/10.1103/PhysRevB.37.785>

13. S. L. Price, M. Leslie, G. W. A. Welch, M. Habgood, L. S. Price, P. G. Karamertzanis and G. M. Day, *Physical Chemistry Chemical Physics* **2010**, *12*, 8478–8490. <https://doi.org/10.1039/c004164e>
14. A. J. Stone, GDMA University of Cambridge, UK, **1999**.
15. D. E. Williams and S. R. Cox, *Acta Crystallographica Section B* **1984**, *40*, 404–417. <https://doi.org/10.1107/S010876818400238X>
16. D. S. Coombes, S. L. Price, D. J. Willock and M. Leslie, *The Journal of Physical Chemistry* **1996**, *100*, 7352–7360. <https://doi.org/10.1021/jp960333b>
17. M. Born, *Mathematical Proceedings of the Cambridge Philosophical Society* **1940**, *36*, 160–172. <https://doi.org/10.1017/S0305004100017138>
18. J. A. Chisholm and S. Motherwell, *Journal of Applied Crystallography* **2005**, *38*, 228–231. <https://doi.org/10.1107/S0021889804027074>
19. S. L. Price, *Chemical Society Reviews* **2014**, *43*, 2098–2111. <https://doi.org/10.1039/C3CS60279F>
20. M. A. Spackman and J. J. McKinnon, *CrystEngComm* **2002**, *4*, 378–392. <https://doi.org/10.1039/B203191B>
21. G. Wang, S. Schönecker, S. Hertzman, Q.-M. Hu, B. Johansson, S. K. Kwon and L. Vitos, *Physical Review B* **2015**, *91*, 224203. <https://doi.org/10.1103/PhysRevB.91.224203>
22. A. T. Anghel, G. M. Day and S. L. Price, *CrystEngComm* **2002**, *4*, 348–355. <https://doi.org/10.1039/B202084J>
23. T. Beyer, G. M. Day, and S. L. Price *J. Am. Chem. Soc.* **2001**, *123*, 5086–5094. <https://doi.org/10.1021/ja0102787>
24. A. Bravais *Etudes Crystallographiques Paris: Academic des Sciences: 1913*.
25. G. Freidal *Bull Soc Fr Miner*, **1907**, *30*, 326.
26. J. D. H. Donnay, D. Harker, *Am Miner*, **1937**, *22*, 463.
27. D. S. Coombes, C. R. A. Catlow, J. D. Gale, M. J. Hardy and M. R. Saunders, *Journal of Pharmaceutical Sciences* **2002**, *91*, 1652–1658. <https://doi.org/10.1002/jps.10148>

## Povzetek

Za izračune termodinamsko stabilnih kristalnih struktur polimorfov benzokaina smo uporabili ab initio metode. Za začetno optimizacijo spojine v plinskem stanju in fleksibilnim torzijskim kotom smo uporabili MP2 metodo in bazni set 6-31G(d,p). S kvantnokemijskimi izračuni smo z iskanjem lokalnih minimumov iskali morebitne stabilne konformere. Tako izračunane morebitne stabilne konformere smo izbrali in z nadaljnjo mrežno minimizacijo preverjali njihovo stabilnost. Stabilnost in karakteristike izračunanih struktur smo analizirali tudi s primerjavo izračunanih vodikovih vezi in primerjavo le-teh z eksperimentalno določenimi podatki. Z morfološkimi študijami molecule benzokaina v globalnem minimumu smo želeli najti morfološko pomembne mreže.

Scientific paper

# Functionalization of Graphene Oxide with 9-aminoanthracene for the Adsorptive Removal of Persistent Aromatic Pollutants from Aqueous Solution

Ali Balati,<sup>1</sup> Mohammad Ghanbari,<sup>2</sup> Sara Karimi Behzad<sup>3</sup>  
and Mostafa M. Amini\*<sup>3</sup>

<sup>1</sup> Environmental Sciences Research Institute, Shahid Beheshti University, G.C., Tehran 1983963113, Iran

<sup>2</sup> Department of Organic Chemistry, Faculty of Chemistry, University of Kashan, Kashan, Iran.

<sup>3</sup> Department of Chemistry, Shahid Beheshti University, G.C., Tehran 1983963113, Iran

\* Corresponding author: E-mail: m-pouramini@sbu.ac.ir  
Tel: +98-21-29903109; fax: +9-21-22431663

Received: 17-03-2017

## Abstract

A novel modified graphene oxide nanocomposite was fabricated via a facial procedure, aiming to removal of the aromatic pollutants from aqueous solution. The graphene oxide (GO) was functionalized with 9-aminoanthracene and produced graphene oxide-9-aminoanthracene (GO-9-AA). FTIR, XRD, TGA, TEM and Raman spectroscopy techniques were used for characterization of the adsorbents. Adsorption of naphthalene (NAP), acenaphthylene (ACN), and phenanthrene (PHN) as a model of polycyclic aromatic hydrocarbons (PAHs) was investigated by GO-9-AA. The adsorbent showed excellent removal efficiency towards PAHs from aqueous solution. Equilibrium data of the adsorption process were successfully fitted with Freundlich model from single solute system, and the maximum adsorption capacities followed the order of NAP > ACN > PHN. The kinetic analysis revealed that the overall adsorption process was fast and successfully fitted with the pseudo-second-order kinetic model. The anthracene ring makes GO-9-AA  $\pi$ -electron rich, thus facilitating  $\pi$ - $\pi$  EDA interaction between NAP, ACN and PHN with GO-9-AA.

**Keywords:** Wastewater, Aromatic pollutant; Graphene oxide, PAHs

## 1. Introduction

Polycyclic aromatic hydrocarbons (PAHs) are a group of organic compounds that contain two or more fused rings of carbon and hydrogen. They are persistent environmental contaminants and usually arise from incomplete combustion of hydrocarbons and other organic materials such as petroleum, coal, gas, garbage, tobacco, wood, and biomass.<sup>1,2</sup> PAHs enter the environment from different sources, including combustion fuel gasses, wastewater, and runoff from the petroleum industry. They were identified in industrial and municipal wastewater, effluents, rain, surface and drinking water, soils, and plants.<sup>3,4</sup> PAHs can transport long distance in air and water due to their chemical persistence and semi-volatile na-

ture and are difficult to biodegrade. Presences of PAHs in the environment are of great concern because many of them are toxic, carcinogenic, and they tend to bioaccumulate in aquatic organisms. Some PAHs are capable of interacting with DNA to promote mutagenic and carcinogenic responses. Therefore, they are considered as priority pollutants by both the US Environmental Protection Agency (EPA) and the European Environmental Agency. So, efficient, low-cost and robust methods to decontaminate waters from PAHs are vital to protect human and environment. Numerous studies have focused on the effective elimination of PAHs from aqueous solutions by different strategies such as photocatalysis, adsorption, electrolysis, organobentonite, and sonication. Among these approaches, adsorption removal of PAHs has been considered as

an efficient technique due to its low-cost, high efficiency and facile operation routes. For the adsorptive removal of PAHs from aqueous environments, various kinds of adsorbents have been extensively investigated. However, the adsorption capacities of aforementioned materials are not sufficient. Therefore, it will be beneficial to develop new adsorbents with higher adsorption capacities for persistent organic pollutant management in the environment.

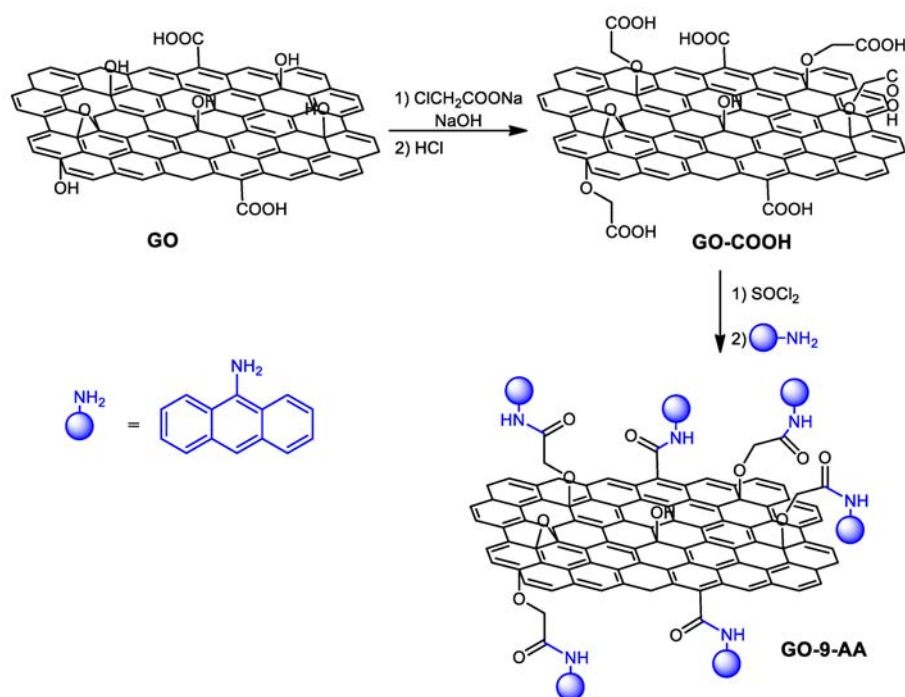
Carbon-based nanomaterials have unique  $\pi$ -electronic structure and been used as an excellent sorbents for the removal of aromatic compounds.<sup>12–15</sup> GO, as a newly found carbon-based nanomaterial with fascinating two-dimensional (2D) atomic structure and only one atomic thickness, have attracted considerable attention in a broad range of application in addressing environmental challenges.<sup>16–18</sup> Due to its large specific surface area (theoretical limit,  $2630 \text{ m}^2 \text{ g}^{-1}$ ), remarkable electronic properties and high ability of modification, potential environmental applications of GO as a superior adsorbent has been recognized for removal of organic and inorganic contaminants from water and gasses.<sup>19,20</sup> GO can be well-dispersed in water due to its abundant hydrophilic groups on its surface such as hydroxyl, carboxylic and epoxide.<sup>21,22</sup> In addition, the interaction between GO and pollutants is closely related to its surface structure which is tunable and flexible.<sup>23,24</sup> The surface of GO usually consists of two parts: unoxidized and oxidized zones. The unoxidized zone is referring to the lowly oxidized GOs while oxidized zones consist of both  $sp^3$  zones and  $sp^2$  clusters. The oxygen-containing functional groups could be found on the surface of GO in the oxidized zones. The  $sp^2$  clusters are

affinitive to non-electrolytic organic compounds by  $\pi$ - $\pi$  stacking or other hydrophobic interactions<sup>26,27</sup> whereas the oxygen-containing functional groups tend to bind hydrophilic species due to hydrogen bonding, ion exchange or coordination effects.<sup>28,29</sup> Due to diverse zones of GO with different adsorption affinity, the adsorption behavior of GO mainly depends on its surface structural feature. Therefore, introduction of a suitable functional group on GO surface can improve its adsorption capacity for the removal of target pollutants. In the current research GO was modified and functionalized with 9-aminoanthracene by formation of the chemical bonds between carboxyl groups of GO and amine groups of 9-aminoanthracene to produce GO-9-AA (Scheme 1). The aim of functionalization of GO with 9-aminoanthracene is to increase the  $sp^2$  clusters in GO for enhancing adsorption of non-electrolytic organic compounds by  $\pi$ - $\pi$  stacking or other hydrophobic interactions. The fabricated composite was utilized for the removal of NAP, ACN and PHN as a model of PAHs and adoption mechanism of aforementioned PAHs was also proposed. To the best of our knowledge, this research is the first example of GO-9-AA fabrication and its application for the removal of NAP, ACN and PHN from aqueous solution.

## 2. Experimental

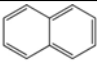
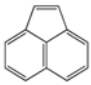
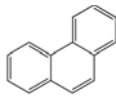
### 2.1. Materials

All reagents were the analytical grade and used without further purification. Graphite powder (~ 325 mesh si-



Scheme 1. Schematic illustration of GO-9-AA fabrication

Table 1. Physicochemical properties of the selected PAHs

PAH's	Structure	Molecular weight (g mol <sup>-1</sup> )	Vapour pressure at 25 °C Pa	Water solubility (g L <sup>-1</sup> )	log K <sub>ow</sub>
Naphthalene C <sub>10</sub> H <sub>8</sub>		128	10.4	31~	3.37
Acenaphthylene C <sub>12</sub> H <sub>8</sub>		152	0.9	3.93	4.00
Phenanthrene C <sub>14</sub> H <sub>10</sub>		178	0.02	1.2	4.57

ze, 99.9995%) was obtained from Alpha Aesar Company (Karlsruhe, Germany). Sulfuric acid (H<sub>2</sub>SO<sub>4</sub>), potassium persulfate (K<sub>2</sub>S<sub>2</sub>O<sub>8</sub>), phosphorus pentoxide (P<sub>2</sub>O<sub>5</sub>), potassium permanganate (KMnO<sub>4</sub>), hydrogen peroxide (H<sub>2</sub>O<sub>2</sub>), hydrochloric acid HCl, hydrazine hydrate (H<sub>6</sub>N<sub>2</sub>O), nitric acid (HNO<sub>3</sub>), glacial acetic acid, sodium hydroxide (NaOH) and SnCl<sub>2</sub> were purchased from Merck Chemical Company (Darmstadt, Germany). NAP, ACN, PHN and anthracene were purchased from Sigma-Aldrich Chemical Company (Dorset, UK). All aqueous solutions were prepared with ultrapure water (16 MΩ.cm) from the Milli-Q water purification system (Millipore, Bedford, MA, USA). The physicochemical properties of PAHs are shown in Table 1.

### 2. 1. 1. Fabrication of GO

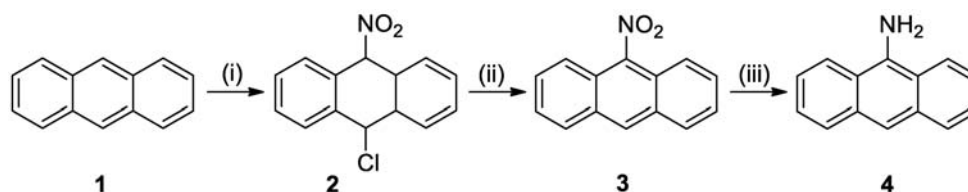
GO was synthesized using modified Hummer's method. Graphite flakes were oxidized using a combination of powerful reagents, i.e., sulfuric acid (H<sub>2</sub>SO<sub>4</sub>), potassium persulfate (K<sub>2</sub>S<sub>2</sub>O<sub>8</sub>) and phosphorus pentoxide (P<sub>2</sub>O<sub>5</sub>). Briefly, 3.0 g of graphite flakes were suspended in 10 mL of H<sub>2</sub>SO<sub>4</sub>. Oxidizing agents K<sub>2</sub>S<sub>2</sub>O<sub>8</sub> and P<sub>2</sub>O<sub>5</sub> were gradually added to the graphite and sulfuric acid mixture and stirred at 90 °C until the flakes were dissolved. The stirring continued for 4 more hours at 80 °C, and the solution was then diluted with 500 ml Milli-Q Millipore water. After dilution, the solution was stirred overnight, and then filtered, washed with deionized water and thereafter dried to get the powdered form of GO. Pre-oxidized GO powder was then subjected to further oxidation with 125 mL of H<sub>2</sub>SO<sub>4</sub> and 15 g of potassium permanganate (KMnO<sub>4</sub>) in an ice bath. After 2 more hours stirring, 130 mL of Milli-Q Millipore water was added to the mixture, and this caused the temperature to rise to 95 °C. After 15 minutes, 15 mL hydrogen peroxide (30%, v/v) was added to reduce manganese to manganese sulfate (Mn → MnSO<sub>4</sub>). Finally, the solution was diluted with 400 mL of Milli-Q Millipore water and yellowish suspension was stirred overnight. GO was filtered and washed thoroughly with HCl and water till the rinsed water pH was found to be approximately 7.

### 2. 1. 2. Preparation of 9-nitroanthracene (3)

9-nitroanthracene (**3**, Scheme 2) was prepared according to a previous report. Briefly, concentrated nitric acid (4 mL) was added dropwise to a suspension of anthracene (**1**) (10.0 g, 56.0 mmol) in glacial acetic acid (40 mL) maintaining the temperature below 30 °C. The reaction mixture was stirred vigorously for 1 h to form a clear solution. Then a mixture of concentrated HCl (50 mL) and glacial acetic acid (50 mL) was added slowly resulting in a pale yellow precipitate of 9-nitro-10-chloro-9,10-dihydroanthracene (**2**). The solution was filtered, and washed with glacial acetic acid (3 × 25 mL) and thoroughly with water until the washings were neutral. The resulting yellow solid was treated with a warm solution (60–70 °C) of 10% NaOH (200 mL), filtered, washed with warm water until the washings were neutral. Finally, the solid was air-dried and recrystallized from glacial acetic acid affording fluffy yellow needles (8.31 g, 67% yield), mp 148–150 °C (lit. 145–146 °C). R<sub>f</sub> = 0.30 (*n*-hexane/EtOAc 9:1). <sup>1</sup>H NMR (300 MHz, CDCl<sub>3</sub>) δ = 8.57 (1H, s), 8.03 (2H, d, *J* = 7.6 Hz), 7.92 (2H, d, *J* = 7.6 Hz), 7.68–7.52 (4H, m).

### 2. 1. 3. Preparation of 9-aminoanthracene (4)

9-aminoanthracene (**4**, Scheme 2) was prepared according to the procedure reported by Janovec et al.,. Briefly, a suspension of 9-nitroanthracene (**3**) (7.24 g, 32.5 mmol) in glacial acetic acid (145 mL) was heated in 70–80 °C for 1.5 h. To the resulting clear solution was added a slurry of SnCl<sub>2</sub> (31.0 g, 163.2 mmol) in concentrated HCl (110 mL) via a dropping funnel. The resulting yellow precipitate was stirred at 80 °C for a further 30 min, cooled to room temperature, filtered, washed with concentrated HCl (3 × 10 mL), treated with a solution of 5% NaOH for approximately 15 min with manual stirring from time to time. Finally, product was collected by filtration, washed thoroughly with water until the washings were neutral and vacuum-dried at 50 °C for 6 h to afford a yellow powder (5.18 g, 83% yield). No further purification was required, M.p 161–166 °C (lit. 153–154 °C). R<sub>f</sub> =



**Scheme 2.** Schematic illustration of 9-aminoanthracene synthesis. Reagents and conditions: (i) concd.  $\text{HNO}_3/\text{HCl}$ ,  $<30\text{ }^\circ\text{C}$ ; (ii)  $\text{NaOH}$  (10%),  $60\text{--}70\text{ }^\circ\text{C}$ ; (iii)  $\text{SnCl}_2/\text{concd. HCl}$ , glacial  $\text{HOAc}$ ,  $70\text{--}80\text{ }^\circ\text{C}$ .

0.39 (*n*-hexane/EtOAc 3:1),  $^1\text{H NMR}$  (300 MHz,  $\text{CDCl}_3$ ):  $\delta = 7.98\text{--}7.94$  (m, 4H), 7.88 (s, 1H), 7.47–7.39 (m, 4H), 4.82 (s, 2H,  $\text{NH}_2$ ).

### 2. 1. 4. Preparation of GO-9-AA

The GO suspension (1 mg/mL) was sonicated in the bath under 100W power for 1 h. The resulting suspension was taken for further carboxylation and amidation. In carboxylation of GO, 1.5 g  $\text{NaOH}$  and 1.5 g sodium chloroacetate were added into 300 mL GO suspension and sonicated in the bath for 1 h to convert hydroxyl and epoxide groups to carboxyl groups. The resulting mixture was neutralized with diluted  $\text{HCl}$ , and purified by repeated centrifugation at 4,000 rpm for 45 min and rinsed with ultrapure water, then evaporated to dryness in vacuum yielding a dark black solid product. The carboxylated graphene oxide,  $\text{GO-COOH}$ , was reacted in 20 mL of  $\text{SOCl}_2$  (containing 2 mL of dimethylformamide) at  $70\text{ }^\circ\text{C}$  for 24 h to convert the carboxyl groups into acyl chlorides, then evaporated to dryness in the vacuum and resuspended in dry acetonitrile containing 9-aminoanthracene (500 mg). The mixture was stirred vigorously at  $50\text{ }^\circ\text{C}$  for 48 h under nitrogen atmosphere, and then the product was purified by repeated centrifugation at 4,000 rpm for 45 min and rinsed with ultrapure water, acetone, and dichloromethane to remove unreacted 9-aminoanthracene. The final product, graphene oxide-9-aminoanthracene (GO-9-AA), was dried at room temperature in vacuum yielding 270 mg.

## 2. 2. Characterization

The fabricated GO-9-AA was characterized by FTIR, XRD, TGA, TEM and Raman spectroscopy. FTIR spectra of materials were recorded within 400 to  $4000\text{ cm}^{-1}$  region with Shimadzu FTIR 8300 spectrometer in KBr matrix. Raman spectra were measured using SENTERRA (2009) (BRUKER, Germany). The TGA data were acquired with Shimadzu TA-50 thermal analyzer (Shimadzu, Japan) at heating rate of  $5\text{ }^\circ\text{C min}^{-1}$  from room temperature to  $800\text{ }^\circ\text{C}$ . High-angle X-ray diffraction patterns were obtained with STOE diffractometer using  $\text{Cu-K}\alpha$  radiation at scanning rate of 3/min from  $2\theta = 5^\circ\text{--}80^\circ$ . The morphology of the GO-9-AA was recorded with Philips CM120 transmission electron microscopy (TEM).

## 2. 3. Batch Adsorption Experimental

All adsorption experiments were carried out in a batch reactor at  $25 \pm 1\text{ }^\circ\text{C}$ . Different concentrations of NAP, ACN and PHN ( $1\text{--}30\text{ mg L}^{-1}$ ) were made by preparation of simulated wastewater of three adsorbates (in pure methanol) with DI water. Adsorption experiments were conducted by adding a specific amount of GO-9-AA to the synthetic wastewater, including water/methanol solution (20% v/v) in 50 mL glass centrifuge tubes sealed with Teflon-lined screw caps. During the adsorption experiments, negligible amounts ( $0\text{--}0.15\text{ }\mu\text{L}$ ) of 0.1 M  $\text{HCl}$  or 0.1 M  $\text{NaOH}$  were added to the solution for adjusting the pH to  $7.0 \pm 0.1$ . After obtaining the equilibrium, the mixture was centrifuged at 6000 rpm for 10 min, and then concentrations of the solutes in the supernatants phase were measured by UV/visible spectrophotometer (UV/Vis 2100 Shimadzu).

## 2. 4. Data Analysis

The equilibrium data of the adsorption experiments were fitted with two conventional isotherm models, i.e. Langmuir and Freundlich to determine the theoretical maximum adsorption capacity of the GO-9-AA. Based on the Langmuir isotherm model, adsorption process takes place on a homogeneous surface by monolayer adsorption, and there is no interaction between adsorbed particles. It is formulated as:

$$q_e = \frac{q_m b C_e}{1 + b C_e} \quad (1)$$

Where  $C_e$  is the equilibrium concentration of the adsorbate in  $\text{mg L}^{-1}$ ,  $q_e$  the amount of PAHs adsorbed at equilibrium in  $\text{mg g}^{-1}$ ,  $q_m$  and  $b$  are the Langmuir constants which demonstrate the adsorption capacity of adsorbent and apparent heat change in  $\text{mg g}^{-1}$  and  $\text{l mg}^{-1}$ , respectively.

Dimensionless constant separation factor ( $R_L$ ) reflects the fundamental characteristics of Langmuir model, and it is expressed as:

$$R_L = \frac{1}{1 + b C_0} \quad (2)$$

Where  $b$  is the Langmuir constant and  $C_0$  is the highest initial concentration of adsorbate  $\text{mg L}^{-1}$ . The



value of  $R_L$  illustrates the types of Langmuir isotherm. Adsorption phenomenon is irreversible ( $R_L = 0$ ), favorable ( $0 < R_L < 1$ ), linear ( $R_L = 1$ ), or unfavorable ( $R_L > 1$ ). The Freundlich isotherm model assumes that adsorption process is multilayer and occurs on heterogeneous surfaces. The Freundlich isotherm model is given by:

$$q_e = K_F C_e^{1/n} \quad (3)$$

Where  $K_F$  ( $\text{mg}^{(n-1)/n} \text{g}^{-1} \text{L}^{-1}$ ) and  $n$  are Freundlich isotherm model constants, representative of the saturation capacity and intensity of adsorption process.

The Kinetics of the adsorption of the NAP, ACN, and PHN onto GO-9-AA were investigated by fitting the adsorption data with pseudo first-order and pseudo-second-order kinetic models. The pseudo-first order assumes that adsorption rate is a proportion with the number of free adsorption sites and it is formulated as:

$$\log(q_e - q_t) = \log q_e - \frac{k_1}{2.303} t \quad (4)$$

Where  $q_e$  and  $q_t$  are the amounts of NAP, ACN and PHN adsorbed ( $\text{mg g}^{-1}$ ) onto GO-9-AA at equilibrium and any time  $t$  (min), respectively, and  $k_1$  is the rate constant of the adsorption process ( $\text{min}^{-1}$ ).

The linear relationship between adsorption rate and the square of the number of unoccupied adsorption sites is an assumption of the pseudo-second order kinetic model, and it is given by:

$$\frac{t}{q_t} = \frac{1}{k_2 q_e^2} + \frac{t}{q_e} \quad (5)$$

Where  $k_2$  is the adsorption rate constant ( $\text{mg g}^{-1} \text{min}^{-1}$ ).

All of the isotherm and kinetic model parameters were obtained by fitting the models in Sigma Plot 12.0.

## 3. Results and Discussion

### 3.1. Preparation of GO-9-AA

After modification of the GO surface by a chlorine group using thionyl chloride, the reaction of highly reactive chlorine with the amino group of 9-aminoanthracene is led to the formation of title sorbent. Pyridine was added to the reaction mixture to react with the side product (HCl). The formation of GO-9-AA nanocomposite was confirmed by IR spectroscopy, elemental analysis, thermal gravimetric analysis, Raman spectroscopy, powder X-ray diffraction and transmission electron microscopy.

## 3.2. Characterization of GO-9-AA

### 3.2.1. FTIR Analysis

The FTIR spectra of GO and GO-9-AA are shown in Figure 1. The appearance of characteristic absorption peaks at 3449, 1735, 1631 and 1067  $\text{cm}^{-1}$  revealed the stretching vibrations of  $-\text{OH}$ ,  $\text{C}=\text{O}$ ,  $\text{C}=\text{C}$ , and  $\text{C}-\text{O}$  functional groups in GO, respectively. After the amidation reaction, several new peaks appeared on the FTIR spectrum of GO-9-AA. The amide characteristic ( $-\text{C}(\text{O})\text{NH}-$ ) stretching vibration peak at 1653  $\text{cm}^{-1}$  indicates that the amide bond formed by reaction between GO and 9-aminoanthracene. Furthermore, the new peak at 1573  $\text{cm}^{-1}$  corresponds to the  $\text{N}-\text{H}$  bending vibration and the peak at 1192  $\text{cm}^{-1}$  for  $\text{C}-\text{N}$  in-plane stretching demonstrates that the 9-aminoanthracene was grafted onto the GO by the amide bond.

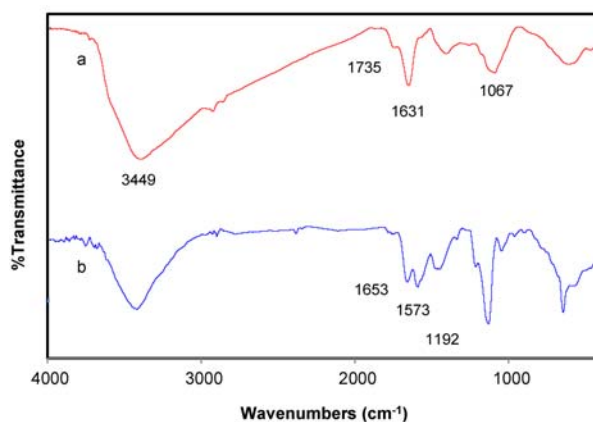


Fig. 1. FT-IR spectra of (a) GO and (b) GO-9-AA

### 3.2.2. Raman Spectroscopy

Raman spectroscopy as a powerful tool has been frequently used to investigate the structural and electronic

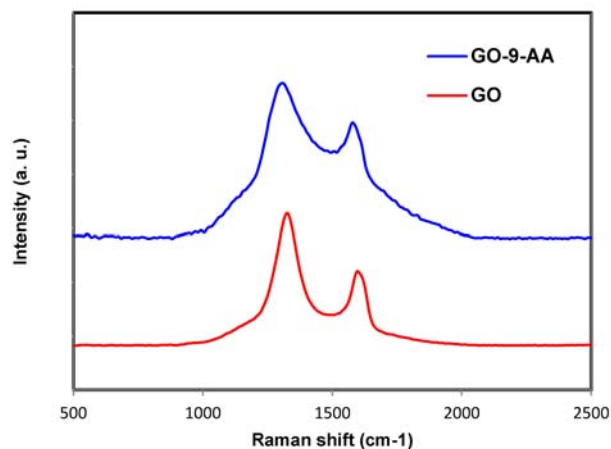


Fig. 2. Raman spectra of GO and GO-9-AA

properties of GO. Figure 2 shows the Raman spectra of the pristine GO and GO-9-AA. As expected, the pristine GO displays a prominent G-band (graphitic band) at  $1598\text{ cm}^{-1}$  which is due to the influence of defects and isolated double bonds, and D-band (disorder band) at  $1326\text{ cm}^{-1}$ . The D-band in carbon materials is associated with the presence of 'disorder' such as defects or simply nanoscale dimensions. The significant structural changes occurring during the amidation reaction were also reflected in the Raman spectra. In GO-9-AA, the G band shifts back to  $1579\text{ cm}^{-1}$  which is relatively close to the G-band of the pristine graphite compared with GO, suggesting that electronic conjugation in GO-9-AA was restored after 9-aminoanthracene grafting on GO structure.<sup>38,39</sup>

### 3. 2. 3. TGA Analysis

Strong evidence for successful functionalization of the GO with 9-aminoanthracene was also provided via TGA analysis (Fig. 3). GO shows slight mass loss from room temperature to  $210\text{ }^{\circ}\text{C}$  and significant mass loss from  $210$  to  $230\text{ }^{\circ}\text{C}$ . Following with slight mass loss up to  $600\text{ }^{\circ}\text{C}$ . The major mass loss at  $\sim 220\text{ }^{\circ}\text{C}$  is caused by pyrolysis of the oxygen-containing functional groups, generating  $\text{CO}$ ,  $\text{CO}_2$ , and steam. In compared with GO, TGA of GO-9-AA shows an enhanced thermal stability due to the removal of oxygen-containing functional groups by amidation reaction. This change led to a new thermal decomposition at  $490\text{--}570\text{ }^{\circ}\text{C}$  which attributed to the formation of amide-bonds of 9-aminoanthracene functional group. This mass changes indicate successful covalent functionalization of GO by 9-aminoanthracene which was also in agreement with the results of FTIR and Raman analysis.

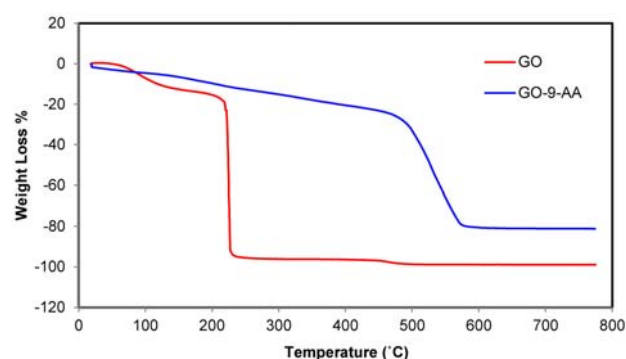


Fig. 3. TGA of GO and GO-9-AA

### 3. 2. 4. XRD Analysis

Figure 4 shows XRD patterns of both pristine GO and GO-9-AA. The peak at  $11.06^{\circ}$  corresponds to the (001) diffraction with an interlayer spacing of approximately  $0.74\text{ nm}$ . As it can be seen, this peak in XRD pattern

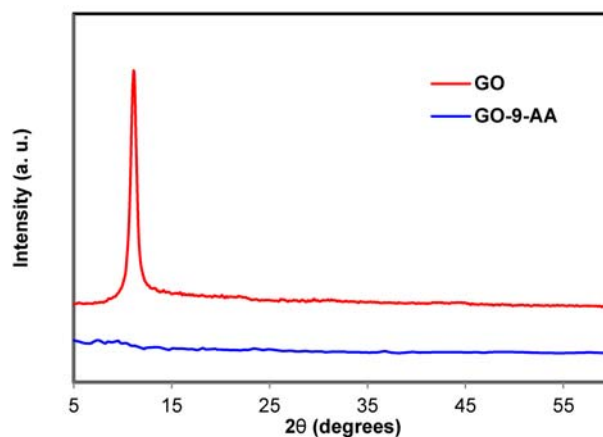


Fig. 4. X-ray diffraction patterns of GO and GO-9-AA

of GO after amidation has been eliminated, suggesting exfoliation of layered in GO-9-AA.

### 3. 2. 5. TEM Analysis

The natural structure of GO could be proved by natural ripples on the GO surfaces. The microstructure of the sorbent before and after modification was investigated by TEM analysis. The TEM images demonstrated that both GO and GO-9-AA nanosheets were transparent (Figure 5). As it can be seen, GO has fairly flat surface compared with that of GO-9-AA and its wrinkles were mainly positioned on the boundary regions of the GO and created scrolls, whereas the surface of GO-9-AA has more aggregations and wrinkles which mostly on the basal planes to make groove regions.

## 3. 3. Adsorption Isotherms

Describing the interaction between adsorbent and the adsorbate is usually the aim of adsorption isotherm models when the adsorption process reaches equilibrium. The isotherm models allow having the most vital parameter for designing an appropriate adsorption system. The adsorption isotherms of NAP, ACN, and PHN on GO-9-AA are shown in Figure 6, and the regression parameters are listed in Table 2. In general, all adsorption isotherms were nonlinear, and the regression parameters are listed in Table 2. The results indicated that the nonlinear correlation coefficients of the Freundlich isotherm model for NAP, ACN, and PHN onto GO were 0.991, 0.997 and 0.997, and onto GO-9-AA were 0.998, 0.997 and 0.997, respectively. The higher correlation coefficients for Freundlich model imply that adsorption process takes place mostly onto heterogeneous regions such as edges, grooves, and wrinkles. The same result has also been reported in the removal of PAHs by other adsorbent materials such as modified periodic mesoporous organosilica, GO and graphene.<sup>45,46</sup> Based on Langmuir isotherm mo-

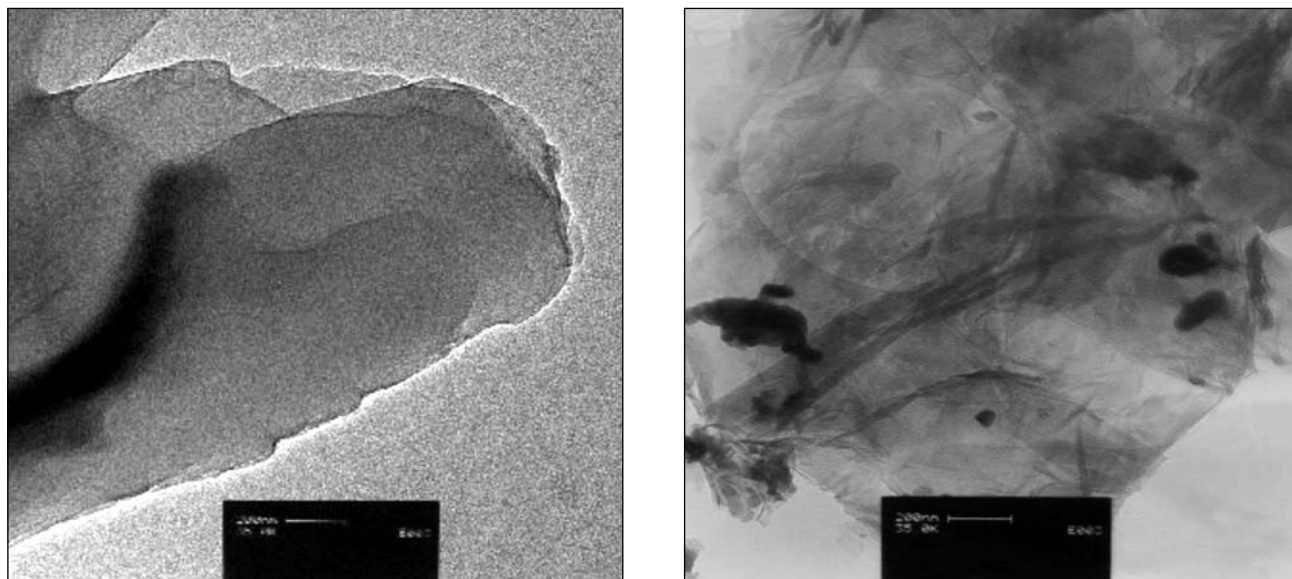


Fig. 5. TEM micrograph of GO (left) and GO-9-AA (right)

Table 2. Isotherm parameters for NAP, ACN, and PHN adsorption onto GO and GO-9-AA

Adsorbates	Langmuir					Freundlich			
	$q_{m,cal}$ ( $\text{mg g}^{-1}$ )	$q_{e,exp}$ ( $\text{mg g}^{-1}$ )	$b$ ( $\text{l mg}^{-1}$ )	$R_L$	$R^2$	$K_f$ ( $\text{mg}^{(n-1)/n}$ $\text{g}^{-1} \text{L}^{-1}$ )	$N$	$R^2$	
GO	NAP	22.93	23.16	0.52	0.18	0.987	9.43	3.40	0.991
	ACN	18.80	21.28	0.38	0.21	0.995	4.93	2.22	0.997
	PHN	17.83	19.30	0.34	0.23	0.988	4.71	2.19	0.997
GO-9-AA	NAP	57.00	78.08	1.31	0.09	0.994	42.18	2.06	0.998
	ACN	46.32	57.60	0.59	0.16	0.995	21.18	2.26	0.997
	PHN	44.50	52.02	0.58	0.17	0.994	18.95	2.32	0.997

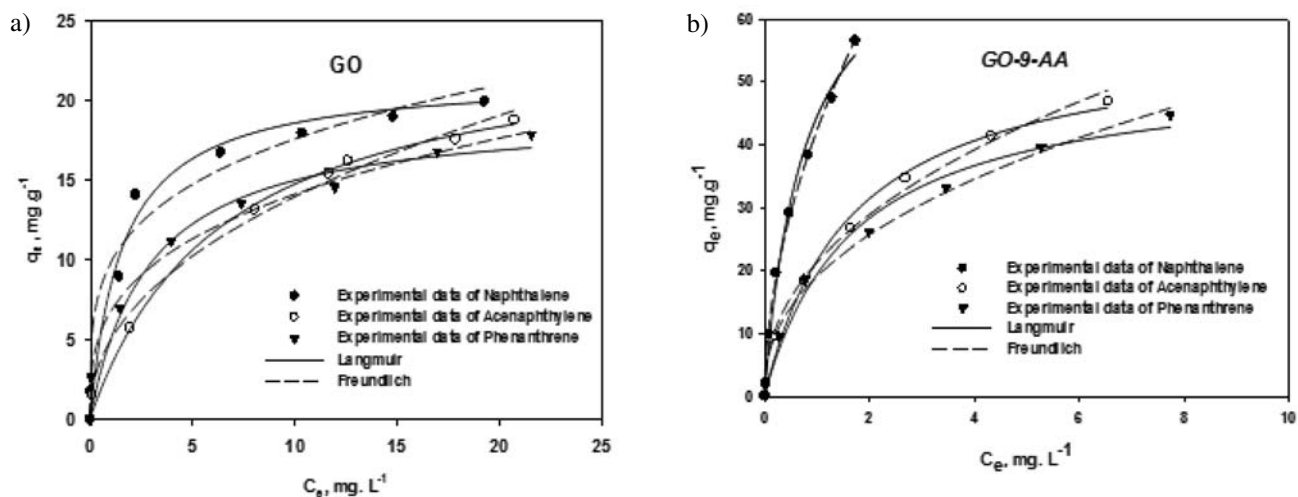


Fig. 6. Adsorption isotherms of NAP, ACN, and PHN onto GO and GO-9-AA at room temperature and pH =7.0

del, maximum theoretical adsorption capacity ( $q_{m,cal}$ ) were obtained 23.16, 21.28 and 19.30  $\text{mg g}^{-1}$  onto GO and 78.08, 57.60 and 52.02  $\text{mg g}^{-1}$  onto GO-9-AA for NAP,

ACN, and PHN, respectively. The same trends were observed for experimental adsorption capacities ( $q_{e,exp}$ ) i.e., 22.93, 18.80 and 17.83  $\text{mg g}^{-1}$  for NAP, ACN and PHN

onto GO and 57.00, 46.33 and 44.50 mg g<sup>-1</sup> onto GO-9-AA, respectively. Separation factor ( $R_L$ ), derived from the Langmuir isotherm model was also calculated (Table 2) to prove the favorableness of the adsorption of three adsorbates onto GO and GO-9-AA. The values of  $R_L$  are calculated in the range of 0.09–0.23 demonstrating a favorable adsorption process of NAP, ACN, and PHN. Adsorption intensity of adsorbates could be attributed to the Freundlich constant ( $1/n$ ). Adsorbates could be easily adsorbed when  $0.1 < 1/n \leq 0.5$ , adsorption process of the adsorbates is difficult when  $0.5 < 1/n \leq 1$ , and when  $1/n > 1$  adsorption is entirely difficult to occur. The  $1/n$  values of NAP, ACN, and PHN onto two adsorbents were calculated in the range of 0.1–0.5 proofing that the adsorbates could be easily adsorbed. Since GO-9-AA showed a notable adsorption capacity in comparison with GO, it was selected to precede extra adsorption experiments.

### 3. 4. Adsorption Kinetics

Rapid treatment of a large volume of drinking water is the main factor which sometimes limits practical application of the adsorbents. In order to investigate the required time for obtaining adsorption equilibrium, kinetic studies were performed. The effect of adsorption time on the removal of NAP, ACN, and PHN by GO-9-AA is shown in Figure 7. Adsorption kinetic data were evaluated with two

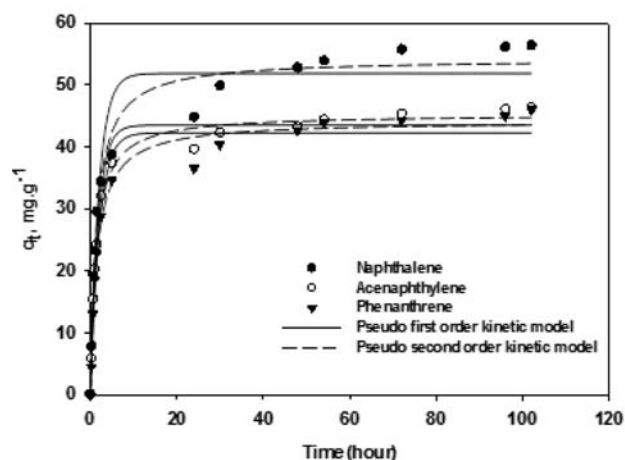


Fig. 7. Adsorption kinetics of NAP, ACN, and PHN on GO-9-AA at room temperature and pH = 7.0.

semi-empirical kinetic models: the pseudo-first and second-order equations. The validity of two models was investigated by nonlinear regression. It can be seen from Figure 7, the adsorption rate was quite fast with the order of magnitude NAP > PHN > ACN within the first 20 h, and then gradually slowed down until equilibrium was reached within 48 h which quite similar to that reported for aromatic compounds. Parameters obtained with two models are summarized in Table 3. As depicted in Figure 7 and Table 3, predicted adsorption data of NAP, ACN, and PHN onto GO-9-AA by pseudo-second order kinetic model showed a quite good agreement with measured data for both fast and the slow adsorption steps (nonlinear correlation coefficients of the model for NAP, ACN, and PHN onto GO-9-AA were 0.991, 0.996 and 0.994, respectively). Constant rates of NAP, ACN, and PHN adsorption, in the liquid phase, are comparable to those calculated for other aromatic hydrocarbons on different adsorbents. The experimental values of  $q_e$  for NAP, ACN, and PHN were 56.3, 46.24 and 45.92 mg g<sup>-1</sup>, respectively, which are consistent with the  $q_e$  values calculated from the pseudo-second order model which summarized in Table 3. The good agreement of adsorption kinetic data with pseudo-second order model indicates that adsorption of the target adsorbates on GO-9-AA is due to a chemical adsorption.

### 3. 5. Comparison of Adsorption Behavior Based on Literature Data

The efficacy of GO-9-AA adsorbent was evaluated in comparison with other adsorbents (Table 4). As it can be seen, the sorption capacity of PAHs on GO-9-AA composites is much higher than other adsorbents.

### 3. 6. Desorption

For the environmental protection and economic purposes, adsorbents should both have adequate capacity to decrease the pollutants concentration to satisfy environmental protection agencies standards and have been recycled and reused in successive cycles because they might have either precious raw substance or consist of hazardous materials. The recycling NAP, ACN, PHN and the regeneration of GO-9-AA are illustrated in Figure 8. The adsorption-desorption experiment results demonstrated that the efficiency of the applied GO-9-AA adsorbent

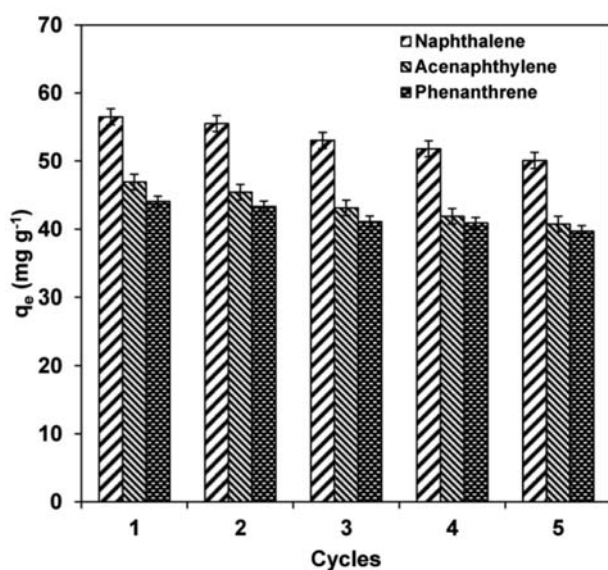
Table 3. Kinetic parameters of NAP, ACN, and PHN adsorption on GO-9-AA

Adsorbates	Pseudo-first-order			Pseudo-second-order			
	$k_1$ (min <sup>-1</sup> )	$q_{e,exp}$ (mg g <sup>-1</sup> )	$R^2$	$q_{e,cal}$	$k_2$ (mg g <sup>-1</sup> min <sup>-1</sup> )	$q_{e,cal} R^2$ (mg g <sup>-1</sup> )	
NAP	56.30	0.50	51.79	0.974	0.71	54.14	0.991
ACN	46.24	0.56	43.41	0.991	0.80	45.21	0.996
PHN	45.92	0.49	42.16	0.985	0.67	44.09	0.994

**Table 4.** Comparison of maximum adsorption capacity of different adsorbents for adsorption of PAHs

Adsorbent	Adsorbate	Adsorption capacity (mg.g <sup>-1</sup> )	Temperature (°C)	Equilibrium Time (hour)	References
SBA-15-NH <sub>2</sub>	NAP	1.63	25	10	44
	ACN	1.01			
	PHN	0.60			
PMO	NAP	46.64	28	50	45
RHAC	NAP	63.60	28	120	46
Activated carbon (Coconut Shell)	PHN	20.22	25	1	47
Multilayer Graphene	PHN	28.1	25	NA	48
MWCNT30	PHN	14.1	25	NA	49
Biochar	PHN	14	25	672	50
C60, Fullerene	NAP	2.3	25	72	51
Activated carbon	NAP	58.36	25	280	52
Zeolite	NAP	29.59	25	6	53
	NAP	78.08			
	PHN	52.02			
GO-9-AA	ACN	57.60	25	72	Present study
	PHN	52.02			

was satisfactory for the removal of target PAHs by removing 94% (56.50 mg g<sup>-1</sup>), 79% (46.92 mg g<sup>-1</sup>), and 74% (44.24 mg g<sup>-1</sup>) of NAP, ACN, and PHN, respectively in the first cycle. As can be noticed on Figure 8, the absorption capacity of GO-9-AA remained essentially the same after five successive cycles of testing. After fifth adsorption-desorption experiments, the efficiency of GO-9-AA was 83.5% (50.09 mg g<sup>-1</sup>), 68% (41.00 mg g<sup>-1</sup>), and 66% (39.90 mg g<sup>-1</sup>) of NAP, ACN, and PHN, respectively. The negligible decrease in the GO-9-AA capacity (around 10%) revealed the good reusability and stability of this adsorbent; therefore, it could be a suitable choice to be used efficiently for the treatment of wastewater polluted by PAHs.

**Fig. 8.** Recycling of GO-9-AA in the adsorption of NAP, ACN, and PHN, at room temperature, and pH = 7.0

### 3. 7. Adsorption Mechanism

Isotherm and kinetic parameters of NAP, ACN, and PHN adsorption on GO-9-AA are listed in Table 2 and 3, respectively. As it can be seen, the maximum adsorption capacity ( $q_e$ ) for three adsorbates are in the following order of magnitude NAP>ACN>PHN onto GO-9-AA. A similar behavior was also observed for the adsorption coefficient ( $K_d = q_e/C_e$ , in Fig.9) values at different equilibrium concentrations. As it depicted in Figure 9, adsorption coefficients for NAP, ACN, and PHN have a similar trend. However, a marked decrease in the  $K_d$  values for the three adsorbates (magnitude of decrease was in the order of NAP>ACN>PHN) was different. Based on the assumptions of Freundlich isotherm model, removal of NAP, ACN, and PHN by heterogeneous adsorption onto GO-9-AA is concerning to the presence of high surface energy sites, such as defects, edges, and groove areas.<sup>60,61</sup> In this case, three adsorbates would primarily be adsorbed with high affinities to these regions. Inherent surface heterogeneity on GO and increasing the amount of groove and folded regions of GO after functionalization (Figure 5) give rise to change in homogeneities into the modified GO. Uneven charge sharing on the GO-9-AA could generate high active region in wrinkles and defect parts from the chemical perspective; as a result, NAP, ACN, and PHN could be adsorbed more in these active sites. As Figure 9 shows, adsorption coefficient values for three adsorbates reduce considerably with increasing concentrations, which is in agreement with the  $K_d-C_e$  curve obtained in the current study for GO-9-AA.

Figure 9 shows that the adsorption of three adsorbates is favorable at a low concentration. Also, the starting point and decreasing slope for NAP is larger than the other two adsorbates, i.e., ACN, and PHN which shows adsorption of NAP is more favorable than ACN, and PHN. Nevertheless, this is not consistent with the hydrophobi-

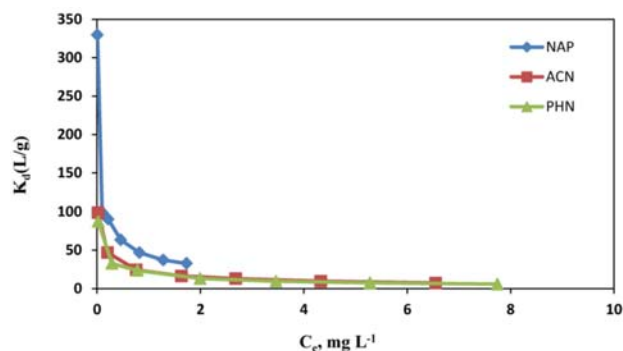


Fig. 9. Adsorption coefficients of NAP, ACN, and PHN onto GO-9-AA in different concentrations

city ( $K_{ow}$ ) trend of the target PAHs, i.e.,  $PHN > ACN > NAP$ . Wang and et al. suggested that different adsorption capacities of PAHs by carbonic adsorbents after eliminating hydrophobic effect might be due to sieving effect. Since adsorption of NAP, especially in the low concentration with approximately high solubility range is more favorable than ACN, and PHN; this shows more heterogeneous regions such as wrinkle surfaces, which have rich  $\pi$ -electron density onto GO-9-AA and readily available for the molecule with a smaller size.

Finally, several possible interactions between GO-9-AA and aromatic compounds (as an adsorbate) are responsible for the adsorption of NAP, ACN, and PHN. These interactions are a hydrophobic effect, electrostatic and electron donor-acceptor (EDA). Based on the adsorption mechanism between aromatic compounds and carbonaceous adsorbents<sup>63</sup> EDA interaction was proposed to be the main mechanism for adsorption of NAP, ACN, and PHN on GO-9-AA. One type of EDA interaction is  $\pi$ - $\pi$  EDA interaction.  $\pi$ - $\pi$  EDA interaction is specific and noncovalent, that exists between electron-rich and electron-poor compounds. The existence of anthracene rings on GO-9-AA makes it more electron-rich; therefore, the  $\pi$ - $\pi$  EDA interactions between three adsorbates and GO-9-AA surface will be stronger and easier.

## 4. Conclusion

GO-9-AA composite was successfully prepared via a facial strategy, characterized and its performance evaluated for the removal of NAP, ACN, and PHN. Incorporation of 9-aminoanthracene in the structure of GO led to both high adsorption capacity and fast removal kinetics that was proved by isotherm and kinetic experiments. The adsorption isotherm and kinetic data were fitted better by Freundlich and pseudo-second-order, respectively. It seems that more conformational change of GO after functionalization with 9-aminoanthracene and stronger electron donor-acceptor interaction between NAP, ACN, and PHN with modified GO are the main reasons for higher

adsorption capacity of GO-9-AA for the removal of the target adsorbates. Furthermore, the adsorption efficacy of GO-9-AA was evaluated in comparison with other adsorbents. The results showed that the adsorption capacity of GO-9-AA for the removal of target PAHs is much higher than other adsorbents. Therefore, GO-9-AA could be considered as a promising adsorbent for the removal of PAHs from water in real world applications.

## 5. Acknowledgements

The financial support from the Iranian National Science Foundation (Grant No. 93026590) and University of Kashan is gratefully acknowledged.

## 6. References

- H. Guo, T. Jiao, Q. Zhang, W. Guo, Q. Peng and X. Yan, *Nanoscale Res. Lett.* **2015**, *10*, 272. <https://doi.org/10.1186/s11671-015-0931-2>
- A. Balati, A. Shahbazi, M. M. Amini, S. H. Hashemi and K. Jadidi, *Eur. J. Environ. Sci.* **2014**, *4*.
- D. P. Arfsten, D. J. Schaeffer and D. C. Mulveny, *cotoxicol. Environ. Saf.* **1996**, *33*, 1–24. <https://doi.org/10.1006/eesa.1996.0001>
- M. Maier, D. Maier and B. Lloyd, *Water Res* **2000**, *34*, 773–786. [https://doi.org/10.1016/S0043-1354\(99\)00230-4](https://doi.org/10.1016/S0043-1354(99)00230-4)
- X. Zhang, S. Xie, M. C. Paau, B. Zheng, H. Yuan, D. Xiao and M. M. F. Choi, *J. Chromatogr. A* **2012**, 1247, 1–9. <https://doi.org/10.1016/j.chroma.2012.05.047>
- S.-S. Cai, J. A. Syage, K. A. Hanold and M. P. Balogh, *Anal. Chem* **2009**, *81*, 2123–2128. <https://doi.org/10.1021/ac802275e>
- Y. Ide, Y. Nakasato and M. Ogawa, *J. Am. Chem. Soc* **2010**, *132*, 3601–3604. <https://doi.org/10.1021/ja910591v>
- W. Chen, L. Duan, L. Wang and D. Zhu, *Environ. Sci. Technol* **2008**, *42*, 6862–6868. <https://doi.org/10.1021/es8013612>
- G. D. Sheng, D. D. Shao, X. M. Ren, X. Q. Wang, J. X. Li, Y. X. Chen and X. K. Wang, *J Hazard Mater* **2010**, *178*, 505–516; <https://doi.org/10.1016/j.jhazmat.2010.01.110>
- Y. Huang, A. N. Fulton and A. A. Keller, *Sci. Total Environ* **2016**, *571*, 1029–1036. <https://doi.org/10.1016/j.scitotenv.2016.07.093>
- P. Zuman and J. Ludvik, *Electroanalysis* **2000**, *12*, 879–888. [https://doi.org/10.1002/1521-4109\(200008\)12:12<879::AID-ELAN879>3.0.CO;2-O](https://doi.org/10.1002/1521-4109(200008)12:12<879::AID-ELAN879>3.0.CO;2-O)
- Z. Wu and L. Zhu, *J Environ Sci* **2012**, *24*, 248–253. [https://doi.org/10.1016/S1001-0742\(11\)60780-8](https://doi.org/10.1016/S1001-0742(11)60780-8)
- D. T. Sponza and R. Oztekin, *Chem. Eng. j.* **2010**, *162*, 142–150. <https://doi.org/10.1016/j.cej.2010.05.014>
- D. T. Sponza and R. Oztekin, *Bioresour Technol* **2010**, *101*, 8639–8648. <https://doi.org/10.1016/j.biortech.2010.06.124>

15. S. Rengaraj, Y. Kim, C. K. Joo and J. Yi, *J. Colloid Interface Sci* **2004**, 273, 14–21.  
<https://doi.org/10.1016/j.jcis.2004.01.007>
16. X. Luo, K. Ma, T. Jiao, R. Xing, L. Zhang, J. Zhou and B. Li, *Nanoscale Res. Lett* **2017**, 12, 99.  
<https://doi.org/10.1186/s11671-017-1864-8>
17. R. Xing, T. Jiao, Y. Liu, K. Ma, Q. Zou, G. Ma and X. Yan, *Polym. Sci.* **2016**, 8, 181.
18. X. Zhao, K. Ma, T. Jiao, R. Xing, X. Ma, J. Hu, H. Huang, L. Zhang and X. Yan, *Sci. Rep* **2017**, 7.
19. G. K. Ramesha, A. Vijaya Kumara, H. B. Muralidhara and S. Sampath, *J. Colloid Interface Sci* **2011**, 361, 270–27720.  
<https://doi.org/10.1016/j.jcis.2011.05.050>
20. T. Jiao, Y. Liu, Y. Wu, Q. Zhang, X. Yan, F. Gao, A. J. Bauer, J. Liu, T. Zeng and B. Li, *Sci. Rep* **2015**, 5, 12451.  
<https://doi.org/10.1038/srep12451>
21. S. Park and R. S. Ruoff, *Nat. Nanotechnol* **2009**, 4, 217–224.  
<https://doi.org/10.1038/nnano.2009.58>
22. M. J. Allen, V. C. Tung and R. B. Kaner, *Chem. Rev* **2009**, 110, 132–145. <https://doi.org/10.1021/cr900070d>
23. D. R. Dreyer, S. Park, C. W. Bielawski and R. S. Ruoff, *Chem. Soc. Rev* **2010**, 39, 228–240.  
<https://doi.org/10.1039/B917103G>
24. X. Yuan, Y. Wang, J. Wang, C. Zhou, Q. Tang and X. Rao, *Chem. Eng. J.* **2013**, 221, 204–213.  
<https://doi.org/10.1016/j.cej.2013.01.090>
25. Y.-B. Luo, J.-S. Cheng, Q. Ma, Y.-Q. Feng and J.-H. Li, *Anal. Methods* **2011**, 3, 92–98.  
<https://doi.org/10.1039/C0AY00624F>
26. R. Kempaiah, S. Salgado, W. L. Chung and V. Maheshwari, *Chem. Commun.* **2011**, 47, 11480–11482.  
<https://doi.org/10.1039/c1cc15096k>
27. C. Braun, C. Cook, C. Merritt and J. Rousseau, *ORG. SYNTH* **1951**, 31, 77–79.  
<https://doi.org/10.15227/orgsyn.031.0077>
28. L. Janovec, G. Suchár, J. Imrich, P. Kristian, V. Sasinková, J. Alföldi and E. Sedláč, *Collect. Czech. Chem. Commun* **2002**, 67, 665–678.  
<https://doi.org/10.1135/cccc20020665>
29. J. Sun, Z. Chen, M. Ge, L. Xu and M. Zhai, *J. Hazard. Mater.* **2013**, 244–245, 94–101.  
<https://doi.org/10.1016/j.jhazmat.2012.11.043>
30. M. S. Morey, S. O'Brien, S. Schwarz and G. D. Stucky, *Chem. Mater* **2000**, 12, 898–911.  
<https://doi.org/10.1021/cm9901663>
31. C. B. Vidal, A. L. Barros, C. P. Moura, A. C. A. de Lima, F. S. Dias, L. C. G. Vasconcellos, P. B. A. Fechine and R. F. Nascimento, *J. Colloid Interface Sci* **2011**, 357, 466–473.  
<https://doi.org/10.1016/j.jcis.2011.02.013>
32. C. Namasivayam and D. Kavitha, *Dyes Pigm.* **2002**, 54, 47–58. [https://doi.org/10.1016/S0143-7208\(02\)00025-6](https://doi.org/10.1016/S0143-7208(02)00025-6)
33. J. Saikia, B. Saha and G. Das, *J. Hazard. Mater.* **2011**, 186, 575–582. <https://doi.org/10.1016/j.jhazmat.2010.11.036>
34. S. Sun, Y. Cao, J. Feng and P. Wu, *J. Mater. Chem. A* **2010**, 20, 5605–5607.
35. K. N. Kudin, B. Ozbas, H. C. Schniepp, R. K. Prud'Homme, I. A. Aksay and R. Car, *Nano Lett.* **2008**, 8, 36–41.  
<https://doi.org/10.1021/nl071822y>
36. A. Lerf, H. He, M. Forster and J. Klinowski, *J. Phys. Chem. B* **1998**, 102, 4477–4482.  
<https://doi.org/10.1021/jp9731821>
37. H.-K. Jeong, Y. P. Lee, R. J. Lahaye, M.-H. Park, K. H. An, I. J. Kim, C.-W. Yang, C. Y. Park, R. S. Ruoff and Y. H. Lee, *J. Am. Chem. Soc* **2008**, 130, 1362–1366.  
<https://doi.org/10.1021/ja076473o>
38. A. Fasolino, J. Los and M. I. Katsnelson, *Nat. Mater* **2007**, 6, 858–861. <https://doi.org/10.1038/nmat2011>
39. O. Glukhova and M. Slepchenkov, *Nanoscale.* **2012**, 4, 3335–3344. <https://doi.org/10.1039/c2nr30477e>
40. Z. Pei, L. Li, L. Sun, S. Zhang, X.-q. Shan, S. Yang and B. Wen, *Carbon.* **2013**, 51, 156–163.  
<https://doi.org/10.1016/j.carbon.2012.08.024>
41. J. Wang, Z. Chen and B. Chen, *Environ. Sci. Technol* **2014**, 48, 4817–4825. <https://doi.org/10.1021/es405227u>
42. L. N. Z. X.G. Luo, *J. Hazard. Mater* **2009**, 171, 340–347.  
<https://doi.org/10.1016/j.jhazmat.2009.06.009>
43. X. Luo, C. Wang, L. Wang, F. Deng, S. Luo, X. Tu and C. Au, *Chem. Eng. J.* **2013**, 220, 98–106.  
<https://doi.org/10.1016/j.cej.2013.01.017>
44. A. Balati, A. Shahbazi, M. M. Amini and S. H. Hashemi, *J water reuse desal.* **2015**, 5, 50–63.
45. C. B. Vidal, A. L. Barros, C. P. Moura, A. C. De Lima, F. S. Dias, L. C. Vasconcellos, P. B. Fechine and R. F. Nascimento, *J. Colloid Interface Sci* **2011**, 357, 466–473.  
<https://doi.org/10.1016/j.jcis.2011.02.013>
46. S. Yakout, A. Daifullah and S. El-Reefy, *Adsorp. Sci. & Technol.* **2013**, 31, 293–302.  
<https://doi.org/10.1260/0263-6174.31.4.293>
47. C. Zhang, X. Zhang, Z. Huang, D. Huang and Q. Cheng, *J Environ Anal Toxicol* **2012**, 2012.
48. J. Zhao, Z. Wang, Q. Zhao and B. Xing, *Environ. Sci. Technol* **2013**, 48, 331–339.  
<https://doi.org/10.1021/es403873r>
49. K. Yang, L. Zhu and B. Xing, *Environ. Sci. Technol* **2006**, 40, 1855–1861. <https://doi.org/10.1021/es052208w>
50. T. H. Nguyen, H.-H. Cho, D. L. Poster and W. P. Ball, *Environ. Sci. Technol* **2007**, 41, 1212–1217.  
<https://doi.org/10.1021/es0617845>
51. X. Cheng, A. T. Kan and M. B. Tomson, *J. Chem. Eng. Data* **2004**, 49, 675–683.  
<https://doi.org/10.1021/je030247m>
52. B. Cabal, C. O. Ania, J. B. Parra and J. Pis, *Chemosphere.* **2009**, 76, 433–438.  
<https://doi.org/10.1016/j.chemosphere.2009.04.002>
53. C.-F. Chang, C.-Y. Chang, K.-H. Chen, W.-T. Tsai, J.-L. Shie and Y.-H. Chen, *J. Colloid Interface Sci* **2004**, 277, 29–34.  
<https://doi.org/10.1016/j.jcis.2004.04.022>
54. B. Pan, D. Lin, H. Mashayekhi and B. Xing, *Environ. Sci. Technol* **2008**, 42, 5480–5485.  
<https://doi.org/10.1021/es8001184>
55. P. Lazar, F. Karlický, P. Jurečka, M. Kocman, E. Otyepková, K. Šafářová and M. Otyepka, *J. Am. Chem. Soc* **2013**, 135,

- 6372–6377. <https://doi.org/10.1021/ja403162r>
56. B. X. D. Lin, *Environ. Sci. Technol* **2008**, 42, 7254–7259. <https://doi.org/10.1021/es801297u>
57. M. S. I. Efremenko, *Langmuir*. **2006**, 22, 3614–3621. <https://doi.org/10.1021/la052100u>
58. X. W. K. Yang, L. Zhu, B. Xing, *Environ. Sci. Technol* **2006**, 40, 5804–5810. <https://doi.org/10.1021/es061081n>
59. W. W. K. Yang, Q. Jing, L. Zhu, *Environ. Sci. Technol* **2008**, 42, 7931–7936. <https://doi.org/10.1021/es801463v>
60. J. J. P. M. Sander, *Environ. Sci. Technol* **2005**, 39, 1606–1615. <https://doi.org/10.1021/es049135l>
61. F.-G. Klärner and T. Schrader, *Acc. Chem. Res* **2012**, 46, 967–978.
62. M. Hardouin–Lerouge, P. Hudhomme and M. Sallé, *Chem. Soc. Rev* **2011**, 40, 30–43. <https://doi.org/10.1039/B915145C>
63. J. Leblond and A. Petitjean, *ChemPhysChem* **2011**, 12, 1043–1051. <https://doi.org/10.1002/cphc.201001050>
64. C. Chen and H. Whitlock Jr, *J. Am. Chem. Soc* **1978**, 100, 4921–4922. <https://doi.org/10.1021/ja00483a063>

## Povzetek

Modificiran grafenov oksid smo pripravili z namenom njegove uporabe kot odstranjevalca aromatskih onesnaževalcev iz vodnih raztopin. Grafenov oksid (GO) smo funkcionalizirali z 9-aminoantracenom in pripravili grafenov oksid 9-aminoantracena (GO-9-AA). Za karakterizacijo adsorbenta smo uporabili naslednje metode: infrardečo spektroskopijo (FTIR), rentgensko praškovno difrakcijo (XRD), termogravimetrično analizo (TGA), transmisijsko elektronsko mikroskopijo (TEM in ramansko spektroskopijo). Kot modelne aromatske ogljikovodike, primerne za preučevanje adsorpcije, smo uporabili naftalen (NAP), acenaftalen (ACN) in fenantren (PHN). Adsorbent GO-9-AA je bil zelo učinkovit v primeru odstranjevanja aromatskih ogljikovodikov iz vodnih raztopin. Ravnotežni podatki adsorpcijskih procesov sledijo Freundlichovemu modelu, maksimalne adsorpcijske kapacitete za preučevane aromatske ogljikovodike pa lahko podamo z zaporedjem NAP > ACN > PHN. Iz podatkov kinetične analize lahko razberemo, da je proces hiter in učinkovit in ustreza kinetičnemu modelu psevdodrugega reda. Obroči antracena na grafenovem oksidu (GO-9-AA) so »bogati« s  $\pi$  elektroni in zaradi tega pospešujejo interakcijo le-tega z aromatskimi ogljikovodiki (NAP, ACN in PHN).



Scientific paper

# The Methodology Applied in DPPH, ABTS and Folin-Ciocalteu Assays Has a Large Influence on the Determined Antioxidant Potential

Helena Abramovič, Blaž Grobin, Nataša Poklar Urih and Blaž Cigić\*

Department of Food Science and Technology, Biotechnical Faculty, University of Ljubljana, Jamnikarjeva 101, 1000 Ljubljana, Slovenia

\* Corresponding author: E-mail: [blaz.cigic@bf.uni-lj.si](mailto:blaz.cigic@bf.uni-lj.si)

Phone: +386 1 320 37 84 Fax: +386 1 256 62 96

Received: 29-03-2017

## Abstract

Antioxidant potential (AOP) is not only the property of the matrix analyzed but also depends greatly on the methodology used. The chromogenic radicals 2,2'-azino-bis(3-ethylbenzothiazoline-6-sulfonic acid) (ABTS<sup>•+</sup>), 2,2-diphenyl-1-picrylhydrazyl (DPPH<sup>•</sup>) and Folin-Ciocalteu (FC) assay were applied to estimate how the method and the composition of the assay solvent influence the AOP determined for coffee, tea, beer, apple juice and dietary supplements. Large differences between the AOP values depending on the reaction medium were observed, with the highest AOP determined mostly in the FC assay. In reactions with chromogenic radicals several fold higher values of AOP were obtained in buffer pH 7.4 than in water or methanol. The type of assay and solvent composition have similar influences on the reactivity of a particular antioxidant, either pure or as part of a complex matrix. The reaction kinetics of radicals with antioxidants in samples reveals that AOP depends strongly on incubation time, yet differently for each sample analyzed and the assay applied.

**Keywords:** Chromogenic radicals, antiradical activity, Folin-Ciocalteu, reaction kinetics, Trolox equivalents, solvent composition

## 1. Introduction

A dozen different methods can be found in the literature<sup>1</sup> for *in vitro* analysis of antioxidant properties of phenolic compounds. Among the most popular are those employing phospho-tungsto-molybdate in Folin-Ciocalteu (FC) reagent or chromogenic radicals such as 2,2'-azino-bis(3-ethylbenzothiazoline-6-sulfonic acid) (ABTS<sup>•+</sup>) and 2,2-diphenyl-1-picrylhydrazyl (DPPH<sup>•</sup>). Such radicals, with unpaired valence electron at one nitrogen atom, can be reduced by compounds with antioxidant properties and the assays are based on spectrophotometric measurements of unreacted radicals at the beginning and after a certain incubation time.

There is a long going debate as to whether results of such *in vitro* assays are relevant, since no correlation between *in vitro* antioxidant properties and health benefits has been confirmed<sup>2</sup> and rates of reaction of antioxidants with radicals are much more important for their effective-

ness than the stoichiometric values obtained by antioxidant assays.<sup>3,4</sup> Despite these limitations a great number of papers are published each year containing data about antioxidant potential (also activity and capacity) and total polyphenol content of various biological, pharmaceutical and food samples.

The incubation time for reaction of antioxidants with radical probe and FC reagent varies substantially between different studies and ranges from minutes to hours. Apart from their structural characteristics (number and position of –OH groups, inductive effects of other substituents present in the antioxidant molecule, steric hindrance/accessibility, packaging of an antioxidant around reactive species) the reactivity of an antioxidant depends significantly on reaction conditions such as solvent polarity, pH, temperature, type and concentration of reactive species.<sup>3,6–14</sup> Since the selection of the method, the time and reaction conditions adopted to evaluate the content of antioxidants in a given sample significantly

impact the determined values and, due to the fact that these parameters in a number of articles are relatively poorly described, it is very difficult to compare the results of AOP obtained for similar samples in different studies.

As shown in numerous studies, green and black tea, green and roasted coffee, apple juice, beer, and cranberry fruits are considered as antioxidant rich foods and exhibit notable AOP.<sup>15–20</sup> The primary purpose of the present study was to demonstrate how the selected method and composition of the assay solvent influence the reactivity of antioxidant compounds in the above mentioned foods with chromogenic radicals, DPPH<sup>•</sup> and ABTS<sup>•+</sup>, and with the FC reagent. The reactivity was evaluated utilizing the approach of reaction kinetics as well as stoichiometric calculations of AOP expressed in Trolox equivalents (TE). ABTS assay was carried out in water and in aqueous buffers pH 7.4 and pH 5.0. DPPH assay was performed in methanol (MeOH) and in mixtures of MeOH with water and aqueous buffers pH 7.4 and pH 5.0. FC assay was carried out only after one protocol.

## 2. Experimental

### 2.1. Sample Material

The samples included in our investigation: green tea (Green tea, Winston's Tea Company, UK), black tea (English breakfast, Winston's Tea Company, UK), green coffee (Finca la Providencia, 100% Arabica, Guatemala), roasted coffee (Green coffee roasted for 13 minutes, final temperature 223 °C; STA Impianti – Combi5), apple juice (100%, Fructal, Slovenia), beer (Pale lager, Union, Slovenia), dried cranberries (Brusnifem, Medex, Slovenia) and dried cranberries with added vitamin C (Cranberry kapseln mit vitamin C, Sunlife productions, Germany), were obtained from local suppliers.

### 2.2. Preparation of Sample Solutions

Coffee beans were ground using a laboratory scale mill and sieved through a No. 30 sieve. Crushed tea leaves were additionally homogenised in a mortar. 6.00 g of ground green or roasted coffee, and 1.00 g of green or black tea were transferred into a beaker and 100 ml boiling MilliQ water poured over. The beaker was covered with a watch glass to minimize evaporation and the suspension was mixed on a magnetic stirrer (300 rpm) for 5 min. Small amounts of evaporated water were compensated by MilliQ water (control by weighing). 100 mg of dietary supplement (dried cranberries, dried cranberries with added vitamin C) were transferred into a 15 ml centrifuge tube and extracted with 10.0 mL of MilliQ water by vortexing at room temperature for 5 min. All samples were filtered through 0.45- $\mu$ m cellulose acetate filters and used for the analysis of AOP within 1 h. Beer and

apple juice were transferred from freshly opened packages.

### 2.3. Reagents and Solvents

ABTS reagent, DPPH<sup>•</sup> reagent, Folin-Ciocalteu reagent, Trolox and ethanol (C<sub>2</sub>H<sub>5</sub>OH, 96%) were purchased from Sigma-Aldrich GmbH (Steinheim, Germany). Methanol (CH<sub>3</sub>OH, 99.9%), sodium carbonate (Na<sub>2</sub>CO<sub>3</sub>), sodium hydroxide (NaOH), acetic acid (CH<sub>3</sub>COOH) and sodium dihydrogen phosphate dihydrate (NaH<sub>2</sub>PO<sub>4</sub> × 2H<sub>2</sub>O) were obtained from Merck (Darmstadt, Germany). Manganese dioxide (MnO<sub>2</sub>) was obtained from Kemika (Zagreb, Croatia). The water used was purified using a Milli-Q system (resistivity >18 M $\Omega$  cm; Millipore).

### 2.4. Folin-Ciocalteu Assay

The FC assay was performed according to the modification of Gutfinger.<sup>21</sup> 50  $\mu$ L of appropriately diluted sample, 700  $\mu$ L of MilliQ water and 125  $\mu$ L of FC reagent (previously diluted 1:2 (v/v) with MilliQ water) were transferred into a 1.5 mL microcentrifuge tube and mixed by vortexing. After 5 min of incubation at 25 °C, an aqueous solution of Na<sub>2</sub>CO<sub>3</sub> (125  $\mu$ L, 20%, w/v) was added, and the sample mixed again and incubated for an additional 55 min at 25 °C. Final dilutions of samples in the test tubes are given in Supporting Information. The absorbance at 765 nm ( $A_{765}$ ) was measured on a Varian Cary 100 BIO UV-VIS spectrophotometer in a polystyrene cuvette with a 1 cm path length. Absorbance of the blank (50  $\mu$ L of MilliQ water instead of the sample) was subtracted from the absorbance of sample (three parallels).

### 2.5. The DPPH and ABTS Assays

The DPPH and ABTS assays were performed according to a modification of the method of Brand-Williams et al.<sup>22</sup> and Re et al.,<sup>23</sup> respectively. The DPPH<sup>•</sup> solution was prepared in MeOH and diluted to the concentration that would give an absorbance of 2.4 at 520 nm in the 1 cm pathlength cuvette. The radical cation of ABTS, ABTS<sup>•+</sup>, was produced by reacting ABTS with MnO<sub>2</sub> in aqueous solution followed by centrifugation and filtration. The ABTS<sup>•+</sup> solution was diluted with MilliQ water to the concentration that would give an absorbance of 2.4 at 734 nm in the 1 cm pathlength cuvette. All the solutions, buffers and solvents were incubated at 25 °C prior to analysis.

The assay solutions were prepared in 1.5 mL micro centrifuge tubes by mixing DPPH<sup>•</sup> or ABTS<sup>•+</sup> solution (500  $\mu$ L) with 450  $\mu$ L of MilliQ water, MeOH, acetate buffer (25 mM, pH 5.0) or phosphate buffer (5 mM, pH 7.4) for the DPPH assay, and MilliQ water, acetate buffer (25 mM, pH 5.0) or phosphate buffer (5 mM, pH 7.4) for the ABTS assay. The reactions were started by the addi-

tion of 50  $\mu\text{L}$  of the sample solution into the assay medium, with thorough mixing. Final dilutions of samples in the test tubes are given in Supporting Information. Each sample was prepared in three parallels. After 60 min incubation at 25  $^{\circ}\text{C}$  the absorbance at 520 nm in the DPPH assay ( $A_{520}$ ) and 734 nm in the ABTS assay ( $A_{734}$ ) was measured on a Varian Cary 100 BIO UV-VIS spectrophotometer in a 1 cm cuvette. The measured absorbance was subtracted from the corresponding absorbance of the controls (50  $\mu\text{L}$  of MilliQ water instead of the sample) after 60 min incubation. The data are expressed as  $dA_{520}$  or  $dA_{734}$ , respectively.

The assay solutions for analysis of the reaction kinetics of investigated antioxidants with DPPH $^{\bullet}$  (in the mixture of MeOH and phosphate buffer pH 7.4, and in MeOH) and ABTS $^{+\bullet}$  (in phosphate buffer pH 7.4 and in water) radicals were prepared in 1 cm quartz cuvettes with the stopper to prevent evaporation, by mixing DPPH $^{\bullet}$  or ABTS $^{+\bullet}$  solution (500  $\mu\text{L}$ ) with 450  $\mu\text{L}$  of the selected solvent. The reaction was started by the addition of 50  $\mu\text{L}$  of the sample solution (final dilutions in the assay solutions are given in Supporting Information) into the assay medium and  $A_{520}$  and  $A_{734}$ , respectively, were continuously monitored at 15 s intervals over 180 min on a Varian Cary 100 BIO UV-VIS spectrophotometer at 25  $^{\circ}\text{C}$ . The measured absorbances were subtracted from the corresponding absorbances of the controls at appropriate time points.

## 2. 6. Statistical Analysis

All samples were prepared in triplicate (three infusions prepared on different days). Each sample was analysed in three parallels. The standard deviations in determined AOP for the parallels were <5% and standard deviations in AOP for different sample preparations were <15%. The coefficient of variation (CV) and Pearson correlation coefficients ( $r$ ) were calculated with program Excel (Microsoft).

## 3. Results and Discussion

### 3. 1. AOP of Selected Drinks and Food Supplements Obtained by DPPH, ABTS and FC Assays

The values of  $A_{765}$ ,  $dA_{520}$  and  $dA_{734}$  determined after 60 min of incubation at selected dilutions (Supporting Information) of investigated beverages and dietary supplements were used to calculate the AOP with the DPPH, ABTS and FC method (Figure 1). For the purpose of comparison, the results were normalized according to the reactivity of Trolox determined under the same conditions and expressed as mmol TE per g of dry matter, or per L of beverage.<sup>13</sup>

From Figure 1 and considering the values for CV of AOPs (Table 1), the method for AOP determination is seen to have a large impact on the values obtained. Furthermore, differences within a single method reveal that the solvent influences the ability of antioxidants to scavenge chromogenic radicals. The notable differences in the determined AOP of investigated samples can be attributed to the fact that the reactivity of antioxidants depends largely on the interaction of antioxidants with the solvent i.e. H-bonds and deprotonation of phenolic –OH group that depends, besides on its pKa, on the pH of the reaction medium.<sup>7,24</sup> In such a complex system, the variety of interactions between the antioxidants that operate via different reaction mechanisms results in the specific overall effect. However, despite the significant differences between samples, some common features can be seen.

**Table 1.** Coefficients of variation (CV) for AOP of samples determined by DPPH, ABTS assays and all methods applied

Sample	CV (%)		
	DPPH	ABTS	all methods
Green tea	16	24	20
Black tea	23	26	24
Green coffee	58	32	51
Roasted coffee	50	31	43
Cranberry	49	36	46
Cranberry with vit. C	4	10	33
Pale lager beer	62	64	70
Apple juice	55	55	57

In general, the highest AOP for the majority of antioxidants, with the exception of green and black teas, was determined in the FC assay, followed by ABTS and DPPH assays in buffer pH 7.4 and in buffer pH 5 and the smallest one determined in MeOH (DPPH) or water (ABTS). For systems with similar compositions of phenolic compounds, e.g. green and black tea and roasted and green coffee, the AOP dependences on reaction medium are also similar. In the reactions of green and roasted coffee antioxidants with chromogenic radicals the influence of the studied solvents on reactivity was much greater with the DPPH assay (more than 100% higher AOP in buffer pH 7.4 than in the other three solvents) than with the ABTS assay. The largest difference in AOP assessed by different methods in different media was observed for beer antioxidants, as compared with the other investigated samples, resulting in three-fold greater AOP determined at pH 7.4 than in MeOH (DPPH $^{\bullet}$ ) and water (ABTS $^{+\bullet}$ ). When considering the effects of the reaction conditions on absolute levels of measured AOPs, the results with apple juice are similar to beer.

Although the main purpose of our study was not to measure the “absolute” AOP, comparison of our results with those in the literature should be considered. The AOP

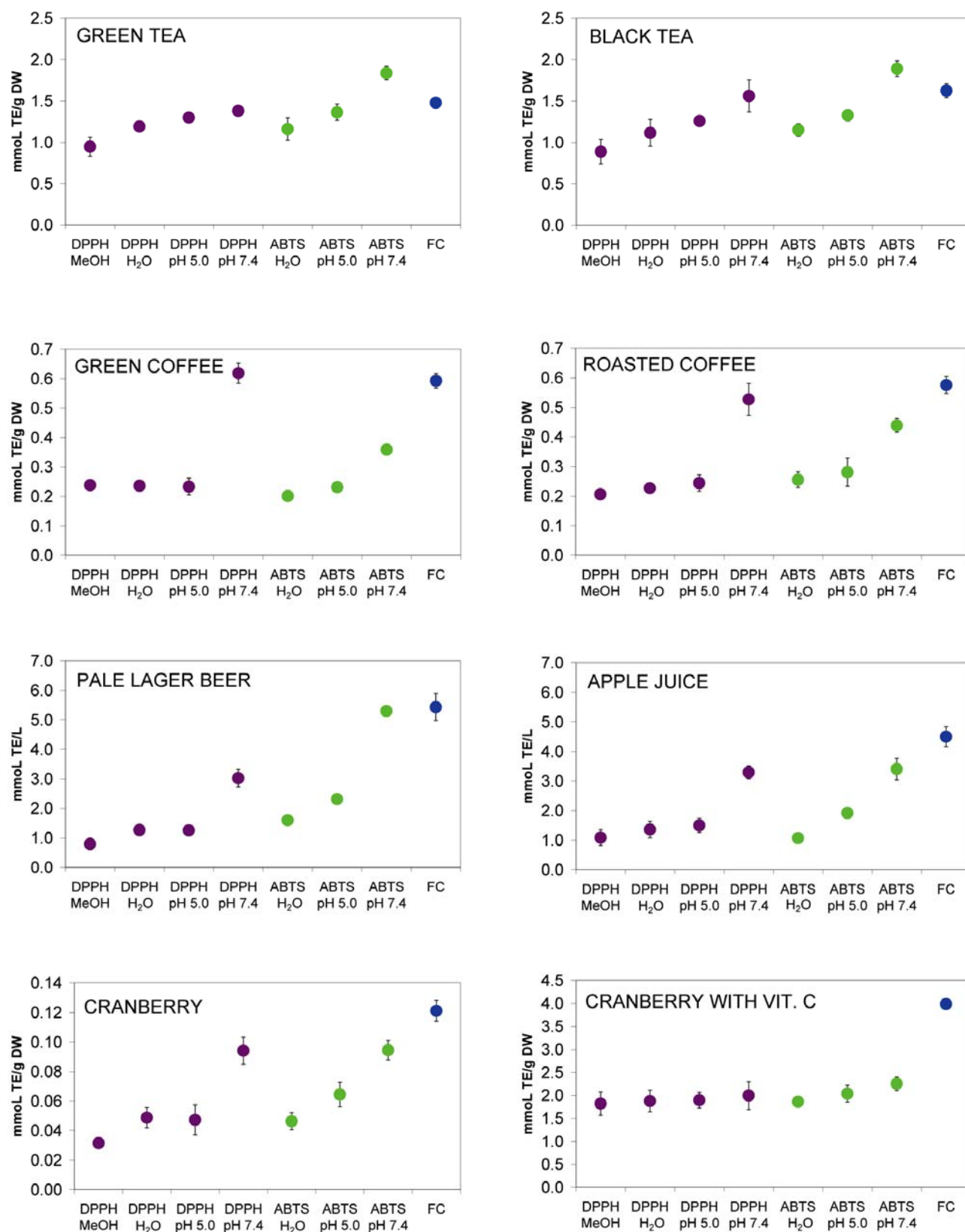


**Figure 1.** Antioxidant potential (AOP) of green tea, black tea, green coffee, roasted coffee, dietary supplement with dried cranberries, dietary supplement with dried cranberries and vitamin C, pale lager beer and apple juice in DPPH, ABTS and FC assays. The AOPs were determined after 60 min incubation of the properly diluted sample with the probe at 25 °C in the particular solvent. They are expressed as Trolox equivalents in mmol/g of dry weight or mmol/L of beverage.

in original papers was normalized according to the reactivity of Trolox.<sup>13</sup> The results reveal that the AOP values determined in our study are similar to those published elsewhere.<sup>15,16,18–20,25,26</sup> In general, the highest AOP values determined by these authors were those determined using the FC method. This is consistent with the results of our study. It should be noted that the DPPH and ABTS assays in their studies were conducted in MeOH or in water, where we have also obtained lower AOP values than in the FC assay, too.

Comparison of values of AOP for food supplements, for dried cranberries and for dried cranberries with added vitamin C, shows significant differences in absolute AOP values as well as in the influence of the solvent on the obtained AOP. The AOP of dried cranberries with added vit. C is almost two orders of magnitude higher than that of dried cranberry fruits, which in comparison to literature AOP data is of similar range though somewhat lower,<sup>17,27</sup> most probably due to losses incurred during drying and storage, since the published data were obtained by analysing fresh fruit. The labelled content of ascorbic acid (AA) in the enriched cranberry food supplement amounts to 1.4 mmol/g. Since Trolox and AA have similar molar reactivities in reactions with chromogenic radicals,<sup>13</sup> it can be estimated that approx. 75% of AOP of investigated sample can be attributed to the AA. The large contribution of AA to the AOP of dried cranberries with added vit. C is reflected in the results obtained by FC assay, being twofold greater than those obtained by chromogenic radicals, as was observed for AA.<sup>13</sup>

### 3. 2. The Influence of Solvent on the Kinetics of Reaction of Antioxidants with ABTS<sup>•+</sup> and DPPH<sup>•</sup> Radicals in Selected Drinks and Food Supplements

The kinetics of reaction of antioxidants in selected samples with chromogenic radicals were analyzed in solvents giving the lowest (water for ABTS<sup>•+</sup> or MeOH for DPPH<sup>•</sup>) and the highest (buffer pH 7.4 for both, ABTS<sup>•+</sup> and DPPH<sup>•</sup>) values of AOP after 60 min incubation. In order to compare the influence of incubation time on the value of AOP, the  $dA_{520}$  and  $dA_{734}$  values determined at 15 s intervals were normalized to the corresponding values obtained after 60 min incubation of the selected sample with chromogenic radical in a particular solvent. The determined value of AOP depends greatly on the time of incubation (Figure 2), the effect being dependent on the sample, the type of assay and the solvent. However, for both tests the shape of curves reveals a fast phase followed by a slow one.

The fast phase, often completed in the range of seconds, is mainly attributable to the oxidation of existing phenolic –OH groups.<sup>12,28–31</sup> The rate constants however depend greatly on the type of antioxidant and the solvent

composition.<sup>3,12</sup> In the present section we have not focused on the kinetics of the fast phases but rather on the amplitude that is directly proportional to the determined AOP, in order to show how incubation time influences its value. For both chromogenic radicals, with the exception of cranberry extract, beer and apple juice analyzed with DPPH<sup>•</sup> radical in MeOH, at least 50% of the “60 min” amplitude was reached after 1 min incubation.

At prolonged incubation times the kinetic profiles for the ABTS assays in buffer pH 7.4 and in water are similar. However, it is important to note that, despite similar kinetic profiles, the calculated AOP for all samples is much higher in buffer pH 7.4 than in water (Figure 1). For beer, where, as compared to other samples, the largest difference in AOP determined by ABTS assays in water and buffer pH 7.4 was observed after 60 min (3.3-fold), the difference in AOP would be even larger if AOP was calculated after prolonged incubation.

Comparison of kinetic profiles for DPPH assays in MeOH and buffer pH 7.4 reveals the same pattern for all analysed samples. The kinetics are much faster at pH 7.4 and, for green tea and coffee, the absorbance virtually levels off after 30 min, and only minor changes are observed up to 3 h incubation. In contrast to the DPPH assay at pH 7.4, the kinetics in MeOH are much slower and AOP depends greatly on the time of incubation. It should be stressed that a large relative AOP increase after prolonged incubation in MeOH does not mean that AOP in MeOH is higher than in buffer pH 7.4. For the majority of samples, AOP determined after 60 min incubation with DPPH in buffer pH 7.4 is ≈3-fold that in MeOH (Figure 1). Generally most of the amplitude of the slower phase can be attributed to secondary modifications of partially oxidized polyphenols and formation in the test tube of compounds with antioxidant properties.<sup>32</sup> It is known that oxidative cross-coupling that leads to the formation of dimers some, of which possess radical scavenging activity themselves, can contribute significantly to the overall AOP.<sup>6,33</sup> However, even for an early stage, the contribution to the initial amplitude of antioxidants formed from partially oxidized polyphenols cannot be neglected, especially for the solvents that increase the reaction rates. The presence in the sample of mixtures of antioxidants that differ in rate constant for their reaction with chromogenic radicals and have different propensities for secondary transformations undoubtedly results in a complex kinetic profile, as has been observed, even when oxidation of model compounds was analyzed.<sup>6,34</sup>

The solvent type is responsible for electron and/or hydrogen atom transfer which are characteristic not only in sequential proton loss electron transfer (SPLET) but also in hydrogen atom transfer, proton-coupled electron transfer and other mechanisms of the reaction of antioxidants with radicals.<sup>35</sup> Moreover, the change of hydrogen ion concentration (different buffer pH, or acidic methanol) may alter the dominant reaction mechanism.

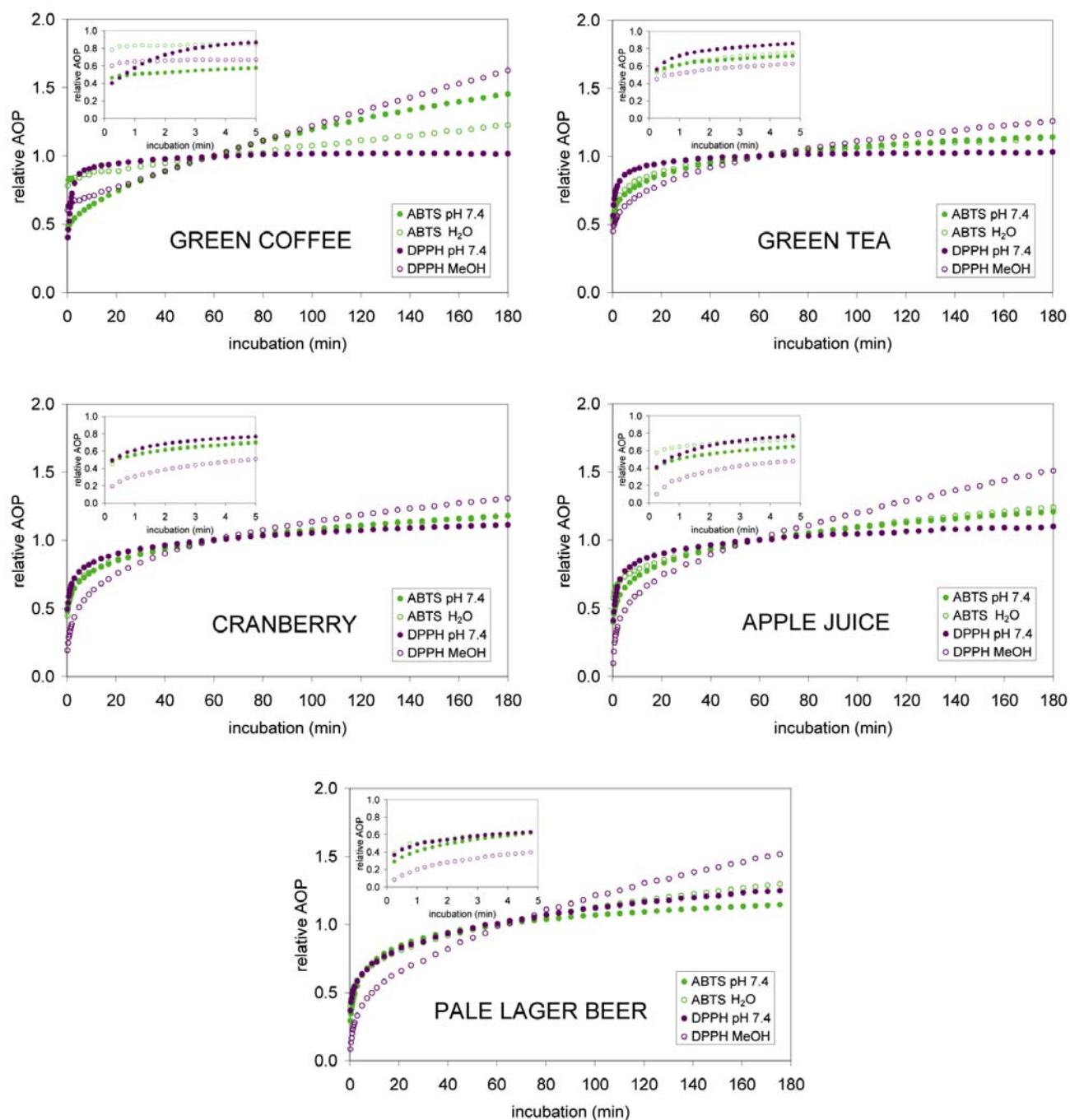


**Figure 2.** Influence of incubation time at 25 °C on the antioxidant potential (AOP) determined for green tea, green coffee, dietary supplement with dried cranberries, pale lager beer and apple juice in DPPH assay in methanol or DPPH assay in the mixture of methanol and buffer pH 7.4, and ABTS assays in MilliQ water or buffer pH 7.4. The  $dA_{520}$  and  $dA_{734}$  values obtained at certain time point were divided by  $dA_{520}$  or  $dA_{734}$  values measured after 60 min incubation in the particular solvent to give the relative AOP at a certain time point in comparison to the 60 min incubation for each of the four assays.

SPLET, which includes oxidation of the deprotonated form of the phenolic compound,  $ArO^-$  to  $ArO^*$ , is the predominant reaction mechanism of the phenolic compounds with different radicals in protic solvents.<sup>28,36–38</sup> Since the oxidation of the deprotonated form of phenolic compounds ( $ArO^- \rightarrow ArO^* + e^-$ ) (very fast) is preferred

over that of the corresponding phenol ( $ArOH \rightarrow ArO^* + H^+ + e^-$ ) (slow), in aqueous medium which supports the deprotonation of the phenol well and has higher H-bond accepting ability than MeOH, the oxidation of phenols is expected to be faster than in pure MeOH.<sup>7</sup> That is most likely the reason for the smaller initial amplitude observed

in MeOH (Figure 2). Solvents with high H-bond accepting ability strongly decrease the rate of abstracting hydrogen from ArOH and thus favour electron transfer processes from ArO<sup>-</sup>.<sup>28,39</sup> The AOP at neutral and basic pH, is expected to be higher than that in mildly acidic pH or absence of buffer (Figure 1), bearing in mind that the acid/base equilibrium of the –OH group at higher pH is shifted to the deprotonated form, ArO<sup>-</sup>. It must be considered that not only a difference in the reaction rates but also modifications of partially oxidized polyphenols, resulting in the formation of secondary antioxidants, contribute to AOP.

The large influence of incubation time on the determined AOP with DPPH in MeOH, which is the most common solvent for this type of assay, points to the importance of controlling time and temperature in the experiment. The fact that the AOP depends greatly on experimental conditions is often neglected and many papers, in which AOP of various samples is determined, are published each year without a detailed description of the experimental conditions.

Despite the above noted limitations, methods for evaluating AOP will remain useful tools for rapid assessment of the amounts of redox active compounds in complex matrices. There is, nevertheless, sufficient evidence that assays for estimating AOP should be performed under controlled and well defined conditions, that are properly described in the methods section, in order to enable comparison with published results.

### 3. 3. Correlation Between AOPs Determined in Different Assays and Different Solvents

Pearson correlation coefficients of AOPs for eight samples, determined in different assays and solvents, are listed in Table 2. In general the *r* values are large and for only four combinations are the values not significant at  $\alpha = 0.05$ . The strong correlations have also been observed for combinations of FC, ABTS and DPPH assays of food samples.<sup>15,40</sup> The correlations in our study that are not sig-

nificant at  $\alpha = 0.05$  were determined for DPPH in MeOH when correlated to the AOP obtained in DPPH and ABTS assays at pH 7.4 and FC assay. This is to be expected as the reactivity of ionized polyphenols in neutral and basic pH solutions is certainly different from that in MeOH. The correlation within ABTS and DPPH assays performed in different solvents was weakest for both radicals when AOP was determined at pH 7.4. Higher *r* values were observed when DPPH and ABTS assays at pH 7.4 were correlated to the FC assays than to the AOP values determined with chromogenic radicals in other solvents.

It should be stressed out that overall good correlation coefficients do not guarantee that AOPs determined by the two methods give similar TE values. For example, we have found strong correlation ( $r = 0.94$ ; significant at  $\alpha = 0.001$ ) between AOP determined with ABTS assay in pH 5 buffer and AOP determined by FC assay, but 90% higher AOP was on average determined by FC assay.

### 3. 4. Correlation Between AOPs Determined for Complex Samples and Model Antioxidants

In order to determine whether the influence of type of assay and of solvent composition on the reactivity of a model antioxidant is similar to that for complex samples where particular model antioxidant is a major redox active compound correlation analyses were performed (Table 3). The reactivities of model antioxidants that are important constituents of samples included in this study have been analyzed under the same conditions.<sup>13</sup> For both tea samples the highest *r* values were determined with catechin (CTH) and epigallocatechin gallate (EGCG) which are major constituents of tea polyphenols.<sup>16,41</sup> Additionally, for gallic acid (GA), that is a constituent of EGCG, the best correlation, although not statistically significant, was observed with tea samples. High correlations have been observed for green and roasted coffee with chlorogenic (CGA) and caffeic acids (CA) that are major polyphenolic compounds in coffee.<sup>20,42</sup> Cranberries contain a complex mixture of polyphenols with flavonoids as major con-

**Table 2.** The values of Pearson correlation coefficient for correlation between antioxidant potentials determined in various assays

		DPPH				ABTS	
		MeOH	H <sub>2</sub> O	pH 5	pH 7.4	H <sub>2</sub> O	pH 7.4
DPPH	H <sub>2</sub> O	0.97***					
	pH 5	0.96***	1.00***				
	pH 7.4	0.67	0.80*	0.80*			
ABTS	H <sub>2</sub> O	0.91**	0.97***	0.95***	0.77*		
	pH 5	0.83*	0.94***	0.93***	0.93***	0.95***	
	pH 7.4	0.54	0.71*	0.70	0.93***	0.78*	0.91**
FC	FC	0.69	0.80*	0.78*	0.95***	0.82*	0.94***

\*\*\* values are significant at the  $\alpha = 0.001$  level, \*\* are significant at the  $\alpha = 0.01$  and \* are significant at the  $\alpha = 0.05$  level

**Table 3.** The values of Pearson correlation coefficient for antioxidant potentials of food samples and model polyphenols determined in various assays

	GA	CGA	CTH	EGCG	CA	AA
Green tea	0.64	0.42	0.85**	0.75*	0.26	0.27
Black tea	0.46	0.63	0.92**	0.76*	0.50	0.40
Green coffee	-0.33	0.99***	0.66	0.47	0.96***	0.67
Roasted coffee	-0.08	0.95***	0.82*	0.54	0.86**	0.70
Cranberry	0.07	0.88**	0.86**	0.53	0.75*	0.73*
Cranberry with vit. C	-0.21	0.71*	0.46	-0.08	0.50	0.98***
Pale lager beer	0.33	0.70	0.83*	0.53	0.51	0.66
Apple juice	0.04	0.89**	0.81*	0.52	0.74*	0.75*

\*\*\* values are significant at the  $\alpha = 0.001$  level, \*\* are significant at the  $\alpha = 0.01$  and \* are significant at the  $\alpha = 0.05$  level

stituents,<sup>27,43</sup> which can be related to the high correlation with CTH. The fact that AA is the predominant antioxidant in vit. C enriched cranberry supplement is reflected in the excellent correlation with AA. For apple juice<sup>44,45</sup> and beer,<sup>18,46</sup> in which the major polyphenols are hydroxycinnamic acid and flavan-3-ols, the best correlation is observed with model antioxidants within these groups.

The data presented in Table 3 clearly show that the type of assay and the solvent composition have similar influences on the reactivity of a particular antioxidant, either pure or as part of a complex matrix.

## 4. Conclusions

Spectrophotometric methods for assessing the amount of redox active compounds in complex matrices as DPPH, ABTS and FC assays are widespread and are applied in areas of agricultural and food science, chemistry and pharmacy. We have shown that the small variations in experimental protocols that are often encountered in the literature can result in considerable differences in the reactivity of antioxidants in food samples and dietary supplements. This confirms that antioxidant activity/potential is not an inherent property of a compound but is strongly influenced by the nature of the reactive target species as well as by the environment in which the reaction takes place.

## 5. Abbreviations

A, absorbance; AA, ascorbic acid; ABTS<sup>+</sup>, 2,2'-azino-bis-3-ethylbenzothiazoline-6-sulfonic acid; AOP, antioxidant potential; ArOH, phenolic compound; CA, caffeic acid; CGA, chlorogenic acid; CTH, catechin; CV, coefficient of variation; DPPH<sup>•</sup>, 2,2-diphenyl-1-picrylhydrazyl; EGCG, epigallocatechin gallate; FC, Folin-Ciocalteu; GA, gallic acid; MeOH, methanol; r, Pearson correlation coefficient; SPLET, sequential proton loss electron transfer; TE, Trolox equivalents

## 6. Acknowledgments

This work was supported by Slovenian Research Agency contract P4-0121. The authors would like to thank Roger H. Pain for his valuable suggestions and discussion of the paper.

## 7. References

1. S. Chanda, R. Dave, *Afr. J. Microbiol. Res.* **2009**, *3* (13), 981–996.
2. R. G. Berger, S. Lunkenbein, A. Ströhle, A. Hahn, *Crit. Rev. Food Sci. Nutr.* **2012**, *52*, 162–171.  
<https://doi.org/10.1080/10408398.2010.499481>
3. J. Xie, K. M. Schaich, *J. Agric. Food Chem.* **2014**, *62* (19), 4251–4260. <https://doi.org/10.1021/jf500180u>
4. M. C. Foti, *J. Agric. Food Chem.* **2015**, *63*, 8765–8776.  
<https://doi.org/10.1021/acs.jafc.5b03839>
5. M. Foti, G. Ruberto, *J. Agric. Food Chem.* **2001**, *49*, 342–348. <https://doi.org/10.1021/jf0006527>
6. P. Goupy, C. Dufour, M. Loonis, O. Dangles, *J. Agric. Food Chem.* **2003**, *51* (3), 615–622.  
<https://doi.org/10.1021/jf0259381>
7. G. Litwinienko, K. U. Ingold, *Acc. Chem. Res.* **2007**, *40*, 222–230. <https://doi.org/10.1021/ar0682029>
8. L. Bertalanič, T. Košmerl, N. Poklar Ulrih, B. Cigić, *J. Agric. Food Chem.* **2012**, *60* (50), 12282–12288.  
<https://doi.org/10.1021/jf3041512>
9. A. L. Dawidowicz, D. Wianowska, M. Olszowy, *Food Chem.* **2012**, *131* (3), 1037–1043.  
<https://doi.org/10.1016/j.foodchem.2011.09.067>
10. A. L. Dawidowicz, M. Olszowy, *Eur. Food Res. Technol.* **2013**, *236* (6), 1099–1105.  
<https://doi.org/10.1007/s00217-013-1982-1>
11. J. Anissi, M. El Hassouni, A. Ouardaoui, K. A. Sendide, *Food Chem.* **2014**, *150*, 438–447.  
<https://doi.org/10.1016/j.foodchem.2013.11.009>
12. T. Prevc, N. Šegatin, N. Poklar Ulrih, B. Cigić, *Talanta* **2013**, *109*, 13–19.  
<https://doi.org/10.1016/j.talanta.2013.03.046>



13. H. Abramovič, B. Grobin., N. Poklar Ulrih, B. Cigić, Submitted for publication.
14. A. L. Dawidowicz, M. Olszowy, *Eur. Food Res. Technol.* **2010**, *231* (6), 835–840. <https://doi.org/10.1007/s00217-010-1333-4>
15. A. Floegel, D.-O. Kim, S.-J. Chung, S. I. Koo, O. K. Chun, *J. Food Compos. Anal.* **2011**, *24* (7), 1043–1048. <https://doi.org/10.1016/j.jfca.2011.01.008>
16. P. Carloni, L. Tiano, L. Padella, T. Bacchetti, C. Customu, A. Kay, E. Damiani, *Food Res. Int.* **2013**, *53* (2), 900–908. <https://doi.org/10.1016/j.foodres.2012.07.057>
17. J. Namiesnik, K. Veerasilp, M. Kupaska, K.-S. Ham, S.-G. Kang, Y.-K. Park, D. Barasch, A. Nemirovski, S. Gorinstein, *Eur. Food Res. Technol.* **2013**, *237* (5), 819–829. <https://doi.org/10.1007/s00217-013-2041-7>
18. S. S. Mitić, D. Đ. Paunović, A. N. Pavlović, S. B. Tošić, M. B. Stojković, M. N. Mitić, *Int. J. Food Prop.* **2014**, *17* (4), 908–922. <https://doi.org/10.1080/10942912.2012.680223>
19. C. S. G. Kitzberger, M. B. D. Scholz, M. D. Benassi, *Food Res. Int.* **2014**, *61*, 61–66. <https://doi.org/10.1016/j.foodres.2014.04.031>
20. T. Pilipczuk, B. Kusznerewicz, D. Zielińska, A. Bartoszek, *J. Food Sci. Technol.* **2015**, *52*, 5736–5744. <https://doi.org/10.1007/s13197-014-1646-6>
21. T. Gutfinger, *J. Am. Oil Chem. Soc.* **1981**, *58*, 966–968. <https://doi.org/10.1007/BF02659771>
22. W. Brand-Williams, M. E. Cuvelier, C. Berset, *Lebensm. Wiss. Technol.* **1995**, *28*, 25–30. [https://doi.org/10.1016/S0023-6438\(95\)80008-5](https://doi.org/10.1016/S0023-6438(95)80008-5)
23. R. Re, N. Pellegrini, A. Proteggente, A. Pannala, M. Yang, C. Rice-Evans, *Free Radic. Biol. Med.* **1999**, *26* (9–10), 1231–1237. [https://doi.org/10.1016/S0891-5849\(98\)00315-3](https://doi.org/10.1016/S0891-5849(98)00315-3)
24. M. Musialik, G. Litwinienko, *Org. Lett.* **2005**, *7* (22), 4951–4954. <https://doi.org/10.1021/ol051962j>
25. J. Lachman, M. Šulc, J. Sus, O. Pavlíková, *Hort. Sci.* **2006**, *33* (3) 95–102.
26. I. Juranović, Cindrić, M. Kunšić, M. Zeiner, G. Stinger, G. Rusak, *Croat. Chem. Acta* **2011**, *84* (3), 435–438.
27. E. J. Borowska, B. Mazur, R. G. Kopciuch, B. Buszewski, *Food Technol. Biotechnol.* **2009**, *47* (1), 56–61.
28. M. C. Foti, C. Daquino, C. Geraci, **2003**, *J. Org. Chem.* *69* (7), 2309–2314. <https://doi.org/10.1021/jo035758q>
29. O. Friaa, D. Brault, *Org. Biomol. Chem.* **2006**, *4*, 2417–2423. <https://doi.org/10.1039/b602147f>
30. R. B. Walker, J. D. Everette, *J. Agric. Food Chem.* **2009**, *57*, 1156–1161. <https://doi.org/10.1021/jf8026765>
31. M. Musialik, R. Kuzmicz, T. S. Pawłowski, G. Litwinienko, *J. Org. Chem.* **2009**, *74* (7), 2699–2709. <https://doi.org/10.1021/jo802716v>
32. H. Hotta, S. Nagano, M. Ueda, Y. Tsujino, J. Koyama, T. *Biochim. Biophys. Acta* **2002**, *1572*, 123–132. [https://doi.org/10.1016/S0304-4165\(02\)00285-4](https://doi.org/10.1016/S0304-4165(02)00285-4)
33. X. L. Jin, R. T. Yang, Y. J. Shang, F. Dai, Y. P. Qian, L. X. Cheng, B. Zhou, Z. L. Liu, *Chin. Sci. Bull.* **2010**, *55*, 2885–2890. <https://doi.org/10.1007/s11434-010-3064-0>
34. P. Terpine, H. Abramovič, *Food Chem.* **2010**, *121*, 366–371. <https://doi.org/10.1016/j.foodchem.2009.12.037>
35. A. L. Dawidowicz, M. Olszowy, *Talanta* **2012**, *97*, 312–317. <https://doi.org/10.1016/j.talanta.2012.04.036>
36. C. Iuga, J. R. Alvarez-Idaboy, N. Russo, *J. Org. Chem.* **2012**, *77* (8), 3868–3877. <https://doi.org/10.1021/jo3002134>
37. R. L. Prior, X. Wu, K. Schaich, *J. Agric. Food Chem.* **2005**, *53*, 4290–4302. <https://doi.org/10.1021/jf0502698>
38. Y. J. Shang, B. Y. Liu, M. M. Zhao, *Czech J. Food Sci.* **2015**, *33*, 210–216. <https://doi.org/10.17221/611/2014-CJFS>
39. M. Bietti, M. Salamone, G.A. DiLabio, S. Jockusch, N.J. Turro, *Org. Chem.* **2012**, *77*, 1267–1272. <https://doi.org/10.1021/jo201454c>
40. S. Dudonné, X. Vitrac, P. Coutière, M. Woillez, J. M. Mérillon, *J. Agric. Food Chem.* **2009**, *57* (5), 1768–1774. <https://doi.org/10.1021/jf803011r>
41. Y. Zuo, H. Chen, Y. Deng, *Talanta* **2002**, *57* (2), 307–316. [https://doi.org/10.1016/S0039-9140\(02\)00030-9](https://doi.org/10.1016/S0039-9140(02)00030-9)
42. C. L. Ky, J. Louarn, S. Dussert, B. Guyot, S. Hamon, M. Noirot, *Food Chem.* **2001**, *75*, 223–230. [https://doi.org/10.1016/S0308-8146\(01\)00204-7](https://doi.org/10.1016/S0308-8146(01)00204-7)
43. E. Pappas, K. M. Schaich, *Crit. Rev. Food Sci. Nutr.* **2009**, *49*, 741–781. <https://doi.org/10.1080/10408390802145377>
44. K. Kahle, M. Kraus, E. Richling, *Mol. Nutr. Food Res.* **2005**, *49*, 797–806. <https://doi.org/10.1002/mnfr.200500064>
45. M. Ceymann, E. Arrigoni, H. Schärer, A. Bozzi Nising, R. F. Hurrell, *J. Food Compos. Anal.* **2012**, *26* (1–2), 128–135. <https://doi.org/10.1016/j.jfca.2011.12.002>
46. M. Dvorakova, P. Hulin, M. Karabin, P. Dostalek, *Czech J. Food Sci.* **2007**, *25*, 182–188.

## Povzetek

Antioksidativni potencial (AOP) ni samo lastnost analiziranega vzorca, ampak je v veliki meri odvisen tudi od uporabljenih metodologij. Na primeru kromogenih radikalov 2,2'-azino-bis(3-etilbenzotiazolin-6-sulfonske kisline) (ABTS<sup>+</sup>), 2,2-difenil-1-pikrilhidrazila (DPPH<sup>•</sup>) in Folin-Ciocalteu (FC) metode smo pokazali, kako izbor metode in sestava topila, v katerem poteka reakcija, vplivata na določeno vrednost AOP kave, čaja, piva, jabolčnega soka in prehranskih dopolnil. V splošnem smo največje AOP vrednosti določili s FC metodo. Reakcijski medij ima velik vpliv na določeno vrednost AOP s kromogenima radikaloma, saj smo v pufru s pH 7,4 določili nekajkrat večji AOP kot v vodi ali metanolu. Izbor metode in sestava reakcijskega medija imata podoben vpliv na reaktivnost posameznega antioksidanta, tako čistega kot v mešanici z ostalimi antioksidanti. AOP je močno odvisen tudi od časa inkubacije, toda različno za posamezne vzorce in izbrane metode.

Scientific paper

# Synthesis, Crystal Structures and Catalytic Oxidation of Manganese(III) Complexes Derived from Salen-Type Schiff Base *N,N'*-Bis(5-nitrosalicylidene)ethane-1,2-diamine

Qing-Bin Li, Yong-Jun Han, Gan-Qing Zhao and Ling-Wei Xue\*

College of Chemistry and Chemical Engineering, Pingdingshan University, Pingdingshan Henan 467000, P.R. China

\* Corresponding author. E-mail: pdsuchemistry@163.com

Received: 05-04-2017

## Abstract

Two mononuclear Schiff base manganese(III) complexes,  $[\text{MnL}(\text{N}_3)(\text{OH}_2)] \cdot \text{CH}_3\text{OH}$  (**1**) and  $[\text{MnL}(\text{NCS})(\text{OH}_2)] \cdot \text{H}_2\text{O}$  (**2**), where L is the dianionic form of *N,N'*-bis(5-nitrosalicylidene)ethane-1,2-diamine, have been prepared and characterized by elemental analysis, IR and UV-Vis spectroscopy and single crystal X-ray diffraction. The Mn atom in each complex is in an octahedral coordination. Molecules of the complexes are linked through intermolecular hydrogen bonds. Catalytic properties for epoxidation of styrene by the complexes using PhIO and NaOCl as oxidant have been studied.

**Keywords:** Synthesis, Crystal structure, Schiff base, Manganese complex, Catalytic oxidation

## 1. Introduction

Schiff bases with salen-type are a kind of versatile ligands in coordination chemistry.<sup>1</sup> In recent years extensive studies have been made on the chemistry of manganese(III) complexes derived from Schiff bases due to their important role in several metalloenzymes and to understand their catalytic activities in many organic reactions.<sup>2</sup> Manganese complexes have interesting biological activities.<sup>3</sup> The involvement of manganese in many biological systems is well established. Manganese(III) salen complexes are among the most efficient catalysts for the epoxidation of various olefins with high selectivity and yield. Epoxidation of olefins catalyzed by manganese(III) salen complexes has been studied extensively since Kochi and coworkers described in 1986 that they are highly effective, chemoselective, and stereoselective catalysts.<sup>4</sup> Azide and thiocyanate are widely used because of their diverse binding modes which yield different types of molecules such as dimers, tetramers, one-, two-, or three-dimensional arrays.<sup>5</sup> In order to investigate the influence of the azide and thiocyanate ligands on manganese(III) complexes with tetradentate Schiff base ligands, as well as the catalytic oxidation property, we report here the synthesis, characterization, crystal structures and catalytic oxidation property of two new complexes  $[\text{MnL}(\text{N}_3)(\text{OH}_2)] \cdot$

$\text{CH}_3\text{OH}$  (**1**) and  $[\text{MnL}(\text{NCS})(\text{OH}_2)] \cdot \text{H}_2\text{O}$  (**2**), where L is the dianionic form of *N,N'*-bis(5-nitrosalicylidene)ethane-1,2-diamine.

## 2. Experimental

### 2.1. Materials and Methods

Manganese perchlorate, sodium azide and ammonium thiocyanate obtained from commercial sources were of analytical grade and used without further purification. 5-Nitrosalicylaldehyde and *N,N'*-ethane-1,2-diamine were purchased from Aldrich. The Schiff base  $\text{H}_2\text{L}$  was prepared according to the literature method.<sup>6</sup> Iodosylbenzene (PhIO) was prepared by the hydrolysis of iodobenzene diacetate.<sup>7</sup> Styrene and styrene oxide were purchased from Aldrich and used in epoxidation experiment without further purification. The styrene oxide was used as standard sample in GC analysis. CHN elemental analyses were carried out with a Finnigan EA 1112 elemental analyzer. IR spectra were performed on a Nicolet 470 spectrometer with KBr pellets in the 4000–400  $\text{cm}^{-1}$  region. UV-Vis spectra were recorded on a Lambda 35 spectrometer. The crystal determination was carried out on a Bruker SMART 1000 CCD area diffractometer. GC experiments were performed with Agilent 5977A Network

GC systems.  $^1\text{H}$  and  $^{13}\text{C}$  NMR data were recorded on a Bruker 300 MHz instrument.

**Caution!** Perchlorate and azide complexes of metal ions are potentially explosive. Only a small amount of material should be prepared, and it should be handled with caution.

## 2. 2. Synthesis of $[\text{MnL}(\text{N}_3)(\text{OH}_2)] \cdot \text{CH}_3\text{OH}$

The mixture of  $\text{NaN}_3$  (0.065 g, 1.00 mmol) and  $\text{Mn}(\text{ClO}_4)_2 \cdot 6\text{H}_2\text{O}$  (0.362 g, 1.00 mmol) in 50 mL methanol was stirred for half an hour with heating, then  $\text{H}_2\text{L}$  (0.358 g, 1.00 mmol) was added to the solution and the reaction continued to stirred for 1 h. After filtration, the deep brown filtrate was allowed to stand at room temperature for a week to deposit brown crystals of the complex in 37.2% yield. *Anal.* Calc. for  $\text{C}_{17}\text{H}_{18}\text{MnN}_7\text{O}_8$ : C, 40.57; H, 3.60; N, 19.48. Found: C, 40.38; H, 3.72; N, 19.35%. IR data (KBr;  $\nu$ ,  $\text{cm}^{-1}$ ): 3450 (m, br), 2041 (s), 1634 (s), 1601 (s), 1559 (w), 1501 (m), 1451 (s), 1343 (w), 1301 (m), 1093 (s), 948 (m), 853 (s), 799 (w), 693 (w), 545 (s). UV-Vis data in acetonitrile [ $\lambda_{\text{max}}$  (nm)]: 298, 343.

## 2. 3. Synthesis of $[\text{MnL}(\text{NCS})(\text{OH}_2)] \cdot \text{H}_2\text{O}$

The mixture of  $\text{NH}_4\text{NCS}$  (0.076 g, 1.0 mmol) and  $\text{Mn}(\text{ClO}_4)_2 \cdot 6\text{H}_2\text{O}$  (0.362 g, 1.00 mmol) in 50 mL methanol was stirred for half an hour with heating, then  $\text{H}_2\text{L}$  (0.358 g, 1.00 mmol) was added to the solution and the reaction continued to stirred for 1 h. After filtration, the deep brown filtrate was allowed to stand at room temperature for a week to deposit brown crystals of the complex in 45.0% yield. *Anal.* Calc. for  $\text{C}_{17}\text{H}_{16}\text{MnN}_5\text{O}_8\text{S}$ : C, 40.40; H, 3.19; N, 13.86. Found: C, 40.53; H, 3.33; N, 13.70%. IR data ( $\text{cm}^{-1}$ ): 3445 (m, br), 2067 (s), 1634 (s), 1601 (s), 1561 (w), 1500 (m), 1446 (s), 1345 (w), 1298 (w), 1102 (s), 993 (m), 951 (m), 855 (s), 799 (w), 696 (w), 547 (s). UV-Vis data in acetonitrile [ $\lambda_{\text{max}}$  (nm)]: 298, 343.

## 2. 4. X-ray Diffraction

Suitable single crystals of the complexes were mounted at the top of glass fibres and scanned on a Bruker SMART 1000 CCD area diffractometer with a  $\text{MoK}\alpha$  radiation ( $\lambda = 0.71073 \text{ \AA}$ ) at 298(2) K. The unit cell dimensions were obtained with the least-squares refinements and the structures were solved and refined by direct methods with SHELXTL-97 program.<sup>8</sup> The final refinement was performed by full-matrix least-squares techniques with anisotropic thermal parameters for the non-hydrogen atoms on  $F^2$ . The water and hydroxyl hydrogen atoms (O3 and O8 for **1** and **2**) were located from difference Fourier maps, with O–H and H...H distances restrained to 0.85(1)

and 1.37(2)  $\text{Å}$ , respectively. The remaining hydrogen atoms were placed geometrically, with  $U_{\text{iso}}(\text{H})$  restrained to 1.2  $U_{\text{eq}}(\text{C})$  and 1.5  $U_{\text{eq}}(\text{C}_{\text{methyl}})$ . Multi-scan absorption correction was applied by using the SADABS program.<sup>9</sup> Crystallographic data are summarized in Table 1.

**Table 1.** Crystal and structure refinement data for the complexes

	<b>1</b>	<b>2</b>
Formula	$\text{C}_{17}\text{H}_{18}\text{MnN}_7\text{O}_8$	$\text{C}_{17}\text{H}_{16}\text{MnN}_5\text{O}_8\text{S}$
FW	503.32	505.35
Crystal system	Monoclinic	Monoclinic
Space group	$P2_1/n$	$P2_1/c$
$a/\text{Å}$	13.8160(9)	13.936(2)
$b/\text{Å}$	12.2649(8)	12.707(2)
$c/\text{Å}$	13.8286(9)	13.067(2)
$\beta/^\circ$	117.280(1)	116.187(2)
$V/\text{Å}^3$	2082.7(2)	2076.5(5)
$Z$	4	4
$\mu/\text{mm}^{-1}(\text{Mo-K}\alpha)$	0.696	0.793
Reflections/parameters	11921/308	11814/301
Independent reflections	4529	4516
Obs. reflections [ $I \geq 2\sigma(I)$ ]	3836	3623
Restraints	4	6
$F(000)$	1032	1032
Goodness of fit on $F^2$	1.081	1.050
$R_1, wR_2$ [ $I \geq 2\sigma(I)$ ] <sup>a</sup>	0.0297, 0.0816	0.0411, 0.1148
$R_1, wR_2$ (all data) <sup>a</sup>	0.0380, 0.0890	0.0538, 0.1294

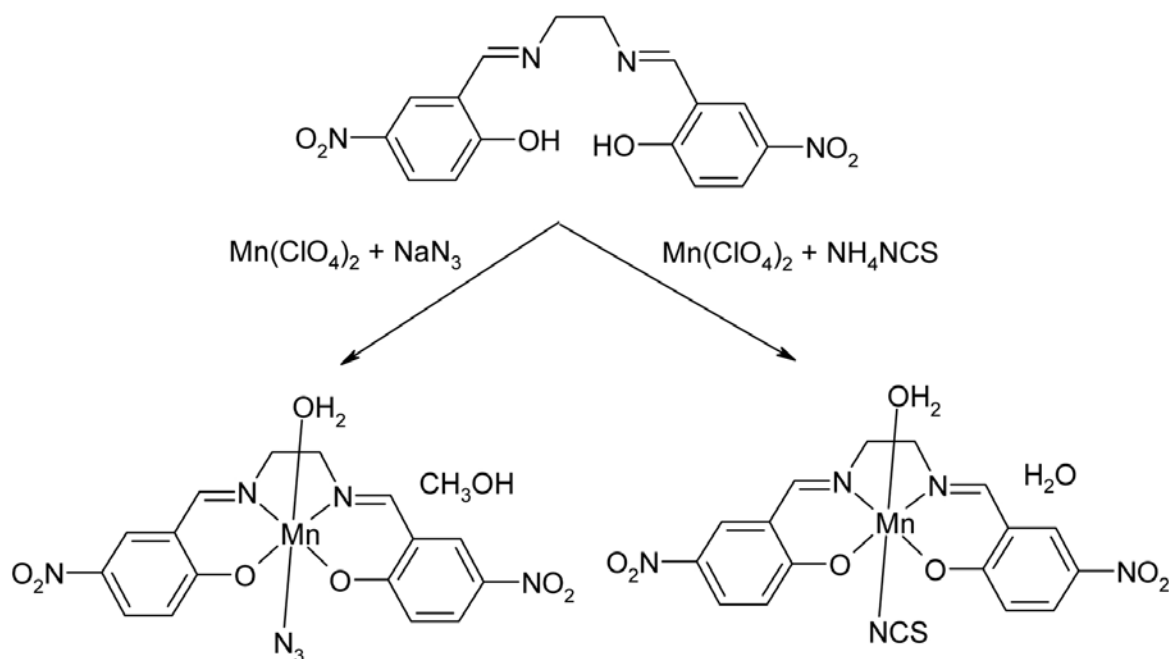
$$^a R_1 = \sum \|F_o\| - |F_c| / \sum \|F_o\|, wR_2 = [\sum w(F_o^2 - F_c^2)^2 / \sum w(F_o^2)^2]^{1/2}$$

## 2. 5. General Method for Styrene Oxidation

The oxidation reactions were carried out at room temperature in acetonitrile under nitrogen atmosphere with constant stirring. The composition of the reaction mixture was 2.00 mmol of styrene, 2.00 mmol of chlorobenzene (internal standard), 0.10 mmol of Mn(III) complex (catalyst) and 2.00 mmol iodobenzene or sodium hypochlorite (oxidant) in 5.00 mL freshly distilled acetonitrile. When the oxidant was sodium hypochlorite, the solution was buffered to pH 11.2 with  $\text{NaH}_2\text{PO}_4$  and  $\text{NaOH}$ .<sup>10</sup> The composition of reaction medium was determined by GC with styrene and styrene epoxide quantified by the internal standard method (chlorobenzene). All other products detected by GC were mentioned as others. For each complex the reaction time for maximum epoxide yield was determined by withdrawing periodically 0.1 mL aliquots from the reaction mixture and this time was used to monitor the efficiency of the catalyst on performing at least two independent experiments. Blank experiments with each oxidant and using the same experimental conditions except catalyst were also performed.

### 3. Results and Discussion

Complexes **1** and **2** were synthesized according to the procedure as described in Scheme 1.



Scheme 1. The synthetic procedure for the complexes

#### 3.1. Crystal Structure Description of the Dioxomolybdenum Complexes

The structures of complexes **1** and **2** are shown in Figs. 1 and 2, respectively. Selected bond lengths and bond angles are listed in Table 2. The distances and angles related to the hydrogen bonding are listed in Table 3.

Single-crystal X-ray structural analysis revealed that both complexes are similar. The asymmetric unit of each complex contains a mononuclear manganese complex molecule and a solvent molecule, *viz.* methanol for **1** and water for **2**. The Mn atoms in the complexes are in octahedral environment consisting of the N<sub>2</sub>O<sub>2</sub> donor set of the Schiff base ligands, the oxygen donor of water ligands, and the terminal nitrogen donor of the azide or thiocyanate ligand. The equatorial plane of the octahedral coordination is defined by the phenolate oxygen and imino nitrogen of the Schiff base ligands, with the Mn atoms deviate from the least-squares planes by 0.061(2) Å for **1** and 0.089(2) Å for **2**. The Ni–N and Ni–O bond lengths are comparable to the corresponding values observed in manganese complexes with Schiff base ligands.<sup>11</sup> The axial Mn1–N5 and Mn1–O3 bond lengths are longer than the equatorial bonds, which is caused by Jahn-Teller effects expected for d<sup>4</sup> high spin manganese(III) systems.<sup>12</sup> The azide and thiocyanate ligands are quasi-linear, with

angles of 178.8(2)° for **1** and 177.8(3)° for **2**. The plane defined by N1–N2–O1–O2 forms dihedral angles of 17.9(3)° and 13.1(3)° for **1**, and 14.8(3)° and 16.7(3)° for **2**, with C1–C6 and C11–C16 benzene rings, respectively.

Table 2. Selected bond lengths (Å) and angles (°) for the complexes

<b>1</b>			
Mn1–O1	1.8745(12)	Mn1–O2	1.8844(12)
Mn1–N1	1.9737(14)	Mn1–N2	1.9766(13)
Mn1–O3	2.3031(15)	Mn1–N5	2.2288(17)
O1–Mn1–O2	91.61(5)	O1–Mn1–N1	91.80(6)
O2–Mn1–N1	174.92(6)	O1–Mn1–N2	174.25(6)
O2–Mn1–N2	92.72(6)	N1–Mn1–N2	83.63(6)
O1–Mn1–N5	95.91(6)	O2–Mn1–N5	93.58(6)
N1–Mn1–N5	89.82(7)	N2–Mn1–N5	87.60(6)
O1–Mn1–O3	89.72(6)	O2–Mn1–O3	90.32(6)
N1–Mn1–O3	85.93(6)	N2–Mn1–O3	86.47(6)
N5–Mn1–O3	173.05(6)		
<b>2</b>			
Mn1–O1	1.8830(16)	Mn1–O2	1.9107(16)
Mn1–N1	1.981(2)	Mn1–N2	1.979(2)
Mn1–O3	2.297(2)	Mn1–N5	2.205(3)
O1–Mn1–O2	93.49(7)	O1–Mn1–N2	172.49(9)
O2–Mn1–N2	91.63(8)	O1–Mn1–N1	91.36(8)
O2–Mn1–N1	172.62(8)	N2–Mn1–N1	83.04(9)
O1–Mn1–N5	92.31(9)	O2–Mn1–N5	94.78(9)
N2–Mn1–N5	92.74(10)	N1–Mn1–N5	90.58(10)
O1–Mn1–O3	91.55(8)	O2–Mn1–O3	89.49(8)
N2–Mn1–O3	83.00(8)	N1–Mn1–O3	84.81(8)
N5–Mn1–O3	174.06(9)		

In the crystal structure of **1**, the manganese complex molecules are linked by water molecules through intermolecular hydrogen bonds of O–H...O to form dimers.

The dimers are then connected *via* O–H...N hydrogen bonds to form 2D layers (Fig. 3). In the crystal structure of **2**, the manganese complex molecules are linked by water molecules through intermolecular hydrogen bonds of O–H...O to form dimers. The dimers are then connected by water molecules to form 2D layers (Fig. 4).

**Table 3.** Distances (Å) and angles (°) involving hydrogen bonding of the complexes.

<i>D</i> –H... <i>A</i>	<i>d</i> ( <i>D</i> –H)	<i>d</i> (H... <i>A</i> )	<i>d</i> ( <i>D</i> ... <i>A</i> )	Angle( <i>D</i> –H... <i>A</i> )
<b>1</b>				
O3–H3A...O8	0.85(1)	1.88(1)	2.716(2)	168(3)
O3–H3B...O2 <sup>i</sup>	0.84(1)	2.16(1)	2.967(2)	163(3)
O3–H3B...O1 <sup>i</sup>	0.84(1)	2.60(2)	3.188(2)	128(2)
O8–H8...N5 <sup>ii</sup>	0.87(1)	1.96(1)	2.185(3)	167(3)
O8–H8...N6 <sup>ii</sup>	0.87(1)	2.61(1)	3.461(3)	167(3)
<b>2</b>				
O3–H3A...O8	0.85(1)	1.88(1)	2.696(30)	162(3)
O3–H3B...O2 <sup>iii</sup>	0.85(1)	1.99(1)	2.819(3)	164(3)

Symmetry codes: (i)  $1 - x, -y, -z$ ; (ii)  $3/2 - x, 1/2 + y, 1/2 - z$ ; (iii)  $-x, 2 - y, 1 - z$ .

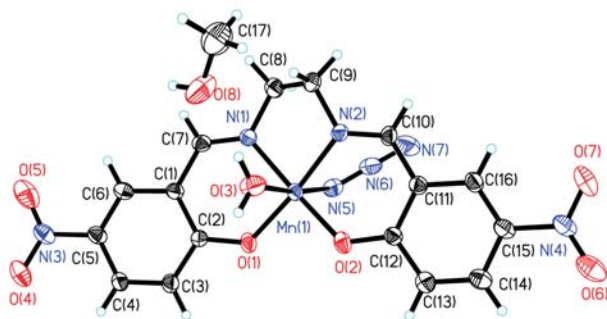


**Figure 1.** Molecular structure of **1** at 30% probability thermal ellipsoids.

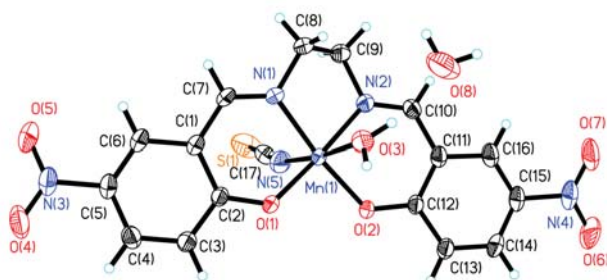


**Figure 2.** Molecular structure of **2** at 30% probability thermal ellipsoids.

### 3. 2. Infrared and Electronic Spectra

IR spectra of the manganese(III) complexes are very similar. The complexes exhibit broad bands cen-

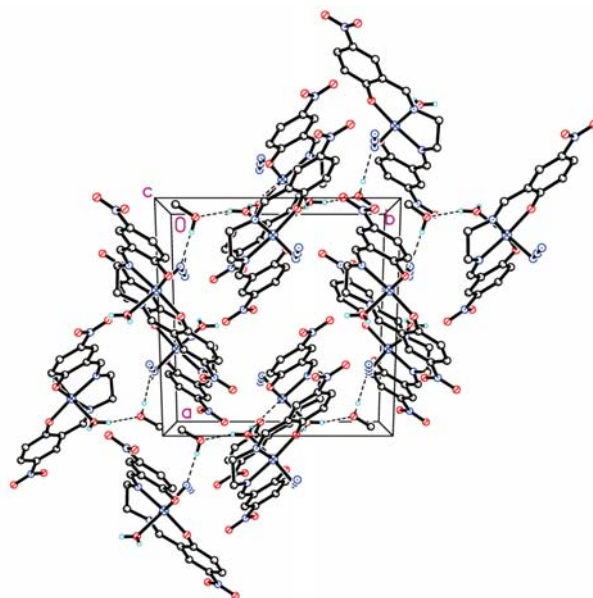


**Figure 3.** Molecular packing of **1**. Intermolecular hydrogen bonds are shown as dashed lines.

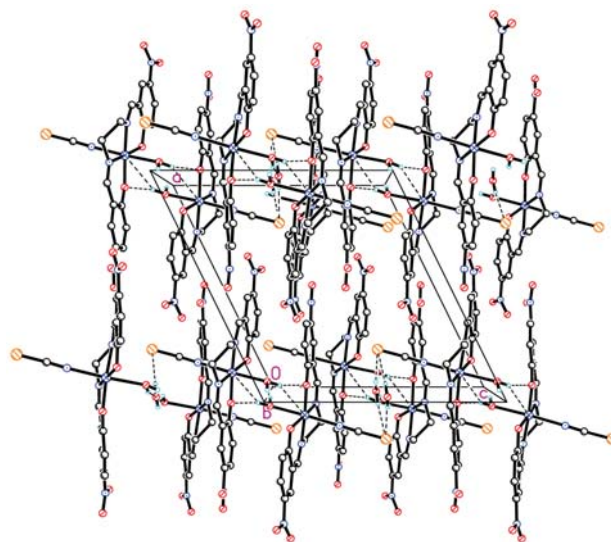


**Figure 4.** Molecular packing of **2**. Intermolecular hydrogen bonds are shown as dashed lines.

tered at *ca.* 3450  $\text{cm}^{-1}$ , indicative of the presence of coordinated and/or lattice water or methanol molecules. The strong bands indicative of  $\nu(\text{C}=\text{N})$  are located at 1601  $\text{cm}^{-1}$ . The shift of the strong bands towards lower frequencies, compared to the spectrum of the free Schiff base, is consistent with the imino nitrogen coordination. The asymmetric and symmetric vibrations of the nitro groups are located at about 1451 and 1301  $\text{cm}^{-1}$ , respectively. The intense absorption for the stretching vibrations of the azide ligand in **1** and the thiocyanate ligand in **2** are observed at 2041  $\text{cm}^{-1}$  and 2067  $\text{cm}^{-1}$ , respectively.

UV-Vis spectra for diluted acetonitrile solutions of the complexes were registered. The absorption at 298 nm and 343 nm are due to the benzene and azomethine chromophore  $\pi \rightarrow \pi^*$  transitions, respectively.

### 3. 3. Oxidation of Styrene by the Complexes

Oxidation of styrene was carried out at room temperature with the complexes as the catalysts and PhIO and NaOCl as oxidants. The deep brown color of the solutions containing the complexes and the substrate was intensified after the addition of oxidant indicating the formation of oxo-metallic intermediates of the catalysts.<sup>13</sup> After completion of oxidation reaction of the alkene, the solution regains its initial color which suggests that the regeneration of the catalysts takes place. The percentage of conversion of styrene, selectivity for styrene oxide, yield of styrene oxide for each complex and reaction time to obtain maximum yield using both the oxidants are given in Table 4.

The two complexes as catalysts convert styrene most efficiently in the presence of PhIO or NaOCl. It is easily observed that there is no obvious difference for the catalytic properties between the two complexes, as a result of similar structures. The complexes are selective towards the formation of styrene epoxide. When the reactions were carried out with PhIO, styrene conversions are 89% and 87% for **1** and **2**, respectively. When the reactions were carried out with NaOCl, styrene conversions are 75% and 76% for **1** and **2**, respectively. <sup>1</sup>H NMR data for the product ( $\delta$ , ppm, CDCl<sub>3</sub>): 2.76 (t, 1H), 3.09 (t, 1H), 3.82 (t, 1H), 7.28 (m, 5H). <sup>13</sup>C NMR data for the product ( $\delta$ , ppm, CDCl<sub>3</sub>): 51.0, 52.3, 125.5, 128.1, 128.5, 137.7. The catalytic properties of the complexes are comparable to those of the molybdenum complexes.<sup>14</sup>

Table 4. Catalytic results

	Time (h)	Oxidant	Conversion (%)	Epoxide yield (%)	Selectivity (%)	Other
1	2.0	PhIO	89	77	83	17
	3.0	NaOCl	75	62	80	20
2	2.0	PhIO	87	79	85	15
	3.0	NaOCl	76	65	78	22

## 4. Supplementary Material

1060283 for **1**, and 1060284 for **2** contain the supplementary crystallographic data for this paper. These data can be obtained free of charge at <http://www.ccdc.cam.ac.uk/const/retrieving.html> or from the Cambridge Crystallographic Data Centre (CCDC), 12 Union Road, Cambridge CB2 1EZ, UK; fax: +44(0)1223-336033 or e-mail: [deposit@ccdc.cam.ac.uk](mailto:deposit@ccdc.cam.ac.uk).

## 5. Acknowledgments

This research was supported by the National Sciences Foundation of China (No. 20676057 and 20877036) and Top-class foundation of Pingdingshan University (No. 2008010).

## 6. References

- (a) L. K. Das, C. J. Gomez-Garcia, A. Ghosh, *Dalton Trans.* **2015**, 44, 1292–1302; <https://doi.org/10.1039/C4DT02823F>  
(b) S. Chakraborty, C. R. Bhattacharjee, P. Mondal, S. K. Prasad, D. S. S. Rao, *Dalton Trans.* **2015**, 44, 7477–7488. <https://doi.org/10.1039/C4DT03989K>
- (a) M. Z. Rong, J. Wang, Y. P. Shen, J. Y. Han, *Catal. Commun.* **2012**, 20, 51–53; <https://doi.org/10.1016/j.catcom.2011.11.035>  
(b) S. Majumder, S. Hazra, S. Dutta, P. Biswas, S. Mohanta, *Polyhedron* **2009**, 28, 2473–2479; <https://doi.org/10.1016/j.poly.2009.04.034>  
(c) M. Salavati-Niasari, F. Davar, M. Bazarganipour, *Dalton Trans.* **2010**, 39, 7330–7337. <https://doi.org/10.1039/b923416k>
- (a) N. Zhang, C.-Y. Huang, D.-H. Shi, Z.-L. You, *Inorg. Chem. Commun.* **2011**, 14, 1636–1639; <https://doi.org/10.1016/j.inoche.2011.06.027>  
(b) L. Z. Zhang, T. Ding, C. L. Chen, M. X. Li, D. Zhang, J. Y. Niu, *Russ. J. Coord. Chem.* **2011**, 37, 356–361; <https://doi.org/10.1134/S1070328411040117>  
(c) N. Patel, H. Parekh, M. Patel, *Transition Met. Chem.* **2005**, 30, 13–17.
- K. Srinivasan, P. Michaud, J. K. Kochi, *J. Am. Chem. Soc.* **1986**, 108, 2309–2320. <https://doi.org/10.1021/ja00269a029>
- (a) H.-H. Li, Z.-L. You, C.-L. Zhang, M. Yang, L.-N. Gao, L. Wang, *Inorg. Chem. Commun.* **2013**, 29, 118–122; <https://doi.org/10.1016/j.inoche.2012.12.023>  
(b) Z.-L. You, D.-M. Xian, M. Zhang, *CrystEngComm* **2012**, 14, 7133–7136; <https://doi.org/10.1039/c2ce26201k>  
(c) M. Zhang, D.-M. Xian, N. Zhang, Z.-L. You, *J. Coord. Chem.* **2012**, 65, 1837–1846; <https://doi.org/10.1080/00958972.2012.684383>  
(d) X.-S. Zhou, Z.-L. You, D.-M. Xian, D.-P. Dong, *Chinese J. Inorg. Chem.* **2013**, 29, 850–854.
- M. R. Bermejo, A. Castineiras, J. C. Garcia-Monteagudo, M. Rey, A. Sousa, M. Watkinson, C. A. McAuliffe, R. G. Pritchard, R. L. Beddoes, *J. Chem. Soc. Dalton Trans.* **1996**, 14, 2935–2944. <https://doi.org/10.1039/DT9960002935>
- H. Saltzman, J. G. Sharefkin, *Organic Syntheses Collect*, Vol. V, Wiley, New York, 1973.
- G. M. Sheldrick, *SHELXTL-97, Program for X-ray Crystal Structure Solution*, Göttingen (Germany): Univ. of Göttingen, 1997.

9. G. M. Sheldrick, *SADABS, Siemens Area Detector Absorption (and Other) Correction*, Göttingen (Germany): Univ. of Göttingen, 1997.
10. W. Zhang, E. N. Jacobsen, *J. Org. Chem.* **1991**, *56*, 2296–2298. <https://doi.org/10.1021/jo00007a012>
11. (a) N. Aurangzeb, C. E. Hulme, C. A. McAuliffe, R. G. Pritchard, M. Watkinson, M. R. Bermejo, A. Sousa, *J. Chem. Soc. Chem. Commun.* **1994**, *18*, 2193–2195; <https://doi.org/10.1039/c39940002193>  
(b) M. Watkinson, M. Fondo, M. R. Bermejo, A. Sousa, C. A. McAuliffe, R. G. Pritchard, N. Jaiboon, N. Aurangzeb, M. Naeem, *J. Chem. Soc. Dalton Trans.* **1999**, *1*, 31–42; <https://doi.org/10.1039/a805555f>  
(c) Z.-L. You, T. Liu, N. Zhang, M. Zhang, D.-M. Xian, H.-H. Li, *Inorg. Chem. Commun.* **2012**, *19*, 47–50; <https://doi.org/10.1016/j.inoche.2012.01.034>  
(d) Z.-H. Pan, G.-Q. Zhao, L.-W. Xue, W.-C. Yang, *Synth. React. Inorg. Met.-Org. Nano-Met. Chem.* **2016**, *46*, 1759–1764; <https://doi.org/10.1080/15533174.2015.1137068>  
(e) X.-M. Hu, G.-Q. Zhao, L.-W. Xue, W.-C. Yang, *Inorg. Nano-Met. Chem.* **2017**, *47*, 91–94;  
(e) N. Lah, S. Grabner, P. Bukovec, *Acta Chim. Slov.* **2015**, *62*, 255–260.
12. M. R. Bermejo, M. Fondo, A. Garcia-Deibe, A. M. Gonzalez, A. Sousa, J. Sanmartin, C. A. McAuliffe, R. G. Pritchard, M. Watkinson, V. Lukov, *Inorg. Chim. Acta* **1999**, *293*, 210–217. [https://doi.org/10.1016/S0020-1693\(99\)00260-1](https://doi.org/10.1016/S0020-1693(99)00260-1)
13. E. N. Jacobsen, In: I. Ojima (Ed.), *Catalytic Asymmetric Synthesis*, VCH, Weinheim, 1993, p. 159.
14. (a) Q. Liu, J. Lin, J. Liu, W. Chen, Y. Cui, *Acta Chim. Slov.* **2016**, *63*, 279–286;  
(b) M. Liang, D.-H. Zou, *Acta Chim. Slov.* **2016**, *63*, 180–185. <https://doi.org/10.17344/acsi.2015.2169>

## Povzetek

Sintetizirali smo dva enojedna manganova(III) kompleksa s Schiffovo bazo kot ligandom,  $[\text{MnL}(\text{N}_3)(\text{OH}_2)]\text{-CH}_3\text{OH}$  (**1**) in  $[\text{MnL}(\text{NCS})(\text{OH}_2)]\text{-H}_2\text{O}$  (**2**), kjer je L dianion spojine *N,N'*-bis(5-nitrosaliciliden)etan-1,2-diamin, ter ju okarakterizirali z elementno analizo, IR in UV-Vis spektroskopijo ter z monokristalno rentgensko difrakcijo. Mn atom ima v obeh kompleksih oktaedrično koordinacijo. Molekule kompleksov so povezane preko intermolekularnih vodikovih vezi. Določili smo katalitične lastnosti kompleksov za epoksidacijo stirena z uporabo PhIO in NaOCl kot oksidantov.

Scientific paper

# Sodium Saccharin as an Effective Catalyst for Rapid One-pot Pseudo-five Component Synthesis of Dihydropyrano[2,3-*g*]chromenes under Microwave Irradiation

Leila Moradi\* and Maryam Aghamohammad Sadegh

Department of Organic Chemistry, Faculty of Chemistry, University of Kashan, P.O. Box 8731753153, Kashan, I. R. Iran

\* Corresponding author: E-mail: l\_moradi@kashanu.ac.ir

Tel: +9855912336, Fax: +983155912397

Received: 06-04-2017

## Abstract

One-pot microwave-assisted synthesis of dihydropyrano[2,3-*g*]chromenes catalyzed by sodium saccharin as an efficient, mild and green catalyst was studied. The method presented is a safe and eco-friendly approach for the multicomponent synthesis of dihydropyrano[2,3-*g*]chromene derivatives with many merits including short reaction times (in comparison with other reported results), high yields and easy work up.

**Keywords:** Dihydropyrano[2,3-*g*]chromenes; Sodium saccharin; Pseudo-five component reactions; Microwave irradiation

## 1. Introduction

One pot multicomponent reactions (MCRs) with high atom economy<sup>1,2</sup> play an important role in combinatorial chemistry. Consequently, this field has attracted great attention in recent years.<sup>3–5</sup> During MCRs, target compounds are produced with greater efficiency by generating structural complexity in a single step from three or more reactants.<sup>6,7</sup>

Chromenes and their derivatives have a wide range of applications in various fields of chemistry, biology and pharmacology.<sup>8</sup> Some of these compounds exhibit spasmolytic, diuretic, anticoagulant, anticancer and antimicrobial activities.<sup>9–11</sup>

During attempts to synthesize the title compounds, some shortcomings were observed, such as long reaction time. Consequently, to overcome this drawback, the microwave irradiation method was used in the present study. Microwave irradiation (MW) as a form of electromagnetic energy that falls at the lower-frequency end of electromagnetic spectrum (300–300000 MHz), uses the ability of some liquids and solids to transform electromagnetic radiation into heat to drive chemical reactions.<sup>12,13</sup> In fact, use of microwaves has some advantages, such as spectacular decrease of the reaction time, improved conversions, formation of cleaner products and wide scope for the development of new reaction conditions.<sup>14–16</sup>

Development of catalytic systems composed of low-cost, clean, environmentally benign and commercially available materials, has been a challenge in organic synthesis. Saccharin as an artificial sweetener with no food energy, has been employed extensively in a variety of foods and beverages, such as drinks, juices, cookies, medicines, toothpaste and gelatin. It is also used in cosmetics, pharmaceutical products and nutritive and non nutritive sweeteners.<sup>17–20</sup>

Recently, sodium saccharin as a basic green and easy available compound was used as catalyst in some organic syntheses.<sup>21,22</sup> We now report a new efficient and simple synthetic method, taking place via addition and subsequently cyclization of 2,5-dihydroxy-1,4-benzoquinone, arylaldehydes and malononitrile in the presence of a catalytic amount of sodium saccharine under microwave irradiation. Green and low-cost catalyst, easy workup, short reaction time in comparison with other reported results,<sup>23</sup> are just some of the advantages of the presented method.

## 2. Experimental

### 2.1. Materials and Apparatus

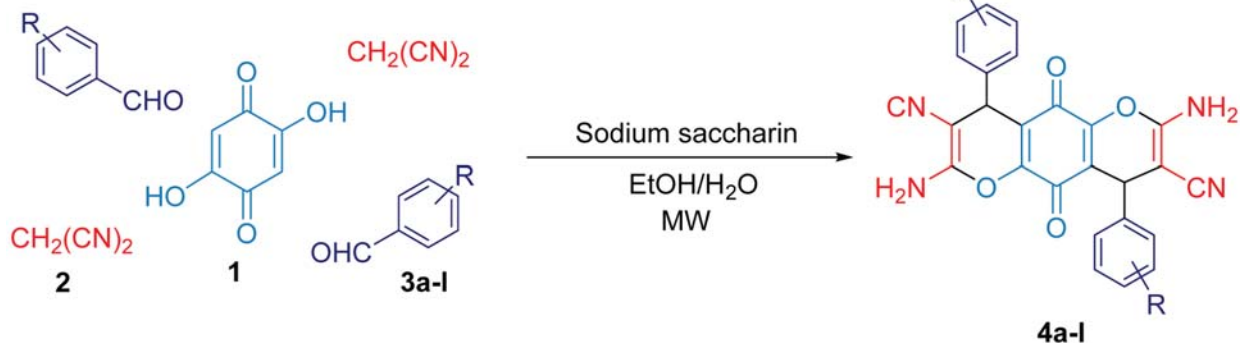
All chemicals were obtained from Merck and Sigma–Aldrich and used as received. Melting points were de-



terminated in an open capillary using a Thermo Scientific 9300 apparatus. FTIR spectra were recorded with a Perkin–Elmer FTIR 550 spectrometer.  $^1\text{H}$  NMR and  $^{13}\text{C}$  NMR spectra were recorded in DMSO- $d_6$  using Bruker DRX-400 spectrometer operating at 400 and 100 MHz, respectively. The elemental analyses (CHN) were obtained from a Carlo Erba model EA 1108 analyzer carried out on Perkin–Elmer 240c analyzer. Microwave-assisted reactions were performed with a Milestone ETHOS EZ apparatus, keeping irradiation power fixed and monitoring the internal reaction temperature. Mass spectra were recorded on a Finnigan MAT 44S by Electron Ionization (EI) mode with an ionization voltage of 70 eV.

## 2. 2. General Procedure for the Synthesis of Dihydropyrano[2,3-*g*]chromenes

A mixture of arylaldehyde (2.0 mmol), malononitrile (0.13 g, 2.0 mmol), 2,5-dihydroxy-1,4-benzoquinone (0.14 g, 1.0 mmol),  $\text{H}_2\text{O}/\text{EtOH}$  (1:1, 5 mL) and a catalytic amount of sodium saccharin (10 mol%) was irradiated in a microwave oven (100 W) at 30 °C for appropriate times. After completion of the reaction (monitored by TLC), the precipitated product was separated from the reaction mixture by simple filtration and then washed with EtOH to afford the products (Scheme 1).



Scheme 1. Synthesis of dihydropyrano[2,3-*g*]chromene derivatives catalyzed by sodium saccharin under microwave irradiation.

## 2. 3. Spectral and Analytical Data

**2,7-Diamino-4,9-bis(4-nitrophenyl)-5,10-dioxo-4,9-dihydropyrano[2,3-*g*]chromene-3,8-dicarbonitrile (4a).** Brown powder ( $\text{C}_{26}\text{H}_{14}\text{N}_6\text{O}_8$ ); FTIR (KBr):  $\nu_{\text{max}}$  3345 ( $\text{NH}_2$ ), 3180 (=C–H aromatic), 2196 (CN), 1592 (C=C aromatic)  $\text{cm}^{-1}$ .  $^1\text{H}$  NMR (400 MHz, DMSO- $d_6$ ):  $\delta$  4.7(s, 2H, 2CH), 7.39–8.18 (m, 12H, H–Ar, 2 $\text{NH}_2$ ) ppm. Anal. Calcd for  $\text{C}_{26}\text{H}_{14}\text{N}_6\text{O}_8$ : C 58.00, H 2.62, N 15.61%. Found: C 58.10, H 2.61, N 15.65%.

**2,7-Diamino-4,9-bis(2-hydroxyphenyl)-5,10-dioxo-4,9-dihydropyrano[2,3-*g*]chromene-3,8-dicarbonitrile (4b).** Orange powder ( $\text{C}_{26}\text{H}_{16}\text{N}_4\text{O}_6$ ); FTIR (KBr):  $\nu_{\text{max}}$  3459(OH), 3303 ( $\text{NH}_2$ ), 3180 (=C–H aromatic), 2189

(CN), 1579 (C=C aromatic) ( $\text{cm}^{-1}$ .  $^1\text{H}$  NMR (400 MHz, DMSO- $d_6$ ):  $\delta$  3.67 (2H, bs, 2OH), 4.74 (s, 2H, 2CH), 6.6–7.1 (m, 12H, H–Ar, 2 $\text{NH}_2$ ) ppm. Anal. Calcd for:  $\text{C}_{26}\text{H}_{16}\text{N}_4\text{O}_6$ : C 65.00, H 3.36, N 11.66%. Found: C 65.10, H 3.33, N 11.65%.

**2,7-Diamino-4,9-di-ortho-tolyl-5,10-dioxo-4,9-dihydropyrano[2,3-*g*]chromene-3,8-dicarbonitrile (4c).** Brown powder ( $\text{C}_{28}\text{H}_{20}\text{N}_4\text{O}_4$ ); FTIR (KBr):  $\nu_{\text{max}}$  3182 ( $\text{NH}_2$ ), 3053 (=C–H aromatic), 2201 (CN), 1596 (C=C aromatic) ( $\text{cm}^{-1}$ .  $^1\text{H}$  NMR (400 MHz, DMSO- $d_6$ ):  $\delta$  2.48 (s, 6H, 2 $\text{CH}_3$ ), 5.37 (s, 2H, 2CH), 6.95–7.30 (m, 12H, H–Ar, 2 $\text{NH}_2$ ) ppm. Anal. Calcd for  $\text{C}_{28}\text{H}_{20}\text{N}_4\text{O}_4$ : C 70.58, H 4.23, N 11.76%. Found: C 70.61, H 4.22, N 11.75%.

**2,7-Diamino-4,9-diphenyl-5,10-dioxo-4,9-dihydropyrano[2,3-*g*]chromene-3,8-dicarbonitrile (4d).** Brown powder ( $\text{C}_{26}\text{H}_{16}\text{N}_4\text{O}_6$ ); FTIR (KBr):  $\nu_{\text{max}}$  3296 ( $\text{NH}_2$ ), 3179 (=C–H aromatic), 2202 (CN), 1595 (C=C aromatic)  $\text{cm}^{-1}$ .  $^1\text{H}$  NMR (400 MHz, DMSO- $d_6$ ):  $\delta$  4.46 (s, 2H, 2CH), 7.24–7.40 (m, 12H, H–Ar, 2 $\text{NH}_2$ ) ppm. Anal. Calcd for  $\text{C}_{26}\text{H}_{16}\text{N}_4\text{O}_6$ : C 69.64, H 3.60, N 12.49%. Found: C 69.61, H 3.62, N 12.46%.

**2,7-Diamino-4,9-bis(4-chlorophenyl)-5,10-dioxo-4,9-dihydropyrano[2,3-*g*]chromene-3,8-dicarbonitrile**

**(4e).** Brown powder ( $\text{C}_{26}\text{H}_{14}\text{N}_4\text{O}_4\text{Cl}_2$ ); FTIR (KBr):  $\nu_{\text{max}}$  3317 ( $\text{NH}_2$ ), 3173 (=C–H aromatic), 2197 (CN), 1591 (C=C aromatic) ( $\text{cm}^{-1}$ .  $^1\text{H}$  NMR (400 MHz, DMSO- $d_6$ ):  $\delta$  4.45 (s, 2H, 2CH), 7.29–7.32 (m, 12H, H–Ar, 2 $\text{NH}_2$ ) ppm. Anal. Calcd for  $\text{C}_{26}\text{H}_{14}\text{N}_4\text{O}_4\text{Cl}_2$ : C 60.36, H 2.73, N 10.83%. Found: C 60.28, H 2.75, N 10.81%.

**2,7-Diamino-4,9-bis(4-bromophenyl)-5,10-dioxo-4,9-dihydropyrano[2,3-*g*]chromene-3,8-dicarbonitrile (4f).** Brown powder ( $\text{C}_{26}\text{H}_{14}\text{N}_4\text{O}_4\text{Br}_2$ ); FTIR (KBr):  $\nu_{\text{max}}$  3321 ( $\text{NH}_2$ ), 3179 (=C–H aromatic), 2199 (CN), 1589 (C=C aromatic) ( $\text{cm}^{-1}$ .  $^1\text{H}$  NMR (400 MHz, DMSO- $d_6$ ):  $\delta$  4.45 (s, 2H, 2CH), 7.22–7.51 (m, 12H, H–Ar, 2 $\text{NH}_2$ ) ppm. Anal. Calcd for:  $\text{C}_{26}\text{H}_{14}\text{N}_4\text{O}_4\text{Br}_2$ : C 51.51, H 2.33, N 9.24%. Found: C 51.60, H 2.36, N 9.26%.

**2,7-Diamino-4,9-bis(2,4-dichlorophenyl)-5,10-dioxo-4,9-dihydropyrano[2,3-g]chromene-3,8-dicarbonitrile (4g).** Brown powder ( $C_{26}H_{12}N_4O_4Cl_4$ ); FTIR (KBr):  $\nu_{max}$  3326 ( $NH_2$ ), 3178 (=C–H aromatic), 2203 (CN), 1590 (C=C aromatic)  $cm^{-1}$ .  $^1H$  NMR (400 MHz, DMSO- $d_6$ ):  $\delta$  5.00 (s, 2H, 2CH), 7.34–8.52 (m, 10H, H–Ar, 2NH $_2$ ), ppm.  $^{13}C$  NMR (100 MHz, DMSO- $d_6$ ):  $\delta$  33.2 (CH), 56.08, 117.2, 119.9, 128.4, 129.1, 132.4, 133.4, 139.8, 147.5, 158.7, (C-alkene and Ar), 177.3 (2C=O) ppm. MS  $m/z$  (%): 586 ( $M^+$ ), 522 (3), 431 (9), 366 (25), 339 (41), 274 (82), 186 (32), 115 (44), 91 (100), 65 (58). Anal. Calcd for  $C_{26}H_{12}N_4O_4Cl_4$ : C 53.24, H 2.04, N 9.55%. Found: C 53.78, H 2.09, N 9.32%.

**2,7-Diamino-4,9-bis(3-nitrophenyl)-5,10-dioxo-4,9-dihydropyrano[2,3-g]chromene-3,8-dicarbonitrile (4h).** Brown powder ( $C_{26}H_{14}N_6O_8$ ); FTIR (KBr):  $\nu_{max}$  3345 ( $NH_2$ ), 3207 (=C–H aromatic), 2195 (CN), 1593 (C=C aromatic)  $cm^{-1}$ .  $^1H$  NMR (400 MHz, DMSO- $d_6$ ):  $\delta$  4.71 (s, 2H, 2CH), 7.39–8.15 (m, 12H, H–Ar, 2NH $_2$ ), ppm;  $^{13}C$  NMR (100 MHz, DMSO- $d_6$ ):  $\delta$  36.2 (CH), 56.7, 117.0, 119.3, 123.0, 130.07, 130.5, 135.2, 145.4, 147.2, 148.2, 158.8 (C-alkene and Ar), 177.52 (2C=O) ppm. MS  $m/z$  (%): 538 ( $M^+$ ), 417 (2), 348 (4), 281 (4), 257 (9), 222 (12), 152 (14), 131 (21), 104 (75), 91 (26), 76 (73), 57 (55), 43 (100). Anal. Calcd for  $C_{26}H_{14}N_6O_8$ : C 57.99, H 2.60, N 15.61%. Found: C 58.00, H 2.40, N 15.88%.

**2,7-Diamino-4,9-bis(thiophen-2-yl)-5,10-dioxo-4,9-dihydropyrano[2,3-g]chromene-3,8-dicarbonitrile (4i).** Brown powder ( $C_{22}H_{12}N_4O_4S_2$ ); FTIR (KBr):  $\nu_{max}$  3333 ( $NH_2$ ), 3102 (=C–H aromatic), 2195 (CN), 1576 (C=C aromatic)  $cm^{-1}$ .  $^1H$  NMR (400 MHz, DMSO- $d_6$ ):  $\delta$  3.80 (s, 2H, 2CH), 6.90–8.73 (m, 10H, H–Ar, 2NH $_2$ ), ppm.  $^{13}C$  NMR (100 MHz, DMSO- $d_6$ ):  $\delta$  76.4, 129.7, 131.02, 135.7, 139.1, 140.9, 153.9 (C-alkene, C-thiophene), 187.6 (2C=O) ppm. MS  $m/z$  (%): 460 ( $M^+$ ), 374 (8), 342 (12), 314 (18), 160 (92), 147 (15), 133 (30), 109 (34), 76 (38), 66 (50), 49 (100). Anal. Calcd for  $C_{22}H_{12}N_4O_4S_2$ : C 57.39, H 2.60, N 12.17, S 13.91%. Found: C 57.10, H 2.60, N 12.10, S 13.33%.

**2,7-Diamino-4,9-bis(4-hydroxyphenyl)-5,10-dioxo-4,9-dihydropyrano[2,3-g]chromene-3,8-dicarbonitrile (4j).** Brown powder ( $C_{26}H_{16}N_4O_6$ ); FTIR (KBr):  $\nu_{max}$  3417 (OH), 3346 ( $NH_2$ ), 3219 (=C–H aromatic), 2198 (CN), 1599 (C=C aromatic)  $cm^{-1}$ .  $^1H$  NMR (400 MHz, DMSO- $d_6$ ):  $\delta$  4.10 (s, 2H, 2CH), 6.90–8.30 (m, 12H, H–Ar, 2NH $_2$ ), 11.08 (s, 2H, 2OH) ppm.  $^{13}C$  NMR (100 MHz, DMSO- $d_6$ ):  $\delta$  34.2 (2CH), 75.5, 107.2, 114.6, 115.5, 117.1, 123.2, 134.3 (C-alkene and Ar), 160.96, 164.4 (2C=O) ppm. MS  $m/z$  (%): 480 ( $M^+$ ), 454 (9), 313 (48), 274 (25), 238 (38), 198 (18), 187 (46), 170 (100), 94 (69). Anal. Calcd for  $C_{26}H_{16}N_4O_6$ : C 65.00, H 3.33, N 11.66%. Found: C 64.88, H 3.59, N 11.1%.

**2,7-Diamino-4,9-di(*para*-tolyl)-5,10-dioxo-4,9-dihydropyrano[2,3-g]chromene-3,8-dicarbonitrile (4k).**

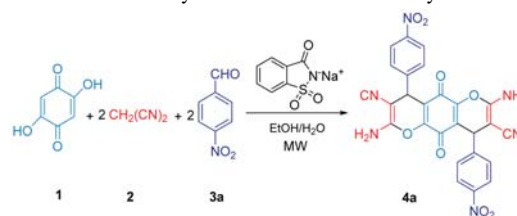
Brown powder ( $C_{28}H_{20}N_4O_4$ ); FTIR (KBr):  $\nu_{max}$  3436 ( $NH_2$ ), 2922 (=C–H aromatic), 2198 (CN), 1584 (C=C aromatic)  $cm^{-1}$ .  $^1H$  NMR (400 MHz, DMSO- $d_6$ ):  $\delta$  2.25 (s, 6H, 2CH $_3$ ), 4.45 (s, 2H, 2CH), 6.94–7.86 (m, 12H, H–Ar, 2NH $_2$ ) ppm. MS  $m/z$  (%): 476 ( $M^+$ ), 388 (2), 313 (48), 265 (11), 299 (8), 168 (21), 140 (42), 115 (34), 104 (72), 91 (40), 69 (80), 42 (100). Anal. Calcd for  $C_{28}H_{20}N_4O_4$ : C 70.58, H 4.20, N 11.76%. Found: C 70.91, H 4.10, N 11.91%.

**2,7-Diamino-4,9-bis(4-methoxyphenyl)-5,10-dioxo-4,9-dihydropyrano[2,3-g]chromene-3,8-dicarbonitrile (4l).** Brown powder ( $C_{28}H_{20}N_4O_6$ ); FTIR (KBr):  $\nu_{max}$  3321 ( $NH_2$ ), 2926 (=C–H aromatic), 2196 (CN), 1584 (C=C aromatic)  $cm^{-1}$ .  $^1H$  NMR (400 MHz, DMSO- $d_6$ ):  $\delta$  3.65 (s, 6H, 2OCH $_3$ ), 4.45 (s, 2H, 2CH), 6.72–7.20 (m, 12H, H–Ar, 2NH $_2$ ) ppm. MS  $m/z$  (%): 508 ( $M^+$ ), 445 (16), 380 (45), 355 (8), 339 (28), 290 (34), 274 (49), 198 (39), 128 (22), 105 (80), 91 (100), 77 (28). Anal. Calcd for  $C_{28}H_{20}N_4O_6$ : C 66.14, H 3.93, N 11.02%. Found: C 66.70, H 3.70 and N 11.10%.

### 3. Results and Discussion

In the initial stages of the presented research optimization of the catalyst amounts, solvent and power of microwave irradiation were investigated. In the first step, catalyst optimization was studied. For determining the best quantity of sodium saccharin, 2 mmol of 4-nitrobenzaldehyde, 2 mmol of malononitrile and 1 mmol of 2,5-dihydroxybenzoquinone were used (as a model reaction). The reaction was performed in the presence of various amounts of the catalyst. As shown in Table 1, it is clearly observed that 0.019 g (10 mol%) of sodium saccharin lead to the highest yield of **4a** (Table 1, entry 5).

**Table 1.** Effect of catalyst amounts on the time and yield of **4a**<sup>a</sup>



Entry	Cat. (mol%)	Time (min)	Yield (%) <sup>b</sup>
1	–	20	–
2	2	15	47
3	5	12	71
4	8	10	83
5	10	8	90
6	12	8	90
7	15	8	88
8 <sup>c</sup>	10	19 <sup>d</sup>	88

<sup>a</sup> 1 mmol of **1**, 2 mmol of **2** and 2 mmol of **3a** in 5 mL EtOH/H $_2$ O (1:1) and power of 100 W. <sup>b</sup> Isolated yield. <sup>c</sup> Thermal condition (35 °C). <sup>d</sup> Time in hours.

The obtained results show that excellent yield was achieved using 10 mol% (0.019 g) of sodium saccharin (Table 1, entry 5). It should be considered that due to the very low solubility of products in general organic solvents, homogeneous catalysts are the best choice for the synthesis of dihydropyrano[2,3-*g*]chromenes.

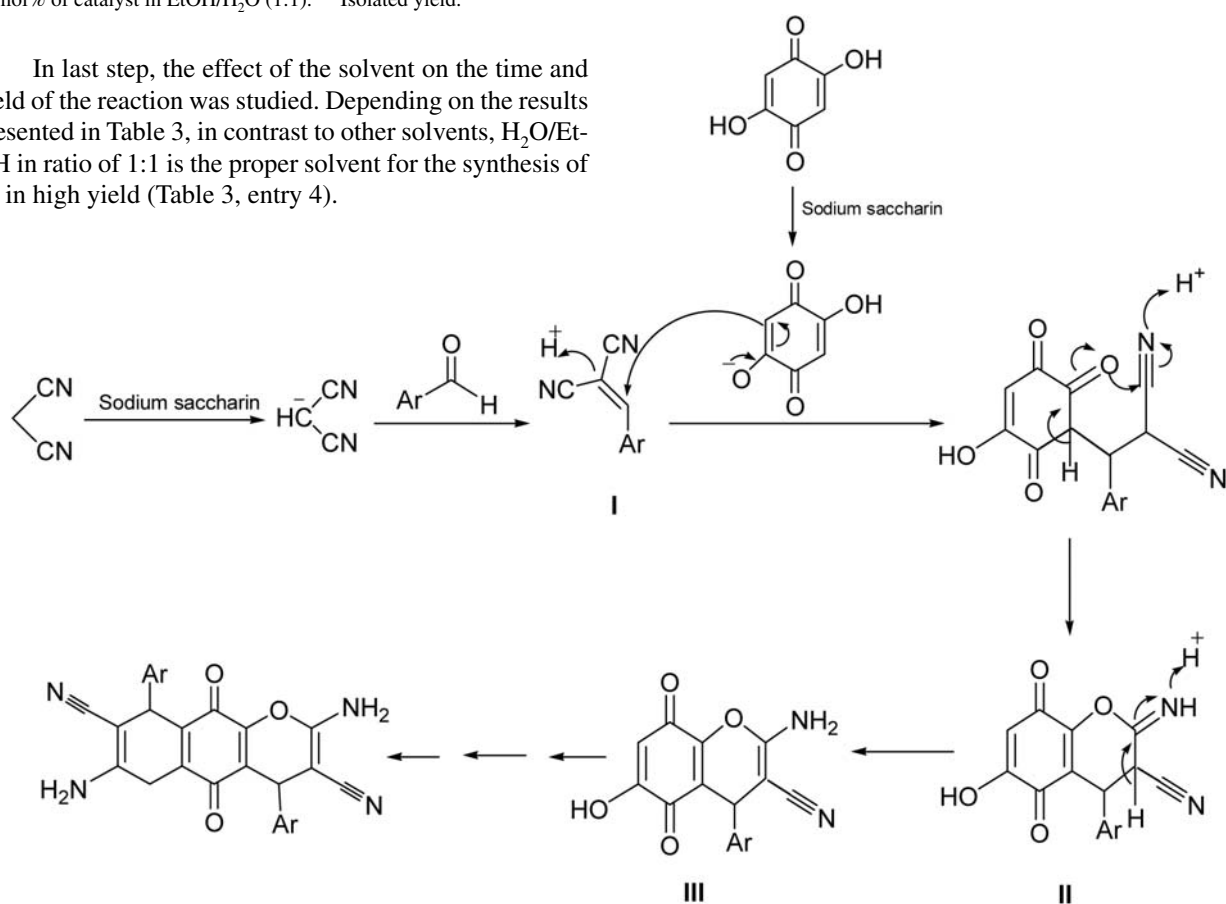
In continuation of the research, the power of microwave irradiation was examined. Model reaction was run at several powers. Results in Table 2 show that the power of 100 W was the optimized condition for the synthesis of **4a** (Table 2, entry 4).

**Table 2.** Optimization of microwave power<sup>a</sup>

Entry	Power (W)	Time (min)	Yield (%) <sup>b</sup>
1	100	2	50
2	100	4	55
3	100	6	70
4	100	8	90
5	100	10	90
6	200	5	55
7	200	8	42
8	300	5	45
9	300	8	40

<sup>a</sup> 1 mmol of **1**, 2 mmol of **2** and 2 mmol of **3a** in the presence of 10 mol% of catalyst in EtOH/H<sub>2</sub>O (1:1). <sup>b</sup> Isolated yield.

In last step, the effect of the solvent on the time and yield of the reaction was studied. Depending on the results presented in Table 3, in contrast to other solvents, H<sub>2</sub>O/EtOH in ratio of 1:1 is the proper solvent for the synthesis of **4a** in high yield (Table 3, entry 4).



**Scheme 2.** The plausible mechanism of dihydropyrano[2,3-*g*]chromenes formation

**Table 3.** Solvent effect on synthesis of **4a**<sup>a</sup>

Entry	Solvent	Time (min)	Yield (%) <sup>b</sup>
1	EtOH	5	35
2	H <sub>2</sub> O	8	70
3	CH <sub>3</sub> CN	12	65
4	EtOH/H <sub>2</sub> O (1:1)	8	90
5	EtOH/H <sub>2</sub> O (1:2)	8	75
6	MeOH	8	41
7	Dioxane	10	52

<sup>a</sup> 1 mmol of **1**, 2 mmol of **2** and 2 mmol of **3a**, in the presence of 10 mol% of sodium saccharin and power of 100 W. <sup>b</sup> Isolated yield.

According to the optimization results, the procedure was extended to various aldehydes (with electron withdrawing and electron donating groups). As can be seen in Table 4, aldehydes containing electron withdrawing groups (especially at the *para* position), have the highest yields (Table 4, entries 1, 8), also low yield products were obtained using aldehydes with a group at the *ortho* position (Table 4, entries 2, 3, 7). As a result, the reaction proceeded very efficiently and led to the formation of dihydropyrano[2,3-*g*]chromene derivatives **4a–l** in high yields and in short reaction times. The structures of **4a–l** was deduced from their FTIR, mass spectroscopy, elemental analysis, <sup>1</sup>H NMR and <sup>13</sup>C NMR techniques.

**Table 4.** Pseudo-five-component synthesis of dihydropyrano[2,3-g]chromene derivatives 4<sup>a</sup>

Entry	Product	ArCHO 3a-l	Time (min)	Yield (%) <sup>b</sup>	m.p. (C)	Ref.
1	4a		8	90	290–293	23
2	4b		14	80	264–266	23
3	4c		16	78	280–282	23
4	4d		19	82	287–289	23
5	4e		13	85	273–275	23
6	4f		16	85	264–266	23
7	4g		19	80	263–265	–
8	4h		13	90	242–244	–
9	4i		13	85	258–260	–
10	4j		18	80	208–210	–
11	4k		18	78	260–263	–
12	4l		18	82	>300	–

<sup>a</sup> 1 mmol of **1**, 2 mmol of **2** and 2 mmol of **3a-l**, in the presence of 10 mol% of sodium saccharin in EtOH/H<sub>2</sub>O (1:1), and power of 100 W. <sup>b</sup> Isolated yield.

A plausible mechanism of the reaction is presented in Scheme 2. In the first step of the reaction, acidic proton of malononitrile has been separated by sodium saccharin as a basic catalyst. Then, the Knoevenagel condensation of malononitrile anion and aldehyde leads to the intermediate **I**. In the next step, cyclization and tautomerization lead via **II** to the product **III**. The same process occurs on the other side of 2,5-dihydroxy-1,4-benzoquinone (due to its special structure) and finally, a dual chromene structure is produced.

The efficiency of sodium saccharin in comparison with other catalysts in the synthesis of dihydropyrano[2,3-g]chromenes was also investigated. Results presented in Table 5 clearly show that sodium saccharin can be mentioned as a powerful, highly efficient catalyst for the synthesis of dihydropyrano[2,3-g]chromenes under microwave irradiation.

**Table 5.** The effect of various catalysts on the synthesis of **4a** under optimized conditions

Entry	Catalyst (10 mol %)	Time	Yield (%) <sup>a</sup>
1	Meglumine	15	43
2	[BMIM]BF <sub>4</sub> <sup>b</sup>	8	57
3	Sodium phthalimide	10	70
4	Sodium benzoate	25	64
5	NEt <sub>3</sub>	20	75
6	Saccharin	30	52
7	Sodium saccharin	8	90

<sup>a</sup> Isolated yield. <sup>b</sup> 0.02 g.

## 4. Conclusion

We have developed an efficient, novel and eco-friendly method for the synthesis of dihydropyrano[2,3-g]chromenes in the presence of sodium saccharin as the catalyst under microwave irradiation. The procedure described provides clean reaction conditions with easy work-up, simple filtration and short reaction times with high yields of products.

## 5. Acknowledgments

We thank the Research Council of the University of Kashan for support of this work.

## 6. References

- B. M. Trost, *Science* **1991**, *55*, 1471–1477. <https://doi.org/10.1126/science.1962206>
- J. Collins, *J. Chem. Edu.* **1995**, *72*, 965–970. <https://doi.org/10.1021/ed072p965>
- C. Hulme, M. Ayaz, G. Martinez-Ariza, F. Medda, A. Shaw, Recent Advances in Multicomponent Reaction Chemistry, In Small Molecule Medicinal Chemistry: Strategies and Technologies, W. Czechtizky, P. Hamley (Eds.), Wiley & Sons, Inc, New Jersey, **2015**, pp. 965–970. <https://doi.org/10.1002/9781118771723.ch6>
- A. Dömling, A. D. Alqahtani, General Introduction to MCRs: Past, Present, and Future, in Multicomponent Reactions in Organic Synthesis, J. Zhu, Q. Wang, M.-X. Wang (Eds), Wiley-VCH Verlag GmbH & Co. KGaA, Weinheim, Germany, **2014**, pp. 1–43.
- B. H. Rotstein, S. Zaretsky, V. Rai, A. K. Yudin, *Chem. Rev.* **2014**, *114*, 8323–8359. <https://doi.org/10.1021/cr400615v>
- H. Bienaymé, C. Hulme, G. Oddon, P. Schmitt, *Chem. Eur. J.* **2000**, *6*, 3321–3329. [https://doi.org/10.1002/1521-3765\(20000915\)6:18<3321::AID-CHEM3321>3.0.CO;2-A](https://doi.org/10.1002/1521-3765(20000915)6:18<3321::AID-CHEM3321>3.0.CO;2-A)
- I. Ugi, *Pure. Appl. Chem.* **2001**, *73*, 187–191. <https://doi.org/10.1351/pac200173010187>
- W. S. Shehab, A. A. Ghoneim, *Arab. J. Chem.* **2011** <https://doi.org/10.1016/j.arabj.2011.10.008>
- S. R. Parker, H. C. Cutler, J. M. Jacyno, R. A. Hill, *J. Agric. Food. Chem.* **1997**, *45*, 2774–2776. <https://doi.org/10.1021/jf960681a>
- R. C. Gadwood, B. V. Kamdar, L. A. Cipkus Dubary, M. L. Wolf, M. P. Smith, W. Watt, S. A. Mizesak, V. E. Groppi, *J. Med. Chem.* **1993**, *36*, 1480–1487. <https://doi.org/10.1021/jm00062a022>
- L. Tang, Y.S. Yang, R.Y. Ji, *Pub. Chem. Med.* **2008**, *43*, 162–168.
- S. Ravichandran, E. Karthikeyan, *Int. J. Chem. Tech. Res.* **2011**, *3*, 466–470.
- R. Gedye, F. Smith, K. Westaway, H. Ali, L. I. Bald, L. Laberge, J. Rousell, *Tetrahedron Lett.* **1986**, *27*, 279–282. [https://doi.org/10.1016/S0040-4039\(00\)83996-9](https://doi.org/10.1016/S0040-4039(00)83996-9)
- R. Das, D. Mehta, H. Bhardawa, *Int. J. Res. Dev. Pharm. L. Sci.* **2012**, *1*, 32–39.
- A. R. Mekeimer, K. U. Sadek, *Chinese. Chem. Lett.* **2009**, *20*, 271–274. <https://doi.org/10.1016/j.cclet.2008.11.025>
- M. Jha, S. Guy, T. Y. Chou, *Tetrahedron Lett.* **2011**, *52*, 4337–4341. <https://doi.org/10.1016/j.tetlet.2011.06.052>
- A. Talevi, A. V. Enrique, L. E. Bruno-Blanch, *Bioorg. Med. Chem. Lett.* **2012**, *22*, 4072–4074. <https://doi.org/10.1016/j.bmcl.2012.04.076>
- M. Tripathi, S. Khanna, M. Das, *India. Food Addit. Contam.* **2006**, *23*, 1265–1275. <https://doi.org/10.1080/02652030600944395>
- Z. Jakopin, M. Dolenc, *Synth. Commun.* **2008**, *38*, 3422–3438. <https://doi.org/10.1080/00397910802149105>
- N. Gencer, D. Demir, F. Sonmez, M. Kucukislamoglu, *Bioorg. Med. Chem.* **2012**, *20*, 2811–2821. <https://doi.org/10.1016/j.bmc.2012.03.033>
- F. Matloubi Moghaddam, G. R. Koozehgiri, M. G. Dekaminy, *Monatsh Chem.* **2004**, *135*, 849–851.
- H. Kiyani, F. Ghorbani, *Heterocycl. Lett.* **2013**, *3*, 359–369

23. A. Shaabani, R. Ghadari, S. Ghasemi, M. Pedarpour, A. H. Rezayan, A. Sarvary, S. W. Ng, *J. Comb. Chem.* **2009**, *11*, 956–959. <https://doi.org/10.1021/cc900101w>

## Povzetek

Raziskalo smo »one-pot« sintezo dihidropirano[2,3-g]kromenov pod pogoji obsevanja z mikrovalovi in z uporabo natrijevega saharinata kot učinkovitega, milega in zelenega katalizatorja. Metoda predstavlja varen in okolju prijazen pristop k multikomponentni sintezi dihidropirano[2,3-g]kromenskih derivatov; odlikujejo jo mnoge prednosti v primerjavi z ostalimi doslej objavljenimi pristopi, kot so krajši reakcijski časi, višji izkoristki in enostavnost izolacije.

Scientific paper

# Adsorptive Removal of Malachite Green from Model Aqueous Solutions by Chemically Modified Waste Green Tea Biomass

Cerasella Indolean,<sup>\*1</sup> Silvia Burcă<sup>1</sup> and Andrada Măicăneanu<sup>\*2</sup><sup>1</sup> Department of Chemical Engineering, Babeş-Bolyai University, 11 Arany Janos st., RO-400028, Cluj-Napoca, Romania<sup>2</sup> Department of Chemistry, Indiana University of Pennsylvania, Indiana, PA 15705, USA\* Corresponding author: E-mail: cella@chem.ubbcluj.ro; sanda.maicaneanu@iup.edu  
tel: +40 264 593833 ext. 5761. fax: +40 264 590818

Received: 08-02-2017

## Abstract

The adsorption of malachite green (MG) from aqueous solution by waste green tea (WGT) biomass was investigated. A series of experiments in batch conditions were conducted in order to assess the MG removal on WGT, following adsorbent quantity and temperature influences. Maximum removal efficiency for untreated WGT was 89% (4 g biomass, 100 mL solution of 94 mg/L, 316 K). It was found that the adsorption of MG increased by increasing temperature from 296 to 316 K. Thermodynamic parameters ( $\Delta H^\circ$ ,  $\Delta S^\circ$ ,  $\Delta G^\circ$ ) were calculated, and indicated that dye adsorption onto the studied biomass was endothermic and non-spontaneous. Six chemical treatments were tested (four acidic –  $H_3PO_4$ ,  $H_2SO_4$ , HCl, and tartaric acid, one oxidant –  $H_2O_2$ , and one basic – NaOH) in order to study the chemical groups responsible for MG adsorption onto WGT biomass. The alkali and acidic treatments led to an increase of adsorption efficiency up to 92% and 95% ( $H_2SO_4$ ) respectively. The FTIR spectroscopy results emphasized the modifications of the biomass surface and how these are influencing the adsorption process.

**Keywords:** Waste green tea, chemical treatment, adsorption, malachite green, SEM analysis

## 1. Introduction

Dyes are usually used in industries such as textile, paper, drug, rubber, food, cosmetic, plastic, printing, etc., activities, which have as result considerable amount of colored wastewater. Dye is the first contaminant to be recognized in wastewater, because not only damage the aesthetic nature of freshwater, which will reduce sun penetration, but also many of them possess a serious threat for human beings, aquatic life, and for environment, in general.<sup>1</sup>

The presence of very small amounts of dyes in water (less than 1 ppm for some dyes) is highly visible and undesirable.<sup>2</sup> Thus, the development of clean-up technologies for the treatment of water contaminated with dyes is of major interest.<sup>3</sup> A number of technologies are available to control and reduce the water pollution with dye contaminants. Among them are coagulation<sup>4</sup>, filtration<sup>5</sup>, ion-exchange,<sup>6</sup> electrolysis,<sup>7</sup> advanced oxidation processes<sup>8</sup>, foam flotation,<sup>9</sup> etc. The removal of dyes in an economic

way remains an important problem, although a number of systems have been developed using adsorption techniques.<sup>10</sup> Adsorption is a well-known equilibrium separation process and an effective method for water decontamination applications. Among many techniques for water re-use, adsorption has been found to be superior in terms of ease of operation, low initial cost, flexibility and simplicity of design, and insensitivity to toxic pollutants.<sup>11</sup> Also, adsorption does not result in the formation of harmful substances due to partial degradation as some chemical or biological methods would.<sup>12</sup> Adsorption of most of the adsorbents including agricultural by-product is controlled by physical forces, with some exception of chemisorption.<sup>1</sup> The main physical forces controlling adsorption are van der Waals forces, hydrogen bonds, dipole-dipole  $\pi$ - $\pi$  interactions, etc.<sup>13</sup>

Many low-cost adsorbents, such as rice husk, wheat bran, coconut bunch waste, orange peel, banana peel, garlic peel, papaya seed, pineapple stem waste, sunflower stalks, silk cotton hull, maize cob, etc., which are able to

bind dyes molecules, have been previously researched and evaluated.<sup>14</sup>

Waste green tea could be also an economical alternative for dyes removal from wastewater. Tea plant, called *Camellia sinensis*,<sup>15</sup> is native to South-East Asia, but is cultivated today in over 30 countries in several areas of the world and belongs to the genus *Camellia*, *Theaceae* family.<sup>16</sup> Taking into consideration the quantity of tea and tea based drinks consumed annually, which gives rise to a disposal problem, utilization of such waste is extremely desirable.<sup>17–18</sup>

The cell wall of tea consist of cellulose and hemicelluloses, lignin, condensed tannins, and structural proteins. In short, tea waste have a good potential as dyes scavengers from aqueous solution since its constituents contain several functional groups.<sup>19</sup> Previous studies have centered their attention on the preparation of waste tea activated carbon<sup>17,20</sup> or on various treatments involving acetylation, isopropyl alcohol, formaldehyde, HNO<sub>3</sub>, pressure, and ultrasound.<sup>17,20–24</sup>

The aim of this study was to realize malachite green (MG) adsorption onto chemically modified waste green tea (WGT). Influence of the adsorbent quantity and temperature over the MG removal were also considered in order to investigate the WGT potential as a biosorbent. Influence of carboxyl, carbonyl, sulfonate, sulfhydryl, phosphate, and hydroxyl groups from the biomass surface over the adsorption of MG onto untreated and chemically modified WGT were detailed. Equilibrium and kinetic studies on the untreated WGT – MG system were considered in a previous paper.<sup>25</sup>

## 2. Materials and Methods

### 2.1. Adsorbent

The adsorbent, WGT, was collected from a local tea shop. The used green tea leaves were washed several times with distilled water to remove any adhering dirt and repeatedly boiled in distilled water until the filtered water was clear. Then it was oven dried at 80 °C for 48 h. Finally, the WGT sample was ground and sieved to obtain grains in the 200–400 μm range that will be further used in the adsorption experiments.

### 2.2. Characterization of the Biosorbent

#### 2.2.1. Elemental Analysis

In order to obtain information about the elemental composition of the studied materials, the C, H, N, S, and O content of untreated and chemically modified WGT, before and after MG adsorption (for all considered treatments) was determined. Elemental analysis was carried out using Thermo Finnigan Flash EA 1112 Series equipment. The biosorbent sample was added into a tin capsule and analysed at 900 °C under O<sub>2</sub> atmosphere.

#### 2.2.2. SEM Analysis

Scanning electron microscope images were obtained with a JEOL (USA) JSM 5510 LV apparatus on samples coated with a thin layer of gold under vacuum to improve electron conductivity and image quality.

### 2.3. Preparation of MG Solutions

MG, *N,N,N,N*-Tetramethyl-4,4'-diaminotriphenyl-carbenium oxalate, is a cationic (basic) dye,<sup>26</sup> which has a positive charge that is delocalized on the entire compound by resonance. It belongs to triphenylmethanes family and is amphipathic (behaves as a polar and non-polar compound). MG is commonly used for dyeing textiles and paper, as well as is an antiparasitic and antifungal agent in aquaristics.<sup>14</sup>

Malachite green was purchased from Penta (Czech Republic) and used without further purification. Stock solution (1000 mg/L) of MG were prepared using distilled water and stored in the refrigerator. Experiments were carried out using solutions obtained by dilution of the stock solution to the desired concentration. MG concentration was determined using a double beam UV-visible spectrophotometer (GBC Cintra 202) at λ = 618 nm.

### 2.4. Adsorption Experiments

Adsorption process was conducted in batch conditions, in dynamic regime (magnetic stirring at 300 rpm), through the contact of a certain amount of adsorbent (1–5 g) with a volume of 100 mL MG dye aqueous solution 94 mg/L. The adsorption process was realized until equilibrium was reached (240 min, established from preliminary experiments). Residual dye concentration in solution was determined, at established time intervals after a preliminary centrifugation (5 min at 10000 rpm) and appropriate dilution.

In order to determine the effect of temperature on the adsorption process, experiments were carried out at three different temperatures 296, 306, and 316 K. The experiments were realized using 100 mL solution of 94 mg/L and 4 g WGT.

Adsorption efficiency expressed as percentage was calculated with equation (1):<sup>27,28</sup>

$$E = \frac{C_0 - C_e}{C_0} \cdot 100 \quad (1)$$

where, C<sub>0</sub> and C<sub>e</sub> are MB initial and equilibrium concentrations, respectively (mg/L).

The amount of the adsorbed dye (MG) onto the WGT biomass was expressed as adsorption capacity (q<sub>e</sub>, mg/g) and calculated as shown in equation (2):<sup>16,27</sup>

$$q_e = \frac{(C_0 - C_e) \cdot V}{m} \quad (2)$$

where, V is solution volume (L), and m is WGT quantity (g).



All the experiments were repeated three times, the values presented were calculated using averaged concentration values.

## 2. 5. Chemical Treatments for WGT Biomass

### 2. 5. 1. $\text{H}_3\text{PO}_4$ Treatment

10 g of WGT were mixed with 50 mL 50%  $\text{H}_3\text{PO}_4$  solution at room temperature for 24 h in a 500 mL beaker with a stirring speed of 150 rpm so that the reagent was fully incorporated into the raw material.<sup>29</sup> After this treatment, the modified WGT was filtered and washed with distilled water several times until 7 pH and filtered. Later on, the adsorbent was oven-dried at 105 °C for 12h.

### 2. 5. 2. $\text{H}_2\text{SO}_4$ Treatment (Preparation of Activated Carbon from WGT)

The activated carbon was prepared by contacting WGT with  $\text{H}_2\text{SO}_4$  98% for 24 h (1:1 acid volume to WGT weight). After that, the charred material was washed several times in distilled water until the pH of the solution becomes neutral.<sup>30,31</sup> Chemical treated WGT was dried first in air, overnight, and then in an oven at 90–100 °C for 8–10 hours.

### 2. 5. 3. HCl Treatment

10 g of WGT were slowly stirred (150 rpm) in 100 mL HCl 1N for 4 hours. The treated cellulosic WGT was left overnight in contact with HCl solution and thereafter was washed with distilled water several times until neutral pH and filtered. The HCl-treated WGT biomass was dried in a hot air oven at 80°C until constant weight (24 hours).

### 2. 5. 4. Tartaric Acid Treatment

15 g of WGT were mixed with 100 mL of 2 M tartaric acid. The mixture was stirred at 200 rpm for 4 hours. The modified WGT was subsequently washed with distilled water until neutral and filtered. The treated WGT was dried at 80 °C for 24 h.

### 2. 5. 5. $\text{H}_2\text{O}_2$ Treatment

10 g of WGT were mixed with 50 mL of 25%  $\text{H}_2\text{O}_2$  and kept in contact for 3 h at room temperature, in a closed vessel and then boiled for 15 min. The sample was washed with distilled water to neutral pH, filtered and dried in an oven at 80 °C until constant weight.<sup>32</sup>

### 2. 5. 6. NaOH Treatment

10 g of WGT were mixed with 150 mL 1% NaOH solution for 6 h at room temperature.<sup>30</sup> The cellulosic sample was then washed thoroughly with distilled water

until the sample was neutralized and dried in the oven at 80 °C for 24 h.

The material obtained after each individual chemical treatment was grounded and passed through several sieves in order to obtain the desired particle size (200–400  $\mu\text{m}$ ). Finally, the resulting material was stored in airtight containers for further use.

## 2. 6. FTIR Analysis

The FTIR spectra (1.2 mg WGT samples mixed with 300 mg KBr) were obtained using JASCO 615 FTIR spectrometer, 500–4000  $\text{cm}^{-1}$ , resolution 2  $\text{cm}^{-1}$ .

## 3. Results and Discussion

### 3. 1. Elemental Analysis

Untreated and chemically treated WGT elemental analysis performed before and after MG adsorption showed that after treatment, in some cases (exception acidic treatments with  $\text{H}_3\text{PO}_4$ ,  $\text{H}_2\text{SO}_4$ , and tartaric acid), carbon content decreases from the initial 52.27% (untreated WGT) to values ranging from 44.83% for NaOH treatment to 45.80% for  $\text{H}_2\text{O}_2$ , Table 1. The organic content of the material decreases significantly due to the delignification process that takes place.<sup>32</sup> In the case of  $\text{H}_2\text{SO}_4$  treatment, carbon content increases to 56.83% due to the formation of a new active carbon material (biochar). Elemental analysis of WGT samples after MG adsorption showed an increase of the carbon content in all cases, confirming the fact that organic dye is adsorbed onto the surface of the studied materials.

### 3. 2. SEM Analysis

The surface morphology of untreated WGT, before (a) and after (b) adsorptive removal of MG was determined by SEM and is presented in Figure 1.

The raw WGT surface is shown to be rough and consists of many strands of fibrous-like materials (Figure 1a).

SEM image confirmed the amorphous and heterogeneous structure of WGT. Considerable changes in surface morphology after biosorption are noted as surface protuberances become less obvious and the surface becomes smoother (Figure 1b).

### 3. 3. The Effect of Adsorbent Quantity

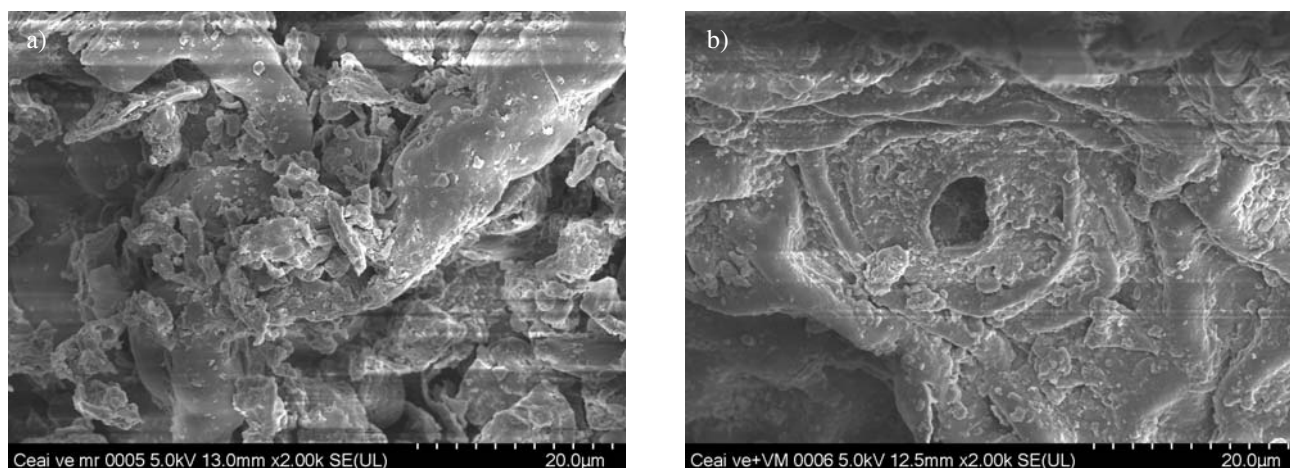
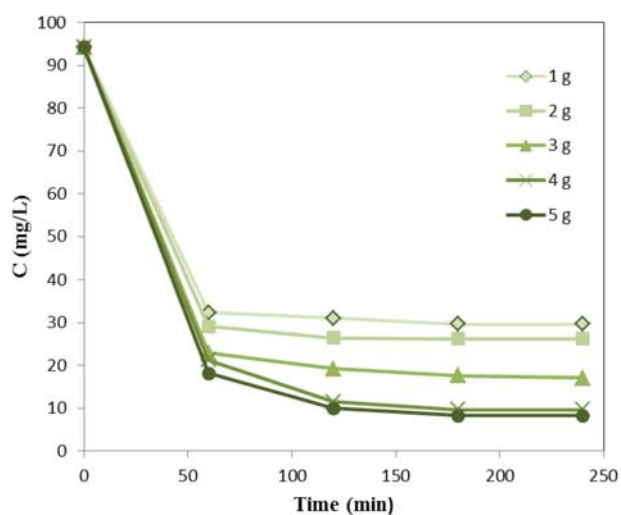
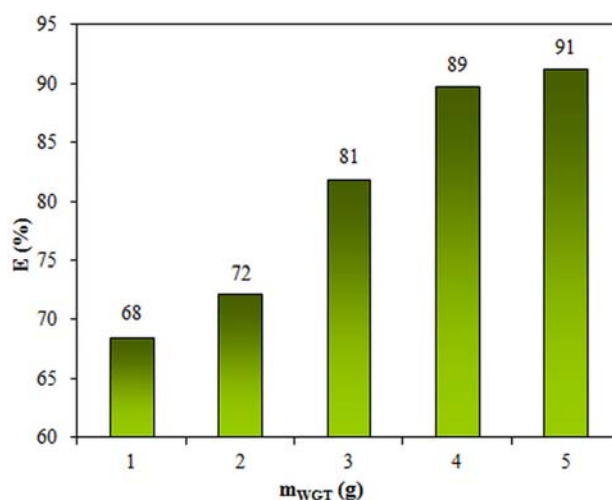
The adsorption of MG onto WGT was investigated by changing the adsorbent quantity, from 1 to 5 g, using particles of 200–400  $\mu\text{m}$  in diameter, 100 mL dye aqueous solution, 94 mg/L, magnetic stirring (300 rpm), for 240 minutes, until the equilibrium was reached, Figure 2.

As presented in Figure 3 with the increasing amount of adsorbent the adsorption efficiency increase too, due to

**Table 1.** Elemental analysis of WGT untreated and chemically modified, before and after MG adsorption (1% error)

Nr. crt.	Component	C (%)	H (%)	N (%)	O* (%)
1	WGT untreated – before adsorption	52.27	6.31	3.86	37.56
2	WGT untreated – after adsorption	53.71	5.92	3.26	37.11
3	WGT treated with H <sub>3</sub> PO <sub>4</sub> – before adsorption	54.06	3.56	1.76	40.62
4	WGT treated with H <sub>3</sub> PO <sub>4</sub> – after adsorption	58.78	4.07	2.47	34.98
5	WGT treated with H <sub>2</sub> SO <sub>4</sub> – before adsorption	56.83	5.64	3.46	34.07
6	WGT treated with H <sub>2</sub> SO <sub>4</sub> – after adsorption	60.26	5.72	3.86	30.16
7	WGT treated with HCl – before adsorption	48.19	6.59	3.67	41.55
8	WGT treated with HCl – after adsorption	49.71	6.60	4.30	39.39
9	WGT treated with tartaric acid – before adsorption	53.23	6.26	3.34	37.17
10	WGT treated with tartaric acid – after adsorption	54.07	6.49	4.13	35.31
11	WGT treated with H <sub>2</sub> O <sub>2</sub> – before adsorption	45.80	6.28	3.71	44.21
12	WGT treated with H <sub>2</sub> O <sub>2</sub> – after adsorption	46.13	6.15	3.93	43.79
13	WGT treated with NaOH – before adsorption	44.83	6.13	3.28	45.76
14	WGT treated with NaOH – after adsorption	48.25	6.34	3.09	42.32

\* Calculated by difference

**Figure 1.** Scanning electron micrographs of untreated WGT before (a) and after (b) adsorptive removal of MG.**Figure 2.** Influence of the WGT quantity (untreated) over the evolution of concentration in time (296 K, 94 mg/L, 100 mL, 200–400 µm, 300 rpm, 240 min).**Figure 3.** The effect of untreated WGT quantity over the adsorption efficiency (296 K, 94 mg/L, 100 mL, 200–400 µm, 300 rpm, 240 min).

an increase of surface area and the availability of more adsorption sites, with more active functional groups.<sup>16,27</sup>

Taking into consideration that by changing the WGT quantity, from 4 to 5 g, the increase in adsorption efficiency is small ( $E_{4g} = 89\%$  and  $E_{5g} = 91\%$ ), and that higher quantities are difficult to handle in terms of sampling and separation from the aqueous solution, further experiments were carried on using 4 g of WGT.

### 3. 4. The Effect of Temperature

It well known that temperature plays an important role in the adsorption processes. A study of temperature dependence for the adsorption process gives valuable information about the enthalpy and entropy changes accompanying the adsorption processes.<sup>28</sup>

The adsorption of MG onto WGT was investigated in the 23–43 °C (296–316K) range. As it can be observed from Figure 4 an increase in temperature led to a higher quantity of dye removed, indicating that in this system adsorption takes place as an endothermic process. Similar findings were reported for other sorbent types.<sup>33–36</sup>

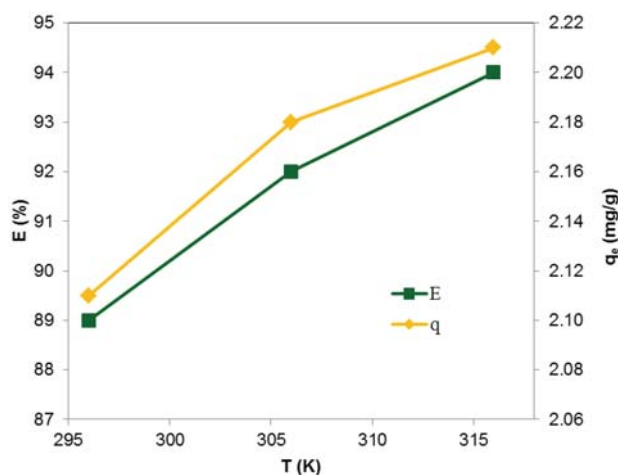


**Figure 4.** The effect of temperature on MG adsorption onto untreated WGT; (296 K, 94 mg/L, 100 mL, 4 g, 200–400 μm, 300 rpm, 240 min).

### 3. 5. Thermodynamic Analysis

The parameters such as free energy change ( $\Delta G^\circ$ ), enthalpy change ( $\Delta H^\circ$ ), and entropy change ( $\Delta S^\circ$ ) can be estimated by the change of equilibrium constant with temperature.<sup>33</sup>

The Gibbs free energy change ( $\Delta G^\circ$ ) was calculated from equations (3) and (4), while the change of enthalpy ( $\Delta H^\circ$ ) and entropy ( $\Delta S^\circ$ ) were obtained using Van't Hoff equation (5):

$$\Delta G^\circ = \Delta H^\circ - T\Delta S^\circ \quad (3)$$

$$\Delta G^\circ = -RT \ln K_d \quad (4)$$

$$\ln K_d = -\frac{\Delta H^\circ}{RT} + \frac{\Delta S^\circ}{R} \quad (5)$$

where, R is the universal gas constant ( $8.314 \times 10^{-3}$  kJ/Kmol), T is absolute temperature (K), and  $K_d$  is the distribution coefficient ( $K_d = q_e/C_e$ ) (L/g).<sup>9,37</sup>

Slope and intercept values of  $\ln(q_e/C_e)$  versus  $1/T$  plot, Figure 5, were used to calculate  $\Delta H^\circ$  and  $\Delta S^\circ$ . The values of the thermodynamic parameters are depicted in Table 2.

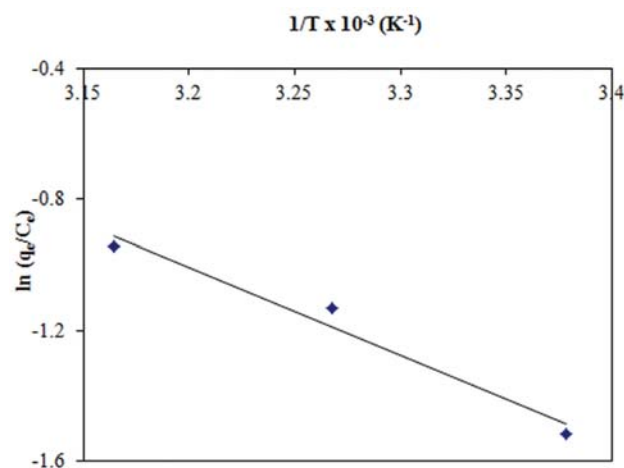


**Figure 5.**  $\ln(q_e/C_e)$  versus  $1/T$  plot for the estimation of thermodynamic parameters for MG adsorption onto untreated WGT.

The Gibbs free energy, which indicates the degree of spontaneity of the adsorption process,<sup>16</sup> decreased with increasing of temperature, indicating that a better adsorption is obtained at higher temperatures, and the process is more spontaneous at 316 K. The relatively small values of  $\Delta G^\circ$ , although positives, suggested that the adsorption process can be possible in a certain temperature range (between 296–316 K, in the present work).<sup>38–40</sup>

Positive value of  $\Delta H^\circ$  (22.42 kJ/kmol) shows the endothermic nature of the adsorption. This fact indicates the possibility of physical adsorption, since the heat of chemisorption generally falls into a range of 80–200 kJ/mol.<sup>41</sup> The low value of  $\Delta S^\circ$  may imply that no remarkable change in entropy occurred during the MG adsorption onto WGT. In addition, the positive value of  $\Delta S$  reflects the increased of randomness at the solid-solution interface during adsorption.<sup>42</sup>

**Table 2.** Thermodynamic parameters for MG adsorption onto untreated WGT at various temperatures; (94 mg/L, 100 mL, 4 g, 200–400 μm, 300 rpm, 240 min).

$\Delta S^\circ$ (kJ/mol K)	$\Delta H^\circ$ (kJ/mol)	$\Delta G^\circ$ (kJ/mol)		
		296 K	306 K	316 K
0.063	22.42	3.735	3.103	2.472

### 3. 6. The Effect of Chemical Treatments of WGT Biomass Onto MG Adsorption Process

The influence of chemical treatments on adsorption efficiency of WGT is illustrated in Figure 5.

Generally, the acidic treatments change the negatively charged surface of the WGT biomass to positively charged and thus decrease the electrostatic attractions between biomass surface and the cationic molecules (of MG, for example).<sup>43</sup> Acid treatments allows the hemicellulose hydrolyze, especially xylan present in the lignocelluloses. Hemicelluloses can be degraded into xylose, mannose, acetic acid, galactose, glucose, etc. Phenolic compounds are also formed during acidic treatments from the partial breakdown of lignin.<sup>44</sup>

Tartaric acid treatment of the WGT biomass conducts to an increase of the amount of MG removed from the synthetic wastewater aqueous solutions, this chemical pretreatment converting the biomass to highly adsorbing material in terms of higher percentage of MG removed onto the modified tea surface, probably due to an increase of carboxylic groups number on the WGT surface, result that is in good agreement with others from literature.<sup>45,46</sup> The adsorption efficiency of MG increases from 89% (for untreated material) to 93% (after tartaric acid treatment).

WGT biomass treated with HCl led to a decrease of adsorption efficiency (from 89% for untreated material to 75% for HCl treatment), fact which can be attributed to the decrease in electronegativity of the biosorbent surface due to the presence of the residual  $H^+$  ions<sup>47,48</sup> Due to the fact that generally, the acid treatments lead to a decrease of adsorption, the still high values of adsorption efficiency obtained could be associated with the amount of organic matter present in the treated biomass.<sup>49</sup>

$H_3PO_4$  and  $H_2SO_4$  treatments were considered due to the fact that a different material can be obtained, acti-

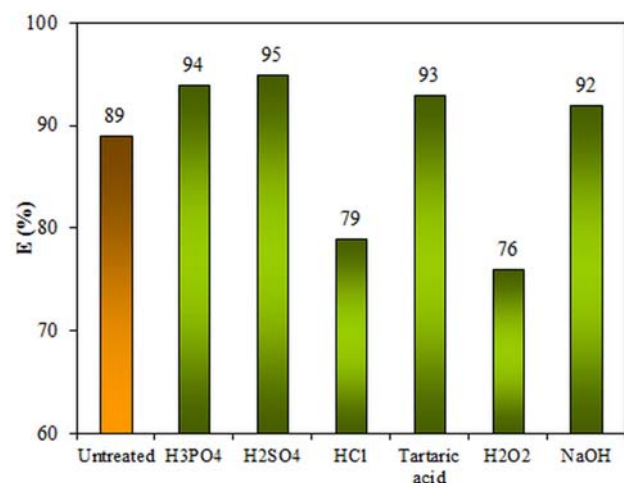


**Figure 6.** Effect of chemical treatments over the adsorption efficiency of MG onto WGT; (296 K, 94 mg/L, 100 mL, 4 g, 200–400  $\mu$ m, 300 rpm, 240 min).

vated carbon (or biochar), which is commonly utilized due to its large adsorption capacity, fast adsorption kinetics, and relatively ease of regeneration.<sup>19,29</sup>

The activated carbon obtained from WGT biomass after  $H_3PO_4$  and  $H_2SO_4$  treatments provided better results for the adsorption efficiency that increases from 89 (for untreated biomass) to 94, and 95%, respectively (Figure 6), results that are in good agreement with other from the literature.<sup>16,50</sup>

In the case of alkali treatment such as NaOH, the increasing of adsorption efficiency can be explained by the fact that after treatment, hydrolysis reactions can occur, causing high dissolution of organic substances from the biomass.<sup>43</sup> The hydrolysis reactions can lead to the formation of more hydroxylic ( $HO^-$ ) and carboxylate ( $COO^-$ ) groups in the treated biomass, which enhance the cationic adsorption.<sup>51</sup> The mechanism of alkali treatment is believed to be saponification of intramolecular ester bonds crosslinking xylan hemicellulose and other component, for example, lignin.<sup>43</sup> Dilute NaOH treatment of lignocellulosic materials caused swelling, leading to a decrease in the degree of polymerization, a decrease in crystallinity, separation of structural linkages between lignin and carbohydrates, and disruption of the lignin structure.<sup>30</sup>

After NaOH treatment, the WGT biomass had a better adsorption efficiency, an increase from 89 to 92% was noted. This treatment is very efficient, with a high increase in adsorption efficiency, fact that can be attributed to the changes on the biomass surface (increase in surface area, average pore volume, and pore diameter),<sup>52</sup> in addition to the already described effects of alkali treatment.<sup>30,43,47,51</sup>

As it can be seen in Figure 6, the treatment of WGT biomass with  $H_2O_2$  leads to a decrease in efficiency (76% by comparison with 89% for the untreated material), fact that confirm the hypothesis that if the concentration of oxidant agent is high (25%  $H_2O_2$ ), the modification of functional groups of the basic structure of the material takes place and the delignification of cellulosic WGT begins to occur.<sup>53</sup>

### 3. 7. Fourier Transform Infrared Spectroscopy (FTIR)

FTIR analysis is an important method for identifying the functional groups responsible for the retention of the dye molecules onto biomass surface. FTIR spectra were obtained for MG dye removal instead of onto untreated (Figure 7) and NaOH treated (Figure 8), before and after biosorption.

The increasing, decreasing, and shifted signals corresponding to different functional groups, were interpreted to indicate which groups participated in the adsorption process. The fact that no significant reduction in number of bands after adsorption for both untreated and treated WGT (Figures 7 and 8) was observed, could indicate that the studied process occurs mainly as physisorption).<sup>32</sup>

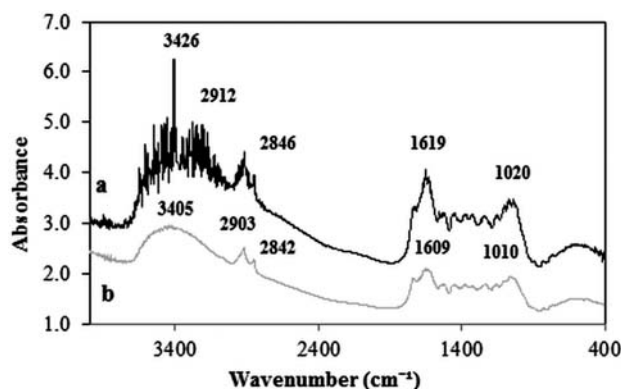


Figure 7. FTIR spectra of untreated WGT before adsorption (a) and after MG adsorption (b).

As it can be seen in Figure 7, the groups affected by the MG adsorption include  $\text{-OH}$ ,  $\text{N-H}$  (stretching), secondary amines,  $\text{SO}_3$  (stretching),  $\text{-C-C-}$ , and amine groups. In the spectrum of untreated WGT biomass (before adsorption), Figure 7a, a broad band from  $3600$  to  $3000\text{ cm}^{-1}$  for  $\text{-OH}$  groups of phenols/carboxyls was observed. The strong band attributed to the hydroxyl group (at  $3426\text{ cm}^{-1}$ ) might be an indication of high cellulose content. After adsorption the aspect of this band is rather flat, and the maximum is shifted to  $3405\text{ cm}^{-1}$ , suggesting the MG adsorption onto WGT surface takes place. Alkane  $\text{C-H}$  vibrations were identified at  $2919$  and  $2886\text{ cm}^{-1}$  for the untreated WGT before adsorption and shifted at  $2903$  and  $2842\text{ cm}^{-1}$  for the WGT after adsorption, a fact which can be explained by the change in the lignocellulosic structure.<sup>16,54</sup> A distinct band at  $1619\text{ cm}^{-1}$  was observed, Figure 7, that was shifted at  $1609\text{ cm}^{-1}$  after MG adsorption, a band that was probably the result of the stretching vibration of  $\text{C=O}$  and  $\text{C-N}$  (Amide I) peptidic bond of proteins.<sup>55</sup> Bands at  $1020\text{ cm}^{-1}$  (before adsorption) and  $1010\text{ cm}^{-1}$  (after adsorption) that could be attributed to the stretching vibration of the  $\text{C-O}$  groups, shifted after adsorption. The fingerprint region demonstrates the existence of sulfur or phosphate groups ( $800\text{--}400\text{ cm}^{-1}$ ).

All these changes identified in the FTIR spectra sup-

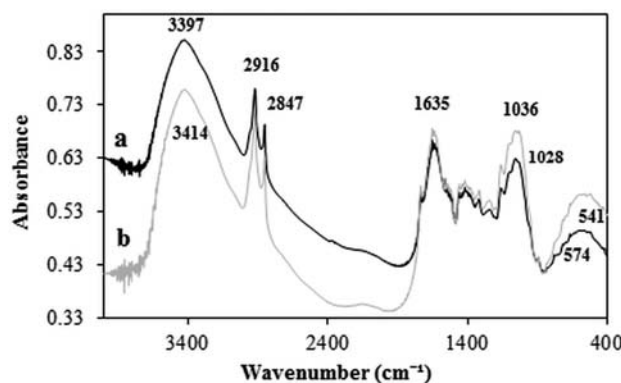


Figure 8. FTIR spectra of WGT treated with NaOH before adsorption (a) and after MG adsorption (b).

port the fact that MG dye adsorption onto WGT surface occurred.

Spectra of NaOH treated WGT before and after MG dye adsorption are depicted in Figure 8. The broad absorption peak at around  $3397\text{ cm}^{-1}$  corresponds to the  $\text{O-H}$  stretching vibrations due to inter- and intra-molecular hydrogen bonding of cellulosic polymeric compounds (macromolecular associations), such as alcohols, phenols, and carboxylic acids, as in pectin, cellulose, and lignin, thus, showing the presence of hydroxyl groups on the adsorbent surface.<sup>47</sup> After MG adsorption this band was shifted at  $3414\text{ cm}^{-1}$ , a fact which supports the MG adsorption. The band at  $2916\text{ cm}^{-1}$  is attributed to the  $\text{C-H}$  stretching vibration of aliphatic acids, while the band at  $1635\text{ cm}^{-1}$  is due to asymmetric stretching vibrations of  $\text{C=O}$ , from carboxyl acid groups.<sup>17,31</sup> The other prominent band at  $1028\text{ cm}^{-1}$  was shifted at  $1036\text{ cm}^{-1}$  and is due to  $\text{C-O}$  stretching vibration from cellulose. Moreover, in the case of treated WGT biomass after adsorption, a remarkable shift in positions of  $\text{-OH}$  and  $\text{C=O}$  bands was observed, which indicates that MG is bound mostly at these groups.<sup>56–59</sup> The changes in FTIR spectra confirm the binding of MG with functional groups present on the adsorbent surface. Similar observations were also reported by Pirbazari et al.<sup>25</sup> The proposed adsorption mechanism would involve the connection realized between a lone pair of the oxygen atom in  $\text{-OH}$  and  $\text{C=O}$  and the nitrogen atom  $=\text{N}^+(\text{CH}_3)_2$  in the MG molecule.

## 4. Conclusions

The efficiency of waste green tea biomass in removing malachite green dye from aqueous solution has been investigated. The removal efficiency increases with the increase of biomass quantity until no further significant change was observed ( $4\text{--}5\text{ g}$ ) and an increase in temperature, and hence the adsorption process is endothermic in nature. Six chemical treatments were tested (four acidic, one basic, and one oxidant) in order to study, first, the chemical groups responsible for the adsorption of MG onto WGT biomass, and secondly, which chemical treatment gives better results in terms of adsorption efficiency by comparison to the untreated material. For WGT biomass, the alkali ( $\text{NaOH}$ ) and acidic ( $\text{H}_2\text{SO}_4$ ,  $\text{H}_3\text{PO}_4$ , and tartaric acid) treatments led to increases of the adsorption efficiency from  $89\%$  (untreated WGT) to  $92\%$  ( $\text{NaOH}$ ),  $93\%$ ,  $94\%$  and  $95\%$  for acidic treatments (tartaric acid,  $\text{H}_3\text{PO}_4$ , and  $\text{H}_2\text{SO}_4$ , respectively).

It can be concluded that this green approach, eco-friendly, and economic cellulosic biomass, could be a promising adsorbent in environmental pollution cleanup. Also, chemical treatments applied to lignocellulosic adsorbents, improved adsorption efficiencies. Further detailed economical analysis (e.g. materials and operating costs) could be used in order to design practical engineering application in the future.

## 5. References

1. M. T. Yagub, T. K. Sen, S. Afroz and H. M. Ang, *Adv. Colloid Interface Sci.*, **2014**, *209*, 172–184. <https://doi.org/10.1016/j.cis.2014.04.002>
2. I. M. Banat, P. Nigam, D. Singh and R. Marchant, *Bioresour. Technol.*, **1996**, *58*, 217–227. [https://doi.org/10.1016/S0960-8524\(96\)00113-7](https://doi.org/10.1016/S0960-8524(96)00113-7)
3. Z. Aksu, *Process Biochem.*, **2005**, *40*(3–4), 997–1026. <https://doi.org/10.1016/j.procbio.2004.04.008>
4. B. H. Tan, T. T. Teng and A. K. M. Omar, *Water Res.*, **2000**, *34*, 597–601. [https://doi.org/10.1016/S0043-1354\(99\)00151-7](https://doi.org/10.1016/S0043-1354(99)00151-7)
5. A. I. Zouboulis, N. K. Lazaridis and A. Grohman, *Separ. Sci. Technol.*, **2002**, *37*, 403–416. <https://doi.org/10.1081/SS-120000795>
6. B. Bolto, D. Dixon, R. Eldridge, S. King and K. Linge, *Water Res.*, **2002**, *36*, 5057–5065. [https://doi.org/10.1016/S0043-1354\(02\)00231-2](https://doi.org/10.1016/S0043-1354(02)00231-2)
7. L. Szpyrkowicz, J. Naumczyk and F. Zilio-Grandi, *Water Res.*, **1995**, *29*, 517–524. [https://doi.org/10.1016/0043-1354\(94\)00176-8](https://doi.org/10.1016/0043-1354(94)00176-8)
8. S. Esplugues, J. Giménes, S. Contreras, E. Pascual and M. Rodriguez, *Water Res.*, **2002**, *36*, 1034–1042. [https://doi.org/10.1016/S0043-1354\(01\)00301-3](https://doi.org/10.1016/S0043-1354(01)00301-3)
9. P. Mavros, A. C. Daniilidou, N. K. Lazaridis and L. Stergiou, *Environ. Technol.*, **1994**, *15*, 601–616. <https://doi.org/10.1080/09593339409385467>
10. S. Dawood and T. K. Sen, *Water Res.*, **2012**, *46*, 1933–1946. <https://doi.org/10.1016/j.watres.2012.01.009>
11. I. H. Dakhil, *J. Kerbala Univ.*, **2013**, *1*, 5–14.
12. C. Crini, *Bioresour. Technol.*, **2006**, *97*, 1061–1085. <https://doi.org/10.1016/j.biortech.2005.05.001>
13. H. Ali, *Water Air Soil Pollut.*, **2010**, *213*, 251–273. <https://doi.org/10.1007/s11270-010-0382-4>
14. A. Bhatnagar and M. Sillanpää, *Chem. Eng. J.*, **2010**, *157*, 277–296. <https://doi.org/10.1016/j.cej.2010.01.007>
15. D. Podstawczyk, A. W. Krowiak, K. Chojnaka and Z. Sadowski, *Bioresour. Technol.*, **2014**, *160*, 161–165. <https://doi.org/10.1016/j.biortech.2014.01.015>
16. N. S. Mokgalaka, R. I. McCrindle and B. M. Botha, *J. Anal. Atom. Spectrom.*, **2004**, *19*, 1375–1378. <https://doi.org/10.1039/b407416e>
17. E. Akar, A. Altinişik and Y. Seki, *Ecol. Eng.*, **2013**, *52*, 19–27. <https://doi.org/10.1016/j.ecoleng.2012.12.032>
18. N. T. Zaveri, *Life Sci.*, **2006**, *78*, 2073–2080. <https://doi.org/10.1016/j.lfs.2005.12.006>
19. B. H. Hameed, *J. Hazard. Mater.*, **2009**, *161*, 753–759. <https://doi.org/10.1016/j.jhazmat.2008.04.019>
20. M. Auta and B. H. Hameed, *Chem. Eng. J.*, **2011**, *171*, 502–509. <https://doi.org/10.1016/j.cej.2011.04.017>
21. A. Fazal and U. Rafique, *J. Water Sustain.*, **2012**, *2*(4), 259–270.
22. J. Shah, M. R. Jan, A. Ul Haq, and M. Zeeshan, *J. Saudi Chem. Soc.*, **2015**, *19*, 301–310.
23. C. -H. Weng, Y. -T. Lin, D. -Y. Hong, Y. C. Sharma, S. -C. Chen *et al. Ecol. Eng.*, **2014**, *67*, 127–133. <https://doi.org/10.1016/j.ecoleng.2014.03.053>
24. A. E. Pirbazari, E. Saberikbah, M. Badrouh and M. S. Emami, *Water Resour. Ind.*, **2014**, *6*, 64–80. <https://doi.org/10.1016/j.wri.2014.07.003>
25. S. Burcă, A. Măicăneanu and C. Indolean, *Rev. Roum. Chim.*, **2016**, *61*(6–7), 541–547
26. [http://www.pentachemicals.eu/specifikace/specifikace\\_892.pdf](http://www.pentachemicals.eu/specifikace/specifikace_892.pdf)
27. W. Amey and V. N. Ganvir, *Int. Res. J. Environ. Sci.*, **2013**, *2*, 53–55.
28. J. Zhang, Y. Li, C. Zhang and Y. Jing, *J. Hazard. Mater.*, **2008**, *150*, 774–782. <https://doi.org/10.1016/j.jhazmat.2007.05.036>
29. M. H. Kalavathy, T. Karthikeyan, S. Rajgopal and L. R. Miranda, *J. Colloid Interf. Sci.*, **2005**, *292*, 354–362. <https://doi.org/10.1016/j.jcis.2005.05.087>
30. A. Ronda, M. A. Martín-Lara, M. Calero and G. Blázquez, *Ecol. Eng.*, **2013**, *58*, 278–285. <https://doi.org/10.1016/j.ecoleng.2013.07.013>
31. R. Gnanasambandam and A. Protor, *Food Chem.*, **2000**, *68*, 327–332. [https://doi.org/10.1016/S0308-8146\(99\)00191-0](https://doi.org/10.1016/S0308-8146(99)00191-0)
32. M. Suchy and D. S. Argyropoulos, *Japan TAPPI J.*, **2002**, *1*, 1–18.
33. M. -H., Baek, C. O. Ijagbemi, O. Se-Jin, D. -S. Kim, *J. Hazard. Mater.*, **2010**, *176*, 820–828.
34. F. Deniz, and S. Karaman, *Chem. Eng. J.*, **2011**, *170*, 67–74. <https://doi.org/10.1016/j.cej.2011.03.029>
35. S. Venkata Mohan, S. V. Ramaianah and P. N. Sharma, *Biochem. Eng. J.*, **2008**, *38*, 61–69. <https://doi.org/10.1016/j.bej.2007.06.014>
36. A. Saeed, M. Sharif and M. Iqbal, *J. Hazard. Mater.*, **2010**, *179*, 564–572. <https://doi.org/10.1016/j.jhazmat.2010.03.041>
37. W. Yang, S. Yajuan, L. Ping and L. Bo, *J. Chinese Inst. Food Sci. Technol.*, **2011**, *4*, 83–89.
38. Liu, L., Liu, J., Li, H., Zhang, H., Liu, J. and Zhang, H., *BioResources*, **2012**, *7*(3), 3555–3572.
39. D. M. Gligor, and A. Maicaneanu, In *Clay: Types, Properties and Uses*, edited by Humphrey J. P.; Boyd D. E.; Hauppauge, NY: Nova Science Publishers Inc., **2011**, pp. 1–62.
40. M. Macoveanu, D. Bilba, N. Bilba, M. Gavrilescu, and G. Soreanu, *Procese de schimb ionic în protecția mediului; Bucharest: Matrix Rom*, **2002**.
41. M. A. Hossain and Md. L. Hossain, *Int. J. Adv. Res.*, **2014**, *2*, 360–374.
42. Y. Liu and Y. J. Liu, *Sep. Purif. Technol.*, **2008**, *61*, 229–242. <https://doi.org/10.1016/j.seppur.2007.10.002>
43. E. Pehlivan, T. Altun and Ş. Parlayici, *Food Chem.*, **2012**, *135*, 2229–2234. <https://doi.org/10.1016/j.foodchem.2012.07.017>
44. R. Abdallah and S. Taha, *Chem. Eng. J.*, **2012**, *195–196*, 69–76. <https://doi.org/10.1016/j.cej.2012.04.066>
45. L. W. Low, T. T. Teng, N. Morand and B. Azahari, *APCBEE Procedia*, **2012**, *1*, 103–109. <https://doi.org/10.1016/j.apcbee.2012.03.018>

46. Y. Feng, H. Zhou, G. Liu, J. Qiao, J. Wang, H. Lu, L. Yang, and Y. Wu, *Bioresource Technol.*, **2012**, *125*, 138–144.  
<https://doi.org/10.1016/j.biortech.2012.08.128>
47. H. Yazici, M. Killç, M. Solak, *J. Hazard. Mater.*, **2008**, *151*, 669–675.  
<https://doi.org/10.1016/j.jhazmat.2007.06.042>
48. N. Gupta, A. K. Kushwaha and M. C. Chattopadhyaya, *Arabian J. Chem.*, **2016**, *9*, S707–S716.  
<https://doi.org/10.1016/j.arabjc.2011.07.021>
49. K. G. Bhattacharyya and A. Sharma, *J. Hazard. Mater.*, **2004**, *113*, 97–109.  
<https://doi.org/10.1016/j.jhazmat.2004.05.034>
50. A. P. Batista, L. P. Romão, M. L. Arguelho, C. A. Garcia, J.P. Alves et al., *J. Hazard. Mater.*, **2009**, *163*, 517–523.  
<https://doi.org/10.1016/j.jhazmat.2008.06.129>
51. T. Gu, *Green Biomass Pretreatment for Biofuels Production*; Ohio: Springer, **2013**.  
<https://doi.org/10.1007/978-94-007-6052-3>
52. A. Wankhade and V. N. Ganvir, *Int. Research J. Environ. Sci.*, **2013**, *2–4*, 53–55.
53. G. Blázquez, M. Calero, A. Ronda, G. Tenorio, and M. A. Martín-Lara, *J. Ind. Eng. Chem.*, **2014**, *20*, 2754–2760.  
<https://doi.org/10.1016/j.jiec.2013.11.003>
54. H. Eroglu, E. Varoglu, S. Yapıcı and A. Sahin, *Chem. Eng. J.*, **2010**, *165*, 563–572.  
<https://doi.org/10.1016/j.cej.2010.09.074>
55. Z. Chen, H. Deng, C. Chen, Y. Yang, and H. Xu, *J. Environ. Health Sci. Eng.*, **2014**, *12*, 63–73.  
<https://doi.org/10.1186/2052-336X-12-63>
56. J. -F. Gao, Q. Zhang, J. -H. Wang, X. -L. Wu, S. -Y. Wang et al. *Bioresource Technol.*, **2011**, *102*, 805–813.  
<https://doi.org/10.1016/j.biortech.2010.08.119>
57. P. Thamilarasu and K. Karunakaran, *Canadian J. Chem. Eng.*, **2013**, *91*, 9–18.  
<https://doi.org/10.1002/cjce.20675>
58. A. Cabuk, S. Ilhan, C. Filik and F. Caliskan, *Turk. J. Biol.*, **2004**, *29*, 23–28.
59. J. R. Njimou, A. Măicăneanu, C. Indolean, C. P. Nanseu-Njiki, E. Ngameni, *Environ. Technol.*, **2016**, *37*, 1369–1381.  
<https://doi.org/10.1080/09593330.2015.1116609>

## Povzetek

Proučevana je bila adsorpcija barvila malahitno zeleno (MG) iz vodne raztopine na odpadno biomaso zelenega čaja (WGT). Izvedena je bila serija šaržnih eksperimentov z namenom ugotoviti vpliv temperature in količine biomase na adsorpcijo. Maksimalna kapaciteta odstranitve z neobdelano biomaso WGT je bila 89% (4 g biomase, 100 mL raztopine s koncentracijo 94 mg/L, 316 K), pri tem se je kapaciteta adsorpcije večala od 296 do 316 K. Izračunani termodinamski parametri ( $\Delta H^\circ$ ,  $\Delta S^\circ$ ,  $\Delta G^\circ$ ) kažejo, da je adsorpcija endotermna in nespontana. Testiranih je bilo 6 kemijskih predobdelav biomase ( $H_3PO_4$ ,  $H_2SO_4$ , HCl, vinska kislina,  $H_2O_2$  in NaOH) z namenom ugotoviti skupine, odgovorne za adsorpcijo. Obdelava z NaOH in  $H_3PO_4$  je povečala adsorpcijsko kapaciteto na 92% in 95%. FTIR spektroskopija je pokazala modifikacijo površine biomase in s tem vpliv na adsorpcijo.





## **DRUŠTVENE VESTI IN DRUGE AKTIVNOSTI SOCIETY NEWS, ANNOUNCEMENTS, ACTIVITIES**

### **Vsebina**

Kemijski laboratorij celjske kraljice (ob 580 letnici kronanja češke kraljice Barbare Celjske) .....	S67
Poročilo o delu v letu 2016 .....	S77
Koledar znanstvenih in strokovnih srečanj .....	S81
Navodila za avtorje .....	S86

### **Contents**

Chemical Laboratory of Celje Queen (at 580 <sup>th</sup> Anniversary of Bohemian coronation of Queen Barbara of Celje) .....	S67
Report for 2016 .....	S77
Scientific meetings – chemistry, chemical technology and chemical engineering .....	S81
Instructions for authors .....	S86



# Kemijski laboratorij celjske kraljice (ob 580 letnici kronanja češke kraljice Barbare Celjske)

Stanislav Južnič

\* Corresponding author: E-mail: juznic@hotmail.com

Telephone: 031 814 742

## Povzetek

Barbara Celjska je bila gotovo najbogatejša alkimistka vseh časov. Prispevek skuša pojasniti kakšni poskusi so potekali v njenem laboratoriju in nakazati, katere tehniške kemijske naprave je utegnila pri tem uporabljati. Ker je bila večina le-teh iz zlahka lomljivih snovi, bi bilo njihovo iskanje bržkone brez haska, saj ni veliko upanja za njihovo ohranitev.

**Ključne besede:** Barbara Celjska, Zgodovina alkimije, 15. stoletje, Celje, Češka, Samobor

## 1. Uvod

Herman II Celjski si je svoje talente raje omislil zunanaj debelih bukev, tako da mu je latinščina ostala španska vas. Toliko več pa je dal na učenost svojih otrok, kjer mu je sekira najbolj padla v med prav pri najmlajši Barbari<sup>1</sup> in pri posvojenki Ani.<sup>2</sup>

Dne 11. 2. 1437 so v zlati Pragi cesarjevo soprogo Barbaro Celjsko okronali za češko kraljico. To je bil svojevrsten višek družbenega vzpona tedaj petinštiridesetletne gospe, ki od nekdanj ponazarja značilno slovensko zgodbo o uspehu pod tremi celjskimi zvezdami.

Barbara Celjska nikakor ni bila zgolj vladarica, temveč se je obenem nadvse uspešno ukvarjala z laboratorij-



Slika 1: Barbarin Samoborski grad z nekdanjim laboratorijem v kletnih prostorih kot je videti danes: je črna kraljica tam postorila kaj zlata?

skimi poskusi tiste vrste, ki jih danes radi krstimo za alkimijo. V Samoboru med Zagrebom in našo mejo je preživela veliko časa kot cesarjeva vdova. Ker je bila daleč najbogatejša gospa v tedanji ogrsko-hrvaški kraljevini, si je lahko marsikaj privoščila. Nosila je seveda tudi ogrsko-hrvaško krono, kajpada ne na vsakdanjih sprehodih. Tedanja ogrsko-hrvaška kraljevina pa ni bila kar tako, saj je ob deželah omenjenih v svojem imenu obsegala še današnjo Slovaško, Romunijo, dele Avstrije in Slovenije.<sup>3</sup>



Slika 2: Vladarica Barbara Celjska.

## 2. Alkimija v somoborski kleti

Barbari je ljubezen do nekoliko bolj okultnih ved vsadil že oče Herman II., ki je hranil eno izmed tobož pristnih kup Svetega Graala (St. Grail, Graal) v svojem

gradu Rogatec.<sup>4</sup> Skupaj s sinom, Barbaro, njeno hčerko in zetoma pa se je prevzetni Herman dal včlaniti za povrhu v Red Zmaja,<sup>5</sup> ki je imel kar nekaj okultnih podstati.

Barbarin Samoborski dvorec seveda tudi ni bil od muh, v njegovi kleti pa si je zvedava gospa uredila alkimistični laboratorij. Njeni zapisi niso ohranjeni, saj vladarici Barbari seveda ni bilo treba objavljati knjig in pisati o svojih dosežkih. Raje je pustila, da so o njenih tehnikah poročali drugi.

Dobro pričevanje o njenem delu dobimo iz zapisov njenega sodobnika, češkega alkimista Johannes iz Laaza (Laatz), ki je bil bržkone doma na Moravskem. Johannes iz Laaza je deloval večinoma v Italiji, kjer se je ukvarjal z zlatotvorstvom in preobrazbo kovin. Njega dni to ni bilo tako nenavadno, kot bi bilo danes, je pa bil vmes seveda svojevrsten riziko. Zaradi neuspehov pri vedno znova objavljeni preobrazbi kovin se je vrli Johannes postopoma zameril raznoraznim laškimi vladarjem in je moral bežati iz Italije. Dobil je celo za svoj poklic nič kaj laskavi vzdevek Lasnioro (Laz-nien-oro, »Laz brez zlata«). Ko si je na vrat na nos obrusil pete in pustil nejeverne Italijane za svojim hrbtom, je na veliko potoval in obiskoval številne znane alkimiste, da bi jim z zvijačo ali kako drugače izpulil skrivnostne formule na katerih je slonela tehnika njihovega pečanja s kemijskimi pretvorbami. Seveda se je zvečine slabo odrezal, saj je velika večina tedanjih alkimistov svoja znanja skrbno skrivala pred zvedavimi očmi vsiljivcev.

Ko je nadobudni Laaz takole vandral brez pravega haska, si je spotoma nabral kar nekaj novic o zmogljivosti Barbarinega kemijskega laboratorija. Beseda je dala besedo in ukaželjni Laaz si je že brusil pete pred vrati Barbarine graščine da bi obiskal še dvor kraljice Barbare v Samoboru. Tam so ga Barbarini pomočniki sprejeli precej bolje,

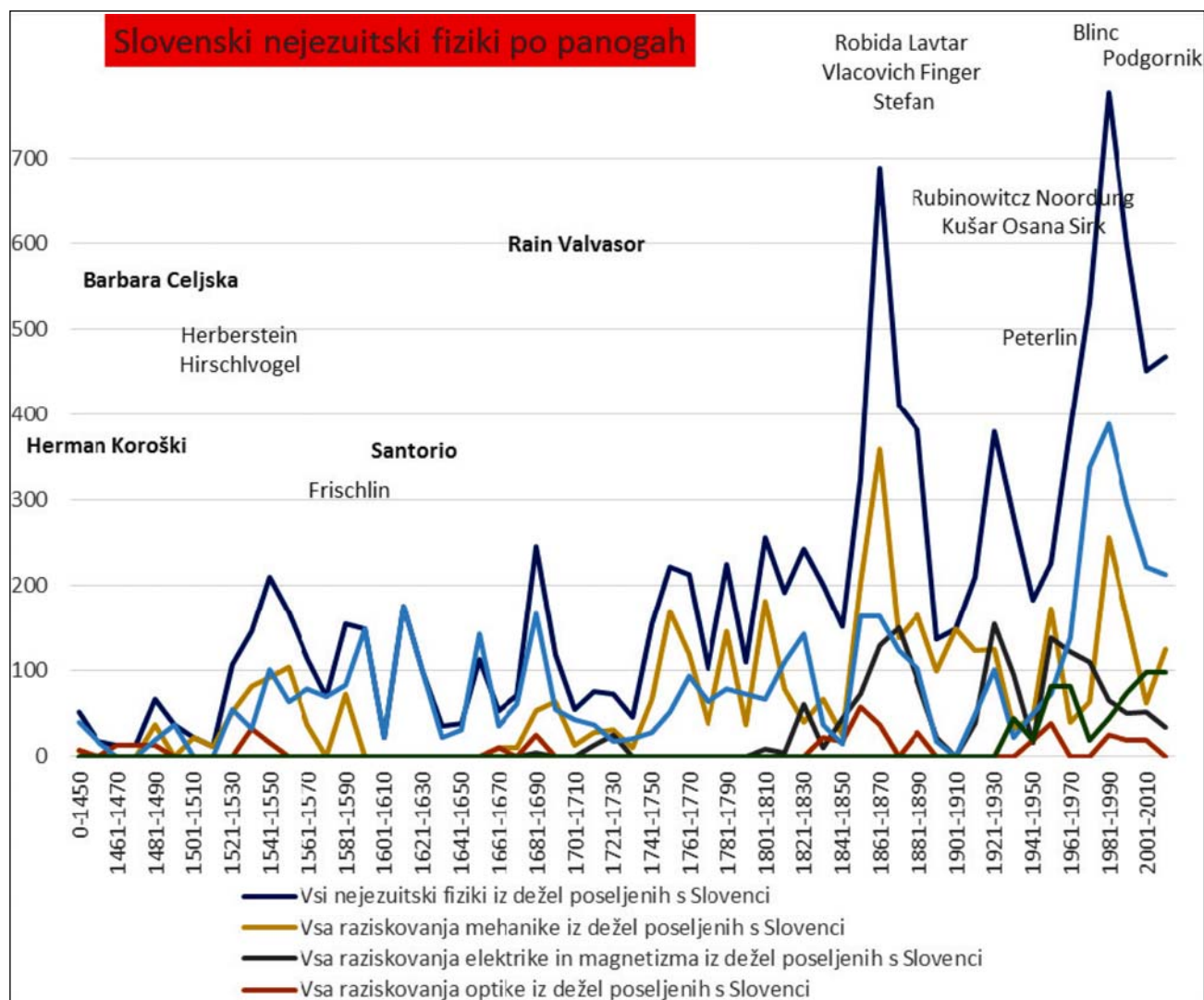


Slika 3: V hrvaški Krapini izdan dokument o Barbarini poroki z povabilom na prihajajočo poroko podpisan dne 6. Novembra 1405 (Magyar Nemzeti Levéltár – Országos Levéltár - Diplomataikai Levéltár (MNL OL DL), Budapest, signatura 78655)

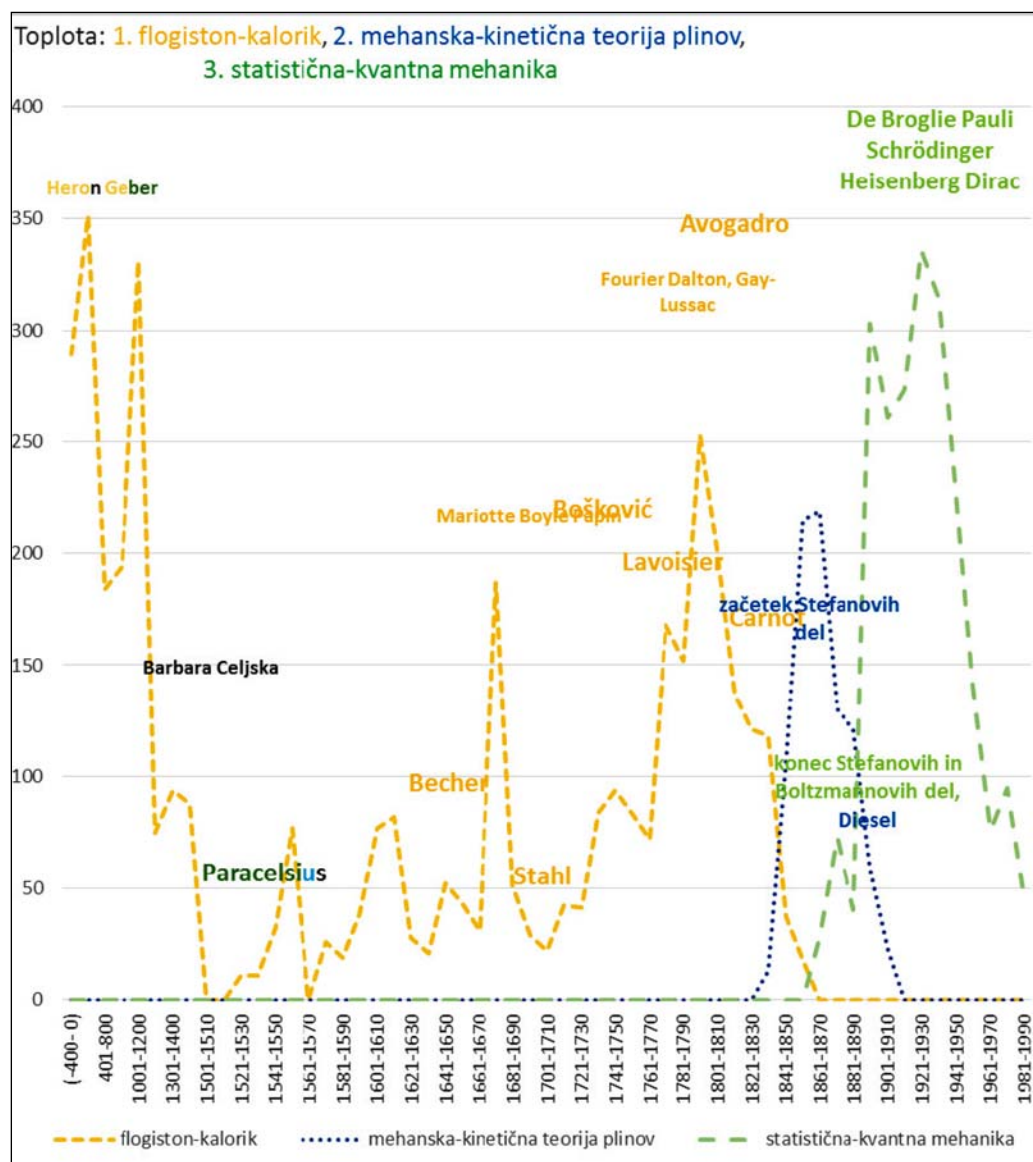
kot je bil sicer vaje. Barbari je Laazova pozornost namreč kar dišala, saj je bil Laaz kljub številnim spodsrljam v alkimističnih krogih dokaj znana osebnost in ne samo pavliha. Laaz je namreč sestavil spis *Tractatus aureus de lapide philosophorum* kjer je takoj sprva in znova na koncu v svojem *Tractatus II de lapide philosophico* zatrjeval, da je bil svoj čas študent slovečega alkimista Antona iz Firenc (Antonius de Florentia),<sup>6</sup> ki naj bi ga svoj čas spravili s sveta v Pragi v svojevrstnem obračunu tedanje, llahko bi rekli, alkimistične mafije. Spis je Laaz sicer datiral nekako osem let po obisku Barbarinega laboratorija, vendar pa so Laazovi izumi in mnenja že mnogo prej krožili med smetano tedanje evropske kemije in alkimije. Prav bogata kraljica Barbara je bila daleč najbolje obveščena med vsemi sodobniki, ki so se njega dni ukvarjali s tehnikami proizvodnje novih materialov, tako da so novice v njen laboratorij trumoma pritekale in je pogosto kar stežka ločevala zrna od plev. Laazove ideje pa so se ji zdele nadvse pomembne, saj si je Laaz v svojem traktatu

med drugim privoščil opise pridobivanja živega srebra, žvepla, in arzena v povezavi s slovitimi vedeži, kot sta bila legendarni Hermes in Tomaž Akvinski.<sup>7</sup> Idrijski živosrebrni rudnik njega dni resda še ni obratoval, kljub temu pa je zvečine špansko živo srebro igralo odločilno vlogo pri domnevnih ali resničnih pretvorbah kemijskih spojin. Barbarin nečak Ulrik je že dobrih ducat let pred Laazovim obiskom Barbarinega laboratorija romal v Španijo, tako da je imela Barbara španskega živega srebra od nekdanj dovolj na razpolago.

Zadnji del Laazovega teksta je bil posvečen opatu Johannesu Trithemiusu, ki je slovel po svojem tajnopisu. Nekoliko nagajivi Laaz je celo priporočal uporabo sperme, ženskih tekočin in krvi po trojni destilaciji, ki se je njega dni postopoma uvajala v kemijo po Arabskih predlogah sposojenih pri Kitajcih,<sup>8</sup> čeravno je severnoitalijanski inovator Taddeo Alderotti razvil svojo inačico frakcionirne destilacije že nekaj let predno so bili na voljo potopisi Marka Pola. Barbara zaradi dvornih igrin in mahinacij ni



Graf 1: Kemijska raziskovanja Barbare Celjske v primerjavi z dosežki drugih znanstvenikov povezanih s slovenskimi deželami.



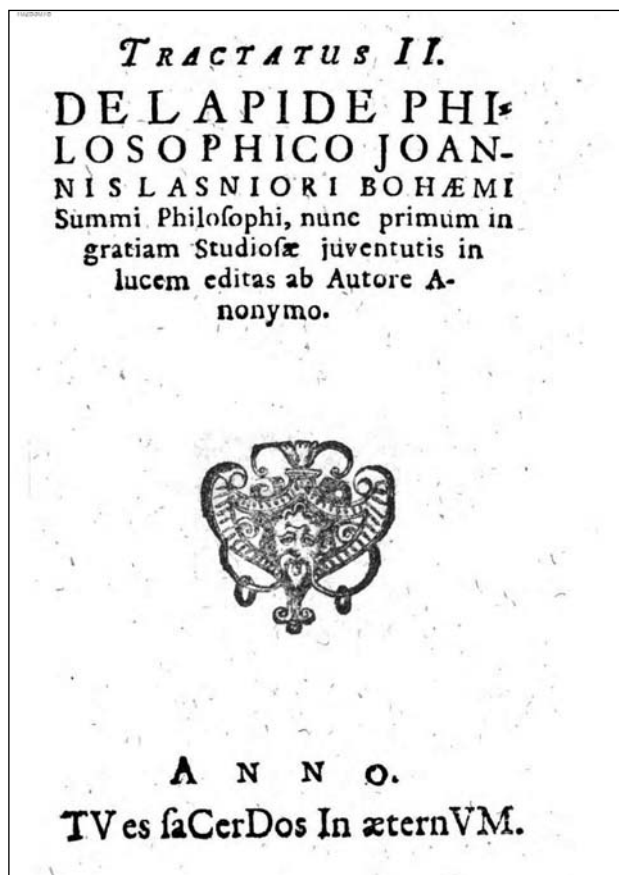
Graf 2: Kemijska raziskovanja Barbare Celjske v primerjavi z dosežki drugih znanstvenikov v svetovnem merilu.

spremljala svojega soproga na njegovo cesarsko kronanje v Rim, čeravno si je veliko obetala od vmesnih obiskov italijanskih laboratorijev. Zato so bile njene povezave z italijanskimi tehnološkimi inovatorji slabše kot si je želela in so ji Laazove informacije o laških novotarijah prišle nadvse prav.

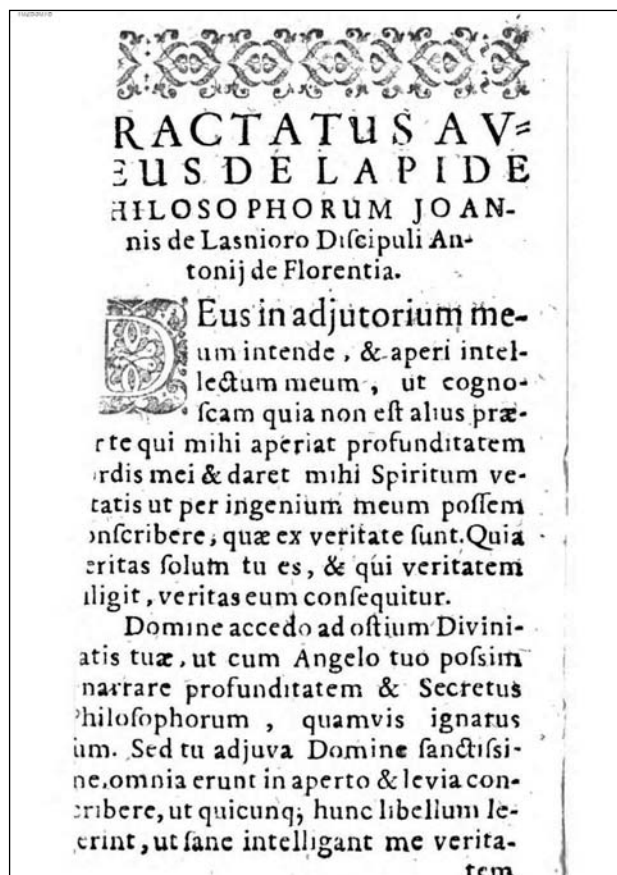
Da bi naredila prijeten vtis na Laaza, ga je cesarica vdova Barbara povabila v svoj laboratorij. Govorila sta morda kar po češko, saj so Barbari tuji jeziki šli nadvse dobro od rok. Tisti čas se je pisalo leto 1540 in alkimistične pretvorbe so bile vedno bolj priljubljeno pečanje mnogih. To kar je Laaz videl v Barbarinem kletnem samoborskem laboratoriju in poskuse, opravljene v njegovi navzočnosti, je premeteni Laaz opisal v knjigi *Via Universalis* (»Univerzalna pot«.), ki jo lahko imamo za svojevrstno Laazovo tehniško zapuščino. Del teksta iz tega

Laazovega dela je bil pozneje objavljen v sedmi izdaji alkimističnega dela *Currus Triumphalis Antimonii* (»Zmagujoči antimonov voz« ali »Triumfalni antimonov voz«.), pripisanega alkimistu Basilu Valentinu. Pri pisanju domnevnega benediktinca z dobrodušno pametnim obrazom na naslovnici knjige Basila Valentina je šlo bržkone za prvovrstno potegavščino, eden izmed piscev, ki so se skrivali za posrečeno domisljico pa je bil navdušeni Paracelzijanec leipziški profesor Joachim Tancke, ki je pri potegavščini pomagal tamkajšnjemu solastniku proizvodnje soli Johannu Thöldeji iz mesta Hesse. Pri čiščenju soli se je seveda možakar naučil veliko kemije, kar mu je zelo prav prišlo v knjigah, ki so se prodajale za med.

Johannes iz Laaza je takole osmisli svoj nepozabni obisk v Barbarinem laboratoriju: »*Ko sem od več strani slišal o kraljici, vdovi kralja Sigismunda, blagega spomina,*



Slika 4: Naslovnica Laazove knjige



Slika 5: Laazov začetek knjige

da je večča v fizikalni umetnosti, sem stopil k njej, da bi jo preizkusil. Ta žena mi je odgovarjala zelo premeteno. Videl sem, da je vzela živo srebro in arzenik ter še nekaj drugega, kar je ona sama vedela. Iz tega je naredila prašek, od katerega se je baker pobelil. Dobljeno snov je bilo mogoče drgniti ne da bi pokazala pravo barvo. Preizkusa s kladivom pa ta snov ni prenesla. Tako je ogoljufala mnoge ljudi«.

Poskus je Laaz seveda poznal iz alkimistične literature in ga je tudi sam mnogokrat svojeručno zastavil. Gre za spajanje bakra z živim srebrom in arzenom, pri čemer spojina dobi lepo srebrno barvo. Barva jer bila namreč temeljna reč pri tedanjih alkimistih<sup>9</sup> in ostaja velepomembna tudi danes. Že neznanec, ki je pisal pod imenom Pseudo-Demokrit, je v 2. stoletju odkril skrivnost tovrstnega

navideznega spreminjanja bakra v srebro. Takšni poskusi v egipčanski Aleksandriji njega dni niso bili nič nenavadnega, strokovnjaki so si pač brez slabih namenov skušali pridobiti potrebne veščine za cenejše pridobivanje kovin, ki so bile videti kot zlahodne. Pri tem niso imeli v mislih prevare, podobno kot v sodobni industriji tankih prevlek nezaželene lastnosti izdelka prekrijemo s nekaj molekulami zaželene trdote, barve in bleska.

Laaz seveda ni ostal le pri tem in je Barbaro nagovarjal, da naj mu pokaže kaj še zna pametnega postoriti v svojem laboratoriju. Barbara si ni dala dvakrat reči in je svoje pomočnice in pomočnike zdajci-takojci pritegnila k

demonstracijam novih tehnik, ki si jih je Laaz takole zapomnil:

»Prav tako sem videl pri njej, da je segret baker posipala z nekim praškom, ki se je vpil v baker in je baker obarval kot bi bil fino srebro. Ko se je baker ponovno strdil, je postal baker, kakor je bil prej. Pokazala mi je še več takih lažnih umetnosti.«

Seveda je Barbara pričakovala Laazovih pohval in se je brzkone nadejala še kakšnega nasveta z njegove strani. Takšen postopek nikakor ni bil posebna novost za Laaza, saj je bil prav tako poznan v alkimistični literaturi. Že Stockholmski papirus star kakih sedemnajst stoletij, ki ga je švedski generalni konzul prinesel domov iz egipčanskih Teb, govori o beljenju bakra (halkoy leukosis) med svojimi 154 recepti kjer so pomembno mesto zavzemale imitacije zlata in srebra. Opravlja se z arzenom, tako da so na Barbarin način realgar (rdeči arzenov sulfid,  $\alpha\text{-As}_4\text{S}_4$ ) in arzenik (strupen prah, arzenov tri-oksidi) vrgli v raztaljeni vreli baker. Ker se je očitno premalo navdušeni Laaz še vedno obotavljal s pričakovanimi pohvalami, je še vedno dokaj čedna kraljica naročila nov poskus, ki naj bi Laaza še bolj osupnil:

»Drugič je vzela crocus martis (Crocus martis – dobesedno »marsov žafran«, železov oksid s formulo  $(\text{FeSO}_4)$ , ki običajno vsebuje delež nečistosti), bakreno apno in druge praške. Snovi je pomešala in s tem cementirala



**Slika 6:** Naslovnica *Basilica chimica* Oswalda Crolla pripisane Basilu Valentinu, ki jo je Volf Engelbert Turjaški imel v svoji ljubljanski knjižnici v prostorih sodobnega NUKa.



**Slika 7:** Barbara Celjska portretirana kot Venera, ki je bila ekvivalentna bakru v njenih laboratorijskih poskusih (Vir: Konrad Kyeiser, Bellifortis, manuscript 1360, folio 002v, Bibliothèque municipale de Besançon, first half of the fifteenth century, "Liber de septem signis", Bellifortis-fragment).



**Slika 8:** Celjska kot temno modra Venera še bolj podobna bakru, ki ga je skušala pozlatiti v svojem laboratoriju



**Slika 9:** Barbara na koncilu v Konstanci (Vir: Kronika Ulricha Richenthala).



enake dele zlata in srebra. Kovina je imela na zunaj in odnotraj videz finega zlata, ko pa se je raztalila, je izgubila zlato barvo. S tem je prevarala mnoge trgovce».

V drugem postopku uporabljen *crocus martis* (žafan železa) oziroma železov dva-oksidi je rumene barve, medtem ko je bakrov oksid rdeče barve. Cementacija se v tem kontekstu alkimiji imenuje postopek odvajanja zlata od srebra.

Kovine in kovinske okside so tedanji strokovnjaki razžarili v posebni posodi skupaj z navadno soljo in galico (tako imenovanem cementu). Na takšen način očiščeno zlato je bilo celo čistejše od naravnega. Tako zlato se je v poznejši dobi Paracelzove jatrokemije uporabljalo za kot zdravilo. Bolnikom so ga dajali v obliki tankih zlatih lističev, ali tekočega pitnega zlata, torej zlata topljenega v zlatotopki, ali v zmesi alkohola in limonovega soka.

Laaz pa je iz vse te kolobocije vendarle očitno potegnil ta kratko. Njegovo pričevanje se namreč zaključuje takole: »Videl sem mnogo goljufij in prevar, zato sem ji to očital. Ona pa me je hotela zapreti, a ušel sem ji z Božjo pomočjo.«<sup>10</sup>

Seveda je bil znani prevarant v resnici Laaz, Barbara pa najbrž zlepa ne, saj je imela pod palcem toliko cvenka, da ji ja ni bilo treba prigoljufati dodatnih zaslužkov. Žal pa Laaz nekako ni hotel poročati o spornem zaključku svojega sodelovanja v Barbarinem laboratoriju, ki je moral biti kaj vratolomen in vznemirljiv.

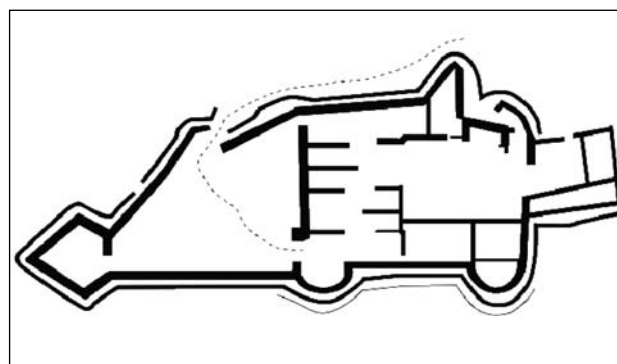


**Slika 10:** Vladarica Barbara Celjska se pridno smehlja za bodoče rodove med koncilom v Konstanci, a med nasmehi si seveda misli svoje.

Barbara je zavoljo takšnih in drugačnih Laazovih potegavščin resda kmalu prišla ob dober glas, saj se je v Samoborju in Medvedgradu, seveda pa tudi v bližnjem Zagrebu, vrli bratje Hrvati še dandanes spominjajo kot črne kraljice.<sup>11</sup> Iz njenega spodnještajerskega okolja pa so kmalu izšli prvovrstni učenjaki, ki so predavali predvsem na Dunajski univerzi. Prvi med njimi je bil Bernhard Perger iz Ščavnice v Slovenskih goricah, po nemško imenovanih Stainz.<sup>12</sup>



**Slika 11:** Samoborski grad od znotraj v današnjem stanju: kaj neki je ostalo od Barbarinega letnega laboratorija?



**Slika 12:** Tloris gradu Samobor formalno v posesti Celjske hiše, kjer si je Barbara Celjska uredila znameniti kletni laboratorij.

V Pergerjevih deških letih se je dokončno skrhalo dotedanja moč njegovih gospodarjev, knezov celjskih. Ob začetku Pergerjevih najstniških let je lepe oči zatisnila mogočna cesarica Barbara Celjska, dobrih pet let za njo pa še njen nečak Ulrik kot zadnji Celjan. Eden od povodov za celjski danes in nikoli več je bila pomanjkljiva skrb za univerzitetno izobrazbo, saj Celjani kljub silni moči in znanju niso obvladovali nobenega univerzitetnega mesta, niti se niso posebej trudili za ustanovitev kakšne nove univerze. Tako se je Perger slaba tri leta po umoru Ulrika Celjskega leta 1459 odpravil po znanje na dunajsko uni-

verzo, ki je prav tedaj slovela po Peuerbachovih in Regiomontanusovih predavanjih. Perger je bil humanist bolj italijanske usmeritve, ki si jo je prisvojil v mladih študijskih letih. Med njegovimi nasprotniki na dunajski univerzi je bil predvsem nemški humanist Konrad Celtis, ki je našega junaka v zbadljivi pesmi imenoval celo »zahrbtnega Slovana«.



Slika 13: Triindvajsetletna kraljica Barbara Celjska na koncilu v Konstanci

### 3. Zaključek

Čeravno nimamo vpogleda ne v Barbarino zbirko eksperimentalnih naprav, ne v naravoslovni del njene knjižnice, si vendarle lahko predstavimo okoliščine njene raziskovalne vneme. Kemijski in alkimistični vzgibe njenih snovanj utegnejo biti naravnost vznemirljivi. Barbarin družbeni položaj je bil seveda nekajkrat previsok, da bi si belila glavo z objavljanim dosežkom, ki pestijo vsakdan navadnih smrtnikov. Gotovo bo dodatno predstavo o njih kmalu bolje predočil ohranjeni del njene zasebne korespondence skupaj z obračuni njenih nemajhnih izdatkov ob nabavah pripomočkov za poskuse in kemijskih snovi.

### 4. Literatura

1. J. Mlinar, *Podoba Celjskih grofov v narativnih virih*. Ljubljana: Historia znanstvena zbirka Oddelka za zgodovino Filozofske fakultete v Ljubljani 11, **2005**, 55; I. Sivec, *Kraljica s tremi kronami*. Mengeš: ICO, **2016**, 27.
2. M. Lukanc, *Ana Celjska*. Celje: Pokrajinski muzej, **2016**, 12.
3. [https://www.academia.edu/31751274/Queen\\_Sisters\\_Barbara\\_and\\_Anna\\_of\\_Celje](https://www.academia.edu/31751274/Queen_Sisters_Barbara_and_Anna_of_Celje)
4. S. Likar, *Vloga viteških redov na obrambnem i karitativne*



Slika 14: Barbara in njen soprog v Konstanci obkrožena z vsemi vladarskimi častmi

*področju s poudarkom na Nemškem viteškem redu na Slovenskem*, Diplomatska naloga. Teološka Fakulteta Univerze v Ljubljani, mentor Bogdan Kolar, **2007**, 61-62.

5. A. Žižek, *ABC Arhivska Barbara Celjska*. Celje: Zgodovinski arhiv/Pokrajinski muzej, **2015** (nepaginirano), 8
6. B. Láng, *Unlocked Books: Manuscripts of Learned Magic in the Medieval Libraries of Central Europe*. Penn State Press, **2010**, 157.
7. J. Laaz, *Tractatus II de lapide philosophico/ Tractatus aureus de lapide philosophorum*, **1611** (nepaginirano), 8.
8. D. Grdenić, *Alkemija*. Zagreb: Jasenski i Turk, **2003**, 195.
9. D. Grdenić, *Alkemija*. Zagreb: Jasenski i Turk, **2003**, 50, 52
10. R. Fugger Germadnik, *Barbara Celjska 1382-1451*. Celje: Zgodovinski arhiv/Pokrajinski muzej, **2010**, 32; I. Sivec, *Kraljica s tremi kronami*. Mengeš: ICO, **2016**, 244-245, 252-256; B. Láng, *Unlocked Books: Manuscripts of Learned Magic in the Medieval Libraries of Central Europe*. Penn State Press, **2010**, 156, 211; N. Petraeus, (ur.): *Fr. Basilii Valentini Chymische Schriften*. Hamburg, **1717, 1740**; H. Kopp, *Die Alchemie in älterer und neuerer Zeit*. Heidelberg: Carl Winters, **1886**, 1: 60-61; U. Büttner, & E. Schwär, *Barbara von Cilli - Empress, Femme Fatale, and Vampire*, V: (ur. U. Büttner, E. Schwär), *Konstanzer Konzilgeschichte*, Constance: Publisher Stadler, **2014**, 63-68.

11. S. Paušek-Baždar, Königin Barbara zu Cilli als Alchimistin in Samobor. *Godišnjak Njemačke narodnostne zajednice* 15/1, **2008**, 275, 279; A. Žvab, Baročna alkimija na Kranjskem. *Kronika*. 2, **2016**, 202; S. Katanec, *The Perquisite of a Medieval Wedding: Barbara of Cilli's Acquisition of Wealth, Power, and Lands*. Magistrska teza, Budapest, **2014**, 9, 10.
12. Glede kraja Pergerjevega rojstva je več tehničnih inštitucij (C. Faustman, Cornelia & D. Luger, Humanist und Naturwissenschaftler? Bernhard Perger zwischen Kanzleihumanismus, griechischer Philologie und dem Erbe Georgs von Peuerbach, in: *Wissensheft und Kultur an der Zeitenwende. Renaissance/Humanismus, Naturwissenschaften und universitärer Alltag im 15. Und 16. Jahrhundert* (ur. Helmuth Grössing & Kurt Mühlberger), Vienna: University Press, **2012**, 143, 146, 148, 150).

## Abstract

### Chemical Laboratory of Celje Queen (at 580<sup>th</sup> Anniversary of Bohemian coronation of Queen Barbara of Celje)

Barbara of Cilli was certainly the richest female alchemist of all times. The article tries to explain what kind of experiments she carried out in her laboratory and indicate which technical chemical plant she likely has used. The major part of her expensive tools was made from easily breakable materials, therefore any contemporary pursuit to locate them will be probably in vain, because there is not much hope for their preservation.

**Keywords:** Barbara of Cilli, History of Alchemy, 15<sup>th</sup> Century, Cilli, Bohemia, Samobor in Croatia



## POROČILO PREDSEDNIKA SLOVENSKEGA KEMIJSKEGA DRUŠTVA O DELU DRUŠTVA V LETU 2016

V letu 2016 je bilo društvo aktivno na številnih področjih. Morda smo bili še vedno deležni nekaterih pozitivnih vplivov na delovanje društva (mednarodno leto kemije, 60-letnica ustanovitve društva, 60-letnica izdajanja društvene revije *Acta Chimica Slovenica*). Prav tako pa se na žalost še vedno čuti gospodarska in ekonomska kriza, kar smo še posebej boleče občutili konec leta 2016, ko smo prejeli obvestilo ARRS, da so nam sicer odobrili enako finančno pomoč pri izdajanju društvene revije za naslednji dve leti (2017 in 2018), vendar se zaradi nezmožnosti proračuna Republike Slovenije znesek zmanjša za skoraj 40 odstotkov (na 18.142 EUR letno).

**Slovenski kemijski dnevi** so bili v letu 2015 prvič organizirani v Ljubljani, na novi Fakulteti za kemijo in kemijsko tehnologijo Univerze v Ljubljani, v skupni organizaciji Slovenskega kemijskega društva in FKKT Univerze v Ljubljani, v letu 2016 pa smo jih po nekaj letih spet organizirali v Portorožu, v Kongresnem centru Metropol, od 28. do 30. septembra. Udeleženci konference so bili z izbiro lokacije zelo zadovoljni, zato bodo Slovenski kemijski dnevi 2017 tudi organizirani v Portorožu.

Programski odbor, ki sem mu predsedoval, v njem pa so bili še prof. Marija Bešter Rogač, prof. Zorka Novak Pintarič, prof. Marjan Veber in prof. Janez Plavec, je pripravil zanimivo in kvalitetno srečanje. Na posvetovanju je bilo predstavljenih več kot 100 prispevkov v obliki predavanj in posterjev. Delo je potekalo plenarno in v dveh vzporednih sekcijah. Udeleženci konference so bili zelo zadovoljni s kvaliteto znanstvenih in strokovnih prispevkov. Na konferenci je sodelovalo 17 sponzorjev. Posebej želim omeniti in se zahvaliti družbi Kemomed d.o.o., ki je bila ob svoji 20-letnici delovanja glavni sponzor naše konference.

Prenarni predavatelji so bili: **prof. Vojko Vlachy**, FKKT Univerze v Ljubljani; **prof. József Karger-Kocsis**, Fakulteta za inženirstvo Univerze za tehnologijo in ekonomiko iz Budimpešte; **Prof. Thomas Carell**, LM Univerza München; **Prof. Claus Hélix-Nielsen**, FKKT Univerze v Mariboru in Danska tehnična univerza, Lyngby ter **Prof. Anton Meden**, FKKT Univerze v Ljubljani.

Poleg petih plenarnih predavanj je bilo sedem polurnih »keynote« vabljenih predavanj (**Franc Perdih**, **Miha Grilc**, **Matej Huš**, **Ivanka Jerić**, **Jurij Svete**, **Bojan Pahor** in **Nataša Zabukovec Logar**) ter dva promocijska seminarja.

V letniku *Acta Chimica Slovenica* 2016(63) so izšle štiri številke s skupno 108 originalnimi znanstvenimi in strokovnimi prispevki na skupno 720 straneh z dvokolonskim tiskom. Tretja številka je bila posvečena tragično

preminulemu direktorju Kemijskega inštituta, profesorju Janku Jamniku. V uredništvo je prispelo preko 1200 prispevkov, vendar jih na začetku zaradi neustrezne tehnične priprave in dokumentacije zavrne več kot 80 % brez recenzije. Slaba polovica recenziranih člankov je pozitivno ocenjenih. Objavljeni članki pokrivajo aktualna področja organske, anorganske, fizikalne in analize kemije, kemije materialov, kemijskega, biokemijskega in okoljskega inženirstva ter splošne, uporabne in biomedicinske kemije. Pisani so v angleškem jeziku s slovenskim povzetkom. V slovenskem delu revije – Društvenih vesteh, so bila objavljena sekcijška poročila, ter seznam diplomskih, magistrskih in doktorskih del na širšem področju kemije v letu 2016 na slovenskih univerzah. V društvenih vesteh sta bila objavljena tudi dva slovenska strokovna prispevka o sintezni biologiji za proizvodnjo biobutanola in o prvih korakih Nikole Tesle v kemijske vede. Faktor vpliva (Impact Factor) za *Acta Chimica Slovenica* za leto 2015 znaša  $IF = 1,167$  in se je ob prizadevnemu delu urednikov precej zvišal ( $IF = 0,61$  za 2014).

Na internetu na strani <http://acta.chem-soc.si> objavljamo elektronsko verzijo *Acta Chimica Slovenica*, kar povečuje branost ter mednarodno odmevnost revije. Članki, objavljeni v ACSi, so povzeti še v Chemical Abstracts Plus, Current Contents (Physical, Chemical and Earth Sciences), Science Citation Index Expanded in Scopus.

Ob izidu vsake številke se je sestel uredniški odbor. Člani so pregledali opravljeno delo, načrtovali naslednje številke in usklajevali uredniško politiko. V letu 2016 so potekale priprave na tematsko številko Cutting Edge, ki bo izšla septembra 2017. Zanj je do oktobra 2016 prispelo 14 prispevkov mlajših raziskovalcev, večina člankov je še v recenzentskem postopku.

Začeli smo pripravljati posvečeno številko akademiku profesorju Mihi Tišlerju ob njegovem 90. rojstnem dnevu; izbran je bil uredniški odbor in poslana obvestila vabljenim avtorjem. Za to posvečeno številko je predvidena četrta številka v letu 2017. Prav tako smo začeli urejati uporabo licence Creative Commons v letu 2017, ki ureja avtorske pravice objavljenih člankov.

Konec leta 2014 in v začetku 2015 smo prenovili društveno domačo stran, ki je zdaj moderneje urejena in optimalno deluje na različnih napravah (računalniki, tablični računalniki, pametni telefoni). Upam, da vam božžje vseč, predvsem pa je pomembno to, da so vse informacije (o društvu, o njegovih aktivnostih, o preteklih in bodočih dogodkih, vstopno mesto za revijo *Acta Chimica Slovenica*, vstopno mesto za informacije o Slovenskih kemijskih dnevih) dostopne na enem mestu, na domači strani

društva.

Nekaj informacij o financiranju izdajanja Acta Chimica Slovenica in na splošno o financah za delovanje društva. Nekaj let smo zbirali presežke v poslovnem skladu za "težke čase". Za leto 2015 smo precej večje odhodke še uspeli pokriti s sredstvi iz poslovnega sklada. Sofinanciranje izdajanja ACSi s strani ARRS za leti 2015 in 2016 je bilo na letni ravni za več kot 9.000 EUR nižja od prejšnje letne pogodbene vrednosti za leti 2013 in 2014. Kot povedano že zgoraj, pa se je pogodbena vrednost za leti 2017 in 2018 na letni ravni znižala še za približno 11.000 EUR. Nižja pogodbena vrednost je posledica zmanjšanja sredstev, ki jih država namenja za financiranje slovenske znanosti preko ARRS. Upamo, da bomo del izpada sredstev države uspeli pokriti iz prihodkov konferenec Slovenski kemijski dnevi.

Zahvaljujem se inštitucijam, ki finančno podpirajo njeno izdajanje (obe FKKT (Ljubljana in Maribor)), Kemijski inštitut, Inštitut Jožef Stefan in Fakulteta za farmacijo Univerze v Ljubljani; z objavo oglasa so v letu 2016 od slovenskih podjetij pomagali Krka iz Novega mesta, Donau Lab Ljubljana in MTI Pavlič d.o.o. iz Novega mesta. Največji finančni podpornik je še vedno država Slovenija preko dvoletne pogodbe o sofinanciranju. Kot povedano zgoraj, pa so se finančna sredstva v nekaj letih več kot prepolovila.

V aprilu 2015 je bilo Slovensko kemijsko društvo na letni skupščini, ki je potekala v Ljubljani, sprejeto v **ECTNA – European Chemistry Thematic Network Association**. V letu 2016 smo se udeležili letne skupščine, ki je potekala v Gdansk na Poljskem.

Člani Slovenskega kemijskega društva so bili v letu 2016 zelo dejavni na področju mednarodnega sodelovanja. Poleg dvostranskega sodelovanja s kemijskimi društvi sosednjih in drugih srednjeevropskih držav, je bilo pomembno delovanje naših članov v mednarodnih združenjih IUPAC, EuCheMS, EFCE, EPF in ECA. Nekatere pomembne aktivnosti:

1. 6. EuCheMS evropski kemijski kongres, 11. do 15. september 2016, Sevilla, Španija;
2. pred EuCheMS kongresom je 10. in 11. septembra potekala generalna skupščina EuCheMS);
3. Letno srečanje IUPAC ChemRAWN odbora, 30. junij in 1. julij 2016, Bergen, Norveška (udeležil se ga je titularni član V. Kaučič);
4. IUPAC CHEMRAWN XXI (21<sup>st</sup> IUPAC Conference on Chemical Research Applied to World Needs, World Conference on Solid Urban Waste Management) je potekala aprila 2016 v Rimu, Italija (kot član Future Action Committee-ja konference se je srečanja udeležil V. Kaučič);
5. Letna skupščina ECTNA je potekala od 24. do 26. aprila 2016 v Gdansk na Poljskem (udeležila sta se je M. Veber in V. Kaučič);
6. 48. Mednarodna kemijska olimpijada je bila julija 2016 v Tbilisiju, Gruzija. Naši dijaki so dosegli od-

lične rezultate: Uroš Prešern (gimnazija Novo mesto) je dobil srebrno medaljo, Tristan Kovačič (gimnazija Novo mesto), Martin Rihtaršič in Vid Kermelj (oba gimnazija Škofja Loka) pa so dobili bronaste medalje. Vsem čestitke za ta uspeh! Mentorja ekipe sta bila dr. Andrej Godec in dr. Darko Dolenc, oba FKKT, Ljubljana;

7. European Symposium on Computer Aided Process Engineering – ESCAPE-26 je potekal v Portorožu od 12. do 15. junija 2016. Konferenco je organiziral je prof. Zdravko Kravanja s sodelavci iz FKKT Univerze v Mariboru;
8. 46<sup>th</sup> IUPAC World Polymer Congress (MACRO 2016) je potekal od 17. do 21. julija 2016 v Istanbulu, Turčija.

V Ljubljani, 14. 3. 2017  
Venčeslav Kaučič

## Poročilo o delu Sekcije mladih kemikov za leto 2016

Sekcija mladih kemikov je namenjena študentom vseh treh stopenj in drugih strokovnjakom na področju kemije in sorodnih ved do 35 let. V Sekcijo mladih kemikov je bilo do konca leta 2016 včlanjenih 59 članov, kar je za šest več kot preteklo leto. Z letom 2016 je Sekcija mladih kemikov SKD postala članica novonastale svetovne mreže mladih kemikov IYCN (International Younger Chemist's Network), ki deluje v sklopu IUPAC. Posamezni člani SMK so bili tudi izvoljeni v organe in delovne skupine IYCN.

Znotraj delovnih skupin SMK smo se člani srečevali v prostorih Kemijskega inštituta in UL FKKT. Med glavnimi dejavnosti SMK v letu 2016 bi izpostavil zlasti promocijo naravoslovja med osnovnošolskimi učenci. Člani SMK so aktivno sodelovali z Javnim zavodom RTV Slovenija pri oblikovanju vsebin s področji naravoslovja, zlasti pri demonstraciji naravoslovnih poskusov za oddajo Firbcologi in Male sive celice.

Člani Sekcije mladih kemikov smo v sodelovanju s člani Sekcije za spektroskopijo SKD in Katedro za analizo kemijo UL FKKT oblikovali in izvedli delavnico za učence osmega in devetega razreda OŠ, ki obiskujejo izbirna predmeta Kemija v šoli in Kemija v življenju.

Aleš Zupančič,  
predsednik Sekcije mladih kemikov

## Poročilo o delu komisije za slovensko kemijsko terminologijo in nomenklaturu v letu 2016

Komisija za slovensko kemijsko terminologijo in nomenklaturu je tudi v preteklem letu sodelovala pri delu Tehniške komisije Sekcije za terminološke slovarje pri Inštitutu za slovenski jezik ZRC SAZU. Člani tehniške komisije za področje kemije in kemijske tehnologije so Andrej Šmalc in Leon Čelik iz ljubljanske ter Peter Glavič iz mariborske podružnice Slovenskega kemijskega društva.

V letu 2016 se je nadaljevalo sodelovanje pri novi izdaji splošnega tehniškega slovarja, ki obsega tudi pripravljane gradiva s področja kemije, kemijske tehnologije in kemijske tehnike. Po reorganizaciji leta 2014 se delo opravlja dopisno, osnovno gradivo s pripombami članov pa se obravnava na rednih sejah po tri ure tedensko. V letu 2016 je bila dokončana obdelava gesel črke O.

Nadaljevalo se je tudi pripravljane gradiva za predvideni slovarkemijske tehnike. Slovar bo obsegal pomembnejše pojme s tega področja in bopredstavljaj pomembno dopolnitev splošnega tehniškega slovarja. Delo je zelo obsežno, saj z naglim razvojem vseh področij tehnike sproti naraščajoča tudi število novih pojmov, ki jih je treba še terminološko obdelati. Slovar pripravlja ožja (štiričlanska) skupina članov širše Tehniške komisije (v sestavi P. Glavič, A. Šmalc, L. Čelik za kemijo in kemijsko tehnologijo in A. Skušek za mehanski del procesne tehnike) na rednih sejah, ki so na Inštitutu za slovenski jezik pri ZRC SAZU dvakrat mesečno po dve uri. Glavnina dela se opravi doma, na vsaki seji se obravnavajo vnaprej pripravljena in obdelana gesla, njihovi popravki in dopolnitve pa se dokončno obravnavajo na naslednji seji ob pregledu zapisnika. Na ta način se je delo precej pospešilo, tako da je bilo v letu 2016 dokončno obdelano in vneseno v slovar vse gradivo do vključno črke Ž – skupaj 1012 gesel, pri čemer je treba omeniti, da so tu všteta tudi nekatera že prej obdelana, ki so bila le popravljena. Delo se nadaljuje z obdelavo manjkajočih gesel, ki so se pojavila vzporedno ob redni obdelavi že zbranih.

V letu 2016 so komisiji priskočili na pomoč Fakulteta za kemijo in kemijsko tehnologijo Univerze v Ljubljani, Fakulteta za kemijo in kemijsko tehnologijo Univerze v Mariboru, Helios Količevo, Lek Ljubljana, Krka Novo mesto in Melamin Kočevje, s prispevki v skupnem znesku 4100 EUR. Zaradi pomanjkanja sredstev za delo poteka priprava slovarja kemije in kemijske tehnike pretežno *pro bono*, saj smo mnenja, da bi bilo škoda prekiniti delo, ki je do praktično treh četrtin že opravljeno in je za dokončno slovaropisno obdelavo pripravljenih že okrog 7600 gesel.

Poleg rednega dela v zvezi s slovarjem je komisija v preteklem letu strokovno pregledala še standarde SIST ISO 80000-2 Matematika, 80000-4 Mehanika, 80000-5 Termodinamika ter 80000-9 Atomska in jedrska fizika (prav tako *pro bono*). Nova izdaja standarda SIST ISO 80000 postopno nadomešča izdajo SIST ISO 80000 iz obdobja 20082013.

Za leto 2017 je predvideno nadaljnje sodelovanje pri pripravi gradiva za novo izdajo Slovenskega tehniškega slovarja in dodatno zbiranje in obdelavo gradiva za novi slovar kemijske tehnike ter začetek končnih redakcijskih del v zvezi s pripravo računalniške oblike slovarja za objavo na spletu, ki bo omogočala sprejemanje pripomb in novih gesel ter s tem sprotno dopolnjevanje slovarja.

Andrej Šmalc

## Poročilo o delu sekcije Eurachem Slovenija

Kakovost proizvodov in življenja prebivalcev RS je v veliki meri odvisno od meritev, ki jih opravljajo kemijski laboratoriji v industriji (kakovost proizvodov in hrane, varovanje okolja), zdravstvu, raziskovalnih inštitutih, fakultetah in drugih laboratorijih v javnem in zasebnem sektorju. Zagotavljanje primerljivosti rezultatov meritev je tako ena ključnih potreb vsake družbe, vpete v globalni svet. Laboratoriji dokazujejo svojo usposobljenost z akreditacijo po mednarodnih standardih kot npr ISO EN 17025: General requirements for the competence of testing and calibration laboratories, pri tem pa so ključni mednarodni strokovni standardi in strokovna harmonizirana vodila. EURACHEM aktivno deluje na področju priprav harmoniziranih vodil za (bio) kemijske laboratorije, ki temeljijo na ključnih mednarodnih dokumentih, kot sta "JCGM 200:2012 International vocabulary of metrology – Basic and general concepts and associated terms (VIM) in Guide to the Expression of Uncertainty in Measurement (GUM). Delo EURACHEMa poteka v več delovnih skupinah, Raziskovalci in strokovnjaki iz Slovenije so aktivno vključeni v tri delovne skupine (Validacija analitskih postopkov, Medlaboratorijska preskušanja in Izobraževanje), prav tako pa sodelujemo kot polnopravni člani z volilno pravico na vsakoletni Generalni skupščini. Prenos znanja v slovensko okolje se izvaja preko enodnevnih seminarjev, šol kakovosti, predavanj študentom ter ciljanim izobraževanjem na zahteve posameznih laboratorijev. V letu 2016 se je na seminarjih povečalo število udeležencev iz laboratorijev v zdravstvu, predvsem na šoli kakovosti v organizaciji SIQ. To usposabljanje je Zbornica laboratorijske medicine Slovenije ovrednotila z 20 točkami SILM. Od 28. 3. do 8. 5. 2016 je na evropski ravni za naše člane potekal brezplačen e-seminar o merilni negotovosti. Dr. Nineta Hrastelj Majcen se je udeležila generalne skupščine EURACHEM v Gentu v Belgiji, od 10.5. do 13. 5. 2016. V letu 2016 pa so potekale aktivne priprave nekaterih članov društva za izvedbo delavnice »9<sup>th</sup> Proficiency testing in analytical chemistry, microbiology and laboratory medicine – Current Practice and Future Directions«, ki bo od 9.–12. oktobra 2017 v Portorožu.

Dr. Nineta Hrastelj

## Poročilo Sekcije za kristalografijo za leto 2016

Sekcija za kristalografijo pri Slovenskem kemijskem društvu je v letu 2016 sodelovala s hrvaškim kristalografskim društvom iz Zagreba pri organizaciji 24. zaporednega srečanja slovenskih in hrvaških kristalografov. Srečanje je potekalo na hrvaškem v Bolu na Braču. Kot vsako leto je bila tudi tokrat udeležba mednarodna, zato je bil uradni jezik srečanja angleščina. S skupnim trudom s hrvaškimi kolegi pa smo uspeli organizirati srečanje s sredstvi donatorjev in sponzorjev tako, da smo obdržali tradicijo, da za udeležence kotizacije ni bilo.

Podobno kot na prejšnjih konferencah, so se tudi tokrat povabili za sodelovanje odzvali ugledni, mednarodno uveljavljeni plenarni predavatelji. To so bili Mariusz Jaskolski (Poznan, Poljska), »Handling crystal pathologies in macromolecular crystallography«; Lee Brammer (Sheffield, Združeno kraljestvo), »Flexibility, Dynamics and Chemical Reactions in Solids: Molecular Crystals to Framework Materials«; Goran Dražić (Ljubljana, Slovenija), »Direct imaging and quantification of crystal structures at the atomic level using  $C_s$  corrected scanning transmission electron microscope«; Michele Zema (Chester, Združeno kraljestvo), »Crystallography and Society: outcomes of IYCr 2014«; Željko Skoko (Zagreb, Hrvaška), »Thermally stable crystals – acrobatics on the nanoscale«.

Konferenca je bila po udeležbi rekordna. Udeležilo se je 98 kristalografov, ki so s kakovostnimi prispevki v obliki krajših predavanj osvetlili številna področja kristalografije. Srečanje je bil tako spet priložnost za izmenjavo spoznanj, navezavo stikov in intenzivno učenje mlajših kolegov.

Zaradi omejenih sredstev v raziskovalnih programih ni projektov, se slovenski kristalografi v letu 2016 žal nismo mogli udeležiti drugih srečanj, kjer smo sicer pogosto prisotni (Evropsko kristalografsko srečanje ECM30 v Baslu in Evropske konference o praškovni difrakciji EPDIC15 v Bariju).

Aktivno poteka delo za pripravo jubilejnega 25. Slovensko-hrvaškega kristalografskega srečanja, ki bo junija 2017 v Ljubljani. Srečanje bo potekalo v prostorih nove stavbe Fakultete za kemijo in kemijsko tehnologijo, ki je glavni institucionalni soorganizator srečanja. Trenutno stanje prijav kaže, da bo dogodek uspešen tako po udeležbi kot po vsebini.

*prof. dr. Anton Meden*

Sekcija za živilsko kemijo (Food Chemistry Division, FCD) Evropskega združenja za kemijske in molekularne znanosti (European Association of Chemical and Molecular Sciences - EuCheMS), kjer predstavljamo Slovensko kemijsko društvo. V okviru tega smo med drugim sodelovali pri izborih tematik mednarodnih simpozijev, ki jih organizira FCD. Med te aktualne tematike spadajo: nova živila in nanomateriali, bioaktivne sestavine in mikro-nutrienti, kemijske reakcije in interakcije sestavin v živilih, živilska kemija in bioekonomija, kakovost in varnost hrane, funkcionalna živila in sestavine s funkcionalnimi lastnostmi, pigmenti in aditivi v živilih, potvorbe, avtentičnost in sledljivost in nove metode v živilski kemiji. Poleg tega smo bili člani Sekcije za živilsko kemijo aktivni tudi na področju izobraževanja in popularizacije kemije in še posebej živilske kemije. Te aktivnosti smo med drugim izvajali tudi na svojih inštitucijah, kjer smo pripravili delavnice za osnovnošolce in srednješolce.

V planu za leto 2017 smo predvideli aktivno udeležbo na mednarodnih simpozijih. Načrtujemo večjo udeležbo na EuroFoodChem XIX (Budimpešta, 4.-6. 10. 2017), ki je najpomembnejši simpozij, ki ga organizira FCD. Tudi letos se bomo udeležili sestanka FCD, kjer bomo predstavili naše delo in z ostalimi člani FCD naredili načrt dela za prihodnje leto. Sekcija za živilsko kemijo bo v letu 2017 sodelovala na Slovenskih kemijskih dnevih, ki bodo od 20. do 22. septembra v Portorožu.

*Irena Vovk*

## Sekcija za živilsko kemijo

Člani Sekcije za živilsko kemijo so v letu 2016 sodelovali s prispevki na Slovenskih kemijskih dnevih, ki jih je organiziralo Slovensko kemijsko društvo v Portorožu. Aktivno smo sodelovali tudi pri različnih dejavnostih



# KOLENDAR VAŽNEJŠIH ZNANSTVENIH SREČANJ S PODROČJA KEMIJE IN KEMIJSKE TEHNOLOGIJE

## SCIENTIFIC MEETINGS – CHEMISTRY AND CHEMICAL ENGINEERING

### 2017

#### July 2017

---

- 2 – 5                    4<sup>TH</sup> EUCHEMS INORGANIC CHEMISTRY CONFERENCE – EICC-4  
Copenhagen, Denmark  
Information:            <http://www.euchems.eu/events/4th-euchems-inorganic-chemistry-conference-eicc-4/>
- 2 – 6                    INTERNATIONAL SYMPOSIUM ON MACROCYCLIC AND SUPRAMOLECULAR  
CHEMISTRY IN CONJUNCTION WITH ISACS: CHALLENGES IN ORGANIC  
MATERIALS & SUPRAMOLECULAR CHEMISTRY  
Cambridge, United Kingdom  
Information:            <http://www.rsc.org/events/detail/17933/international-symposium-on-macrocyclic-and-supramolecular-chemistry-in-conjunction-with-isacs-challenges-in-organic-materials-and-supramolecular-chemistry>
- 2 – 7                    16<sup>TH</sup> EUROPEAN POLYMER CONGRESS  
Lyon, France  
Information:            <http://www.europolyfed.org/home>
- 2 – 8                    3<sup>RD</sup> INTERNATIONAL MASS SPECTROMETRY SCHOOL (IMSS)  
Dubrovnik, Croatia  
Information:            <http://www.imss.nl/>
- 3 – 6                    2<sup>ND</sup> INTERNATIONAL CONFERENCE ON NEW PHOTOCATALYTIC MATERIALS FOR  
ENVIRONMENT, ENERGY AND SUSTAINABILITY (NPM -2)  
Ljubljana, Slovenia  
Information:            <http://chem-soc.si/news-1/2.-mednarodna-konferenca-new-photocatalytic-materials-for-environment-energy-and-sustainability-npm-2>
- 3 – 7                    ISSNP 2017 – INTERNATIONAL SUMMER SCHOOL ON NATURAL  
PRODUCTS  
Naples, Italy  
Information:            <http://www.issnp.org/>
- 7 – 10                   10<sup>TH</sup> INTERNATIONAL SYMPOSIUM ON CATALYSIS IN MULTIPHASE REACTORS  
(CAMURE-10) & 9<sup>TH</sup> INTERNATIONAL SYMPOSIUM ON MULTIFUNCTIONAL  
REACTORS (ISMR-9)  
Tsingtao (Qingdao), PR China  
Information:            <http://camure2017.csp.escience.cn/dct/page/1>
- 9 – 13                   16<sup>TH</sup> INTERNATIONAL MEETING ON BORON CHEMISTRY  
(IMEBORON XVI)  
Hong Kong, China  
Information:            [www.imeboron16.org](http://www.imeboron16.org)
- 9 – 13                   EuCOMC 2017 – 22<sup>ND</sup> EUROPEAN CONFERENCE ON ORGANOMETALLIC  
CHEMISTRY  
Amsterdam, The Netherlands  
Information:            <http://www.eucomc2017.amsterdam/>

- 9 – 14 46<sup>TH</sup> IUPAC WORLD CHEMISTRY CONGRESS (IUPAC-2017)  
São Paulo, Brazil  
Information: [www.IUPAC2017.org](http://www.IUPAC2017.org)
- 23 – 27 16<sup>TH</sup> ECSSC – 16<sup>TH</sup> EUROPEAN CONFERENCE ON SOLID STATE CHEMISTRY  
Glasgow, UK  
Information: <https://ecssc16.com/>
- 23 – 29 RACI CENTENARY CONGRESS  
Melbourne, Australia  
Information: <http://www.racicongress.com>
- 24 – 26 5<sup>TH</sup> INTERNATIONAL CONFERENCE ON GREEN CHEMISTRY  
AND TECHNOLOGY  
Rome, Italy  
Information: <http://greenchemistry.alliedacademies.com/>

---

**August 2017**

- 13 – 17 SE2017 – 200 YEARS OF SELENIUM RESEARCH  
Stockholm, Sweden  
Information: <http://se2017.se/>
- 16 – 18 CHEMICAL IDENTIFIER  
Bethesda, MD United States  
Information: <http://www.inchi-trust.org>
- 20 – 23 GLS-13 – 13<sup>TH</sup> INTERNATIONAL CONFERENCE ON GAS-LIQUID AND  
GAS-LIQUID-SOLID REACTOR ENGINEERING (GLS-13)  
Brussels, Belgium  
Information: <http://www.gls13.com/>
- 27 – 30 EUROPACAT 2017  
Florence, Italy  
Information: <http://www.europacat2017.eu/index.html>
- 28 – 31 17<sup>TH</sup> IUPAC INTERNATIONAL SYMPOSIUM ON MACROMOLECULAR COMPLEXES  
(MMC-17)  
Tokyo, Japan  
Information: <http://www.waseda.jp/assoc-mmc17/>
- 28 – Sept. 1 EuroAnalysis 2017  
Stockholm, Sweden  
Information: <http://euroanalysis2017.se/>
- 28 – Sept. 2 11ICHC – 11<sup>TH</sup> INTERNATIONAL CONFERENCE ON THE HISTORY OF CHEMISTRY  
Trondheim, Norway  
Information: <http://www.ntnu.edu/11ichc>

---

**September 2017**

- 3 – 6 3<sup>RD</sup> EuGSC – 3<sup>RD</sup> EuCheMS CONGRESS ON GREEN AND SUSTAINABLE CHEMISTRY  
York, UK  
Information: <http://www.euchems.eu/events/3rd-eugsc-3rd-euchems-congress-on-green-and-sustainable-chemistry/>
- 3 – 6 20<sup>TH</sup> INTERNATIONAL SYMPOSIUM ON INDUSTRIAL CRYSTALLIZATION  
Dublin, Ireland  
Information: <http://isic20.com/>
- 3 – 8 21<sup>ST</sup> EUROPEAN CONFERENCE ON THERMOPHYSICAL PROPERTIES  
Graz, Austria  
Information: <http://ectp2017.tugraz.at/>

- 4 – 7 11 EUROPEAN CONFERENCE ON THEORETICAL AND COMPUTATIONAL CHEMISTRY – 11EUCO-TCC  
Barcelona, Spain  
Information: <http://www.11euco-tcc.org/>
- 5 – 8 THERMODYNAMICS 2017  
Edinburgh, UK  
Information: <http://www.thermodynamics2017.efconference.co.uk/>
- 10 – 13 GDCh SCIENTIFIC FORUM CHEMISTRY 2017 - ANNIVERSARY CONGRESS »GDCh – 150 YEARS  
Berlin, Germany  
Information: <https://veranstaltungen.gdch.de/tms/frontend/index.cfm?l=7210&modus=>
- 10 – 14 81<sup>ST</sup> PRAGUE MACROMOLECULAR MEETING  
Prague, Czech Republic  
Information: <http://www.imc.cas.cz/sympo/81pmm/>
- 11 – 14 EUROPEAN SYMPOSIUM ON COMMUNION AND CLASSIFICATION 2017  
Izmir-Seferihisar, Turkey  
Information: <http://efce.info/ESCC+2017.html>
- 17 – 20 BloodSurf2017  
Clemson, SC United States  
Information: <http://www.ireviakine.net/Bloodsurf/>
- 17 – 22 INTERNATIONAL SYMPOSIUM ON IONIC POLYMERIZATION – IP 2017  
Durham, United Kingdom  
Information: <https://www.dur.ac.uk/soft.matter/ip2017/>
- 19 CUTTING EDGE 2017  
Ljubljana, Slovenia  
Information: <http://www.cutting-edge.si/>
- 20 – 22 SLOVENIAN CHEMICAL DAYS 2017  
Portorož, Slovenia  
Information: <http://chem-soc.si/slovenski-kemijski-dnevi>
- 24 – 27 ECPC17 – 2ND EUROPEAN CONFERENCE ON PHYSICAL CHEMISTRY  
Corsica, France  
Information: <http://ecpc17.com/>
- 26 – 27 EuCheMS GENERAL ASSEMBLY  
Rome, Italy  
Information: <http://www.euchems.eu/about-us/2017-general-assembly-rome-italy/>
- 27 – 29 11<sup>TH</sup> INTERNATIONAL SYMPOSIUM ON BIOORGANIC CHEMISTRY (ISBOC-11)  
Konstanz, Germany  
Information: <https://www.uni-konstanz.de/isboc-11/about-isboc-11/>

---

**October 2017**

- 1 – 5 EPIC 2017 – 6<sup>TH</sup> EUROPEAN PROCESS INTENSIFICATION CONFERENCE 2017  
Barcelona, Spain  
Information: <http://www.wcce10.org/index.php/en/>
- 1 – 5 WCCE10 – 10<sup>TH</sup> WORLD CONGRESS OF CHEMICAL ENGINEERING INCORPORATING THE 11<sup>TH</sup> EUROPEAN CONGRESS OF CHEMICAL ENGINEERING (ECCE11)  
Barcelona, Spain  
Information: <http://www.wcce10.org/index.php/en/>

- 1 – 5 4<sup>TH</sup> EUROPEAN CONGRESS OF APPLIED BIOTECHNOLOGY – ECAB3  
Barcelona, Spain  
Information: <http://www.wcce10.org/index.php/en/>
- 2 – 5 7<sup>TH</sup> IUPAC INTERNATIONAL CONFERENCE ON GREEN CHEMISTRY  
Moscow, Russian Federation  
Information: <http://greeniupac2017.muctr.ru>
- 4 – 6 XIX<sup>TH</sup> EUROFOODCHEM CONFERENCE  
Budapest, Hungary  
Information: <http://www.eurofoodchem2017.mke.org.hu/index.php>
- 9 – 12 9<sup>TH</sup> WORKSHOP ON PROFICIENCY TESTING IN ANALYTICAL CHEMISTRY,  
MICROBIOLOGY AND LABORATORY MEDICINE  
Portorož, Slovenia  
Information: <http://eurachempt2017.eu/>
- 9 – 13 POLYCHAR 25 – 25<sup>TH</sup> ANNUAL WORLD FORUM ON ADVANCED MATERIALS  
Kuala Lumpur, Malaysia  
Information: <http://www.25POLYCHAR.org.my>
- 11 – 13 IUPAC-FAPS 2017 POLYMER CONGRESS ON SMART MATERIALS FOR EMERGING  
TECHNOLOGY  
Jeju Island, Republic of Korea  
Information: <http://www.faps2017.org>
- 11 – 13 5<sup>TH</sup> MS FOOD DAY  
Bologna, Italy  
Information: <http://www.spettrometriadimassa.it/Congressi/5MS-FoodDay/>
- 12 – 14 EWCC 2017 – EAST-WEST CHEMISTRY CONFERENCE 2017  
Skopje, Macedonia  
Information: <http://ewcc2017.org/>

---

**November 2017**

- 5 – 9 HPLC 2017 – THE 46<sup>TH</sup> INTERNATIONAL SYMPOSIUM ON HIGH PERFORMANCE  
LIQUID PHASE SEPARATIONS AND RELATED TECHNIQUES  
Jeju Island, Republic Of Korea  
Information: <http://www.hplc2017-jeju.org>
- 26 – 29 EMEC 18 – 18<sup>TH</sup> EUROPEAN MEETING ON ENVIRONMENTAL CHEMISTRY  
Porto, Portugal  
Information: <http://emec18.eventos.chemistry.pt/>

**2018**

---

**February 2018**

- 21 – 23 ChemCYS 2018 – 14<sup>TH</sup> CHEMISTRY CONFERENCE FOR YOUNG SCIENTISTS  
Blankenberge, Belgium  
Information: <http://chemcys.be/>

---

**April 2018**

- 15 – 18 PETROMASS 2018 – XI. INTERNATIONAL MASS SPECTROMETRY CONFERENCE  
ON PETROCHEMISTRY, ENVIRONMENTAL AND FOOD CHEMISTRY  
Bled, Slovenia  
Information: <http://www.petromass2018.com/>

---

**June 2018**

- 4 – 6 IIS PRAGUE 2018 – 13<sup>TH</sup> INTERNATIONAL SYMPOSIUM ON THE SYNTHESIS AND APPLICATIONS OF ISOTOPES AND ISOTOPICALLY LABELLED COMPOUNDS  
Prague, Czech Republic  
Information: <http://www.iis-prague2018.cz/>
- 4 – 7 POLYMERS AND ORGANIC CHEMISTRY 2018 (POC 2018)  
Montpellier, France  
Information: <https://iupac.org/event/polymers-organic-chemistry-2018-poc-2018/>

---

**July 2018**

- 8 – 13 27<sup>TH</sup> IUPAC INTERNATIONAL SYMPOSIUM ON PHOTOCHEMISTRY  
Dublin, Ireland  
Information: <https://iupac.org/event/27th-iupac-international-symposium-photochemistry/>

---

**August 2018**

- 26 – 30 ECC7 – 7<sup>TH</sup> EuCheMS CHEMISTRY CONGRESS  
Liverpool, UK  
Information: <https://www.euchems2018.org/>

---

**September 2018**

- 16 – 19 DISTILLATION & ABSORPTION CONFERENCE 2018  
Firenze, Italy  
Information: <http://www.aidic.it/da2018/>

---

**October 2018**

- 4 – 7 N-LIGANDS2018 – 7<sup>TH</sup> EuCheMS CONFERENCE ON NITROGEN-LIGANDS  
Lisbon, Portugal  
Information: <http://www.n-ligands2018.com/>
- 14 – 18 14<sup>TH</sup> IUPAC INTERNATIONAL CONGRESS OF PESTICIDE CHEMISTRY  
Rio de Janeiro, Brazil  
Information: <https://iupac.org/event/14th-iupac-international-congress-of-pesticide-chemistry/>
- 16 – 21 22<sup>ND</sup> INTERNATIONAL CONFERENCE ON ORGANIC SYNTHESIS (22-ICOS)  
Florence, Italy  
Information: <http://www.22-icos-florence.it>

# Acta Chimica Slovenica

## Author Guidelines

### Submissions

Submission to ACSi is made with the implicit understanding that neither the manuscript nor the essence of its content has been published in whole or in part and that it is not being considered for publication elsewhere. All the listed authors should have agreed on the content and the corresponding (submitting) author is responsible for having ensured that this agreement has been reached. The acceptance of an article is based entirely on its scientific merit, as judged by peer review. There are no page charges for publishing articles in ACSi.

### Submission material

Typical submission consists of:

- full manuscript (Word file, with title, authors, abstract, keywords, figures and tables embedded, and references);
- supplementary files:
  - **Statement of novelty** (Word file),
  - **List of suggested reviewers** (Word file),
  - ZIP file containing **graphics** (figures, illustrations, images, photographs),
  - **Graphical abstract** (single graphics file),
  - **Proposed cover picture** (optional, single graphics file),
  - **Appendices** (optional, Word files, graphics files).

### Submission process

Submission process consists of 5 steps. Before submission, authors should go through the checklist at the bottom of these guidelines page and prepare for submission:

#### Step 1: Starting the submission

- Choose one of the journal sections.
- Confirm all the requirements of the **checklist**.
- Additional plain text comments for the editor can be provided in the relevant text field.

#### Step 2: Upload submission

- Upload full manuscript in the form of a Word file (with title, authors, abstract, keywords, figures and tables embedded, and references).

#### Step 3: Enter metadata

- First name, last name, contact email and affiliation for all authors, in relevant order, must be provided. Corresponding author has to be selected. Full postal address and phone number of the corresponding author has to be provided.
- **Title and abstract** must be provided in plain text.
- Keywords must be provided (max. 6, separated by semicolons).

- Data about contributors and supporting agencies may be entered.
- **References** in plain text must be provided in the relevant text filed.

#### Step 4: Upload supplementary files

- **Statement of novelty** in a Word file must be uploaded
- **List of suggested reviewers** with at least three reviewers must be uploaded as a Word file.
- All **graphics** have to be uploaded in a single ZIP file. Graphics should be named Figure 1.jpg, Figure 2.eps, etc.
- **Graphical abstract image** must be uploaded separately.
- **Proposed cover picture** (optional) should be uploaded separately.
- Any additional **appendices** (optional) to the paper may be uploaded. Appendices may be published as a supplementary material to the paper, if accepted.
- For each uploaded file the author is asked for additional metadata which may be provided. Depending of the type of the file please provide the relevant title (Statement of novelty, List of suggested reviewers, Figures, Graphical abstract, Proposed cover picture, Appendix).

#### Step 5: Confirmation

- Final confirmation is required.

### Article Types

**Review articles** are welcome in any area of chemistry and may cover a wider or a more specialized area, if a high impact is expected. Manuscripts normally should not exceed 40 pages of one column format (letter size 12, 33 lines per page). Authors should consult the ACSi editor prior to preparation of a review article.

**Scientific articles** should have the following structure:

1. Title (max. 150 characters),
2. Authors and affiliations,
3. Abstract (max. 1000 characters),
4. Keywords (max. 6),
5. Introduction,
6. Experimental (Results and Discussion),
7. Results and Discussion (Experimental),
8. Conclusions,
9. Acknowledgements (if any),
10. References.

The sections should be arranged in the sequence generally accepted for publications in the respective fields. Scientific articles should report significant

and innovative achievements and exhibit a high level of originality.

**Short communications** generally follow the same order of sections, but should be short (max. 2500 words) and report a significant aspect of research work meriting separate publication.

**Technical articles** report applications of an already described innovation. Typically, technical articles are not based on new experiments.

## Preparation of Submissions

**Text** of the submitted articles must be prepared with Word for Windows. Normal style set to single column, 1.5 line spacing, and 12 pt Times New Roman font is recommended. Line numbering (continuous, for the whole document) must be enabled to simplify the reviewing process. For any other format, please consult the editor. Articles should be written preferably in English. Correct spelling and grammar are the sole responsibility of the author(s). Papers should be written in a concise and succinct manner. The authors shall respect the ISO 80000 standard, and IUPAC Green Book rules on the names and symbols of quantities and units. The Système International d'Unités (SI) must be used for all dimensional quantities.

**Graphics** (figures, graphs, illustrations, digital images, photographs) should be inserted in the text where appropriate. The captions should be self-explanatory. Lettering should be readable (suggested 8 point Arial font) with equal size in all figures. Use common programs such as Word Excel to prepare figures (graphs) and ChemDraw to prepare structures in their final size (8 cm for single column width or 17 cm for double column width) so that neither reduction nor enlargement is required. In **graphs**, only the graph area determined by both axes should be in the frame, while a frame around the whole graph should be omitted. The graph area should be white. The legend should be inside the graph area. The style of all graphs should be the same. **Figures and illustrations** should be of sufficient quality for the printed version, i.e. 300 dpi minimum. **Digital images and photographs** should be of high quality (minimum 250 dpi resolution). On submission, figures should be of good enough resolution to be assessed by the referees, ideally as JPEGs. High-resolution figures (in JPEG, TIFF, or EPS format) might be required if the paper is accepted for publication.

**Tables** should be prepared in the Word file of the paper as usual Word tables. The captions should be above the table and self-explanatory.

**References** should be numbered and ordered sequentially as they appear in the text, likewise methods, tables, figure captions. When cited in the text, reference numbers should be superscripted, following punctuation marks. It is the sole respon-

sibility of authors to cite articles that have been submitted to a journal or were in print at the time of submission to ACSi. Formatting of references to published work should follow the journal style; please also consult a recent issue:

1. J. W. Smith, A. G. White, *Acta Chim. Slov.* **2008**, *55*, 1055–1059.
2. M. F. Kemmere, T. F. Keurentjes, in: S. P. Nunes, K. V. Peinemann (Ed.): *Membrane Technology in the Chemical Industry*, Wiley-VCH, Weinheim, Germany, **2008**, pp. 229–255.
3. J. Levec, Arrangement and process for oxidizing an aqueous medium, US Patent Number 5,928,521, date of patent July 27, **1999**.
4. L. A. Bursill, J. M. Thomas, in: R. Sersale, C. Collela, R. Aiello (Eds.), *Recent Progress Report and Discussions: 5th International Zeolite Conference*, Naples, Italy, 1980, Gianini, Naples, **1981**, pp. 25–30.
5. J. Szegezdi, F. Csizmadia, Prediction of dissociation constant using microconstants, [http://www.chemaxon.com/conf/Prediction\\_of\\_dissociation\\_constant\\_using\\_microconstants.pdf](http://www.chemaxon.com/conf/Prediction_of_dissociation_constant_using_microconstants.pdf), (assessed: March 31, 2008)

Titles of journals should be abbreviated according to Chemical Abstracts Service Source Index (CASSI).

## Special Notes

- Complete characterization, **including crystal structure**, should be given when the synthesis of new compounds in crystal form is reported.
- Numerical **data should be reported with the number of significant digits corresponding to the magnitude** of experimental uncertainty.
- **The SI system of units and IUPAC recommendations** for nomenclature, symbols and abbreviations should be followed closely. Additionally, the authors should follow the general guidelines when citing spectral and analytical data, and depositing crystallographic data.
- **Characters** should be correctly represented throughout the manuscript: for example, 1 (one) and I (ell), 0 (zero) and O (oh), x (ex), D7 (times sign), B0 (degree sign). Use Symbol font for all Greek letters and mathematical symbols.
- The rules and recommendations of the **IUBMB** and the **International Union of Pure and Applied Chemistry (IUPAC)** should be used for abbreviation of chemical names, nomenclature of chemical compounds, enzyme nomenclature, isotopic compounds, optically active isomers, and spectroscopic data.
- **A conflict of interest** occurs when an individual (author, reviewer, editor) or its organization is involved in multiple interests, one of which could possibly corrupt the motivation for an act in the other. Financial relationships are the most easily identifiable conflicts of interest, while conflicts can occur also as personal relationships, academic competition, etc. **The Edi-**

**tors** will make effort to ensure that conflicts of interest will not compromise the evaluation process; potential editors and reviewers will be asked to exempt themselves from review process when such conflict of interest exists. When the manuscript is submitted for publication, **the authors** are expected to disclose any relationships that might pose potential conflict of interest with respect to results reported in that manuscript. In the Acknowledgement section the source of funding support should be mentioned. The statement of disclosure must be provided as Comments to Editor during the submission process.

- **Published statement of Informed Consent.** Research described in papers submitted to ACSi must adhere to the principles of the Declaration of Helsinki (<http://www.wma.net/e/policy/b3.htm>). These studies must be approved by an appropriate institutional review board or committee, and informed consent must be obtained from subjects. The Methods section of the paper must include: 1) a statement of protocol approval from an institutional review board or committee and 2), a statement that informed consent was obtained from the human subjects or their representatives.
- **Published Statement of Human and Animal Rights.** When reporting experiments on human subjects, authors should indicate whether the procedures followed were in accordance with the ethical standards of the responsible committee on human experimentation (institutional and national) and with the Helsinki Declaration of 1975, as revised in 2008. If doubt exists whether the research was conducted in accordance with the Helsinki Declaration, the authors must explain the rationale for their approach and demonstrate that the institutional review body explicitly approved the doubtful aspects of the study. When reporting experiments on animals, authors should indicate whether the institutional and national guide for the care and use of laboratory animals was followed.
- Contributions authored by **Slovenian scientists** are evaluated by non-Slovenian referees.
- Papers describing **microwave-assisted reactions** performed in domestic microwave ovens are not considered for publication in *Acta Chimica Slovenica*.
- *Manuscripts that are not prepared and submitted in accord with the instructions for authors are not considered for publication.*

## Appendices

Authors are encouraged to make use of supporting information for publication, which is supplementary material (appendices) that is submitted at the same time as the manuscript. It is made available on

the Journal's web site and is linked to the article in the Journal's Web edition. The use of supporting information is particularly appropriate for presenting additional graphs, spectra, tables and discussion and is more likely to be of interest to specialists than to general readers. When preparing supporting information, authors should keep in mind that the supporting information files will not be edited by the editorial staff. In addition, the files should be not too large (upper limit 10 MB) and should be provided in common widely known file formats so as to be accessible to readers without difficulty. All files of supplementary materials are loaded separately during the submission process as supplementary files.

## Proposed Cover Picture and Graphical Abstract Image

Authors are encouraged to submit illustrations as candidates for the journal Cover Picture as well as graphical abstracts. Graphical abstract contains an image that appears as a part of the entry in the table of contents in both online and printed edition. The pictures may be the same. The illustrations must be related to the subject matter of the paper. Usually both proposed cover picture and picture for graphical abstract are the same, but authors may provide different pictures as well.

**Graphical content:** an ideally full-colour illustration of resolution 300 dpi from the manuscript must be proposed with the submission. Graphical abstract pictures are printed in size 6.5 × 4 cm (hence minimal resolution of 770 × 470 pixels). Cover picture is printed in size 11 × 9.5 cm (hence minimal resolution of 1300 × 1130 pixels).

### Statement of novelty

Statement of novelty is provided in a Word file and submitted as a supplementary file in step 4 of submission process. Authors should in no more than 100 words emphasize the scientific novelty of the presented research. Do not repeat for this purpose the content of your abstract.

### List of suggested reviewers

List of suggested reviewers is a Word file submitted as a supplementary file in step 4 of submission process. Authors should propose the names, full affiliation (department, institution, city and country) and e-mail addresses of three potential referees. For each reviewer at least one reference relevant to the scientific field should be provided as well. Appropriate referees should be knowledgeable about the subject but have no close connection with any of the authors. In addition, referees should be from institutions other than (and preferably countries other than) those of any of the authors.

## How to Submit

Users registered in the role of author can start submission by choosing USER HOME link on the top of



the page, then choosing the role of the Author and follow the relevant link for start of submission. Prior to submission we strongly recommend that you familiarize yourself with ACSi style by browsing the journal, either in print or online, particularly if you have not submitted to the ACSi before or recently.

## Correspondence

All correspondence with the ACSi editor regarding the paper goes through this web site and emails. Emails are sent and recorded in the web site database. All emails you receive from the system contain relevant links. **Please do not answer the emails directly but use the embedded links in the emails for carrying out relevant actions.** Alternatively, you can carry out all the actions and correspondence through the online system by logging in and selecting relevant options.

## Proofs

Proofs will be dispatched via e-mail and corrections should be returned to the editor by e-mail as quickly as possible, normally within 48 hours of receipt. Typing errors should be corrected; other changes of contents will be treated as new submissions.

## Submission Preparation Checklist

As part of the submission process, authors are required to check off their submission's compliance with all of the following items, and submissions may be returned to authors that do not adhere to these guidelines.

1. The submission has not been previously published, nor is it under consideration for publication in any other journal (or an explanation has been provided in Comments to the Editor).
2. All the listed authors have agreed on the content and the corresponding (submitting) author is responsible for having ensured that this agreement has been reached.
3. The submission files are in the correct format: manuscript in MS Word; diagrams and graphs are created in Excel and saved in one of the file formats: TIFF, EPS or JPG; illustrations are also saved in one of these formats (See **Author guidelines** for details).
4. The manuscript has been examined for spelling and grammar (spell checked).
5. The **title** (maximum 150 characters) briefly explains the contents of the manuscript.
6. Full names (first and last) of all authors together with the affiliation address are provided. Name of author(s) denoted as the corresponding author(s), together with their e-mail address, full postal address and telephone/fax numbers are given.
7. The **abstract** states the objective and conclusions of the research concisely in no more than 150 words.
8. Keywords (maximum six) are provided.
9. **Statement of novelty** is prepared as a Word file.
10. The text adheres to the stylistic and bibliographic requirements outlined in the **Author guidelines**.
11. Text in normal style is set to single column, 1.5 line spacing, and 12 pt. Times New Roman font is recommended. All tables, figures and illustrations have appropriate captions and are placed within the text at the appropriate points.
12. Mathematical and chemical equations are provided in separate lines and numbered (Arabic numbers) consecutively in parenthesis at the end of the line. All equation numbers are (if necessary) appropriately included in the text. Corresponding numbers are checked.
13. Tables, Figures, illustrations, are prepared in correct format and resolution (see **Author guidelines**).
14. The lettering used in the figures and graphs do not vary greatly in size. The recommended lettering size is 8 point Arial.
15. Separate files for each figure and illustration are prepared. The names (numbers) of the separate files are the same as they appear in the text. All the figure files are packed for uploading in a single ZIP file.
16. Authors have read **special notes** and have accordingly prepared their manuscript (if necessary).
17. References in the text and in the References are correctly cited. (see **Author guidelines**). All references mentioned in the Reference list are cited in the text, and *vice versa*.
18. Permission has been obtained for use of copyrighted material from other sources (including the Web).
19. The names, full affiliation (department, institution, city and country), e-mail addresses and references of three potential referees from institutions other than (and preferably countries other than) those of any of the authors are prepared in the word file.
20. Full-colour illustration or graph from the manuscript is proposed for graphical abstract.
21. **Appendices** (if appropriate) as supplementary material are prepared and will be submitted at the same time as the manuscript.

## Privacy Statement

The names and email addresses entered in this journal site will be used exclusively for the stated purposes of this journal and will not be made available for any other purpose or to any other party.

ISSN: 1580-3155



---

## Koristni naslovi

---



Slovensko kemijsko društvo  
www.chem-soc.si  
e-mail: chem.soc@ki.si



Wessex Institute of Technology  
www.wessex.ac.uk



SETAC  
www.setac.org



European Water Association  
<http://www.ewa-online.eu/>



European Science Foundation  
www.esf.org



European Federation of Chemical Engineering  
<https://efce.info/>



International Union of Pure and Applied Chemistry  
<https://iupac.org/>

---

## Novice evropske zveze kemijskih društev (EuCheMS) najdete na:



EuCheMS: Brussels News Updates  
<http://www.euchems.eu/newsletters/>



Izdajo pripravili  
**Neil G. Connolly, Ture Damhus**  
**Richard M. Hartshorn, Alan T. Hutton**

PRIPOROČILA IUPAC 2005

## **NOMENKLATURA ANORGANSKE KEMIJE**

ISBN 978-961-90731-8-6

Obseg: 367 str.

Kemijska nomenklatura oz. poimenovanje kemijskih elementov in spojin je potrebno zato, da se vsi, ki jih uporabljajo, med seboj lahko sporazumevajo. Najpomembnejše pri tem je, da je poimenovanje spojin enotno in enoznačno, saj mora biti zagotovljeno, da si pod določenim imenom vsi predstavljajo isto kemijsko spojino.

Z razvojem kemije in celotne splošne znanosti je bilo v preteklosti odkritih ali sintetiziranih ogromno število kemijskih spojin, kar se bo v prihodnosti brez dvoma nadaljevalo s še večjo intenziteto. Vzporedno z odkritji in raziskavami pa se je razvijalo in prilagajalo tudi poimenovanje kemijskih spojin. IUPAC (Mednarodna unija za čisto in uporabno kemijo) skrbi za vsklajeno delovanje na tem področju. V predgovoru k originalu knjige, ki sledi le-temu, je zato natančno opisano, kako je Mednarodna unija poimenovanje kemijskih spojin spremljala, zasledovala in

spreminjala, kadar je bilo to potrebno zaradi jasnosti ali možnosti različnih razumevanj.

Pred nami je tako v letu 2008 prevod »Nomenclature of Inorganic Chemistry, IUPAC Recommendations 2005« v slovenskem jeziku, le tri leta po izidu izvirnika. Zadnja slovenska nomenklatura anorganske kemije je bila izdana leta 1986, njen obseg pa je bil 86 strani (brez preglednic). Nova izdaja prevoda obsega skoraj 400 strani strokovno izjemno zahtevnega teksta. Slovenski prevod je pripravil Andrej Šmalc, z recenzijo in z nekaterimi dodatnimi dejavnostmi v zvezi s pripravo za tisk pa mu je pomagal Primož Šegedin. Za obsežno in strokovno korektno opravljeno delo se obema iskreno zahvaljujem.

**Venčeslav Kaučič**  
 Predsednik Slovensko kemijsko društvo

Slovensko kemijsko društvo  
 Slovenian Chemical Society



Publikacijo lahko kupite v Slovenskem kemijskem društvu,  
 Hajdrihova 19, 1000 Ljubljana

Naročilo oddate preko društvene spletne strani:

<http://www.chem-soc.si/publikacije/nomenklatura-anorganske-kemije>

**Cena: 17,50 EUR**

DODATNI 10% POPUST  
ZA UNIVERZE



**DONAU LAB** Ljubljana  
Member of LPPgroup

Donau Lab d.o.o., Ljubljana  
Tbilisjska 85  
SI-1000 Ljubljana  
www.donaulab.si  
office-si@donaulab.com

## TINYCLAVE

Kovinska posoda 10 ml  
Do 100 bar  
-20 do +300 °C

**€ 2.310<sup>+DDV</sup>**

- Izmenljiva reaktorska posoda, dobavljiva v stekleni ali kovinski izvedbi (nerjaveče jeklo s PTFE insertom oz. Hastelloy). Vse posode so izmenljive in kompatibilne z osnovnim pokrovom.
- Prostornina modela Tinyclave: 10 do 25 ml  
Prostornina modela Miniclave: 100 do 300 ml

## MINICLAVE

Kovinska posoda 100 ml  
Do 100 bar  
-20 do +300 °C

**€ 2.708<sup>+DDV</sup>**



**büchiglasuster**  
Pilot Plant and Reactor Systems  
switzerland



## KEMIJSKI PRIROČNIK

Opisi posameznih kemikalij so opremljeni tudi s CAS in s številkami carinske tarife, ki je usklajena s kombinirano nomenklaturou EU.

Vsebina knjige je prilagojena dosežkom mednarodnih organizacij (Organizacija za hrano in kmetijstvo – FAO, Organizacija za ekonomsko sodelovanje in razvoj OECD, Svetovna zdravstvena organizacija WHO...), ki so v osemdesetih letih prejšnjega stoletja postavljale temelje nove svetovne politike pri obravnavi kemijskih snovi in njihovega vpliva na človekovo okolje.

Priročnik je rezultat dela strokovnjakov Fakultete za farmacijo in Fakultete za kemijo in kemijsko tehnologijo. Podatki so zbrani iz različnih virov, ki so bili dosegljivi v strokovni literaturi, na spletnih straneh, v uradnih listih in drugih sprejemljivih publikacijah.

Ker je takšen način obravnave nevarnih kemikalij pripravljen v slovenščini, je knjiga pomemben prispevek uresničevanju nacionalnega programa o kemijski varnosti.

Avtorji knjige so Prof. Dr. Aleš Krbavčič, Prof. Dr. Aleš Obreza, Prof. Dr. Marija Sollner-Dolenc, Prof. Dr. Branko Stanovnik in Mag. Milan Škrli.

Vsebinsko priročnik zajema opise blizu 800 kemikalij, IUPAC kemijski nomenklaturni sistem za organske in neorganske spojine, opis svetovnega usklajenega sistema za razvrščanje in označevanje kemikalij (GHS), mednarodni sistem merskih enot, pregled aktivnih snovi in preparatov za zaščito rastlin registriranih v RS in osnovne farmakološko toksikološke lastnosti nekaterih kemijskih funkcionalnih skupin.

Priročnik predstavlja monografije nevarnih kemikalij, opisuje njihove kemijske in fizikalne lastnosti, praktično uporabo ter njihov vpliv na žive organizme in okolje. Namenjena je strokovnjakom, ki delujejo na področju kemije, farmacije, veterine, agronomije pa tudi poslovnim osebam, ki se ukvarjajo s proizvodnjo in prometom z nevarnimi kemikalijami ter nadzirajo njihov promet.

Priročnik nudi veliko koristnih podatkov osebam, ki so pogosto v stiku z naravnim okoljem (lovci, čebelarji, ribiči, ekologi), ki skrbijo za zaščito rastlin (gozdarstvo, poljedelstvo, sadjarstvo) in živali (veterina). V tem pogledu so posebno predstavljene kemikalije, katerih uporaba je dovoljena v Sloveniji na področju kmetijstva, sadjarstva in gozdarstva.

Publikacija je izredno primerena kot učbenik za študente kemije, kemijske tehnologije, farmacije in drugih sorodnih znanosti.

V publikaciji so zajete zakonske določbe glede razvrščanja in označevanja kemikalij v prometu, obnem z uredbo Evropskega parlamenta in Sveta o razvrščanju, označevanju in pakiranju snovi ter zmesi, ki se začne izvajati za snovi s 1. decembrom 2010, za zmesi pa s 1. junijem 2015.



**Cena knjige v elektronski obliki (CD-ROM) znaša 15 EUR**

# SLOVENSKI KEMIJSKI DNEVI 2017

Portorož, Kongresni center - Grand Hotel Bernardin

20. - 22. september 2017

Slovensko kemijsko društvo  
Slovenian Chemical Society



## KOTIZACIJA

	Plačilo pred 1. 9. 2017	Plačilo po 1.9.2017
<b>Člani društva</b> (zaposleni in zaposleni študenti 3. stopnje)	240 EUR	260 EUR
<b>Nečlani</b>	260 EUR	280 EUR
Študenti (1. in 2. stopnja, nezaposleni študenti 3. stopnje) ter upokojenci- <b>člani društva</b>	30 EUR	45 EUR
Študenti (1. in 2. stopnja in nezaposleni študenti 3. stopnje) - <b>nečlani</b>	45 EUR	60 EUR

## POMEMBNEJŠI DATUMI

Spletna prijava in oddaja povzetkov	30. junij 2017
Obvestilo o sprejetju povzetkov	21. julij 2017
Program konference	1. september 2017
Zadnji rok za plačilo kotizacij po redni ceni	1. september 2017

**Dobrodošli so prispevki  
z vseh področij  
kemijskih znanosti**

Lepo vabljeni na **23. Slovenske kemijske dneve**, ki jih znova organiziramo v **Portorožu**, v Kongresnem centru Grand Hotela Bernardin.

Svoje dosežke lahko predstavite v obliki **predavanj in posterjev**. Poskrbeli smo za odlične plenarne in vabljene predavatelje, manjkal pa ne bo tudi čas za druženje, sklepanje poznanstev in poslovnih priložnosti.

Programski in organizacijski odbor: Marija Bešter Rogač (FKKT UL), Zorka Novak Pintarič (FKKT UM), Darja Lisjak (IJS), Venčeslav Kaučič, predsednik (SKD), Janez Plavec (KI) in Marjan Veber (FKKT UL).







# Strast do pametnih premazov

Visoki **standardi, znanje**, strast do **inovacij** ter želja po nenehnih izboljšavah – to je okolje v katerem že več kot 150 let nastajajo Heliosovi **pametni premazi.**

Rešitve, ki zadostijo široki paleti potreb ustvarjajo vez, zaradi katere kupci postanejo naši partnerji in tako rastemo – skupaj.

# BODITE NEUSTAVLJIVI

## MAGNEZIJ Krka 300



Granulat za pripravo napitka vsebuje magnezijev citrat in vitamin B<sub>2</sub>.



Magnezij in vitamin B<sub>2</sub> prispevata k zmanjšanju utrujenosti in izčrpanosti ter normalnemu delovanju živčnega sistema.



Magnezij prispeva tudi k delovanju mišic.



- ✔ Okus po pomaranči in limeti. ✔ Brez konzervansov.
- ✔ Brez umetnih barvil, arom in sladil. ✔ Ena vrečka na dan.

Prehransko dopolnilo ni nadomestilo za uravnoteženo in raznovrstno prehrano. Skrbite tudi za zdrav življenjski slog.

[www.krka.si](http://www.krka.si)

 KRKA

*Naša inovativnost in znanje  
za učinkovite in varne  
izdelke vrhunske kakovosti.*

NOVO

# Acta Chimica Slovenica

## Acta Chimica Slovenica

Linen fiber felt useful as fiber material for preparation of fully bio-based fiber reinforced composites. Actually described is the hydrophobic modification by bio-based treatment using natural Tung Oil. 'See more details on page 373

Year 2017, Vol. 64, No. 2

